Fluctuations of mountain glaciers in northern Norway throughout the Holocene

JOSHUA ROBERT LEIGH

Fluctuations of mountain glaciers in northern Norway throughout the Holocene

JOSHUA ROBERT LEIGH

THESIS SUBMITTED FOR THE DEGREE OF

DOCTOR OF PHILOSOPHY

DEPARTMENT OF GEOGRAPHY

DURHAM UNIVERSITY

2021

I. ABSTRACT

Mountain glaciers are an intrinsic part of the cryosphere and their short response times make them crucial indicators of climate change. Comprehensive investigations into long- and short-term glacier fluctuations are essential in developing reliable reconstructions of past climate variability and play a fundamental role in underpinning numerical models for the predictions of glacier behaviour in a changing climate. This thesis presents changes of mountain glaciers in central Troms and Finnmark County northern (Arctic) Norway, since the recession of the Scandinavian Ice Sheet (SIS; 14,000-11,000 cal. yrs BP), throughout the Holocene, and during the 20th and early-21st century.

A new method for identifying and mapping very small glaciers from remotely sensed imagery is developed; implementing this new approach has enabled the identification of an additional 78 ice bodies not included within prior glacier inventories. Subsequent remote sensing over the period 1989-2018 reveals considerable glacier recession, when glaciers (n = 219) shrank by 35 km^2 (-35%). A subset of 15 glaciers reveals them to have lost ~69% of their area between LIA maxima and 2018 (from 10 km^2 to 3.1 km^2 respectively). The corollary of this is that, given 90% of the studied glaciers were <0.5 km^2 in 2018, it is likely that many will melt completely before the end of the 21st century.

By combining extensive glacial and periglacial geomorphological mapping with calibrated and relative age dating, the first moraine chronology within the Rotsund Valley (Kåfjord Alps) has been established. This Holocene chronology is one of the most extensive records of small mountain glaciers across mainland Troms and Finnmark county, filling a critical gap in our knowledge on the patterns of Holocene glacier fluctuations in an area particularly susceptible to rapid climatic changes. Mountain glaciers in this region likely reached their maximum extent between ~12,000 and ~10,500 cal. yrs BP, roughly corresponding with the end of the Younger Dryas (YD; 12,900-11,700 cal. yrs BP). Subsequently glacier recession was however, interrupted by a major moraine forming event ~8,200 cal. yrs BP. Maximum Neoglacial regrowth/readvance occurred ~4,600 cal. yrs BP with the most recent glacial maximum achieved during the Little Ice Age (LIA), in the early- to mid-19th century (1814-1877).

II. CONTENTS

List of Figures

List of Tables

III. LIST OF ABBREVIATIONS AND TRANSLATIONS

Table I. *List of abbreviations (sorted alphabetically) and translations of key terms in Sami and Norwegian that are used in this thesis and on regional maps etc.*

Abbreviations	
AO	Arctic Oscillation
[cal.] yrs BP	[Calibrated] years Before Present
CDE	Colour Development Index
CI	Confidence Interval(s)
DDA	Discrete Debris Accumulation
DEM	Digital Elevation Model
GIS	Geographic Information System
GPS	Global Positioning System
HTM	Holocene Thermal Maximum
ID	[Glacier] Identification
IPCC	Intergovernmental Panel on Climate Change
ka	Kiloannum (1,000 years)
LGM	Last Glacial Maximum
LIA	Little Ice Age
LOI	Loss on Ignition
NAO	North Atlantic Oscillation
NGI	Inventory of Norwegian Glaciers
NGU	Norges Geologiske Undersøkelse *(English: Geological Survey of Norway)*
NVE	Norges Vassdrags og Energidirektora (*English: Norwegian Water Resources and Energy Directorate)*

m a.s.l.	meters above sea level
RSF	Rock Slope Failure
R-value	[Schmidt hammer] Rebound value
SIS	Scandinavian Ice Sheet
SLL/5LL	Single Largest Lichen / [mean of the] Five Largest Lichen
YD	Younger Dryas

Sami	
Jiehkki	glacier (or ice cap)
Vággi	small river valley
Johka	river
Gáisá	summit of a mountain
Gáisi	tall mountain (with year-round snow)

Norwegian	
Bre (breen)	glacier (the glacier)
Jøkul	glacier/ice cap
Fonn	Glacier/snowpatch
Vann (vannet)	[body of] water (the [body of] water)
Vatn (vatnet)	a (small) lake (the lake)
Løsmasse	loose material
Elv (elva)	river (the river)
Dal (dalen)	valley (the valley)

IV. GEOLOGICAL TIMELINE; KEY CLIMATIC EVENTS AND TERMINOLOGY

Table II. *Simplified geological timeline and outlining of the key climatic events since the Last Glacial Maximum (LGM). Dates presented below and throughout the thesis are ages common era (CE) or denoted as cal. yrs BP (unless otherwise stated).*

Period	Epoch	Stage
Quaternary *2.588 million BP-present*	Anthropocene* *mid-20th century-present*	Anthropogenic climate change *1900s-ongoing*
	Holocene *11,700 cal. yrs BP-present*	Little Ice Age (LIA)[1] *1300s-1850*
		Neoglacial *6,000-2,000 cal. yrs BP*
		8.2 ka event (Finse Event)[2] *8,400-8,000 cal. yrs BP*
		Holocene Thermal Maximum (HTM)[3] *11,00-5,000 cal. yrs BP*
		Boreal *9,000-7,500 cal. yrs BP*
		Erdalen Event *10,100-9,500 cal. yrs BP*
		Pre-Boreal *11,300-9000 cal. yrs BP*
		Younger Dryas (YD) *12,800-11,700 cal. yrs BP*
		Allerød oscillation *13,600-12,800 cal. yrs BP*
	Pleistocene *2,580,000-11,700 cal. yrs BP*	Older Dryas *13,900-13,600 cal. yrs BP*
		Bølling oscillation *14,600-14,000 cal. yrs BP*
		LGM *27,000-24,000 cal. yrs BP*

*The Anthropocene is still debated and as of yet is not a formally recognised geological Epoch, (see Zalasiewicz *et al.*, 2017). It is, however, included as it recognises the rapid anthropogenically forced climate change of the 20th and 21st centuries.

[1]The termination of the LIA with glaciers reaching their maximum extent is temporally variable across Norway from 1750 in the south to 1930 in the north (cf. Nesje *et al.*, 2008).

[2]The 8.2 ka event peaks at 8,200 cal. yrs BP (Alley *et al.*, 1997).

[3]Occurring after 8,000 cal. yrs BP across Europe, HTM temperatures were warmest over the period 7,500-5,500 cal. yrs BP (cf. Renssen *et al.*, 2009).

V. ACKNOWLEDGMENTS

I am very grateful to my dedicated supervisors, Chris Stokes, Dave Evans, Liss Andreassen, and Rachel Carr, whose expert guidance, boundless enthusiasm, and gentle encouragement helped me through my Ph.D. Their detailed comments and suggestions throughout the past four years have contributed greatly to my published work and this thesis. Their support has been invaluable, making the whole process a great experience and has truly helped me grow as a researcher and writer.

I owe tremendous thanks to all those who assisted me in the field: Robert Leigh, James Linighan, Richard Jones, and Callum Pearson. Thank you all for your hard graft, good company, dedication to the task at hand, and for just putting up with me in the field! The weather of northern Norway is thanked for sparing me a complete soaking; those few days of sun and blue skies made the landscape come alive and being treated to a display of the aurora borealis was phenomenal! No thanks are given to the hordes of biting insects that ravaged us morning and night at our 2019 base camp.

I must thank all my friends (no one mentioned, no one forgotten), particularly those who joined me cycling, climbing, and on my many adventures across the UK and abroad. The time spent engaged in sport and culture has been invaluable to me and has been the means to clear my head and an opportunity to talk through ideas and worries. Other members of the Physical Geography cluster of Durham University's Department of Geography are thanked for discussion, ideas, and help troubleshooting.

My family, especially my partner Charlotte (who is my rock), and Mum and Dad have been immeasurably supportive throughout the last four years; it has been a roller coaster and without all their love and support, this would not have been possible.

Finally, I must briefly acknowledge my GCSE / A-level Geography teachers all of whom inspired me, sending me down the road that led to this thesis. Alongside the lyrics and music of Enter Shikari (especially their 2012 album "A Flash Flood of Colour") which never fails to disappoint and has proven to comfort me at times of hardship and energise me at times of activity.

VI. ACKNOWLEDGEMENT OF FUNDING

This research was funded by the Natural Environment Research Council as part of the IAPETUS Doctoral Training Programme (NE/ L002590/1).

Additional financial support for fieldwork was provided by the Alpkit Foundation and Lexus Norway kindly provided a vehicle for use during fieldwork.

VII. DECLARATION AND STATEMENT OF COPYRIGHT

I confirm that no part of the material presented in this thesis has previously been submitted by me or any other person for a degree in this or any other university.

In all cases, where relevant, material from the work of others has been acknowledged.

Joshua R. Leigh
Department of Geography
Durham University

CHAPTER 1

Introduction

Looking across the recently deglaciated foreland and onto Sorbmejiehkki (glacier ID 121) form the crest of the large lateral moraine.
Photograph date: 29th August 2018 (by J.R. Leigh)

“This is an expedition,

Into the Arctic tundra!

. . .

as we witness the ice-caps melt

Instead of being spurred into changing our ways

We're gonna invest in military hardware to fight for the remaining oil that’s

left beneath the ice!

But what happens when it's all gone!

You haven't thought this through have you boys!”

(Reynolds, 2012)

1.1. Introduction and rationale

Since the 1800s the fjords and coastal mountains of northern Norway have attracted the attention of mountaineers, artists, and scientists alike. During several early Arctic expeditions, the French painter Auguste E.F. Mayer (1805-1890) depicted many striking scenes of ships and crews exploring the northern fjords and mountains, from Lofoten to Svalbard. The physicist and glaciologist James D. Forbes (1809-1868) collected observations of many Norwegian glaciers during his 1851 expedition around Norway and provides a documentary account of the Lyngen Peninsula as "a mountainous peninsula . . . the summits covered with perpetual snow and are the feeders of numerous glaciers which in their general aspect perfectly resemble those of Switzerland" (Forbes, 1853, p. 74). Early photographers Knud Knudsen (1832–1915; one of Norway's first professional photographers) and Axel Lindahl (1841-1906; a Swedish photographer specialising in the landscape of northern Norway) captured imagery from across Norway with many of their images, sometimes by chance, providing a unique snapshot of glacier extent at the turn of the 20th century (e.g. Figure 1.1). The famous Yorkshire mountaineer William C. Slingsby (1849–1929), whom the Norwegians named the "Father of Norwegian Mountaineering", was amongst the first mountaineers to explore the mountains and glaciers of northern Norway and writes: "in the mountains of Lyngen, Nature has developed her wilds and most eerie forms" (Slingsby, 1904, p. 414). In her accounts of mountaineering on Lyngen in 1898, Aubrey Le Blond (1860-1934; the first president of the Ladies Alpine Club) beautifully describes the view from the summit of Istinden (1,495 m a.s.l.): "Glaciers with free rifts in their waves of ice swept majestically between the peaks which stood like minster spires to the north. Tiny lakes looked up at us with wide-open sapphire eyes from every little hollow. Clouds drifted lazily here and there, casting deep purple shadows on the hillsides. Not a sound fell on the ear. We seemed detached from the earth" (Le Blond, 1908, p. 47).

The Arctic landscape and glaciers of northern Norway are now, however, under threat of significant environmental change as a result of a warming climate, forced by human activities. This has brought a range of environmental consequences such as the shrinking of glaciers, melting of permafrost, degradation of Arctic ecosystems, and increasing vulnerability of local communities to environmental risk (West and Hovelsrud, 2008; Øseth, 2011).

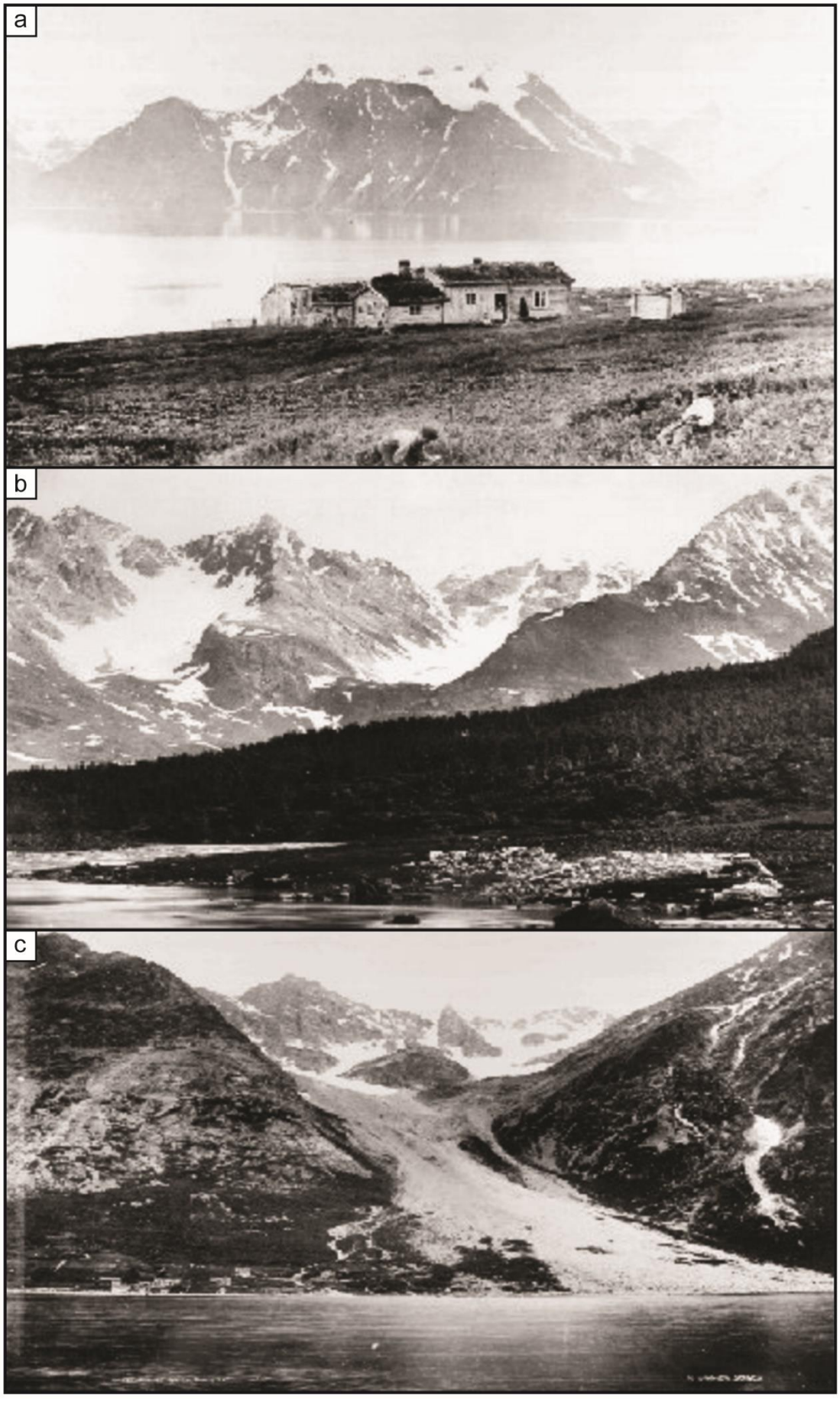
a
b
c

Figure 1.1. *Landscape photographs of the Lyngen Peninsula by Axel Lindahl and Knud Knudsen: (a) a view of the mountain Store Reindalstiden and glacier Støvelbreen (glacier ID 190; approx. 69°44'"N, 20°15'E) from the hamlet of Djupvik on the eastern side of Lyngenfjord taken by Axel Lindhal in 1880 (photograph identifier: NTRMF39-016), (b) a view from Jægervatnet on the western side of north Lyngen showing glaciers Trollbreen (left; glacier ID 202; approx. 69°42'N, 20°01'E) and Forholtbreen (right; glacier ID 204; approx. 69°42'N, 20°00'E) taken by Axel Lindhal in 1910 (photograph identifier: NTRMF39-02181), (c) a view from Kjosen fjord central Lyngen that shows two small, unnamed, glaciers (right; glacier ID 220 and left; glacier ID 222; approx. 69°36'N, 20°6'E) taken by Knud Knudsen in 1885 (photograph identifier: NTRMF39-01710). Photographs from the "Digital Museum" archive (www.digitaltmuseum.org).*

The present-day anthropogenic climate forcing is unprecedented and indisputable (e.g. IPCC, 2021), with the evidence backed up by a 100% consensus within the global scientific community (Powell, 2015, 2017; Skuce *et al.*, 2016). The result of 20th and early-21st century climate change can in some sense be considered as an end to the Holocene, with many scientists now considering the presence of a new epoch, *the Anthropocene* (1950-present). This concept, however, continues to be debated (cf. Waters *et al.*, 2016; Zalasiewicz *et al.*, 2017, 2018). Regardless of nomenclature, the evidence is clear that in the last decade (2010-2020), anthropogenically-induced warming reached approximately +1°C (likely between 0.8°C and 1.2°C) above pre-industrial levels (1850-1900), with a rate of temperature increase at approximately 0.2°C per decade (Allen *et al.*, 2018).

One of the most visible signs of climate warming is the dramatic shrinkage of mountain glaciers (IPCC, 2019, 2021). Indeed, in recent years public perception of climate change and engagement with climate science has grown (Milfont *et al.*, 2017; Thackeray *et al.*, 2020), accompanied by the rise of mass activist movements (e.g. the "School Strike for Climate, Extinction Rebellion). This has (re-)highlighted the, often irreversible, damage climate change is having on our environment. Viewed through the lens of glaciology, events such as ceremonies to mark/mourn the disappearance and "death" of glaciers (e.g. Okjökull in Iceland and the Pizol glacier in Switzerland) symbolise a new era of environmental consciousness (Johnson, 2019; Árnason and Hafsteinsson, 2020; Craps, 2020; Morehouse and Cigliano, 2021).

In Arctic Norway, glacier change since the curtailment of natural climate variability is substantial (Andreassen *et al.*, 2012b; Giesen *et al.*, 2014; Stokes *et al.*, 2018; Weber *et al.*, 2020), in part owing to the intensification of surface air temperature warming north of 60°N (Arctic Amplification; Serreze and Barry, 2011; IPCC, 2019, 2021). Furthermore, temperature and precipitation in this region, key variables in the "health" of glaciers, are substantially influenced by large-scale atmospheric circulation patterns; the Arctic Oscillation (AO) and North Atlantic Oscillation (NAO) (Thompson and Wallace, 1998; Nesje *et al.*, 2000b; Hurrell *et al.*, 2003; Rasmussen, 2007; Nesje and Matthews, 2011; Bonan *et al.*, 2019). The maritime glaciers of northern Norway are, therefore, highly sensitive to climatic perturbations (Winkler and Nesje, 2009; Winkler *et al.*, 2009; Andreassen *et al.*, 2012b). An in-depth understanding of former glacial extent in northern (Arctic) Norway is also key to improving our understanding of climate variability and plays a critical role in assessing the magnitude of contemporary glacier change in a longer-term context (e.g. Oerlemans, 1994, 2005; Wittmeier *et al.*, 2015; Roe *et al.*, 2017; IPCC, 2019, 2021).

Despite the potential to improve our understanding of Arctic, European, and global climatic change since the termination of the Younger Dryas (YD), research into the patterns of Holocene fluctuations of mountain glaciers in mainland northern Norway remains sparse. The need for robust constraints on glacier change at 100-1000-year timescales persists and is vital in the formation of predictions on the future response of glaciers (Mackintosh *et al.*, 2017). An improved chronology for the mountain glaciers of northern (Arctic) Norway has the potential to provide crucial insights into climate variability at high latitudes, as well as processes governing long-term glacial dynamics and landscape change.

This thesis focuses on examining the number, extent, and rate of change in mountain glaciers throughout the central Troms and Finnmark region over contemporary timescales (e.g. 20th/21st centuries), establishing the timing and extent of the Little Ice Age (LIA) maximum (the period of most recent glacial advance), and constraining the timing of the maximum extent for these mountain glaciers following the YD, and throughout the Holocene.

1.2. Aims and objectives

This thesis has two overarching aims:

1. To put the observed centennial-millennial scale changes in glacier extent into a present-day context.
2. To reconstruct glacial changes of the central Toms and Finnmark region of Arctic Norway, with a particular emphasis on the Holocene glacial chronology since the recession of the Scandinavian Ice Sheet (SIS).

To address these aims five key objectives are outlined:

1. Identify the number and extent of present-day glaciers throughout the central Troms and Finnmark region (paying particular attention to very small glaciers that may previously have eluded national scale glacier inventories) and examine the extent to which these glaciers have shrunk during the rapid, anthropogenically-forced, climate change of the late-20th and early-21st centuries.
2. Identify the presence and establish the age of LIA moraines fronting a series of small valley glaciers in an area of central Troms and Finnmark County that has not previously been investigated.
3. Compile a detailed map of the glacial and periglacial geomorphology throughout the central Toms and Finnmark region using remotely sensed imagery (including satellite imagery, aerial orthophotographs, and digital elevation models (DEMs)).
4. Extend the established chronology to determine the ages for the full suite of moraines beyond the LIA maximum moraines, using a combination of dating techniques.
5. Compare the application of calibrated and relative dating techniques (Schmidt hammer and soil chronosequencing) whist simultaneously establishing a dataset for the development of Schmidt hammer and soil chronosequence calibration curves for the region and collecting data for absolute dating (terrestrial cosmogenic nuclide dating (TCND)).

1.3. Thesis structure and results

This thesis is compiled with a traditional study area overview and literature review followed by a series of research papers (either published, submitted, or prepared for peer-reviewed journals) that tackle the outlined objectives (Section 1.2.). A brief discussion of the overall findings is then presented, followed by the concluding remarks.

1.3.1. Chapter 2

This chapter provides an overview of the research topic and characterises the study area, outlining previous work on the glacial geomorphology and Holocene glacier fluctuations of mainland Norway. It provides a chronological summary of key climatic events from the YD to the present-day, with a particular focus on glacier change since the LIA maximum. There is no stand-alone methods section as methods are described in detail in each relevant results chapters (Chapters 3-6).

1.3.2. Chapter 3

Leigh, J.R., Stokes, C.R., Carr, R.J., Evans, I.S., Andreassen, L.M. and Evans, D.J.A., 2019. Identifying and mapping very small (<0.5 km^2) mountain glaciers on coarse to high-resolution imagery. *Journal of Glaciology* **65**(254), pp. 873-888. DOI: 10.1017/jog.2019.50

This paper details approaches to the identification and mapping of very small (<0.5 km^2) glaciers which are prevalent in northern Norway, highlighting not only the subjectivity in their mapping but also the extent to which the advent of extensive, high-resolution imagery (e.g. <1 m pixel resolution) can enable the identification of previously unmapped glaciers. A range of examples of minimum size-thresholds are discussed, and attention is drawn to the 2012 Inventory of Norwegian Glaciers (Andreassen *et al.*, 2012a) which excludes glaciers smaller than 0.01 km^2. The existence of glaciers, in the study area, below this 0.01 km^2 minimum size-threshold is demonstrated. A simple survey of multiple observers was undertaken, showing that when unguided there was considerable inconsistency in mapping results between

experts; yet, when guided by a newly developed 'glacier scoring system', between-user differences, specifically with regards to the total number of mapped glaciers, decreased by up to ~80%. The 'glacier scoring system' allows users to classify glaciers as either *certain*, *probable*, or *possible* and helps in facilitating the mapping of glaciers smaller than 0.01 km^2 on high-resolution imagery (e.g. <1 m pixel resolution).

In this paper, I undertook the initial mapping, wrote the manuscript, and designed and made the figures. Further mapping (for the purpose of cross comparison) was conducted by Stokes C.R. and Carr R.J. and is outlined in the text. All authors contributed ideas, advised in the creation and function of the 'glacier scoring system', and provided feedback on the text. The paper has been peer-reviewed and published in *Journal of Glaciology*.

1.3.3. Chapter 4

Leigh, J.R., Stokes, C.R., Evans, D.J.A., Carr, R.J. and Andreassen, L.M., 2020. Timing of Little Ice Age maxima and subsequent glacier retreat in northern Troms and western Finnmark, northern Norway. *Arctic, Antarctic, and Alpine Research* **52**(1), pp. 281-311. DOI: 10.1080/15230430.2020.1765520

Having identified a study area in Arctic Norway, that has for the most part evaded detailed investigations, this paper undertakes both LIA glacial reconstructions for selected glaciers (glaciers ID: 115, 117, 121, and 123; approx. 69°44'N, 20°38'E), alongside regional scale glacier change assessments using 1950s historic maps, and satellite imagery from 1989 to 2018. Lichenometric dating revealed that LIA maximum moraines were formed between 1814 (±41 yrs) and 1877 (±28 yrs), which is before the early twentieth-century LIA maximum proposed on the nearby Lyngen Peninsula but younger than LIA maximum limits in southern and central Norway. Remote sensing provides a broader analysis of contemporary glacier change and, in light of the work conducted by Leigh et al. (2019) and presented in Chapter 3, the analysis of high-resolution aerial orthophotographs enabled the identification and subsequent mapping of an additional 78 ice bodies, of which 23 were classified as *certain* glaciers. When examining glacier change, between 1989 and 2018, the total area of glaciers within the study area (n = 219 in 1989) shrank by ~35 km^2 (35%), with very small glaciers (<0.5 km^2) experiencing the highest relative (%) rates of shrinkage. As of 2018, 90%

of the glaciers in the study area were smaller than 0.5 km^2. Based on the results presented and comparisons with other similar studies, it is considered that many glaciers in the central Troms and Finnmark region may disappear within the next 50-100 years.

In this paper I undertook the fieldwork, remote sensing, data analysis, compiled the detailed surficial/geomorphological map, wrote the manuscript, and designed and made the figures. All authors contributed ideas and feedback on the text. The paper has been peer-reviewed and published in *Arctic, Antarctic, and Alpine Research*.

1.3.4. Chapter 5

Leigh, J.R., Evans, D.J.A., Stokes, C.R., Andreassen, L.M. and Carr, R.J., 2021 Glacial and periglacial geomorphological map of mountain terrain, central Troms and Finnmark County, Arctic Norway. *Journal of Maps* **17**(2), pp. 348-366. DOI: 10.1080/17445647.2021.1950580

This map and accompanying manuscript depicts the glacial and periglacial geomorphology of a ~6,800 km^2 region of central Toms and western Finnmark County, Arctic Norway, including the glaciers studied in Chapter 4. The detailed glacial and periglacial geomorphological mapping provides the foundation for new interpretations of mountain glacier dynamics and landscape response to deglaciation throughout the region, enabling crucial interpretations of glacier dynamics and landscape response to climate change.

The mapping reveals complex suites of landform assemblages that include previously unmapped components of the geomorphological record, pertaining to the interaction of glacial and periglacial regimes in mountainous terrain (e.g. eskers, complex ridge systems, pronival ramparts, rock glacierized moraines, and frost heave structures). Of particular interest for future glacial geochronological studies are the extensive moraine systems mapped throughout the region, which are utilised in Chapter 6. In total we identified >14,500 individual moraine crests, with moraine ridges covering a total area of ~62 km^2. It is concluded that the map resulting from this work further demonstrates the utility of high-resolution aerial imagery and digital elevation models for mapping glacial and periglacial geomorphology across large swaths of rugged and poorly accessible terrain.

In this paper I undertook the remote sensing and map production, alongside making the figures and writing the accompanying manuscript. Evans D.J.A. and Stokes C.R. helped with the interpretation of landforms and all authors contributed ideas and feedback on the text. The paper has been peer-reviewed and published in the *Journal of Maps*.

1.3.5. Chapter 6

Leigh J.R., Stokes C.R., Evans D.J.A., Jones R.S., Carr J.R. and Andreassen L. M. Reconstructing the Holocene glacial history of northern Troms and western Finnmark, northern Norway

Building on the mapping in Chapter 5, this chapter uses a combination of calibrated and relative dating techniques to establish the timing of major moraine forming events by mountain glaciers of central Troms and Finnmark County, alongside regional assessments of SIS dynamics and glacier change since the termination of the YD. The first Holocene glacial chronology in the Rotsund Valley, central Troms and Finnmark County is established and combined with detailed mapping from Chapter 5 to reveal a complex picture of early-Holocene deglaciation and late-Holocene glacier (re)advance. Schmidt hammer dating indicates that mountain glaciers attained their maximum extent between 12,125 (11,120-13,174) and 10,588 (9,587-11,601) cal. yrs BP, subsequently undergoing recession with a series of neoglacial moraines being formed around 4,690 (4,108-5,287) cal. yrs BP. The use of soil chronosequencing as a relative age dating technique is shown to hold promise for moraine dating, especially at sites where large boulders suitable for Schmidt hammer dating are absent.

The regional mapping of the most credible ice sheet and glacier margins indicates that they were likely more extensive and were more dynamic than previously depicted. Furthermore, we provide new evidence and reconstructions of plateau icefields, during the period 13,000 cal. yrs BP to the present-day, in the central mountain regions of our study area that have previously been unreported.

This chapter has been written up and prepared as a manuscript, and it is planned to be submitted for peer-review with *Boreas*. In this chapter I undertook the fieldwork, data analysis, compiled the revised ice sheet outlines, wrote the manuscript,

and designed and made the figures. All authors contributed ideas and feedback on the text.

1.3.6. Chapter 7

Here, the main themes connecting the four results chapters (Chapters 3-6) are drawn out and discussed in turn. The themes are (1) mapping very small glaciers and tracking their evolution over time to assess centennial-scale glacier change; (2) detailed LIA glacier reconstructions based on new site specific geomorphological mapping and a regionally controlled dating framework; (3) regional scale glacial and periglacial mapping across the central Troms and Finnmark region; (4) using regional mapping and localised dating to better understand the Holocene history of mountain glaciers in northern (Arctic) Norway. To conclude this chapter, potential future research avenues are presented to stimulate further investigations across this dynamic and highly responsive region of Arctic Norway.

1.6.7. Chapter 8

The final chapter outlines the overall conclusions of this thesis in relation to the objectives presented in Chapter 1.

1.6.8. Reference list

A full reference list for all the chapters.

1.3.9. Appendix A and B

Appendix A includes a low-resolution copy of the main map from Chapter 5. A high-resolution PDF version of the map can be downloaded following this link: https://doi.org/10.1080/17445647.2021.1950580.

Appendix B includes a table detailing all key objects (e.g. glaciers, moraines, samples) and their locations, taken from Google Earth and displayed in degrees, minutes, seconds.

CHAPTER 2

Study area introduction and a review of Holocene glacial landsystems and glacial history of northern Norway

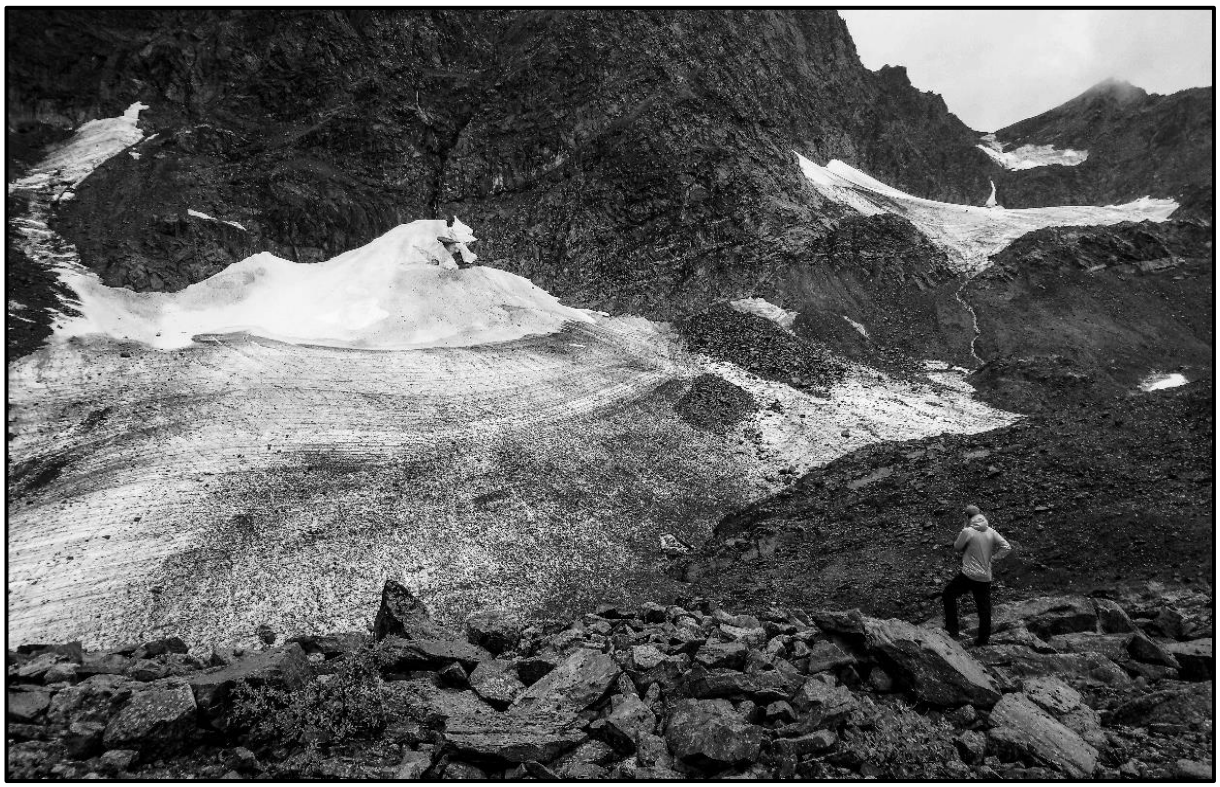

Looking across a dying glacier (glacier ID 123)

Photograph date: 13th September 2018 (by J.R. Leigh)

“There was never a broadcast made of such urgency

'Cos at no time before us

Did we grasp the scope of this emergency?”

(Reynolds, 2015b)

2.1. Introduction to 21st century glacier distribution and climate of Norway

For the purpose of this thesis, guided by the glacial areas as described in the Inventory of Norwegian Glaciers (Andreassen *et al.*, 2012a), mainland Norway is defined as southern, central, and northern Norway. Southern Norway extends south of 65°N, central Norway covers the area between 65°00'N and 67°99'N, and northern Norway extends north of 68°N, well above the arctic circle.

According to the most recent iteration of the Inventory of Norwegian Glaciers (Andreassen *et al.*, 2012a), southern and central Norway combined contain a total of 2,295 glaciers, equal to 73% of all mapped glaciers across mainland Norway, and include the two largest glaciers; Jostedalsbreen (southern Norway) and Vestre Svartisen (central Norway). Jostedalsbreen is a plateau ice cap with an area of ~473 km^2, divided into 82 individual glacier units based on drainage divides. Vestre Svartisen is also a plateau ice cap, with an area of ~219 km^2 and divided into 46 individual glacier units (Andreassen *et al.*, 2012a). Northern Norway contains 848 glaciers, the largest of which is Øksfjordjøkelen, with an area of ~39 km^2 and divided into 14 individual glacier units (Andreassen *et al.*, 2012a). Of the 3,143 glacier units on mainland Norway (Andreassen *et al.*, 2012a) the estimates of total ice volume range from 257 to 300 km^3, with a value of 271 ±28 km^3, considered the most reliable ice volume estimation during the mid-2000s (Andreassen *et al.*, 2015).

Data from the Norwegian Meteorological Institute for the period 1971-2000 (defined as the 'normal period') provides insight into the climate of Norway. Precipitation data (Figure 2.1a) shows western and central Norway having the highest average annual precipitation; these are coastal areas that are among the wettest in Europe (~3500-4000 mm a year, 1971-2000). Precipitation decreases in northern Norway (Fig. 2.1a) but some areas along the coast receive >2,000 mm annually. Furthermore, the mountains on Norway's western coast produce a rain shadow, decreasing precipitation to the east (Hanssen-Bauer *et al.*, 2015). Norway's annual temperature is approximately 1.3°C, but there is substantial regional variation based on latitude and elevation (Figure 2.1b). For example, in coastal areas of Western Norway, the mean annual temperature is >6°C, whereas in the village of Šihččajávri (continental Norway's coldest village; Kautokeino municipality, Troms and Finnmark County) the mean annual temperature is -2.8°C and, in the high mountains, mean

annual temperatures are ~-4°C (Hanssen-Bauer *et al.*, 2015). Comparing the period 1971-2000 against the period 1985-2014 shows that precipitation for Norway as a whole has increased by 7%, with the greatest precipitation increase during the spring months (Hanssen-Bauer *et al.*, 2015). Temperatures across Norway are also increasing at a rate of +0.5°C per decade (between 1976 and 2014), with the strongest temperate changes felt in northern Norway (Hanssen-Bauer *et al.*, 2015). Changes in both precipitation and temperature are decreasing snowfall and snow depth, especially in coastal regions (Dyrrdal, 2009; Dyrrdal *et al.*, 2013). Lower snow accumulation during the autumn and winter months, compounded with higher winter and spring temperatures, is also triggering an earlier snowmelt (Rizzi *et al.*, 2018), forcing a feedback of accelerated spring surface warming due to changes in surface albedo (Déry and Brown, 2007).

The climatic conditions of Norway are predominantly modulated by two atmospheric pressure phenomena, the North Atlantic Oscillation (NAO) and Arctic Oscillation (AO). In Arctic Norway, the AO has been shown to better correlate with glacier mass balance than the NAO (Andreassen *et al.*, 2012b). The NAO is the interannual variability in ocean and atmosphere circulation patterns across the North Atlantic and Nordic Seas and is defined by the strength of the Icelandic Low and the Azores High (Nesje *et al.*, 2000b; Hurrell *et al.*, 2003). When sea-level pressure is below normal in the Azores, it is generally above normal over Iceland and *vice versa* (Nesje *et al.*, 2000b; Hurrell *et al.*, 2003). In a positive NAO phase there will be a stronger difference in pressure between the two regions; westerly winds dominate, triggering a northward shift in the jet stream, increasing the strength and frequency of Atlantic storminess, and resulting in mild and wet winter conditions across Scandinavia (Nesje *et al.*, 2000b; Hurrell *et al.*, 2003; Rasmussen, 2007). Thus, a positive NAO generally results in glaciers in areas of maritime western Norway having a positive net mass balance (Nesje *et al.*, 2000b).

The AO affects the mid-to-high latitudes of the Northern Hemisphere and modulates the north-south location of the mid-latitude jet stream (Thompson and Wallace, 1998; Wang and Ikeda, 2000). During a period of positive AO the polar vortex forms a tight circle, with lower-than-average air pressure across the Arctic, driving storms further north and increasing precipitation over northern Scandinavia (Rogers and Mchugh, 2002; Rasmussen, 2007).

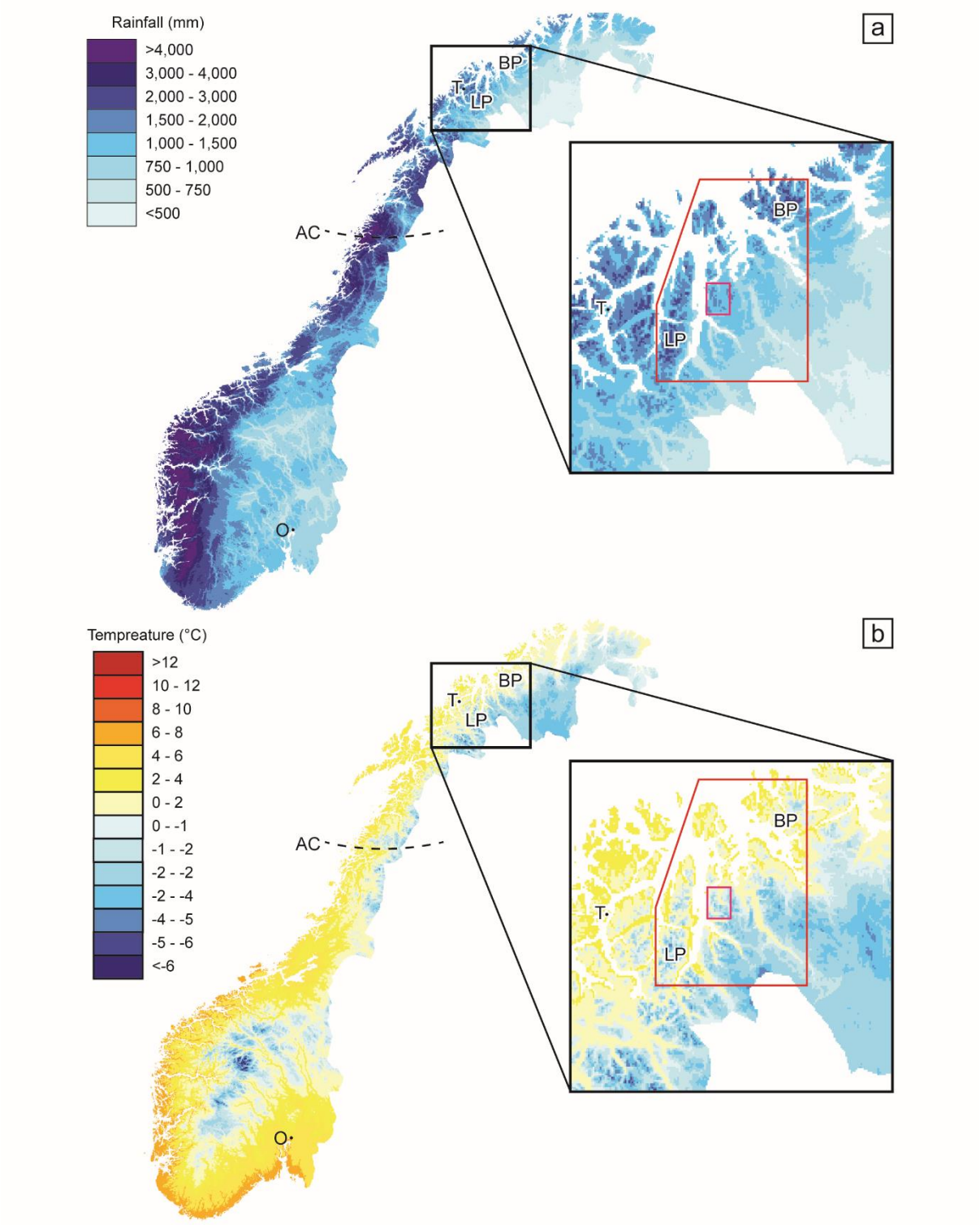

Figure 2.1. *(a) Annual precipitation (mm) across Norway in the 'normal' period 1971-2000; (b) Average annual air temperature (°C) across Norway in the 'norma'l period 1971- 2000. Large red outline shows the study area, inset red rectangle denotes Rotsund Valley site and the letter initials represent; O: Oslo, AC: Arctic circle, T: Tromsø, LP: Lyngen Peninsula, BP: Bergsfjord Peninsula. Imagery source: www.senorge.no/index.html?p=klima.*

2.2. Arctic amplification

An important consideration in the climate of northern (Arctic) Norway is that warming across this region is likely to be greater than that of the rest of Norway (and the northern hemisphere) because of Arctic amplification (AMAP, 2012; Barcaza *et al.*, 2017; Thoman *et al.*, 2020; Norwegian Polar Institute, 2021). Arctic amplification is a feature of the global climate system, whereby temperature variability in the Arctic region (60°N-90°N) is greater than variability for the northern hemisphere, or the globe as a whole, owing primarily to sea ice and snow cover feedbacks (Serreze and Francis, 2006; Serreze and Barry, 2011). The concept of Arctic amplification can be traced back as early as 1896, when it was first hypothesised that changes in the concentration of atmosphere carbon dioxide could change surface temperature, with any such temperature change being especially large in polar latitudes (Arrhenius, 1896). Since its discovery, Arctic amplification has been evidenced in palaeoclimatic records, the instrumental record, and climate models (Serreze and Barry, 2011).

Since the turn of the 20th century, observational and modelling studies have shown pronounced Arctic surface air temperatures relative to the rest of the globe (e.g. Serreze and Barry, 2011; Koenigk *et al.*, 2013; Pithan and Mauritsen, 2014; Stjern *et al.*, 2019; England *et al.*, 2021). Between the 1920s and 1940s the Arctic warmed by 1.7°C before a period of cooling lasting until the 1970s, this warming occurred before the strongest increases in anthropogenic greenhouse gas emissions and is generally considered a factor of natural climate variability (Delworth and Knutson, 2000; Bengtsson *et al.*, 2004; Johannessen *et al.*, 2004; Serreze and Francis, 2006). The warming in the Arctic since the 1970s is, however, thought to result primarily from human activities and the observed warming of 2.7°C, over the period 1971-2017 is more than twice the rate of the northern hemisphere average mean warming (Koenigk *et al.*, 2013; Box *et al.*, 2019).

There are four key drivers that underpin Arctic amplification; sea ice loss, land surface albedo feedback, horizontal heat flux convergence, and cloud cover (cf. Serreze and Barry, 2011).

Arctic sea ice cover, during the autumn, winter, and spring months, provides insulation to the relatively warm waters of the Arctic Ocean and the colder atmosphere. A reduction of the insulating sea ice therefore generates a warming of the overlying atmosphere (cf. Kim *et al.*, 2019). A further feedback is triggered as the darker open

water absorbs more solar radiation, increasing the heat content in the top layer, furthering melt and creating an enduring heat within the upper ocean layer that impedes the subsequent seasons ice growth (Screen and Simmonds, 2010; Serreze and Barry, 2011; Pithan and Mauritsen, 2014; Kim *et al.*, 2019).

Land surface albedo feedback operates in a similar manner to that of the sea-ice feedback; surface temperature warming leads to an earlier and more extensive snow-melt, resulting in a more extensive exposure of the darker underlying surface and stronger absorption of solar radiation (Brown *et al.*, 2010b; Serreze and Barry, 2011; Pithan and Mauritsen, 2014; Thackeray and Fletcher, 2016). The localised changing surface albedo and reduced snow cover is also a key factor in glacier shrinkage (e.g. Naegeli and Huss, 2017; Johnson and Rupper, 2020; Zhang *et al.*, 2021). Bare ice has a low surface albedo (around 0.3), absorbing more shortwave radiation and increasing surface melting, and therefore decreasing extent and duration of snow cover on the glacier surface and expanding the glacier area prone to surface melting over a longer duration (Paul *et al.*, 2005; Benn and Evans, 2010; Naegeli and Huss, 2017; Johnson and Rupper, 2020). Indeed, Naegeli and Huss (2017) found that sensitivity of glacier-wide mass balance per 0.1 albedo decrease is of the same order as a 10% precipitation change.

Horizontal heat flux convergence in the atmosphere and ocean leads to changes in Arctic temperature and also influences sea ice and cloud cover (Serreze and Barry, 2011). It has been suggested that between 1979 and 2008, an increasing poleward energy transport was responsible for 50% of the decadal warming trend in the Arctic (Yang *et al.*, 2010). Additionally, Arctic air temperatures are coupled with Atlantic Multi-decadal Oscillation, which is in turn linked to the strength of ocean thermohaline circulation responsible for bringing warm surface waters poleward (Chylek *et al.*, 2009; Yang *et al.*, 2010).

Arctic cloud cover, while reducing net shortwave radiation, heightens downward longwave radiation and results in a net warming over the course of a year (Serreze and Barry, 2011). The effect of cloud cover is seasonal. During the summer, when surface albedo is low, clouds reduce the downward solar flux and have a cooling effect. Conversely, in the winter, clouds contain greater quantities of liquid water, increasing the retention of longwave radiation and have a stronger influence on surface warming (Intrieri *et al.*, 2002; Serreze and Barry, 2011). Overall, the net warming effect of Arctic clouds contrasts with lower latitudes, where clouds have a net cooling effect (Vavrus

et al., 2009). Furthermore, as atmospheric carbon dioxide concentrations increase there is the possibility that it might trigger a runaway feedback cycle, whereby reduction in winter sea ice may destabilize the atmosphere. This would promote atmospheric convection and produce thicker winter cloud cover with a higher water vapor content, which in turn would strengthen longwave radiation flux, increase surface warming, and further decrease sea ice cover (Abbot *et al.*, 2009).

The interplay of the feedback cycles that initiate Arctic warming is complex, and while sea ice albedo is often cited as a key driver, there are different processes at work together, all of which are compounded by anthropogenically forced climate change (Serreze and Barry, 2011). Warming in the Norwegian Arctic is of particular concern for the survival of the many glaciers and ice caps across the region and for the large areas of mountain permafrost. Observational studies in northern Norway have shown that even large glaciers are not immune to the impacts of Arctic amplification. For example, Langfjordjøkelen (northern Norway) has been observed to have the highest rates of thinning of all glaciers across mainland Norway (Andreassen *et al.*, 2012b). Furthermore, Arctic amplification is expected to become stronger during coming decades, with the impacts of this likely to ripple out from the Arctic region (Serreze and Barry, 2011; AMAP, 2017).

2.3. Study area

The study areas (Figure 2.2) of this thesis are in northern (Arctic) Norway (between 69°10' and 70°20'N), within the central region of Troms and Finnmark County (formerly Troms County and Finnmark County). While some areas have been the focus of previous studies (e.g. the Lyngen and Bergsfjord Peninsula) many regions have not (e.g. the Kåfjord Alps) and therefore this investigation fills an important research gap (see Chapter 1).

Throughout the study area (Figure 2.2) the 2012 Inventory of Norwegian Glaciers (Andreassen *et al.*, 2012a) records a total of 309 glaciers. Of these 309 glaciers only six (2%) are larger than 5 km^2, 41 (13%) are between 1 and 5 km^2, and 268 (87%) are smaller than 1 km^2, with 234 (76%) of these smaller than 0.5 km^2. The methods used within the 2012 Inventory of Norwegian Glaciers for the mapping of glaciers from remotely sensed imagery uses a minimum size-threshold of 0.01 km^2 on 30 m resolution Landsat imagery (Andreassen *et al.*, 2012a). It is, therefore, possible that additional small glaciers (e.g. those smaller than 0.01 km^2) exist throughout the region and elsewhere (see Chapter 3).

Geologically, the area is complex, predominantly characterised by metasedimentary rocks formed during the Caledonian orogeny (Andersen, 1968) and broadly comprising lithologies of amphibolite, quartzite, gneiss, and schist (Lindahl *et al.*, 2005; Augland *et al.*, 2014; Geological Survey of Norway, 2015). Additionally, the central mountain chain of the Lyngen Peninsula and majority of the Bergsfjord Peninsula are underlain by gabbro, olivine gabbro, and metagabbro of Cambrian age (Randal, 1971; Geological Survey of Norway, 2015; Wittmeier *et al.*, 2015). Lithological units have been grouped into regional nappes, for example: Tromsø Nappe, Lyngen Nappe, Vaddas Nappe, and Kåfjord Nappe (Coker-Dewey *et al.*, 2000). The bedrock has been mapped extensively and is recorded in detailed 1:50,000 maps published by the Geological Survey of Norway (Norges Geologiske Undersokelse; NGU). The treeline in this region is generally low and forest limits reach an average of ~400 m around the fjords and ~500 m a.s.l on the inland plateau (Meier *et al.*, 2005). Above this vegetation is Arctic heath/tundra (Te Beest *et al.*, 2016). Decreasing vegetation prevalence with elevation and surface age results in large proportions of exposed bedrock at high elevations and within recently deglaciated terrain.

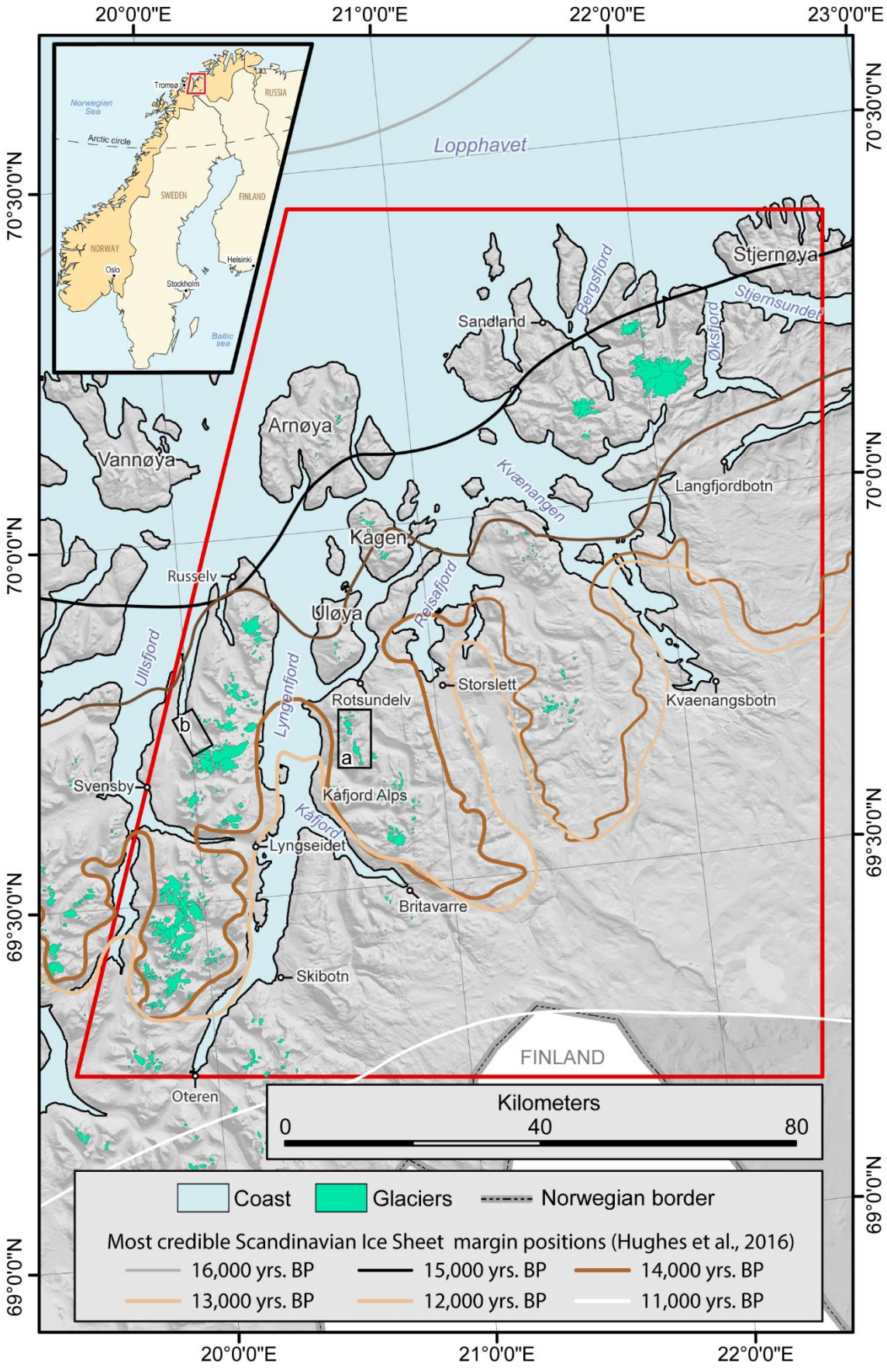
20°0'0"E
21°0'0"E
22°0'0"E
23°0'0"E
70°30'0"N
70°0'0"N
69°30'0"N
69°0'0"N
Lopphavet
Stjernøya
Sandland
Bergsfjord
Øksfjord
Stjernsundet
Arnøya
Vannøya
Kvænangen
Langfjordbotn
Kågen
Russelv
Vløya
Reisafjord
Ullsfjord
Lyngenfjord
Storslett
Rotsundelv
Kvaenangsbotn
b
a
Svensby
Kåfjord Alps
Kåfjord
Lyngseidet
Britavarre
Skibotn
FINLAND
Oteren
Kilometers
0
40
80
Coast
Glaciers
Norwegian border
Most credible Scandinavian Ice Sheet margin positions (Hughes et al., 2016)
16,000 yrs. BP
15,000 yrs. BP
14,000 yrs. BP
13,000 yrs. BP
12,000 yrs. BP
11,000 yrs. BP
Tromsø
RUSSIA
Norwegian Sea
Arctic circle
SWEDEN
FINLAND
NORWAY
Oslo
Helsinki
Stockholm
Baltic sea

Figure 2.2. *Study area location map in central Troms and Finnmark County; northern Norway. Large red outline shows the study area, inset rectangles show field sites (a) the Rotsund Valley, and (b) Strupskardet. Glacier outlines (turquoise) are from the 2012 Inventory of Norwegian Glaciers* (Andreassen *et al.*, 2012a) *and the SIS outlines show the "most credible" margins at 1,000 year timesteps taken from Hughes et al. (2016). Base image is a hill shaded 2 m digital elevation model (Arctic DEM; Porter et al., 2018).*

The region also has a diverse geography, with small mountain ranges, broad fjords, coastal islands, and upland plateaus being the dominant features (Figure 2.2). In the west, the Lyngen Peninsula comprises a ~90 km long mountain range, known as the Lyngen Alps, orientated north-south and formed of mostly flat-topped mountains, divided by deeply incised glacial valleys and flanked by two large fjords: Ullsfjord to the west (75 km long) and Lyngenfjord to the east (82 km long). The Lyngen Alps reach elevations of ≤1,834 m a.s.l and produce a rain shadow to the east of the mountains (Whalley *et al.*, 1989). Andreassen et al. (2012a) record 148 glaciers on the Lyngen Peninsula, some of which are small cold-based plateau icefields covering the highest flat topped summits (e.g. Jiehkkevárri).

North-east of the Lyngen Peninsula are a series of islands (Figure 2.2), the largest four being Arnøya (~276 km^2), Kågen (~86 km^2), Uløya (~78 km^2), and Laukøya (~36 km^2). Arnøya has five broad valleys all orientated north-south and interconnected with smaller subsidiary valleys and cirques. The remaining four islands are characterised by small steeply incised valleys, most of which contain LIA type moraines at the cirque threshold and larger end moraines at the valley mouth. Only 23 cirques across all four islands host present-day glaciers, ice patches, or perennial snow, the remaining are ice/snow free (Andreassen *et al.*, 2012a).

To the east of Lyngenfjord is a small mountain range (colloquially referred to as the Kåfjord Alps; Figure 2.2 and 2.3), with mountain peaks reaching a maximum elevation of 1,355 m a.s.l in the north (Nordmannviktinden) and 1,408 m a.s.l. in the south (Ádjit). There are 44 glaciers recorded in these mountains and the largest two (glacier ID 157 and 158; approx. 69°34'N, 20°47'E) are classified as plateau glaciers (Andreassen *et al.*, 2012a). The southern extent of the Kåfjord Alps range is cross-cut by Kåfjord (a subsidiary of Lyngenfjord) before it continues south towards the Norwegian border, but the mountains here do not retain the name (Figure 2.2). East

of the Kåfjord Alps are a series of broad U-shaped valleys (Rotsunddalen, Kildalen, and Reisadalen).

Approximately 30 km east of the Kåfjord Alps, and at the eastern edge of Reisadalen, there is a small mountain plateau area (Figure 2.2), peaking at 1,339 m a.s.l. (Riehppegáisá), and henceforth referred to as the Riehppe plateau. The Riehppe Plateau is the highest point in the Reisadalen area, covering around 40 km^2 and divided into a northern and southern plateau by a small valley (Rokkilhohka). In total, Andreassen et al. (2012a) record 24 glaciers across the Riehppe plateau, all above 700 m a.s.l. The largest glaciers (ID 109, 110, 111, and 113; approx. 69°44'N, 21°27'E) are connected, but have separate drainage divides, and collectively cover an area of ~1.54 km^2 and an elevation range of 1,212-980 m a.s.l.

Between the two large fjords, Reisafjord (30 km long, ≤14 km wide) and Kvaenangen (72 km long, ≤18 km wide), in the central northern sector of our study area lies a headland and small massif (the Kvænangstinden massif; Figure 2.2), with mountain peaks up to 1,178 m a.s.l (Store Kvænangstinden) and hosting 15 small glaciers (Andreassen *et al.*, 2012a). The largest valley in this range is the north-west orientated Meilandsdalen, predominantly filled by a large moraine dammed lake (Storvatnet; 0.4 km^2) and rock glacier complex originating from the eastern valley wall. At the valley head there are several small perennial ice/snow masses, and one small glacier (glacier ID 74, 0.14 km^2; Andreassen et al., 2012; approx. 69°58'N, 21°22'E).

In the north-east of the study area is the Bergsfjord Peninsula (Figure 2.2), a rugged mountainous area, with several high-elevation plateaus, interwoven by glacial valleys and surrounded by fjords and inlets. The largest surrounding fjords are the Stjernsundet strait (36 km long, ≤4 km wide) to the north-east, Langfjorden (35 km long, ≤3 km wide) to the south, and Kvaenangen (15 km long, ≤15 km wide) to the south-west. The north/north-west of the peninsula is exposed to the open sea (Lopphavet). Andreassen et al. (2012) record 44 glaciers on the Bergsfjord Peninsula, several of which combine to form three large icefields: Øksfjordjøkelen (38.6 km^2), Langfjordjøkelen (7.5 km^2), and Svartfjelljøkelen (4.1 km^2).

Finally, the southern and south-eastern portions of the study area can broadly be categorised as continental upland plateau, stretching up to and beyond the Norwegian border (Figure 2.2). The ≤4 km wide valley Reisadalen dissects the plateau and forms the main topographic depression running in a south-easterly direction towards the south-westernmost part of the Finnmark plateau. There are no present-

day glaciers in this region and studies suggest that the SIS likely retreated from this area between 11,000 and 10,000 yrs BP (Figure 2.2) (Hughes *et al.*, 2016). The area is largely inaccessible by road or foot and has an average elevation of ~770 m a.s.l. There is sparse vegetation cover, meaning that the surface geology, which is predominantly covered by a veneer of sediment, is clearly visible from remotely sensed imagery.

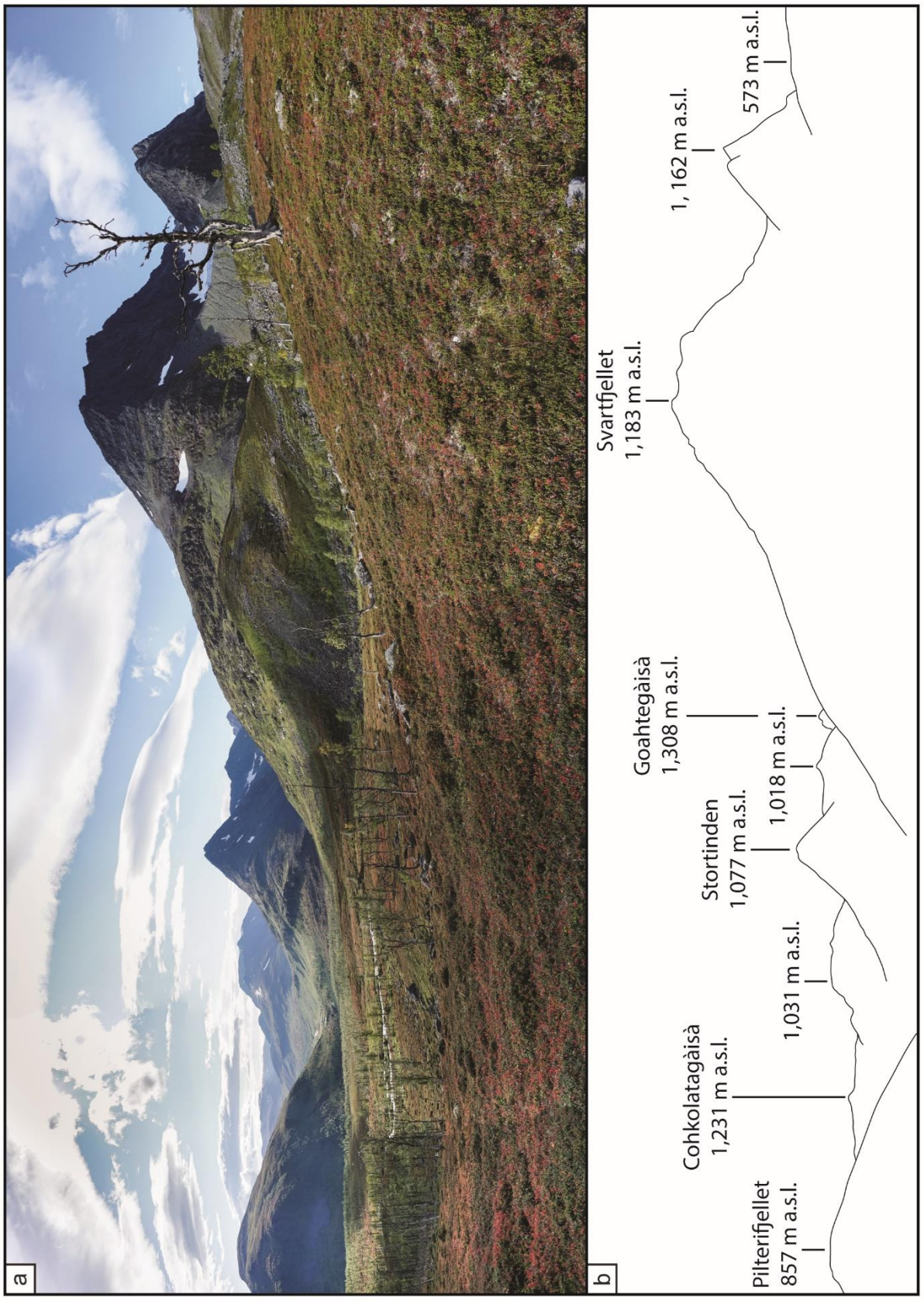

Figure 2.3. (a) *Panorama looking due south into the Rotsund Valley of the* Kåfjord Alps (image source: J.R. Leigh)*; (b) annotated sketch of the main peaks.*

2.4. A review of Holocene glacial landsystems, glacier reconstructions, and key climatic events

2.4.1. Glacial geomorphology and landsystems

Adopting a landsystems approach, individual geomorphological elements (flutings, moraines, eskers etc.) can be grouped into units (e.g. a succession of end moraines or an area of hummocky terrain) that help define an area of land, shaped by a specific process or processes that differs from the surrounding landscape (Speight, 1963; Evans, 2003c). Features across a landscape, similar in form and setting, can also be grouped, from which interpretations of origin and age can be made; building up a picture of landform stratigraphy within a site and/or across a region (e.g. Clayton and Moran, 1982; Evans, 2003c; Bickerdike *et al.*, 2018a). The grouping of geomorphological units and interpretation as to their origins forms the basis of the landsystems concept (cf. Evans, 2003a). One key ability of landsystem classifications is the way in which analysis of mapped units leads to interpretations of 'glaciation styles' (Brugger *et al.*, 1983; Brodzikowski and van Loon, 1987; Owen, 1998; Evans, 2003a), which in turn are used to reconstruct past environments, evolutions in the landscape history, and even specific processes that were active at prior glacier margins (e.g. Boulton and Eyles, 1979; Owen and Derbyshire, 1989; Evans, 1990a, 2003c; Evans and England, 1992; Krüger, 1994; Ó Cofaigh *et al.*, 1999; Evans *et al.*, 2002; McDougall, 2013).

Landsystem interpretations also enable the derivation of morphostratigraphic units, essential for assessment of palaeoglaciological and palaeoclimatic variables (e.g. Lukas, 2006; Nesje, 2009; Benn and Evans, 2010; Boston *et al.*, 2015; Lowe and Walker, 2015; Chandler and Lukas, 2017; Bickerdike *et al.*, 2018b). Morphostratigraphic analysis within a control site (e.g. where landform and geochronological analysis has been undertaken) helps define features of associated age (e.g. the YD) and thereby facilitates identification of similar features in adjacent valleys and across a region (cf. Lukas, 2006). This allows for locations lacking in site specific controls (e.g. owing to logistical issues, or lack of dateable material) to be included in analysis, building a bigger picture of glacial history throughout a region. Investigations that have combined landsystem and morphostratigraphic analysis have proven highly successful in reconstructions of prior ice masses throughout Norway

(e.g. Dahl *et al.*, 2002; Evans *et al.*, 2002; Nesje, 2009; Aa and Sønstegaard, 2019; Wittmeier *et al.*, 2020) and across the globe (e.g. Darvill *et al.*, 2017; Le Roy *et al.*, 2017; Bickerdike *et al.*, 2018b; Braumann *et al.*, 2020; Dowling *et al.*, 2021).

Glaciated terrains have been increasingly characterised by their landsystem signatures and these range from those that define ice-sheet margins (e.g. Alexanderson *et al.*, 2002; Colgan *et al.*, 2003; Van der Wateren, 2003; Kehew *et al.*, 2012; Evans *et al.*, 2014), to plateau icefields (e.g. Rea and Evans, 2003; Evans *et al.*, 2006b, 2012; Evans, 2010), glaciated valleys (e.g. Eyles, 1983; Owen and Derbyshire, 1989; Spedding and Evans, 2002; Benn *et al.*, 2003), and even paraglacial environments (e.g. Ballantyne, 2002, 2003; Mercier, 2008a). Glacial landsystems lie on a spectrum, whereby evolution and transition between glacial styles and dynamics varies not only with time and climate, but also with topography, ice thermal conditions, and debris supply (Johnson, 1980; Eyles, 1983; Evans, 2003a, 2013a; Robinson *et al.*, 2008; Benn and Evans, 2010; Bennett *et al.*, 2010; Evans *et al.*, 2013, 2017a).

The mapping of sediment-landform assemblages enables the compilation of glacial landsystem models, facilitating continued improvement of our understanding of process-form relationships in glacial geomorphology, and helping to explain the spatial and temporal evolution of modern and/or historically deglaciated landscapes (e.g. Evans and Rea, 1999; Evans and Twigg, 2002; Golledge, 2007; Evans *et al.*, 2008; Evans, 2011). By linking geomorphological features to specific processes, glacial landsystem models play a key role in supplementing other palaeoglaciological investigations (Evans *et al.*, 1999b; Evans and Twigg, 2002; Benn and Lukas, 2006). Furthermore, Evans (2009b, 2011, 2013a; Evans *et al.*, 2013, 2017a) highlights the increasing need for modern landsystem analogues that document observable changes in glacial systems, as they are crucial to reconstructing spatial and temporal variability in palaeo-landsystem signatures.

Across central Troms and Finnmark County, five key glacial landsystems have predominated following deglaciation of the SIS, each of which will be discussed in turn: plateau icefield, active temperate, glaciated valley, and paraglacial landsystems.

2.4.1.1. Plateau icefield landsystems

Mountain plateaux, surrounded by deep valleys and fjords, can form an area of refugia and/or act as an inception point for glaciers during cold periods (Ives *et al.*, 1975; Evans *et al.*, 2002, 2016b, 2016a; Rea and Evans, 2003). Work at present-day plateau icefields across the Arctic (e.g. Norway, Iceland, and Canada) has facilitated the development of the plateau icefield landsystem. This broadly identifies two types/phases of plateau icefield glaciation: (1) that of large-scale ice cover whereby the mountain summits and surrounding areas are submerged under ice and the plateau exerts minimal control on ice flow, and (2) the small-scale plateau summit ice centre feeding ice to the surrounding valleys (e.g. Figure 2.4), with ice flow dictated by topography and ice presence controlled by elevation and climate (Ó Cofaigh *et al.*, 1999, 2003; Rea and Evans, 2003, 2007; Evans *et al.*, 2006b).

The nature of plateau icefields is often that of cold-based ice feeding into valley glacier systems and, as such, the geomorphological evidence of plateau icefield landsystems can be difficult to interpret, with limited or no evidence on the plateau itself (Rea *et al.*, 1998). Where evidence on the plateau is absent, landforms and deposits in the surrounding lowlands can be indicative of icefield presence and extent (e.g. Rea *et al.*, 1998; McDougall, 2001, 2013; Rea and Evans, 2003; McDougall and Evans, 2015; Bickerdike, 2016; Bickerdike *et al.*, 2018b, 2018a), although many such landforms are similar to those of glaciated valley landsystems (Eyles, 1983; Benn *et al.*, 2003), into which plateau outlets will often develop over time during glaciation. Careful assessment of the geomorphological record across plateau environments is therefore required to differentiate between valley glacier and plateau icefield landsystems. Where geomorphological evidence is present on the plateau this is generally in the form of moraines, erratics, meltwater channels, glacial erosional forms, sediments and areas of differential bedrock weathering (cf. Rea and Evans, 2003). In some cases, it may be possible to trace ice-marginal moraines and trimlines up-valley onto the plateau itself, providing a quantifiable link between the valley and plateaux deposits (Whalley *et al.*, 1995a; McDougall, 1998, 2001; Rea *et al.*, 1998; Evans *et al.*, 2002, 2006b). A final point of note regarding plateau icefield geomorphology is that in cases of cold-based ice conditions, periglacial features and even Tertiary weathering residues that pre-date glacierisation (e.g. blockfield) may be preserved across plateaux (Dahl, 1966; Whalley *et al.*, 1981, 1997; Gellatly *et al.*, 1988; Kleman,

1994; Rea *et al.*, 1996; Marr *et al.*, 2018). This has given rise to significant debate on palaeonunataks and refugia in glaciated mountain terrains for nearly a century (see Ives, 1978; Ballantyne, 2013 and references therein) and sometimes under-estimations of former ice cover (cf. Sissons, 1980; Rea *et al.*, 1998; McDougall, 2001; McDougall and Evans, 2015)

The presence of plateau icefields has important implications for the Equilibrium-Line Altitude (ELA) interpretations of mountain glaciations (cf. Manley, 1955, 1959; Sissons, 1980; Rea *et al.*, 1998; Carr and Coleman, 2007). Ice-mass input from plateaux to outlet glaciers can substantially alter their ELA, and the larger the plateau area that contributes ice mass, the greater the ELA shift (Rea *et al.*, 1998, 1999; Rea and Evans, 2007). In essence, the area-altitude relationship is such that smaller plateau icefields need higher elevations to survive and the higher the elevation the more likely it is the ice will be cold based. Conversely lower elevation plateau icefields will have warmer ice and more complex thermal regimes (Manley, 1955, 1959). Reconstructions of past climate based on ELA estimations of valley glaciers not influenced by any potential icefield on the surrounding plateau are therefore likely to be erroneous (Rea *et al.*, 1999; Evans *et al.*, 2002). Gellatly et al. (1986) and Rea et al. (1999) note that, if a plateau icefield with a positive mass balance is situated above the regional firn line, it will likely be self-sustaining. Moreover, if it extends to the plateau rim, it will likely contribute mass to a glacier in the valley below via ice avalanching creating a “fall glacier” or “reconstituted glacier”, a glacier that is sustained even though it lies below the regional ELA. In a warming climate, however, plateau icefields can become highly sensitive to excess melt due to their generally smaller ice thicknesses spread over larger areas of similar elevation and thus a rise in ELA will result in a larger volume of ice more susceptible to melt; this causes non-linear responses and rapid ice wastage (e.g. Rea *et al.*, 1999; Boston *et al.*, 2015; Åkesson *et al.*, 2017; Boston and Lukas, 2019; Weber *et al.*, 2019, 2020; Weber, 2020).

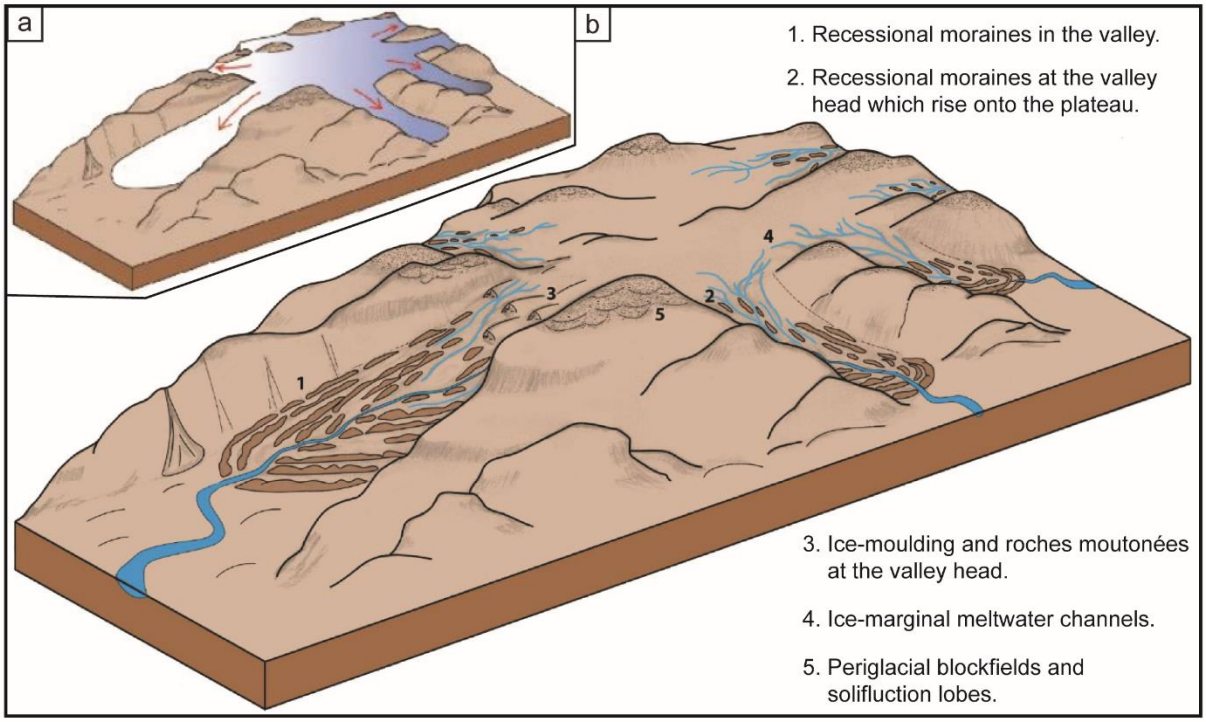

Figure 2.4. *Conceptual diagram of a plateau icefield glacier complex and associated landforms: (a) a plateau icefield glacier complex feeding individual outlet valley glacier systems; (b) conceptual model of the plateau icefield landsystem, that likely characterised glaciated upland areas, emphasising the key glacial landforms that can be used to infer glacier extent and glaciation style. Adapted from Bickerdike et al. (2018a, p. 205 and 210).*

In northern Norway, plateau icefield systems have been identified on the Lyngen Peninsula (e.g. Jiehkkevárri; Figure 2.5) and Bergsfjord Peninsula (e.g. Whalley *et al.*, 1981, 1995a, 1997; Gellatly *et al.*, 1986, 1988; Rea *et al.*, 1996, 1998, 1999; Evans *et al.*, 2002) and, although there are areas of remnant icefields on plateau areas in the mountain areas centred between these two regions, there have been no detailed assessments of their prior extent.

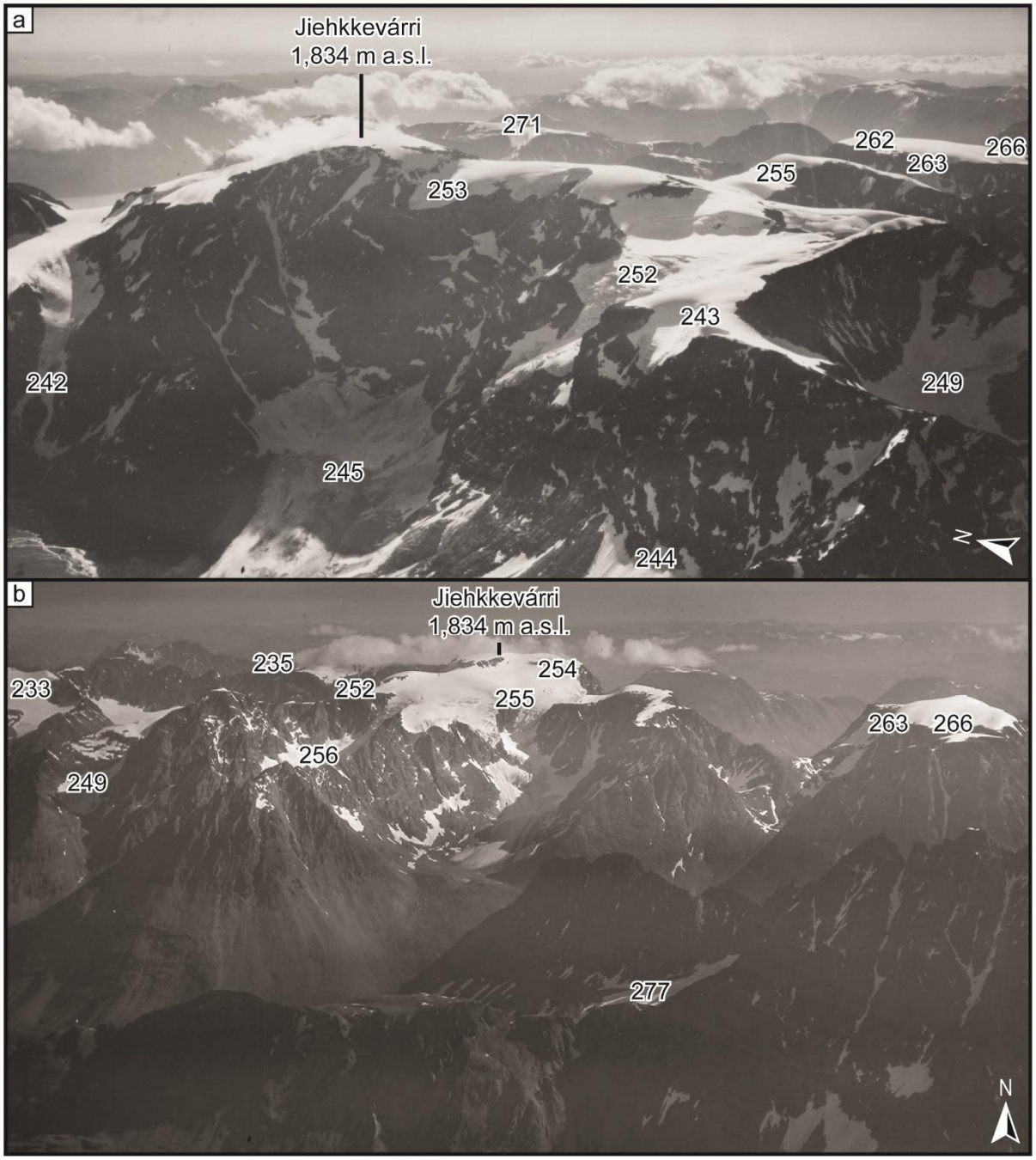

Figure 2.5. *Oblique air photographs from 1952 showing the mountain of Jiehkkevárri and the Jiehkkevárri icefield, located on southern Lyngen (approx. 69°28'N, 19°52'E): (a) looking east, (b) looking north. NVE splits the icefield into several glaciers based on drainage divides, with glacier IDs shown. Both (a) and (b) were photographed on the 31.07.1952 by Widerøes Flyveselskap. Image source: (a) National Library of Norway; (b) Perspektivet Museum.*

2.4.1.2. Active temperate glacier margin landsystems

Temperate glaciers are those which are mainly wet-based for at least part of the year, found in areas where winter snowfall and summer melt rates are high, and the ground is underlain only by discontinuous permafrost (cf. Evans, 2003b; Benn and Evans, 2010). It has been well established that temperate glaciers are highly sensitive and will respond to even short-term changes in climate, resulting in an advance or oscillatory fluctuation over a series of years, even during a period of net recession, hence their active nature (Boulton, 1986; Evans, 2003b; Chandler *et al.*, 2016a, 2016b, 2016c, 2020a, 2020b; Evans *et al.*, 2019b). At high elevations and higher latitudes a frozen zone around the margin can also develop during the winter when the cold temperatures penetrate the ice and underlying sediments (Harris and Bothamley, 1984; Krüger, 1996; Evans and Twigg, 2002; Evans and Hiemstra, 2005). Commonly, active temperate glaciers are considered to form in lowland settings or outlet glacier forelands. However, in higher elevation maritime regions (e.g. the west coast of Norway) mountain glaciers are also seen to behave in the same manner (e.g. Matthews *et al.*, 1995; Winkler and Matthews, 2010). Indeed, alpine cirque glaciers have also been shown to behave with the same characteristics as larger temperate glaciers, responding on daily and seasonal time-scales (cf. Sanders *et al.*, 2010, 2018) and not behaving simply as rigidly rotating ice bodies with little to no internal deformation (McCall, 1952; Lewis, 1960; Weertman, 1971).

Evans and Twigg (2002) and Evans (2003b) explain that the active temperate glacier landsystem is characterised by three depositional domains: (1) extensive, low amplitude moraines, (2) incised and terraced glacifluvial forms, and (3) small scale subglacial landform assemblages (Evans *et al.*, 2017a; Evans, 2018; Evans *et al.*, 2019b; Chandler *et al.*, 2020b). An example of these features in an Arctic, outlet glacier foreland can be found at *Hoffellsjökull* south-east Iceland (Figure 2.6).

The characteristic moraines in the active temperate glacier foreland/margin are small (e.g. <5 m high) push and squeeze moraines, often linked to annual winter advances (Price, 1970; Evans, 2003b; Lukas, 2012) and often accompanied by subdued, overridden ridges formed during a prior advance (Krüger, 1994; Evans and Twigg, 2002; Evans *et al.*, 2016c, 2017a). The shape of the push moraines commonly mirrors that of the glacier front (e.g. Figure 2.6) and, if undisturbed after formation, can form ridges hundreds of meters in length (Price, 1970; Matthews *et al.*, 1979). Glacial

flutes have also been recorded on the proximal side of moraines (e.g. Figure 2.6) and this has linked the processes of push moraine formation and subglacial bedform production; push moraines can result from deformation of subglacial sediments and their extrusion and/or advection to sub-marginal positions where they are used in the construction of moraine ridges (Krüger, 1993, 1994, 1995, 1996; Matthews *et al.*, 1995; Evans and Twigg, 2002; Hiemstra *et al.*, 2015). These studies also show that quasi-stationary ice fronts will construct larger, often multi-crested push moraine complexes.

Large areas of glaciofluvial deposits such as sandur, recessional ice-contact fans, and kame terraces are common on active temperate glacier forelands (e.g. Figure 2.6), either occupying incisions through or wrapped around moraines and/or interspersed with glacially smoothed bedrock (Krüger, 1994; Evans, 2003b; Evans *et al.*, 2017a; Evans, 2018; Chandler *et al.*, 2020b, 2020a). These deposits are often heavily incised and reworked by meltwater and the melt out of ice cores in cases of buried glacier ice (Price, 1969, 1971; Evans and Twigg, 2002; Evans, 2009a). When mapped, the often complex network of active, inactive, and abandoned meltwater channels reveals and records the many adjustments to streamflow resulting from changes to ice margin position (and related meltwater patterns and intensities) proglacial lake outflow, surface runoff, and resulting patterns of aggradation and erosion (Evans and Twigg, 2002; Marren, 2002). The presence of proglacial lakes is not uncommon, formed in overdeepenings or impounded by moraines, debris, and/or bedrock (Liermann *et al.*, 2012). Proglacial lakes become large sediment sinks (Fleisher *et al.*, 2003; Carrivick and Tweed, 2013) and the resulting glaciolacustrine sediment are thought to be primed for deformation during glacial overriding, and provide ample material for push moraine development (e.g. Sharpe and Cowan, 1990; Bennett *et al.*, 2000b, 2000a; Ó Cofaigh and Evans, 2001; Evans, 2003b; Evans *et al.*, 2006a).

As noted earlier, the widespread minor flutings on till surfaces are a subglacial landform assemblage, originating from till deformation and grooving (Hoppe and Schytt, 1953; Boulton, 1976; Gordon *et al.*, 1992; Benn, 1994). The till surfaces themselves are often thin (e.g. <2 m) and have been interpreted as being emplaced by subglacial deformation and lodgement (Gordon *et al.*, 1992; Boulton *et al.*, 2001b; Evans and Twigg, 2002; Van Der Meer *et al.*, 2003; Evans *et al.*, 2010a).

There are few detailed investigations into glacier thermal regime across the central Troms and Finnmark area of northern Norway, but many glacier investigations and reconstructions indicate the widespread presence of temperate ice conditions across a spectrum of glacier sizes (e.g. Griffey and Whalley, 1979; Kverndal and Sollid, 1993; Rea *et al.*, 1996; Bakke *et al.*, 2005a). Furthermore, reviewing the widespread high-resolution aerial orthophotographs that cover the Troms and Finnmark region, it is possible to identify many forelands that host a suite of features that are attributable to active temperate glacier margins, some of which are investigated in detail in this thesis (Chapters 4, 5, and 6).

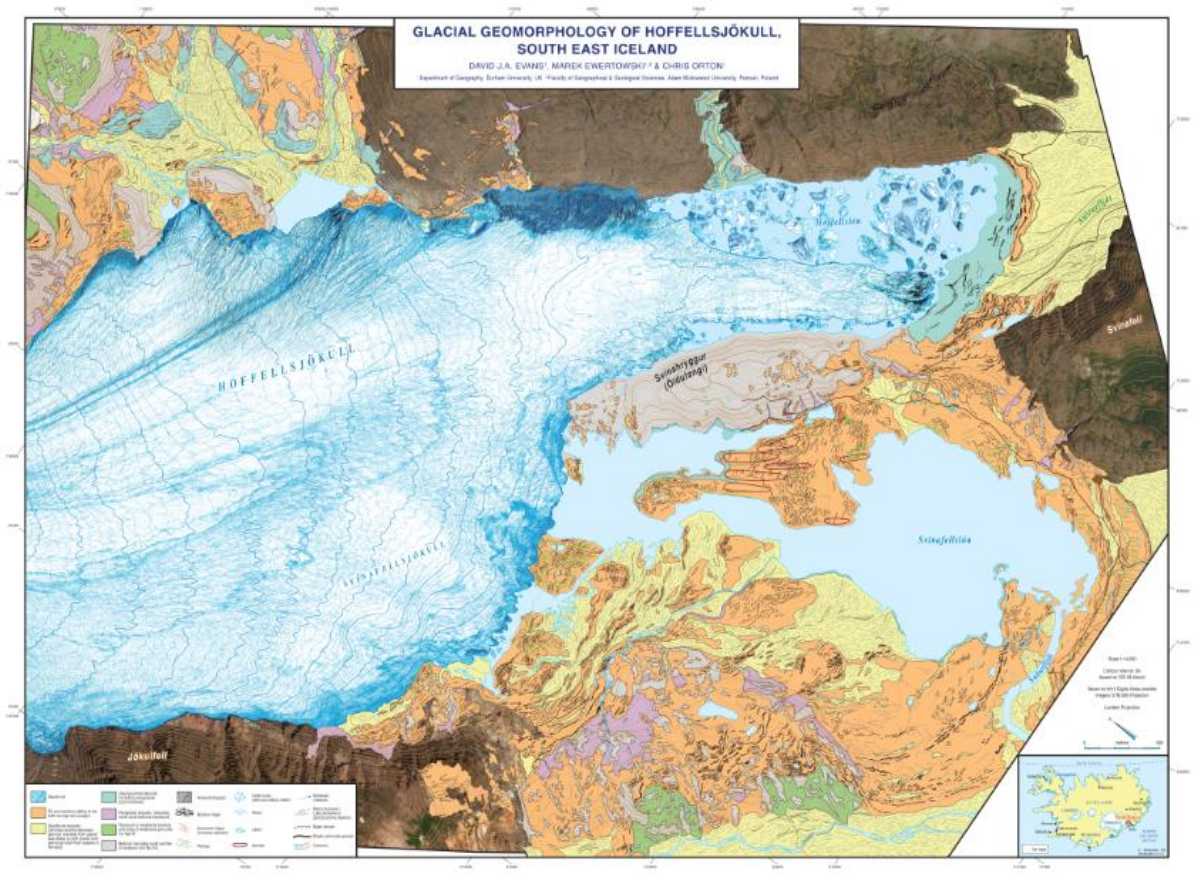

Figure 2.6. *A 1:14 500 scale glacial geomorphology and surficial geology map of Hoffellsjökull, south-east Iceland showing signs of active temperate glacier recession* (Evans *et al.*, 2019b, p. 258).

2.4.1.3. Glaciated valley landsystem

The glaciated valley landsystem incorporates a range of depositional and erosional features specific to topographically confined glaciers specific to a range of climates, timescales, and glacial thermal regimes (e.g. Boulton and Eyles, 1979; Eyles, 1983; Spedding and Evans, 2002; Benn *et al.*, 2003; Glasser *et al.*, 2009; Mackintosh *et al.*, 2017). Importantly for palaeoglaciological investigations, the unique geomorphological elements of each valley landsystem carry a climatic signal that may cover many 100s-1,000s of years (cf. Mackintosh *et al.*, 2017).

It is suggested by Benn et al. (2003) that there are three recurring factors which dominate the processes and forms within the glaciated valley landsystem: topography, debris input, and sediment transport. The transport of sediments with the glaciated valley landsystem can be formed in two modes: coupled ice margins and decoupled ice margins (Benn *et al.*, 2003). Coupled ice margins are developed at glaciers with efficient transfer of sediment from the glacier through the proglacial fluvial system. Conversely, decoupled ice margins are developed where inefficient fluvial systems are unable to remove the sediment from glacier margins (Benn *et al.*, 2003). Transport of sediment within the glaciated valley landsystem involves either 'active' subglacial debris transport or 'passive' supraglacial debris transport and glacifluvial mechanisms which transport sediments over, beneath, and away from the glacier (e.g. Boulton, 1978; Kirkbride and Spedding, 1996; Johnson and Menzies, 2002; Kirkbride, 2002; Egholm *et al.*, 2012; Kirkbride and Deline, 2013). The dominance of any one of these sediment transport process will result in a different response in the glacial and proglacial environments. In cases of slow ice flow velocity, where the supraglacial debris supply exceeds that of debris evacuation the debris cover will spread up-glacier. Continued supply increases debris load and so glaciers that are largely free of debris transition into debris-covered glaciers (cf. Kirkbride, 2000, 2011; Westoby *et al.*, 2020).

Generally, valley glaciers have a substantial debris supply, which results in the development of voluminous moraine systems through a variety of processes (e.g. pushing, squeezing, dumping, and melt out). Possibly the most impressive of the depositional landforms of glaciated valley landsystems are those of lateral moraines (e.g. Figure 2.7), forming ridges 100s of meters high, with sharp crests, and steep, sometimes unstable, slopes. Lateral moraines are often found plastered along steep bounding rock walls, slowly diverging down valley and forming large troughs or

‘ablation valleys’ (Oestreich, 1906) between the distal slope and valley side, which become sinks for glaciofluvial sediment and colluvium.

The formation of large lateral moraines is an incremental process, with the glacier building the moraine over consecutive years. This can result in an age-elevation gradient through their layered internal structures (Humlum, 1978), which often contain chronological evidence that spans the whole Neoglacial period (Osborn, 1986; Reyes and Clague, 2004). Where meltwater discharge is low and/or tightly confined at the glacier terminus position, lateral moraines often form arcuate ridges that mirror the glacier terminus at its maximum extent (latero-frontal moraines), with the frontal portions being formed via a combination of pushing and dumping and reflecting an increase in the active transportation of debris with proximity to the glacier centre-line (Evans *et al.*, 2010b; Hanáček *et al.*, 2011; Lukas and Sass, 2011; Bowman *et al.*, 2018). If latero-frontal moraines become sufficiently large, they also play a role in modulating glacier flow and flow direction and can result in glacier damming. In such circumstances periods of glacier growth are limited to ice thickening, but it is possible for parts of a glacier snout to breach a moraine crests to form “breach lobes” (Owen, 1994; Kirkbride, 2000; Benn *et al.*, 2003; Evans *et al.*, 2010b, 2016b; Hewitt, 2013; Žebre and Stepišnik, 2015). Depending on the valley properties, it is not uncommon for lateral moraines of differing size to develop on either side of the valley, a factor known as ‘within valley asymmetry’ (cf. Matthews and Petch, 1982; Benn, 1989; Evans, 1999b).

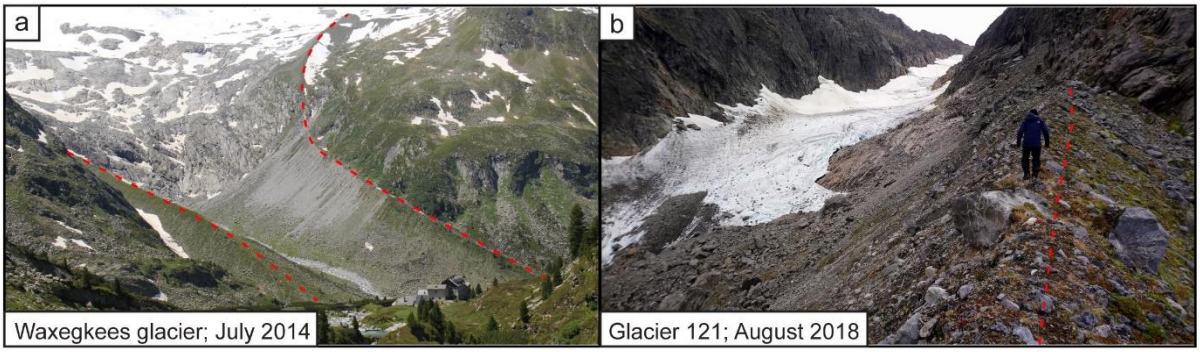

Figure 2.7. *Large lateral moraines found in (a) Austria and (b) Norway. (a) Relatively uniform lateral moraines fronting the glacier Waxegkees, with their upper reaches being less stable, as seen by the lack of vegetation on the higher slope (Image date: 03/07/2014). (b) a steep sided lateral moraine plastered to the true left valley wall. This contrasts with no lateral moraine at this point on the opposite side of the valley (Image*

date: 31/08/2018, approx. location 69°44'31"N, 20°40'14"E). In both (a) and (b) glacially smoothed bedrock is seen it the upper reaches of the valley and abundant surficial material is seen in the valley bottom. Photographs: J.R. Leigh.

Inset within the latero-frontal moraine complex it is common to find sequences of recessional moraines, demarcating the glacier terminus position during a period of glacier stability and/or readvance during net retreat. Recessional moraine assemblages provide a detailed archive of glacier oscillations which in turn can be linked to changes in glacier behaviour and climate (Werner, 1993; Nesje and Dahl, 2000; Lukas and Bradwell, 2010).

In broad areas of chaotic hummocky moraine the patterns of glacier response and climate become less clear (Sissons, 1974, 1977). Hummocky moraine has been evidenced at valley glacier sites across the globe and has sparked continued debate as to formation process and paleoclimate significance (Benn, 1992; Hambrey *et al.*, 1997; Lukas, 2005; Graham *et al.*, 2007). While historically the term has been used descriptively (e.g. Sissons, 1974, 1977, 1979; Benn, 1992; Attig and Clayton, 1993; Bennett and Boulton, 1993; Johnson and Clayton, 2003), more recent work limits the term hummocky moraine, to describe moraine deposits formed through specific processes such as the melt out of debris-mantled ice (e.g. Sharp, 1985; Johnson and Mickelson, 1995; Andersson, 1998; Evans and Twigg, 2002; Schomacker, 2008; Benn and Evans, 2010) or sequences of ice-marginal moraines formed during active, oscillatory ice retreat (e.g. Benn and Lukas, 2006; Bickerdike *et al.*, 2018b; Boston and Lukas, 2019; Chandler *et al.*, 2020c, 2021).

In Norway there are various accounts of “hummocky topography”, “hummocky fields”, and “hummocky moraine” (e.g. Larsen *et al.*, 1998; Knudsen *et al.*, 2006; Sutinen *et al.*, 2014), but there are very few landform studies distinctly categorising hummocky moraine through detailed morphological and sedimentological investigations. In Jæren, south-west Norway, Knudsen (2006) assess the morphology and sedimentology of hummocky moraine of the Høgjæren plateau and define two separate areas, one formed as a result of an active wet-based glacier and the other from a stagnant ice margin. They note that these landforms are similar to those of the characteristic Scottish hummocky moraine (Knudsen *et al.*, 2006). Within the Rotsund Valley field site, areas of chaotic ridge and furrow networks have been mapped in detail (Leigh *et al.*, 2020, 2021; Chapters 4 and 5 respectivly) and classified as areas

of discrete debris accumulation (sensu Whalley, 2009, 2012) on the basis that no sediment landform investigations were undertaken to unequivocally assess their origins (cf. Benn and Evans, 2010).

In contrast to the debris laden lower reaches, the upper parts of the glaciated valley landsystem are likely to be defined by areas of ice-moulded bedrock (see Figure 2.7), accompanied by various medium and small scale erosional features such as roches moutonnées, whalebacks, and striations (Benn *et al.*, 2003; Glasser and Bennett, 2004).

A further distinct feature of the glaciated valley landsystem is that of rock glaciers (Figure 2.8); tongues or lobate masses of angular debris that resemble small glaciers, with distinctive inset ridges and furrows across their surface, and are/were moving downslope due to the deformation of internal ice lenses or frozen sediments (Martin and Whalley, 1987). The size of rock glaciers varies, from small localised lobate structures within a larger stable feature to massive ice-debris accumulations that fill an entire valley (e.g. Millar and Westfall, 2008).

The genesis of rock glaciers and rock glacier classification remain highly contentious issues, with two conflicting schools of thought arguing that rock glaciers are either glacial or periglacial (e.g. Martin and Whalley, 1987; Whalley and Martin, 1992; Hamilton and Whalley, 1995; Whalley *et al.*, 1995b; Haeberli, 2000, 2005; Berthling, 2011; Hedding, 2016b). This simplistic and mutually exclusive twofold classification of rock glaciers is, however, difficult to apply in many situations, and Benn et al. (2003) suggest that it is more likely that these ice-debris accumulations form a continuum. At one end of the spectrum rock glaciers have been shown to have evolved from heavily debris covered glacier termini (e.g. Johnson, 1980; Whalley, 1992; Shroder *et al.*, 2000; Jones *et al.*, 2019b), but many researchers have evidenced the downslope deformation of non-glacial landforms owing to the creep of interstitial ice (e.g. Gray, 1970; Lindner and Marks, 1985; Wilson, 1990; Millar and Westfall, 2008). As such, rock glaciers do not pertain solely to the glaciated valley landsystem, but also to the paraglacial and periglacial landsystems.

Owing to the high preservation potential of rock glaciers when active, inactive, and relict, they represent an important climatic and palaeoclimatic resource, the significance of which was first summarised by Humlum (1998). Humlum (1998) suggests that while glaciers and rock glaciers can form within the same climatic conditions, rock glaciers are also able to develop under drier conditions (e.g. Humlum,

1998; Hughes *et al.*, 2003; Azócar and Brenning, 2010; Bockheim, 2014). The palaeoclimatic significance of rock glaciers has been reaffirmed by research which indicates that they might represent an archive of Holocene and even Lateglacial climatic conditions (Frauenfelder and Kääb, 2000; Millar and Westfall, 2008; Winkler and Lambiel, 2018). Furthermore, irrespective of origin and age, rock glaciers containing present-day ice are thought likely to play an increasingly important role in water preservation in arid and semi-arid environments over the coming years. This is due to the insulation provided by overlying rocky debris making the hydrologically valuable ice volumes more resilient to climate warming (Rangecroft *et al.*, 2015; Jones *et al.*, 2018a, 2019a, 2021; Schaffer *et al.*, 2019). The inclusion of rock glaciers within regional landsystem assessments and a better understanding of their origins and likely ice content are therefore essential if we are to understand their role in providing water for local communities in the future (e.g. Jones *et al.*, 2018a, 2019a, 2021; Schaffer *et al.*, 2019).

Most Holocene glacier investigations across northern Norway have focused on the glaciated valley landsystem, with papers predominantly documenting glacier fluctuations and retreat, and the development of rock glaciers and proglacial lakes (e.g. Whalley, 1971, 1973, 1976, 1992; Griffey and Whalley, 1979; Ballantyne, 1990; Gordon *et al.*, 1992; Bakke *et al.*, 2005a; Greig, 2011; Stokes *et al.*, 2018; Wittmeier *et al.*, 2020). The extensive network of interconnected valleys hosting numerous individual glaciers has created an extensive array of landforms across all scales and serves as a relatively untapped resource for reconstructions of former glacier extent and climatic conditions. As with other investigations, the focus of the valley systems in the Troms and Finnmark region is the Lyngen area, yet even this isolated peninsula has many valley systems that are yet to be documented in detail.

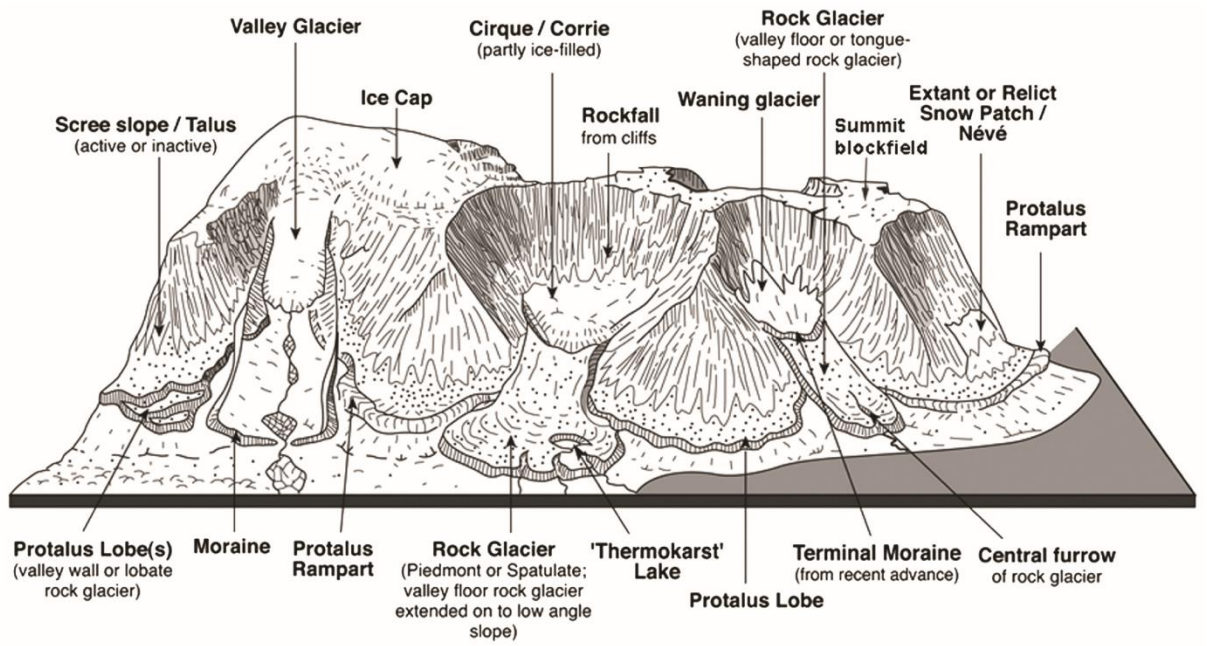

Figure 2.8. *Idealised representations of the types of rock glacier and discrete debris accumulations found in mountain areas (cf. Whalley, 2009, p. 92).*

2.4.1.4. Cirque glacier landsystem

In some mountain settings, present-day cirque glaciers occupying the upper reaches of the glaciated valley landsystems often represent the final stages of deglaciation, but at sites outlying the main area of glacierization and/or in sub-optimal settings, the cirque glacier landsystem can also represent periphery glaciation, especially where these cirques are poorly formed (Dahl *et al.*, 1997; e.g. Harrison *et al.*, 1998; Evans, 1999c, 2007, 2016; Bendle and Glasser, 2012; Bickerdike, 2016). The maximum extent of cirque glaciers is typically demarcated by a prominent moraine ridge (e.g. Colhoun and Synge, 1980; Harrison *et al.*, 1998; Paasche *et al.*, 2007; García-Ruiz *et al.*, 2014; Bickerdike *et al.*, 2016), with this terminal moraine occasionally formed of several superimposed ridges indicating that several glacial maxima of (near) equal magnitude have occurred (e.g. Clapperton, 1971; Bennett *et al.*, 1999; Žebre and Stepišnik, 2015). Inset within the terminal moraine there are often a series of recessional moraines which can extend to within only a short distance of the cirque backwall (e.g. Williams, 1973; Colhoun and Synge, 1980; Dahl *et al.*, 1997; Paasche *et al.*, 2007; García-Ruiz *et al.*, 2014). The recessional moraine sequences within a cirque indicate active retreat, whereas sites where only a terminal moraine is present indicate rapid and uninterrupted deglaciation (cf. Benn and Evans, 2010; Bendle and

Glasser, 2012; Bickerdike *et al.*, 2018a). It has also been noted that, within the cirque landsystems, moraines frequently enclose areas of hummocky terrain (Brynjólfsson *et al.*, 2012; Bickerdike, 2016; Bickerdike *et al.*, 2016), indicative of the high debris to ice ratios that are present, owing to proximity of cirque walls as debris source areas and short (potentially negligible) transport distances.

In deglaciated cirques around the base of the walls, and particularly at the headwall, it is common to find pronival ramparts (e.g. Ballantyne, 1987; Shakesby, 1997; Curry *et al.*, 2001; Wilson *et al.*, 2020), formed as a result of passive transport of rocky debris over a perennial snowbank (cf. Hedding, 2016a). Recent research by Matthews et al. (2017) has, however, shown that it is possible for pronival ramparts to have a complex evolutionary history. In particular, they evidence one rampart that has transitioned into that of a moraine, as a result of glacier development in the recess between the foot of the rampart and the bedrock cliff, which they propose to have occurred during the Neoglaciation with a glacier active in this area as recently as the LIA (Matthews *et al.*, 2017). Indeed, the impounding and sheltering properties of pronival ramparts has been suggested to play a role in the development of very small glaciers in sub-optimal settings (Colucci, 2016). Even within cirques that have not experienced glacial conditions since the LGM, relict pronival ramparts formed during more recent cold periods (e.g. the YD or Neoglacial) are a useful indicator as to the limits of both glaciation and severe cold conditions, in both vertical and horizontal extent (e.g. Ballantyne, 1986; Ballantyne and Kirkbride, 1986; Grab, 1996; Lukas, 2006; Hedding *et al.*, 2007; Hedding, 2016a). Within cirques pronival ramparts are thus a component of the cirque glacier landsystem that also exists within the periglacial landsystem and can transition between the two landsystems.

2.4.1.5. Paraglacial and periglacial landsystems

The term paraglacial, as first defined by Church and Ryder (1972), was used to describe the landscape and processes that are non-glacial, but are nonetheless conditioned by prior glaciation. More recently, Ballantyne (2003) defined paraglacial as “non-glacial earth-surface process, sediment accumulations, landforms, landsystems and landscapes that are directly conditioned by glaciation and deglaciation” (Ballantyne, 2003, p. 432). Slaymaker (2009) adds that paraglaciation is long-term landscape transition of a landsystem unadjusted to prior glacial disturbance

and present-day processes. The paraglacial landsystem is, therefore, related to the relaxation of a landscape over timescales of 10s to 10,000s of years and influenced by ongoing process at varying spatial scales. As a result, a paraglacial landsystem can substantially outlast the period of deglaciation (Iturrizaga, 2011). Ballantyne (2003) categorises the paraglacial landsystem into six key components: rock slopes, drift-mantled slopes, glacier forelands, and alluvial, lacustrine and coastal systems (e.g. Ryder, 1971; Matthews *et al.*, 1998; Ballantyne, 2000, 2002, 2003; Curry, 2000; Mercier, 2008a, 2008b; Bourriquen *et al.*, 2018; Strzelecki *et al.*, 2020).

All of the six paraglacial landsystem subdivisions exist across Norway. The most relevant for this thesis is that of the paraglacial rock slope landsystem (e.g. Ballantyne, 2000, 2002, 2003; McColl, 2012; Ballantyne and Stone, 2013; Cossart *et al.*, 2013; Curry, 2021). At the most extreme end of the spectrum, potential catastrophic rock slope failure (RSF) puts people and infrastructure at high levels of risk (e.g. Huggel *et al.*, 2012; Harbitz *et al.*, 2014; Böhme *et al.*, 2015; Purdie *et al.*, 2015; Hilger *et al.*, 2018). In the Lyngenfjord area of northern Norway (see Figure 2.2) the rock slopes have been conditioned by stress regimes of numerous glacial cycles and are considerd primed for failure (Böhme *et al.*, 2020; Vick *et al.*, 2020); one of the most prime examples is the Jettan rockslide complex (Figure 2.9) composed of an approximate 9 million m^3 of material. If it were to catastrophically fail it would inundate the fjord, producing a tsunami wave that would overwhelm the nearby villages, including Lyngseidet, which is the administrative centre of Lyngen Municipality with a population of ~800 people (Blikra and Christiansen, 2014; Eriksen *et al.*, 2017; Eckerstorfer *et al.*, 2018; Norges Geologiske Undersogelse, 2019; Statistics Norway, 2020). Further important implications of paraglacial RSFs are those of sediment supply to glacial valleys (e.g. McCarroll *et al.*, 1998; Ballantyne, 2002, 2008; Wilson, 2009; Schleier *et al.*, 2015), the formation and expansion of rock glaciers (e.g. Whalley *et al.*, 1986; Whalley and Martin, 1992; Shroder *et al.*, 2000; Haeberli *et al.*, 2006; Harrison *et al.*, 2008; Monnier and Kinnard, 2015; Charbonneau and Smith, 2018), and even the development of cirques (Turnbull and Davies, 2006; Cave and Ballantyne, 2016; Coquin *et al.*, 2019). Evans (2021) however, rejects a RSF origin for cirque formation, reaffirimg the traditional glacial origin hypothesis (e.g. McCall, 1972; Evans and Cox, 1974; Richardson and Holmlund, 1996; Brook *et al.*, 2006; Benn and Evans, 2010; Evans, 2013b; Ipsen *et al.*, 2018).

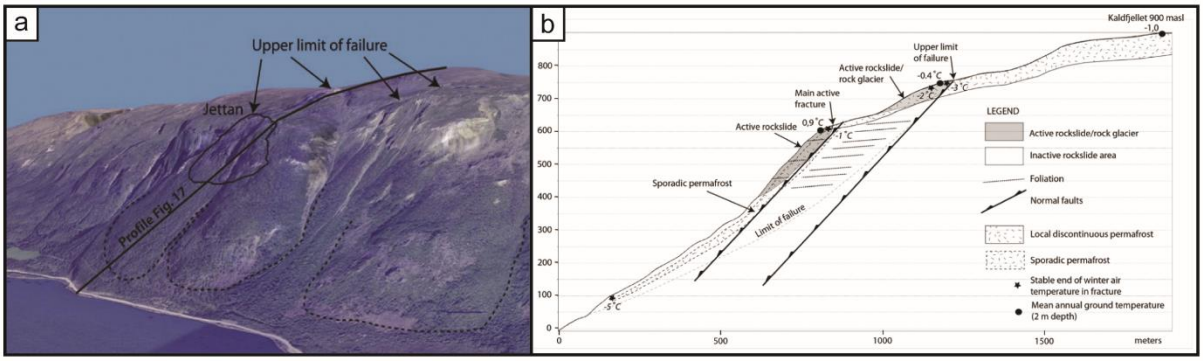

Figure 2.9. *The Jettan rockslide complex (approx. 69°33'23"N, 20°24'48"E): (a) 3D render showing the backscarp (solid polygon), large failure lobes (dotted polygons) and active moving area (solid line); (b)* an annotated west-east p*rofile of the Jettan rockslide with permafrost limits marked. Image modified from Blikra and Christiansen (2014).*

Periglacial environments are defined as those which experience freeze–thaw cycles, deep seasonal freezing, and/or those which exist within the permafrost domain (French, 2017; Ballantyne, 2018). Furthermore, as summarised by Slaymaker (2009), periglacial environments form irrespective of glacial environments and thus their proximity to glacier margins is coincidental. The periglacial realm has also been subdivided into six periglacial environments: polar deserts, Arctic tundra, Arctic and subarctic boreal forest, maritime periglacial, alpine periglacial, and mid-latitude high plateau periglacial (French, 2017; Ballantyne, 2018). The periglacial landsystem therefore encompasses the development of landforms, regolith cover, sediments and subsurface structures in cold non-glacial environments of the past and present (e.g. Evans *et al.*, 2017c; Giles *et al.*, 2017; Murton and Ballantyne, 2017; Ballantyne, 2018; Serrano *et al.*, 2018; Evans, 2020; Murton, 2021), although it should be noted that they can also develop as a result of paraglacial processes within deglaciating(/ed) environments (Wilson, 2009, 2017). Murton and Ballantyne (2017) make a distinction between lowland periglacial landsystems and upland periglacial landsystems: (1) lowland periglacial landsystems are those <400 m a.s.l., generally lacking steep slopes, and overlain by thick bands of Quaternary sediments; (2) upland periglacial landsystems comprise landscapes characterised by steep slopes, >400 m a.s.l. with and thin or discontinuous band of superficial cover. It is however, noted that the upland and lowland periglacial landsystems are transitional, grading into one another (Murton and Ballantyne, 2017). Furthermore, as with the paraglacial landsystem, the periglacial

landsystem is divided into six key components: plateau landsystems, sediment-mantled hillslope landsystems, rock-slope landsystems, slope-foot landsystems, valley landsystems, and buried landsystems (Murton and Ballantyne, 2017).

In northern Norway, most of the land surface is currently underlain by discontinuous permafrost with sporadic permafrost extending as low as ~150 m a.s.l. (Gisnås *et al.*, 2017). During the Lateglacial, YD, and Holocene cold periods, it is possible that permafrost was more extensive and reached lower elevations than the present-day (e.g. Isarin, 1997; Lilleøren *et al.*, 2012). Indeed Sanjaume and Tolgensbakk (2005, 2009) have linked geomorphological evidence on raised beaches to presence of submarine permafrost on the Varanger Peninsula, northern Norway, following SIS deglaciation around 15,000-12,000 cal. yrs BP.

Seasonal ground freezing and snow activity can also produce periglacial landforms (e.g. Matthews *et al.*, 1998; Berthling *et al.*, 2001; Boelhouwers *et al.*, 2003; Harris *et al.*, 2008) and as a result, the total elevation profile of the Troms and Finnmark region can be considered part of the periglacial landsystem, whether active or relict. Periglaciation manifests throughout the Troms and Finnmark study area in a broad spectrum of landforms and processes, across a range of temporal and spatial scales, and in both active and relict features. At the broad scale, large areas of mountain terrain and upland plateau display a wide range of periglacial surface deformation features (e.g. Figure 2.10) including: patterned ground, block-field, gelifluction, and ploughing boulders (e.g. Svensson, 1962, 1963; Whalley *et al.*, 1981; Gellatly *et al.*, 1988; Rea *et al.*, 1996; Farbrot *et al.*, 2008; Hjort *et al.*, 2014). In a more localised context, features like the Jettan rockslide complex, while paraglacailly initated, is presently undergoing periglacial deformation, with deep seated permafrost within its fissures and seasonal freezing throughout the topmost layers (see Figure 2.9; Blikra and Christiansen, 2014; Eckerstorfer *et al.*, 2018). Periglaciation also likely plays an important role in the development and/or preservation of the numerious rock glaciers throughout northern Norway (cf. Martin and Whalley, 1987; Whalley and Martin, 1992; Berthling, 2011) which now exist within the periglacial domain and are thus influenced by periglacial proccess (cf. Haeberli, 1985; Berthling, 2011). Periglacal landsystems, therefore, exist not only as a standalone landsystem but also crossover with those of the paraglacial and glacial landsystems.

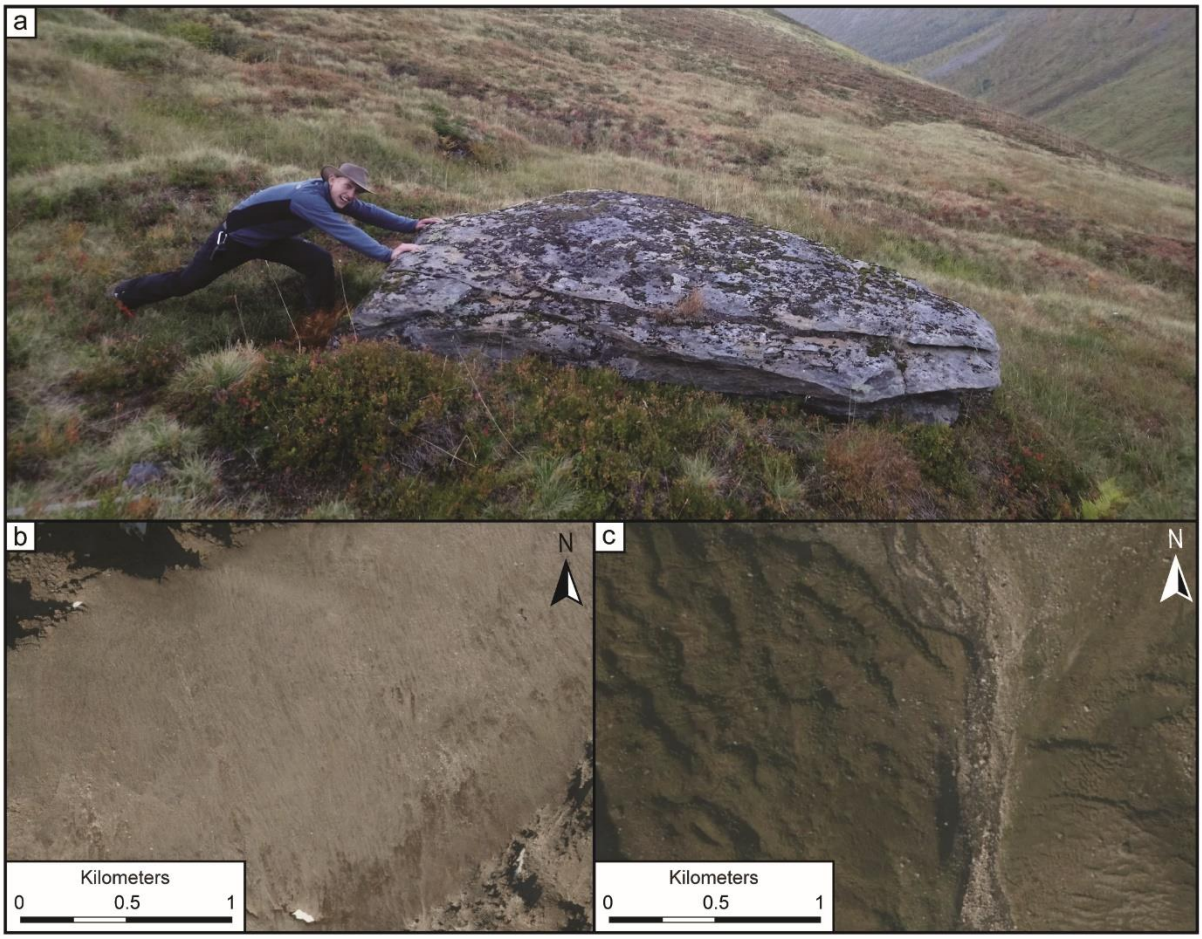

Figure 2.10. *Periglacial surface deformation features from within the Rotsund Valley region of the Troms and Finnmark study area: (a) ploughing boulder on the Rotsund Valley hillslope (approx. 69°43'19"N, 20°42'7"E); (b) sorted stripes on the plateau summit of Litledalsfjellet (1,235 m a.s.l.); (c) gelifluction lobes in the floor of Sahávággi, within the boundaries of outermost (presumed YD) moraine. Image source: (a) J.R. Leigh, (b and c) norgeibilder.no*.

2.4.1.6. Landsystems transitions

The above review demonstrates the most common landsystem types found within the central Troms and Finnmark study area. It should, however, be noted that the extent and location of these glacial landsystems are time transgressive when considered in a context of changing climate, and hence spatial and temporal changes will be recorded in the present-day landform signatures (e.g. Rea *et al.*, 1998; Evans *et al.*, 2002, 2008; Benn *et al.*, 2003; Rea and Evans, 2003; Golledge, 2007; Bickerdike, 2016; Bickerdike *et al.*, 2018b, 2018a). On the Bergsfjord Peninsula of northern Norway, Evans et al. (2002) show how regional glaciation style switches from large outlet glaciers to plateau icefields feeding locally confined valley glaciers, the latter often having readvanced and overridden earlier landforms. Moreover, as glaciers receded during the Holocene, valley glaciers were detached from the plateau icefields (Evans et al., 2002). The importance of plateau ice masses to the modern day glaciology of the region is clear in that they not only remain on many high summits, but also influence the valleys that they continue to drain into (e.g. Gellatly *et al.*, 1989; Whalley *et al.*, 1995a; Ó Cofaigh *et al.*, 1999; Andreassen *et al.*, 2000a, 2005, 2012b; Evans *et al.*, 2002; Rea and Evans, 2003; Weber *et al.*, 2019, 2020).

The importance of glacial landsystem change in time and space has recently been demonstrated by Bickerdike (2016) and Bickerdike et al. (2018a, 2018b) employing palaeoglaciological reconstructions. They show that glacial landsystems across Britain during the Loch Lomond Stadial (YD) evolved within and between catchments, with the largest ice masses having thinned and retreated, with eventual deglaciation causing them to become topographically controlled as isolated ice caps and valley systems, which then shrank to individual cirque glaciers before disappearing altogether. The reconstructions of the deglaciation in Britain are likely representative of the patterns of deglaciation that have occurred and continue to occur throughout Norway (Rea *et al.*, 1998; Evans *et al.*, 2002), where isolated plateau icefields are found feeding larger outlet glaciers while the smaller independent valley systems have mostly retreated into isolated cirques.

2.4.2. Climate history and Norwegian glacier reconstructions since the Younger Dryas

Even though a vast number of Norwegian glaciers are in remote settings, there remains a rich history of exploration and documentation of the country's ice masses. Some of the first reports of glacier activity can be found, by chance, in the historical record, for example in tax relief requests from as early as the mid-1300s, owing to the damage and/or destruction of farm buildings and/or higher pastures due to glacial and periglacial disasters (Grove, 1988, 2004a).

Since the turn of the 20th century there has been a renewed interest in the science of Norwegian glaciers and glaciations, with some of the earliest scientific studies in northern Norway looking to monitor glacier flow speeds and terminus positions (e.g. Rekstad, 1892, 1900, 1904, 1910, 1915). The rise of global transport, a better understanding on anthropogenic climate change, and new and improved methods of defining and dating historic glacier fluctuations, have all facilitated an increase in the quantity of reports pertaining to Norwegian glaciers. A regional bias in reporting does, however, remain, with southern and central Norway having received greater interest, likely due to the ease of accessibility of these areas. Northern Norway can still be considered as relatively remote with large areas having received very little or no attention.

The following sub-sections will describe our understanding of Norwegian glacial history in relation to key climatic events which are commonly used to subdivide the Holocene. The sub-sections follow a chronological order, starting from a brief review of YD ice conditions, moving through the Holocene record, and finishing with an overview of current knowledge on Norwegian glacier extent in the 20th and early-21st centuries.

2.4.2.1. Glaciation in Norway during the Younger Dryas

The prevailing model of YD (12,800–11,700 yrs BP) ice extent is that most of mainland Norway, with the exception of coastal areas, would have been covered by the SIS (Figure 2.2 and 2.6) as it experienced a period of readvance during deglaciation from its Last Glacial Maximum (LGM) extent (e.g. Hughes *et al.*, 2016). Our understanding of YD ice margin positions of the SIS are well established, owing to moraines which

can be (and have been) mapped more or less continuously around the Norwegian coast (Andersen *et al.*, 1995b, 1995a). The timing of the YD maximum does, however, show regional variation, although this could in part be due to the revision of older radiocarbon dates and/or development of new geochronological techniques such cosmogenic nuclide dating (cf. Goehring *et al.*, 2008; Mangerud *et al.*, 2016). Constraints on SIS thickness remain poorly developed, owing to the difficulties in establishing these details from the geomorphological record (e.g. Linge *et al.*, 2006; Goehring *et al.*, 2008; Lane *et al.*, 2020). Furthermore, recent research at inland mountain sites within Norway and Sweden are challenging the long-held view of a landscape completely submerged under cold based ice (e.g. Figure 2.11), suggesting that some mountain areas were ice-free prior to the YD, becoming exposed around 20,000-16,000 cal. yrs BP (Lane *et al.*, 2020).

In northern Troms and Finnmark County there are good age constraints on the deglaciation of the larger fjords and coastal mainland. Ice-sheet margin positions have been dated at numerous sites by radiocarbon and cosmogenic nuclide dating. This indicates that the YD ice-sheet margin stood at fjord heads around 15,000 cal. yrs BP (e.g. Junttila *et al.*, 2010; Romundset *et al.*, 2011, 2017; Stokes *et al.*, 2014; Hughes *et al.*, 2016; Anjar *et al.*, 2020), before rapidly evacuating fjords by around 11,000 cal. yrs BP (Nydal, 1960; Corner, 1980; Forwick and Vorren, 2002; Stokes *et al.*, 2014; Hughes *et al.*, 2016; Anjar *et al.*, 2020) and then retreating substantially inland by 10,000 cal. yrs BP (e.g. Bjune *et al.*, 2004; Jensen and Vorren, 2008; Hughes *et al.*, 2016; Anjar *et al.*, 2020).

There is also new evidence suggesting that, after the SIS retreated from the small islands around the Troms and Finnmark coast (~15,700 cal. yrs BP), the remaining mountain glaciers experienced a Lateglacial readvance, culminating at 13,900 ±700 cal. yrs BP (Wittmeier *et al.*, 2020). At their maximum extent during this period, the mountain glaciers of Arnøya (the confluent Snøfonn and Rødhetta glacier and Nymoen glacier; glacier ID 60, 62, and 63, respectively) extended to the fjord but remained land-terminating. Other glacial chronologies from northern Norway record SIS deposits attributable to the Older Dryas with moraines in the Kongsfjorden and Vardø regions dating to ~14,300 and 13,600 cal. yrs BP, respectively (Romundset *et al.*, 2017). Furthermore, Anjar et al. (2020) suggest glacial erratics were deposited at Nordkinn around ~14,900 cal. yrs BP, and that a recessional at Sirbma dates to between 12,600 and 14,000 cal. yrs BP. Subsequent to the Arnøya Lateglacial

maximum, during the early-YD, the glaciers experienced a period of retreat before a short stabilisation with several substantial moraine complexes forming between 12,300 and 11,500 cal. yrs BP (Wittmeier *et al.*, 2020). The study by Wittmeier et al. (2020) presents an exciting development in our understanding of Arctic mountain glaciers, as it shows similarities with the Southern Hemisphere glacier record from New Zealand and Patagonia (e.g. Putnam *et al.*, 2010; Sagredo *et al.*, 2018; Mendelová *et al.*, 2020), thereby questioning the long-held concept of a "bipolar seesaw" of inter-hemispheric climate variability (cf. Stocker and Johnsen, 2003; Pedro *et al.*, 2011). Instead, Wittmeier et al. (2020) indicate a generally coherent pattern of glacier and summer temperature across hemispheres during the Lateglacial. Further research does, however, need to be conducted across other sites in the islands and coastal mountains of northern Norway to help corroborate these early findings.

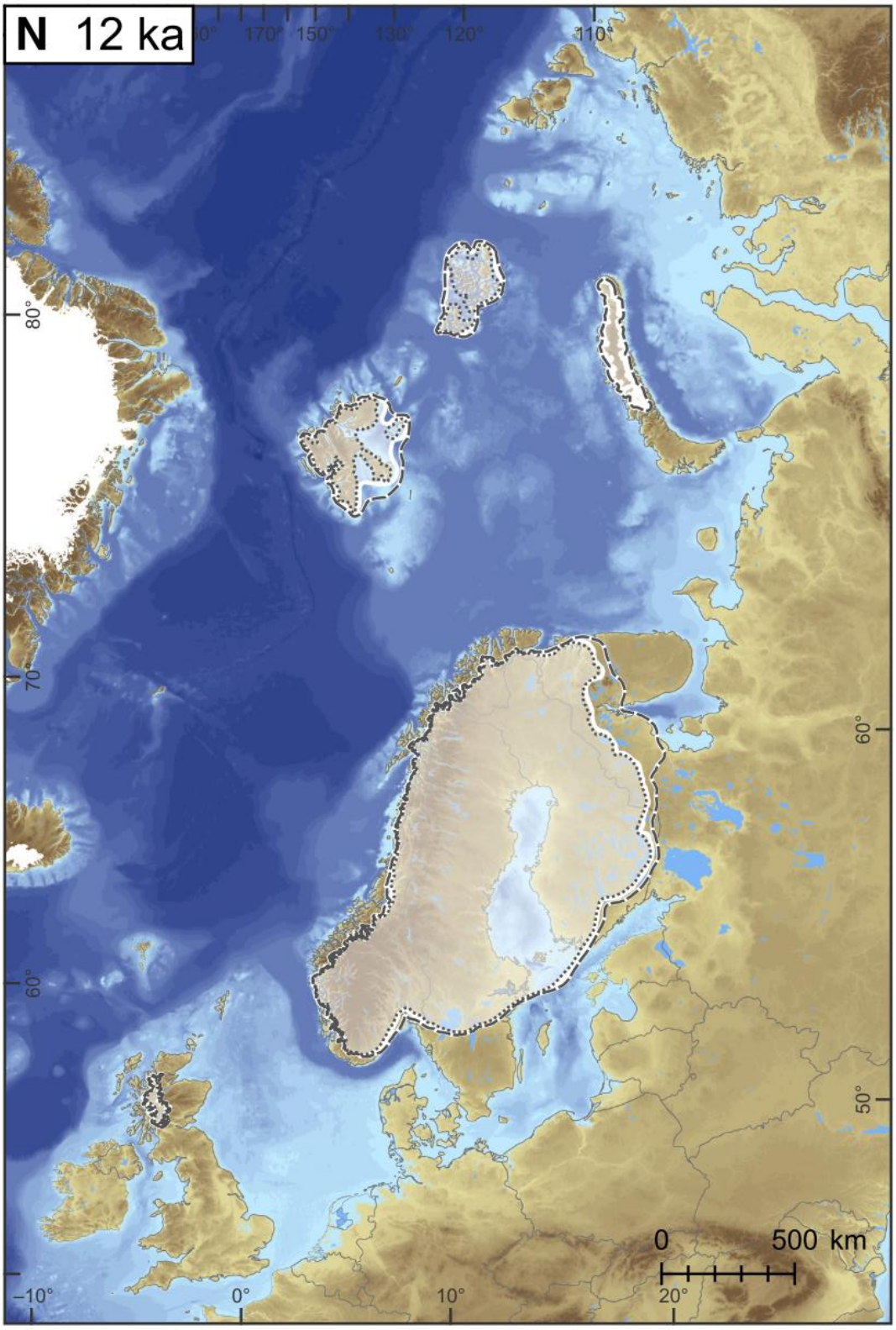

Figure 2.11. *DATED-1 time-slice reconstruction of the extent of the Eurasian ice sheets at 12,000 cal. yrs BP with the SIS shown as a single ice mass. There are three lines to represent uncertainty in the data: maximum (black dashed), minimum (black dotted) and most-credible (solid white line and shaded white area). Reproduced from Hughes et al.* (2016, p. 20).

2.4.2.2. Early-Holocene (Preboreal-Boreal transition) climatic events

Following the recession of the SIS, a period of cooling during the early-Holocene transition from Preboreal to Boreal is evidenced across Norway by large moraine sequences of between one to two moraines, inset from YD moraines yet substantially (~1-4 km) outside of LIA moraines (Nesje *et al.*, 1991; Dahl *et al.*, 2002; Matthews *et al.*, 2008). Formation ages for moraines of this sort were first established by Nesje (1984) in Erdalen, a valley in the northwest of Jostedalsbreen (approx. location 61°50'36"N 7°10'35"E) at an elevation of 480–550 m a.s.l. An age of ~9,100 cal. yrs BP (8,810 ^{14}C yrs BP) was obtained by radiocarbon dating of peat proximal to the outer moraine (c; Rye *et al.*, 1987; Nesje *et al.*, 1991). As a result, the major glacier expansion episodes between 10,100 and 9,500 cal. yrs BP are known, across Scandinavia, as “Erdalen Event(s)” (Dahl *et al.*, 2002). The timing of the Pre-Boreal to Boreal “Erdalen Events” of the early-Holocene roughly correlate with Bond Events 6 and 7 (~9,400 and ~10,300 cal. yrs BP respectively), periods of enhanced Holocene ice-rafting that caused increased volumes of cold, fresh water to be added to the North Atlantic and resulted in an alteration of ocean circulation and climate (Bond *et al.*, 1997, 1999, 2001). The timing of the moraine formation at the Erdalen type site was reaffirmed by Matthews et al. (2008) who used ^{10}Be cosmogenic nuclide dating to assign ages of 10,116 ±1,095 and 9,782 ±1,163 cal. yrs BP for the two moraines (Figure 2.12). They note, however, that the precision of the technique was not able to adequately differentiate the inner and outer Erdalen Event moraines (Matthews *et al.*, 2008). The reaffirmation of an early-Holocene age for the Erdalen moraines via TCND has also shown that ages obtained through radiocarbon dating of buried peat deposits are a reliable means to ascertain close minimum age estimates of glacial deposits (Matthews *et al.*, 2008). This is of particular importance at sites lacking surfaces suitable for rock surface exposure dating.

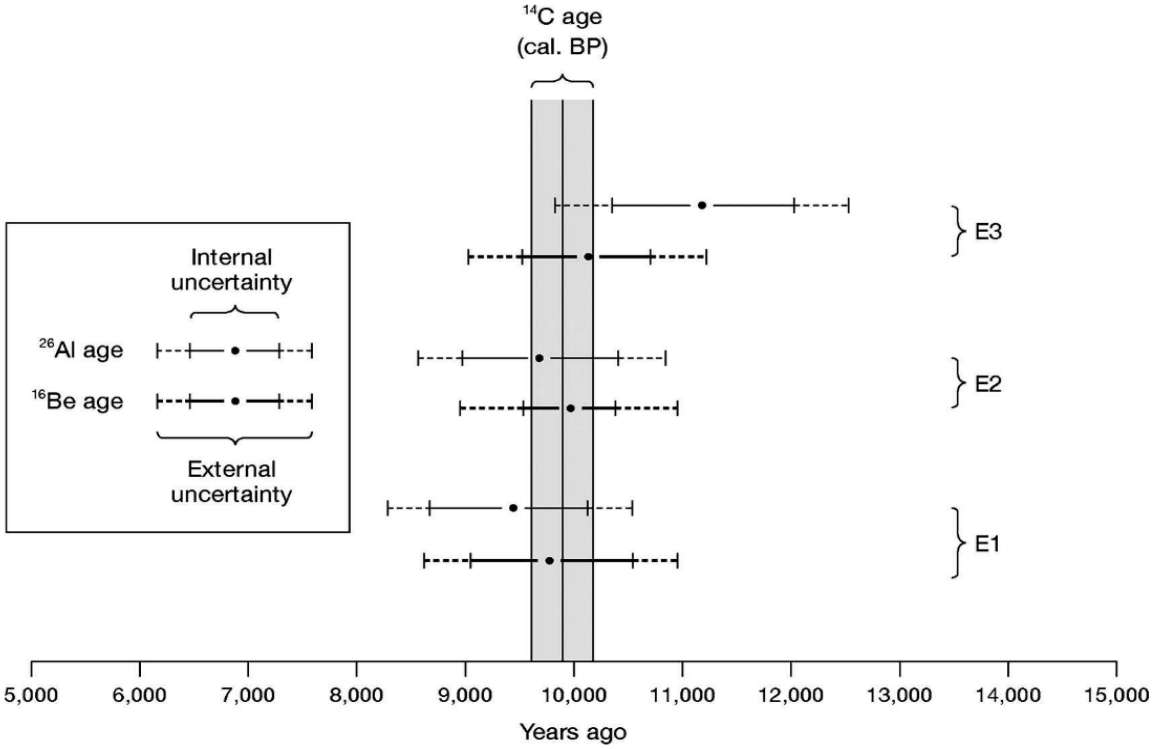

Figure 2.12. *Cosmogenic ^{10}Be and ^{26}Al ages from the Erdalen Event type moraines with internal and external uncertainties (± 1σ) of the shaded band (shaded) indicating the independent evidence of age from ^{14}C dating of peat (Matthews et al., 2008, p. 1161).*

The first Erdalen Event readvance, which occurred between 10,100 and 10,050 cal. yrs BP, has been linked to a major (150-200% relative to early-21st century values) increase in winter snowfall (Dahl *et al.*, 2002). The cause of the second Erdalen Event readvance (9,860-9,530 cal. yrs BP) has been more difficult to determine. The reactivation of existing glaciers triggered by a drop in summer temperature or an increase in winter precipitation due to a shift in prevailing wind direction have both been postulated, with the former considered more likely (Dahl *et al.*, 2002). Simultaneous with glacier readvance, there were other environmental responses, such as vegetation regression linked to reductions in summer temperatures (Paus *et al.*, 2006, 2019).

Moraine evidence and glaciogenic lake sediments attributable to the Erdalen Event(s) are found across southern Norway at both outlet and cirque glaciers (Nesje, 1984; Nesje *et al.*, 1991, 2000a, 2001; Dahl *et al.*, 2002; Bakke *et al.*, 2005c; Matthews *et al.*, 2008; Shakesby *et al.*, 2008; Matthews and Winkler, 2011; Aa and Sønstegaard, 2019). There are, however, sites in southern Norway where no evidence is found for

Erdalen Event glacier readvance, such as at Skriufonnen in northern Rondane, where a lower elevation continental cirque glacier was absent over the period 10,000 to 4,000 cal. yrs BP (Kvisvik *et al.*, 2015).

In central and northern Norway there is a less clear picture of glacier readvance during the Preboreal to Boreal transition, and this is likely, in part, linked to the presence of the SIS across the region. At the mountain Høgtuva (south of the Svartisen ice caps) there are a series of small plateau, outlet, valley and cirque glaciers which are amalgamated under the name of Høgtuvbreen (Jansen *et al.*, 2016). Høgtuvbreen is proposed to have been confluent with Svartisen during the early-Holocene, with suggestions that a series of moraines (termed Rombak moraines) at Altermarka, a site ~20 km down valley from Høgtuvbreen, were formed around 10,360 ± 160 and 10,100 ± 320 cal. yrs BP (Andersen, 1968; Andersen *et al.*, 1995a; Blake and Olsen, 1999; Jansen *et al.*, 2016). Radiocarbon dating of sediments from Lake Vardfjelltjønna, only 10 km down valley from Høgtuvbreen (and 10 km up valley from Altermarka), indicate that this area was deglaciated at 10,650 ± 65 cal. yrs BP, calling into question the ages of the moraines at Altermarka and indicating that Høgtuvbreen would have been a separate ice-mass during the Preboreal to Boreal transition. Yet there are no deposits mapped or dated that can be attributed to the Erdalen Event (Jansen *et al.*, 2016).

In the Troms and Finnmark region of northern Norway there is also a mixed picture of early-Holocene glacial activity. In Lyngenfjord, Corner (1980) describes a rapid retreat of the SIS through the fjord, leaving it ice-free by ~10,200 cal. yrs BP (Corner, 1980; Stokes *et al.*, 2014). In the nearby mountains of the central and western areas of the Lyngen Peninsula several moraines are attributed to early-Holocene events. Firstly, Ballantyne (1990) tentatively suggests that the outermost moraines within Fornesdalen were formed during the Preboreal, on the basis that they are located at the margins of a transection glacier complex and are overridden by Holocene colluvial and rock-fall deposits. Secondly, within Strupskardet, Bakke et al. (2005a) correlated the sediments of Aspvatnet with a series of three latero-frontal push moraines with bracketing ages that fall within the range of the two Erdalen Events; Moraine 10 situated ~880 m outside the LIA moraine and dated to between 10,400 and 10,300 cal. yrs BP, Moraine 11 inset by approximately 50 m and dated to between 9,800-9,400 cal. yrs BP, and Moraine 12 situated ~660 m outside the LIA moraine and dated to between 9,300 and 8,900 cal. yrs BP (Bakke *et al.*, 2005a). Conversely, on

the island of Arnøya and the Bergsfjord Peninsula, to the north and north-east of Lyngen, respectively, Wittmeier et al. (2015, 2020) show there to be no evidence for valley and outlet glacier readvance in the period following the YD and before the LIA.

2.4.2.3. The Holocene Thermal Maximum

The HTM, sometimes also known as the 'Holocene Climate Optimum' or 'Holocene Thermal Optimum', is a global period of relatively warm climate between 11,000 and 5,000 years ago (Wanner *et al.*, 2008; Renssen *et al.*, 2012). However, in regions of the Northern Hemisphere it has been hypothesized that the presence of large ice masses (e.g. the Laurentide Ice Sheet, Greenland Ice Sheet, and SIS) delayed the onset of the HTM as they effectively provided regional atmospheric cooling, counteracting the orbitally forced summer insolation (Carlson *et al.*, 2007; Renssen *et al.*, 2009; Widmann, 2009; Blaschek and Renssen, 2013; Sejrup *et al.*, 2016).

In Scandinavia it is believed that final deglaciation of the SIS occurred shortly after 10,000 cal. yrs BP (Cuzzone *et al.*, 2016; Hughes *et al.*, 2016). At this time the ELA of the SIS was likely above that of its summit, meaning there would have been very little or no accumulation area (Cuzzone *et al.*, 2016; Hughes *et al.*, 2016). The resulting reduction in accumulation would therefore result in a shrinking ice margin and a thinning of the entire ice sheet, with newly exposed mountain summits and ridgelines further dividing the decaying ice into individual masses, each with independent patterns of flow and retreat (Linge *et al.*, 2007; Goehring *et al.*, 2008; Hughes *et al.*, 2016; Stroeven *et al.*, 2016). The remnants of the SIS would likely have formed domes over three areas: the Jotunheimen area in southwest Norway, Jämtland (in the central Norwegian-Swedish border area) and the final portion disappearing from the Sarek Mountains of northern Sweden after 9,700 cal. yrs BP (Boulton *et al.*, 2001a; Stroeven *et al.*, 2016). The regional cooling from the decaying ice sheet resulted in modelled European summer temperatures at the early-Holocene (e.g. before 8,000 cal. yrs BP) of around 0.5-1°C below the HTM level (Renssen *et al.*, 2009).

The disappearing SIS gave rise to Holocene warming in Europe, with regional climate reconstructions having indicated the highest temperatures in Scandinavia occurred over a 2,000-year period between ~7,500 and ~5,500 cal. yrs BP (Renssen *et al.*, 2009; Widmann, 2009). The emergence of ice-free mountain peaks (nunataks) from the decaying SIS provided a refugia for pioneer tree species such as, *Juniperus*

communis (Common Juniper), *Betula nana* (Dwarf Birch), and *Betula pubescens* (Downey Birch), which became established after ~10,830 cal. yrs BP at ice free continental sites across Norway, Sweden, and Finland (e.g. Matthews and Whittaker, 1987; Paus, 1995; Barnekow, 1999; Seppä *et al.*, 2004; Birks and Birks, 2008; Birks, 2015). The growth of Birch species was the result of the HTM summer temperature increase, not only ice recession (Kullman and Kjällgren, 2006). Reconstructions of fauna and flora establishment during the HTM (e.g. Figure 2.13), indicate that Scandinavian summer temperatures were likely 1.5-2.4°C warmer than the 1961–1990 World Meteorological Organisation climate normals (Rosén *et al.*, 2001; Seppä and Birks, 2002; Heikkilä and Seppä, 2003; Bjune *et al.*, 2004; Velle *et al.*, 2005; Kullman and Kjällgren, 2006).

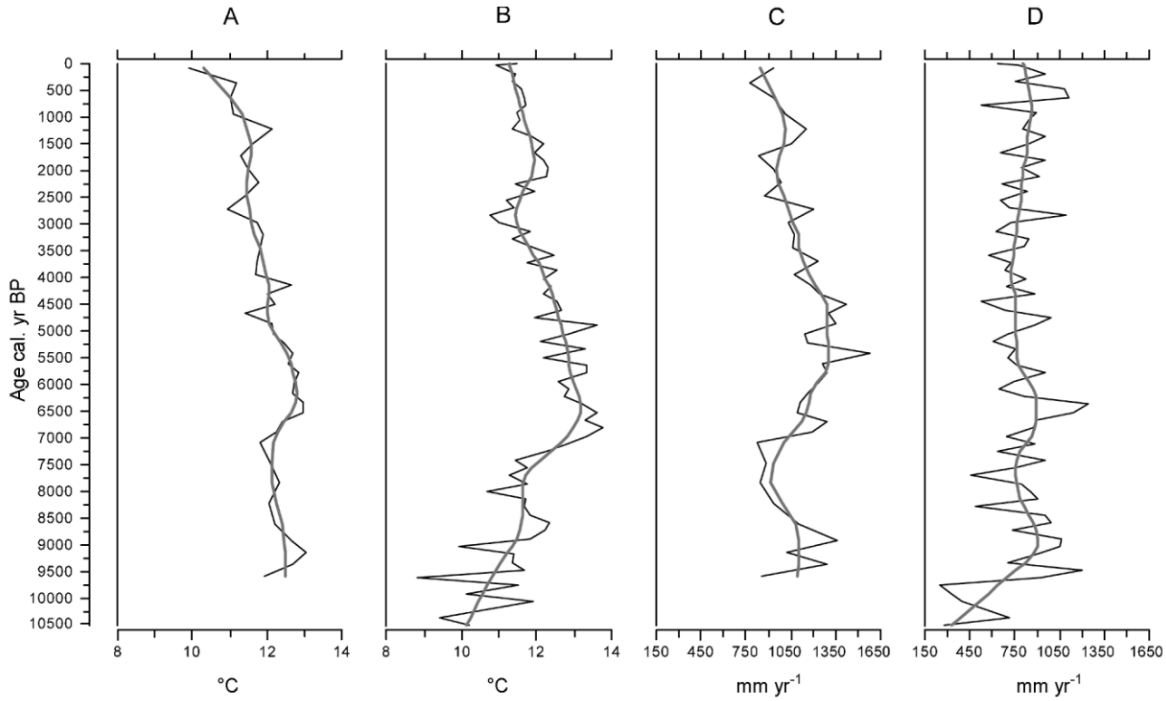

Figure 2.13. *Holocene inferred mean July temperature from proxy records recovered from lake (a) Barheivatn (69°42'N, 19°51'E; the Lyngen Peninsula) and (b) Dalmutladdo (69°10'N, 20°43'E; Skibotn valley at the Norwegian-Finnish border) and inferred mean annual precipitation from (c) Barheivatn and (d) Dalmutladdov (Bjune et al., 2004, p. 218)*.

The high summer temperatures and low winter precipitation that occurred during the HTM caused a drastic reduction in the extent of glacierisation across Norway (Nesje *et al.*, 2008; Nesje, 2009) and between 6,600 and 6,300 cal. yrs BP, most glaciers across Scandinavia are thought to have melted completely (Seppä and Birks, 2002; Bjune *et al.*, 2005; Seppä *et al.*, 2005; Antonsson and Seppä, 2007; Nesje *et al.*, 2008; Nesje, 2009; Renssen *et al.*, 2009, 2012). Evidence to support the disappearance of Norwegian glaciers is found within the pro-glacial sediment archive. Downstream of present-day glaciers, minerogenic rock-flour produced through glacierization is captured and stored in lake basins as bluish-grey sandy and/or clayey silt, sandwiched between non-glacial sediments (Karlén, 1976, e.g. 1981; Nesje and Dahl, 1991b, 1991a; Matthews *et al.*, 2005). Consequently, when the glaciers are smaller or non-existent the levels of glacial sediments found in these deposits are smaller or absent and the concentrations of organic sediments in the lake are much higher (Dahl *et al.*, 2003). Sites across the whole of mainland Norway, including at the Bergsfjord and Lyngen Peninsula (Bakke *et al.*, 2005a; Wittmeier *et al.*, 2015), display an absence of glacial sediments during the mid-Holocene, indicating that these glaciers may have melted completely (Nesje *et al.*, 2008; Nesje, 2009).

In contrast to the above, while most studies have shown Norwegian glacier disappearance during the HTM, Bakke et al. (2010) showed that in Nordland, central Norway, the Okstindbreen icefield and its outlet glacier Austre Okstindbreen existed continuously throughout the Holocene, providing the first account of glacier survival in Norway, during the HTM. The glacier reconstructions of Austre Okstindbreen indicate that the glacier was at its smallest ~7,710 cal. yrs BP (Bakke *et al.*, 2010). Furthermore, in the period 6,950-4,940 cal. yrs BP, overlapping with the Scandinavia HTM (~7,500 and ~5,500 cal. yrs BP), there where at least four short-lived phases of increased glacier activity where the local ELA fluctuated around 1,600-1,500 m a.s.l., only ~260 m higher than ELA in 2010 (Bakke *et al.*, 2010). The findings of Bakke et al. (2010) highlight the potential for high-elevation Arctic glaciers across Scandinavia in the continental-maritime zone to have persisted throughout the Holocene. This demonstrated how compiling glacier records from varied methods (e.g. pro-glacial sediment archives, dated moraines, and historical imagery) it is possible to identify even small short-lived and intermittent fluctuations of glacial activity (Bakke *et al.*, 2010).

2.4.2.4. The 8.2 ka event

Within the period of warming described in the previous section a rapid and short-lived climatic deterioration occurred between 8,400 and 8,000 cal. yrs BP (e.g. Figure 2.14) with peak cold temperatures around 8,200 cal. yrs BP which lasted for only ~150 years (Alley *et al.*, 1997; Alley and Ágústsdóttir, 2005; Kobashi *et al.*, 2007). This period of cooling centred around 8,200 cal. yrs BP around is termed the "8.2 ka event".

The 8.2 ka event became formerly recognised when it was identified in the GISP2 Greenland ice core, where high-resolution analyses show a reduction in $\delta^{18}O$ and therefore cooling, reaching a maximum temperature decrease over central Greenland of between 3.3 and 7.4°C, depending on the modelling relationship applied (e.g. Johnsen *et al.*, 1992; Alley *et al.*, 1993; Cuffey *et al.*, 1994; Leuenberger *et al.*, 1999; Alley and Ágústsdóttir, 2005). While the exact temperature over Greenland remains debated there is an apparent general consensus that the 8.2 ka event resulted in a regional cooling of 1-3°C across the Northern Hemisphere (Kobashi *et al.*, 2007; Matero *et al.*, 2017). Recent evidence of cooling in the Southern Hemisphere in locations such as Madagascar (Voarintsoa *et al.*, 2017, 2019) and New Zealand (Augustinus *et al.*, 2008) challenge the solely Northern Hemispheric view of an 8.2 ka event climatic deterioration. Evidence throughout the Southern Hemisphere is, however, limited. The need for more high-resolution paleoclimate data from the Southern Hemisphere has been highlighted as a key aim of future paleoclimate studies (Voarintsoa *et al.*, 2019).

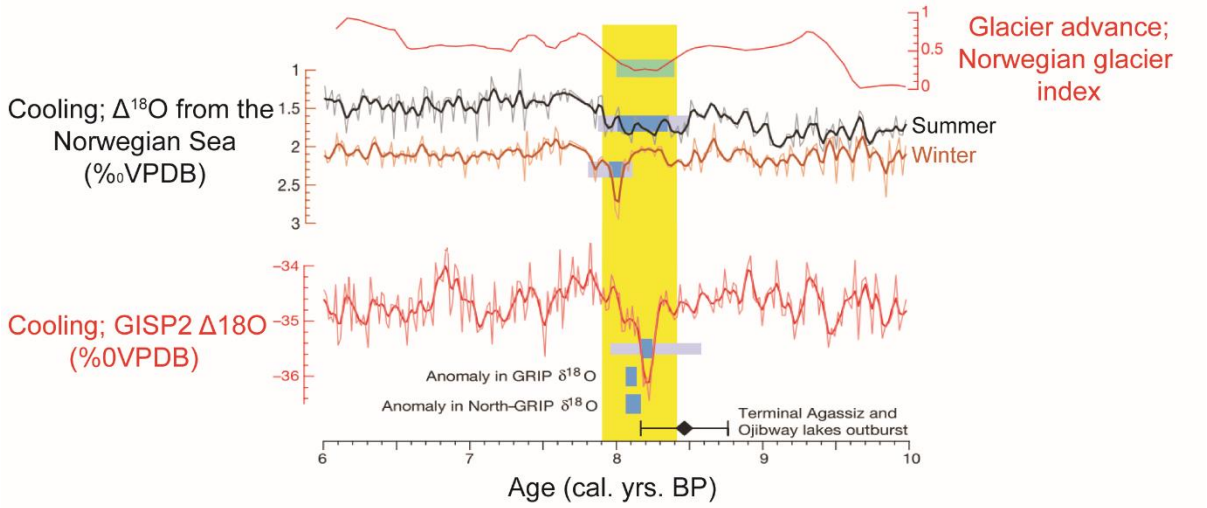

Figure 2.14. *A selection of climate proxy records used to identify anomalies around 8,200 cal. yrs BP. The black diamond with error bar alongside the age axis indicates the best age estimate for the meltwater flood from lakes Agassiz and Ojibway. Heavy coloured blocks indicate peak events, lighter blocks highlight broader anomalies, and the yellow band marks an interval spanning three conspicuous maxima in ^{14}C production. Figure modified from Rohling and Pälike (2005, p. 276).*

There are several key hypotheses that can explain the underlying trigger for the abrupt warming centred around 8,200 cal. yrs BP. The first hypothesis is related to the curtailment of North Atlantic Deepwater formation and its associated northward heat transport. This was due to a catastrophic freshwater influx into the North Atlantic during an abrupt (0.5-5 year) drainage of lakes Agassiz and Ojibway due to the disintegration of the Laurentide Ice Sheet (e.g. Renssen *et al.*, 2002; Teller *et al.*, 2002; Clarke *et al.*, 2004). An alternative hypothesis is associated with a decrease in solar activity associated with solar insolation lowering around 8,400-8,000 cal. yrs BP (e.g. Karlén and Kuylenstierna, 1996; Bond *et al.*, 1997, 2001; Muscheler *et al.*, 2004). More recently, however, Matero et al. (2017) proposed that it was not the drainage of the Agassiz and Ojibway lakes that caused the weakening of the Atlantic Meridional Overturning Circulation but rather the collapse of the Hudson Bay ice saddle of the Laurentide Ice Sheet. This initiated a 100-year-long meltwater pulse into the Labrador Sea with a volume of ~ 883,000 km^3 (≈4.24 m sea level rise). The ice saddle collapse theory has been gaining traction with new studies measuring salinity from central Labrador Shelf (Lochte *et al.*, 2019), examining the geomorphology and establishing new radiocarbon ages in the Hudson Bay area of Manitoba (Gauthier *et al.*, 2020),

and compiling models for studying the ice saddle collapse and associated meltwater pulse (Matero *et al.*, 2020).

2.4.2.4.1. The 8.2 ka (Finse) event in Norway

In Norway, some of the first evidence associated with the 8.2 ka event was found within lake and terrestrial sites throughout the Finse region, north-east of the Hardangerjokulen ice cap in southern Norway (approx. location 60°34'25"N, 7°30'54”E). At these sites, distinct glaciogenic sediments mark a short-lived glacial advance, subsequently termed the “Finse event” (Dahl and Nesje, 1994, 1996). Across Norway the terms “8.2 ka event” and “Finse event” are used synonymously but, for the purposes of this thesis the term “8.2 ka event” is preferred.

Across Norway, evidence for an 8.2 ka glacial readvance (e.g. Figure 2.14) is found almost solely within pro-glacial lake and stream-bank mire sediment archives; pro-glacial sediment cores often show a distinct minerogenic layer between 8,500 and 8,000 cal. yrs BP (cf. Nesje, 2009). Very few studies have been able to attribute any specific moraine to the 8.2 ka event (Aa and Sønstegaard, 2019). The lack of moraine evidence attribute to the 8.2 ka event has been considered to be the result of a larger LIA advance, which exceeded any limits achieved during the 8.2 ka event and thereby removed any older moraines in the process (Matthews *et al.*, 2008; Shakesby *et al.*, 2008; Aa and Sønstegaard, 2019). Shakesby et al. (2008), however, suggested that an apparent absence of 8.2 ka event moraines is actually due to the fact that the majority of geochronological investigations focus on the larger glaciers, whose cumulative mass enabled larger advances in the late-Holocene. They proposed that if evidence of 8.2 ka moraines is to be found, the most likely sites would be those of small, isolated, high-altitude glaciers (Shakesby *et al.*, 2008).

A number of studies have failed to find any substantial evidence of glacier activity during the 8.2 ka event (e.g. Lie *et al.*, 2004; Bakke *et al.*, 2005b; Kvisvik *et al.*, 2015), particularly notable in the few Holocene records from northern Norway. For example, within the central Troms and Finnmark region of northern Norway, a lack of reported evidence attributable to the 8.2 ka event is significant. In the lake sediment cores from Aspvatnet on the Lyngen Peninsula, no glacier-derived sediments were deposited between 8,800 and 3,800 cal. yrs BP, indicating that Lenangsbreen had melted completely during this time (Bakke *et al.*, 2005a). Similarly, in the valley Sør-

Tverrfjorddalen on the Bergfjord Peninsula none of the three lakes (Jøkelvatnet, Store Rundvatnet, and Storvatnet) show conclusive evidence of glacial activity between 10,000 and 4,100 cal. yrs BP. This suggests that the glacier (Langfjordjøkelen) had melted during this period, and that a low-amplitude increase in key detrital parameters (e.g. magnetic susceptibility and Titanium count rates) occurring ~8,200 cal. yrs BP cannot be isolated from a signal derived purely from a decrease in organic productivity caused by a generally cooler climate at this time (Wittmeier *et al.*, 2015). Finally, the Holocene moraine chronology from the nearby island of Arnøya shows no glacier advances after the YD, until the LIA, with this presumed to reflect the small size of the Rødhetta Glacier (1.1 km^2) and warm summers during the Holocene, until the onset of the LIA (Wittmeier *et al.*, 2020).

2.4.2.5. Late-Holocene Neoglacial events

The initiation of glacial regrowth and subsequent century- to millennial-scale glacier expansion episodes during the late-Holocene are termed Neoglaciation or Neoglacial events (Denton and Porter, 1970; Matthews, 2007). Matthews (2007) examined European glacial records from the Alps and Scandinavia and suggested that up to 17 key Neoglacial events can be identified during the late-Holocene. The events are likely correlated with periods of low solar irradiance, but additional forcing factors are also noted, including Milankovitch forcing and volcanic forcing (e.g. Karlén and Kuylenstierna, 1996; Matthews, 2007; Helama et al., 2010; Werner et al., 2013; Schurer et al., 2014; Sigl et al., 2015; Spielhagen and Bauch, 2015).

Across Scandinavia, Neoglaciation occurred during a period of cooling over the time interval 6,000-2,000 cal. yrs BP (Nesje et al., 2008; Nesje, 2009; Solomina et al., 2015). The reforming of glaciers during Neoglaciation across Norway is shown to be time-transgressive, with the development of glaciers responding to regional variations in winter precipitation, summer temperature, wind drift of snow, and glacier hypsometry (Nesje, 2009). Most regions of southern, central, and northern Norway are shown to have evidence of glacial activity (re)initiating around 4,000 years ago (Figure 2.15).

One potential issue in defining and identifying glacial readvance during the start of the late-Holocene is related to the most recent and most expansive Neoglacial event being that of the LIA (see Section 2.2.3.), which may have overridden and destroyed

the evidence of any earlier advances. Yet even where large-scale terrestrial evidence of Neoglacial glacier activity is absent, the pro-glacial sediment archive (e.g. sediments found in proglacial lakes or mires) has recorded events, during which glaciers were larger than at the present-day (e.g. Matthews et al., 2005; Matthews and Dresser, 2008; Bakke et al., 2010; Wittmeier, 2015).

In southern and central Norway there are a number of studies that investigate late-Holocene glacial history for a range of glacier types and sizes, which is critical to providing a comprehensive overview of glacial and climatic conditions during this period. At Folgefonna (western, southern Norway) the small plateau glaciers are shown to have been absent from the catchment after 9,600 cal. yr BP and subsequently began their regrowth at ~5,200 cal. yrs BP, with a marked increase in glacier size indicated at around 2,200, 1,600, and 1,050 cal. yrs BP (Bakke et al., 2005b). After the complete melt of Hardangerjøkulen (southern Norway) during the HTM, the ELA only lowered enough (~1,710 m a.s.l.) to initiate Neoglacial regrowth around 4,800 BP, with the subsequent 1,000 years showing high-frequency glacier fluctuations (Dahl and Nesje, 1994, 1996; Nesje *et al.*, 1994). Furthermore, Dahl and Nesje (1994) suggest that it is only after 2,900 cal. yrs BP that all glaciers of the Hardangerjøkulen were continuously present, a pattern not evidenced at other large ice caps. Modelling the evolution of Hardangerjøkulen from the mid-Holocene by Åkesson et al. (2017) suggests that between 4,000 and 3,800 BP, ice grew preferentially on high topography, and that the north-eastern outlets (Midtdalsbreen and Blåisen) started to develop earlier than the south-western outlet (Rembesdalskåka). The modelled growth in ice volume was fastest during the period 2,300-1,300 cal. yrs BP, whereby the volume of Hardangerjøkulen tripled in under 1,000 years (Åkesson *et al.*, 2017).

In the Rondane mountains (eastern, southern Norway) cirque glacier regrowth appears to have taken place around 4,000 years ago (Kvisvik et al., 2015). A similar pattern was found across the Jostedalsbreen region, with an apparent three-phase Neoglaciation; glacier regrowth occurred around 6,150-4,500 cal. yrs BP followed by two major phases between 4,500-2,700 cal. yrs BP and ~ 2,700 cal. yrs BP, with lake sediment records indicating up to 33 low-amplitude advances during the Neoglaciation (Nesje *et al.*, 2000a).

At the alpine icefield Okstindbreen (northern, central Norway), glaciers survived the HTM and, as such, did not experience Neoglacial regrowth but rather periods of

readvance during Neoglaciation (Bakke *et al.*, 2010). The most substantial periods of advance in the late-Holocene were centred around 4,200, 2,700, 1,300 cal. yrs BP and ~150 yrs BP, with these glacial advances noted as being synchronous with other northern Hemisphere sites including Svalbard, Iceland, and the European Alps (Bakke *et al.*, 2010).

There are, at present, only two studies in northern Norway that give detailed insight as to the timing of Neoglacial activity. These are based upon lake sediment analysis and they highlighted that there are no moraines attributable to pre-LIA Neoglacial events (Bakke *et al.*, 2005a; Wittmeier *et al.*, 2015). On the Lyngen Peninsula, Lenangsbreen is proposed to have reformed after 3,800 cal. yrs BP (Bakke et al., 2005b). On the Bergsfjord peninsula, the Langfjordjøkelen ice cap started reforming ~4,110 cal. yrs BP (Wittmeier *et al.*, 2015). The Neoglaciation of the Troms and Finnmark region in northern Norway seems, therefore, to have occurred later than that of southern and central Norway, with slight regional differences likely attributable to the elevation and catchment size differences between valley glaciers on the Lyngen Peninsula compared with plateau ice caps on the Bergsfjord peninsula.

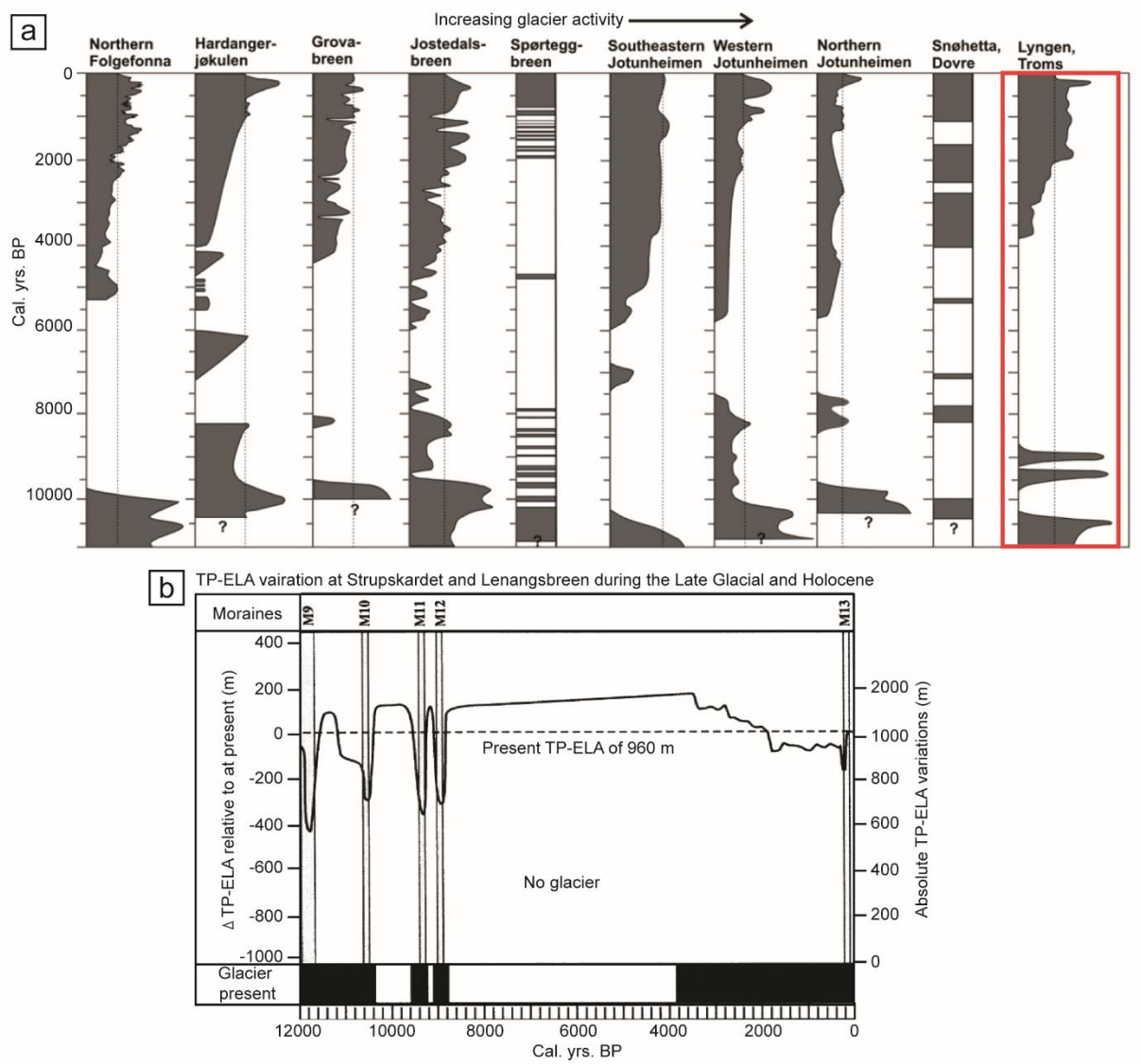

Figure 2.15. *Schematic diagrams showing fluctuations of Norwegian glaciers (a) glacier reconstructions of 10 different Norwegian glaciers during the Holocene, highlighting the disappearance of all showcased glaciers during the HTM and their Neoglacial regrowth (reproduced from Nesje et al., 2008, pp. 13); (b) modified graph of glacier activity and reconstructed temperature-precipitation-wind ELA for Lenangsbreen in Strupskardet over the last 12,000 years (modified from Bakke et al., 2005). Red rectangle in (a) highlights the study are shown in (b).*

2.4.2.6. The Little Ice Age

The most widespread and recent glacier advance across Norway was that of the LIA, triggered by climatic deterioration beginning around 1300 (Grove, 2001, 2004a, 2004b; Matthews and Briffa, 2005) and following the warmer and stable climatic conditions of the 'Medieval Warm Period/Medieval Climate Optimum' (900-1300; e.g. Brázdil *et al.*, 2005; Helama *et al.*, 2009). The occurrecne of a global LIA remains debatable but increasing evidence is emerging of southern hemispheric glaciers (e.g. those in New Zealand and Patagonia) having expirenced substantail readvance during the 18th/19th centuries, thereby pointing more firmly towards a worldwide LIA overlain by vairable regional patterns of glacial maxima (Winkler, 2000; Harrison *et al.*, 2007; Glasser *et al.*, 2011; Putnam *et al.*, 2012; Meier *et al.*, 2018; Carrivick *et al.*, 2020; Shakesby *et al.*, 2020).

While the contentinal European Alps expirenced a relatively uniform LIA maximum in the mid-19th century (Ivy-Ochs *et al.*, 2009 and references therein), mainland Norway appears to exhibit a marked regional asynchronicity in the timing and magnitude of the LIA maximum. Glaciers in south Norway attained their maximum extent in the mid-1700s, up to 180 years before glaciers in the north (Ballantyne, 1990; Grove, 2001, 2004a, 2004b; Winkler, 2003; Solomina *et al.*, 2016). When examining the potential differences in the patterns of Norwegian LIA maxima, there needs to be consideration to not only the climatic conditions but also to difficulties in dating young surfaces, the availability of historical records, and the southern Norway research bias.

2.4.2.6.1. The Little Ice Age in southern Norway

The most well documented glaciers throughout southern Norway are those fed from the Jostedalsbreen ice cap. There have been numerous scientific reports of Jostedalsbreen and its outlet glaciers, alongside knowledge obtainable from other sources such as newspapers, journals, private letters, government papers, photographs, maps and other technical and non-technical documents (Østrem *et al.*, 1976). Of particular value are the unique accounts of the mid-18th century advance of the outlet glacier Nigardsbreen (approx. location 61°39'16N, 7°16'30"E). Information recorded by farmers in the valley documents an advance of the glacier in 1735 onto the cultivated land and impacting on the nearby farm house (Østrem *et al.*, 1976). By

1743 the glacier had advanced far enough that the farm buildings had been completely destroyed (Østrem *et al.*, 1976). Owing to the devastation imparted on the local families in the wake of Nigardsbreen's advance, a government minister, Mr. M. Foss, visited the site, recorded the damage and noted that by 1748 the ice had started to retreat from its extended position (Foss, 1802). Nigardsbreen has never re-attained this maximum extent (Grove, 1988). The record of advance culminating around 1743 and recession initiating around 1748 pinpoints the near exact timing of Nigardsbreen's LIA glacier maximum and this site is, therefore, a key reference for many glacial geochronological studies in the Jostedalsbreen region and throughout southern Norway.

Bickerton and Matthews (1992) use the Nigardsbreen historical record to establish families of lichenometric dating curves, providing a means to date surfaces exposed since the LIA maximum with proposed error margins of as little as ±10% over LIA timescales. Following the initial lichenometric test of Bickerton and Matthews (1992), Bickerton and Matthews (1993) expanded the glacial chronology into the forelands of seven other Jostedalsbreen outlet glaciers, using geomorphological mapping and lichenometry to assess timing and synchronicity of LIA maxima and subsequent moraine forming events (Bickerton and Matthews, 1993). While there is some variation on the timing of the LIA maximum, most outlet glaciers attained their maximum extent during the 1700s (18th century; Table 2.1). Given that the age of the Lodalsbreen terminal moraines conflicts with early observations, it is postulated that lichen snow-kill in the early-1800s, due to increased avalanching at this time, is responsible for smaller lichens and hence a younger calibrated age (Bickerton and Matthews, 1993). Only at Stegaholbreen is the mid-1800s glacier maximum considered reliable, as it is supported by the vegetation trimline and supporting historical documentation (Bickerton and Matthews, 1993). Bickerton and Matthews (1993) note that this late advance is exceptional yet provide little discussion as to why this glacier reached its maximum later than all other glaciers in the region, noting only that Stegaholbreen has long response times of around 24 years.

This detailed knowledge on the timing and extent of LIA glacierisation enabled further studies to examine the necessary ELA depression required for glaciers to advance to these maximum positions. At Jostedalsbreen, an accumulation area ratio method has shown that an ELA depression of 70 m (relative to that of the 1990s) would have been required for glaciers to reach their LIA maximum position (Torsnes *et al.*,

1993). Furthermore, given that changes in glacier size represent an indirect and delayed signal of climatic perturbations, the geomorphological signature of glaciers can be used to determine a distinct palaeo-temperature signal (Oerlemans, 2005). Using the available data on past glacier extent from Jostedalsbreen, Imhof et al. (2012) not only reaffirmed the notion that Norwegian glaciers in the western maritime area are highly correlated with the NAO (Dahl *et al.*, 2003; Nesje and Dahl, 2003; Nesje, 2005), but also concluded that the long and gently sloping outlet glaciers (e.g. Nigardsbreen and Lodalsbreen) have a roughly 20-year lag time in responding to changes in the local climate. In contrast, short and steep outlets (e.g. Bøyabreen and Briksdalsbreen) react within only five years of any climatic changes (Imhof *et al.*, 2012).

Table 2.1. *Lichenometrically derived ages using different methodological approaches for the Jostedalsbreen terminal moraines, considered to represent the LIA maximum (Bickerton and Matthews, 1993).*

Glacier	Age derived from families of lichenometric dating curves	Age derived from single lichenometric dating curves; 5LL	Age derived from single lichenometric dating curves; SLL
Austerdalsbreen	1786 (1761-1795)	1764	1762
Bergsetbreen	1793 (1786-1795)	1789	1786
Fåberstølsbreen	1706 (1690-1725)	1702	1695
Lodalsbreen	1826 (1822-1833)	1826	1833
Stegaholbreen	1863 (1857-1871)	1857	1862
Tuftebreen	1790 (1771-1807)	-	1771
Bødalsbreen	1755 (1742-1763)	1755	1742

East of Jostedalsbreen, the Jotunheimen mountains contain 287 glaciers (Andreassen *et al.*, 2012a). There have been numerous studies investigating the timing and extent of the LIA maximum in this region (Matthews and Shakesby, 1984; Matthews, 1991a, 2005; Bickerton and Matthews, 1993; Matthews *et al.*, 2005; Baumann *et al.*, 2009). However, unlike Jostedalsbreen, there are no historical documents. Instead glacier reconstructions rely on various geochronological techniques such as lichenometric dating, radiocarbon dating, and distal lake/mire sediment analysis (cf. Baumann, 2009). Of the many geochronological studies conducted across Jotunheimen, one of the most comprehensive is that of Matthews

(2005), who investigated the forelands of 16 glaciers and assessed sub-regional patterns of glacier fluctuations, and compared them at a regional scale to those of Jostedalsbreen. The sub-regional assessment shows synchronicity in LIA maxima of a west to east transect of Jotunheimen, with the regional LIA maximum having occurred around 1743-1750 (Matthews, 2005). Although the terminal moraine age estimations have a broad range (from 1699 to 1790), the extremes are considered outliers and thus unrepresentative of the true LIA maximum extent (Matthews, 2005). The revised moraine chronology of Matthews (2005) boasts impressively small error margins of between ±4.5-5.7 years and ±12.4-34.5 years for the youngest and oldest surfaces, respectively. This claims improved accuracy over the previously published chronology of Erikstad and Sollid (1986), which indicated that Jotunheimen's LIA maximum occurred around 1780-1820. Finally, Matthews (2005) explained the few outlying ages resulted from two factors; (1) in the case of the youngest ages, moraine overriding resulted in deposition of fresher boulders and thus later lichen colonisation; (2) in the case of the oldest outlying ages, higher moisture availability resulted in anomalously fast lichen growth and hence the larger lichen sizes were considered anomalous and non-representative of true moraine age.

At the Hardangerjøkulen ice cap (south of Jostedalsbreen) analysis of lacustrine sediments indicates glacier readvance occurred after the 1300s and this is corroborated by radiocarbon dating of subglacial plant remains found in till deposits on recently exposed nunataks in the region (Elven, 1978; Dahl and Nesje, 1994). Lichenometric dating is used to assess the timing of the LIA maximum, with a date of 1750 being assigned to the prominent end moraines of Midtdalsbreen and Blåisen (Andersen and Sollid, 1971).

2.4.2.6.2. The Little Ice Age in central Norway

In central Norway research into the LIA glacial history focuses around the Svartisen ice caps, Vestre Svartisen and Østre Svartisen. The Svartisen (outlet) glaciers have been the focus of important scientific debate with conflicting reports on timings of LIA maximum (e.g. Karlén, 1979; Innes, 1984a; Winkler, 2003).

As with the glaciers of southern Norway, there is some historical documentation of glacier advance in the Svartisen region that lends support to an 18th century LIA maximum. In the 1723 land registry (Matrikkel), there are descriptions of the advances

of Engabreen (the largest north-western outlet glacier from Vestre Svartisen; approx. location 66°42'N, 13°44'E) which affected three farms, with later reports indicating that by 1725 the ice was advancing so quickly that there was not enough time to harvest the growing crops and ultimately resulting in one farmstead (Strosteenøren) being destroyed (Rekstad, 1892; Hoel and Werenskiold, 1962; Grove, 2004a). An account from the turn of the 19th century described Engabreen as ending so close to the fjord that the ice front was washed by the sea (Rekstad, 1892). By 1810, however, the ice front was documented as having retreated from an extended position, demarcated by seven small but clearly defined moraines (Vargas Bedemar, 1819; Theakstone, 1965).

Attempts to define late-Holocene glacier advances for 25 glaciers around central Norway, focusing on the Svartisen glacier, were conducted by Karlén (1979), combining radiocarbon dating and lichenometry. Karlén (1979) reported glaciers having reached maximum positions at 2,800, 1,900, 1,500-1,300, 1,100, and 600 C^{14} yrs BP and that, since the 1300s, there have been frequent glacier expansions with no dominant moraine forming event at any one given time. The lichenometric methods and results of Karlén (1979) were, however, called into question by Innes (1984a) who provided evidence to show that earlier lichenometric dating curves underrepresent lichen grown. A clear example of prior dating inaccuracies is shown at a moraine previously dated to 1780-1830 (Karlén, 1979), yet later evidenced by historical photographs to have been formed around 1910 (Innes, 1984a). A full re-examination of lichen growth in the region led Innes (1984a) to conclude “a careful reevaluation of these curves is required before either the lichenometric evidence for glacial fluctuation dates is accepted . . . or the lichenometric dating of other phenomena in the area is attempted” (Innes, 1984a, p. 350).

An in-depth reassessment of the Svartisen and Okstindan LIA maxima has been carried out by Winkler (2003), who developed new lichenometric dating curves building on the assessment of Innes (1984a). The revised dates of the outermost moraines (of likely LIA origin), resulting from revised local dating curves, are shown in Table 2.2 and indicate a 1700s LIA maximum at Svartisen. The revised 1700s LIA maxima for Svartisen (Winkler, 2003) are now broadly considered the most accurate, reformulating the discussion around regional asynchronicity in LIA maxima and lending greater support to the presence of a mid-18th century (~1750) LIA maximum for southern and central Norway.

Table 2.2. *Lichenometrically-derived ages of LIA terminal moraines from two contrasting investigations within the Svartisen region. The first dates by Karlén (1979) were revised by Winkler (2003) and show substantial differences in calculated moraine ages. The ages of Winkler (2003) are now generally considered to be the most reliable.*

Glacier	Date according to Karlén (1979)	Date according to Winkler (2003)
Øvre Beiarbre	≈1500	1746
Nordre Bogvatnbre	≈1475	1762
Fykanåga No. 14	≈1550	1785
Fykanåga No. 13	≈1475	1761
Langvassåga No. 25	≈1450	1733
Langvassåga No. 23	≈1475	1756
Langvassåga No. 22	≈1600	1798
Langvassåga No. 21	≈1450	1746
Langvassåga No. 20	≈1550	1780
Kjølbreen	≈1475	1754
Flatisen	≈1650	1796
Fingerbreen	≈1475	1747
Austerdalsisen	≈1475	1749
Kampliisen	≈1450	1740
Langvassåga No. 26	≈1625	1809
Fykanåga No. 12	≈1625	1813

2.4.2.6.3. The Little Ice Age in northern Norway

The remoteness of the glaciers of northern Norway has provided fewer opportunities for people to record historical observations of glaciers. However at some key sites in the Lyngen and Bergsfjord areas there are some historical accounts that provide insight into the 19th and 20th century glacier extents, including for example the reports compiled by J.D. Forbes (1853), A. Geikie (1866), W.C. Slingsby (1898), G. Hastings (1899), A. Le Blond (1908), and A. Helland (1905).

The most extensive historical accounts are at Øksfjordjøkelen and its outlet glaciers on the Bergsfjord Peninsula, of which Jøkelfjordbreen (now known as Isfjordjøkelen and Nerisen, glacier ID 47 and 48, respectively; approx. location 70° 8'N, 22°4'E) has received the most attention. In 1851, J.D. Forbes visited the area and, in his memoirs, recounted that this glacier is the only glacier in Norway presently washed by the sea, and that the “fall of masses of ice into the fjord occasions frequent

commotions . . . the waves occasioned by the frequently overflowing of the huts of the natives" (Forbes, 1853, pp.78). In 1859 it was reported that Jøkelfjordbreen was starting to disintegrate, with the rockface beneath becoming partially exposed (Hardy, 1862). Around 30 years later a description and illustration of Jøkelfjordbreen (Figure 2.16) depicts the glacier as two separate units (Geikie, 1866). Since the mid-1800s, local residents have described the recession of Isfjordjøkelen and Nerisen (Helland, 1905), and in the early 1900s ice was collected from the fjord in front of Nerisen to be used in the fishing industry. The 130 years of documentation of the Jøkelfjord glaciers led Gellatly et al. (1989) to conclude that the two glaciers Isfjordjøkelen and Nerisen became detached between 1859 and 1865 and they found no evidence of these two glaciers being reconnected ever since (e.g. Figure 2.16).

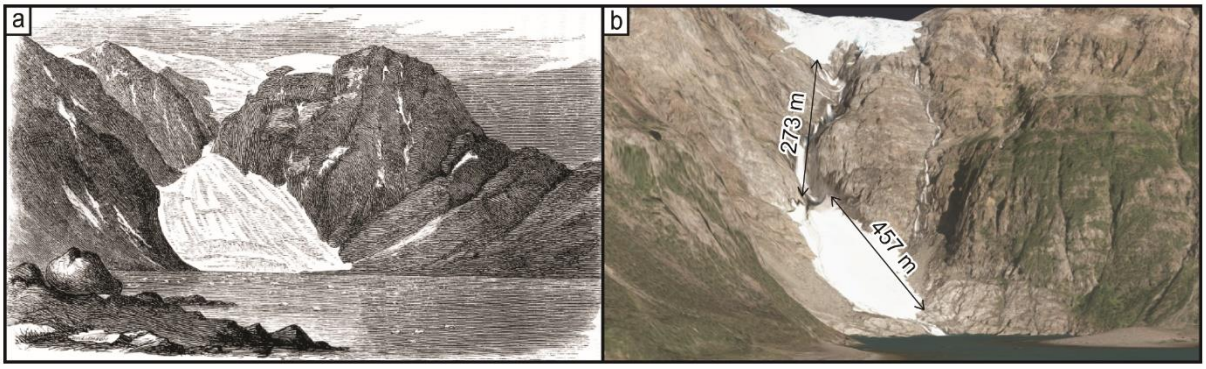

Figure 2.16. *(a) Sketch of the of Jokuls Fjord Glacier (Isfjordjøkelen and Nerisen; ID 47 and 48) from Geikie (1866, p. 149). (b) A 3D render of Isfjordjøkelen and Nerisen using 2015 aerial photographs (image source: norgeibilder.no; image date: 21.08.2015).*

Additional accounts of the northern outlets of Øksfjordjøkelen suggest that the glaciers (ID 39 and 41; approx. location 70°15'N, 22°6'E) almost reached into Nuvsfjorden and are described as being of "true alpine character . . . accompanied by moraines or trails of thick masses carried forward on the surface of the ice" (Forbes, 1853, pp. 81). During the 1870s there is also reference to the retreat of two unnamed hanging glaciers in the valley Øvre Tverdal (described as located on the western side of Øksfjord, opposite the Øksfjord church; approx. location 70°12'N, 22°10'E) and given the locality description it is likely they are referring to glaciers ID 34 and 38 (Helland, 1905). A local businessman, Mr C. Buck, based in Bergsfjord, reported that Isdaljøkelen (glacier ID 43; a western outlet of Øksfjordjøkelen, approx. location

70°10'N, 21°54'E) reached down to 88 m a.s.l. at around 1886. Above Bergsfjord, the large glacier Svartfjelljøkelen (ID 26; approx. location 70°14'N, 21°54'E) was noted in 1862 to almost reach the large lake Bergsfjordvatnet (97 m a.s.l.; Geikie, 1866), extending to ~135 m a.s.l. Subsequently, between 1890 and 1895, Svartfjelljøkelen retreated by 20-25 m (Helland, 1905).

While there are some accounts pertaining to a select few glaciers in the Lyngen and Bergsfjord regions during the 1800s, there are, to the authors knowledge, only a small number of peer-reviewed manuscripts that set out to establish specific constraints on the age and/or glacier extent at the LIA maximum. These are Ballantyne (1990), Bakke et al. (2005a), Wittmeier et al. (2015, 2020), Stokes et al. (2018), and Weber et al. (2020) which are spread across three different areas and discussed in turn.

On the Lyngen Peninsula, Ballantyne (1990) provides details on the LIA maximum, forming the basis for many subsequent glacial reconstructions in the region. Using lichenometry, dendrochronology, and some historical imagery, Ballantyne (1990) set out to date the timings of maximum LIA extent for 21 glaciers, covering a range of sizes, the smallest being south Kvalvikdalsbreen (glacier ID 227, 0.07 km^2, 69°31'43"N, 20°2'11"E) and the largest being Sydbreen (glacier ID 257, 4.29 km^2, 69°27'N, 19°54'E). In total there are four sets of moraines dating to LIA advances: “M1 *Subgroup 2* moraines” (found at six sites, dated to 1919-1930); “M1 *Subgroup 1* moraines” (found at 13 sites, dated to 1910-1920); “M2 moraines” (found at four sites, dated to 1825-1880); and “M3 moraines” (found at 11 sites, dated to mid-1700s). At four of the six sites where M1 *Subgroup 1* moraines are found there are no additional moraines within the vegetation trimline, leading Ballantyne (1990) to conclude that this moraine formed in the early-20^{th} century (1919-1930), representing a late-LIA maximum for Lyngen (and northern Norway more generally). Due to their small size, four glaciers, Kjosen (glacier ID 222, 0.24 km^2, 69°36'N, 20°6'E), Bredalsbreen (glacier ID 234, 0.18 km^2, 69°31'N, 20°01'E), north Veidalsbreen (glacier ID 264, 0.84 km^2, 69°25'N 19°53'E), and Rypedalsvatnbreen (glacier ID 238, 0.27 km^2, 69°30'N 19°57'E), were able to respond quickly and more extensively to the short-term climatic deterioration of low summer temperatures and high winter precipitation between 1870 and 1915 (Ballantyne, 1990).

Elsewhere on the Lyngen Peninsula, Bakke et al. (2005) used the lichenometric dating framework established by Ballantyne (1990) to date the LIA maximum of

Lenangsbreen (ID 199 and 201; approx. location 69°43'N, 20°3'E). By measuring lichen growing on the innermost moraine within their sequence (M13), they determined that it was formed during the period 1890-1928, with a corresponding lowering of the ELA by ~164 m (Bakke *et al.*, 2005a). Stokes et al. (2018) also used Ballantyne's (1990) maps to reconstruct glacier area (n = 10 glaciers) and length (n = 9 glaciers) over the period 1750-1915 and 1915-1953 (with the latter period representing the LIA glacier maximum) and concluded that glacier areas shrank by 1.6 km^2 between 1750 and 1915 and by 5.8 km^2 between 1915 and 1953.

On the Bergsfjord peninsula, Wittmeier et al. (2015) combined their own mapping and analysis of pro-glacial lake sediments from Langfjordjøkelen ice cap with the dating of Ballantyne (1990) and Bakke et al. (2005). The map of valley of Sør-Tverrfjorddalen (Langfjordjøkelen's foreland; approx. location 70°11'N, 21°42'E) depicts 13 moraines and an initial assessment of vegetation cover indicates that M12 and M13 are those relating to the LIA advance (Wittmeier *et al.*, 2015). Subsequent age-depth modelling of lake sediments led them to conclude that M13 was formed ~1925, however they state the maximum LIA glacier extent is demarcated by M12 which they claim was formed decades before, yet no specific date is provided (Wittmeier *et al.*, 2015). Finally, Weber et al. (2020) produced a detailed LIA glacier extent map of Langfjordjøkelen using their own mapping combined with the dating of Wittmeier et al. (2015). The extent of Langfjordjøkelen in 1925 (the supposed LIA maximum; Wittmeier et al., 2015) is shown to be 14.9 km^2 and Weber et al. (2020) note that earlier topographic maps from 1907 had overestimated glacier extent by ~38%.

On the coastal island of Arnøya (north-east of Lyngen), Wittmeier et al. (2020) established absolute ages of LIA moraines using cosmogenic nuclide dating. Through detailed field surveying and mapping, a sequence of three distinct LIA moraines (defined as M11, M12, M13) are identified fronting the Rødhetta glacier (ID 62; approx. location 70° 9'31"N, 20°43'31"E) and at least one LIA moraine is identified in each of the two neighbouring cirques. The ages of M11 and M12 are averaged from multiple samples and show formation during glacial expansion in the mid-1500s (480 ±20 yrs BP) and early-1600s (390 ±100 yrs BP), respectively. However, no age is established for the innermost moraine (M13; Wittmeier et al. 2020). The proposed LIA maximum on Arnøya of 1540 is, therefore, around 400 years earlier than on the Lyngen Peninsula and around 200 years sooner than in central and southern Norway.

When reviewing the historical documentation and scientific literature it is clear that the LIA maximum in northern Norway is a complex and contentious issue, with different sources pointing to different timings, with varying degrees of accuracy and reliability. There remains good rationale to scrutinise the various lines of reasoning and a need for further research across the region to better resolve the intricacies of variable independent factors (climate, locations, glacier hypsometry etc.) that might result in an apparent asynchronous response of glaciers in northern Norway.

2.4.2.7. Glacial extent and change in the 20th and 21st century

Since the termination of the LIA and the start of the 20th century, the vast majority of mountain glaciers and ice caps globally have been in a period of sustained recession, interrupted only by minor, localised readvances (Barry, 2006; Zemp *et al.*, 2008). This period has coincided with the start of widespread observational measurements and the start of many glacier monitoring programs (e.g. Hoel and Werenskiold, 1962) alongside the advent of aerial and satellite photography. It is now possible to gain a unique understanding of short-term changes to glaciers and examine these in a (long-term) climatic context.

While natural variability of glacier extent has a role to play in the decline of glaciers in the early- to mid-1900s (Marzeion *et al.*, 2014), since the 1980/90s, anthropogenically forced climate change is considered to be the driving factor in glacier mass loss (Reichert *et al.*, 2002; Roe *et al.*, 2017). In the period 1991-2010, it is estimated that the fraction of global glacier mass loss attributable to anthropogenic activity was 69% (Marzeion *et al.*, 2014) and that the rates of mass loss during this period are historically unprecedented (Zemp *et al.*, 2015). The current state of glaciers has been summarised by the IPCC in a special report on the cryosphere, which stated with very high confidence that “over the last decades, global warming has led to widespread shrinking of the cryosphere, with mass loss from ice sheets and glaciers” (IPCC, 2019, p. 4), and it is assessed that between 2006 and 2015 glaciers outside of Greenland and Antarctica experienced average mass loss of 220 ±30 Gt per year (IPCC, 2019).

In Norway, glaciers attained their LIA maximum extent asynchronously (see Section 2.3.2.6.) and thus experienced an asynchronous pattern of retreat, with glaciers in the south slowly retreating in the 1800s whilst those in the north were still

advancing (Ballantyne, 1990; Nussbaumer *et al.*, 2011). Between the 1930s and 1950s glacier data from across Norway indicates a more synchronous pattern of significant net retreat (Nesje *et al.*, 2008). Yet, after the 1960s glaciers started to behave differently, with local and regional variations in glacial behaviour being observed (Andreassen *et al.*, 2000b). Furthermore, there have been several periods of readvance during the 20th century of varying magnitude and duration with maritime glaciers, particularly those in western Norway, reacting fastest to climatic fluctuations (Hoel and Werenskiold, 1962; Theakstone, 1965, 1990; Bickerton and Matthews, 1993; Nesje, 2005; Nesje *et al.*, 2008; Winkler and Nesje, 2009; Nesje and Matthews, 2011; Winsvold *et al.*, 2014).

In Scandinavia, during the 1990s, most maritime glaciers started a phase of rapid advance triggered by a period of positive net mass balance in the winters between 1989/90 and 1994/95 (Nesje and Matthews, 2011). The positive mass balance was related to a positive NAO index and resulted in annual winter precipitation of 1,192 mm, 160% greater than the 1961-1990 normal (Nesje and Matthews, 2011). A key example of short term advances is found at the Jostedalsbreen ice cap, where the short and steep outlet glacier Briksdalsbreen (ID 2316; Figure 2.17), with response times of 10-15 years, has undergone several periods of readvance (Hoel and Werenskiold, 1962; Andreassen *et al.*, 2005; Nesje, 2005; Winkler *et al.*, 2009; Nesje and Matthews, 2011). During the periods 1901-1910, 1921-1931, 1974-1980, 1998-1996 Briksdalsbreen has been readvancing, with a 61 m glacier advance peaking in 1994 (Nesje and Matthews, 2011). After 1997, however, Briksdalsbreen has been steadily retreating, with the greatest annual retreat of 130 m in 2003/2004 (Nesje, 2005; Nesje and Matthews, 2011). The same advance phase in the 1990s was not observed in continental glaciers, where mass balance is smaller, and hence these ice-masses underwent steady recession instead (Andreassen *et al.*, 2005; Nesje *et al.*, 2008).

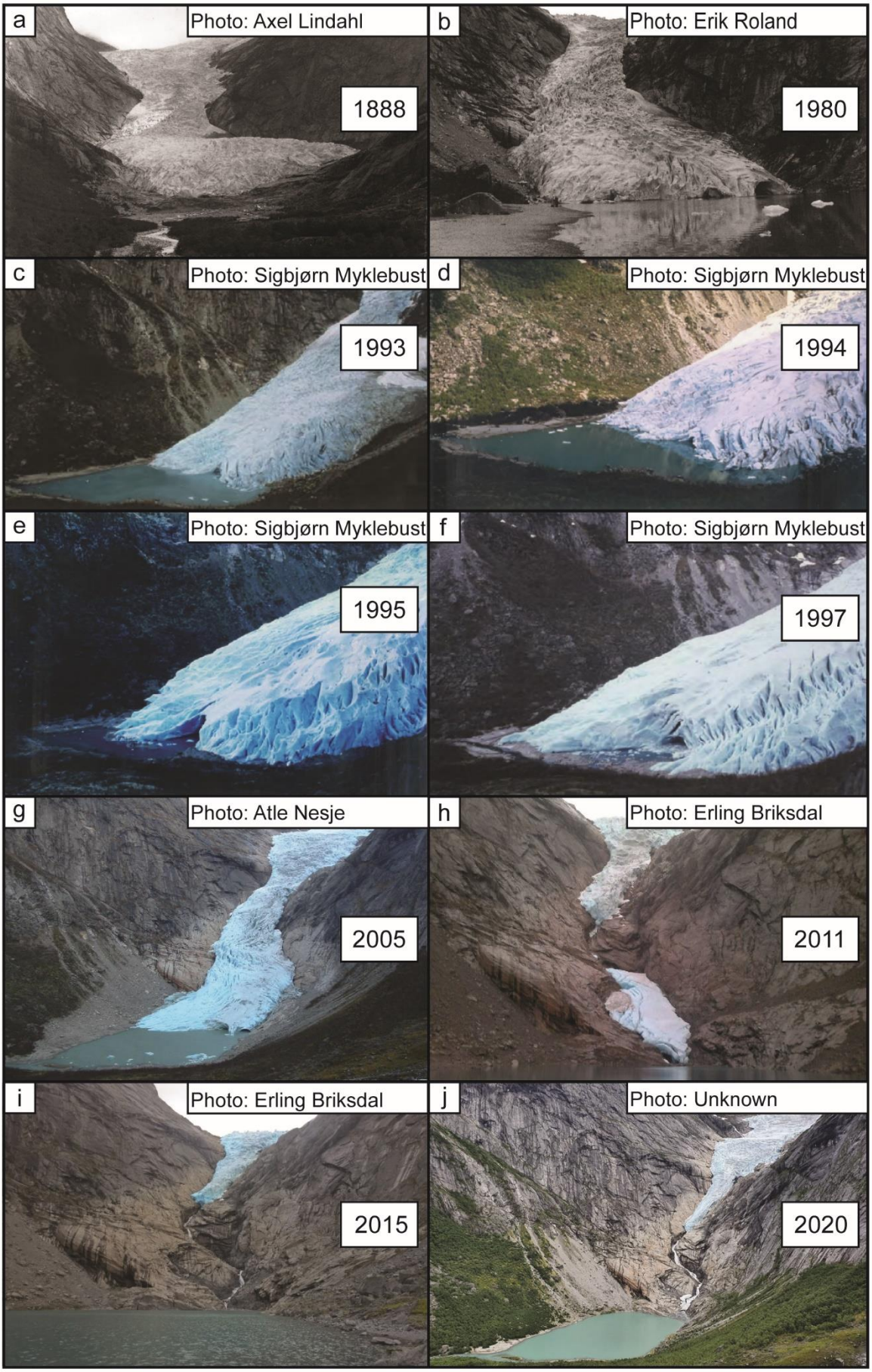
a
Photo: Axel Lindahl
1888
b
Photo: Erik Roland
1980
c
Photo: Sigbjørn Myklebust
1993
d
Photo: Sigbjørn Myklebust
1994
e
Photo: Sigbjørn Myklebust
1995
f
Photo: Sigbjørn Myklebust
1997
g
Photo: Atle Nesje
2005
h
Photo: Erling Briksdal
2011
i
Photo: Erling Briksdal
2015
j
Photo: Unknown
2020

Figure 2.17. *Photographs of Briksdalsbreen from 1888-2020, showing the late-20th century readvance between 1993 and 1997 (approx. location 61°40'N, 6°52'E). Panels c-f are reproduced from Nesje and Matthews (2011) and the remaining panels are imagery from NVE's archive of glacier photographs (http://glacier.nve.no/Glacier/viewer/gpp/en/).*

At the Langfjordjøkelen ice cap in northern Norway, the Langfjord East outlet glacier (ID 54; approx. location 70°07'33"N, 21°47'01"E) has been the focus of mass balance observations since 1989. Langfjord East is the only glacier in northern Norway that has long-term observational data and is therefore a key indicator of glacier condition across the region. The annual balance of Langfjord East over the period 1989-2009 does not, however, reflect the late-20th century advance of southern Norway (cf. Andreassen *et al.*, 2012b). Instead, between 1989 and 2009 Langfjord East lost approximately -0.87 m water equivalent per year (Andreassen *et al.*, 2012b). Furthermore, over the period 1966-2008 volume, area, and length reduced by 46% (-0.180 km^3), 38% (-2 km^2) and 20% (-1.1 km) respectively (Andreassen *et al.*, 2012b). Langfjord East was the only observed glacier across mainland Norway to have negative mass balance during an apparent period of transient mass surplus during the 1990s (Andreassen *et al.*, 2005, 2012b; Nesje and Matthews, 2011). Additional work reconstructing the glacial extent of the Langfjordjøkelen ice cap during the 1915 LIA maximum has revealed an ice extent of 14.9 km^2, which had shrunk to 6.4 km^2 by 2018, representing a >50% reduction in area at a rate of ~9% (0.9 km^2) per decade (Weber *et al.*, 2020). The glacier shrinkage at Langfjordjøkelen since the LIA maximum, when measured as a percentage of total area, is greater than for any other glacier in mainland Norway, with this having been linked to the enhanced warming across this region as a result of Arctic amplification (Weber *et al.*, 2020). Similarly, on the nearby Lyngen Peninsula, Stokes et al. (2018) provided the first regional assessment of glacier change since LIA maximum and showed a reduction in glacier area of ~0.3% per year between the proposed 1915 LIA maximum (Ballantyne, 1990) and 1988. This was followed by a hiatus in recession before continued and sustained retreat of ~1% per year between 2001 and 2014. The results from Lyngen show that it is the smallest glaciers (e.g. those <0.05 km^2) at low elevations (e.g. below 1,400 m a.s.l.) which are most susceptible to climate warming (Stokes *et al.*, 2018).

Across Norway more generally, Andreassen et al. (2020) have compiled a review on glacier change since 1960 for 131 glaciers with long-term observational data. In total the glacierized area has decreased from 817 km^2 in the 1960s to 734 km^2 in the 2010s with an overall surface elevation change of -15.5 m, equal to -0.27 m water equivalent per year over the ~50 year period (Andreassen *et al.*, 2020). All glaciers examined underwent net shrinkage (area and length) and thinning, and are now at record minima within the observational record (Andreassen *et al.*, 2020).

With the concurrence of glacier change assessments across Norway showing net glacier recession during the late-20th/early-21st century, some authors have hypothesized that many of the present-day glaciers most vulnerable to climate change (e.g. those <0.05 km^2, at low elevations, and/or or in sub-optimally orientated cirques) are likely to disappear by 2100 (e.g. Nesje *et al.*, 2008; Andreassen *et al.*, 2012b; Stokes *et al.*, 2018; Weber *et al.*, 2019, 2020). Indeed, it is likely that many small sub-optimally situated glaciers have already melted completely (Parkes and Marzeion, 2018), as demonstrated by Baumann et al. (2009), who have recorded the disappearance of 13 glaciers in the Jotunheimen region of southern Norway since the LIA. Furthermore, modelling of Norwegian glaciers has also shown them to be highly sensitive to climatic changes. For example, the Hardangerjøkulen ice cap is projected to disappear completely within 100 years given a 2.7°C temperature increase (Åkesson *et al.*, 2017), a value within the future climate projections for southern Norway (Hanssen-Bauer *et al.*, 2015). A temperature rise of 2.3°C is suggested to cause a rise in ELA of ~350 m (Nesje *et al.*, 2008). Regional modelling studies show agreement with site-specific investigations, indicating that, dependent on emission scenario, total annual mass changes will be in a deficit of between 117 and 179 m water equivalent during the period 2000–2100 (Mutz *et al.*, 2016).

Glacier recession over the coming decades is an important research issue for Norway, because glaciers are critical to hydropower, water management, and tourism (Aall and Hoyer, 2005; Stewart *et al.*, 2016; Hanssen-Bauer *et al.*, 2017; Andreassen *et al.*, 2020). Additionally, glacier recession results in new and/or increasing risk for nearby communities and infrastructure (e.g. Engeset *et al.*, 2005; Hartmeyer *et al.*, 2020), and threatens irreversible changes to the local environment and ecosystems (e.g. Wrona *et al.*, 2016; Stibal *et al.*, 2020). This reaffirms the need for accurate maps of glaciers, rates and magnitude of glacier recession, and past glacier extent.

2.4.3. Summary

There has been much work investigating glacial geomorphology and developing reconstructions of glacial dynamics across mainland Norway, but there are numerous sites in northern Norway that require further in-depth investigation. Of particular interest are the smaller mountain glaciers situated throughout northern Norway, for which very little is known. To assess the present-day state of these glaciers and then examine their retreat over recent decades and their fluctuations throughout the Holocene is a non-trivial task.

In the study area (Figure 2.2) there is considerable ambiguity as to the total number of (very small) mountain glaciers, the timing and extent of glacial maxima throughout the Holocene, most notably in the presence of mid-Holocene climatic events (Bakke *et al.*, 2005a; Wittmeier *et al.*, 2015, 2020), the onset of Neoglaciation (Bakke *et al.*, 2005a; Wittmeier *et al.*, 2015, 2020), and the timing and extent of LIA maximum (Ballantyne, 1990; Wittmeier *et al.*, 2015, 2020). This leads to important, but previously unanswered research questions: (1) what are the present-day rates of change for mountain glaciers throughout Troms and Finnmark County and how do these compare with the rest of Norway?; (2) when did these mountain glaciers attain their most recent glacial maximum?; (3) to what extent did mountain glaciers fluctuate during the Holocene following the retreat of the SIS from the region?

Evidently, throughout Troms and Finnmark County detailed scrutiny of available historical documentation, aerial photographs and satellite imagery is required, combined with establishing robust age constraints from key glacial features. This forms the key aims for this study. The resulting output will help better understand the impact of anthropogenically forced climate change in a region highly susceptible to enhanced warming and environmental degradation, and has important implications for the interpretation of other paleoenvironmental and climatic records in northern Norway.

CHAPTER 3

Identifying and mapping very small (<0.5 km^2) mountain glaciers on coarse to high-resolution imagery

Leigh J.R.[1], Stokes C.R.[1], Carr J.R.[2], Evans I.S.[1], Andreassen L.M.[3], Evans D.J.A.[1]

[1]Department of Geography, Durham University, Durham, UK; [2]School of Geography, Politics and Sociology, Newcastle University, Newcastle upon Tyne, UK; [3]Norwegian Water Resources and Energy Directorate (NVE), Oslo, Norway

The mountain Goahtegáisá (1,038 m a.s.l., 69°41'23"N, 20°38'44"E) in the Kåfjord Alps surrounded by very small ice/snow units.
Photograph date: 29th August 2018 (by J.R. Leigh)

A version of this chapter has been published as:

Leigh J.R., Stokes C.R., Carr J.R., Evans I.S., Andreassen L.M., Evans D.J.A. 2019. Identifying and mapping very small (<0.5 km2) mountain glaciers on coarse to high-resolution imagery. *Journal of Glaciology*, **65**(254), 73-888.

“Listen, everything you love is about to disappear
I feel it coming, there's something in the air
But this is living, oh it's modern living”
(Reynolds, 2020)

3.1. Abstract

Small mountain glaciers are an important part of the cryosphere and tend to respond rapidly to climate warming. Historically, mapping very small glaciers (generally considered to be <0.5 km^2) using satellite imagery has often been subjective due to the difficulty in differentiating them from perennial snowpatches. For this reason, most scientists implement minimum size-thresholds (typically 0.01-0.05 km^2). Here, we compare the ability of different remote sensing approaches to identify and map very small glaciers on imagery of varying spatial resolutions (30-0.25 m) and investigate how operator subjectivity influences results. Based on this analysis, we support the use of a minimum size-threshold of 0.01 km^2 for imagery with coarse to medium spatial resolution (30-10 m). However, when mapping on high resolution imagery (<1 m) with minimal seasonal snow cover, glaciers <0.05 km^2 and even <0.01 km^2 are readily identifiable and using a minimum threshold may be inappropriate. For these cases, we develop a set of criteria to enable the identification of very small glaciers and classify them as *certain, probable,* or *possible.* This should facilitate a more consistent approach to identifying and mapping very small glaciers on high-resolution imagery, helping to produce more comprehensive and accurate glacier inventories.

3.2. Introduction

Numerous studies have revealed unprecedented global glacier recession during the late-20th and early-21st century, which has been linked to anthropogenically-induced climate change (e.g. Haeberli *et al.*, 2007; Marzeion *et al.*, 2014; Zemp *et al.*, 2015). Although there has been significant mass loss from the large polar ice sheets (Shepherd *et al.*, 2012), the combined melt from mountain glaciers and ice caps between 2003 and 2009 accounted for 29 ±13% of observed sea level rise, approximately equal to the loss from both the Greenland and Antarctic ice sheets (IPCC, 2013). Furthermore, it has been proposed that the combined melt from 'uncharted glaciers' (i.e. glaciers that are not currently included in global glacier inventories) may account for as much as 42.7 mm (31% of a total 137.1 mm sea level equivalent from glaciers globally, excluding the Greenland and Antarctic ice sheets) of sea level rise between 1901 and 2015 (Parkes and Marzeion, 2018).

The development of satellite remote sensing over the last 30-40 years revolutionised our ability to map and monitor glacier extent, reducing a previous reliance on historical records or field-based measurements of glacier change (Andreassen *et al.*, 2002; Pellikka and Rees, 2009). Moreover, recent advances in satellite technology and data availability have dramatically improved the spatial, temporal, and spectral resolution of imagery (Roy *et al.*, 2017). A clear example of this is the Swiss Glacier Inventory SGI2010 which was derived from manual mapping of 0.25 m resolution aerial orthophotographs (Fischer *et al.*, 2014). Other recent glacier inventories such as the Inventory of Norwegian Glaciers (Andreassen *et al.*, 2012a) have also utilised orthophotographs as a means of validating their glacier maps which were compiled from satellite imagery.

Prompted in part by the Global Land Ice Measurements from Space (GLIMS) initiative, there has been a large body of work assessing which remote sensing techniques are most appropriate for mapping glaciers in different settings (Racoviteanu *et al.*, 2009; Paul *et al.*, 2010, 2013; Raup and Khalsa, 2010). However, there has been less focus on very small glaciers (generally considered to be <0.5 km^2), sometimes referred to as 'glacierets' (Lliboutry, 1965; WGMS, 1989; Cogley *et al.*, 2011), ice aprons (Benn and Evans, 2010), and/or 'niche glaciers' (Groom, 1959; Grove, 1961), with various (and sometimes conflicting) definitions regarding the classification and mapping of these units (Fischer, 2018). Despite their small area,

however, mapping very small glaciers is important for several reasons. First, their widespread distribution and frequent occurrence means they likely account for ~80-90% of the total number of glaciers located in mid- to low-latitude mountain ranges (Fischer *et al.*, 2014; Paul and Mölg, 2014; Pfeffer *et al.*, 2014; Huss and Fischer, 2016). Second, very small glaciers act as a reservoir for water storage, moderating interannual variability in streamflow constituting a significant part of the hydrological system in mountain areas (Barnett *et al.*, 2005) and, with a warming climate, are critical in terms of increasing concern about future water security (Huss, 2011; Rangecroft *et al.*, 2013; Huss and Fischer, 2016). Third, smaller glaciers are highly sensitive to climate change and typically exhibit the shortest response times to a given climate forcing (Grudd, 1990; Oerlemans, 1994; Nesje *et al.*, 2008; Federici and Pappalardo, 2010). However, they can also be disproportionately influenced by local topography, such that when they survive in heavily-shaded cirques, they may be sustained for longer than expected (Demuth *et al.*, 2008; DeBeer and Sharp, 2009; Evans, 2009c). Fourth, monitoring the evolution of very small glaciers could reveal new insights regarding their fate over longer timescales e.g. their disappearance versus transitioning into debris-covered and/or rock glaciers, which may also have implications for catchment hydrology (Capt *et al.*, 2016; Jones *et al.*, 2018a, 2018b, 2019a). Finally, it is important to correctly classify very small glaciers because of their relevance to issues of environmental protection in some parts of the world, especially where they may exist within national parks (Fraser, 2017; Tollefson and Rodríguez-Mega, 2017).

Despite their importance and ubiquity, there is very little guidance on how to distinguish very small glaciers (<0. 5 km^2) from perennial snowpatches when compiling remotely sensed glacier inventories or change assessments. In practice, most researchers simply define a minimal size-threshold, commonly somewhere between 0.05 and 0.01 km^2 (Table 3.1). All units below this size-threshold are then ignored or removed, due to the large uncertainty in differentiating between snowpatches and glaciers (Lindh, 1984; Paul and Mölg, 2014; Lynch *et al.*, 2016). This approach is likely to be appropriate for coarse to medium resolution satellite imagery (e.g. Landsat, 80-15 m; Sentinel, 20-10 m), but the last decade has seen a huge growth in much higher resolution satellite imagery (e.g. GeoEye-1, 0.46 m; Planet labs, 3-0.75 m; Pleiades-1, 0.5 m; SPOT, 1.5 m; WorldView, 0.31 m etc.). Alongside this, there has been an increase in the amount of imagery acquired via Unmanned Aerial Vehicles (UAVs)

and, although they only cover small areas, they can provide centimetre-resolution imagery for glacier mapping. These new data sources should therefore permit the identification of very small glaciers, and perhaps render minimum size-thresholds of 0.05 to 0.01 km^2 inappropriate. Indeed, some more recent studies using high resolution imagery (e.g. 0.25 m) have no minimum size-threshold and, as a result, glaciers as small as ~0.001 km^2 have been mapped (Huss and Fischer, 2016).

Given the anticipated growth in high-resolution imagery for glacier mapping, the aim of this paper is to explore ways of improving the objectivity and consistency of mapping very small glaciers (<0.5 km^2 and especially those <0.05 km^2) on high-resolution satellite imagery and aerial photographs. First, we draw attention to the differences in the area and number of very small glaciers identified when using (a) imagery of varying resolutions and (b) different mapping approaches (automated, semi-automated, manual). This is achieved by analysing satellite imagery and aerial orthophotographs with pixel resolutions from 30 to 0.25 m and applying a range of common approaches for mapping of glaciers. Secondly, we develop new criteria to help the objective identification and mapping of very small glaciers using high-resolution imagery. These criteria are developed with the aim of reducing uncertainty and increasing the accuracy and completeness of glacier inventories where high resolution imagery is available.

Table 3.1. *Example of minimum size-thresholds used in previous remote sensing studies mapping glacier changes, listed in chronological order.*

Authors	Study area	Image spatial resolution (m)	Minimum glacier size (km^2)
Barcaza et al. (2017)	Southern Andes	30	0.01
Ganyushkin et al. (2017)	Altai Mountains	0.5-30	0.01
Tielidze et al. (in review)	Caucasus Mountains	1.5-30	0.01
Earl and Gardner (2016)	North Asia	30	0.02
Lynch et al. (2016)	Kamchatka Peninsula	15-30	0.02
Racoviteanu et al. (2015)	Eastern Himalaya	0.5-90	0.02
Burns and Nolin (2014)	Cordillera Blanca	3.2-79	0.01
Paul and Mölg (2014)	Northern Andes	<15-30	0.05
Pfeffer et al. (2014)	Global	≤30	0.01
Xiang et al. (2014)	Poiqu River basin	15-79	0.01
Bliss et al. (2013)	Antarctic periphery	15-200	0.01
Jiskoot et al. (2012)	East Greenland	14.5-15	2
Andreassen et al. (2012b)	Norway	30	0.0081
Frey et al. (2012)	Western Himalayas	30	0.02
Rastner et al. (2012)	Greenland	15-2,000	0.05
Bajracharya et al. (2011)	Hindu Kush-Himalayan region	≤90	0.02
Bhambri et al. (2011)	Garhwal Himalayas	2.5-90	0.25
Kamp et al. (2011)	Himalaya Range of Zanskar	15-79	0.05
Paul et al. (2011)	European Alps	<30-90	0.01
Bolch et al. (2010)	Canadian Cordillera	≤30	0.05
Narama et al. (2010)	Tien Shan Mountains	1.8-30	0.01
DeBeer and Sharp (2009)	Monashee Mountains	4-30	0.01

3.3. Study area

The study area lies within the Kåfjord/Nordreisa municipalities, of northern Norway (Figure 3.1). This area was selected because it contains numerous small glaciers and snowpatches, often partially obscured by shadow and some with thin debris cover, making it a particularly challenging environment and therefore suitable for testing approaches to identify and map very small glaciers.

The study area (Figure 3.1c) is a minor mountain range, with peaks ranging from 1,183 m a.s.l. to 1,320 m a.s.l., dominated by valley and cirque-type glaciers within an elevation range of ~600 to ~1,200 m a.s.l. Many glaciers tend to exist in sheltered and shadowed locations, with generally thin (<1 m) and patchy debris cover on some termini (Figure 3.2). To the west is a major fjord system (Lyngen Fjord) and there are subsidiary fjords to the north and south. The glaciers are subject to a maritime climate. As such, they are particularly sensitive to climate fluctuations (De Woul and Hock, 2005) and their mass balance is heavily influenced by variations in the Arctic Oscillation (Andreassen *et al.*, 2012b; Kjøllmoen *et al.*, 2018). Precipitation

primarily falls as snow between October and May, while rainfall can occur throughout the year (Vikhamar-Schuler *et al.*, 2010). Average monthly temperature typically varies from -10 to 15°C, with the hottest months (June to September) reaching average daily highs of up to 16°C (station number 91740, 6 m a.s.l: www.eKlima.no).

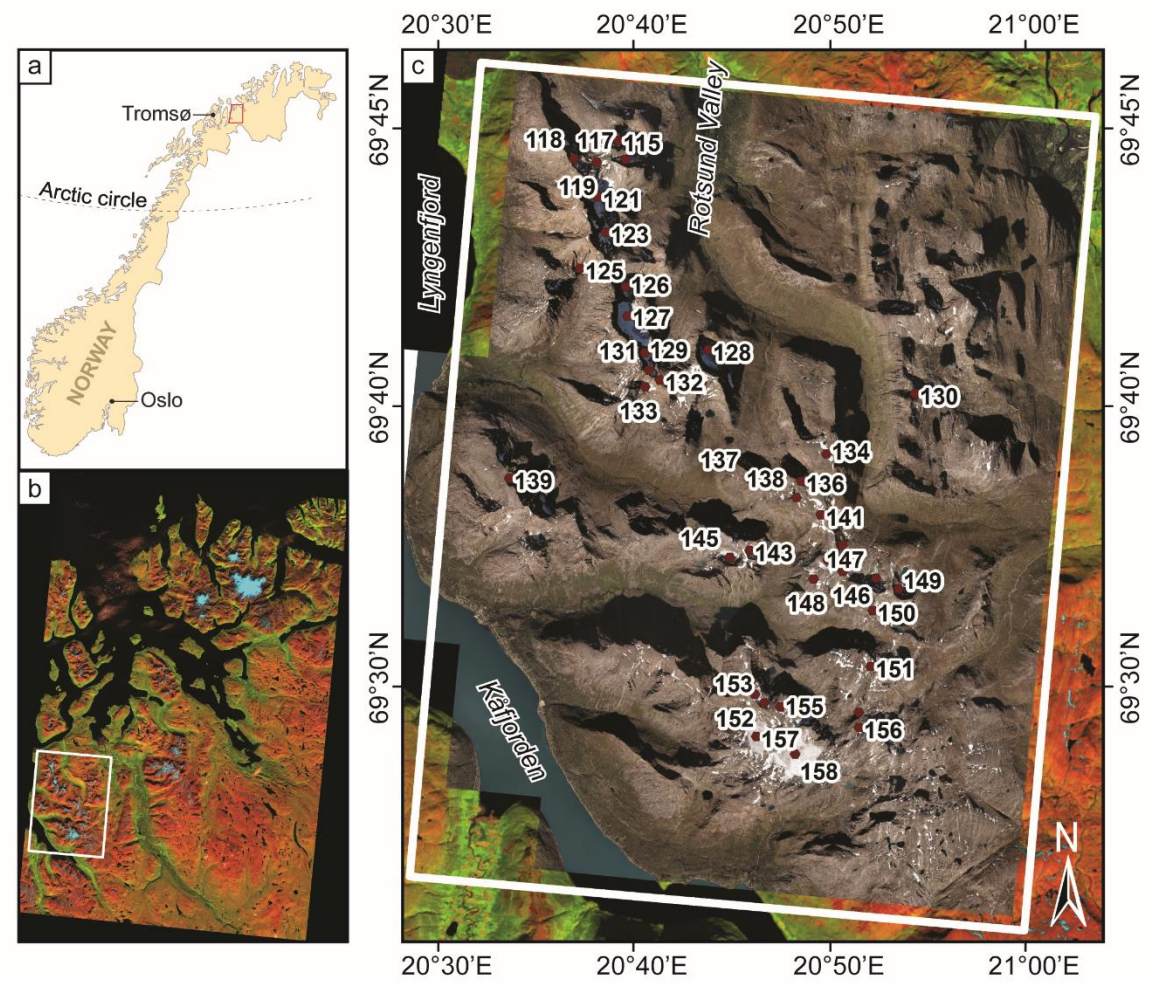

Figure 3.1. *Study site location within the Kåfjord/Nordreisa municipalities; northern Norway. Red rectangle in (a) represents location of image (b), white rectangle in (b) represents location of image (c). The base image of (b) and (c) is a Landsat 8 scene (path 196, row 11) displayed as a false colour composite (R-G-B; 5-4-3). In (c) aerial orthophotographs (0.25 m resolution) are overlain on the Landsat imagery. Note: Numbers in (c) are glacier IDs from the Norwegian Glacier Inventory (NGI).*

Glaciers in Norway have been mapped by the Norwegian Water Resources and Energy Directorate (NVE) and their characteristics are detailed in the Inventory of Norwegian Glaciers (Andreassen *et al.*, 2012a), henceforth referred to as the NGI (Norwegian Glacier Inventory). This most recent glacier inventory was produced using

medium-resolution Landsat imagery and a TM3/TM5 band ratio method (Andreassen *et al.*, 2008; Paul and Andreassen, 2009), with all units below 0.0081 km^2 excluded from the inventory. The mapped units were manually classified as 'glaciers', 'possible snowfields', or 'snow' and additional manual corrections were made where necessary. Within the study area (Figure 3.1c) the NGI records 40 glaciers, with a total glacial extent of 12.09 km^2 (Figure 3.3), and an additional seven units classified as possible snowfields with a total area of ~0.85 km^2 (Andreassen *et al.*, 2012a). The recorded glaciers range in size from 2.48 km^2 to 0.04 km^2 (Andreassen *et al.*, 2012a). Only 10% of the glaciers are >1 km^2 but they account for ~49% of the total glacial area.

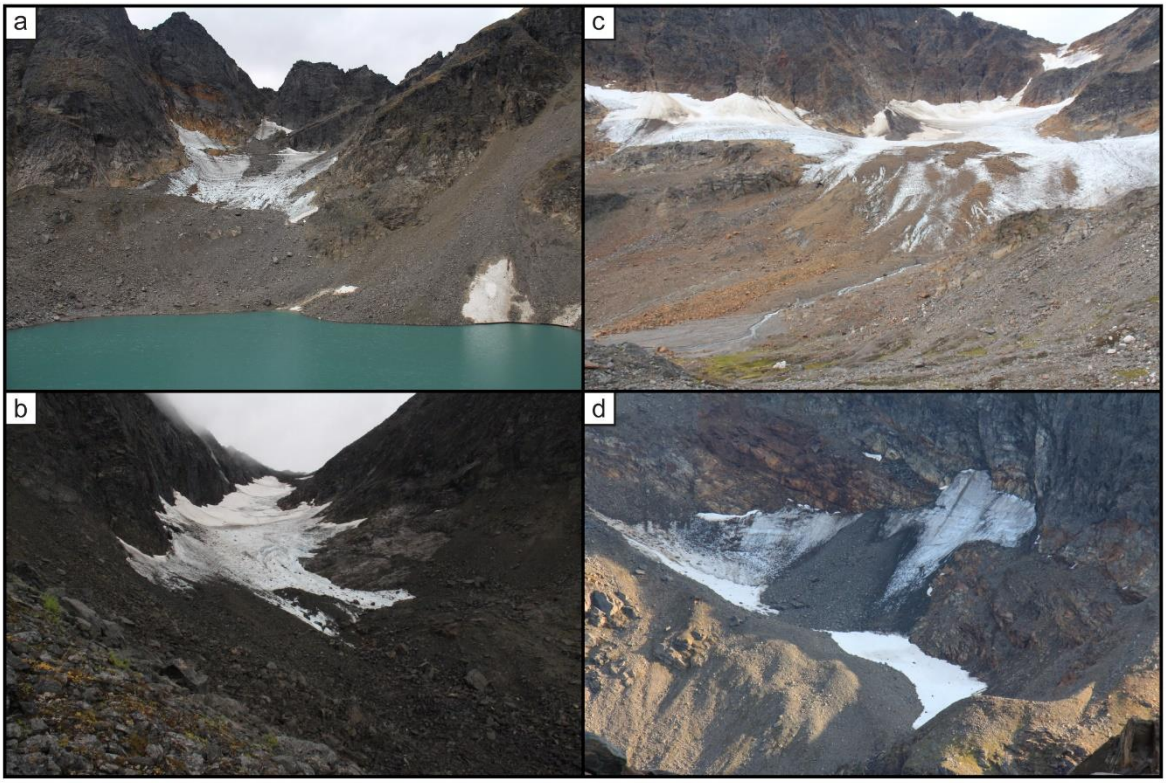

Figure 3.2. *An example of the type of glaciers within the study area, which are partly obscured by debris cover. Images A, B, and C show glaciers 115, 117, and 121, respectively (Andreassen and others, 2012b). Image D shows a very small (~0.03 km^2) glacier, not included within the NGI. All users mapped and classified glaciers A-C as certain. Users 1 and 2 mapped and classified the glacier in D as certain, but User 3 did not map this unit (see Discussion). Locations shown on Figure 3.1c.*

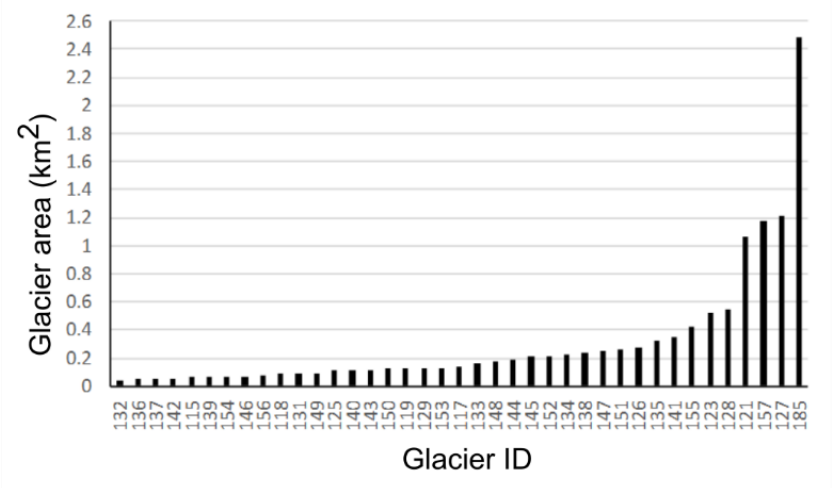

Figure 3.3. *Overview of glacier size distribution within the study site (see Figure 3.1) as recorded in the NGI. Only 10% of glaciers are >1 km^2 while 85% of glaciers are ≤0.5 km^2.*

3.4. Methods

Obtaining suitable imagery in maritime Norway is challenging. Frequent cloud cover means the number of appropriate satellite scenes each year can be very low (Marshall *et al.*, 1994; Andreassen *et al.*, 2008). Furthermore, due to the high latitude of this study area, late-lying snow is prevalent, limiting image collection to between July and September. In this study, aerial orthophotographs, Landsat 8 OLI, and Sentinel-2A imagery were selected to determine the effect that different image resolutions have on the way that very small glaciers are identified and mapped (Table 3.2).

The four most common mapping techniques (automated mapping, automated mapping with a size-threshold, semi-automated mapping, and manual mapping) were performed on Landsat 8 OLI (30 m resolution), pan-sharpened Landsat 8 OLI (whereby a 15 m resolution panchromatic image was merged with the 30 m resolution multispectral image to create a single 15 m resolution colour image), and Sentinel-2A (10 m resolution) imagery. Only manual mapping was conducted on the orthorectified aerial photographs (with resolution 0.25 m). Furthermore, because there remains considerable debate about how to define very small glaciers (Fischer, 2018), glaciers were mapped following the definition of Cogley et al. (2011), i.e. a glacier is defined as “a perennial mass of ice, and possibly firn and snow . . . showing evidence of past or present flow” (Cogley *et al.*, 2011, p. 45). Note that the definition of a glacier by Cogley et al. (2011) was preferred because of the emphasis on evidence of flow, which

is different from the GLIMS definition of a glacier whereby “a glacier or perennial snow mass, identified by a single GLIMS glacier ID, consists of a body of ice and snow that is observed at the end of the melt season . . .” (Raup and Khalsa, 2010, p. 4).

The first approach, automated mapping using a band ratio method (Williams *et al.*, 1991; Pellikka and Rees, 2009), was used on the multispectral satellite imagery. The high reflectivity of ice and snow in the visible and near-infrared wavelengths (VNIR: 0.4-1.2 micrometres; Bands 1-4 on Landsat 8 OLI) compared to a very low reflectivity in the shortwave infrared (SWIR: 1.4-2.5 micrometres; Band 5 on Landsat 8 OLI), is used to automatically delineate glacier extents (Racoviteanu *et al.*, 2009). Band ratio images were computed in ERDAS Imagine software from the raw multispectral imagery (e.g. OLI Band 3/OLI Band 5) and converted to a binary image with ice/snow classified as 1, and the remaining surfaces classified as 0 (Shapiro and Stockman, 2001). Some researchers also implement an additional threshold (e.g. Band 1) which can sometimes improve mapping in shadowed areas. This approach does not always lead to a marked improvement, and it was not used for our assessment. Following the conversion to a binary image, the resulting image was compared against a false colour composite of the multispectral imagery (bands 5, 4, and 3 as Red, Green, Blue) to find the most suitable (albeit subjective) threshold value to isolate glaciers from non-glaciers (Raup *et al.*, 2007). A median (3 x 3 kernel) filter was then applied to the binary image to reduce noise from isolated pixels outside the glaciers and to close small voids within the glaciers (such as those created by discontinuous debris cover).

The second mapping approach uses the automatically mapped glacier outlines from approach one to assess the impact of implementing different minimum size-thresholds for glacier inventories. To assess size-thresholds, the automated maps were copied and then all mapped units below a minimum glacier area of (a) 0.05 km^2 or (b) 0.01 km^2 were removed.

The third approach was semi-automated mapping, also conducted on the multispectral satellite imagery. Initial glacier outlines were generated automatically, as in approach one, and outlines were then manually edited (by a single user) to attempt to correct areas where the automated process had obviously failed to accurately map glacier outlines (usually in association with debris cover, heavy shading, or proglacial lakes). Glacier ice was identified using an R-G-B (5-4-3) false colour composite whereby ice has a distinct blue colour (Andreassen *et al.*, 2012a). Furthermore, any

units that were perceived by the operator to be incorrectly mapped as glaciers were removed, whilst any glaciers perceived as missing were added by manual digitisation.

The fourth approach, also applied to the multispectral satellite imagery, was manual mapping. Here, all potential glacier units were identified and mapped in ArcMap by a single user drawing a polygon-shapefile around their perceived boundaries. To ensure accuracy in mapping, especially around areas of shade, each individual image was viewed using multiple band combinations of Red-Green-Blue as 5-4-3, 4-3-2, and 3-2-1 (Andreassen *et al.*, 2012a). To investigate the impact of subjective interpretation by individual users, different experts with prior experience of mapping glaciers (identified as User 1, User 2, and User 3) undertook manual mapping on the Landsat 8 imagery (see Table 3.2).

Finally, a manual technique was used to map glacier outlines on the aerial orthophotographs. All glacier units were outlined manually by the three different users as individual polygon-shapefiles.

Table 3.2. *List of imagery used in this study and the associated mapping technique. User 1, User 2, and User 3 are each experts with previous glacier mapping experience.*

Imagery and date	Mapping technique used *(km^2)*
Landsat 8 22.07.2016	Automated
	Automated (removing units <0.01)
	Automated (removing units <0.05)
	Semi-automated
	Manual (User 1)
	Manual (User 2)
	Manual (User 3)
Landsat 8 (pansharpened) 22.07.2016	Automated
	Automated (removing units <0.01)
	Automated (removing units <0.05)
	Semi-automated
	Manual (User 1)
Sentinel-2A 20.09.2017	Automated
	Automated (removing units <0.01)
	Automated (removing units <0.05)
	Semi-automated
	Manual (User 1)
Orthophotographs 18.08.2016	Manual (User 1)
	Manual (User 2)
	Manual (User 3)

3.5. Results

The results of the different mapping techniques applied to different imagery are displayed in Table 3.3, which also includes summary statistics of the glaciers mapped in the NGI (Andreassen *et al.*, 2012a). Note that the NGI data were mapped using a semi-automated approach from Landsat 7 (ETM+) imagery captured in 2001. In part, this explains the difference in total number of units and size of glaciers mapped, as there are 15-16 years between the acquisition dates of the NGI and this study.

Table 3.3. *Results of mapping glaciers using multispectral satellite imagery at 30 m, 15 m, and 10 m resolution and 0.25 m aerial photographs. Note: the top row of data is the results of mapping conducted in 2001 taken from the Inventory of Norwegian Glaciers (NGI).*

Imagery	Resolution *(m)*	Technique used (km^2)	Glacier units *count*	Glacier unit difference with NGI *count*	Total area (km^2)	Mapped area difference with NGI (km^2)	Min. glacier size (km^2)	Max. glacier size (km^2)	Median glacier size (km^2)	Mean glacier size (km^2)
NGI (Landsat 7)	30	Semi-Automated	40	N/A	12.09	N/A	0.0378	2.4813	0.1358	0.3022
Landsat 8 OLI	30	Automated	623	583	18.61	6.52	0.0009	4.1877	0.0630	0.0299
		Automated (removing units <0.01)	220	180	16.92	4.83	0.0108	4.1877	0.0270	0.0769
		Automated (removing units <0.05)	58	18	13.26	1.17	0.0504	4.1877	0.0815	0.2285
		Semi-Automated	68	28	12.80	0.71	0.0117	2.2154	0.0774	0.1883
		Manual (User 1)	60	20	12.33	0.02	0.0243	2.1292	0.0881	0.2055
		Manual (User 2)	23	-17	10.22	-1.86	0.0377	2.5818	0.2463	0.4445
		Manual (User 3)	44	4	12.94	0.85	0.0160	2.3480	0.1604	0.2941
Landsat 8 OLI (Pansharpened)	15	Automated	3144	3104	12.76	0.67	0.0002	1.7836	0.0009	0.0041
		Automated (removing units <0.01)	153	113	8.55	-3.54	0.0101	1.7836	0.0189	0.0559
		Automated (removing units <0.05)	28	-12	6.07	-6.02	0.0502	1.7836	0.0849	0.2167
		Semi-Automated	65	25	11.06	-1.03	0.0158	2.1602	0.0706	0.1702
		Manual (User 1)	66	26	11.35	-0.74	0.0177	2.1754	0.0695	0.1720
Sentinel-2A	10	Automated	966	926	10.70	-1.39	0.0001	1.9486	0.0010	0.0107
		Automated (removing units <0.01)	121	81	9.28	-2.81	0.0100	1.9486	0.0225	0.0767
		Automated (removing units <0.05)	29	-11	7.37	-4.72	0.0538	1.9486	0.0969	0.2542
		Semi-Automated	71	31	9.75	-2.34	0.0150	1.9874	0.0851	0.1373
		Manual (User 1)	61	21	11.15	-0.94	0.0156	2.1338	0.0851	0.1828
Orthophotographs	0.25	Manual (User 1)	53	13	9.52	-2.56	0.0171	1.9995	0.0754	0.1797
		Manual (User 2)	58	18	8.57	-3.52	0.0022	1.8705	0.0500	0.1477
		Manual (User 3)	117	77	8.92	-3.17	0.0004	1.8266	0.0121	0.0763

3.5.1. Satellite imagery

3.5.1.1. Automated and semi-automated mapping

The unedited automated approach resulted in the highest numbers of mapped glacier units, regardless of image resolution (Table 3.3). The greatest number of units mapped (n = 3,144) were derived from applying the automated approach to the pan-sharpened Landsat 8 (15 m) imagery (Table 3.3). An increase in the quantity of mapped units did not, however, necessarily equate to a greater total mapped area. For example, the total mapped area of 623 units on the Landsat 8 imagery (30 m) was 18.61 km^2, while the total mapped area of 3,144 units on the pan-sharpened Landsat 8 (15 m) was 12.76 km^2 (Table 3.3). The automated approach consistently maps the smallest units (glacial and/or non-glacial) across all image resolutions, and the area of the smallest units mapped decreases with increasing image resolution (Table 3.3). However, the automated approach resulted in a large number of false-positive results, as the majority of units may be outlines of snow or other non-glacial features.

The use of a minimum size-threshold inevitably leads to a reduction in the number of units mapped. Using a minimum size-threshold of 0.01 km^2, compared to no minimum size-threshold, resulted in the removal of 403 (Landsat 8), 2,991 (pan-sharpened Landsat 8), and 845 (Sentinel-2A) mapped units (Table 3.3, Figure 3.4). Increasing the minimum size-threshold to 0.05 km^2 resulted in the removal of 565 (Landsat 8), 3,116 (pansharpened Landsat 8), and 937 (Sentinel-2A) mapped units, compared to our results with no minimum size class. A minimum size-threshold clearly reduces the number of units mapped, but only discriminates on the basis of size, rather than genesis, and so may incorrectly eliminate a substantial number of very small glacier units (Figure 3.4).

The semi-automated approach, where automated outputs were manually edited, substantially reduced both the number of glacier units and the total areal extent when compared to the simple automated approaches alone (Table 3.3). Using the semi-automated approach resulted in the highest number of units on the Sentinel-2A imagery (10 m; 71 units), compared to 68 units on Landsat (30 m) and 65 on pan-sharpened Landsat 8 (15 m) imagery. When comparing the total mapped area from the semi-automated approach, the Sentinel-2A imagery (10 m) gave the smallest total mapped area at 9.75 km^2, a reduction in area of 24% and 12% compared to the

Landsat 8 and pan-sharpened Landsat 8 imagery (30 and 10 m), respectively (Table 3.3). The semi-automated approach involved editing by an experienced user, meaning the likelihood of removing actual glacier units is diminished, but it remains highly subjective.

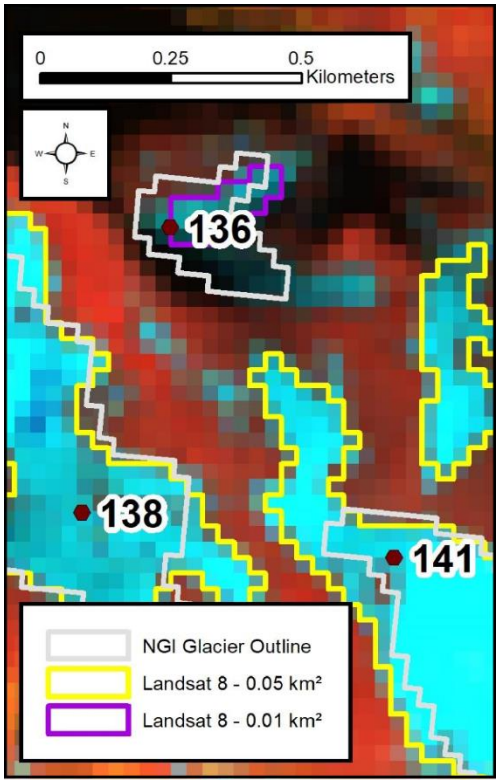

Figure 3.4. *Example of where using a 0.05 km² size-threshold (yellow outlines) eliminates a glacier included in the NGI (ID 136 with an area of 0.0468 km² in that inventory). A significant proportion of the mapped difference is attributed to the heavy shading over the glacier area meaning it falls outside of the required reflective value for the automated method. Note: where only a yellow outline is seen on glaciers 138 and 141, the purple outline is drawn directly underneath and therefore not visible. Background image: Landsat 8 (30 m resolution, R-G-B as 5-4-3). Location shown in Figure 3.1.*

To examine how the above techniques might influence the mapping of both larger and very small glaciers, we separately analysed the outlines of the largest and smallest glaciers found within the study area (as listed in the NGI). The largest NGI glacier in the study site is glacier 158 (Noammerjiehkki) with an area (in 2001) of ~2.48 km² (Andreassen *et al.*, 2012a). When re-mapped using an automated approach, the

resulting areal extent was ~4.19 km^2 on 2016 Landsat 8 imagery (30 m resolution), ~1.78 km^2 on the 2016 pan-sharpened Landsat 8 imagery (15 m), and ~1.95 km^2 on 2017 Sentinel-2A imagery (10 m; Figure 3.5). The automated approach on the 30 m resolution imagery erroneously merges glacier 158 with adjacent units (glaciers 155 and 157), due to seasonal snow obscuring the boundary of glacier 158 and, therefore, resulting in the large area differences between image resolutions. It is possible for such errors to be manually corrected and units are divided into different entities using glacier basins (Andreassen *et al.*, 2012a). Indeed by using a semi-automated approach, users in our study were able to approximate glacier extent beneath the snow cover. Therefore, outlines of glacier 158 derived from different resolution imagery showed far less variance: ~2.22 km^2, 2.16 km^2, and 1.99 km^2 (30 m, 15 m, and 10 m resolution imagery respectively; Figure 3.5, Table 3.3).

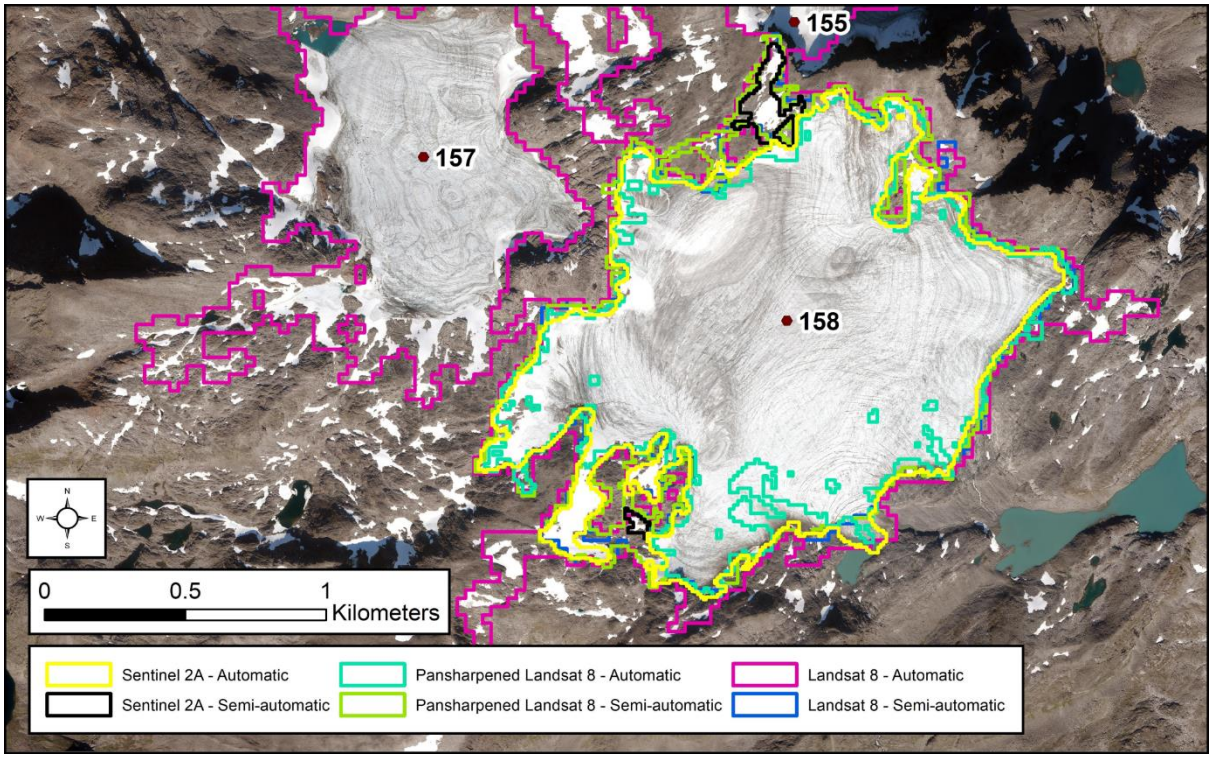

Figure 3.5. *The mapped areal extent of glacier 158 (Noammerjiehkki) when applying automated techniques using the band ratio method on multispectral satellite imagery. The automatic approach on the Landsat 8 (30 m) imagery (pink line) results in the merging of glaciers 157, 158, and 155 into one unit with an areal extent of 4.19 km^2. Closer inspection suggests definition of the three as separate units. Note: To emphasise the substantial differences in outlines between the Landsat 8 automated method and all other methods, only the mapped extent of glacier 158 is shown. All*

other mapped units are removed from this image e.g. glaciers 155 and 157 are not shown for the other imagery types or mapping techniques. Location shown in Figure 3.1.

The smallest glacier in the study site according to the NGI is glacier 130 (Figure 3.6) with an area (in 2001) of ~0.04 km^2 (Andreassen *et al.*, 2012a). When re-mapped using an automated approach on 2016 Landsat 8 imagery (30 m) the resulting areal extent is ~0.03 km^2, but it is measured at ~0.01 km^2 on both the 2016 pan-sharpened (15 m) and 2017 Sentinel-2A imagery (10 m; Figure 3.6). The 0.01 km^2 size-threshold does not affect this unit but the 0.05 km^2 threshold removed it from the map. With a semi-automated approach, the unit is mapped with an area of 0.02 km^2 on the 15 and 10 m resolution imagery. However, the unit was not mapped at the 30 m resolution due to the high uncertainty in distinguishing it as a glacier rather than a snowpatch (Figure 3.6).

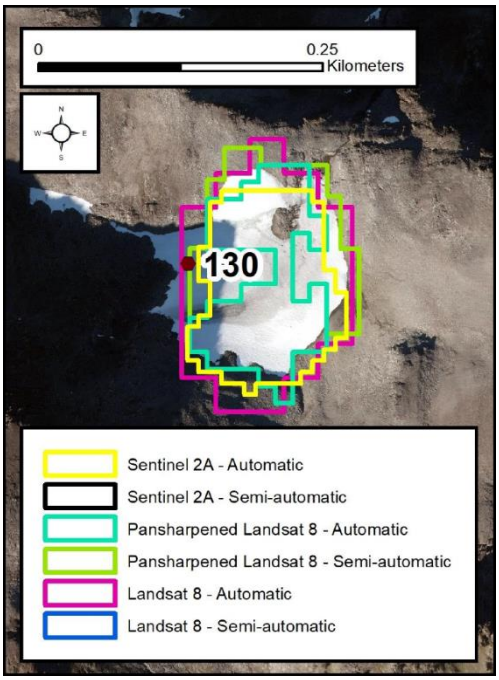

Figure 3.6. *The mapped extent of glacier 130 when applying automated and semi-automated techniques using the band ratio method for multispectral satellite imagery. Note that the glacier was removed by the operator using the semi-automatic approach on the Landsat 8 imagery (30 m), presumably because they thought it was a small snowpatch. The Sentinel-2A semi-automated outline (black) is directly below the automatic outline (yellow). Location shown in Figure 3.1.*

Overall, these results indicate that it is difficult to consistently and objectively map very small glaciers in the study area using both the automatic and semi-automatic approaches. Increasing image resolution (from 30 to 10 m) reduced variance in the mapping of the large glaciers (Figure 3.5), but there was increased variance and uncertainty when mapping very small glaciers (Figure 3.6). Furthermore, there was an inverse relationship between image resolution and total mapped area for both semi-automatic and automatic approaches; more glacier units are mapped on the higher resolution imagery (10 and 15 m) than on the coarse resolution imagery (30 m) yet, the cumulative mapped area of these units is lower (Table 3.3). Minimum size-thresholds will obviously reduce the total number of units mapped (sometimes by >90%) and can result in a substantial decrease in the total mapped area (Table 3.3). Higher resolution (≤10 m) imagery may show that implementing minimum size-thresholds leads to the erroneous removal of genuine glaciers, as in Figure 3.6.

3.5.1.2. Manual mapping

Mapping glaciers manually is more subjective and arguably less consistent than the automated and semi-automated techniques described above. Our results show different glacier outlines from the different users, confirming previous work conducting 'round-robin' experiments with glacier mapping (e.g. Paul *et al.*, 2015). On the Landsat 8 imagery (30 m), there were major differences in both the total area and number of glaciers mapped. For example, Users 2 and 3 mapped fewer glaciers (37 and 16, respectively) than User 1, but User 3 mapped the largest cumulative glacier area (Table 3.3). However, manual mapping resulted in the least amount of difference in the number of mapped units between different image resolutions. In almost all cases, manual mapping reduces the number of units mapped compared with the automated, and semi-automated techniques (Table 3.3). Similar results were also found by Fischer et al. (2014).

When comparing image resolution and individual unit sizes, it is the largest units that experience the greatest absolute differences in mapped size, yet smaller percentage differences. The largest glacier unit manually mapped by each user on the 30 m resolution imagery (2.5818, 2.3480, and 2.1292 km^2) shows maximum difference of ~0.45 km^2 or ~19% (Table 3.3). In contrast, the smallest unit manually mapped by each user on the 30 m resolution imagery (0.0377, 0.00243, and 0.0160 km^2) shows

maximum difference of only ~0.02 km^2 yet this equates to ~81% (Table 3.3). Manual mapping on the 15 and 10 m resolution imagery resulted in a maximum unit size of ~2.18 and 2.13 km^2, respectively, while the minimum unit size was ~0.02 km^2. At resolutions from 30 to 10 m, individual users were able to identify and map glaciers <0.05 km^2. However, no units smaller than <0.01 km^2 were manually mapped, suggesting that there is a lower size limit for confidently identifying glaciers on coarse (30 m) to medium (10 m) resolution imagery.

3.5.2. Aerial orthophotographs; manual mapping

When comparing the manual mapping on high-resolution imagery (aerial orthophotographs, <1 m) against coarse-resolution imagery (Landsat 8 imagery 30 m), it is clear that image resolution affects what is perceived and subsequently mapped as a glacier, especially with regards to the smallest glacier units. While two out of three users mapped more glaciers on coarse (30 m) compared to high-resolution (<1 m) imagery, all three users mapped a smaller total glacier area on the high-resolution imagery (Table 3.3). Again similar results were also found by Fischer et al. (2014). When image resolution is increased from 30 m (Landsat 8 imagery) to 0.25 m (aerial orthophotographs) the largest total area mapped decreases from 12.94 km^2 to 9.52 km^2 (a 26% reduction; Table 3.3). The higher resolution also resulted in smaller units being mapped, the smallest unit decreased from 0.016 km^2 on the Landsat 8 imagery to 0.0004 km^2 on the aerial orthophotographs (a 98% reduction; Table 3.3). The maximum difference between users for the total mapped area is only 0.95 km^2 on the aerial orthophotographs, as opposed to 2.72 km^2 on the Landsat 8 imagery (Table 3.3). This lower total variation on the orthophotographs is caused by lower variation in the mapping of larger glaciers.

When manual mapping using high-resolution aerial orthophotographs, the number of glacier units mapped ranged from 53 to 117, while total glaciated area ranged from 8.57 to 9.52 km^2 (Table 3.3). However, it should be noted that the user who identified the highest number of units did not map the largest cumulative glacier area. This is because 51 of the 117 units mapped (44%) were less than 0.01 km^2 in area and the areas of both the largest units (glaciers 157 and 158) are smaller, resulting in a low cumulative glacier area. The minimum glacier size ranges from 0.0004 to 0.0171 km^2 while the maximum glacier size ranges from 1.8266 to 1.9995

to km^2 (Table 3.3). These results highlight the fact that when manually mapping glaciers on the aerial orthophotographs (<1 m), all operators were able to map very small glaciers, with two out of three users mapping units <0.01 km^2 (Table 3.3).

All users mapped a greater number of glaciers on the aerial orthophotographs than were in the NGI. However, the total area of glaciers has decreased, in part because the aerial orthophotographs are from a more recent date and some glaciers have retreated. Indeed, there are eight examples whereby glacier fragmentation has resulted in more units mapped (e.g. Figure 3.7). Glacier fragmentation, therefore, accounts for a 30%, 16%, and 12% increase in number of glaciers mapped by Users 1, 2, and 3, respectively.

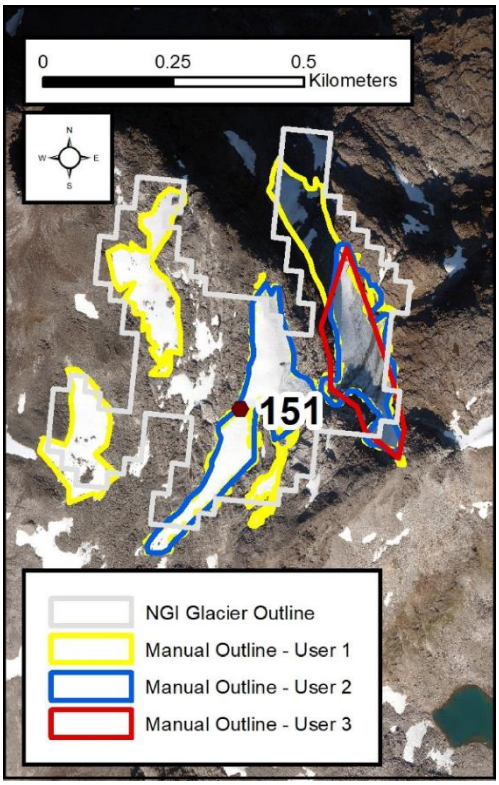

Figure 3.7. *Glacier 151 has fragmented over time. It has been mapped as multiple units by Users 1 and 2, while User 3 has mapped only one portion of the glacier. The grey outline shows the extent of glacier 151 from the NGI, mapped in 2001 from Landsat 7 imagery. Background image: natural colour aerial orthophotograph (0.25 m resolution). Location shown in Figure 3.1.*

To summarise, the results show that increasing image resolution increased the number of glaciers that can be identified and mapped. Furthermore, on the high-resolution imagery (<1 m), it was possible for users to map numerous very small glaciers with individual extents <0.01 km^2 (Table 3.3). The mapping of units <0.01 km^2 by users is attributed to the fact they were able to define specific glacier surface features (e.g. glacier ice, evidence of flow at the surface of the ice) which helped to differentiate glacier units from snowpatches. However, for the smallest units mapped (specifically those <0.01 km^2) there was an increase in differences between users as to what is identified and mapped as a glacier on the high-resolution imagery (<1 m), compared to the lower resolution imagery (30-15 m).

3.6. Discussion and recommendations for future work

There is a large body of literature on the best practice for mapping glaciers >1 km^2 using satellite imagery (e.g. Raup *et al.*, 2007; Paul *et al.*, 2009, 2013; Racoviteanu *et al.*, 2009), but there is little guidance on identifying and mapping very small glaciers (<0.5 km^2), which are often ignored on medium to coarse resolution imagery. This lack of guidance can be problematic given the burgeoning availability of high-resolution satellite imagery and aerial photographs, from which we can now identify these very small glaciers. From the analysis above, we demonstrate that image resolution imagery, and the techniques applied have a substantial impact on the mapped glacial area that results. This is further influenced by the knowledge and experience of the operator, and the methods applied to define a glacier, particularly for glaciers <0.5 km^2. The following sections present a discussion and offer subsequent guidelines to aid in the identification and mapping of very small glaciers.

3.6.1. Mapping approaches on coarse- to medium-resolution imagery (30, 15, and 10 m)

Regardless of image resolution, automated techniques often fail to map the full extent of many units (when compared to high resolution aerial photographs). This is attributed to the inherent problems with automated glacier mapping, typically arising from debris cover, pro-glacial lakes, shadow, remnant snow, ice boundary conditions, and recently deglaciated terrain (Racoviteanu *et al.*, 2009). As such, errors in mapping often require manual correction.

When using the automated and semi-automated approaches, at 30-15 m pixel resolutions, there are very large uncertainties in both the number and total area of glaciers <0.01 km^2. At 15-10 m pixel resolutions especially, maps were overcomplicated by noise from erroneous sources (e.g. late-lying snow). Due to uncertainty in mapping units <0.01 km^2, minimum glacier size-thresholds were applied to the 30 m, 15 m, and 10 m resolution imagery. The results presented here clearly show that, even at the 30 m resolution, it is possible to identify glacier units <0.05 km^2, including those in heavily shaded locations (e.g. Figure 3.4). Such glaciers can be identified based on their basic form and geographical situation (e.g. distinct snow/ice visible, situated in a cirque, evidence of prior valley glaciation). A minimum size-

threshold of 0.05 km^2 may therefore be too large, as it is possible to identify glaciers <0.05 km^2. However, it is difficult to identify glaciers <0.01 km^2, confirming the need for a minimum size-threshold. On the coarse and medium resolution imagery, relative uncertainty in glacier outlines increases with decreasing glacier size (Fischer *et al.*, 2014; Winsvold *et al.*, 2014), but there is still a need for assessment of mapped features falling just below a size-threshold before their removal. Manual correction (e.g. for areas in cast shadow), as shown in Figure 3.8, may increase a glacier's area above a specific threshold and ensure it is included in subsequent analysis (Paul *et al.*, 2016).

Furthermore, when comparing results from manual mapping on the Landsat 8 imagery (30 m), there is a large variation in the number and subsequent area of glaciers mapped. No user in this study mapped any units smaller than 0.01 km^2, the smallest glaciers mapped ranged in size from ~0.02 to ~0.04 km^2 (Table 3.3).

Given the above considerations, we confirm the current literature recommending that mapping on coarse to medium resolution imagery (30-10 m) uses a semi-automated approach with a 0.01 km^2 minimum size-threshold, as per the GLIMS guidelines (Paul *et al.*, 2010).

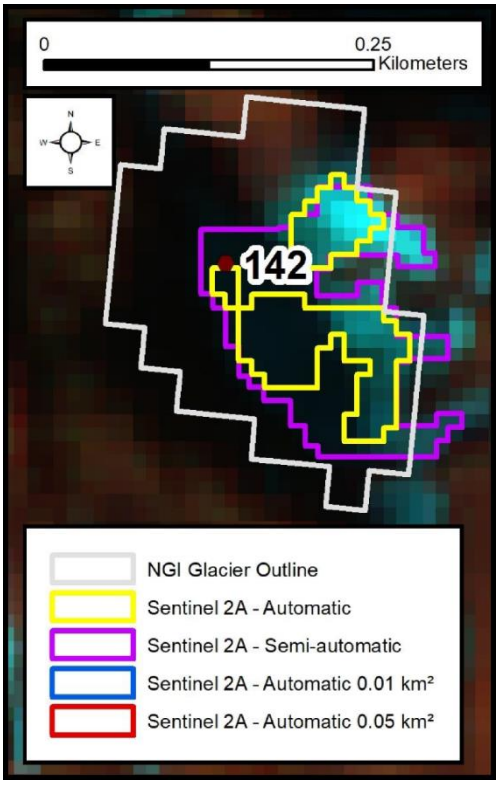

Figure 3.8. *Manually editing the Sentinel-2A imagery automated outlines (yellow outline) of glacier 142 allows all three individual units (with areas of 0.0029, 0.0005, and 0.0077 km^2) to be identified and mapped as one connected unit (purple outline). Without manual rectification the 0.05 and 0.01 km^2 size-threshold remove the automatically mapped glacier units. Background image: Sentinel-2A imagery (10 m resolution, R-G-B as 5-4-3). Location shown in Figure 3.1.*

3.6.2. Mapping approaches on high-resolution imagery (<1 m)

When mapping on the aerial orthophotographs, the application of a minimum glacier size-threshold seems unnecessarily cautious, as the higher resolution enables clear definition of features attributable to a glacier (Fischer *et al.*, 2014). An example of this is found in Figure 3.9, which shows a glacier mapped by all three operators. However, as shown in Table 3.3, large discrepancies remain in the number of units mapped as glaciers by different operators. This difference is again attributed to the increased level of subjectivity because of improved image resolution, especially with regards to distinguishing a snowpatch from a glacier.

A significant point of note is that when mapping on the orthophotographs (<1 m resolution), multiple glaciers with an area <0.01 km^2 were mapped by two out of the three users. Furthermore, as glaciers of varying sizes (plateau, valley, cirque glaciers,

etc.) continue to shrink and fragment under a warming climate it is important that glacier inventories map all parts of a previously mapped glacier and do not ignore those falling below a certain size. Our results suggest that implementing a minimum size-threshold (even of 0.01 km^2) on imagery of <1 m resolution is inappropriate. We now address this issue by developing some criteria to aid the identification of glaciers on high resolution imagery.

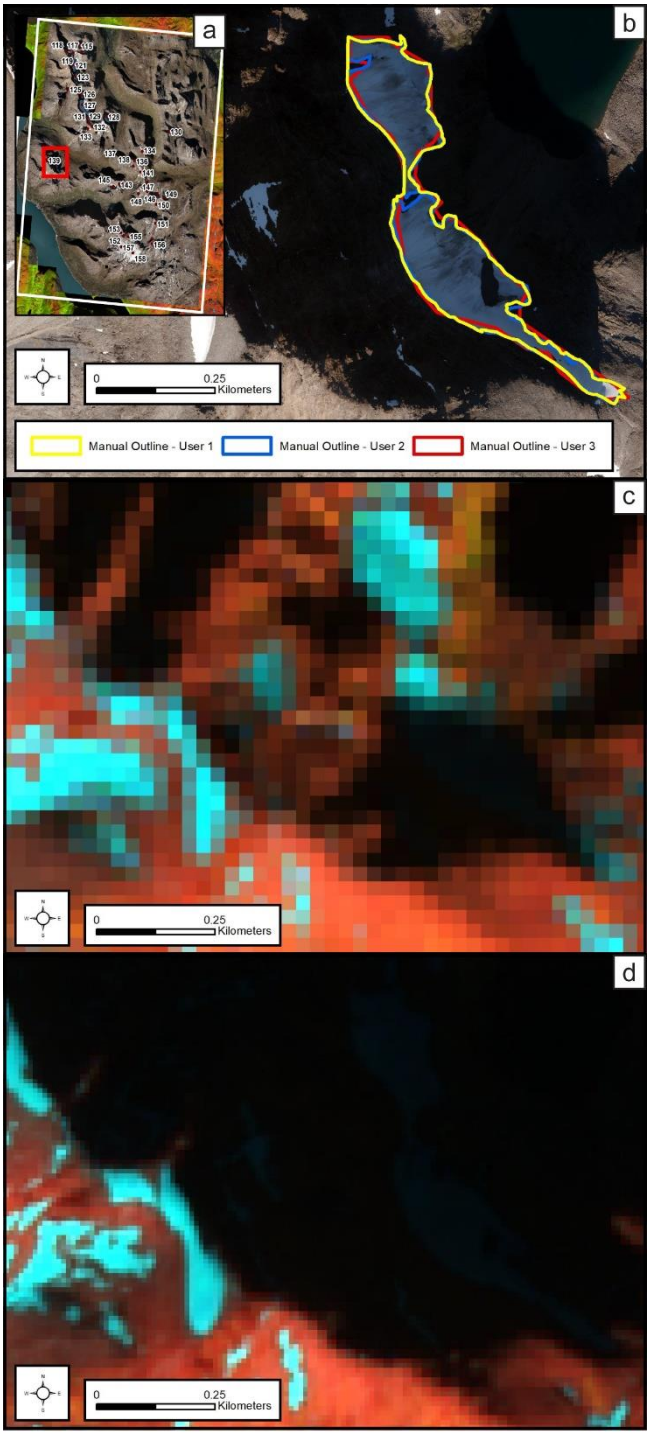

Figure 3.9. (a) *Location of an additional glacier (69°38'8"N, 20°35'24"E; previously unmapped in the NGI) that all users mapped on aerial photographs in (b) but not on the Landsat 8 imagery (30 m resolution, R-G-B as 5-4-3) or Sentinel-2A imagery (10 m resolution, R-G-B as 5-4-3) in (c) and (d) respectively. When the scoring system is used all users mapped this unit as certain This unit is situated in a heavily shaded cirque, bordering a proglacial lake, and with a small amount of debris cover, all factors that hinder mapping on coarse resolution multi-spectral imagery.*

3.6.3. Identifying very small glaciers: a new scoring system

As demonstrated above, a lack of guidance on how to distinguish very small glaciers from snowpatches, when mapping from high-resolution remotely sensed imagery, resulted in significant disparity between results from different mappers. This has been previously highlighted by the GLIMS project, where it was stated that "the methodological interpretation of a glacier as an entity varies widely, prompting the need for standardized methods" (Racoviteanu *et al.*, 2009, p. 54). To our knowledge, no such standardized methods have so far been developed. We therefore propose a new scoring system to increase objectivity when identifying very small glaciers on high-resolution imagery (see Table 3.4). Our scoring system aims to reduce uncertainty and enable more robust and reliable glacier mapping, where image resolution and snow cover conditions permit. The system builds on and extends previous work by Evans (1990b), who identified small glaciers in British Colombia based on three key indicators: crevasses, bergschrunds, and (visible) ice. Furthermore, our scoring system incorporates the glacier definition of Cogley et al. (2011) whereby identification and subsequent glacier classification is weighted towards evidence of past and/or present flow.

Table 3.4. *Glacier identification scoring system for use in high-resolution (e.g. <1 m) remote sensing applications. Summing the feature scores provides degree of confidence in identification as a glacier: 11 to 20 = certain; 6 to 10 = probable; 2 to 5 = possible; 1 = perennial snow. Images from 2016 source: https://www.norgeibilder.no/*

Feature*	Score	Description	Example
Crevasses	5	Cracks and/or fractures, of any width, in the surface of a glacier.	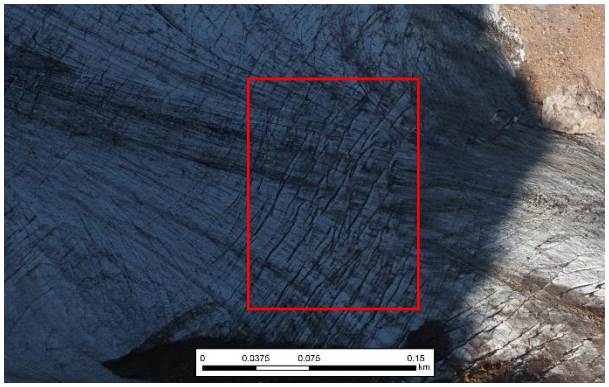
Flow features and deformed stratification	5	Features such as the deformation of glacier banding, presence of foliation, or distinct proglacial debris transport when comparing images from multiple time steps	
Multiple debris bands in ice	3	Parallel stripes of alternating darker/lighter ice observed on the surface of small glaciers resulting from stratification of supraglacial debris in ice.	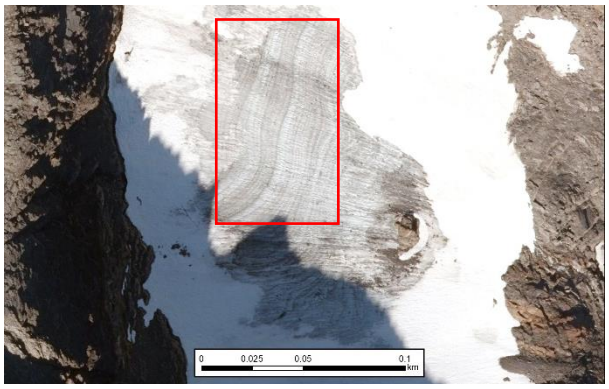
Ice	3	Visible as areas of grey/blue compared to white for nearby snow.	

Bergschrund	2	A crevasse at the head of a glacier or snowpatch adjacent to a rock wall.	
Moraine/s	1	Moraines formed in front of potential glacier units and within the vegetation trimline.	
Unbroken snow accumulation	1	Patches of unbroken white snow appearing convex and/or orientated downslope.	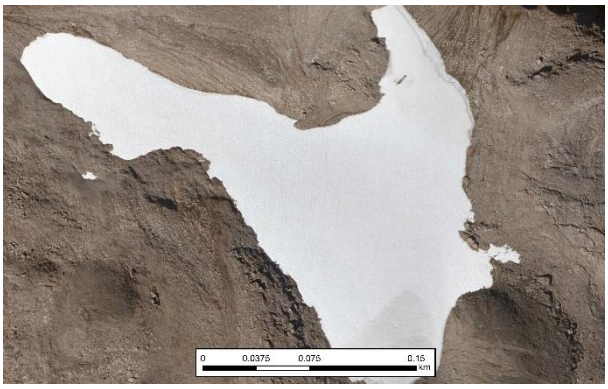

*These features are not visible on coarse (30–15 m) or medium (10 m) resolution imagery

The new scoring system is based upon the examination of each potential glacier unit for specific features; it can be used with a single image but is best when used in conjunction with multiple images from differing years (if available), to confirm that features persist and to allow assessment under different snow cover conditions. This is of particular importance for very small glaciers which can experience ‘accumulation years’ and ‘ablation years’. In the former case snow cover on the ice surface may obscure the ice and any flow features (e.g. deformation of debris banding), thereby giving a different score than if the feature was partially or totally snow free, as it would appear in the latter. Each candidate glacier is scored based on

the features visible on the imagery (Table 3.4) and the resultant total score is used to classify the feature as either a '*certain', 'probable',* or *'possible'* glacier. A total score of 20 'points' is possible depending on the number of specific visible features available. Initially just ice features were included but, on review, inclusion of moraines and snow was considered necessary. Together snow and moraines may reinforce other evidence of glacier presence in helping to inform decisions. Various value systems were tested, but the use of a possible maximum of 20 'points' was considered optimal, as limiting the total score and associated feature values has kept the system simple and efficient.

We recognize four levels of evidence reliability. The clearest evidence of flowing ice is a set of crevasses, or deformation of banding lines and so each of these is awarded 5 points. Un-deformed parallel banding, from stratification of debris-rich versus debris-poor ice, indicates persistence and probably flow and receives 3 points, as does exposed uniform ice. A bergschrund is a single crevasse indicating consolidation or movement away from a headwall, so it does not rate as highly as a set of crevasses and is given 2 points. A moraine indicates that a glacier has been present and may or may not have survived, so it is ancillary evidence and awarded only a single point. Late-summer snow is a normal companion of glacier presence, but this might also be a snowpatch without flowing glacier ice. Snow, therefore, is given a single point. Convexity of a snowpatch has been suggested to indicate a greater likelihood that it hides a glacier (Groom, 1959; Gachev *et al.*, 2016), but under a warming climate many glaciers are downwasting and thinning with a flattening of their surface. Therefore, lack of convexity of a snowpatch does not remove the possibility of buried glacier ice. However, consideration should be made of the incorrect interpretation of snow and associated moraine-like ridges, as it is possible they are periglacial features such as pronival ramparts (Hedding, 2016a, 2016b). Pronival ramparts form at the base of perennial snowpatches and are not glacial in origin (Shakesby, 1997; Hedding and Sumner, 2013; Hedding, 2016a, 2016b). Thus, there is greater uncertainty where only 'snow and moraines' are visible and as such this uncertainty should be noted in any related attributes.

Where a score of 2 to 5 was obtained, the unit should be mapped and classified as only a *possible* glacier and should be marked for review when new imagery is available, or when it can be ground-truthed. A score from 6 to 10 means the unit should be mapped and classified as a *probable* glacier, again marked for future review.

Finally, any unit scoring from 11 to 20 should be mapped as a *certain* glacier. These criteria are relevant irrespective of size. If the unit scores <2, it may be categorised as *snow,* or *perennial snow* if it occurs on multiple images. It can be important to record perennial snowpatches because they contribute not only to the hydrological regime, but can also influence carbon exchange and surface albedo (Zhang, 2005; Woo and Young, 2014; Medeiros *et al.*, 2017; Young *et al.*, 2018). Our approach offers a consistent and easily-applicable system, which should facilitate direct comparison between surveys conducted at different times and/or by different users. Thus, it is hoped that it will improve our ability to identify and monitor very small glaciers.

To test our scoring system, we conducted additional mapping analysis following the criteria laid out in Table 3.4. As a result, there was a considerable reduction in variance between users when mapping glaciers that are classified as *certain* (Table 3.5). Without the scoring system all mapped glaciers are, effectively, classed as *certain,* as there is no scope for classification based on degrees of certainty. Application of the scoring system reduced between-user differences in the total number of glaciers mapped by up to ~80% (Table 3.5). The maximum difference in mean glacier size between users also decreased by ~45% compared to the difference when glaciers were mapped without guidance. However, we note that some variability remains, and this occurs mainly in areas where heavy shading obscures the glacier surface, making it difficult to define surface features, or where remnant snow cover obscures glacier boundaries. Indeed, heavy shading and/or thin debris cover on snow can change its appearance, making it harder to make a definitive classification of snow versus ice. As a result, there is a greater variation in number of *possible* and *probable* glaciers mapped, with some users still mapping more glacier units with these levels of uncertainty. In the case of heavy shading, methods for ‘de-shadowing’ previously employed on multispectral imagery (Richter and Müller, 2005) show potential for use on true colour (RGB) aerial imagery, although these methods still require further research (Shahtahmassebi *et al.*, 2013; Movia *et al.*, 2016). In the case of snow cover, to maximise accuracy, it is important to select images with minimum seasonal snow cover. Even if users are now able to map more glaciers, sub-optimal snow conditions may still lead to uncertainty regarding the exact extent of the glacier area. An example of glaciers that are consistently mapped by all three users, as a direct result of implementing the scoring system, is shown in Figure 3.10. Here, users were able to define glacial boundaries, even in challenging environments, where a high debris

cover possibly obscures a large proportion of glacial ice. In this example (Figure 3.10), all users limited their mapping to the exposed snow/ice, as it is unknown to what extent (if at all) ice exists beneath the debris. Due to this uncertainty in ice content of debris covered areas, extrapolation beyond what is visible should be avoided to minimise uncertainty.

Table 3.5. *Number and area of glacier units digitized from aerial orthophotographs without the scoring system (see also Table 3.3) and after the implementation of the glacier identification scoring system. Showing how the scoring system reduces the number of 'certain' glaciers mapped by each user and greatly increases the consistency between users, although there remains some variability, especially for 'possible' glaciers.*

User	Number of glacier units without the scoring system *area* (km^2)	Number of glacier units with the scoring system *area* (km^2)	Number of 'Certain' glacier units *area* (km^2)	Number of 'Probable' glacier units *area* (km^2)	Number of 'Possible' glacier units *area* (km^2)
1	53 (9.52)	66 (9.67)	40 (8.77)	11 (0.56)	15 (0.34)
2	58 (8.57)	58 (8.57)	45 (8.18)	11 (0.38)	2 (0.01)
3	117 (8.92)	113 (8.88)	36 (7.95)	17 (0.33)	60 (0.61)

A factor that cannot be resolved as a result of image adjustment and/or image acquisition dates is that of extensive/total supraglacial debris cover. In areas where glacial ice is entirely covered by debris, it is simply not possible to accurately define the unit extent and our scoring system is only applicable to debris-free areas (e.g. Figure 3.10). Previous research has shown that mapping the extent of debris covered glaciers can be very difficult, as the debris has very similar characteristics to the surrounding hillslopes from which it was sourced and debris inputs at the margins can make any break in slope between the ice surface and the hillslope difficult to identify (Paul *et al.*, 2013, 2015). Furthermore, debris cover can obscure any ice and/or related flow features used in our classification and remotely sensed data cannot provide information on the internal ice content (Bhambri *et al.*, 2011; Bhardwaj *et al.*, 2014; Lippl *et al.*, 2018). Indeed remote sensing generally fails to provide information about the internal ice content or structure of the unit in these situations, and so in-situ observations would be needed to resolve uncertainty (Whalley *et al.*, 1986; Bosson

and Lambiel, 2016; Capt *et al.*, 2016). Additionally, meltwater streams may be identifiable at the terminus of some debris covered glaciers and may provide an indication of buried glacier ice as opposed to an ice-rock mixture associated with permafrost features (Whalley *et al.*, 1986). The issue of extensive/total debris cover is also relevant to the debate regarding the origin/formation of rock glaciers (Berthling, 2011), whereby similar looking features may have been formed as the result of different geomorphological processes (Martin and Whalley, 1987). Given the additional complexity and large uncertainties associated with mapping extensively debris-covered glaciers from remotely sensed imagery, the use of our new scoring system is restricted to largely non-debris-covered glaciers. However, establishing guidelines for the identification and mapping of largely debris-covered and rock glaciers may be possible in the future, building on work such as Charbonneau and Smith (2018) who used Google Earth imagery to produce an inventory of rock glaciers in the central British Columbia Coast Mountains, Canada.

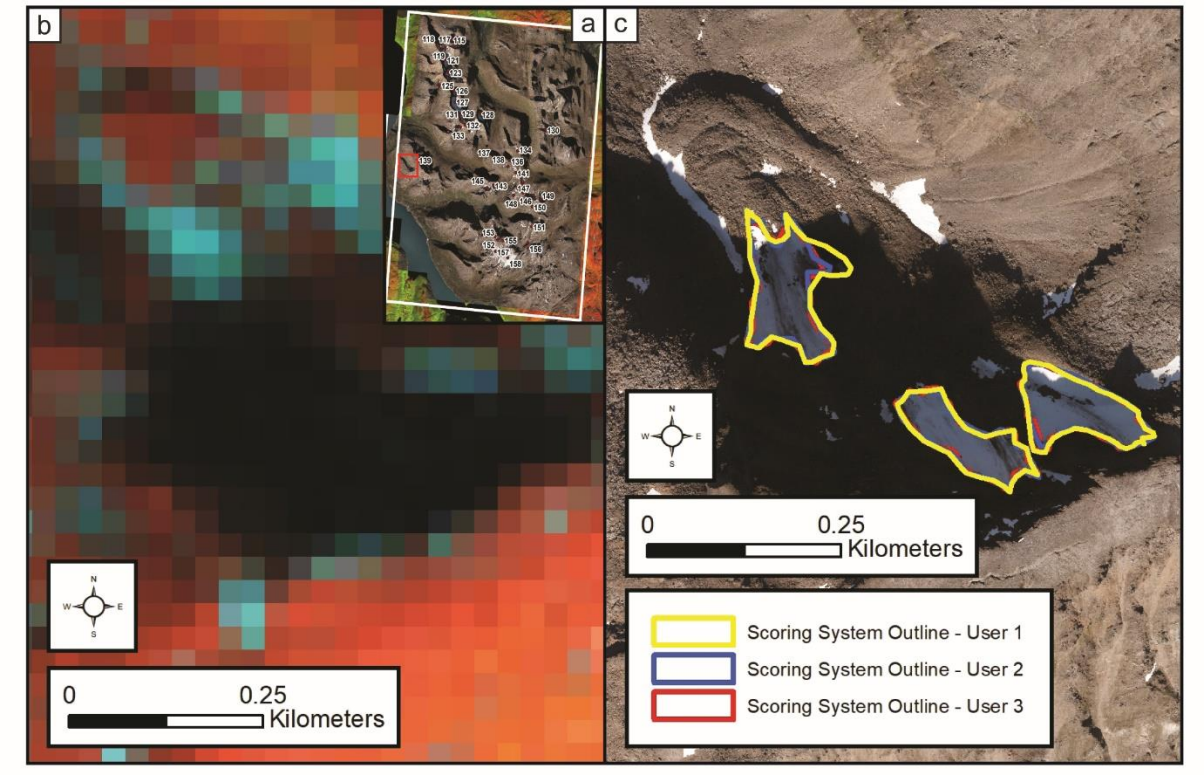

Figure 3.10. *An example of a particularly challenging unit (due to both debris cover and shade) that is only mapped by all three operators when following the scoring system on aerial orthophotographs. (a) Location of the previously unmapped units; (b) Landsat 8 image (30 m resolution, R-G-B as 5-4-3) showing a small area of ice/snow*

as blue yet a large area lies under heavy shadow; (c) natural colour aerial orthophotograph (0.25 m resolution) showing the same area at the same scale, yet the ice/snow unit is easily mapped, even in heavy shadow. Debris surrounding the units means that they are mapped individually, although it is possible they are all connected. This example also shows how user subjectivity still affects scores: as User 1 mapped all units as possible, User 2 mapped all units as certain, and User 3 mapped two as probable and one as possible.

Overall, the system allows users to rank units according to specific features and therefore classify glaciers with degrees of certainty, which increases the information on ice bodies within the study area and provides a more objective, repeatable, and consistent approach. It is however, acknowledged that possible difficulties in acquisition of high-resolution imagery and limitations of time available for inventory production can inhibit mapping of glaciers with exceedingly high levels of detail. In such instances the proposed scoring system may instead be used as a means of validating mapping conducted on satellite imagery, thus providing an objective means of deciding if a unit should or should not be included in a glacier map.

3.7. Conclusions

In this paper we compared how both image resolution and different techniques can influence the mapping of very small glaciers in northern Norway. With 30-15 m pixel resolution imagery, classification errors are prevalent within all methods. It is often not possible to define specific surface features indicative of glacier formation on individual snow/ice units <0.01 km^2. This supports previous work (e.g. Paul *et al.*, 2010) recommending a minimum size-threshold of 0.01 km^2 on imagery of medium to coarse resolution. With increasing image resolution, errors can be mitigated with thorough and systematic assessment of individually mapped units (e.g. reviewing potential glacier units for specific glacial features or manually editing areas erroneously mapped). At 10 m pixel resolution, it is possible to define some individual features characteristic of glaciers, such as crevasses and small terminal moraines. Nonetheless, a minimum size-threshold of 0.01 km^2 is advisable, as it is not possible to identify detailed features on smaller units. On imagery with pixel resolution <1 m, ice/snow units of all sizes can more easily be distinguished even in heavy shading. In this paper, multiple operators were able to map glaciers smaller than 0.01 km^2 on aerial orthophotographs (0.25 m), indicating that a minimum size is inappropriate on high-resolution imagery. However, there are few published guidelines for identifying glaciers on high-resolution imagery. As a result, we have developed a new scoring system that classifies very small glaciers as *certain*, *probable* or *possible*. This is based on detailed ice surface structures (e.g. evidence of flow banding and crevasses) and diagnostic glacial landforms, such as moraines (Table 3.4). This scoring system provides a useful framework to increase the objective mapping of very small glaciers and reduce uncertainties in the next generation of glacier inventories using high-resolution imagery.

3.8. Acknowledgements

Landsat 8 OLI and Sentinel-2A imagery were downloaded free of charge from the USGS Earth Explorer website (https://earthexplorer.usgs.gov) and aerial orthophotographs were kindly provided by the Norwegian Mapping Authority. Prior glacier data as collated by the CryoClim project were also used including glacier outlines downloaded from the NVE website (www.nve.no/hydrology/glaciers/glacier-data). This work will also act as a contribution to the project Copernicus bretjeneste (Copernicus Glacier Service Norway, Contract NIT.06.15.5). We are grateful for the encouraging comments from the late Graham Cogley during the inception of this manuscript. Finally, we thank the Editor (Christoph Schneider) and the diligent reviews provided by Mauro Fischer and an anonymous reviewer.

CHAPTER 4

Timing of 'Little Ice Age' maxima and subsequent glacier retreat in northern Troms and western Finnmark, northern Norway

Leigh J.R.[1], Stokes C.R.[1], Evans D.J.A.[1], Carr J.R.[2], Andreassen L.M.[3]

[1]Department of Geography, Durham University, Durham, UK; [2]School of Geography, Politics and Sociology, Newcastle University, Newcastle upon Tyne, UK; [3]Norwegian Water Resources and Energy Directorate (NVE), Oslo, Norway

Looking north-east from the cirque threshold of glacier 123, down Sorbmevággi and into the main Rotsund Valley.

Photograph date: 13th September 2018 (by J.R. Leigh)

A version of this chapter has been published as:

Leigh, J.R., Stokes, C.R., Evans, D.J.A., Carr, R.J. and Andreassen, L.M., 2020. Timing of Little Ice Age maxima and subsequent glacier retreat in northern Troms and western Finnmark, northern Norway. *Arctic, Antarctic, and Alpine Research*, **52**(1), 281-311.

“Drip, drip, drop, bit by bit
It's the dulcet sound of the glacial melt. . .
They're living in denial (of science!)”
(Reynolds, 2015a)

4.1. Abstract

Glaciers are important indicators of climate change and recent observations worldwide document increasing rates of mountain glacier recession. Here we present ~200 years of change in mountain glacier extent in northern Troms and western Finnmark, northern Norway. This was achieved through: (1) mapping and lichenometric dating of major moraine systems within a sub-set of the main study area (the Rotsund Valley) and (2) mapping recent (post-1980s) changes in ice extent from remotely sensed data. Lichenometric dating reveals that the Little Ice Age (LIA) maximum occurred ~1814 (±41 years), which is before the early-20th century LIA maximum proposed on the nearby Lyngen Peninsula, but younger than LIA maximum limits in southern and central Norway (mid-18th century). Between LIA maximum and 1989, a small sample of measured glaciers (n = 15) shrank a total of 3.9 km^2 (39%), and those that shrank by >50% are fronted by proglacial lakes. Between 1989 and 2018, the total area of glaciers within the study area (n = 219 in 1989) shrank by ~35 km^2. Very small glaciers (<0.5 km^2) show the highest relative rates of shrinkage, and 90% of mapped glaciers within the study area were <0.5 km^2 in 2018.

4.2. Introduction

The most recent period of Holocene glacier expansion is termed the 'Little Ice Age' (Grove, 2001, 2004b). Initiating around 1300, the LIA triggered a global, yet asynchronous, advance of glaciers (Solomina *et al.*, 2016). In many regions the turn of the 20th century, however, marked the end of the LIA with glaciers having entered a period of sustained retreat, interrupted by only minor, localised glacier advances (Overpeck *et al.*, 1997; Grove, 2004b; Winkler *et al.*, 2009). The observed glacial retreat since the LIA has been linked to the anthropogenically-forced warming during the 20th and early-21st centuries (IPCC, 2019). With these trends set to continue, climate warming is likely to be greatly amplified in Arctic regions (Serreze and Barry, 2011). This 'Arctic amplification' is expected to increase mean annual air temperatures within the Arctic Circle by between 4.2°C and 8.3°C (Najafi *et al.*, 2013; IPCC, 2019). There is, therefore, increasing concern about the response of Arctic ice and snow to anthropogenically-forced climate change.

In Norway, 2,534 glaciers cover an area of ~2,692 km^2 (Andreassen *et al.*, 2012a), with an estimated volume of 271 ±28 km^3 (Andreassen *et al.*, 2015), which if melted completely would contribute an estimated ~0.34 mm of sea level rise (Nesje *et al.*, 2008). There is also substantial importance of Norwegian glaciers in relation to energy supply, environmental hazards, and tourism (Andreassen *et al.*, 2012a; Furunes and Mykletun, 2012; Jackson and Ragulina, 2014; Xu *et al.*, 2015). Furthermore, Norwegian glaciers are particularly sensitive to climate fluctuations due to their maritime location, with their mass balance heavily influenced by large-scale atmospheric circulation patterns such as AO and NAO (Nesje *et al.*, 2000b; Thompson and Wallace, 2000; Rasmussen, 2007; Nesje and Matthews, 2011; Bonan *et al.*, 2019). Norway is, therefore, a prime location to study the response of glaciers to climate change~~,~~ but there remain several glacierised regions in Norway, that lack detailed investigation (Stokes *et al.*, 2018). In particular the mapping and dating of LIA glacier extent and subsequent retreat has only been done for a small number of glaciers and glacier regions in Norway (e.g. Ballantyne, 1990; Bickerton and Matthews, 1993; Winkler, 2003; Matthews, 2005; Nussbaumer *et al.*, 2011; Weber *et al.*, 2019), and most of the small glacierised sites within Troms and Finnmark county lack investigation as to their LIA limits. As such, it is unclear when glaciers reached

their LIA maximum in this region and how rates of glacial change have varied after this maximum.

In this paper we: (a) compile detailed geomorphological maps and conduct fieldwork to identify and date LIA moraines (using lichenometry); (b) compare glacier area changes from historical maps and previous glacier inventories, dating from 1907 to 1966; (c) undertake new analysis of satellite imagery (30-15 m spatial resolution) and aerial orthophotographs (<1 m spatial resolution), to map glacier area change over the period 1989 to 2018.

4.3. Study area

The area of investigation is in northern Norway and covers ~9,600 km^2. It is located in central Troms and Finnmark (predominantly in the northern margins of the former Troms County, and includes the Bergsfjord Peninsula of the former Finnmark county; Figure 4.1). The study region is characterised by a range of different glacier sizes; in the north-east on the Bergsfjord Peninsula (region C; Figure 4.1), ice caps and outlet glaciers dominate, while in the mountain belts throughout the central and western regions (region A and B; Figure 4.1), valley and cirque glaciers dominate. Due to the close proximity of large fjord systems and the North Atlantic Ocean, the majority of glaciers in the region are maritime, with relatively high precipitation during the winter and a smaller difference between winter and summer temperature averages than are experienced at similar latitudes inland (Andreassen *et al.*, 2012b). For example, between 1995 and 2018 the January and July mean temperature and total precipitation in the maritime setting of Tromsø (69°39 N, 18°56 E) were -3.1°C / 2,344 mm and 12.3°C / 1,788 mm, respectively. In contrast, the continental climate at Finnmarksvidda (69°22 N, 24°26 E; station no. 97350) has a January and July mean temperature and total precipitation of –13.6°C / 4,55 mm and 13.4°C / 1,728 mm, respectively (data from www.eklima.no). The 'Inventory of Norwegian Glaciers', (henceforth referred to as Andreassen *et al.*, 2012a) defines our study area as "Region 3 - Troms North" (Andreassen *et al.*, 2012a, p. 71) and "Region 2 - Øksfjord" (Andreassen *et al.*, 2012a, p. 71). The glacier inventory covering these two regions is based on Landsat imagery from 2001 and 2006. In total Andreassen et al. (2012a) record 141 glaciers across both regions and provides details on their area, elevation (minimum and maximum), slope, and aspect. The glaciers range in size from 0.01 km^2 to 11.95 km^2. Only ~10% of the glaciers in this region are >1 km^2 in area, but they account for ~67% of the total glacier area; while ~82% of glaciers are <0.5 km^2, but account for only ~23% of the total glacierised area (all values from Andreassen *et al.*, 2012a).

Nearly all prior glaciological research within the broad study area (Figure 4.1) has focused on the ice caps and outlet glaciers of the Bergsfjord Peninsula (region C; Figure 4.1). Data from the Bergsfjord Peninsula as a whole found highly non-linear responses of local plateau-based icefields to climate changes during the YD and throughout the Holocene (Gellatly *et al.*, 1988; Evans *et al.*, 2002; Rea and Evans,

2007). Of particular interest is the Langfjordjøkelen ice cap, where annual mass-balance records are available from 1989. The Langfjordjøkelen mass-balance records reveal mass deficits throughout the period of observation and higher glacier retreat rates compared to elsewhere in Norway (Andreassen *et al.*, 2012b, 2020; Giesen *et al.*, 2014; Wittmeier *et al.*, 2015; Kjøllmoen, 2019).

To address the lack of data on LIA limits in northern Troms, we identified a suitable field site in the Rotsund Valley in the Nordreisa municipality (Figure 4.1). The field site hosts very well-developed moraines fronting several small glaciers within part of a minor mountain range (colloquially referred to as the Kåfjord Alps), with mountain peaks ranging from 1,077 m a.s.l. to 1,320 m a.s.l. The bedrock is composed of Vaddas Nappe and Kåfjord Nappe, broadly comprising metamorphic units of amphibolite, quartzite, gneiss, and schist (Lindahl *et al.*, 2005; Augland *et al.*, 2014; Geological Survey of Norway, 2015). To the west is a major fjord system, Lyngenfjord, and there are also subsidiary fjords north (Rotsundet) and south (Kåfjorden; Figure 4.1). The present-day tree line extends to ~400 m a.s.l. and, above this, alpine tundra is the dominant vegetation. The nearest weather station is at Sørkjosen Airport, ~11 km north-east from the field site (SA; Figure 4.1) and has been operational since 2008 (station number 91740: www.eKlima.no). Average monthly temperature typically varies from -10 to 15°C and precipitation primarily falls as snow between October and May, while rainfall can occur throughout the year (Vikhamar-Schuler *et al.*, 2010).

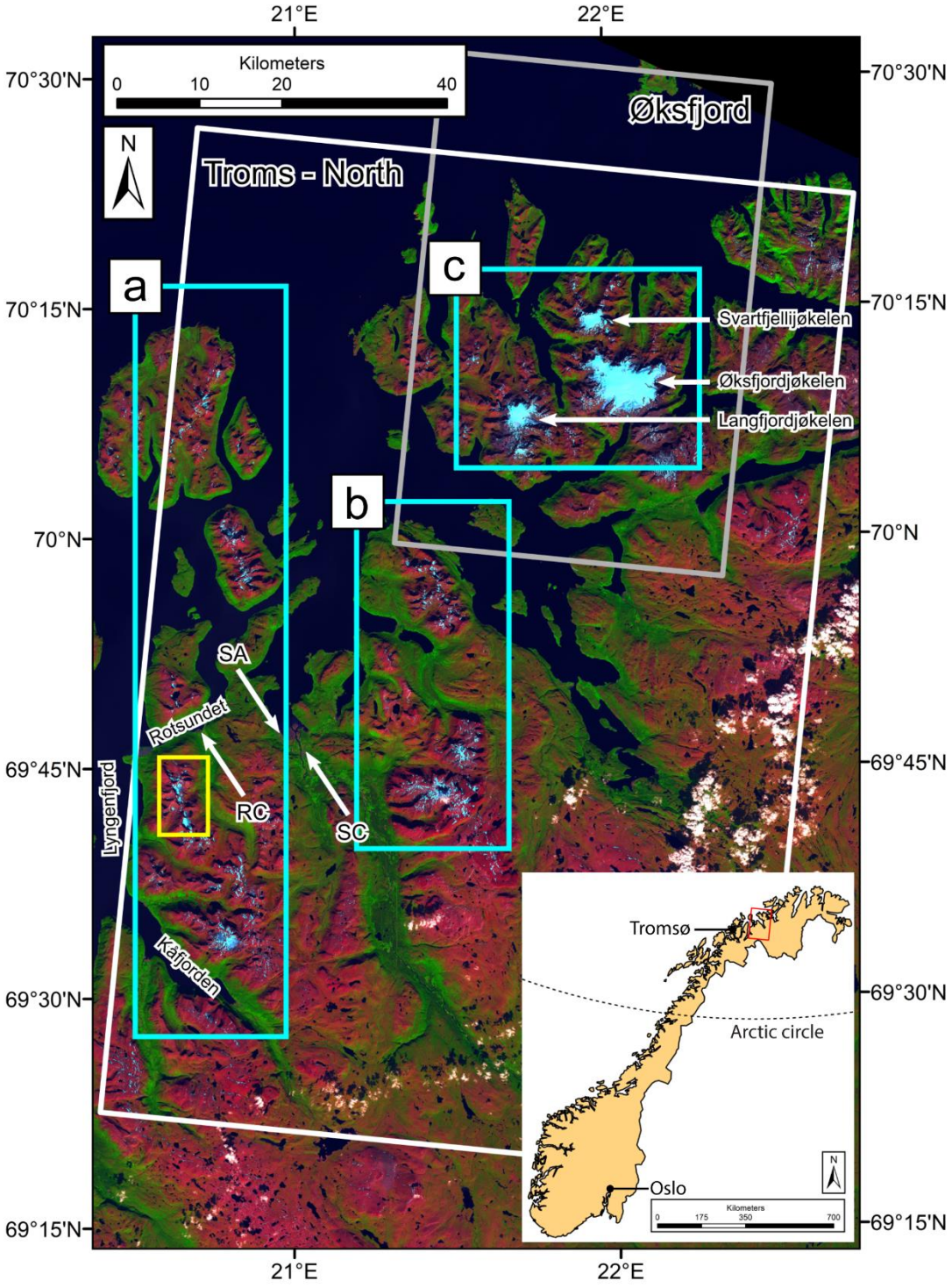

Figure 4.1. *Study area location in Troms and Finnmark county, northern Norway. The white rectangle represents the area under investigation, defined as "Region 3 - Troms North" while the grey rectangle shows "Region 2 - Øksfjord"* (Andreassen *et al.*, 2012a, p. 71)*. Turquoise rectangles indicate the three glacial regions, defined as A, B, and C (the Bergsfjord Peninsula). The yellow rectangle shows the location of the field site within the Rotsund Valley. The location of the Rotsundelv churchyard (RC) and*

Storslett churchyard (SC) used for lichenometric dating controls are highlighted along with the location of the weather station at Sørkjosen Airport (SA). Note: the base image is a 2018 pan-sharpened Landsat 8 scene displayed as a false colour composite; R-G-B as 5-4-3.

The four glaciers under investigation in the Rotsund Valley (glacier ID 115, 117, 121, and 123; Figure 4.2) are located below 1,100 m a.s.l. As of 2018 the smallest glacier is glacier 115, with an area of 0.07 km^2 terminating ~760 m a.s.l. Glacier 115 is also the only glacier in the field site with a proglacial lake (0.3 km^2 and <200 m from the terminus; Figure 4.2b). The largest glacier is glacier 121 with an area of 0.8 km^2, terminating at ~650 m a.s.l (Figure 4.2d). The other two glaciers 117 and 123 have areas of 0.11 and 0.3 km^2 and terminate ~730 and ~600 m a.s.l., respectively (Figure 4.2c, e). Within the forelands of glaciers 115, 117, 121, and 123 moraines occur as both individual features and as multiple ridges forming part of larger moraine systems. Throughout the area, distinct moraines are intermixed with areas of glacifluvial sediments and discrete debris accumulations (DDAs) (*sensu* Whalley, 2009, 2012), exhibiting complex (hummocky) ridge features, and in the recently deglaciated terrain the moraines often border areas of till. The glacial forelands are sparsely vegetated, and the moraines surveyed are unobscured by trees or shrubs. The forelands of all four glaciers were surveyed in the field in August-September 2018, enabling the ground truthing of remotely sensed maps alongside lichenometric dating of moraines.

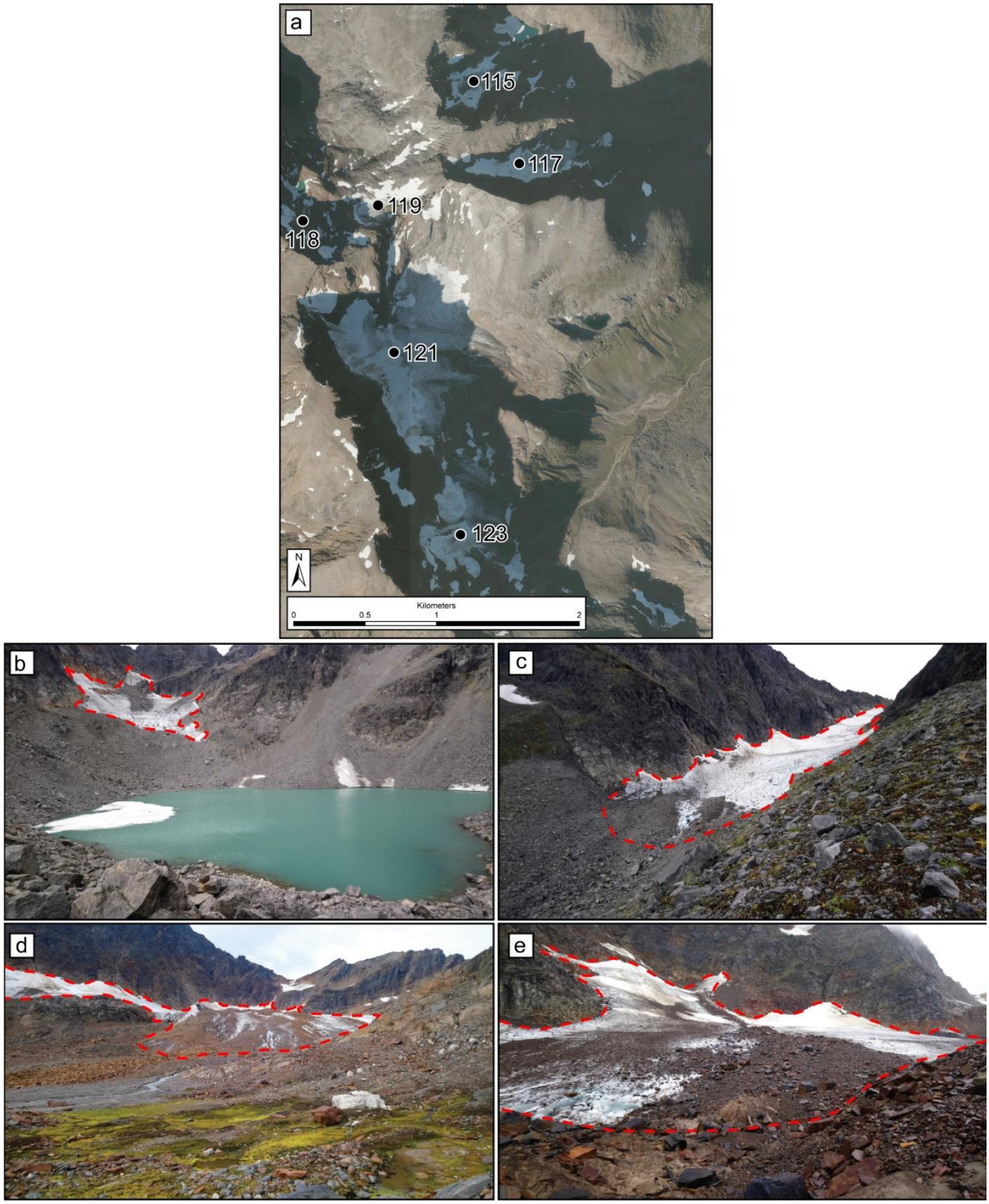

Figure 4.2. (a) *Aerial orthophotographs of the Rotsund Valley field site (2016; www.norgeibilder.no) and photographs of the four glaciers visited in the field; (b) 115, (c) 117, (d) 121, (e) 123. The dashed red line denotes the 2018 glacier extent.*

4.4. Datasets and methods

4.4.1. Geomorphological mapping

Geomorphological mapping of the Rotsund Valley field site (yellow rectangle in Figure 4.1) was conducted using georectified orthophotographs from www.norgeibilder.no at 0.25 m resolution, from 2011 and 2016 (courtesy of the The Norwegian Mapping Authority). Using photographs from different time steps allowed for identification of features under different snow conditions and/or shading. Some late lying snow was present in the imagery at time of capture (16.09.2016) however, this was removed in the maps based on the mapping done in the field and through cross checking on imagery from differing time steps.

The geomorphological map was constructed using a three-stage process: draft maps were digitised from analysis of orthophotographs, which were ground checked in the field, and a final stage of remotely sensed mapping then synthesised all three stages (Chandler *et al.*, 2018). The resulting map (Figure 4.3) was used to reconstruct past glacier extent in the Rotsund Valley, in combination with the lichenometric dating of the moraines. In total, 26 different features were mapped and broadly classified as 'landforms' (e.g. moraine ridges, flutings, pronival ramparts) or 'surficial materials' (e.g. glacier, glaciofluvial sediments, talus) following methods employed for the mapping of Icelandic glaciated landsystems (e.g. Evans *et al.*, 2017b, 2017a, 2019b).

The LIA moraines were initially identified based on their morphostratigraphy (large, sharp-crested, little evidence of slumping and/or reworking), together with a pronounced vegetation trimline. While not vegetation free, the vegetation on these moraines is predominantly scrub vegetation with sporadic larger pioneer species. Whereas moraines further down valley are fully vegetated with grasses, shrubs, and trees. Moraines dated by lichenometry, are labelled from M1 (oldest/furthest from glacier front) to M8 (youngest/closest to glacier front).

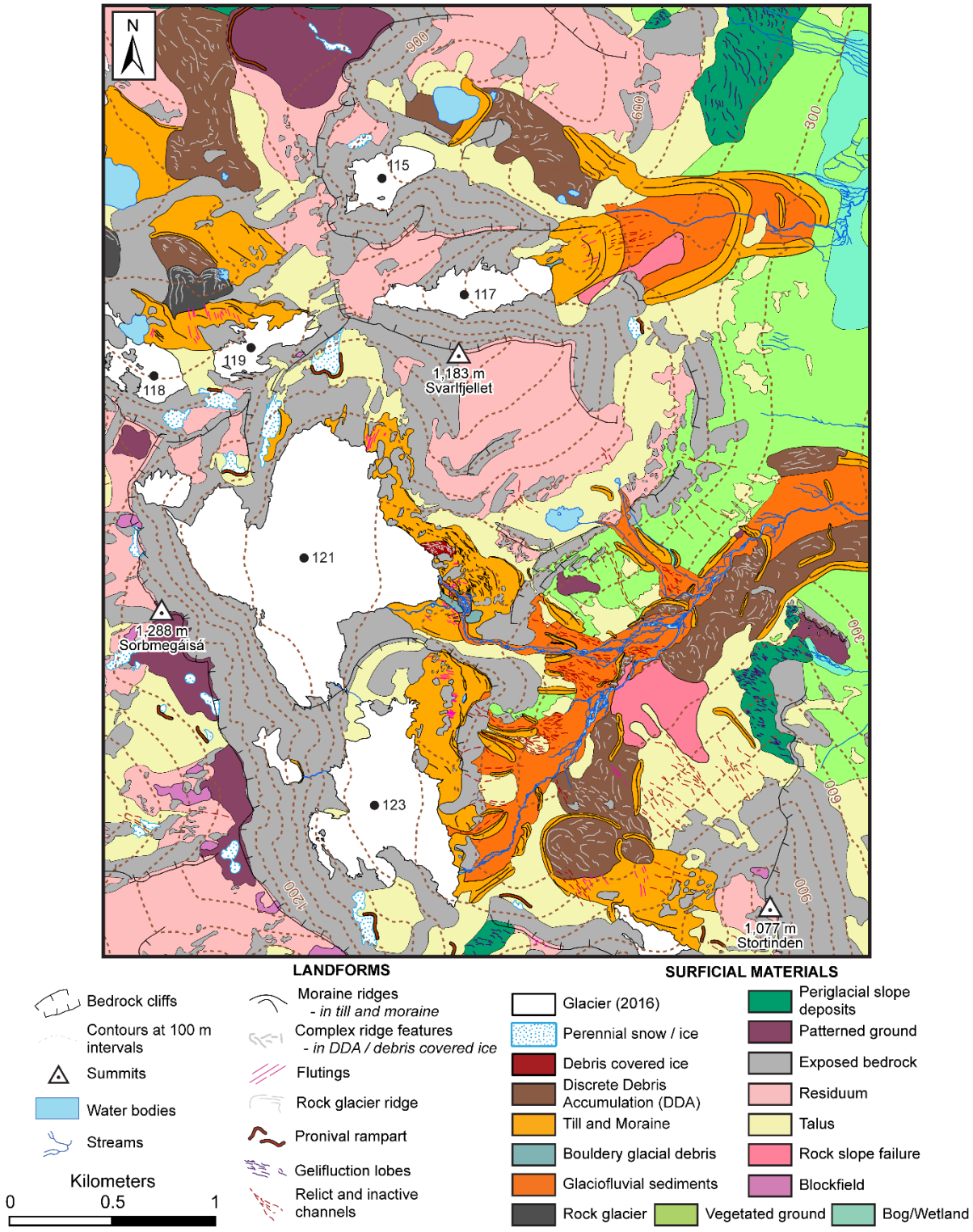

Figure 4.3. *Geomorphological and superficial geological map of the field site within the Rotsund Valley (location shown in Figure 4.1) showing glaciers (ID): 115, 117, 118, 119, 121, and 123. Map based on field mapping and aerial orthophotographs with 0.25 m spatial resolution (image date: 24.08.2016).*

4.4.2. Lichenometry

Lichen size data were collected from moraines within the forelands of glaciers 115, 117, 121, and 123 (see Figure 4.2 and 4.3). Lichenometric measurements were constrained to the yellow-green *Rhizocarpon* lichen (Bickerton and Matthews, 1993; Winkler, 2003; Armstrong, 2011). The diameter of the longest axis of each lichen thalli was measured using a flexible tape to the nearest millimetre (Innes, 1986). Spherical and non-spherical lichens were measured to account for the decrease in the proportion of lichens that have remained circular with time, while any lichens coalesced (fused) over time were avoided (Innes, 1985, 1986; Harrison *et al.*, 2006). We identified coalescence in lichens by presence of a visible black streak of lichen prothallus dividing the specimen (Bradwell, 2010). To mitigate potential biases of incorporating anomalous lichen in our data analysis, any single lichen ≥20% larger than the next largest lichen was removed from the dataset, as is standard practise within lichenometry (Calkin and Ellis, 1980; Loso and Doak, 2006; Solomina *et al.*, 2010; Loso *et al.*, 2014; Pendleton *et al.*, 2017).

Our dating was conducted by indirect lichenometry, which utilises the correlation of lichen sizes on surfaces of unknown age with those on surfaces of known age (Beschel, 1950). Indirect lichenometry provides calculated surface ages that are obtained with the use of calibrated dating curves (Matthews, 2005). Initial construction of dating curves relies on the presence of lichen growing on surfaces of known age, such as headstones, buildings, and independently dated natural surfaces such as boulders on moraines of known age (e.g. Jomelli *et al.*, 2008; Wiles *et al.*, 2010). Within the field site there are no surfaces that can be independently dated, therefore, headstones in nearby churchyards were used as controls. The churchyards are in the villages of Rotsundelv (RC; Figure 4.1) and Storslett (SC; Figure 4.1), approximately 6 km north and 14 km north-east from the field site, respectively. On each headstone, all lichen were measured from both horizontal and vertical faces. It was noted that some headstones recorded the burial of multiple persons at different times and, when reviewing the data, it was clear these headstones carried anomalously smaller lichen relative to the oldest burial date. We therefore infer that the headstone had been cleaned before the new inscription was added and, in these instances, the younger date was used as the control age.

At the field site, lichen size data were collected from siliceous rocks on moraines. Where possible, each moraine was searched for the largest lichen on the distal slope, crest, and proximal slope, thereby mitigating against the influence of micro-environmental variations (Erikstad and Sollid, 1986; Karlén and Black, 2002; Leigh, 2016). On the large, steep-sided, latero-frontal moraines (sometimes in excess of 10 m high) only the crests were searched, due to issues associated with vertical age gradients on these large features (Humlum, 1978). Once a dataset of the largest lichens from the entirety of the moraine had been collected, the mean of the Five Largest Lichen (5LL) was used for analysis (Innes, 1984b; Jomelli *et al.*, 2007; Roof and Werner, 2011). Recent work has also revealed that the 5LL method is not demonstrably inferior to other methods (notably size frequency methods) which require larger lichen-size data sets (Evans *et al.*, 2019a), and in turn require considerably longer periods of time for data collection (which is not always feasible). Overall, implementing the 5LL method provides the greatest comparability to other studies using lichenometric dating throughout Norway and other Arctic regions (Karlén, 1979; Evans *et al.*, 1994; Winkler, 2003; Bakke *et al.*, 2005a; Jansen *et al.*, 2016).

4.4.3. LIA glacier area and length reconstructions

Our LIA reconstructions were based on lichenometric dating and both remotely sensed and field-based moraine mapping. Initially, LIA glacier area reconstructions were made for the four glacier forelands surveyed in the field (glacier 115, 117, 121, and 123). To enable further comparisons of LIA glacier extent, extrapolation of field observations and lichenometric dating was made for 11 other valley/cirque glaciers within the same mountain belt (region A; Figure 4.1). No dating of moraine limits was made for the additional glaciers and therefore, to maintain a reasonable level of comparability, only those glacier forelands with well-defined moraines of similar visual form to those examined in the field (e.g. position down valley from present day glacier, within a marked vegetation trimline) were mapped (Baumann *et al.*, 2009).

To map LIA glacier area, we extrapolated more recent glacier outlines from the 1950s to fit our mapped LIA moraine limits. Following established methods, the oldest glacier outlines (i.e. those digitised from topographical maps or from remote sensing) were extrapolated to the moraine limits in the lower parts of the glacier, following the

extent of lateral moraines or vegetation trimlines (Baumann *et al.*, 2009; Stokes *et al.*, 2018). The extrapolation of glacier polygons for LIA area also involved the re-connection of fragmented ice bodies. For glacier reconstructions where no prior outlines were present (n = 7 glaciers) we instead extrapolated from our 1989, remotely sensed outlines to meet the LIA moraine limits. The Andreassen et al. (2012a) ice divides were also used to ensure individual tributaries were mapped as individual glacier units. Furthermore, for all glaciers where LIA glacier reconstructions were mapped, we also recorded if a proglacial lake was now present within the boundary of the LIA moraine. Finally, to map glacier length we used published glacier centrelines (Winsvold *et al.*, 2014) and either extrapolated or trimmed them to match our glacier outlines. For many of the smaller glaciers included in our study no prior glacier centrelines were available therefore, these were created by manual digitisation perpendicular to contours generated from the Norwegian Mapping Authority N50 Digital Terrain Map (https://kartkatalog.geonorge.no/metadata/e25d0104-0858-4d06-bba8-d154514c11d2).

4.4.4. Remote sensing of 20th-21st century glacier extent

Firstly, glacier outlines from historic 1:100,000 and 1:50,000 topographic maps were provided by the Norwegian Water Resources and Energy Directorate (https://www.nve.no/hydrology/glaciers/glacier-data/, 2016). The glacier outlines (e.g. Figure 4.4) were compiled by Winsvold et al. (2014) and dated to 1907, 1952, 1954, 1955, and 1966. Secondly, new glacier outlines were created for this study using Landsat 5 TM, 7 ETM+, and 8 OLI imagery (courtesy of the U.S. Geological Survey; https://earthexplorer.usgs.gov/) from 1989 to 2018 at roughly five-year time steps, enabling intra-decadal analysis. However, due to challenges obtaining suitable imagery in maritime northern Norway, it was not always possible to maintain equally spaced time steps (Andreassen *et al.*, 2008; Leigh *et al.*, 2019).

Glacier change mapping utilised a well-established semi-automated technique, whereby a band ratio image was developed from the raw multispectral imagery (e.g. TM band 3 / TM band 5 on Landsat 5) and subsequently converted to a binary image (Andreassen *et al.*, 2012a). Adding an additional threshold (e.g. Band 1) is sometimes used, however, in our preliminary mapping it was not shown to provide marked improvements and was not used. Once the band ratio image was produced we then

selected a threshold value to isolate glaciers from non-glaciers, which was visually optimised for each scene by comparing the binary image with a false colour composite (bands 5-4-3 as Red-Green-Blue) of the multispectral imagery (Raup *et al.*, 2007; Racoviteanu *et al.*, 2009; Paul *et al.*, 2013). A median filter (3 × 3 kernel) was then applied to help reduce noise from isolated pixels outside the glaciers and to close small voids within the glaciers (Andreassen *et al.*, 2012a). Finally, once initial glacier outlines had been generated, manual correction of mapped units was undertaken, to account for glaciers cast under shadow and/or debris cover, terminating in proglacial lakes, surrounded by late lying snow, or where lakes/snow patches were erroneously classified as glaciers (Raup *et al.*, 2007; Andreassen *et al.*, 2012a). To ensure accuracy in mapping, especially around areas of shade, each image was viewed using multiple band combinations of Red-Green-Blue as 5-4-3, 4-3-2, and 3-2-1. Additionally, all units mapped on the 1989 satellite imagery, including those which were not included within Andreassen et al. (2012a), were cross-checked on freely available aerial imagery from varying time-steps to validate their identification as glaciers (https://www.norgeibilder.no/). When cross-checking the imagery we assessed the presence of visual indicators of glaciers (crevasses, flow features and deformed stratification, multiple debris bands in ice, ice, bergschrunds, moraines, and unbroken snow accumulation) to categorise each potential glacier unit as a *possible, probable,* or *certain* glacier, following the glacier identification scoring system of Leigh et al. (2019). All units that were considered to score two or more were retained and classified accordingly (11-20 = *certain* glacier; 6-10 = *probable* glacier; 2-5 = *possible* glacier), while any units scoring less than two (e.g. snow/perennial snow) were removed.

Due to the relatively coarse (30-15 m) resolution of Landsat imagery and the associated errors of glacier mapping at this resolution, a minimum size-threshold of 0.01 km^2 was implemented (Paul *et al.*, 2010; Leigh *et al.*, 2019). Therefore, all units <0.01 km^2 on the 1989 imagery were omitted from our maps due to difficulty in differentiating them from a perennial snowpatch. If an individual glacier fragmented over time and any individual unit shrank below 0.01 km^2, it was no-longer mapped. We acknowledge that a glacier unit below our size-threshold does not mean the glacier has disappeared.

In addition to the satellite imagery, a series of historical oblique aerial photographs of the Rotsund Valley field site were used to provide context for glacier

mapping. The oblique photographs aided in the identification of glacier extent, enabled confirmation of glacier confluence, and helped in differentiating snow from ice. The photographs were taken in 1952, by the airline company Wilderøe's Flyveselskap and offer an oblique view south-west into the Rotsund Valley.

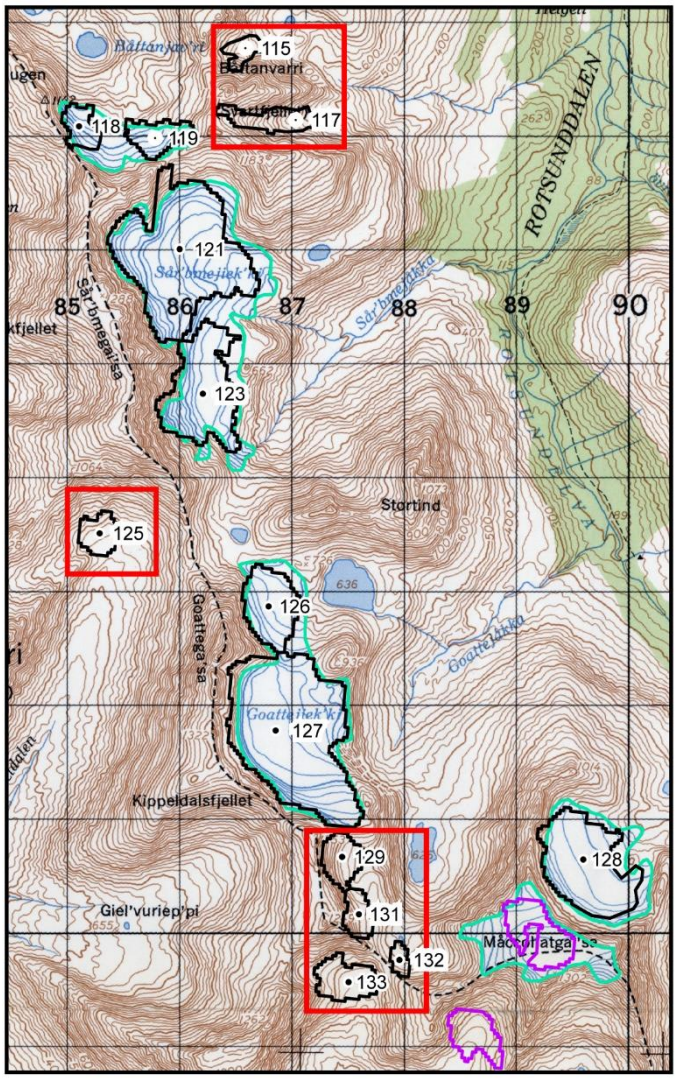

Figure 4.4. *Part of a Norwegian Mapping Authority 1:50,000 topographic map (map sheet: 1634 II) showing the digitised, 1953 glacier outlines (turquoise) in the Rotsund Valley (yellow box - Figure 4.1). The 2001 Andreassen et al. (2012a) glacier outlines (black) are overlaid, with IDs shown. The red boxes highlight seven glaciers in this area that were not included on the 1953 topographic map. The two purple outlines are snow patches mapped in the Andreassen et al. (2012a), one of which was initially mapped as a glacier on the 1953 map. Glaciers 115, 117, 121, and 123 are seen in Figure 4.3. Note: grid squares are 1x1 km.*

4.4.5. Errors and uncertainty in glacier mapping and reconstructions

It is difficult to assess accuracy of the glaciers digitised from the 1:100,000 and 1:50,000 topographic maps, due to the undocumented methods used to map glaciers from the aerial photographs on which the topographic maps are based. Given that we use the same series of historical maps as those of Stokes et al. (2018), error estimates of the mapped glaciers are considered in-line with their estimate of ±5%. It should, however, be noted that throughout the study region, ~20% of glaciers we have mapped were not included on the historic topographic maps (e.g. Figure 4.4).

Potential error associated with glacier mapping from satellite imagery relates not only to the extent in which a glacier's boundaries can be identified and the accuracy of digitisation (both of which are influenced with image resolution), but also issues with georectification. Imagery was checked for georeferencing errors and any imagery that did not align was not used for mapping purposes. It should also be noted that identification of glacier boundaries is also influenced by external factors such as intensity of shading, snow cover, and supraglacial debris (Paul *et al.*, 2013; Winsvold *et al.*, 2014; Leigh *et al.*, 2019). To assess the uncertainty from our semi-automated mapping, we used manually mapped glacier outlines from very high-resolution aerial orthophotographs (2016, 0.25 m resolution) as a benchmark from which we evaluated our glacier outlines from Landsat 8 and pan-sharpened Landsat 8 imagery (2016, 30 and 15 m resolution, respectively). Aerial imagery was used as a benchmark due to its very high resolution and accuracy of georectification compared to Landsat, meaning we were able to define glacier boundaries most accurately, even in areas of heavy shading. The mapping comparison was conducted for a subset of 22 glacier outlines, ~10% of the total number of glaciers mapped on the 1989 imagery (the first mapping time step). Mean percentage difference in glacier area between Landsat 8 imagery (30 m) and aerial orthophotographs (0.25 m) was ±9% and the mean percentage difference was ±6% between pan-sharpened Landsat 8 imagery (15 m) and aerial orthophotographs (0.25 m).

Estimates of error for the LIA areal extent based on our moraine mapping and dating are subject to uncertainties (in terms of both moraine ages and extrapolation of glacier area) which are difficult to quantify. The errors associated with LIA extrapolation are also a factor of moraine identification and preservation; where well-defined intact moraines are present it is easier to map glacier limits. In the case of our

moraine mapping, we restricted the reconstructions to glacier forelands where well-defined end/latero-frontal moraines were identifiable on aerial imagery (e.g. Figure 4.5).

4.4.6. Climate Data

There are no continuous, long-term meteorological records from within the study area. The nearest long-term record is from the city of Tromsø, located ~60-150 km to the west. Climate data were freely accessed via the Norwegian Meteorological Institute (www.eklima.no). In Tromsø, records are combined from station #90440 (located at: 69°39'07.2"N / 18°57'00.0"E / 40 m a.s.l.) and station #90450 (located at: 69° 39' 15.1" N / 18° 56' 12.8" E / 100 m a.s.l.) to gain a continuous record of temperature and precipitation from 1874 to 2018. Station #90440 was shut down in December 1926 while station #90450 was setup in July 1920, providing a period of overlap from which the older data can be homogenised. Following the approach of Andreassen et al. (2012b) and Stokes et al. (2018), the mean of the difference between overlapping months was used to adjust the data prior to 1920. The homogenised temperature data were used to plot mean annual and seasonal temperature alongside total annual and seasonal precipitation, and then also to calculate decadal means. Summer is defined as June-September and winter as October-May (Andreassen *et al.*, 2012b; Stokes *et al.*, 2018).

4.5. Results

4.5.1. Dating moraines within the Rotsund Valley

Within the four surveyed forelands of the Rotsund Valley there were prominent glacial landforms that record a complex glacial history (Figure 4.3). Presumed LIA maximum moraines (termed M1 moraines throughout; see Section 4.4.1.), were found between ~340 and ~690 m a.s.l. and, at the lower elevation, they coincide with a pronounced vegetation trimline (Figure 4.5). Outside of the M1 moraines there are a series of large and well vegetated moraines, sometimes extending down into the treeline and up to ~2 km from the present-day glacier termini.

The forelands outside the M1 moraines lack tree cover but are often covered by an extensive mat of mountain crowberry (*Empetrum nigrum*), bilberry (genus *Vaccinium*), and various mosses (e.g. *Racomitrium canescens* and *Polytrichum juniperinum*), with dispersed yet well-established dwarf-Birch (*Betula nana)*. Within the M1 moraines, where present, vegetation is predominantly grasses and small shrubs. When moving up valley (from the M1 moraines) vegetation becomes sparse and once inside the M3 moraine, vegetation is almost non-existent except for mosses and lichens.

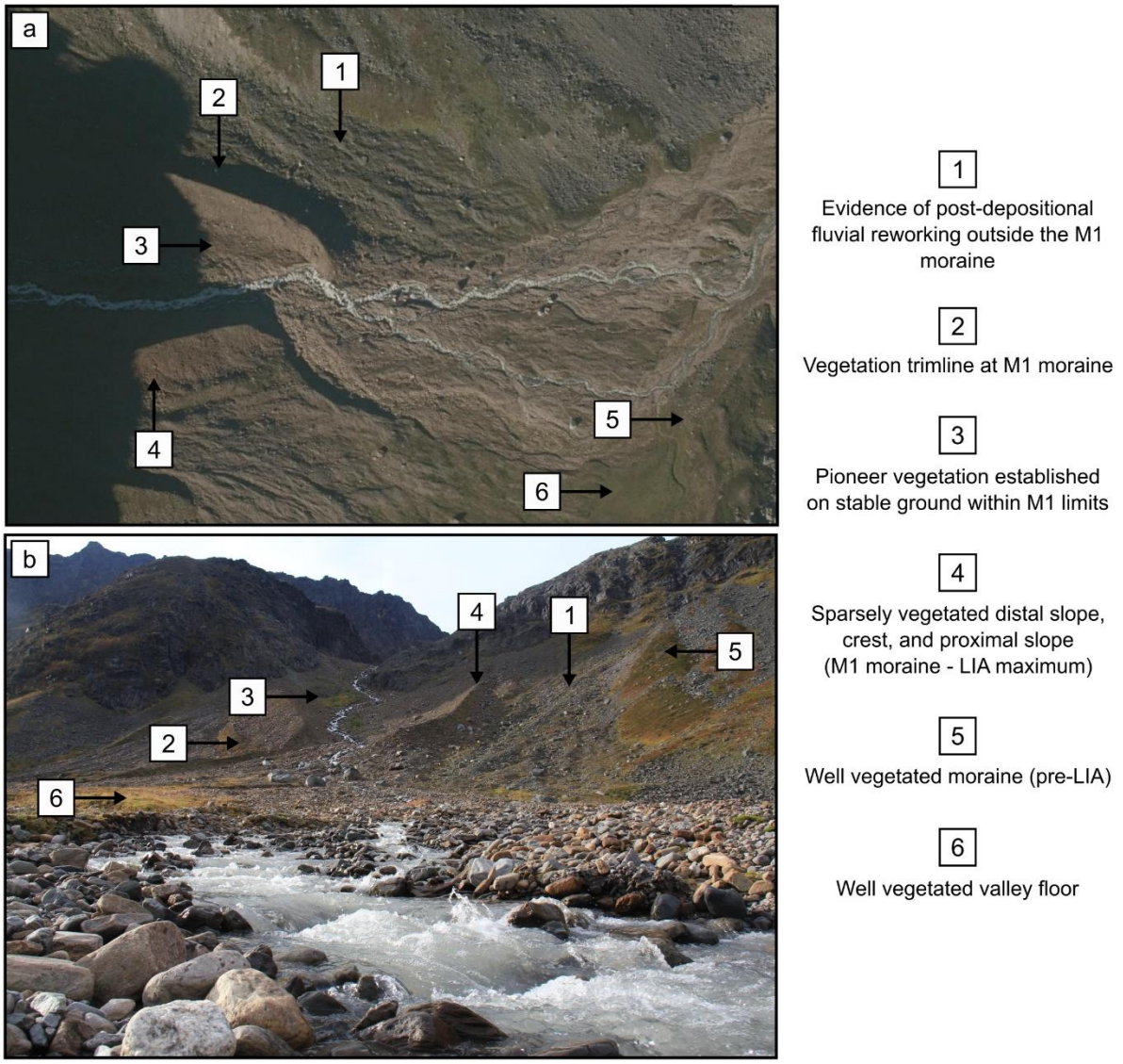

Figure 4.5. *Example of the LIA moraine examined in the field (foreland of glacier 121) which can be seen from: (a) aerial orthophotograph (0.25 m resolution: https://www.norgeibilder.no/; 24.08.2016) and (b) oblique photograph (J.R. Leigh). The M1 moraine is sharp crested, with little evidence of slumping, predominantly unaffected by periglacial slope activity, and on the distal side of the moraine there is a distinct vegetation trimline.*

4.5.1.1. Lichen size data and moraine ages since the LIA

The lichen size data collected in the field shows a pronounced increase in lichen size (largest diameter) with distance from the glacier termini, confirming that lichen size is related to apparent substrate age. Table 4.1 shows the Single Largest Lichen (SLL) and 5LL for each moraine searched. To utilize lichenometry, as a calculated-age dating technique, we established a localised lichenometric dating curve (Figure 4.6). Our lichenometric dating curve was constructed from measurements of lichen growing on headstones within the Rotsundelv and Storslett church yards (Figure 4.1). Once a plot of lichen size and surface age had been made, we used a logarithmic curve ($y = 12.026ln(x) – 26.488$ where x = years before 2018 and y = lichen size) plotted through the largest lichens following established methods (e.g. Innes, 1983; Ballantyne, 1990; Evans *et al.*, 1999a). Due to the limited ages of the fixed points used in our site-specific dating some extrapolation of the curve was unavoidable in order to calculate the ages of moraines that may be older than our oldest control data from the church yards. Extrapolation of lichenometric dating curves is, however, common practice when sufficiently old control surfaces are rare, especially in remote regions (e.g. Ballantyne, 1990; Evans *et al.*, 1999a; Solomina *et al.*, 2010). By using our site-specific dating curve (Figure 4.6) it was, therefore, possible to assign calculated ages to the moraines within the Rotsund Valley. The resulting surface ages (yrs before 2018) range from 204 ±41 yrs to 9 ±2 yrs (Table 4.2), and the detailed moraine chronology for the studied glaciers in the Rotsund Valley is shown in Figures 4.7-4.10.

The M1 moraines exhibit a range of 5LL values from 33.2 to 37.4 mm (Table 4.1), with the oldest and youngest M1 moraine ages calculated at 204 and 196 years old (1814 (±41 yrs) and 1877 (±34 yrs); Table 4.2, Figures 4.7-4.10). The M2 moraines have 5LL values between 23.6 to 27.0 mm and the associated ages vary between 82 and 64 years old (1936 (±16 yrs) and 1954 (±15 yrs); Table 4.2, Figures 4.7-4.10). The younger moraines labelled M3-M8 (where present) have a mixed range of calculated ages and, as a result, document a varying pattern of glacial advance and retreat between each glacier. The youngest moraines investigated are M8 moraines, these moraines are only present on the relatively flat forelands of glacier 121 and 123, <300 m from the present-day glacier terminus (Figure 4.9 and 4.10). The M8 moraines carry no visible lichen specimens and, as a result, are given formation dates of ~2009, based on the lichen lag-times established from the Rotsundelv and Storslett churchyards.

The M8 moraine age is further supported by aerial and satellite imagery which shows the glacier position outside of glacier 121's M8 moraine in 2006, and 20 m inside the moraine in 2011.

Table 4.1. *Lichen size data (Single Largest Lichen (SLL) and mean of the Five Largest Lichen (5LL)) from the moraines within the four glacial forelands of the field site. Glacier IDs are provided as assigned within the Inventory of Norwegian glaciers (Andreassen and others, 2012b).*

Glacier ID	Moraine elv. (m a.s.l)	Assigned moraine ID	SLL (mm)	5LL (mm)
115	660-690	M1	38	37.4
117	570-600	M1	35	33.2
	560-580	M2	32	26.5
	560-570	M3	24	23
121	340-440	M1	41	37
	360-380	M2	27	27
	595	M3	24	23.4
	545	M6	9	8.2
	555	M7	6	5.2
	570	M8	0	0
123	440-450	M1(1)	42	35.6
	425-500	M1(2)	35	33
	455-510	M2	30	23.6
	550-570	M4	14	13.2
	570	M5	13	11.2
	545-600	M6	8	7.4
	550	M8	0	0

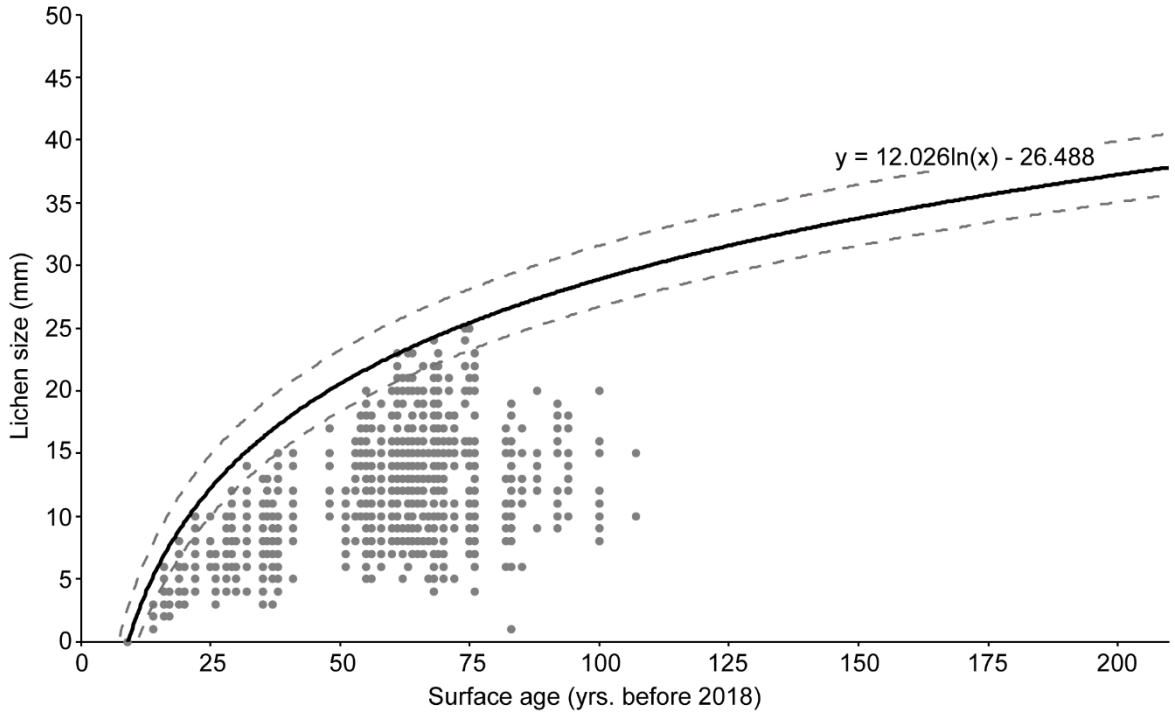

Figure 4.6. *Lichenometric dating curve constructed from lichen growth on dated headstones within the Rotsundelv and Storslett churchyards. The black line represents a logarithmic curve fitted to the largest lichens, while the dotted grey lines represent standardised ±20% lichenometric error margins. The curve has been extrapolated to represent lichen growth over the past 210 years.*

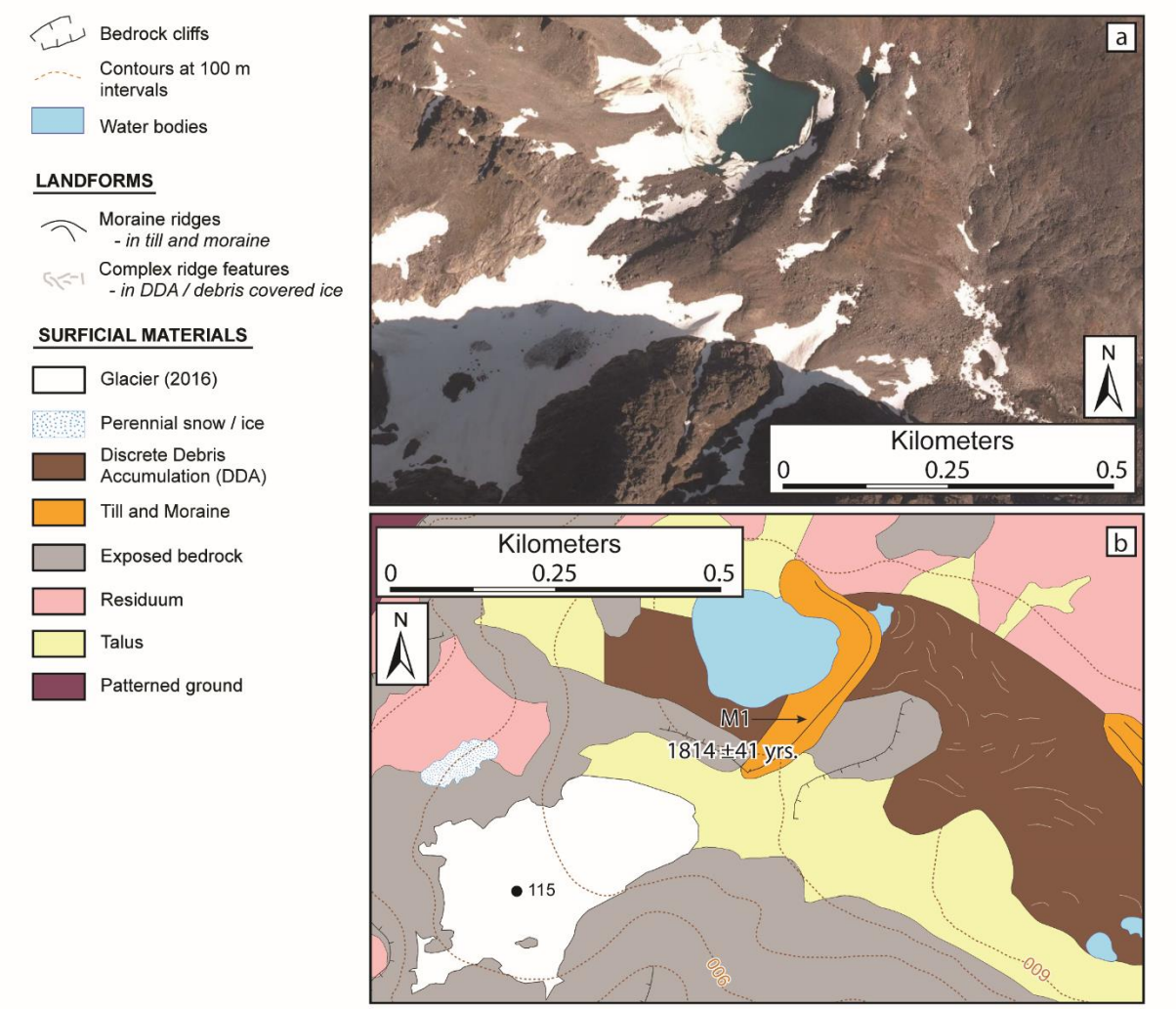

Figure 4.7. *Geomorphological map (b) showing the foreland of glacier 115 (Figure 4.3a) with annotations showing the moraine surveyed for lichenometry and the resulting calculated ages. Map based on field mapping and aerial orthophotographs (image date 24.08.2016) with 0.25 m spatial resolution. Note: due to shading on the 2016 imagery the left image (a) is an aerial photograph from 19.09.2011 (www.norgeibilder.no).*

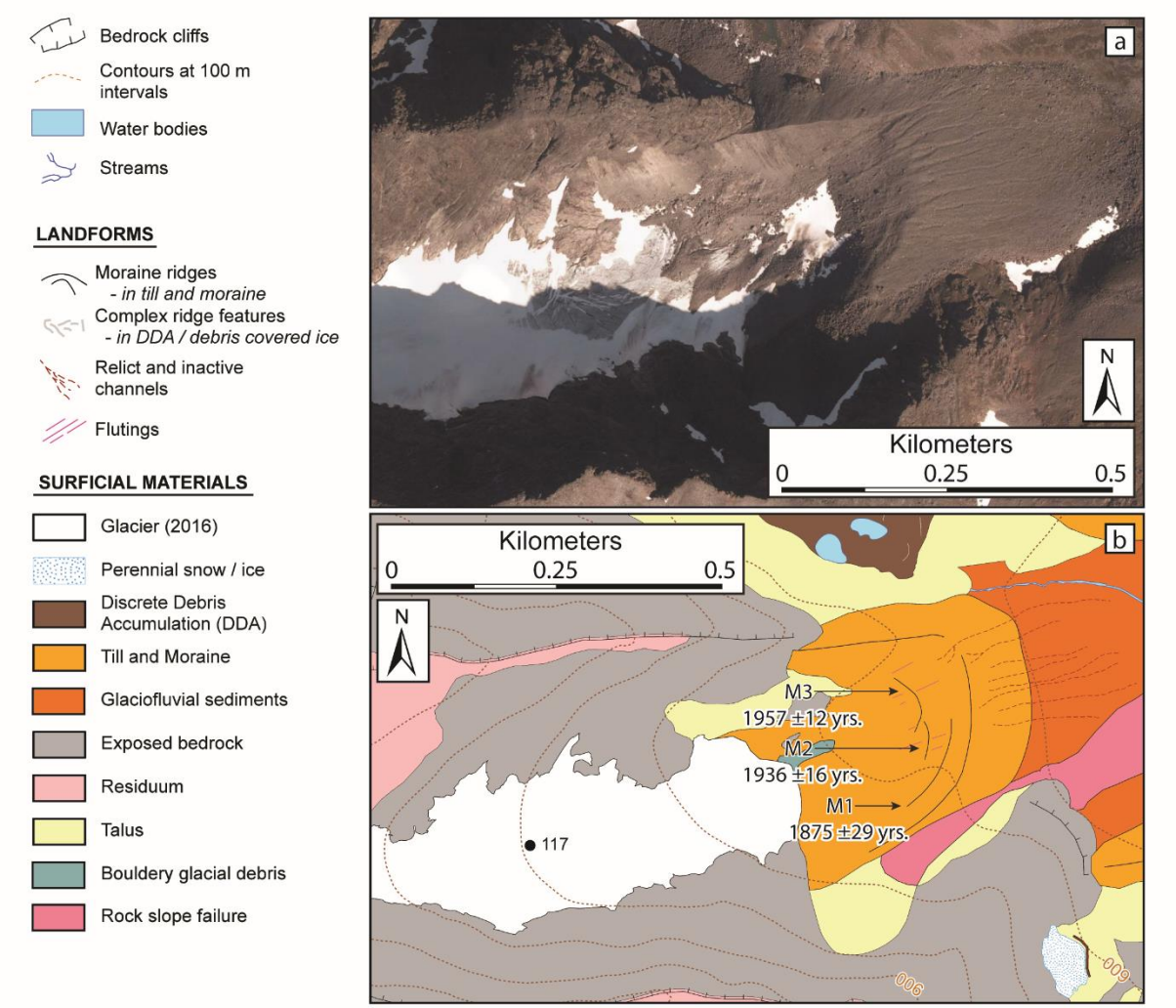

Figure 4.8. *Geomorphological map (b) showing the foreland of glacier 117 (Figure 4.3b) with annotations showing the moraine surveyed for lichenometry and the resulting calculated ages. Map based on field mapping and aerial orthophotographs (image date 24.08.2016) with 0.25 m spatial resolution. Note: due to shading on the 2016 imagery the left image (a) is an aerial photograph from 19.09.2011 (www.norgeibilder.no).*

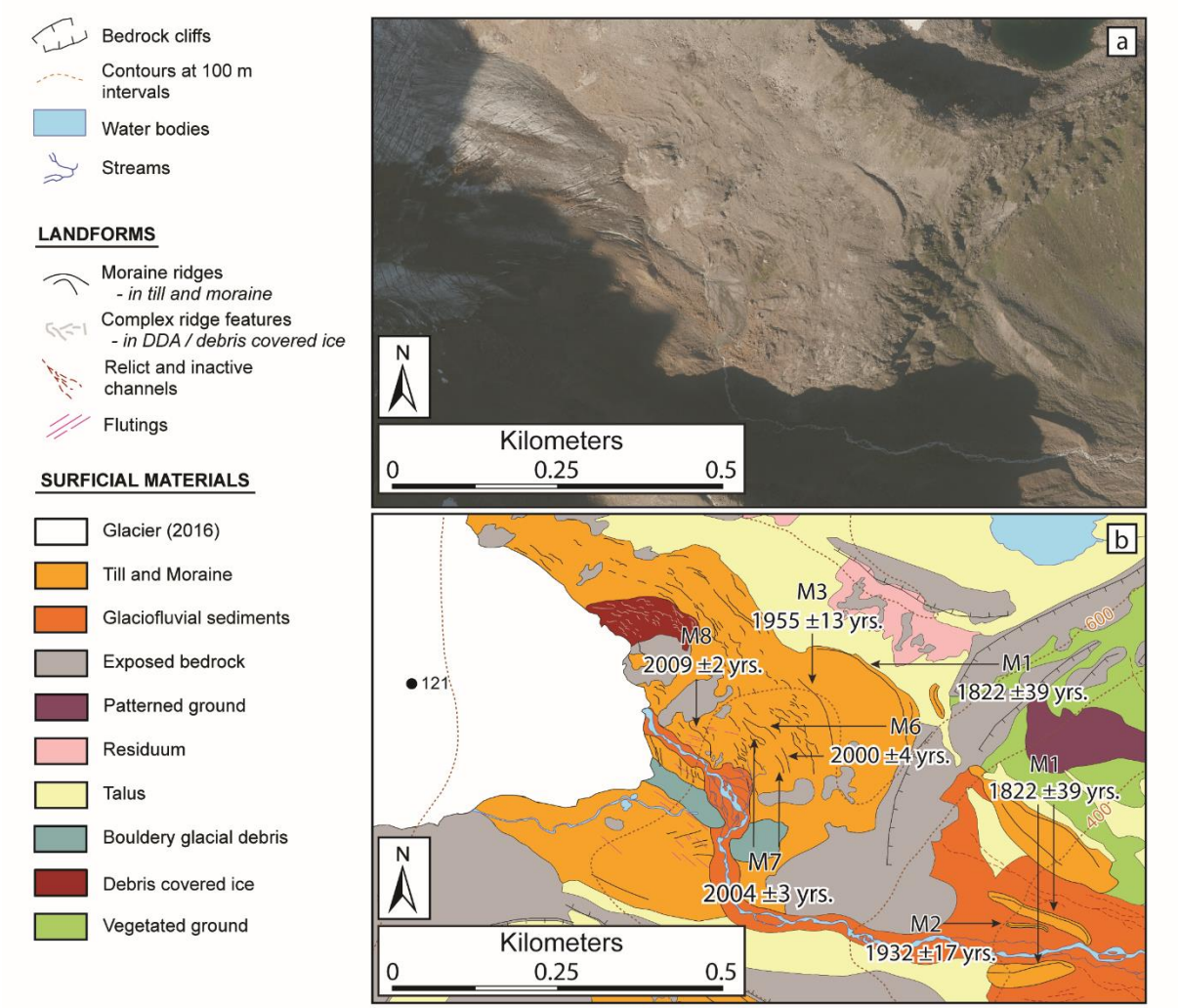

Figure 4.9. *Geomorphological map (a) showing the foreland of glacier 121 (Figure 4.3c) with annotations showing the moraine surveyed for lichenometry and the resulting calculated ages. Map based on field mapping and aerial orthophotographs (image date 24.08.2016; b) with 0.25 m spatial resolution (www.norgeibilder.no).*

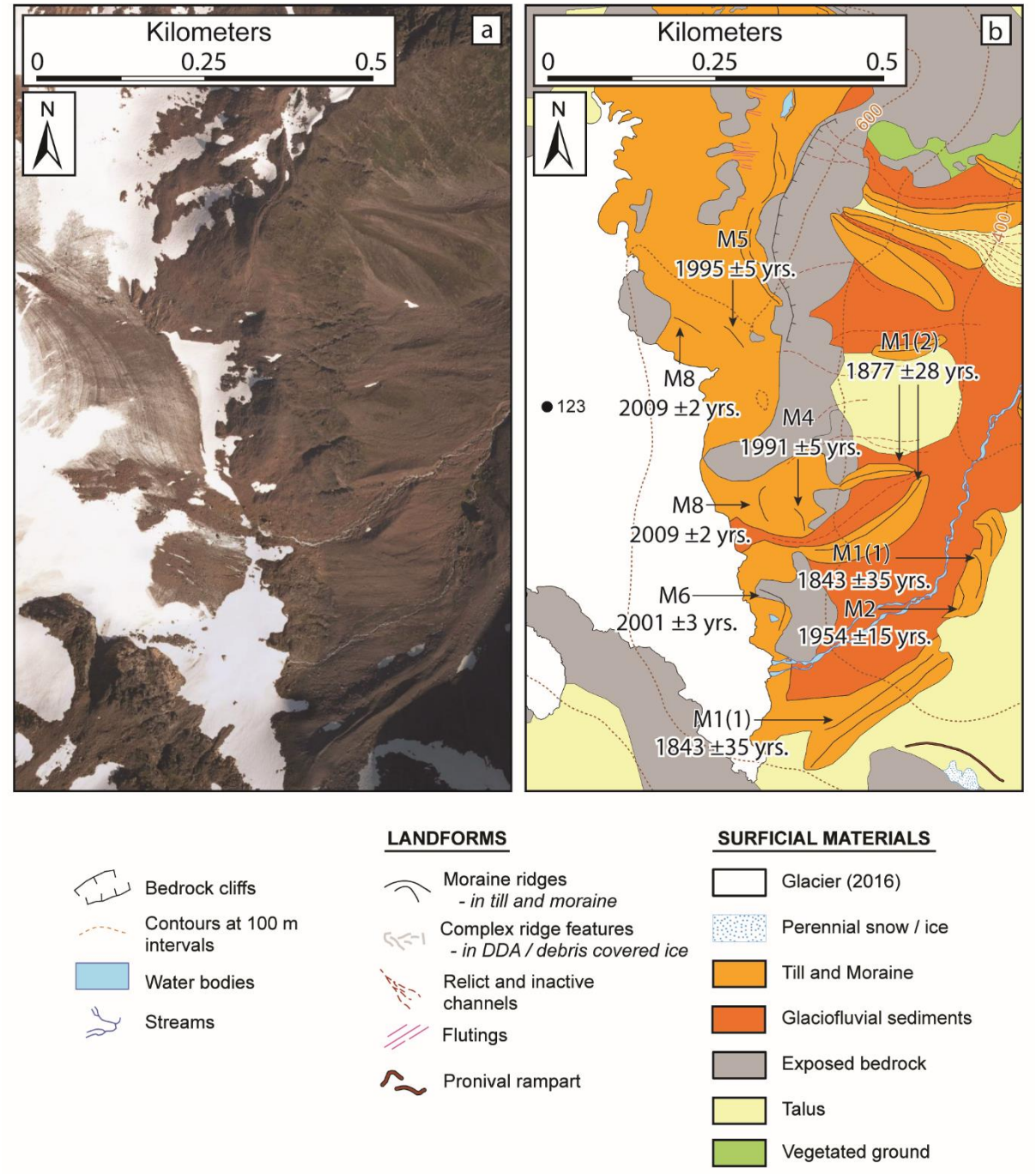

Figure 4.10. *Geomorphological map (a) showing the foreland of glacier 123 (Figure 4.3d) with annotations showing the moraine surveyed for lichenometry and the resulting calculated ages. Map based on field mapping and aerial orthophotographs (image date 24.08.2016) with 0.25 m spatial resolution. Note: due to shading on the 2016 imagery the top image (b) is an aerial photograph from 19.09.2011 (www.norgeibilder.no).*

Table 4.2. *Results of the lichenometric dating providing calculated ages for the moraines under investigation.*

Glacier ID	Moraine	5LL (mm)	Calculated age (yrs before 2018)	Calculated age ±20% (yrs before 2018)	Date (yrs)	Date ±20% (yrs)
115	M1	37.4	204	245-163	1814	1773-1855
117	M1	33.2	143	172-114	1875	1846-1904
	M2	26.5	82	98-66	1936	1920-1952
	M3	23	61	73-48	1957	1945-1970
121	M1	37	196	235-157	1822	1783-1861
	M2	27	85.8	103-69	1932	1915-1949
	M3	23.4	63	76-50	1955	1942-1968
	M6	8.2	18	22-14	2000	1996-2004
	M7	5.2	14	17-11	2004	2001-2007
	M8	0	9	11-7	2009	2007-2011
123	M1(1)	35.6	175	175-140	1843	1808-1878
	M1(2)	33	140.5	169-112	1877	1849-1906
	M2	23.6	64	79-51	1954	1939-1967
	M4	13.2	27	32-22	1991	1986-1996
	M5	11.2	23	28-18	1995	1990-2000
	M6	7.4	17	20-14	2001	1998-2004
	M8	0	9	11-7	2009	2007-2011

4.5.1.2. Historical glacier limits in 1952

Oblique aerial photographs taken of the field site provide a valuable reference for documenting glacier extent (Figure 4.11). In 1952, glacier 115 was flowing into the area now occupied by a moraine dammed lake (formed some after 1952 and before 1989 based on the imagery), constrained by the M1 moraine. There was also evidence of confluence with another ice body (Figure 4.11), which was not verifiable in the field due to a large DDA that either covers any remaining ice or has replaced the ice completely (see Figure 4.2b). The terminus of glacier 117 is just visible and was not past the large latero-frontal moraine (pre-LIA) that encloses the cirque (Figure 4.11). The main area of glacier 121 can be seen filling the entirety of the cirque and was

confluent with glacier 123 to the south-east, while also being connected to the hanging glacier on the cirque headwall by a narrow ice tongue (Figure 4.11). The confirmation of these ice bodies being connected in 1952, lends support to the mapping of this uppermost ice body as a glacier, where it had previously been overlooked in glacier inventories. Glacier 123 was not overtopping the bedrock cliffs at its front and was being funnelled down the narrow gulley on the true right, where the terminus was obscured (Figure 4.11). An additional photograph taken the same year from a different angle shows glacier 117 and 123 and confirms that glacier 117 was within the confines of the M1 moraine and was near the position of the M3 moraine (Figure 4.11). Glacier 123 was a considerable distance from the M1 moraine, just breaching the bedrock lip behind which it currently lies (Figure 4.11).

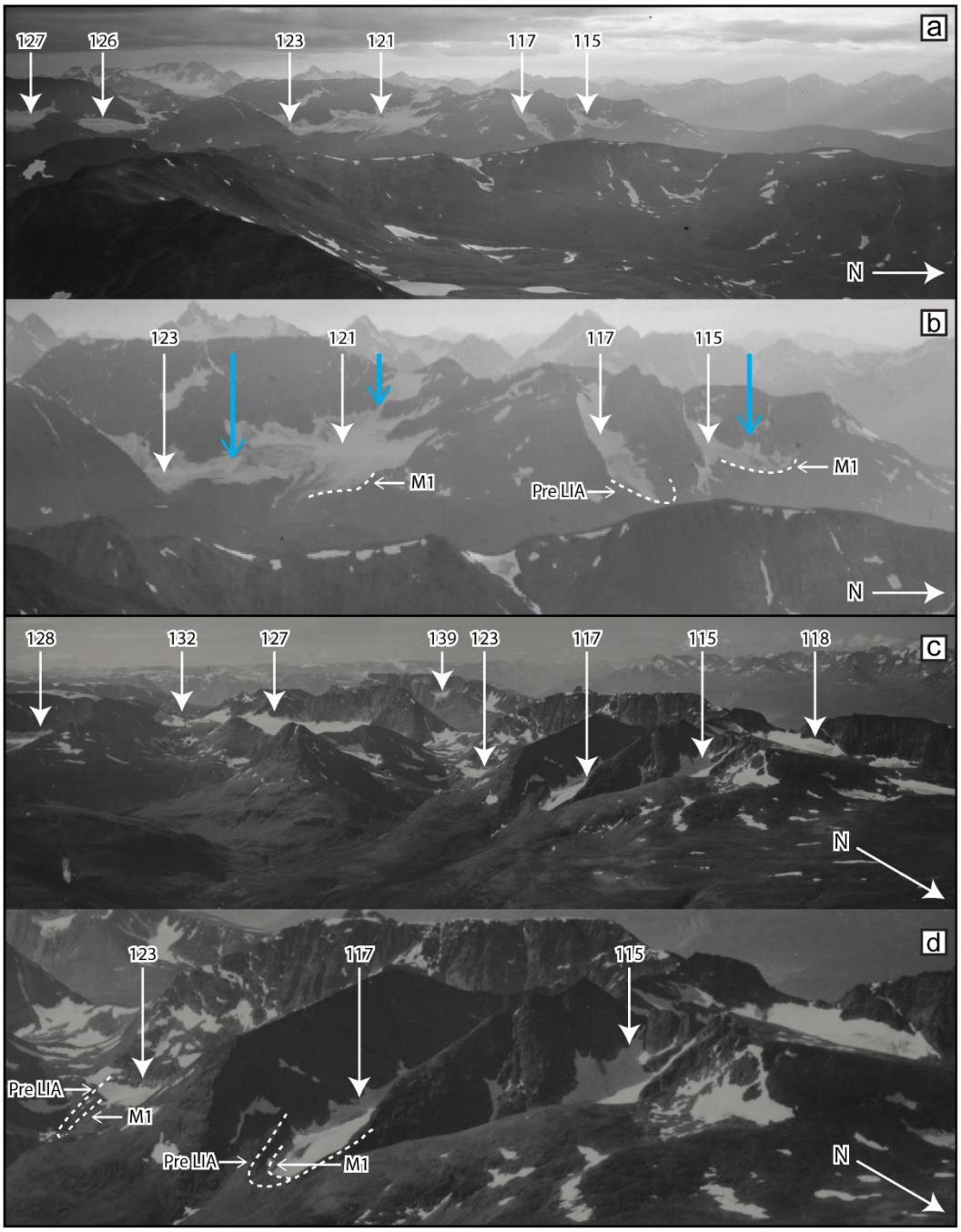

Figure 4.11. *Oblique aerial photographs taken on the 03.08.1952 and the 31.07.1952 (a and c respectively) alongside a zoomed and cropped copy of the aforementioned images (b and d). Glaciers are labelled with corresponding glacier IDs. The dashed lines outline the visible moraines investigated in this study and the blue arrows (b) show where glaciers were confluent with adjoining glaciers/ice bodies. Image source: National Library of Norway (www.nb.no/search?q=wider%C3%B8e%20nordreisa&mediatype=bilder&fromDate=19500101&toDate=19531231).*

4.5.2. Glacier area changes in northern Troms and western Finnmark

4.5.2.1. LIA maximum extent – 1989/2018

The LIA glacial maximum areal extent was mapped for a subset of 15 glaciers (Figure 4.12 and 4.13) all found within region A of our study area (Figure 4.1). Results show that since the LIA maximum (dated to between 1814 (±41 yrs) and 1877 (±34 yrs)) and 1989, the studied glaciers shrunk a total of 3.9 km^2 (39%), and that between LIA maximum and 2018, they shrank a total of 6.9 km^2 (69%). Individual glaciers were between 0.12 km^2 (54%; glacier 115) and 0.56 km^2 (68%; glacier 91) larger during their LIA maximum than in 1989 (Figure 4.12). The largest percentage change between LIA maxima and 1989 was observed at glaciers 91 and 149, which both exhibited a 68% areal reduction, while the smallest percentage change was observed at glacier 121, which shrank only 15% over the same period (Figure 4.12). Overall, mean glacier area reduction from LIA maximum to 1989, (n = 15) equates to ~0.26 km^2 (44%) and from LIA maximum to 2018, equates to ~0.46 km^2 (72%). Notably, of the five glaciers that exhibit glacier loss of >50% between LIA maximum and 1989, all are fronted by at least one proglacial lake (Figure 4.12). The areal extent (and presumably depth) of these lakes varies between, and within forelands, and all lakes are within the extrapolated LIA extent, indicating that at some point during glacier recession they would have been in contact with the glacier.

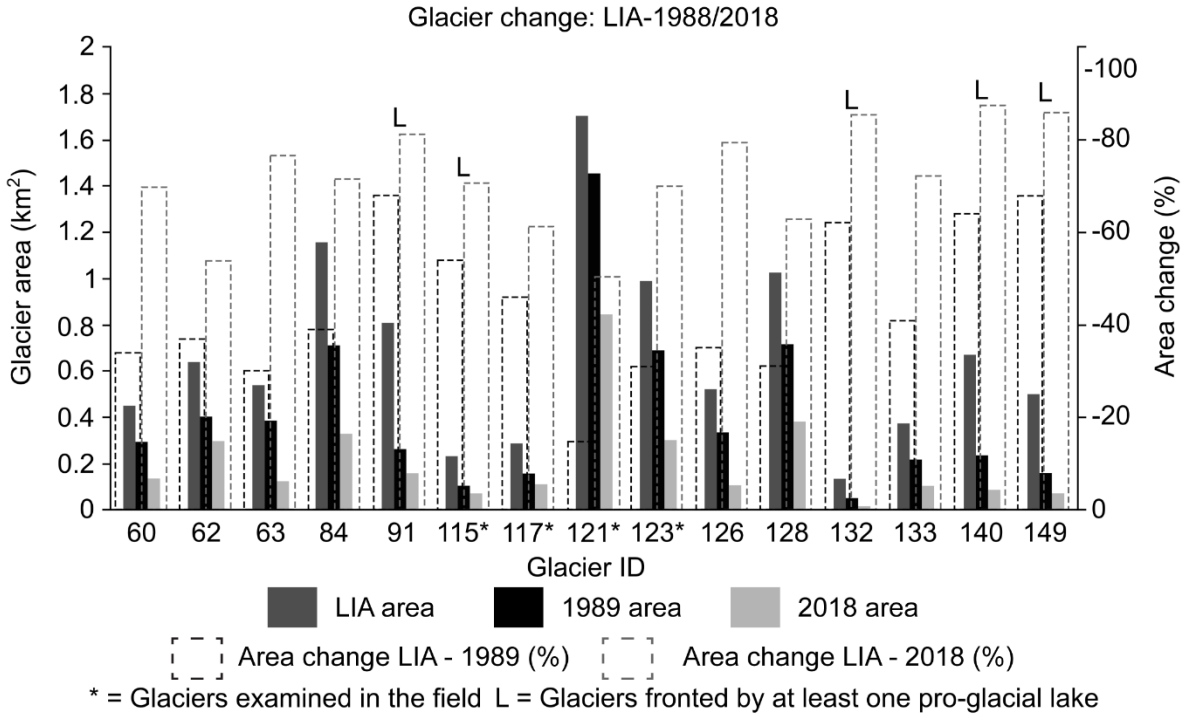

Figure 4.12. *Comparisons of glacial area change between LIA maximum and 1989/2018.*

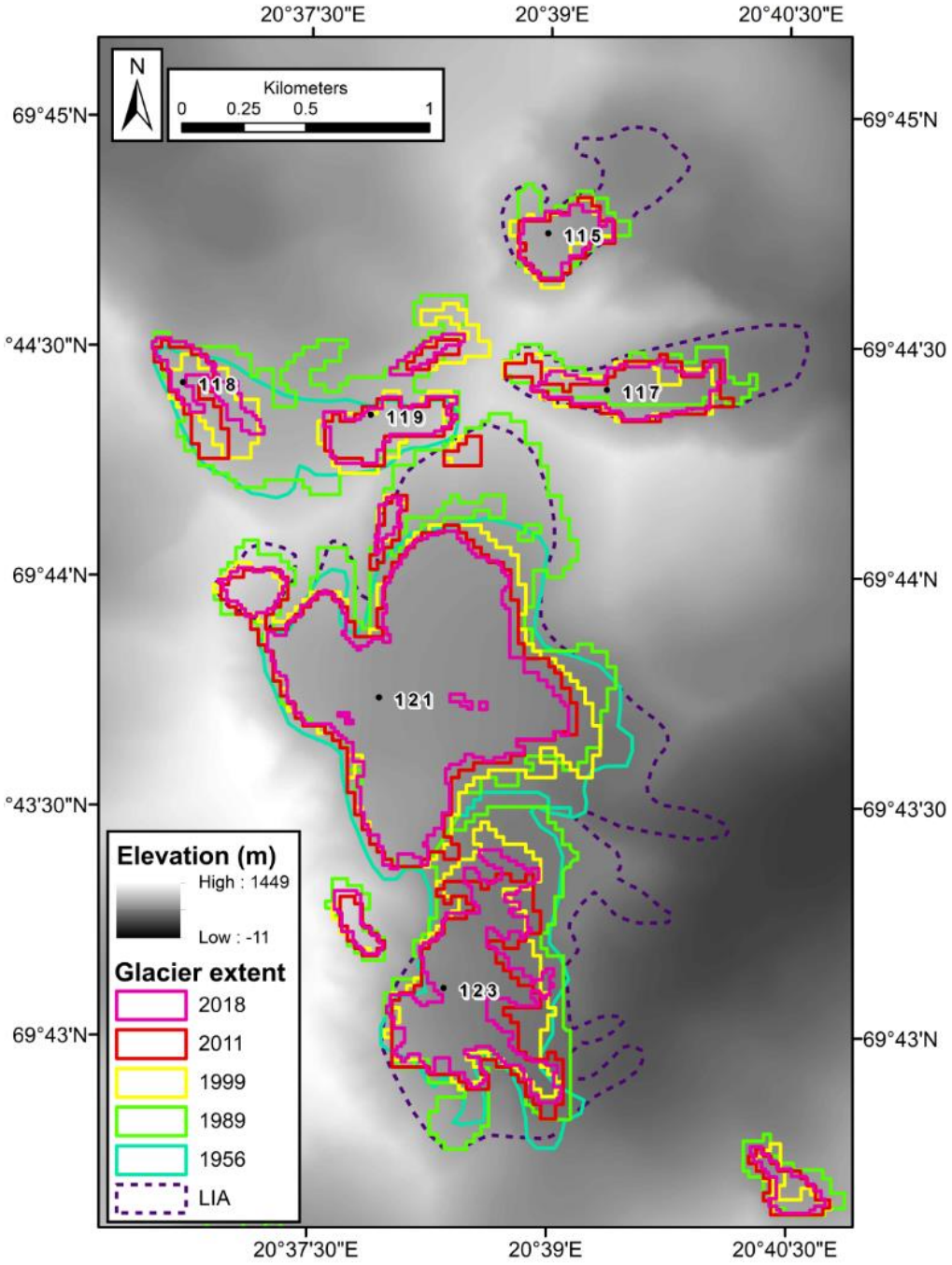

Figure 4.13. *Overview of glacier area change from our Rotsund field site since LIA maximum until 2018 (based upon moraine maps and lichenometric dating) and including glacier outlines from 1956 topographic maps. The background image is the Norwegian Mapping Authority N50 Digital Terrain Map.*

When examining the changes in glacier length for the same glaciers (n = 15), our data indicate that between the LIA maximum and 1989, individual glaciers receded between 1,175 and 52 m (63% and 11%, respectively), and between 1989 and 2018 the same glaciers receded between 545 and 77 m (48% and 5% respectively). When plotting these reductions in glacier length against the reduction in glacier area over the periods LIA-1989 and 1989-2018 there is a general trend of larger glaciers having experienced greater length reductions (Figure 4.14).

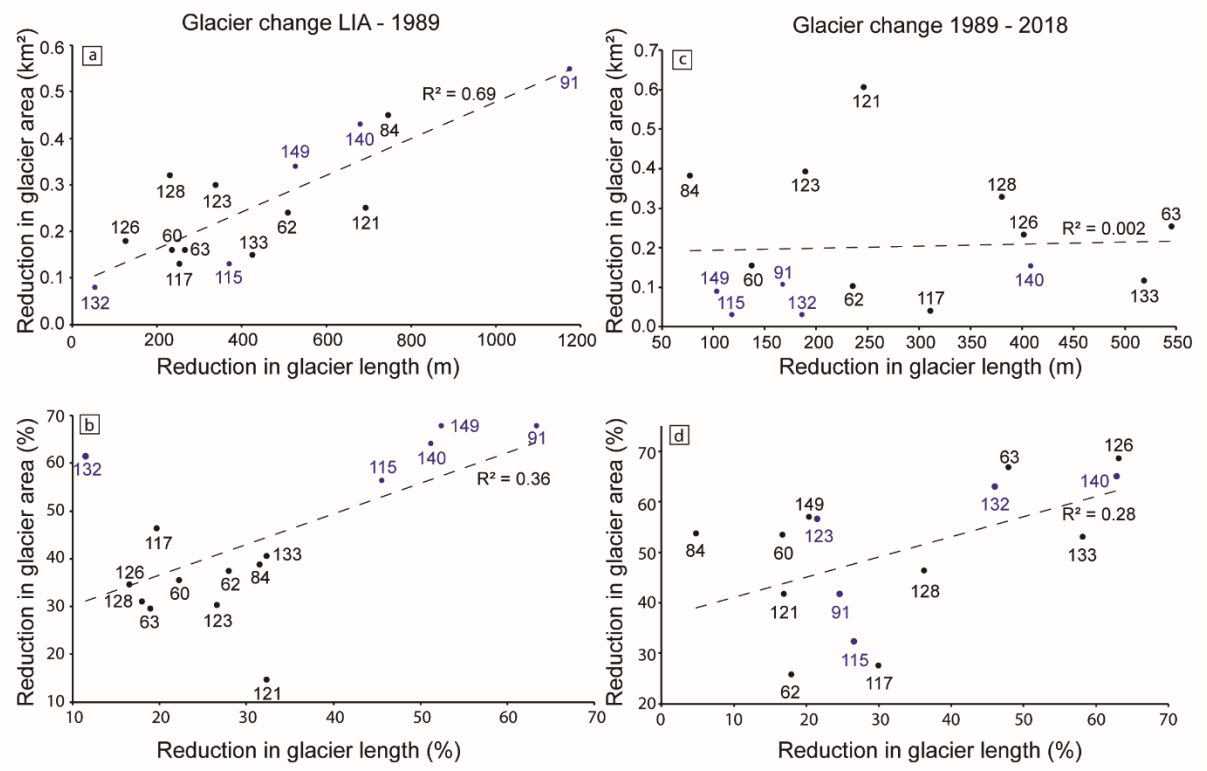

Figure 4.14. *Plots of glacier area and length reduction, as both absolute and percentage values, between the period LIA-1989 (a, b), and 1989-2018 (c, d). Note: the blue circles and corresponding text represent glaciers with at least one pro-glacial lake within the LIA moraine limits and the numbers represent the individual glacier ID's.*

4.5.2.2. 1907-1989

For some of the larger glaciers (n = 84) there is historical data from 1907, 1952, 1954, 1955, 1956, and 1966 (Figure 4.15). Comparing the outlines from the historical 1:100,000 and 1:50,000 topographic maps and our satellite image glacier outlines

reveals steady glacier area loss throughout the 20th century across the whole region, with an anomalous increase observed between some of the 1956 and 1989 outlines (Figure 4.15a V). It should be noted, however, that apart from the 1907 and 1966 outlines (from the Øksfjordjøkelen and Langfjordjøkelen ice caps and surrounding area; Figure 4.15a I), these historical glacier outlines are for different periods and glaciers. When comparing the percentage area change across the dataset, there is a pattern of reduction in glacier area throughout the region (Figure 4.15b). Furthermore, the 59 years between 1907 and 1966 experienced a 9% reduction in glacial area, whereas the 23-year period 1966-1989 experienced a 12% reduction in glacial area (Figure 4.15b I). Our results therefore indicate that the rate of glacial shrinkage was increasing towards the end of the 20th century.

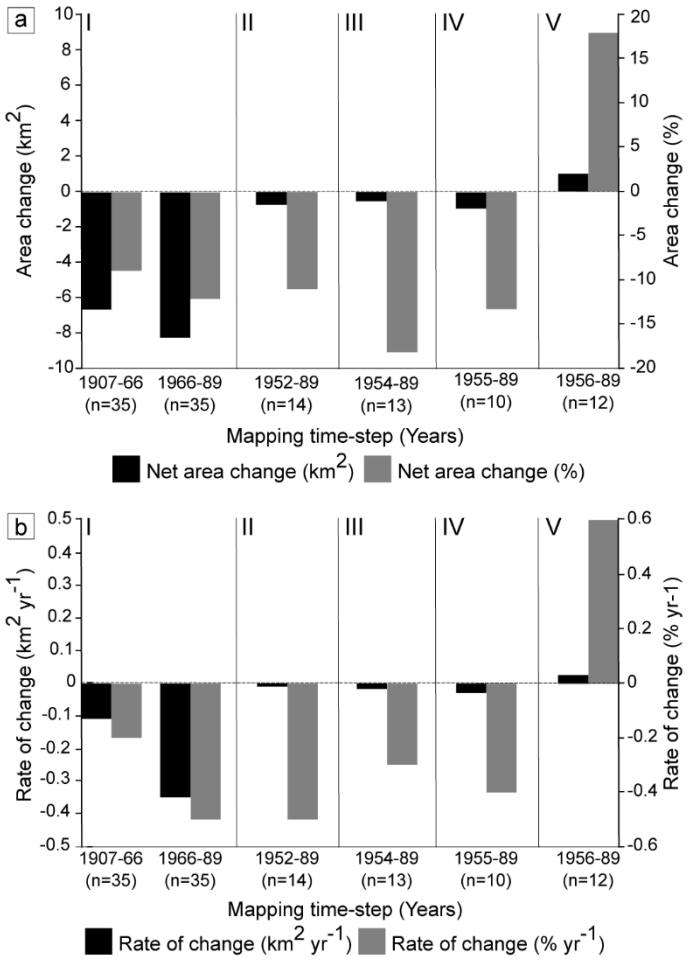

Figure 4.15. *Comparisons of glacier area change between individual sets of historic outlines (from 1: 100 00 Gradteigkart (1907 map) and 1:50 000 Norwegian Mapping Authority topographic maps (1966, 1952, 1954, 1955, and 1956 maps)) and our remotely sensed outlines from 1989. Note: only the outlines in panel I are overlapping*

outlines from different time-steps, the remaining panels II-V represent glacier outlines from different areas within northern Troms at separate time-steps (historic outlines from Winsvold et al., 2014).

4.5.2.3. 1989-2018

In total, 219 glaciers were mapped from the 1989 Landsat 5 satellite imagery, with a total area of 101.8 km^2 (Table 4.3). The total number of glaciers includes 78 newly identified and mapped ice bodies that are not included within the most recent edition of the Inventory of Norwegian Glaciers (Andreassen *et al.*, 2012a; Table 4.3). Of these newly identified glacier units, 23 were classified as *certain* and the remaining 55 were classified as *probable* (n = 10) and *possible* (n = 45; Table 4.3). The 1989, total area of the Andreassen et al. (2012a) glaciers was 94 km^2 and the total area of the additional 78 glaciers found in our study was 7.8 km^2. Of these the area of *certain* glaciers was 2.6 km^2. Additional cloud and snow free imagery and/or ground truthing is needed to confirm or reject the glacial status of the 55 *probable* and *possible* glaciers.

Over the period of satellite observed outlines (1989-2018), the total mapped glacial area of northern Troms and western Finnmark has progressively decreased by 35.4 km^2 (35%), from 101.8 km^2 in 1989 to 66.4 km^2 in 2018 (Table 4.3). The largest net loss, both in absolute area and percentage values (n = -14.1 km^2 and -15%), occurred between 1994 and 1999 (Table 4.3). As some glaciers fragmented as they shrank the number of glacier units mapped increased from 219 in 1989, to 252 in 2018 (Table 4.3). In the study area, 48 glaciers (~22%) have fragmented into two or more individual units over the period of satellite observation (1989-2018). Furthermore, the apparent increase in the number of glaciers over time masks the shrinkage of glacier bodies below our 0.01 km^2 size-threshold; between 1989 and 2018, 36 individual glacier units shrunk below 0.01 km^2 and are, therefore, no longer recorded due to them being too small to accurately map from the coarse resolution Landsat imagery.

Table 4.3. *Summary of remotely sensed glacier area measurements and size over the study period for the whole region of investigation.*

Year	1989	1994	1999	2006	2011	2014	2018
No. of glaciers	219	228	237	243	249	249	252
Total area (km^2)	101.8	96	81.9	81.9	73.7	67.1	66.4
Max. glacier area (km^2)	12.7	12.5	12.4	12.4	12	11.8	11.8
Mean glacier area (km^2)	0.46	0.42	0.35	0.34	0.3	0.27	0.26
No. Glaciers ≥0.5 km^2 (%)	18	16	13	12	10	7	8
No. Glaciers <0.5 km^2 (%)	82	84	87	88	90	93	92
Total area change (km^2)*	n/a	-5.8	-14.1	-0.03	-8.9	-6.6	-0.8
Total area change (%)*	n/a	-6	-15	-0.04	-10	-9	-1
No. of *certain* glaciers	164	167	163	169	174	179	182
Total area (km^2)	96.6	91.4	79	78.7	71.6	65.2	64.6
Max. glacier area (km^2)	12.7	12.5	12.4	12.4	12	11.8	11.8
Mean glacier area (km^2)	0.59	0.55	0.48	0.47	0.41	0.36	0.36
No. Glaciers ≥0.5 km^2 (%)	24	22	19	17	15	10	11
No. Glaciers <0.5 km^2 (%)	76	78	81	83	85	90	89
Total area change (km^2)*	n/a	-5.2	-12.4	-0.28	-7.1	-6.4	-0.64
Total area change (%)*	n/a	-5	-14	-0.4	-9	-9	-1
No. of *probable* glaciers	10	9	9	9	11	15	13
Total area (km^2)	1.3	0.81	0.43	0.37	0.37	0.42	0.36
Max. glacier area (km^2)	0.33	0.26	0.2	0.17	0.08	0.04	0.04
Mean glacier area (km^2)	0.13	0.09	0.05	0.04	0.03	0.03	0.03
Total area change (km^2)*	n/a	-0.52	-0.38	-0.06	0	+0.05	-0.06
Total area change (%)*	n/a	-39	-47	-14	0	+13	-14
No. of *possible* glaciers	45	52	65	65	64	55	57
Total area (km^2)	3.9	3.8	2.5	2.8	2	1.5	1.5
Max. glacier area (km^2)	0.3	0.29	0.21	0.21	0.13	0.08	0.07
Mean glacier area (km^2)	0.09	0.07	0.03	0.04	0.03	0.03	0.03
Total area change (km^2)*	n/a	-0.09	-1.27	+0.31	-0.81	-0.5	+0.03
Total area change (%)*	n/a	-2	-34	+13	-29	-25	+2

*Area change based on the difference between the total area mapped at the previous time step

4.5.3. Climate data

Climate data shows that mean annual temperatures were generally low until the late-1910s, followed by ~20 years of rapid temperature increase (~1.4°C) until end of the 1930s (Figure 4.16a). After 1940, there were ~50 years of mean annual temperature decrease until the late-1980s, after which a clear mean annual temperature increase emerges through to present (~1.1°C; Figure 16a). Between 1874 and 2018, summer temperature has generally remained constant (Figure 4.16b). During the same period, winter temperature generally increased until ~1940 (from ~-1.5°C to ~-0.1°C), then decreased until late-1980s, before warming again until the present (from ~-1.3°C to 0.2°C Figure 16c). 2007 marks the first time within the records that the 10-year average for winter temperature exceeded 0°C (Figure 4.16c), with each subsequent year experiencing higher temperatures. Total annual precipitation patterns exhibit a less varied pattern across the observation period (Figure 4.16a). The winter and summer precipitation values have shown a steady decrease since the early-2000s (Figure 4.16).

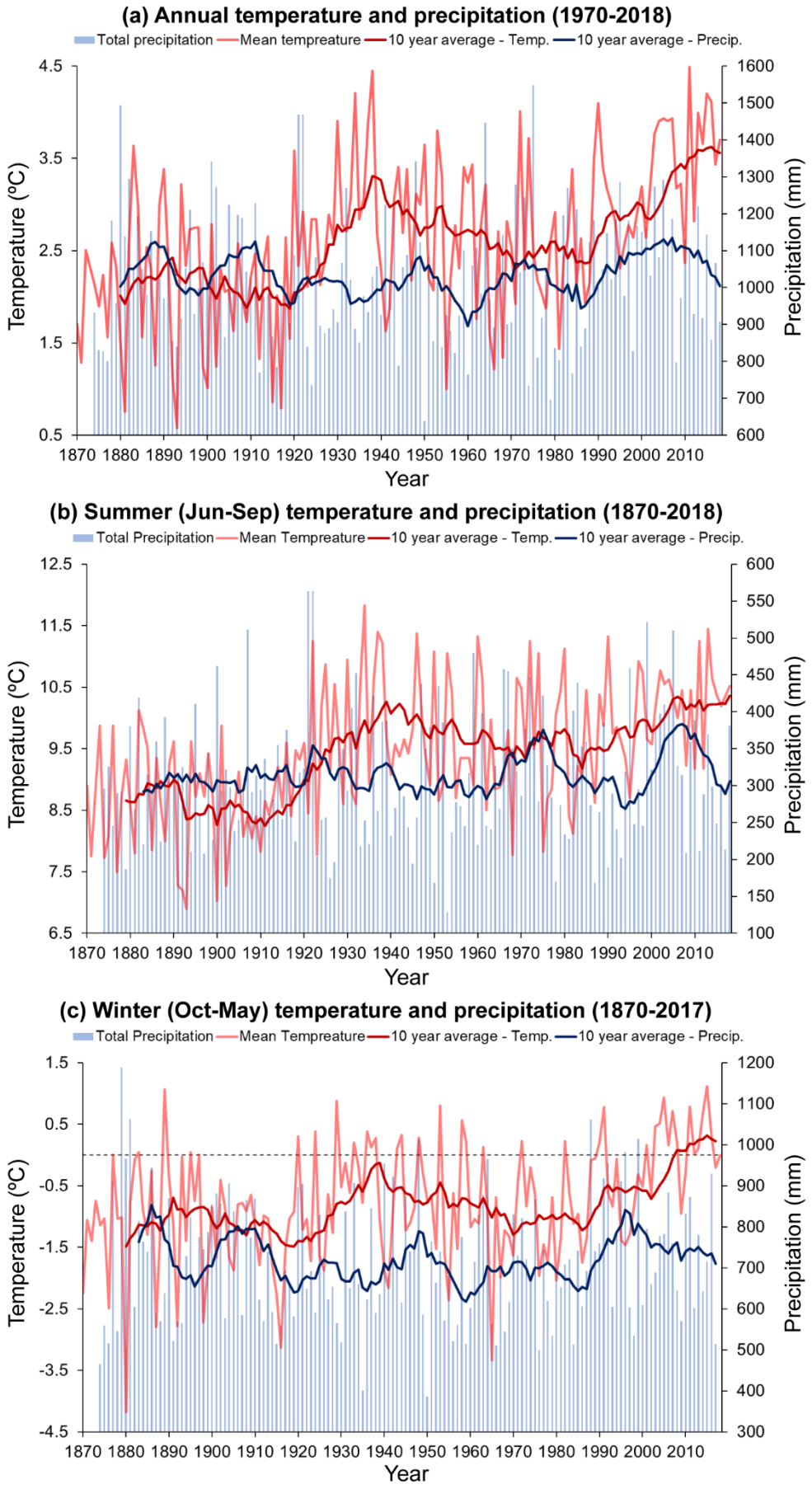
(a) Annual temperature and precipitation (1970-2018)
Total precipitation
Mean tempreature
10 year average - Temp.
10 year average - Precip.
Temperature (ºC)
Precipitation (mm)
Year
(b) Summer (Jun-Sep) temperature and precipitation (1870-2018)
Total Precipitation
Mean Tempreature
10 year average - Temp.
10 year average - Precip.
Temperature (ºC)
Precipitation (mm)
Year
(c) Winter (Oct-May) temperature and precipitation (1870-2017)
Total Precipitation
Mean Tempreature
10 year average - Temp.
10 year average - Precip.
Temperature (ºC)
Precipitation (mm)
Year

Figure 4.16. *Mean annual temperature (a), mean summer (June–September) temperature (b), and mean winter (October–May) temperature (c). Smoothed dark red and blue lines represent 10-year average, dashed line in (c) represents 0°C. Data recorded in Tromsø from two independent weather stations #90440 and #90450 which have been combined to make a continuous record since 1870 (see Section 4.4.6.; accessed via www.eKlima.no).*

4.6. Discussion

4.6.1. Lichenometry and the LIA extent of glaciers within the Rotsund Valley

All the glacier forelands of the Rotsund Valley have moraines that are accessible and suitable for lichenometry (e.g. blocky and showing minimal evidence of post-depositional reworking). Based on LIA moraine characteristics in similar areas (e.g. Winkler, 2003; Baumann *et al.*, 2009; Imhof *et al.*, 2012; Weber *et al.*, 2019), the M1 moraines in the Rotsund Valley (Figures 4.7-4.10) were initially identified from remote sensing as marking LIA maxima, as indicated by their geomorphology, vegetation coverage, and position within glacial forelands (see Section 4.4.1 and Figure 4.5). Our lichenometry confirms this initial hypothesis: the M1 moraines date to between 1814 (±41 yrs) and 1877 (±34 yrs). For the studied glaciers in the Rotsund Valley, it was the glaciers at higher elevations, with additional smaller glaciers/snow patches feeding into them (glacier 115 and 117; Figures 4.2 and 4.11) that an earlier LIA maximum is indicated. In Norway and other mountain regions worldwide, local scale asynchronicity in patterns of glacial advance and retreat has been explained by differences in glacier hypsometry; with glaciers at higher elevations reaching their LIA maxima earlier than neighbouring glaciers at lower elevations (e.g. Nesje *et al.*, 2008; Chenet *et al.*, 2010; Pratt-Sitaula *et al.*, 2011). One potential factor leading to the apparent asynchronicity in LIA maxima of glaciers in the Rotsund Valley (Table 4.2) could, therefore, be explained by glacier hypsometry. Other factors, such as differences in glacier shape, glacier aspect, microclimate, and slope angle may also play a role in modulating the response of glaciers in the Rotsund Valley to changes in climate (Young *et al.*, 2011; Brugger *et al.*, 2019).

On the forelands of glaciers 117, 121, and 123, a smaller yet well-defined moraine ridge (M2) lies immediately within the M1 moraines (Figures 4.8-4.10). The M2 moraines were dated to 1932 (±17 yrs), 1936 (±16 yrs), and 1954 (±15 yrs; Table 4.2). While the M2 moraine fronting glacier 123 seems to have formed ~18-22 years later than the other M2 moraines, we conclude that given all the M2 moraines exhibit markedly similar form, position, and vegetation coverage, they result from the same moraine forming event dating to the early-20th century (Table 4.2). The apparent asynchronicity again resulting from differences in glacier characteristics which at a local scale can modulate individual glaciers responses to climate forcing (Chenet *et al.*, 2010; Pratt-Sitaula *et al.*, 2011; Brugger *et al.*, 2019). Furthermore, the M2

moraines observed in the Rotsund Valley are comparable with a series of moraines fronting nine glaciers on the nearby Lyngen Peninsula, which have previously been dated to between 1910 and 1935, and subsequently attributed to the LIA maximum (Ballantyne, 1990).

The climate data (Figure 4.16) show that winter precipitation was increased for several years between the late-1890s and the 1910s, while between ~1900 and ~1920, annual temperature decreased. We suggest that the observed ~20-year period of lowering temperatures coupled with ~10 years of increased winter precipitation (Figure 4.16) caused the glaciers of northern Troms to experience a small advance or still stand, during a period of net-retreat from the 19th century LIA maximum (M1 moraines; Table 4.2). Consequently, we suggest that the M2 moraines of the early-19th century in our study area of the Rotsund Valley may not document LIA maximum as proposed for the Lyngen Peninsula (Ballantyne, 1990). Instead we conclude that the M2 moraines, of the Rotsund Valley, were formed during a period of rapid climate variability, initiated ~1880 and continuing throughout the 20th century.

The remaining moraines, M3 to M8, document a more recent and rapid retreat from the mid-20th to early-21st century (1955-2009; Table 4.2). In forelands where numerous moraines are present (e.g. the foreland of glacier 121), topography can be considered as the driving factor behind moraine formation (Barr and Lovell, 2014). Shallow glacier beds are likely to result in deposition of smaller, yet more numerous moraines triggered by ice margin fluctuations as a response to minor variations in climate (Barr and Lovell, 2014). Whereas glaciers in steep cirques are less likely to respond to minor climate variations leading to more stable margins and fewer, yet, larger, moraines (Barr and Lovell, 2014). The relatively flat forelands of glaciers 121 and 123 are therefore, likely responsible for the more numerous moraines that are present (Figure 4.9 and 4.10).

In summary, our results show a 19th century LIA maximum (1814-1877; Table 4.2), in contrast to the 20th century LIA maximum (1910-1930) as proposed for the Lyngen Peninsula (Ballantyne, 1990). An early- to mid-19th century LIA maxima in our in northern Troms study area represents a considerably later glacial advance than similar studies from central and southern Norway, which document a mid-18th century LIA maximum (Nesje, 2009 and references therein). The more recent LIA advance found for high-arctic glaciers within Norway, compared to central and southern Norway was thought to be the result from a reduction in summer temperate and an increase in

winter snowfall, corresponding with a northward retreat of the oceanic polar front during the 19th century (Ballantyne, 1990).

4.6.1.1. Comparisons with alternative lichenometric dating curves

We note that the apparent growth rates (Section 4.5.1.1), as calculated from our dating curve (Figure 4.6), are slower than those reported from elsewhere in Norway (e.g. Erikstad and Sollid, 1986; Ballantyne, 1990; Winkler, 2003). To examine the implications of the variable lichen growth rates for calculated substrate ages, we experimented with three additional curves (Figure 4.17), specifically from the Lyngen Peninsula in Troms County at 69°N (Ballantyne, 1990), Svartisen and Okstindan in Nordland county between 66-67°N (Winkler, 2003), and Jostedalsbreen and Jotunheimen in Vestland County between 61-62°N (Erikstad and Sollid, 1986). The resulting ages for the oldest surfaces resulted in a maximum discrepancy of ~142 years (Table 4.4) and the maximum discrepancy for the youngest surfaces was ~14 years, with the lag time before initial lichen colonisation ranging from 9 to 22 years (Table 4.4). This indicates that the existing lichen growth curves for Norway cannot be employed outside of their original study areas, likely because of the different climatic regimes and their controls on lichen growth rates. Indeed, Beschel (1961) coined the term ‘hygrocontinentality’ to explain discrepancies in growth rate as a function of different climatic variables across a range of spatial scales (e.g. <100 km to >4,000 km), which has since been verified by a number of lichenometric investigations (Beschel, 1961; Gribbon, 1964; e.g. Curry, 1969; Ten Brink, 1973; Evans *et al.*, 1999a; Hansen, 2010).

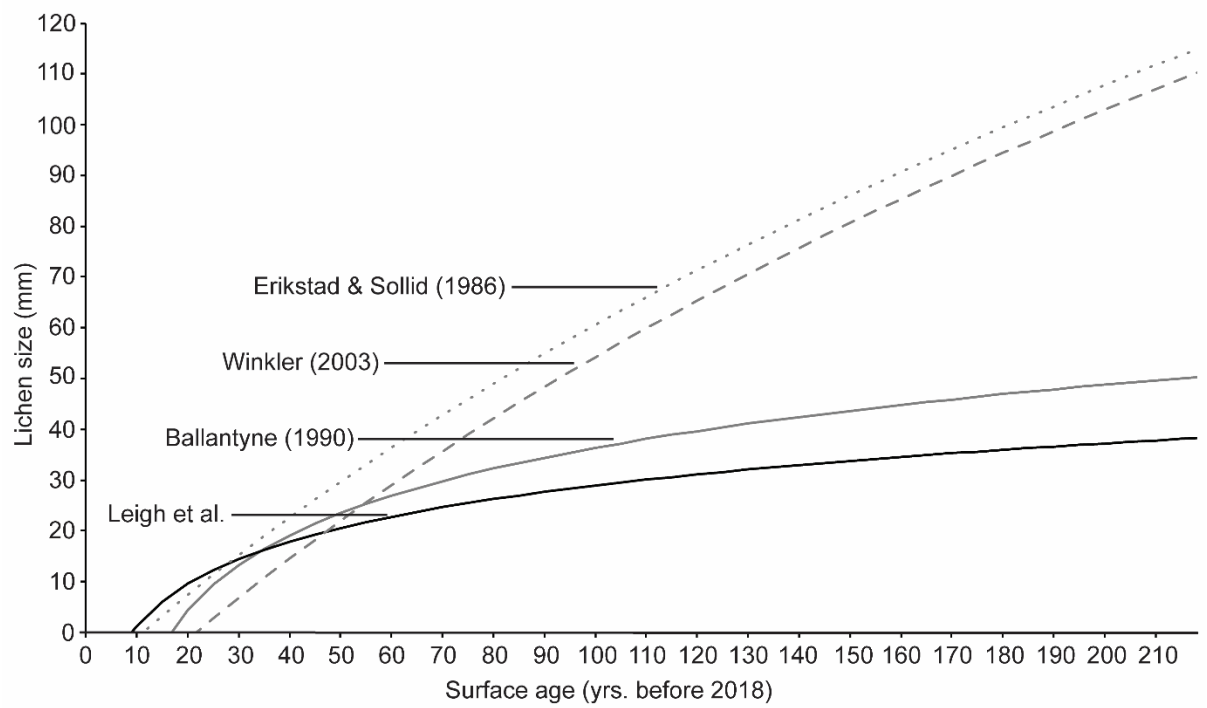

Figure 4.17. *Comparison of different lichenometric dating curves constructed from different areas across Norway; Erikstad and Sollid (1986) from 61-62°N, Winkler (2003) from 66-67°N, and Ballantyne (1990) / Leigh et al. (this paper) from 69°N. All curves have been extrapolated to represent lichen growth over the past 210 years.*

The impact of hygrocontinentality, or indeed climate more generally, on lichen growth relates to two primary factors: (i) the amount of effective precipitation; and (ii) the duration of snow cover (Beschel, 1961; Curry, 1969; Benedict, 1990, 2008; Hamilton, 1995; Evans *et al.*, 1999a; Hansen, 2010). As precipitation is known to differ substantially across Norway, both with latitude and longitude, it is the most likely control on variable lichen growth rates. For example, both Jostedalsbreen and Jotunheimen in Vestland and Svartisen and Okstindan in Nordland County are areas of high precipitation >2,000 mm yr^{-1} (potentially exceeding 4,000 mm yr^{-1} depending on specific location (Figure, 4.18a; http://www.senorge.no/index.html?p=klima); whereas our research in the Rotsund Valley (and the Nordreisa region) is in an area of relatively low precipitation, between 500-700 mm yr^{-1} (Figure 4.18a; http://www.senorge.no/index.html?p=klima). The higher precipitation in Vestland and Nordland Counties has, therefore, resulted in not only a difference in the shape of the age-size curve (Figure 4.17), but a considerable difference in the averaged lichen growth rate over the last 210 years. Furthermore, when taking a simple average growth rate over the 210-year period for the four different sites (Jostedalsbreen,

Svartisen, Lyngen Peninsula, and the Rotsund Valley) and plotting this against the available, local, total precipitation values over the period 2007-2018, areas of higher precipitation result in faster lichen growth rates (Figure 4.18b). For example, the lichen growth rate in Vestland and Nordland counties is three times greater than that in the Rotsund Valley (Figure 4.18b), and even within Troms County, an increase in precipitation across a west to east transect results in the lichen growth rate on the Lyngen Peninsula being around 50% greater than that of the Rotsund Valley (Figure 4.18b).

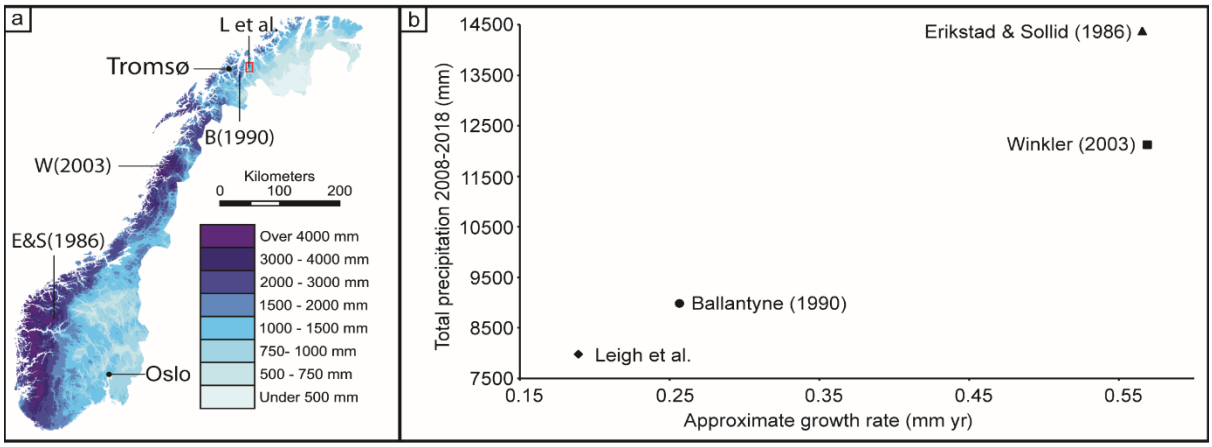

Figure 4.18. *(a) Precipitation map of Norway showing normal annual precipitation (mm yr^{-1}) for the period 1971-2000 (http://www.senorge.no/index.html?p=klima) with the red box highlighting our northern Troms study site. (b) Average lichen growth rate over the past 210 years from Erikstad and Sollid (1986), Winkler (2003), Ballantyne (1990), and Leigh et al. (this paper) compared with total precipitation over the period 2008-2018 (precipitation data from four different weather stations (station no.: 91740, 91080, 79762, 58480 accessed via www.eKlima.no) near the study sites of the aforementioned lichenometric studies). Note: data from station no. 79762 starts in 2007 and therefore to remain consistent across all sites, we used data over the period 2007-2018 for all sites.*

As a result of our investigation into lichen growth as a function of hygrocontinentality (Figure 4.17), it is apparent that the climate of Norway can substantially impact on not only the timing and extent of LIA maximum (as initially outlined by Ballantyne, 1990), but also on the rates of lichen growth and resulting shape of any age-size curves and calculated surface ages (Table 4.4, Figure 4.17).

We, therefore, conclude that given the considerably lower precipitation rates across Nordreisa County, compared to the Lyngen Peninsula (or other sites further south; Figure 4.18), our site-specific dating curve (Figure 4.6) remains the most reliable tool for lichenometric dating within the Rotsund Valley.

Table 4.4. *Results of the lichenometric dating when using dating curves from different areas of Norway (see Figure 4.17) with the associated calculated ages for the moraines under investigation.*

Glacier ID	Moraine	5LL data	Leigh et al. (this paper)		Ballantyne (1990)		Winkler (2003)		Erikstad & Sollid (1986)	
			Age (yrs before 2018)	Date	Age (yrs before 2018)	Date	Age (yrs before 2018)	Date	Age (yrs before 2018)	Date
115	M1	37.4	204	**1814**	107	**1911**	74	**1945**	62	**1956**
117	M1	33.2	143	**1875**	84	**1934**	67	**1952**	56	**1962**
	M2	26.5	82	**1936**	59	**1959**	57	**1961**	47	**1972**
	M3	23	61	**1957**	49	**1969**	52	**1966**	41	**1977**
121	M1	37	196	**1822**	104	**1914**	72	**1946**	61	**1957**
	M2	27	85	**1933**	61	**1957**	57	**1961**	47	**1971**
	M3	23.4	63	**1955**	50	**1968**	52	**1966**	42	**1977**
	M4	8.2	18	**2000**	24	**1994**	32	**1986**	22	**1996**
	M5	5.2	14	**2004**	21	**1997**	29	**1989**	18	**2000**
	M6	0	9	**2009**	17	**2001**	23	**1996**	39	**1979**
123	M1(1)	35.6	175	**1843**	96	**1922**	70	**1948**	59	**1959**
	M1(2)	33	140	**1878**	83	**1935**	67	**1952**	56	**1962**
	M2	23.6	64	**1954**	51	**1967**	53	**1965**	42	**1976**
	M3	13.2	27	**1991**	30	**1988**	39	**1979**	28	**1990**
	M4	11.2	23	**1995**	27	**1991**	36	**1982**	26	**1992**
	M5	7.4	17	**2001**	23	**1995**	32	**1987**	21	**1997**
	M6	0	9	**2009**	17	**2001**	23	**1996**	12	**2006**
	M7	0	9	**2009**	17	**2001**	23	**1996**	12	**2006**

4.6.2. Changes in glacier size: links with climate and topography

4.6.2.1. Little Ice Age maxima to late-20th century

Our LIA reconstructions (Figure 4.12) cover a small subset of 15 glaciers within region A (see Figure 4.1). The results show that the reconstructed glacier area decreased from 10 km^2 at LIA maximum to 6.2 km^2 in 1989, and to 3.1 km^2 in 2018 (Figure 4.12). It is difficult to find a direct comparison of LIA area reconstructions as different studies examine area change over different timeframes, using different methods (e.g. Andreassen *et al.*, 2008; Stokes *et al.*, 2018). A relatively close comparison can, however, be made to glacier area change in Jotunheimen and Hardangerjøkulen (southern Norway). Between LIA maximum (~1750) and 2003, glaciers in Jotunheimen (n = 233) shrank by ~100 km^2 (35%) (Baumann *et al.*, 2009) while between LIA maxium (~1750) and 2013, the Hardangerjøkulen ice cap shrank by ~40.3 km^2 (37%) (Weber *et al.*, 2019). In comparison, our results show a 39% reduction in glacier area over a shorter timeframe (LIA maxima (~1814) to 1989). Comparatively, results from Langfjordjøkelen on the Bergsfjord Peninsula has shown that this ice cap has experienced the highest rates of glacier shrinkage throughout Norway with a greater reduction in length, area, glaciological and geodetic mass balance (Andreassen *et al.*, 2020). Indeed, our data on Langfjordjøkelen reveals that glacier area has reduced from 10.5 km^2 in 1989 to 6.8 km^2 in 2018, representing a 35% (3.7 km^2) reduction in area, over the 29-year period. Furthermore, recent work analysing the mass-balance of Langfjordjøkelen has shown that between 2008 and 2018 the glacier lost ~46 million m^3 of ice, firn and snow, with an accumulated geodetic mass loss of -13.6 m water equivalent during the 10-year period (Kjøllmoen, 2019). A final comparison is also be made against the study of Nussbaumer et al. (2011) who also quantified glacier length changes at Jostedalsbreen since LIA maximum (~1750). They found that the Nigardsbreen outlet glacier from the Jostedalsbreen ice cap receded ~4,500 m (~29%) between LIA maximum and 1990, after which a small, short-lived, re-advance was recorded (Nussbaumer *et al.*, 2011). In comparison, the mean reduction in length of the 15 reconstructed glaciers in our study was ~442 m (~33%) between LIA maximum (~1814) and 1989, with no re-advance recorded during the period of observation.

One substantial trend that was evident in our LIA reconstructions was that all glaciers with area losses >50% between LIA maxima and 1989, appear to have been

fronted by at least one proglacial lake, given the presence of present-day lakes within LIA moraine boundaries. Ice-marginal proglacial lake development and growth generates a series of positive feedbacks which can accelerate glacier recession, primarily as a result of increased ablation through thermal melting and calving (Carrivick and Tweed, 2013). Furthermore, a proglacial lake increases the amount of water at the bed of the glacier, accelerating ice flow velocity, which in turn leads to glacier thinning and increased recession (Carrivick and Tweed, 2013). Proglacial lake development in the study area appears to be the main driver for some glaciers having experienced greater area reductions since LIA maximum than glaciers terminating on land (Figure 4.12).

The relationship between absolute reduction in glacier area and glacier length is strongest over the period LIA-1989 (Figure 4.14a, b). Glaciers that have lost the largest area have, in general, also experienced the greatest length changes. This is not surprising given that most of these were valley glaciers at their LIA maximum and will have experienced most retreat in their lowermost reaches. It is also interesting to note that when only including those glaciers fronted by proglacial lakes (n = 5) the R^2 values increase to 0.9, suggesting that the development of lakes enhances glacier retreat.

For the glaciers where historical mapped extents correspond with the Andreassen et al. (2012a) outlines (n = 84; Figure 4.15), a more detailed examination of glacier change was possible. Overall, glaciers exhibited net retreat during the period 1907-1989, broadly in-line with that in other areas of northern Norway such as Høgtuvbreen in Nordland and Langfjordjøkelen in Finnmark (Andreassen *et al.*, 2000a, 2012b; Theakstone, 2010; Winsvold *et al.*, 2014). Conversely, in region A of our study area (Figure 4.1), the historical outlines dated to 1956 (n = 12 glaciers), appear to show an increase in glacier area (Figure 4.15V). Given no such increase in glacier area for Troms County is reported elsewhere in the literature over this period (1950-1989), coupled with our results showing similar sized glaciers within our study area all exhibiting glacier area loss; it is therefore, believed that this apparent increase in glacier area is an artefact of the historical mapping under-represented the full extent of glaciers in 1956, leading to an apparent increase in glacier area in 1989.

Overall, the larger reduction in glacier area towards the end of the 20th century represents an increasing rate of shrinkage from 0.2% yr^{-1} to -0.5% yr^{-1} (Figure 4.15), which results in a larger shrinkage of glaciers in central Troms and Finnmark

compared to their southern counterparts. Additionally, our study reveals a greater percentage glacier area reduction, which is, in part, attributed to the larger proportion of smaller glaciers throughout the study area.

4.6.2.2. 1989-2018

The identification and mapping of 78 more glaciers (n = 219), than are included within Andreassen et al. (2012a) (n = 141), was possible owing to the use of multiple, overlapping, very high-resolution aerial orthophotographs from different time steps (available from https://www.norgeibilder.no). Cross checking of snow/ice units on aerial orthophotographs (especially those in shadow) was particularly useful when differentiating between a potential very small glacier (<0.5 km^2) and a snowpatch. The 23 additional glaciers classified as *certain*, on the 1989 imagery (Table 4.3), all show evidence of flowing ice in the form of crevassing and/or ice deformation. The mean size of these 23 additional glaciers was only 0.12 km^2 in 1989, and by 2018, the mean size had reduced to 0.03 km^2 (a 75% reduction). The distribution of the 23 additional *certain* glaciers across our study area shows that very small glaciers in mountain valleys and cirques are most easy to overlook by large scale glacier inventories (Leigh et al., 2019); 13 reside within region A, eight reside within region B, one resides within region C, and the final glacier is a standalone unit in western Finnmark. The remaining glaciers classified as *probable* and *possible* on the 1989 imagery (n = 10 and 45 respectively; Table 4.3), show only partial evidence of glacier characteristics. Additional evidence is, however, needed (i.e. additional snow free high-resolution imagery or ground truthing) before the *probable* and *possible* units can be confirmed to be a *certain* glacier or refuted and re-classified as *perennial snow*. The importance of mapping such previously unrecorded units, has been highlighted by Parkes and Marzeion (2018) who note that failure to consider uncharted glaciers may be an important cause of difficulties in closing the Global Mean Sea Level Rise budget during the 20th century.

The overall net area reduction of glaciers within the study area from 101.8 km^2 to 66.4 km^2 between 1989 and 2018 (Table 4.3), is in line with the vast majority of reports on glacier change, both regionally and globally (e.g. Andreassen *et al.*, 2012a; Frey *et al.*, 2012; Haeberli *et al.*, 2013; Stokes *et al.*, 2018). The observed glacier shrinkage indicates an approximate reduction in area of ~1% yr^{-1} between 1989 and

2018, with the largest period of glacier shrinkage between 1994 and 1999 (a net areal reduction of 14.1 km^2 or 15%; Table 4.3). In contrast, a short period of annual cooling between 1995 and 1999, coupled with increased winter precipitation culminating towards the end of the 1990s, was likely responsible for the period of minimal reduction in glacier area between 1999 and 2006. Overall, our results indicate northern Troms and western Finnmark saw a substantial reduction in glacier area towards the end of the 20th century.

The lower total area loss recorded between 2006 and 2018 (Table 4.3), coincided with warmer air temperatures and this apparent anomaly may be explained by the observed recession and fragmentation of small glaciers into heavily shaded positions (Figure 4.16). It has been demonstrated that where glaciers do not extend far beyond the shade of a cirque backwall they are likely to receive greater mass inputs (e.g. increased snow from wind drift and/or avalanching) and be more shielded from direct solar radiation (Kuhn, 1995; DeBeer and Sharp, 2009). In turn, glaciers now situated within deep cirques are likely to have differing responses to climate change than when they were larger, or when compared to larger valley and outlet glaciers within the study area (DeBeer and Sharp, 2007; Brown *et al.*, 2010a). There is, therefore, potential for the retreating glaciers in the mountain belts of central Troms and Finnmark to transition into a state of reduced retreat once a critical threshold has been met (in terms of shielding and mass input), and as a result they may experience reduced rates of mass loss.

Finally, when examining the relationship between absolute reduction in glacier area and glacier length, over the period 1989-2018 (Figure 4.14c, d), the correlation is much weaker than for over longer-time scales (Figure 4.14a, b), i.e. those glaciers that lost a greater absolute area did not always experience a greater length change. This contrasts with the relationships between the LIA and 1989 (Figure 4.14a, b) and is likely to reflect the transition from a valley-influenced hypsometry to a more upland cirque hypsometry. In the case of the valley-influenced hypsometry, the glacier is more prone to rapid change with a greater proportion of the glacier body below the ELA. Due to many glaciers having a valley-influenced hypsometry at the end of the LIA, the warming in the early-20th century would have had had the greatest effect when their frontal positions were further from the ELA. Subsequently, glaciers receded into more sheltered positions within cirques and their shapes have changed to be more circular, and with retreat taking place more evenly around their perimeter.

4.6.2.3. Glacier size and area change

Our study shows that generally smaller glaciers (e.g. <1 km^2) have decreased less in their absolute area (km^2) but experienced a larger relative (%) reduction (Figure 4.19 and 4.20), consistent with findings from other glacierised regions such as; Canada (Tennant *et al.*, 2012), Nepal (Ojha *et al.*, 2016), and Mongolia (Pan *et al.*, 2018). The glaciers in the central and western mountain belts (region A and B; Figure 4.1) have undergone the largest relative reduction in their glacial extent (Figure 4.20) and it is the glaciers that were <0.05 km^2 in 1989 which experienced the largest percentage loss in glacier area. In contrast, some of the largest glaciers within the Troms and Finnmark region have experienced absolute area loss of >0.5 km^2 since 1989, with these values only representing a small relative (%) reduction in area.

As glaciers shrink there is also a tendency for them to disintegrate into smaller individual fragments (Paul et al., 2004) and this was observed throughout northern Troms and western Finnmark, with ~22% of glaciers having fragmented between 1989 and 2018 (Table 4.3, Figure 4.21). Glacier fragmentation results in a positive feedback of increased shrinkage, due to the greater perimeter-to-area ratios of glacier fragments compared to larger parent units (Paul *et al.*, 2004). Changes to the localised thermal radiation regime (e.g. increased bedrock exposure lowering surface albedo) results in higher melt rates. Furthermore, where individual glacier fragments become detached from their tributaries, they receive less (possibly no) input (Paul *et al.*, 2004; Jiskoot and Mueller, 2012; Carturan *et al.*, 2015). Glacier fragmentation further complicates a glaciers' response to climate change and disproportionately affects those glaciers in exposed and/or low elevation positions.

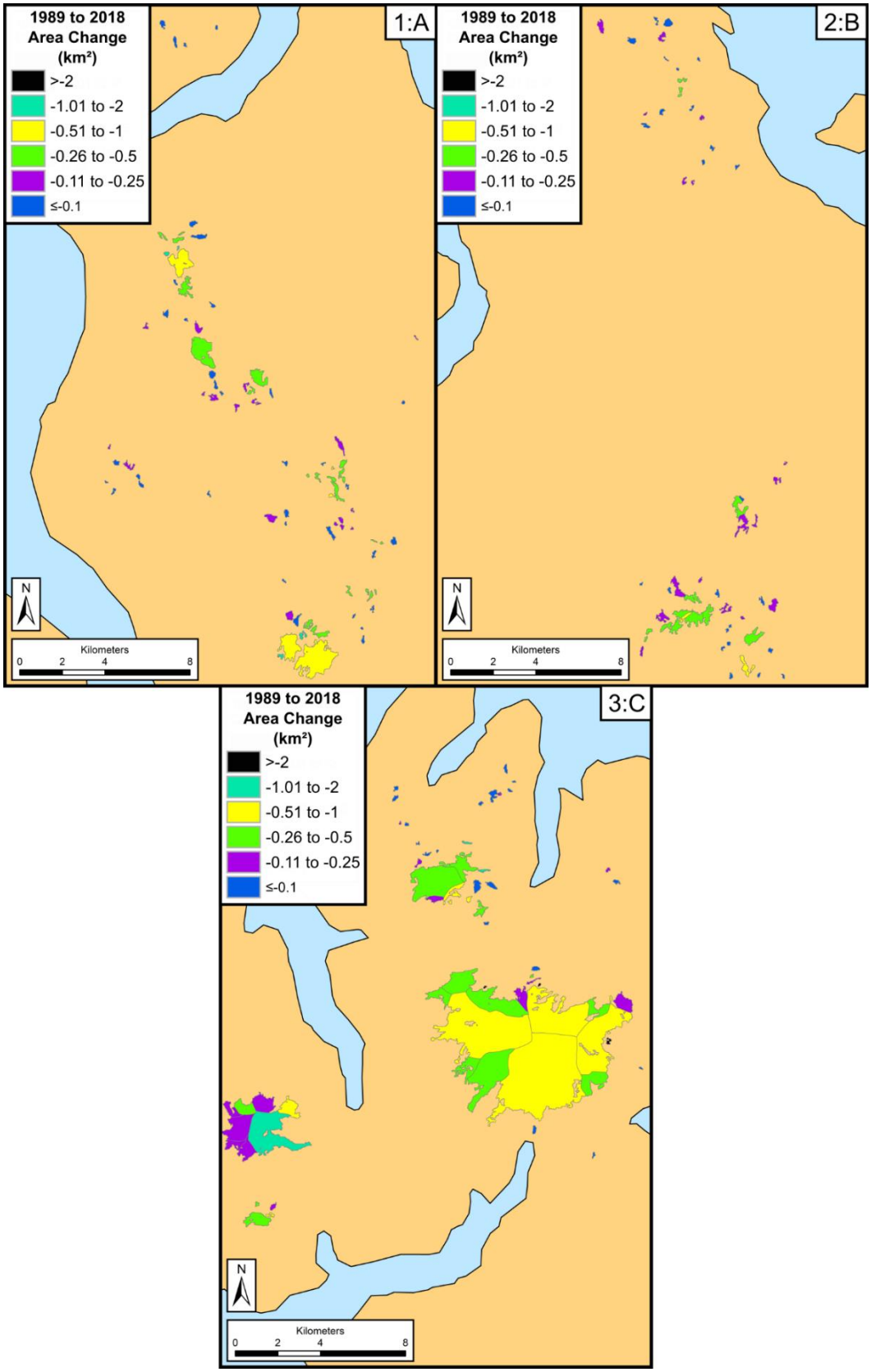

Figure 4.19. *Colour coded map of absolute glacier area change (km²) from 1989 to 2018. Panels 1, 2, and 3, show the predominantly glaciated parts of regions A, B, and, C as outlined in Figure 4.1.*

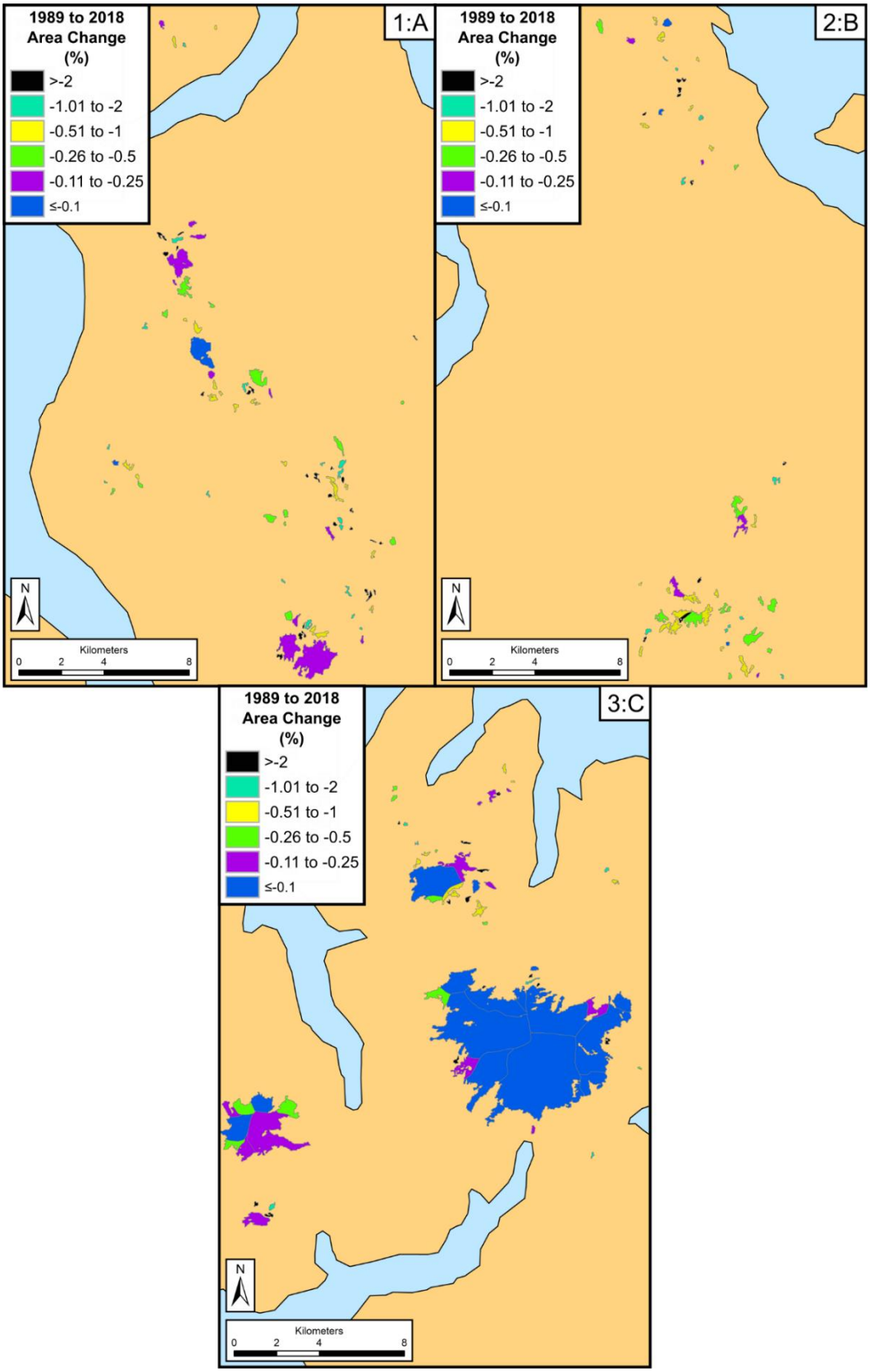

Figure 4.20. *Colour coded map of relative glacier area change (%) from 1989 to 2018. Panels 1, 2, and 3, show the predominantly glaciated parts of regions A, B, and C as outlined in Figure 4.1.*

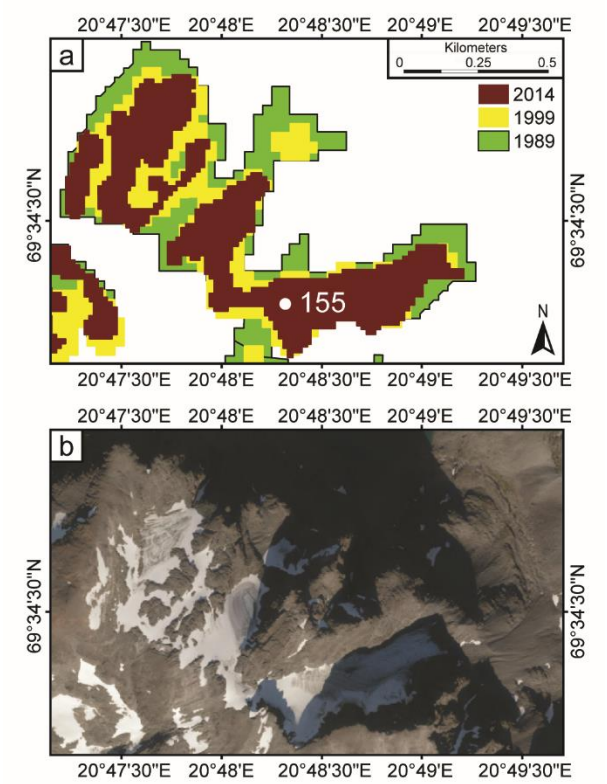

Figure 4.21. *An example of glacier fragmentation over time: (a) glacier ID 155 mapped as one unit in 1989, as two units in 1999 (the main body and an isolated (glacier) ice patch from its central tongue), and as three separate units in 2014 (the 1999 ice patch has shrunk below the 0.01 km² size-threshold); (b) aerial orthophotograph showing glacier 155 in 2016 (https://www.norgeibilder.no; 16.09.2019). Note: while it is possible to discern the very small glacier fragment that shrunk below the 0.01 km² size-threshold on the aerial imagery (0.25 m resolution), it was not possible to accurately map it on the satellite imagery (15 m resolution).*

4.6.3 Future evolution of glaciers in northern Troms and western Finnmark

Climate projections 2071-2100 for Norway indicate a median increase in annual mean air temperature of 4.5°C, with the largest warming occurring in northern Norway (Hanssen-Bauer *et al.*, 2017). Regional temperature predictions for the former Troms County, during the period 2021-2050 indicate a median increase in annual temperature of 1.9 °C (Hanssen-Bauer *et al.*, 2015). Over the period 2021-2050, the precipitation for the former Troms County is set to increase annually by between 2.7 and 23.2%, yet the winter precipitation might either decrease by 6.4% or increase by 19.9% (Hanssen-Bauer *et al.*, 2015). The greater variance in precipitation predictions

highlights the greater uncertainty in future precipitation patterns compared to air temperature changes. Any increase in winter precipitation will, however, be offset by increases in summer temperature that led to a longer ablation season and higher melt (Stokes *et al.*, 2018). Furthermore, due to increasing temperatures - both annually and seasonally - a higher ratio of precipitation falling as rain is expected (IPCC, 2013, 2019; Berghuijs *et al.*, 2014). Increased rainfall throughout the year can increase surface melting of ice and snow and therefore any increased precipitation is unlikely to mitigate the impacts of temperature increase; hence glaciers are likely to continue to retreat and/or down-waste (Oltmanns *et al.*, 2019).

For the Langfjord East outlet glacier on the Bergsfjord Peninsula, Andreassen et al. (Andreassen *et al.*, 2012b) have suggested that there is a possibility it will disappear completely within the next 50-100 years. Furthermore, glacier recession is most acute for glaciers of <0.05 km^2 at elevations <1,400 m a.s.l. (Stokes *et al.*, 2018); as of 2018 these criteria are met for ~60% of mapped glaciers within our study area. Given our dataset indicates that 71% of all mapped glaciers in the study area have lost ≥50% of their area, during the period 1989-2018, it is therefore plausible that many glaciers in the Troms and Finnmark region may disappear within the next 50-100 years (Nesje *et al.*, 2008; Andreassen *et al.*, 2012a, 2012b; Stokes *et al.*, 2018). There is, however, potential for topography to play a role in the preservation of ice bodies which exist in areas of heavy shade and/or debris supply. Glaciers which exist in deep cirques are prone to heavy shading, relatively high mass inputs from snow avalanching and/or wind drift, and increased debris supply (Johnson, 1980; Kuhn, 1995) which in turn has the potential to decouple them from the climate system (DeBeer and Sharp, 2009; Brown *et al.*, 2010a). The presence of topographically induced, glacier-climate decoupling is therefore likely to result in some, cirque glaciers being preserved in the future. As a result there is the possibility that some of these optimally situated ice bodies may outlast the larger glaciers and ice caps located on exposed plateaus, which have no protection from a warming and wetting climate (Hanssen-Bauer *et al.*, 2015; IPCC, 2019).

4.7. Conclusions

This paper presents new data on glacier change throughout central Troms and Finnmark County, northern Norway, from the LIA maxima to 2018; using lichenometry, historical maps, existing glacier inventories, and new remotely sensed glacier outlines. The LIA maxima for a series of small glaciers in the Rotsund Valley occurred between 1814 (±41 yrs) and 1877 (±34 yrs), earlier than has been reported for the larger glaciers on the nearby Lyngen Peninsula. Extrapolation of our LIA reconstructions, to 11 other glacier forelands, has shown that glaciers were between 15% and 68% larger at their LIA maximum than in 1989. Out of the 15 glaciers with LIA reconstructions, all glaciers exhibiting >50% area loss between the LIA maximum and 1989, are fronted by proglacial lakes within the confines of the LIA maximum moraine.

Analysis of historical maps has shown that throughout the first half of the 20th century, glacier recession was minimal (~0.2% yr^{-1}) but between 1966 and 1989, rates of glacier recession had more than doubled (~0.5% yr^{-1}; Figure 4.15). Implementation of a new glacier identification scoring system, using multiple very high-resolution aerial orthophotographs (0.25 m resolution) to cross check mapping of coarse resolution satellite imagery (30-15 m resolution), enabled the identification and mapping of 78 additional glaciers in 1989 (23 of which are classified as *certain*), that were not included in the Inventory of Norwegian Glaciers (Andreassen *et al.*, 2012a). Over the 29-year period of satellite observation (1989-2018), we document a 35.4 km^2 reduction in glacial area (35%) within central Troms and Finnmark County. The greatest glacier area loss occurred between 1994 and 1999, with a net reduction of ~2.8 km^2 yr^{-1} (20% yr^{-1}) linked to a period of annual warming initiated ~1985. Our analysis has confirmed that it is the very small glaciers (<0.5 km^2) that show the highest relative shrinkage and as of 2018, over 90% of glaciers mapped were <0.5 km^2 in their areal extent (Table 4.3). Finally, we suggest where topographical setting permits (e.g. deep shaded cirques), very small glaciers within central Troms and Finnmark County could outlast the larger ice caps located on the elevated and exposed plateaus.

4.8. Acknowledgements

Firstly recognition and appreciation must go to the Alpkit Foundation whose grant provided monetary funding and to Lexus Norway, who provided a vehicle for JRL to use during fieldwork. JRL thanks Robert Leigh and James Linighan for fieldwork assistance. A tremendous thanks must be given to the Norwegian Mountain Rescue and the staff at the University Hospital of North Norway who attended to JRL's field partner after a severe injury and to Henry Patton who was able to drive JRL back to the field site to collect his abandoned equipment. Landsat 5 TM, 7 ETM+, and 8 OLI imagery were downloaded free of charge from the USGS Earth Explorer website (https://earthexplorer.usgs.gov/), and aerial orthophotographs were kindly provided by the Norwegian Mapping Authority (Kartverket). Prior glacier data as collated by the CryoClim project were also used, including glacier out- lines downloaded directly from the Norwegian Water Resources and Energy Directorate (NVE) website (www.nve.no/hydrology/glaciers/glacier-data/). Finally, we thank the editors (A.E. Jennings and J.C. Yde), and we are grateful for the comprehensive reviews provided by an anonymous reviewer and Stefan Winkler, who also shared insight and lichenometric data from the Svartisen region of northern Norway.

CHAPTER 5

Glacial and periglacial geomorphology of central Troms and Finnmark county, Arctic Norway

Leigh J.R.[1], Evans D.J.A.[1], Stokes C.R.[1], Andreassen L.M.[2], Carr J.R.[3]

[1]Department of Geography, Durham University, Durham, UK; [2]Norwegian Water Resources and Energy Directorate (NVE), Oslo, Norway; [3]School of Geography, Politics and Sociology, Newcastle University, Newcastle upon Tyne, UK

Looking across Grøtsundet, to the west of Ullsfjord, into the small valley occupied by the glacier ID 364 (69°51'N, 19°14'E).

Photograph date: 06th September 2018 (by J.R. Leigh)

A version of this chapter has been published as:

Leigh, J.R., Evans, D.J.A., Stokes, C.R., Andreassen, L.M. and Carr, R.J., 2021. Glacial and periglacial geomorphology of central Troms and Finnmark county, Arctic Norway. *Journal of Maps*, **17**(2), 348-366.

“And I know that we've still got time
But I do not think we're invincible
And I'm thinking that it's a sign”
(Reynolds, 2009)

5.1. Abstract

Here we present a glacial and periglacial geomorphological map of a ~6,800 km^2 region of central Troms and Finnmark county, Arctic Norway. The map is presented at a 1:115,000 scale with the aim of characterising the spatial distribution of glacial and periglacial landforms and facilitating the reconstruction of the glacial history of the region during the latter stages of deglaciation from the Last Glacial Maximum and into the Holocene. Mapping was conducted predominantly by manual digitisation of landforms using a combination of Sentinel-2A/2B satellite imagery (10 m pixel resolution), vertical aerial photographs (<1 m pixel resolution), and Digital Elevation Models (10 and 2 m pixel resolution). Over 20,000 individual features have been mapped and include: moraines (subdivided into major and minor moraines), ridges within areas of discrete debris accumulations (DDAs), flutings, eskers, irregular mounded terrain, lineations, glacially streamlined bedrock, possible glacially streamlined terrain, pronival ramparts, rock glaciers (subdivided into valley wall and valley floor, and rock glacierized moraines), lithalsas, contemporary glaciers and lakes. The map records several noteworthy large moraine assemblages within individual valleys, forming inset sequences from pre-YD limits up to the 2018/19 ice margins and represents a valuable dataset for reconstructing Holocene glacial and periglacial activity.

5.2. Introduction

Since the retreat of the Scandinavian Ice Sheet (Mangerund, 2004; Hughes *et al.*, 2016) over continental Norway, the Norwegian Arctic has been subject to a complex pattern of glacial advance and retreat cycles (cf. Nesje *et al.*, 2008; Solomina *et al.*, 2015). The multitude of large scale, and sometimes rapid, glacier fluctuations has produced a complex landscape signature of glacial and periglacial features and surficial materials (Olsen *et al.*, 2013). However, the most recent glacier advance during the Little Ice Age (typically within the past ~200 years: Ballantyne, 1990; Leigh *et al.*, 2020) is thought to have been the most extensive neoglacial advance and has likely overridden glacial deposits formed during the mid- to late-Holocene (Matthews *et al.*, 2000, 2005).

Norway has a rich history of glaciological and geological investigations with fjords of northern Norway having been studied since the late-1800s/early-1900s (e.g. Helland, 1899; Vogt, 1913; Grønlie, 1931). Detailed investigations into the bedrock geology and Quaternary surficial geology have also been carried out across the region, chiefly funded and compiled by the Geological Survey of Norway (Norges Geologiske Undersøkelse: NGU). There have also been several glacier inventories providing information regarding their characteristics and local geomorphology (Østrem *et al.*, 1973; Andreassen *et al.*, 2012a). However, while there is good knowledge about the Quaternary history, the patterns and extent of mountain glaciation across Arctic Norway throughout the Holocene, remains less well examined, especially when compared to southern Norway, or the European Alps. Indeed, within central Troms and Finnmark County only a small number of detailed, site-specific studies have been undertaken with the aim of reconstructing glacier change since the termination of the YD. Areas covered include Ullsfjord (e.g. Holmes and Andersen, 1964), Lyngenfjord (Andersen, 1968), the Lyngen peninsula (e.g. Ballantyne, 1990; Bakke *et al.*, 2005a), the Bergsfjord Peninsula (e.g. Evans *et al.*, 2002; Wittmeier *et al.*, 2015), the Rotsund Valley (Leigh *et al.*, 2020), and the island of Arnøya (Wittmeier *et al.*, 2020). Most of the more isolated mountain and plateau regions of central of Troms and Finnmark County have received little or no attention.

To decipher the intricate assemblages of individual landforms and improve our understanding of the complex mountain and fjord landscape of central Troms and Finnmark County, we have produced a comprehensive, high-resolution (e.g. <1 m)

map of the regions glacial and periglacial geomorphology (main map; Appendix and online: doi.org/10.1080/17445647.2021.1950580). The resulting dataset of this Arctic landscape will provide the foundation for new interpretations of mountain glacier dynamics and landscape response to deglaciation since the termination of the YD (~11,700 yrs BP; Lohne *et al.*, 2012), throughout the Holocene and up to the present day, further refining existing models of mountain glacial landsystems and their use in paleoglaciological reconstructions (Evans *et al.*, 2002, 2016b, 2016b, 2017b, 2018; Benn *et al.*, 2003; Hättestrand and Clark, 2006; Chandler and Lukas, 2017; Darvill *et al.*, 2017; Bickerdike *et al.*, 2018b; Martin *et al.*, 2019; Chandler *et al.*, 2019). Moreover, the mapping of periglacial landforms provides a baseline for a refined understanding of their development, particularly for some of the more controversial, hybrid landforms, such as rock glaciers, that evolve from a range of antecedent conditions and hence demonstrate equifinality (Whalley and Martin, 1992; Evans, 1993; Berthling, 2011). Additionally, the mapping and monitoring of the development of periglacial landforms remains important, especially in Arctic and alpine environments, as it is likely that periglacial processes will play an increasingly dominate role in landscape evolution in the future (Ravanel and Deline, 2011; Huggel *et al.*, 2012; Stoffel and Huggel, 2012; Ballantyne, 2018). The increasing prevalence of periglacial processes will likely result in new and/or increased risk to communities within the periglacial domain such as from RSF or infrastructure damage owing to melting permafrost (e.g. Stoffel *et al.*, 2014; Arenson and Jakob, 2015; Jaskólski *et al.*, 2017; Eriksen *et al.*, 2018; Hjort *et al.*, 2018; Matthews *et al.*, 2018).

In addition to its employment in landsystem developments and applications, this map will also underpin reconstructions of glacial chronologies for the central Troms and Finnmark region, an Arctic area with a cryospheric system particularly susceptible to rapid climate change (IPCC, 2019). This extends the findings of Evans et al. (2002) and Rea and Evans (2007), whose work across the Bergsfjord Peninsula (~12 km north-east of the study area) illustrated the value of comprehensive landsystem mapping across a whole glacierized region with a topographic complexity that dictates the variable nature of post YD glacier-climate responses and hypsometric change in mountain glacier systems, particularly in plateau icefield and fjord head settings.

5.3. Study area and previous work

The mapping conducted in this study focuses on an area of central Troms and Finnmark County (in the northern region of the former Troms County), between ~69°11'-70°02' N and ~19°28'- 21°50'E (Figure 1). Geographically, the area extends from the Lyngen Peninsula (otherwise known as the Lyngen Alps) in the west, to the large valley, Navitdalen in the east; and includes the small, glaciated islands of Uløya and Kågen in the north (Figure 1). The region is predominantly characterized by alpine and plateau type mountain terrains (reaching an altitude of 1,834 m a.s.l; at Jiehkkevárri 69°28'N-19°52'E) with steep sided valleys and fjords in coastal areas, contrasting with inland terrain to the south/south-east comprising an elevated plateau stretching across to the Norwegian border. There is also a considerable west-east precipitation gradient across the study area for example, between 1966 and 2019 total yearly precipitation averages ~997 mm yr^{-1} to the west of our study area (station No. 90490) whereas at the eastern margins (station No. 92350) the total yearly precipitation averages less than half that of the west at only ~468 mm yr^{-1}.

The three largest fjords in the study area are Ullsfjorden (75 km long) and Lyngenfjord (82 km long) flanking the Lyngen Peninsula (to the west and east respectively), and Kvænangen (72 km long). Glaciers are found in the small mountain ranges that border the fjords particularly on the Lyngen Peninsula (Andreassen et al., 2012a; Stokes et al., 2018), and most are valley and cirque glaciers (some connected with several units as glacier complexes such as Strupbreen and Koppangsbreen, IDs 200 and 205 respectively), with several plateau icefields (Whalley *et al.*, 1981; Rea *et al.*, 1999; Stokes *et al.*, 2018), and one small ice cap (Noammerjiehkki, ID 158). In this paper we use the glacier IDs and names following the Inventory of Norwegian glaciers (Andreassen *et al.*, 2012a). Beyond the glacierized areas, most of the land surface is underlain by permafrost, with the lower altitudinal limit of sporadic permafrost potentially reaching as low as ~150 m a.s.l. (Gisnås *et al.*, 2017). Much of the mountain and highland plateau within the study area is, therefore, within the periglacial domain, evidenced by large areas of gelifluction sheets and/or patterned ground and the periglacial reworking of glacial landforms for example permafrost creep or rock glacierization of moraines (Vere and Matthews, 1985; Evans, 1993; Ó Cofaigh *et al.*, 2003; Evans *et al.*, 2016b).

During the last glaciation, the uplands and fjords throughout the area were covered by the Scandinavian Ice Sheet, with the most credible position of the ice sheet margin terminating on the continental shelf ~16,000 yrs BP (Hughes *et al.*, 2016). The northern margin of the study area was deglaciated ~15,000 yrs BP and regional ice stood at the mouths of the major fjords (e.g. Ullsfjorden, Lyngenfjord, and Kvænangen) at ~13-12,000 yrs BP (Stokes *et al.*, 2014; Hughes *et al.*, 2016; Figure 5.1). By ~11,000 yrs BP it had likely receded to the southern limits of our study area (Stokes *et al.*, 2014; Hughes *et al.*, 2016; Figure 5.1). Therefore, in the period since the termination of the YD, the central Troms and Finnmark region was likely characterised by large valley glaciers extending beyond individual cirque basins as well as into valley heads surrounding the numerous plateaux; at that time, there would also have been extensive periglacial activity in the recently deglaciated terrain.

Recent compilation of surficial geological maps from the 1980s to the 1990s such as the 1:50,000 Quaternary geological maps (Bergstrom and Neeb, 1978; Tolgensbakk and Sollid, 1988 etc.) for the entirety of former Troms County was carried out by Sveian et al. (2005) at a 1:310,000 scale. This mapping defined 22 Quaternary superficial deposits (including till, marginal moraine, glaciofluvial deposit, lacustrine deposits etc.) all mapped as closed polygons (through the process of scanning and vectorization of historical maps). The scale of mapping resulted in frequent grouping of large swaths of closely spaced yet independent moraines into one feature, which is especially true for valley head and within valley moraine systems. Additionally, in the recently deglaciated forelands (e.g. since the Little Ice Age) the classification of “Bart Fjell / Bare Rock” is usually accompanied by the description that these areas lack material with more than 50% of the area comprised solely of bedrock (Sveian *et al.*, 2005; NGU, 2021) and, as a result, do not map a wealth of medium- to small-scale glacial geomorphological features including: rock glacierised moraines, minor moraines, flutings etc.

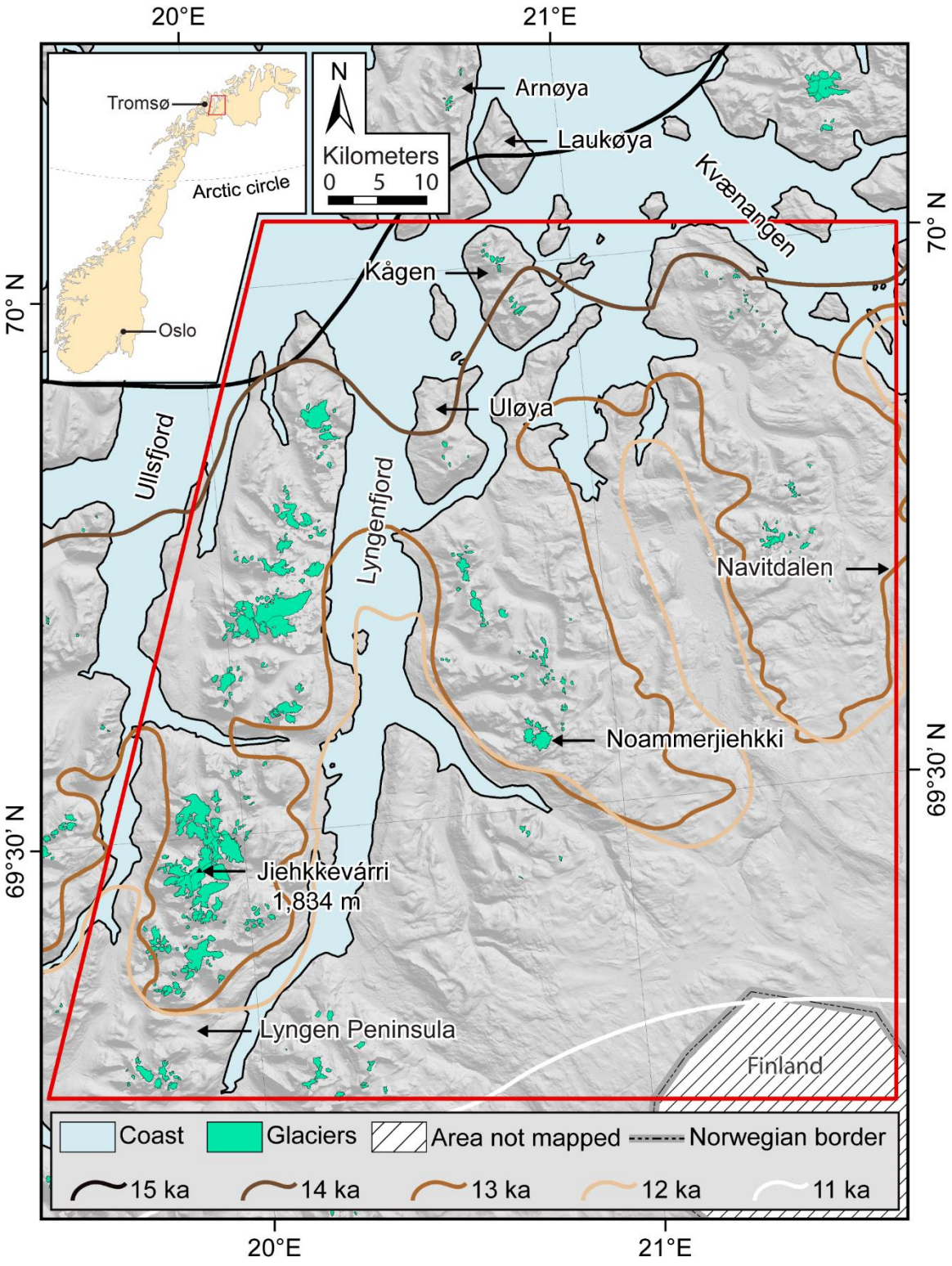

Figure 5.1. *Location map showing the study site (within the red frame) in central Troms and Finnmark county, northern Norway, with site location within Norway shown on the inset map. The inset outlines show the most credible margin of the Scandinavian Ice Sheet as it retreats inland at 1,000-year intervals as reconstructed by Hughes et al. (2016). The base image is a composite of 2 m resolution hill-shaded Arctic DEM tiles*

and the glaciers are shown using glacier outlines from the Inventory of Norwegian Glaciers (Andreassen et al., 2012a).

Furthermore, previous research in the region employing detailed geomorphological mapping in glacial/periglacial investigations include those of Whalley (1976), Griffey and Whalley (1979), Ballantyne (1990), Gordon et al. (1992) and Bakke et al. (2005a), Greig (2011), which all focus on individual valleys or valley features on the Lyngen Peninsula. On northern Lyngen, Whalley (1976) and Griffey and Whalley (1979) identify rock glacier complexes within Strupskardet and Veidalen, respectively. On the true right (eastern/south-eastern) lateral margin of Strupbreen (glacier ID 200; Andreassen *et al.*, 2012a) within Strupskardet, a rock glacier and series of moraines are identified and mapped, with the rock glacier being depicted as an aggregated lateral moraine and rock glacier assemblage diverted around a rock spur and down a small valley-side niche (Whalley, 1976). There have also been several studies of the proglacial lake Strupvatnet (in contact with Strupreeen), dating back to 1898 (cf. Whalley, 1973) which have enabled detailed investigations into lake development and drainage events (e.g. Liestøl, 1956; Aitkenhead, 1960; Whalley, 1971, 1973). On the southern side of Veidalen, a series of moraines and a duel lobed rock glacier originating from two north-facing cirques, occupied by unnamed glaciers ID 188 and 189 (Andreassen *et al.*, 2012a), have been mapped; the rock glacier is depicted as two large and connected lobes, the proximal margins of which were interpreted to be ice-cored hummocks (Griffey and Whalley, 1979). Additional work in Strupskardet by Bakke et al. (2005a) identified moraines fronting the glaciers of Eastern and Western Lenangsbreen (glacier ID 199 and 201, respectively). Their geomorphological map depicts a series of 13 moraines, which are used to reconstruct the glacial history of the Lenangsbreen glacier/s and are associated with other geomorphological features, including meltwater channels, fossil protalus rock glaciers, former shorelines, till, glaciofluvial deposits, blockfields, avalanche deposits, talus, and peat accumulations (Bakke *et al.*, 2005a).

On southern Lyngen, the glacial and periglacial geomorphology constrained within the valley of Fornesdalen is depicted in detail by Ballantyne (1990). He mapped six major moraines fronting Fornesbreen (glacier ID 229) as well as ridges within ‘hummocky drift’ (Ballantyne, 1990). Mapping of rockfall/avalanche deposits incorporated within rock glacier boundaries was also undertaken and highlighted the

areas where post-depositional rock-glacier reworking/overriding has affected the lateral portions of some moraines, although the rock glaciers were considered relict at the time of mapping (Ballantyne, 1990). Whalley (1992) also identified a low elevation rock glacier in Ellendalen, noting that this rock glacier appeared to be an extension of the glacier above and inferred that it was glacial in origin.

5.4. Map production

High resolution geomorphological mapping was conducted using remote sensing analysis, with map production based on a combination of full colour aerial orthophotographs (courtesy of the Norwegian Mapping Authority, www.norgeibilder.no), Sentinel-2A/2B satellite imagery (courtesy of the European Spacey Agency (ESA), downloaded from the U.S. Geological Survey), and the Arctic Digital Elevation Model (DEM; Porter et al. (2018) courtesy of the Polar Geospatial Center).

Features were identified and digitally mapped as either vector lines or polygons using ESRIs ArcGIS software (version 10.5.1). Mapping of all landforms, excluding contemporary glaciers and lakes, was conducted by manual digitisation on the orthophotographs, in preference to satellite images, because they show small scale features that are both absent from previous mapping and undetectable on the satellite imagery. Over 2,000 georeferenced orthophotographs with <1 m resolution from 2016 were used for the mapping. Some differences in lighting are generally unavoidable when using aerial imagery and, in cases where this was obvious, it was not considered to impact on image interpretation and mapping. In areas of intense shading, simple brightness and contrast adjustment in ArcMap helped mitigate the impacts of shading.

Mapping of glaciers and lakes was conducted using multispectral satellite imagery and a semi-automated process, to ensure speed and to provide the most current outlines. We used a semi-automated mapping approach utilising a band ratio method to generate initial outlines, followed by manual correction of mapped units to account for glaciers and lakes which were poorly or erroneously mapped (for further details on semi-automated mapping see Raup *et al.*, 2007; Andreassen *et al.*, 2012a; Du *et al.*, 2016; Song *et al.*, 2017; Watson *et al.*, 2018; Leigh *et al.*, 2019, 2020; Nagy and Andreassen, 2019). Glaciers have also been divided in individual units based on drainage divides provided by Andreassen et al. (2012a). Thus, large glacier complexes, like that around Jiehkkevárri (southern Lyngen), are shown as multiple connected polygons partitioned by solid lines. Following Leigh et al., (Leigh *et al.*, 2019) a minimum size-class of 0.01 km^2 (equal to 100 Sentinel-2A/2B pixels) was implemented for the mapping of glaciers. However, because waterbodies are easier to identify and define on satellite imagery, we used a smaller size-threshold of 0.0004 km^2 (equal to four Sentinel-2A/2B pixels) for lakes.

In the absence of localised ground-truthing we used oblique, three-dimensional views, provided by the online features of ‘Norge i Bilder’ (www.norgeibilder.no), and Google Earth, combined with the imagery provided by ‘Google Maps Street View’, ‘Google Maps Community Photosphere’s’ and ‘Google Maps Community Photographs’ (all freely available online courtesy of Google LLC and its contributors) in order to aid landform identification and for cross checking initial landform interpretations. Cross referencing of the large-scale geomorphological features (e.g. eskers, streamlined bedrock, etc.) was also conducted using Sentinel-2A/2B imagery 2018/19 multispectral satellite imagery with a spatial resolution of 10 m and can be viewed with different band combinations, not solely true colour. Finally, the 2 m resolution ArcticDEM, projected using varying hill-shading parameters to account for potential azmith biasing (cf. Smith and Clark, 2005), provided both topographic context, but also a means of identifying changes in topography associated with small scale geomorphological features.

5.5. Description of mapped landforms

In total, ~23,500 glacial features and 1,200 periglacial features were mapped and are described individually in the following sub-sections.

5.5.1. Moraines

Moraine ridges are prominent ice-marginal landform features of formerly and contemporary glaciated landscapes expressed as linear or curvilinear, elongate features exhibiting positive relief (cf. Benn and Evans, 2010). We note that, at the heads of and within individual valleys, moraines may form continuous ridges (generally <100 m long, <10 m high). Most often, however, moraines occur as fragmentary deposits, and along the sides of fjords and on mountain plateaus some fragmentary ridges can be traced for several kilometres. The moraine crests are generally narrow (e.g. 1-5 m wide), yet the combined proximal–distal widths can form ridges >100 m wide, and larger moraine complexes are composed of multiple closely spaced or superimposed ridges (e.g. Figure 5.2). In some areas there are clusters of “saw-tooth” frontal moraine ridges, exhibiting “teeth” pointing down valley and notches pointing up valley (Matthews *et al.*, 1979; Burki *et al.*, 2009; Evans *et al.*, 2017a, 2019b). Within some recently deglaciated terrain there are series of densely spaced moraines that lie generally <15 m apart, likely reflecting annual or possibly sub-annual deposition at highly active glacier margins (Sharp, 1984; Boulton, 1986; Evans and Twigg, 2002; Evans, 2003b; Lukas, 2012; Reinardy *et al.*, 2013; Chandler *et al.*, 2016b, 2020a). Moraines can also coincide with areas of discrete debris accumulations (DDAs; sensu Whalley, 2009, 2012) that form a complex assemblage of ridges and furrows (see section 5.5.2). Overall, moraines are found throughout the region, but the most extensive and/or complex moraine systems are found along the fjords and/or within individual valleys.

Moraines are subdivided into two categories based upon size. Major moraines, either formed of one large feature or a composite formed by the superimposition of multiple moraine crests, have been mapped as polygons, with the boundaries drawn around the proximal and distal slopes (Figure 5.2). Minor moraines (e.g. those <4 m wide), mostly found within likely Little Ice Age glacier limits (see Leigh *et al.*, 2020), are mapped as lines which are drawn along their crests (Figure 5.2).

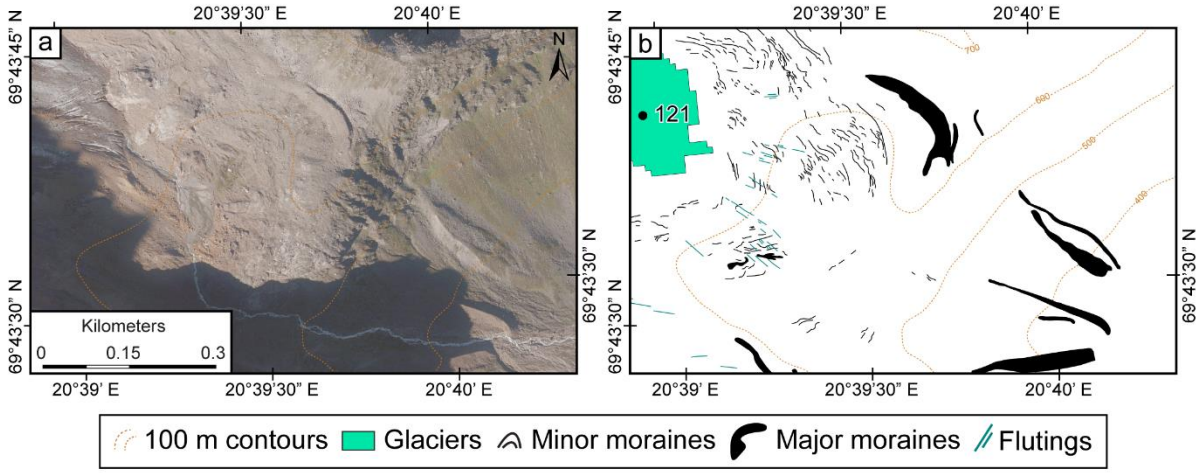

Figure 5.2. *Moraines in the recently deglaciated foreland of glacier ID 121: (a) image from norgeibilder.no (24.08.2016), (b) subset of resulting map (presented at 1:4,000 scale; glacier mapped on Sentinel-2B imagery from 07.09.2018). The densely spaced, small moraines are mapped as lines representing their crests, whereas the broader moraines, in places composed of multiple bifurcating/superimposed ridges (e.g. far right) are mapped as polygons. Note there are also some flutings in the foreland (mapped as lines) which are aligned perpendicular to the moraines. Approximate image location: 69°43'37.85"N, 20°39'10.01"E.*

5.5.2. Ridges within areas of discrete debris accumulations (DDA)

We define small areas (generally <0.2 km^2) of complex, hummocky ridge systems as 'ridges within areas of discrete debris accumulations' (DDAs; sensu Whalley, 2009, 2012). DDA as described by Whalley (2012) is "a non-genetic and descriptive term . . . without any preconceived notion of origin" (Whalley, 2012, p. 3). These features appear as a complex and often disorganised network of ridges and furrows separated by a mix of sediment veneer, boulders, and vegetated ground (Figure 5.3). Ridge crest patterns display no dominant orientation, and ridges are of variable lengths but not exceeding 100 m. Importantly, these DDA ridges differ from moraine ridges because they are short and discontinuous and do not appear to demarcate a clear former ice-margin. Patches of similarly complex ridge systems can be found across the region where they are contained within large latero-frontal moraines.

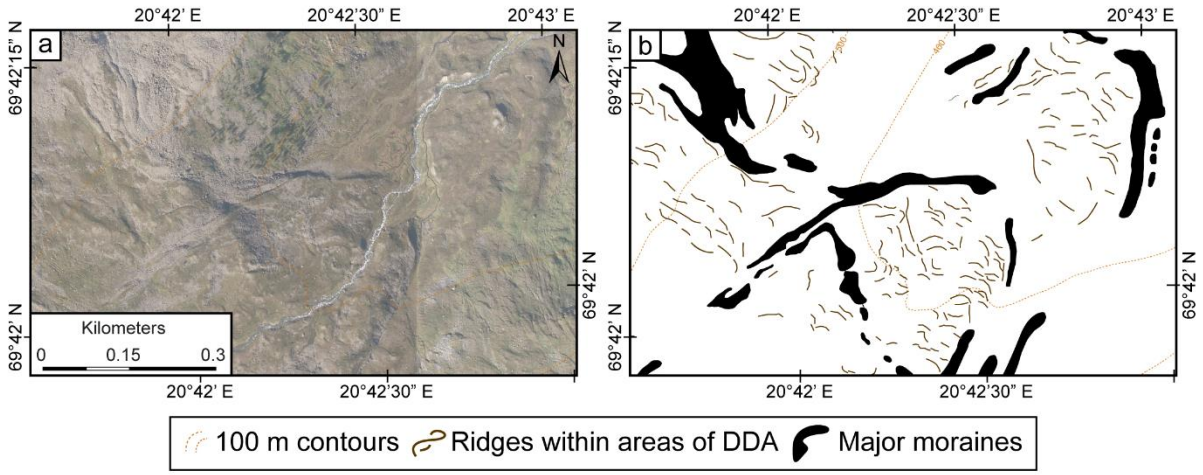

***Figure 5.3**. Ridges within areas of DDA lying inside and abutted up against major moraines: (a) image from norgeibilder.no (24.08.2016), (b) subset of resulting map (presented at 1:4,000 scale). When mapped, these ridges (grey lines) generally show no dominant pattern of orientation. Approximate image location: 69°42'4.18"N, 20°42'21.55"E.*

5.5.3. Flutings

Flutings are closely spaced ridges of sediment aligned parallel to the direction of ice movement and often lying down glacier of embedded boulders or bedrock outcrops (Figure 5.4; e.g. Hoppe and Schytt, 1953; Boulton, 1976; Gordon *et al.*, 1992; Benn, 1994; Evans *et al.*, 2010a). The close grouping of flutings forms a notable ridge and furrow appearance on till covered glacier forelands, aligned at right angles to individual moraines and thereby forming inset arcuate zones separated by moraines and displaying slightly offset alignments (e.g. Figure 5.4). Given their small size, flutings are only visible on the high-resolution orthophotographs and have been mapped as lines.

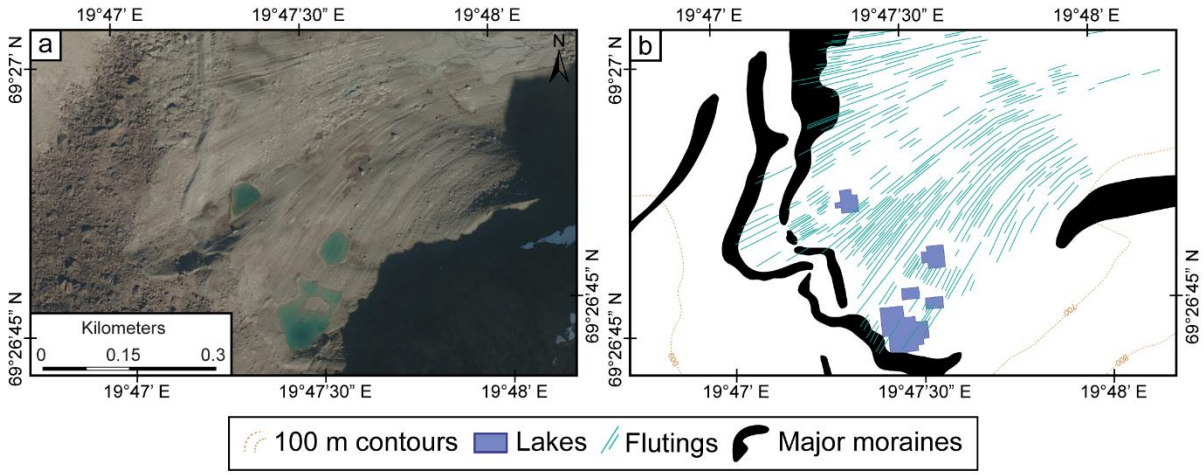

***Figure 5.4**. Flutings on the recently deglaciated foreland of glacier ID 288, showing slight variation in alignment but joining moraine ridges at right angles: (a) image from norgeibilder.no (24.08.2016), (b) subset of resulting map (presented at 1:4,000 scale). Approximate image location: 69°26'54.06"N, 19°47'27.69"E.*

5.5.4. Eskers

A series of distinctive ridges, predominantly in the south-east of the region, have been mapped as eskers. Classification is based on their sinuous planform; extensive length (with consideration of post depositional fragmentation); orientation parallel to sub-parallel with presumed ice flow direction; and oblique to features identified as end moraines (e.g. Price, 1966, 1969; Shilts *et al.*, 1987; Brennand, 2000; Delaney, 2002; Storrar *et al.*, 2014, 2015, 2020). They also appear as lighter-coloured landscape features due to the higher proportion of glaciofluvial material (e.g. sand; Storrar and Livingstone, 2017). Eskers mostly comprise multiple ridges forming integrated networks but can occasionally occur as isolated features (Figure 5.5).

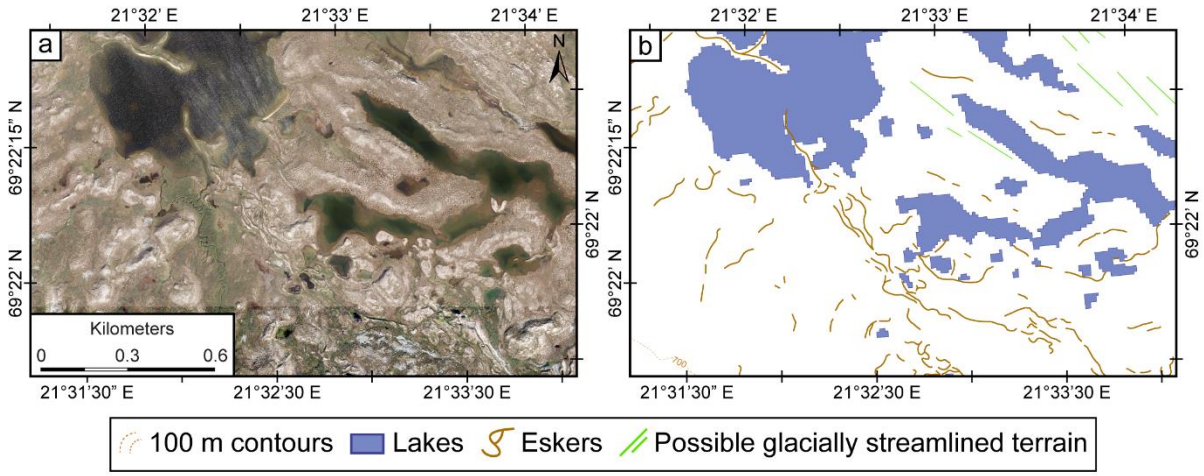

Figure 5.5. *A series of eskers in an area of subdued topography in the plateau region of central Troms and Finnmark: (a) image from norgeibilder.no (24.08.2016), (b) subset of resulting map (presented at 1:8,000 scale). The eskers comprise a simple, linear configuration in the north and a more complex network diverging into multiple flow directions in the east, south-east, and south. Approximate image location: 69°22'6.80"N, 21°32'48.49"E.*

5.5.5. Irregular Mounded Terrain

Irregular mounded terrain comprises series of low relief, disorganized, and irregular mounds, in places intersected by interweaving meltwater channels and small ponds (generally <2,000 m^2, possibly kettle holes; Figure 5.6). This type of terrain broadly occurs as bands ~0.4 km wide and is found only in the south-eastern part of the continental plateau area, near large esker networks. Mapping of individual mounds as polygon features has revealed no pattern to their orientation and shows individual mounds can vary in form from small, simple mounds of ~25 m^2 to larger, branched ridges of ~3,100 m^2 (Figure 5.6). Occasional strips of coarse, bouldery and unvegetated debris occur between mounds. These mounds have a distinctly different morphology to the ridges classified as moraines and/or eskers and, to ensure clarity, we do not classify these landforms genetically. Indeed, the origin of the features is unclear, although a likely genesis could include the incision of meltwater into a thick till cover, the dissection and reworking of extensive and complex esker networks, or the differential melting of highly debris covered glacier ice during the final stages of ice-sheet deglaciation in the region.

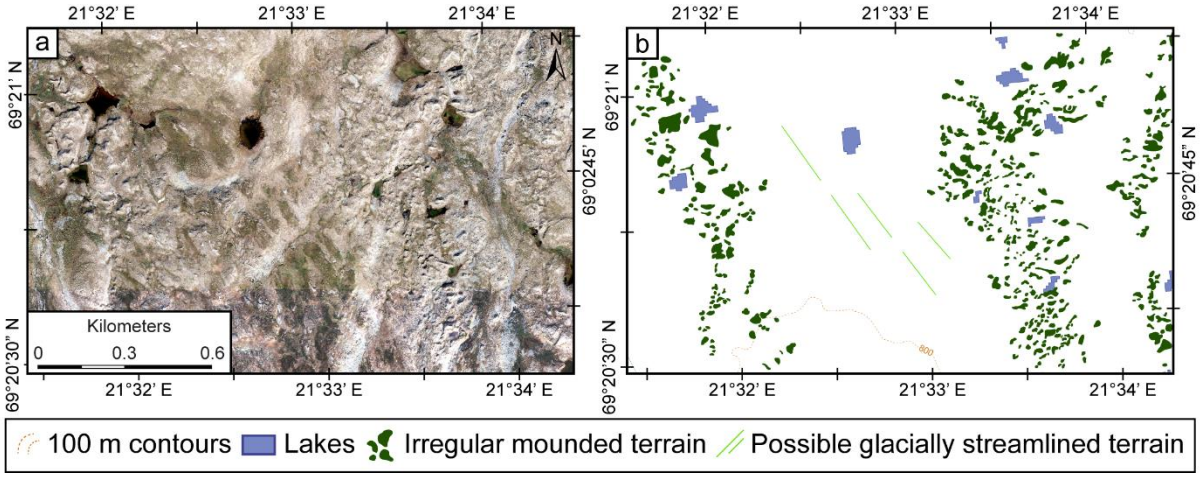

Figure 5.6. *Three swaths of irregular mounded terrain formed in parallel with each other in an area of subdued topography in the plateau region of central Troms and Finnmark: (a) image from norgeibilder.no (24.08.2016), (b) subset of resulting map (presented at 1:8,000 scale). The mounds show no dominant shape or orientation but form bands (≤ 500 m wide) of densely spaced mounds. Approximate image location: 69°20'44.79"N, 21°33'27.13"E.*

5.5.6. Glacial lineations

Glacial lineations are large, straight-crested landforms composed of sediment aligned parallel to the direction of former ice flow and sometimes differentiated as drumlins or mega-scale glacial lineations (found mainly within the large valleys Reisadalen and Navitdalen), with the latter exhibiting much greater length and higher elongation ratios (e.g. Clark, 1993, 1997; Clark *et al.*, 2003; Stokes *et al.*, 2013). Those mapped in this study resemble drumlins and most occur within Reisadalen, a ~3.5 km wide U-shaped valley in the central part of the study area, and on the southwest Finnmark plateau. The lineations are up to 1.4 km long and have been mapped as lines drawn along their crests. Lineations occur near glacially streamlined bedrock features (see Section 5.5.7) with which they are aligned (e.g. Figure 5.7).

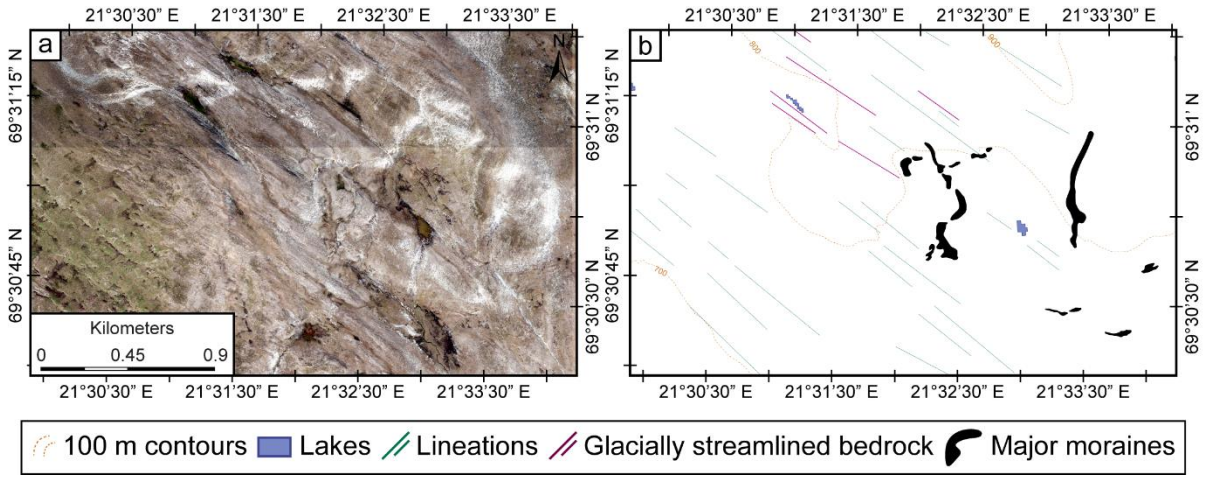

Figure 5.7. *Glacial lineations and associated glacially streamlined bedrock, locally overlain by moraines, and recording a former north-westerly ice flow direction: (a) image from norgeibilder.no (24.08.2016), (b) subset of resulting map (presented at 1:12,000 scale). Approximate image location: 69°30'48.99"N, 21°32'11.01"E.*

5.5.7. Glacially streamlined bedrock

The term 'glacially streamlined bedrock' is used to describe an assortment of (near-) linear landforms composed of bedrock and aligned parallel with the direction of former ice flow, which are mapped as lines. Glacially streamlined bedrock occurs at both small and large scale, meters to hundreds of meters in length and up to several metres in height and width (Figure 5.8). It is important to note that there is potential for identification errors in cases where bedrock structure is aligned closely parallel to streamlined features (Lovell *et al.*, 2011; Darvill *et al.*, 2014), although ice scouring is known to accentuate structural ridges (cf. Bradwell *et al.*, 2008; Livingstone *et al.*, 2010; Krabbendam and Bradwell, 2011; Newton *et al.*, 2018).

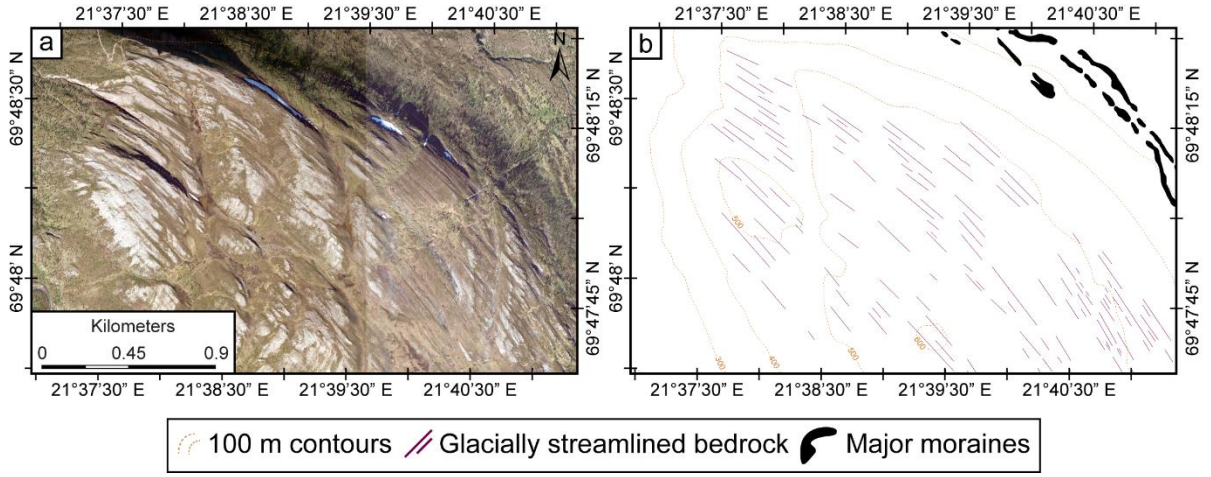

Figure 5.8. *Glacially streamlined bedrock developed across an upland flanked by two glacial valleys: (a) image from norgeibilder.no (24.08.2016), (b) subset of resulting map (presented at 1:12,000 scale). The streamlining gently curves from a mean direction of 334° in the south-east to a mean direction of 300° in the north-west and parallels the orientation of the valleys on either side. Approximate image location: 69°48'9.30"N, 21°38'11.01"E.*

5.5.8. Possible glacially streamlined terrain

Throughout the study area there are areas of subdued streamlined terrain, faintly visible on the aerial imagery as series of linear features largely aligned and with a similar orientation (Figure 5.9). These features are often not discernible on the DEM and, as such, it is therefore difficult to interpret their true form. We have, however, mapped them as linear features, under the classification of 'possible glacially streamlined terrain' and, where mapped, their orientation matches that of other nearby streamlined features (e.g. glacially streamlined bedrock). Caution is, however, advised before any specific interpretation of these features is made, which would clearly benefit from fieldwork e.g. to examine possible striae and/or abrasion surfaces, etc.

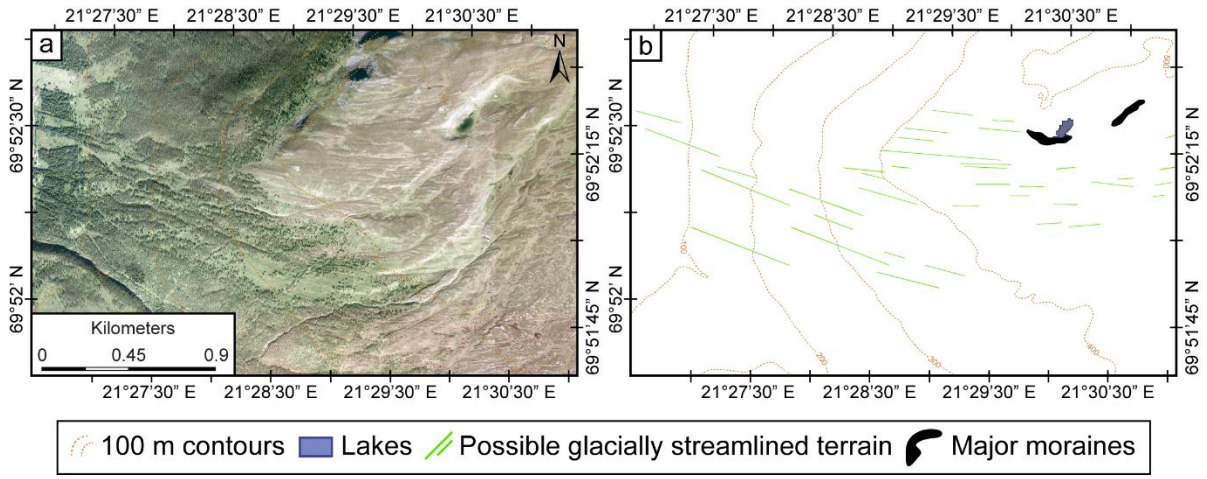

Figure 5.9. *An example of some linear features mapped as possible glacially streamlined terrain: (a) image from norgeibilder.no (24.08.2016), (b) subset of resulting map (presented at 1:12,000 scale). While there appears to be some semblance of ridges aligned parallel to each other and with a similar orientation, they are subdued to the extent they are not all discernible on the DEM. Approximate image location: 69°52'26.50"N, 21°29'48.77"E.*

5.5.9. Pronival ramparts

Pronival ramparts (formerly/alternatively protalus ramparts; Hedding, 2011) are distinctive ridges of open blockwork, formed beneath bedrock cliffs and talus slopes at the downslope margins of past and/or present perennial or semi-permanent snow-patches (e.g. Figure 5.10). They can appear similar in form to moraine ridges but generally have a ridge crest to talus-foot distance of <70 m and there are no glacial erosional forms or evidence of over-deepening of the associated upslope areas. Their widths can vary, and individual ridges can be partially superimposed, but their length is generally <500 m (Ballantyne and Benn, 1994; Shakesby, 1997; Hedding and Sumner, 2013; Hedding, 2016b, 2016a). Active features have a snow-patch occupying their proximal faces. On the high-resolution orthophotographs it is possible to identify the ridges as formed of angular (blocky) debris with little to no soil/vegetation cover on their sides/crest. Pronival ramparts have been mapped as lines drawn along the crest of each individual ridge (Figure 5.10).

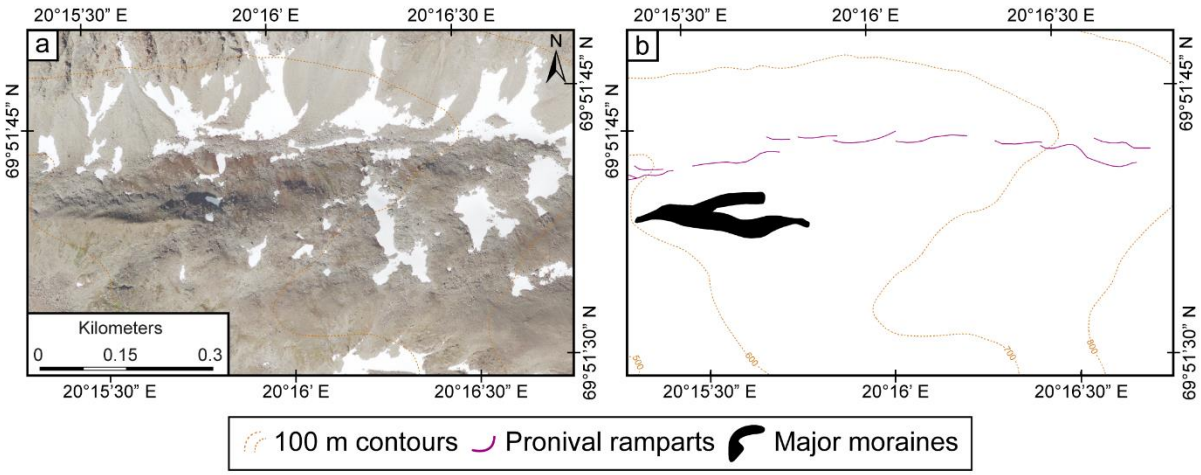

Figure 5.10. *A row of individual pronival ramparts: (a) image from norgeibilder.no (24.08.2016), (b) subset of resulting map (presented at 1:4,000 scale). The ramparts sit at the foot of a talus slope, below a valley rock wall that contains several very small (<0.01 km²) perennial snow patches. There is a lateral moraine to the left of the image, lying distal to the pronival ramparts, indicative of the sequential development of inset parallel ridges of different origins during overall deglaciation of the valley. Approximate image location: 69°51'39.07"N, 20°16'19.02"E.*

5.5.10. Rock glaciers and glacierized landforms

Rock glaciers are identifiable as lobate, ridged masses of angular debris that resemble small glaciers, and are moving or have moved downslope due to the deformation of internal ice lenses or frozen sediments. They may also form from downwasting debris-covered mountain glaciers, although the definition of rock glaciers using genetic versus descriptive criteria is a contentious issue (cf. Whalley and Martin, 1992; Hamilton and Whalley, 1995; Whalley *et al.*, 1995b; Barsch, 1996; Benn *et al.*, 2003; Berthling, 2011; Hedding, 2016b). Smaller lobate, ridged masses can also be developed by the process of rock glacierization of existing landforms (e.g. Thompson, 1957; England, 1978; Matthews and Petch, 1982; Evans, 1993; Matthews *et al.*, 2017), such as moraines or protalus ridges. We avoid inferring formation mechanisms and adopt a purely descriptive approach to mapping rock glaciers, following the protocols used by Dyke et al. (1982) and Evans et al. (2006b, 2016b, 2016b) in mapping landforms in glacierized mountains. A pronounced convex morphology of individual lobes is indicative of an active ice core, while a less distinct, flat and/or collapsed appearance indicates older/relict lobes with a melting/melted ice core (inactive or relict;

Ikeda and Matsuoka, 2002; Sattler *et al.*, 2016); although in most cases the margins of rock glaciers remain identifiable by steep (e.g. 26-36°) front and side slopes (Lindner and Marks, 1985). The rock glaciers we mapped may or may not have a present-day ice core, although this is often not a characteristic that can be immediately determined (cf. Whalley, 2020). We have, therefore, not attempted to quantify ice presence in our classifications. These accumulations of rock debris generally, but not exclusively, have lengths greater than their widths and are immediately recognisable by their bouldery surface of (superimposed) ridges and furrows (Ballantyne and Kirkbride, 1986; Ballantyne and Harris, 1994; Hamilton and Whalley, 1995; Lilleøren and Etzelmüller, 2011). Large rock glaciers can be identified on all imagery types and the ridge structures can be interpreted on the DEM where the elevation difference between ridges is >2 m. Many smaller rock glaciers, however, need to be viewed on the orthophotographs to enable identification of individual ridges within the main landform assemblage. All rock glaciers are depicted by polygons representing their outer margins inset with lines drawn along ridge/lobe crests.

Notwithstanding the ongoing debate surrounding rock glacier origins and classifications (see Berthling, 2011), we categorise rock glaciers as either ‘valley floor rock glaciers’ or ‘valley wall rock glaciers’. We define valley wall rock glaciers (including protalus lobes e.g. ridges at the foot of talus slopes meeting the criteria of a pronival rampart but showing evidence of flow (Blagborough and Breed, 1967; Gray, 1970; Chattopadhyay, 1984; Wilson, 1990; Johnson *et al.*, 2007; Millar and Westfall, 2008; Matthews *et al.*, 2017)) as rock glaciers that appear to have formed independently of glacier ice cores, and presumed to have formed as the result of creep of rock slope failure (RSF) or talus deposits (Figure 5.11a, b). Indeed, protalus lobes evidence the early stages of gravitationally induced deformation of interstitial ice (Lindner and Marks, 1985; Matthews et al., 2013), representing the embryonic form of a rock glacier, a key component in the rock glacier continuum (e.g. Serrano and López-Martínez, 2000; Hedding 2011, Sattler et al., 2016). We define valley floor rock glaciers as features that have clearly evolved at the margins of former debris-charged glaciers, for example those that occur at the foot of a glacial cirque (Figure 15.11c, d). The example of a valley floor rock glacier in Figure 5.11c, d has clearly defined ridges within the rock debris, fills a substantial portion of the cirque, and extends up to the 2018 glacier margin. Figure 5.11c and 5.11d show a valley wall rock glacier that is distinctly separate from that of the main rock glacier on the cirque floor. These two

rock glaciers (Figure 5.11c, d) could, over time, effectively fuse together to form a large complex landform, from which it might not be possible to define separate origins. The ability to identify and map each individual landforms (valley wall and valley floor rock glaciers) at the present day, therefore, provides a unique insight into rock glacier equifinality and the evidence of periglacial processes working in this highly active region.

Finally, we separately define and map 'rock glacierized moraines' on the basis that these moraines display discrete evidence of localised periglacial downslope deformation (cf. Thompson, 1957; Gunnar, 1964; England, 1978; Whalley, 2009). This moraine deformation manifests as part of a moraine transforming from a largely linear or curvilinear feature, such as a lateral or frontal moraine, into a lobate ridged or spatulate form (Figure 5.11e, f). Such moraines may be accompanied by areas of debris within their proximal margins that appear to be deforming either due to permafrost creep of interstitial ice and/or deformation of a buried glacial ice core. The term "rock glacierized" is not strictly genetic, but simply refers to parts of moraines that have been developed into rock glaciers. Rock glacierized moraines are generally found within smaller valleys and are mapped as polygons, with the boundaries drawn around the proximal and distal slopes.

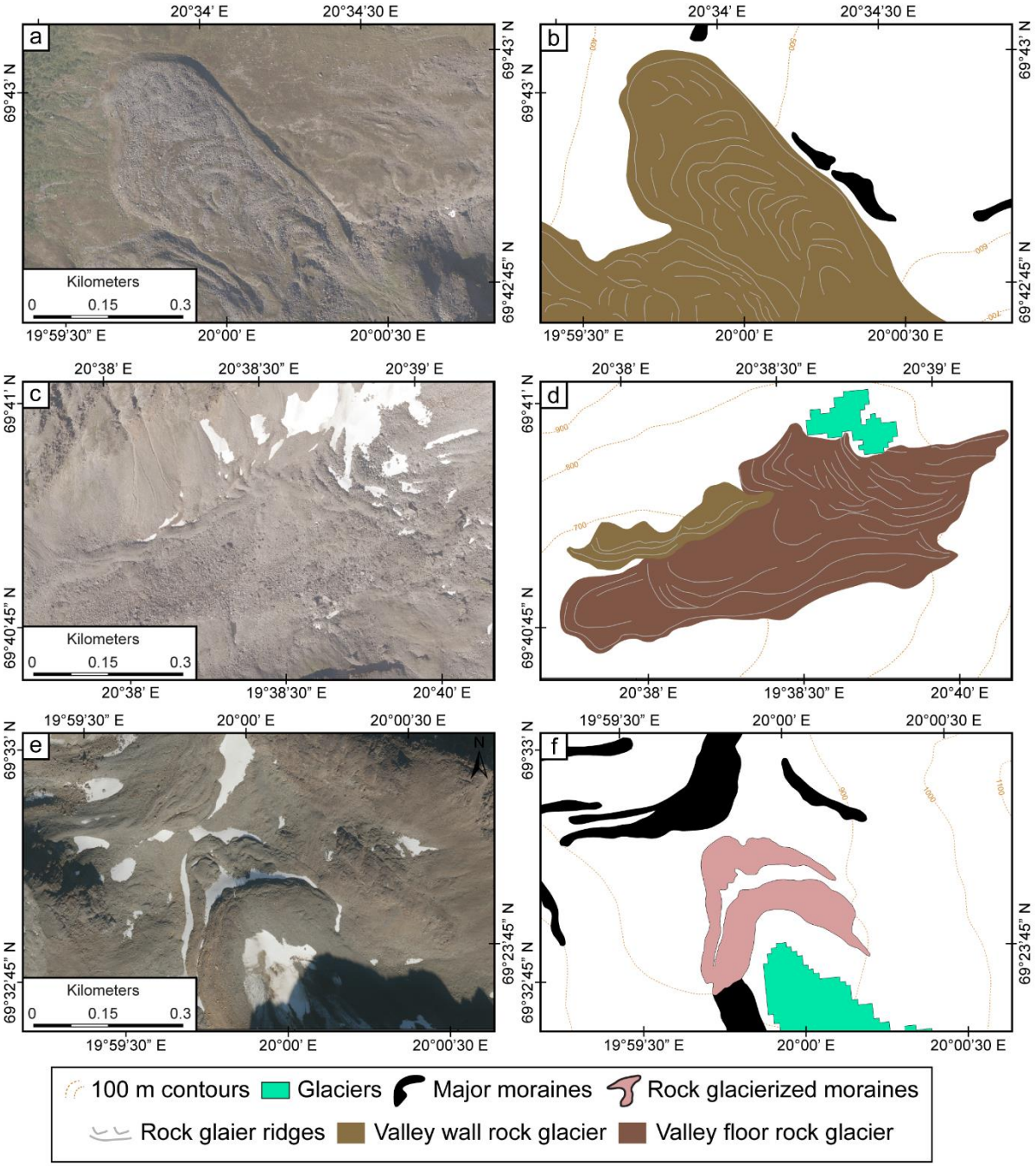

Figure 5.11. *A collection of rock glacierized landforms: (a, b) A large valley wall rock glacier with a clear lobate form, multiple (sometimes bifurcating) surface ridges, and convex profile. (c, d) A large valley floor rock glacier showing multiple, overlapping lobes, formed beneath a very small glacier (not included in the 2012 Inventory of Norwegian Glaciers), and connected to a small valley wall rock glacier on its northern margin. (e,f) Rock glacierized frontal portions of a latero-frontal moraine fronting a small glacier (not included in the 2012 Inventory of Norwegian Glaciers). The rock glacierized section of the moraine is inset with smaller ridges and furrows indicative of post-depositional modification of a glacial ice core. All images from norgeibilder.no*

(24.08.2016) and map subsets at 1:4,000 scale, with glaciers mapped on 2018 satellite imagery. Approximate image locations: 69°42'57.27"N, 20°33'54.42"E; 69°40'50.97"N, 20°38'24.74"E; 69°32'46.83"N, 19°59'55.71"E.

5.5.11. Lithalsas

Lithalsas (or 'mineral palsas') are vegetation-free frost-heaved permafrost mounds (showing little pattern in their formation) rising out of a bog/mire (Harris, 1993; Ballantyne, 2018; Figure 5.12). They can develop into mounds up to ~8 m high with diameters of ~120 m (Pissart *et al.*, 2011; Wolfe *et al.*, 2014). Lithalsas are formed on frost-susceptible substrates including till, alluvium, lake, and marine deposits with high ground water availability (Ballantyne, 2018). Throughout the study site lithalsas were only identified and mapped on the western side of the Lyngen Peninsula, outside the mapped valley moraine limits, and in areas not exceeding 20 m a.s.l. Given their small size, lithalsas are only visible on the high-resolution orthophotographs and have been mapped as polygons.

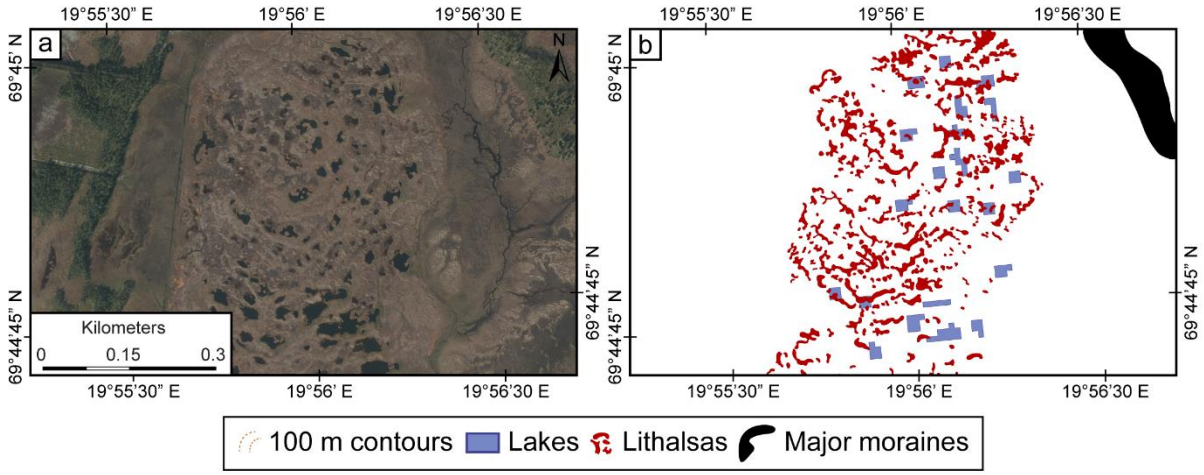

Figure 5.12. *An area of lithalsas at low level and distal to the valley moraine system: (a) image from norgeibilder.no (24.08.2016), (b) subset of resulting map (presented at 1:4,000 scale). The lithalsas are neatly constrained to the wetland area formed from a light-coloured sediment like that of glaciofluvial sediments seen elsewhere in the region. Note however, that most of the closely situated lakes in this wetland are too small to be mapped from satellite imagery and hence are not shown on this map. Approximate image location: 69°44'43.95"N, 19°55'53.87"E.*

5.5.12. Contemporary glaciers and lakes

Mapping of glacier outlines was guided by the prior outlines of Andreassen et al. (2012a) and Leigh et al. (2020). Glaciers are easily identifiable on the multispectral imagery, especially when using a false colour composite of bands 5-4-3 as Red-Green-Blue, whereby glaciers appear as bright, fluorescent blue (e.g. Raup *et al.*, 2007; Andreassen *et al.*, 2012a). Lakes and smaller inland waterbodies are found localized in a basin or constrained by other geomorphological features (e.g. moraines) and are easily identifiable on the multispectral imagery using both true and false colour composites. As the extent of lakes is seasonally variable, the size of mapped polygons is dependent on image capture date. Both glaciers and lakes were mapped as polygons, with the lines drawn around their margins.

A total of 404 glaciers and 3,041 lakes were mapped and these range in size from 0.01 km^2 to 8.15 km^2 for glaciers and 400 m^2 (0.0004 km^2) to 10 km^2 for lakes. Around 84% of all mapped glaciers are in the central and western area and around 41% of lakes are in the south-east of the study area. At the time of image capture (2018/19), we identify 36 ice-contact proglacial lakes (≥0.0004 km^2), of which 53% are on the Lyngen Peninsula.

5.6. Summary and conclusions

This paper presents a new glacial and periglacial geomorphological map of a ~6,800 km^2 region of central Troms and Finnmark county, northern Norway (see main map; Appendix and online: doi.org/10.1080/17445647.2021.1950580). The map reveals complex suites of landform assemblages that include previously unmapped components of the geomorphological record pertaining to the interaction of glacial and periglacial regimes in mountainous terrain. Our mapping also revises and updates the older and more generic superficial geology mapping of the central Troms and Finnmark region (e.g. Bergstrom and Neeb, 1978; Tolgensbakk and Sollid, 1988; Sveian *et al.*, 2005 etc.), most notably by mapping: (1) previously un-mapped and recently deglaciated terrain (up to the 2016 glacier margins, and including the 2018/19 glacier extent), enabling the documentation of small and often poorly-preserved geomorphological features present in these active environments (e.g. annual moraines, flutings, ice-contact proglacial lakes etc.); and (2) individual moraine ridges (with no minimum size-threshold), enabling the identification of closely spaced and occasionally bifurcating moraine ridges indicative of minor fluctuations of glacier margins and these were found at valley heads, within valleys, and at active glacier margins.

Additionally, we note that throughout our study area, and especially across the Lyngen Peninsula, very small glaciers (<0.05 km^2) have supraglacial debris cover at/around their fronts. The debris cover often masks the boundaries of the glaciers, making it difficult to map the full extent of the ice, especially using satellite imagery. This indicates that buried (stagnant) glacier ice is widespread on the heavily debris covered forelands fronting cirque glaciers, which has implications for the development of glacier-derived rock glaciers and rock glacierized moraines. Indeed, Griffey and Whalley (1979) previously noted that it is likely that large rock avalanches supplied the small glaciers 187 and 188 with an abnormally large quantity of debris, leading to the development of the rock glacier in the area.

Of particular interest for future glacial geochronological studies are the extensive moraine systems that are mapped throughout the region, covering a total area of ~63.7 km^2. Large terminal and recessional moraine complexes are mainly located at the heads of and within mountain valleys and were likely formed during the retreat of the Scandinavian Ice Sheet at the termination of the Younger Dryas or

several episodes of glacial advance or still-stands throughout the Holocene. The distribution of glacial valleys near the fjord systems, and the complex moraine systems they contain, indicate that the maritime mountain regions of Troms and Finnmark County experienced extensive alpine-style glaciations (Neoglacial events; Nesje and Kvamme, 1991; Matthews and Briffa, 2005; Matthews and Dresser, 2008; Wanner *et al.*, 2011 etc.), with evidence of ice caps and icefield glaciation limited to and centred on the higher plateaux areas further inland and towards the Norwegian boarder (cf. Evans *et al.*, 2002).

There is a notable decrease in the prevalence of landforms within the glacial/periglacial domain across a west to east transect. The alpine terrain that characterises the central/western side of the study area (e.g. the Lyngen Peninsula, Nordreisa and Kåfjord municipalities, and the islands of Uløya and Kågen) has a high volume of glacial and periglacial landforms. In contrast, the broad valleys, plateaux regions, and smaller mountain belts that characterise the eastern/south-eastern side of our study area have fewer mountain glaciers and, where ice is present, it is more commonly in the form of plateau glaciers covering areas of subdued topography. The distribution of mapped landforms can be attributed not only to the terrain, but also likely reflects the substantial precipitation gradient that is present across our study area from west to east.

The prevalence of permafrost across large areas of land across our study area has resulted in a wide variety of periglacial phenomena, much of which remains outside the scope of our mapping. The most notable features are those associated with seasonally frozen ground (e.g. patterned ground) and mass wasting (e.g. gelifluction). In areas of complex glacial geomorphology extensive periglacial mass wasting can not only alter the appearance and structure of glacial landforms (e.g. rock glacierized moraines; see Section 5.5.10) but can also, mask or subdue the presence, and/or imitate the form, of glacial features. Greater care must, therefore, be taken when mapping the small scale glacial geomorphological features in areas of active periglacial processes.

The map resulting from this work further demonstrates the utility of high-resolution aerial imagery and DEMs (e.g. <1 m orthophotographs, 2 m Arctic DEM), combined with medium-resolution satellite imagery (e.g. 10 m Sentinel-2A/2B), and their associated remote sensing techniques, for mapping glacial and periglacial geomorphology across large swaths of rugged and poorly accessible terrain. Our map

can be used to underpin robust palaeoglaciological reconstructions of plateau and mountain glaciers, enable new interpretations of mountain glacier dynamics in a highly sensitive Arctic region, further refining existing models of mountain glacial landsystems, and can help guide future field investigations throughout the region.

5.7. Acknowledgments

This work would not have been possible without the digital archive of high-resolution aerial imagery provided by www.norgeibilder.no which is a cooperation between the Norwegian Public Roads Administration, the Norwegian Institute of Bioeconomics (NIBIO), and the Norwegian Mapping Authority (Kartverket). The high-resolution Arctic DEMs were provided by the Polar Geospatial Center under NSF-OPP awards 1043681, 1559691, and 1542736. We also thank ESA and USGS for providing free satellite imagery and the Geological Survey of Norway (NGU) for providing freely available geological data (made available by the Norwegian license for public data; NLOD). We thank the editors (Mike Smith and Martin Margold) and are grateful for the diligent reviews of Brian Whalley, Jostein Bakke, and Heike Apps, who provided valuable comments and insight which improved the quality and clarity of the map and accompanying manuscript.

CHAPTER 6

Reconstructing the Holocene glacial history of northern Troms and western Finnmark; northern Norway

Leigh J.R.[1], Stokes C.R.[1], Evans D.J.A.[1], Jones R.S.[1,2], Andreassen L.M.[3], Carr J.R.[4]

[1]Department of Geography, Durham University, Durham, UK; [2]School of Earth Atmosphere and Environment, Monash University, Melbourne, Australia; [3]Norwegian Water Resources and Energy Directorate (NVE), Oslo, Norway; [4]School of Geography, Politics and Sociology, Newcastle University, Newcastle upon Tyne, UK

Selecting rock samples on the Sorbmevággi, valley head moraine

Photograph date: 25th August 2019 (by J.R. Leigh)

“There was a house in a field on the side of a cliff

And the waves crashing below were just said to be a myth

So they ignored the warnings from the ships in the docks

Now the house on the cliff is the wreckage on the rocks. . .

This house was doomed, but they didn't care

They invested in a system that was beyond repair. . .

So this is such exciting time to be alive

Our generation's got to fight to survive

It's in your hands now, whose future?

Our future”

(Reynolds, 2012)

6.1. Abstract

Following the Younger Dryas (YD), Norway experienced several, abrupt, centennial to millennial-scale climate variations throughout the Holocene. Comprehensive investigations into short-term glacier fluctuations are a fundamental tool in developing reliable reconstructions of past climate variability and predictions of glacier behaviour under future climate change. Here we present the first Holocene glacial chronology in the Rotsund Valley, central Troms and Finnmark county, northern Norway, based on calibrated and relative moraine dating using Schmidt hammer and soil chronosequencing. We provide evidence that, following deglaciation of the main ice sheet across the region, mountain glaciers within the Rotsund Valley attained their maximum extent between 12,125 (11,120-13,174) and 10,588 (9,587-11,601) cal. yrs BP and subsequently underwent recession, with several moraine building events interrupting net retreat. A series of Neoglacial moraines appear to have formed around 4,690 (4,108-5,287) cal. yrs BP representing regrowth/readvance of glaciers in the Rotsund Valley. Furthermore, based on these findings and detailed moraine mapping it has been possible to produce an updated ice margin chronology for the Scandinavian Ice Sheet (SIS) and mountain glaciers from 14,000 cal. yrs BP to the present-day (2018/19). Our mapping and glacial chronology reveals a complex picture of early-Holocene deglaciation and late-Holocene glacier regrowth/readvance.

6.2. Introduction

Glaciers are highly sensitive to climatic perturbations and reconstructions of their former extent plays a key role in improving our understanding of climate variability (Oerlemans, 1994, 2005; Wittmeier *et al.*, 2015; Roe *et al.*, 2017; IPCC, 2019). Constraining Holocene fluctuations of Arctic glaciers is, therefore, of critical importance in assessing the magnitude of contemporary glacier change in a longer-term context and investigating the response of glaciers to major circum-Arctic climate events, e.g. the YD, the 8.2 ka event, the Holocene Thermal Maximum (HTM), and the Little Ice Age (LIA).

Research into constraining the number, age, and magnitude of glacier fluctuations across Scandinavia throughout the Holocene is generally focused on the larger ice caps and outlet glaciers in southern regions (cf. Nesje *et al.*, 2008; Nesje, 2009). A better understanding of the fluctuations of mountain glaciers in northern Norway throughout the Holocene is, therefore, required to: (i) assess the asynchronicity of glacier response across a latitudinal gradient that crosses the Arctic Circle, (ii) put the effects of historic rapid climatic fluctuations into a modern-day context, and (iii) help local communities adapt and prepare for future changes in glacier extent.

The glaciers across northern Norway are particularly sensitive to climate fluctuations and can provide clear indications of even short-lived climatic changes (e.g. Grudd, 1990; Andreassen *et al.*, 2000a, 2012b; Bakke *et al.*, 2005a; Oerlemans, 2007; Stokes *et al.*, 2018; Leigh *et al.*, 2020; Weber *et al.*, 2020). The sensitivity of these glaciers to climate fluctuations is predominantly due to their maritime location and sensitivity to variations in the Arctic Oscillation and North Atlantic Oscillation (Rasmussen, 2007). Furthermore, observational data and computer models both indicate an increased sensitivity to global climate change in the Arctic (Miller *et al.*, 2010; Serreze and Barry, 2011; IPCC, 2019; Park *et al.*, 2019). The resulting amplification of Arctic climate change sees substantial regional disparity in temperatures between southern and northern Norway (Ballantyne, 1990; Birks *et al.*, 2005; Bjune *et al.*, 2005; Paasche *et al.*, 2007).

This paper aims to build on and expand site-specific studies whilst simultaneously bringing attention to an area of northern Norway that has, thus far, escaped detailed scrutiny. By undertaking a detailed analysis of glacier extent since

the termination of the YD across central Troms and Finnmark county we develop a better understanding of the complex mountain glacial landsystems that evolved alongside the recession of the SIS (Mangerud, 2008). The combined application of calibrated, and relative age dating enables us to build a picture of mountain glacier change over centennial-to-millennial scale timeframes. This provides a long-term context for 20th/21st century climate change by establishing a chronology for glacier change in the European Arctic region, an area known to be experiencing some of the highest rates of warming today (IPCC, 2019). These aims are met through the following key objectives:

1. Use detailed geomorphological mapping of glacial landforms (Leigh *et al.*, 2021) to reconstruct the patterns of ice-sheet deglaciation and evolution of different glacial landsystems during the Holocene.
2. Determine calibrated formation ages for the sequence of moraines within the Rotsund Valley.
3. Assess the presence of Holocene climatic events recorded within the moraine sequences of small, Arctic, mountain glaciers.

6.3. Holocene glaciations and geomorphological setting

6.3.1. Glacial history: Previous work

Following deglaciation of the SIS, glaciers and ice caps in Norway are thought to have undergone a complex pattern of rapid retreat and progressive readvance throughout the Holocene (Nesje *et al.*, 2008; Nesje, 2009). The most notable of these climatically-driven fluctuations are the readvance/stillstand during the *Erdalen Event* 10,100-9,500 cal. yrs BP (e.g. Dahl *et al.*, 2002), the *8.2 ka cold event* 8,200 cal. yrs BP (e.g. Nesje and Dahl, 2001), the *HTM* 8,000-6,000 cal. yrs BP (e.g. Bjune *et al.*, 2005), the *Neoglacial* 6,000-2,000 cal. yrs BP (e.g. Matthews and Dresser, 2008), the *LIA* 1300-1850/1900 (e.g. Grove, 2004b, 2004a), and a rapid response to present-day (20th-21st century) anthropogenically-forced climate change (e.g. Andreassen *et al.*, 2012a).

A period of cooling during the early-Holocene transition from Preboreal to Boreal, and subsequently termed the Erdalen Event (dating to 10,100-9,500 cal. yrs BP), is evidenced across Norway by substantial moraines inset from the YD limits (Andersen, 1980; Corner, 1980; Nesje and Kvamme, 1991; Dahl *et al.*, 2002; Turner and Marshall, 2011). It is also recorded in environmental responses from non-glacial sites, such as vegetation regression linked to reductions in summer temperatures (Paus *et al.*, 2006, 2019). Erdalen Event moraines are often grouped into two or three major zones, thought to have formed between 10,100 cal. yrs BP and 9,500 cal. yrs BP (e.g. Andersen, 1980; Nesje *et al.*, 1991; Dahl *et al.*, 2002; Bakke *et al.*, 2005c; Matthews *et al.*, 2008; Nesje and Matthews, 2011; Aa and Sønstegaard, 2019). In the Lyngen region of northern Norway, Ballantyne (1990) indicated the presence of likely Preboreal moraines and Bakke et al. (2005a) identified three closely grouped moraines formed during the period 10,400-8,900 cal. yrs BP. On the Bergfjord Peninsula (~70 km NE of Lyngenfjord), reconstructions of Holocene history of the Langfjordjøkelen ice cap do not, however, record the same pattern of advances as those described in the Lyngen region. Rather, Wittmeier et al. (2015) concluded that between 10,000 and 4,100 cal. yrs BP, the northern outlet glacier of Langfjordjøkelen was absent or too small to contribute mineral deposits to the proglacial lakes (Wittmeier *et al.*, 2015).

Over the period 10,000-6,000 cal. yrs BP, Holocene climate was steadily warming (Turner and Marshall, 2011), only interrupted at around 8,200 cal. yrs BP by an abrupt ~160-year long period of cooling (Alley *et al.*, 1997; Rohling and Pälike,

2005; Thomas *et al.*, 2007). This period of cooling is termed the '8.2 ka event' and known as, and/or incorporated within, the Scandinavian 'Finse Event' (Dahl and Nesje, 1994, 1996; Nesje and Dahl, 2001; Nesje *et al.*, 2008; Nesje, 2009). Across Norway, the climatic deterioration of the 8.2 ka event was responsible for substantial readvance and possible regrowth of ice caps and mountain glaciers (Nesje and Dahl, 2001; Seierstad *et al.*, 2002; Nesje *et al.*, 2006; Aa and Sønstegaard, 2019). Very few studies are able to attribute a specific moraine to the 8.2 ka event, but evidence is instead found in pro-glacial lake sediments indicating the ubiquity of increased glacier activity across Norway during a period of mid-Holocene net warming (Nesje *et al.*, 2008; Nesje, 2009).

The warming during the mid-Holocene is referred to broadly as the HTM, during which summer temperatures are thought to have been between 1.5°C and 2°C warmer than at the 20th/21st century boundary (Bjune *et al.*, 2005; Nesje *et al.*, 2008; Nesje, 2009). Across Scandinavia, the peak HTM is thought to have occurred over a 200-year period between 6,600 and 6,300 cal. yrs BP, with this phase having the most reduced glacierization and most glaciers thought to have melted completely (Seppä and Birks, 2002; Bjune *et al.*, 2005; Seppä *et al.*, 2005; Antonsson and Seppä, 2007; Nesje *et al.*, 2008; Nesje, 2009; Renssen *et al.*, 2009, 2012). On the Lyngen Peninsula, northern Norway, no glacier-derived meltwater sediments are found between 8,800 and 3,800 cal. yrs BP, indicating a fully deglaciated catchment with reconstructions of the Equilibrium-Line Altitude (ELA) indicating they were above 1,200 m (Bakke *et al.*, 2005a; Wittmeier *et al.*, 2015).

Following the peak of the HTM, there was a general period of cooling over the time interval 6,000-2,000 cal. yrs BP, which resulted in glaciers reforming across Scandinavia towards the end of this period, commonly referred to as the Neoglaciation (Grove, 2004b, 2004a; Nesje *et al.*, 2008; Nesje, 2009; Wittmeier *et al.*, 2015). Across Norway there was variable regrowth of glaciers during the Neoglaciation, with the development of glaciers responding to regional variations in winter precipitation, summer temperature, wind drift of snow, and glacier hypsometry (Nesje, 2009). For example, valley glaciers on the Lyngen Peninsula in northern Norway are proposed to have reformed after 3,800 cal. yrs BP (Bakke *et al.*, 2005a). The Høgtuvbreen ice cap in the Svartisen area of northern Norway experienced initiation around 4,420-4,300 cal. yrs BP (Jansen *et al.*, 2016); and in Rondane, southern Norway, cirque glacier growth took place around 4,000 years ago (Kvisvik *et al.*, 2015). Throughout the

Neoglacial, proglacial sediments record a series of events during which glaciers were larger than the present-day and these occurred at a millennial-scale (e.g. Matthews *et al.*, 2005; Matthews and Dresser, 2008; Bakke *et al.*, 2010; Wittmeier *et al.*, 2015).

It is generally considered that the culmination of the Norwegian Neoglacial, was the glacial readvance of the LIA (Nesje, 2009). Initiating at around 1300, glaciers (particularly in the northern Hemisphere) began a pattern of asynchronous readvance (Grove, 2001, 2004b, 2004a). Unlike in contentinal Europe, which expierienced uniform LIA maxima during the mid-19th century, Norway experienced considerable regional variability in the extent and timing of LIA maximum (Ballantyne, 1990; Grove, 2001, 2004a, 2004b; Ivy-Ochs *et al.*, 2009; Solomina *et al.*, 2016; Leigh *et al.*, 2020). Hence, the timing of the LIA maximum varies from the mid-18th century in southern Norway to the early-20th century in northern Norway (e.g. Ballantyne, 1990; Winkler, 2003). Regional differences in LIA maxima across Norway appear to be influenced primarily by differences in summer temperature and winter precipitation, with local scale differences being explained, in part, by individual glacier hypsometry (e.g. Ballantyne, 1990; Nesje *et al.*, 2008; Leigh *et al.*, 2020).

Since the culmination of the LIA, most glaciers across Norway (and globally) have experienced net mass loss (e.g. Dyurgerov, 2005; Nesje *et al.*, 2008; Andreassen *et al.*, 2012a; Zemp *et al.*, 2015). Observations of glacier change since the mid-20th century show exceptionally rapid retreat, primarily linked to anthropogenically forced climate change (e.g. Zemp *et al.*, 2015, 2019; Stokes *et al.*, 2018; IPCC, 2019; Leigh *et al.*, 2020). Arctic amplification is also likely to further impact glaciers in northern (Arctic) Norway, many of which may disappear before the end of the 21st century (e.g. Nesje *et al.*, 2008; Serreze and Barry, 2011; Andreassen *et al.*, 2012b; Stokes *et al.*, 2018; IPCC, 2019; Zemp *et al.*, 2019; Leigh *et al.*, 2020).

6.3.2. Study area

The study area covers 6,810 km^2 of the county of Troms and Finnmark (formerly the northern region of Troms County), extending from the Lyngen Peninsula in the west, to Navitdalen in the east and including the small islands of Uløya and Kågen in the north (Figure 6.1). Most glaciers in the region can be considered maritime given their proximity to large fjord systems and the North Atlantic Ocean, coupled with their

exposure to high precipitation during the winter with a smaller range in winter and summer temperatures than for glaciers at similar latitudes further inland (Andreassen *et al.*, 2012b).

Two field sites currently characterised by small, valley and cirque glaciers (the Rotsund Valley and Strupskardet; Figure 6.1a and 6.1b, respectively) were visited in August/September 2018 and 2019 to undertake detailed geochronological investigations. These study areas were chosen because prior glaciological investigations are sporadically spaced throughout the region and pay little or no attention to the small mountain glaciers (e.g. <1 km^2) that account for most ice bodies in central Troms and Finnmark county. For example, the major fjords at the western limits of our study area were included within the earlier works of Andersen (1968) and Corner (1980), while those at the eastern limits have been described by Sollid et al. (1973). The early works used extensive mapping of fjord moraine sequences and raised shorelines, coupled with radiocarbon dating, to build up a picture of ice front positions since the Older Dryas/14,000 cal. yrs BP (e.g. Holmes and Andersen, 1964; Andersen, 1968; Sollid *et al.*, 1973; Corner, 1980) yet their reconstructions often overlook the dynamic, short-lived, and less extensive glacier fluctuations of the Holocene. More recently, work to establish millennial-scale reconstructions of the pace of deglaciation through the main fjord systems across northern Norway has taken place (e.g. Stokes *et al.*, 2014) alongside large scale ice-sheet reconstructions which have tracked the retreat of the SIS from its terminal position on the continental shelf ~25,000 cal. yrs BP, to the Norwegian coastal margin at ~16,000 cal. yrs BP, through the fjords at ~13-12,000 cal. yrs BP, and out onto the upland plateaux at ~11-10,000 cal. yrs BP (Hughes *et al.*, 2016). Only recently has there been a focus on specific valleys with detailed valley chronologies, accompanied by regional assessments of 20^{th}/21^{st} century glacier change (e.g. Bakke *et al.*, 2005a; Stokes *et al.*, 2018; Leigh *et al.*, 2020).

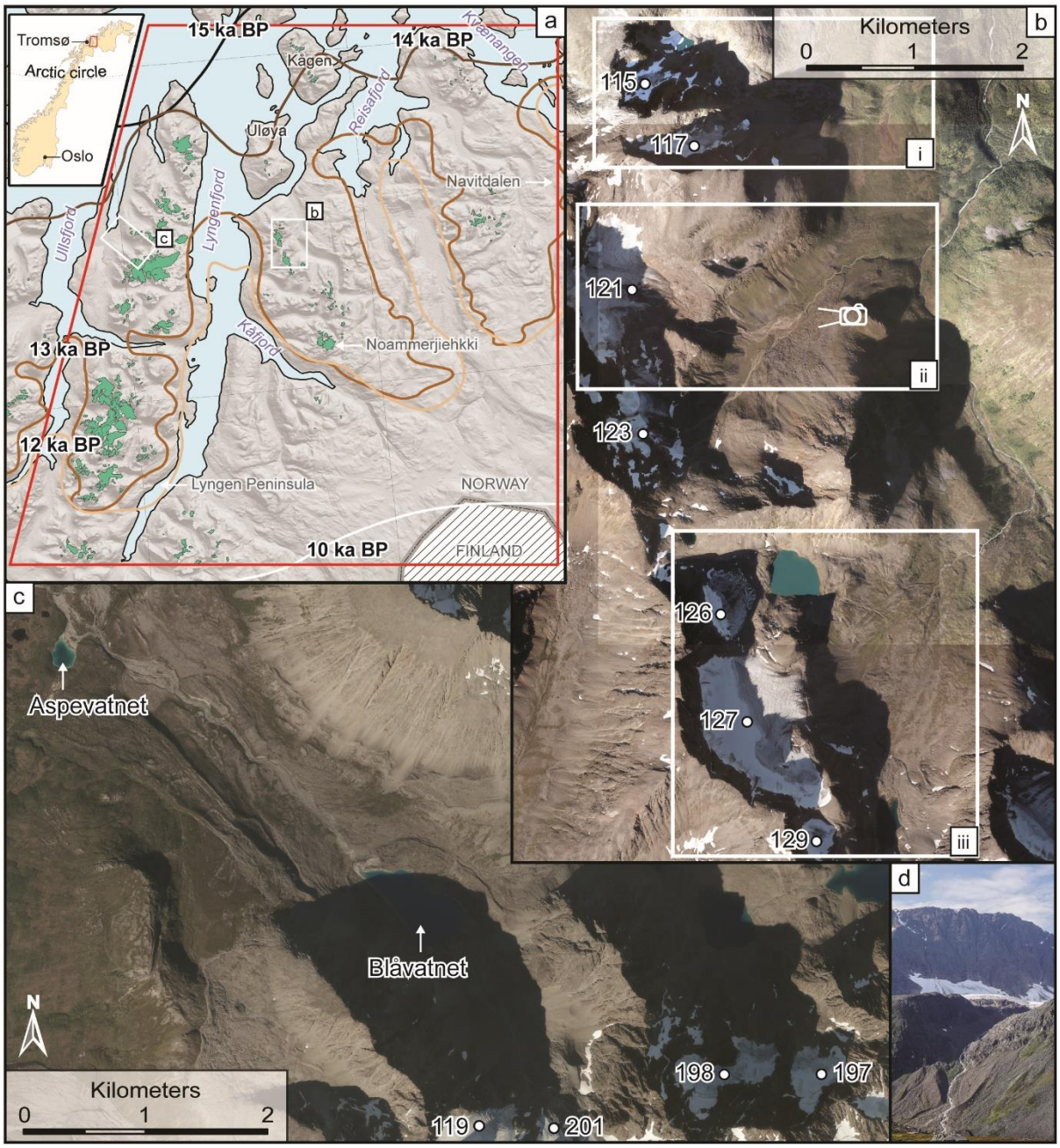

Figure 6.1. *Study area location in Troms and Finnmark county, northern Norway. (a) The red outline represents the study area, the solid lines are the SIS margins from Hughes et al. (2016), and the two white rectangles indicate the field sites: (b) Rotsund valley and (c) Strupskardet. (b) Within the Rotsund Valley the three subsidiary valleys Hjemtverrdalen (i), Sorbmevággi (ii), and Goahtevággi (iii) are identified, and the camera denotes location of photograph (d). (c) The Strupskardet field site. (d) a field site photograph (capture date: 27/08/2019) of Sorbmevággi LIA moraines and glacier 121 sitting below the headwall. The base image in (a) is a hill shaded ArcticDEM*

mosaic with present-day glaciers marked, the imagery in (b) and (c) is 0.25 cm resolution aerial orthophotographs captured 24/08/2016, from www.norgeibilder.no.

6.3.2.1. The Rotsund Valley

The Rotsund Valley (Figure 6.1b) is situated within the Nordreisa Municipality and is flanked on the west by a minor mountain range (colloquially referred to as the Kåfjord Alps). The mountain peaks in this area range from 1,077 m a.s.l. (Stortinden) to 1,320 m a.s.l. (Geaippilvarri) and the bedrock is composed of Vaddas Nappe and Kåfjord Nappe, broadly comprising metamorphic facies of amphibolite, quartzite, gneiss, and schist (Lindahl *et al.*, 2005; Augland *et al.*, 2014; Geological Survey of Norway, 2015). The present-day tree line extends to ~400 m a.s.l. and, above this, alpine tundra is the dominant vegetation. To the west is a major fjord system, Lyngenfjord, and there are also subsidiary fjords to the north (Rotsundet) and south (Kåfjorden; Figure 6.1).

Within the Rotsund Valley, three subsidiary valleys were investigated to develop a detailed chronology that could inform the much broader regional-scale mapping (Leigh *et al.*, 2021): (1) an un-named, west-east orientated valley (henceforth referred to as Hjemtverrdalen; Figure 6.1bi), containing glaciers 115 and 117 and drained by the river Hjemtverrelva; (2) the southwest-northeast orientated valley Sorbmevággi (Figure 6.1bii), containing glaciers 121 (Sorbmejiehkki) and 123 and drained by the river Sorbmejohka; (3) the southwest-northeast orientated valley Goahtevággi (Figure 6.1biii), containing glaciers 126, 127 (Goahtejiehkki), 129, 131, and 132 and drained by the river Goahtejohka. All three valleys have large latero-frontal moraine systems, with the terminus positions of the outermost moraines extending into the main Rotsund Valley at elevations from ~140 to ~340 m a.s.l. LIA moraines are present in the forelands of glaciers 115, 117, 121, 123, and 126, and have previously been dated to between 1814 and 1877 (Leigh *et al.*, 2020).

6.3.2.2. Strupskardet

The valley Strupskardet (Figure 6.1c), in the Lyngen Municipality, is a west-east orientated valley crossing the northern Lyngen Alps. The Lyngen Alps are situated on a ~70 km long peninsula (Lyngen Peninsula), flanked by Lyngenfjord to the east and Ullsfjorden to the west. To the north and south of Strupskardet are mountains ranging

from 1,042 m a.s.l. (Nordre) to 1,625 m a.s.l. (Lenangstinden), with bedrock composed of Lyngsfjellet nappe, comprising ophiolitic gabbro, and metamorphic facies including amphibolite and schist (Randal, 1971; Coker-Dewey *et al.*, 2000; Augland *et al.*, 2014). The present-day tree line extends to ~350 m a.s.l. as a dispersed and stunted tree cover. Within Strupskardet there are two glacier-fed lakes: Aspvatnet (0.4 km^2, 30 m a.s.l.) and Blåvatnet (~0.3 km^2, 189 m a.s.l.). These lakes are fed by glaciers 119, 201 (Lenangsbreen), 198, and 197 and, the river that feeds Aspvatnet is soured by Blåvatnet.

Importantly, previous research by Bakke et al. (2005a) has established independent ages for most moraines within Strupskardet. Moraine ages were determined by combining details from various geomorphological signatures (e.g. former shorelines) and sediment cores from the proglacial lake Aspvatnet. The resulting glacial chronology for Strupskardet proposes moraine ages spanning the past 20,000 cal. yrs BP (Bakke *et al.*, 2005a). The oldest moraines in the sequence (M1 and M2) were correlated to the high sea-level stand during the Risvik-substage in Finnmark (Bakke *et al.*, 2005a). However, ice sheet reconstructions and dating indicate this area would have been covered by the ice sheet with its terminus on the continental shelf (c.f. Stokes et al., 2014; Hughes et al., 2016). Thus, the age of the pre-YD moraines should be considered as conjectural (Bakke, *pers. comm.*). Nonetheless, for the (post-)YD moraines, reliable ages were established. The moraines enclosing lake Blåvatnet (M8 and M9; ~2.3 km from the present-day glacier front) were proposed to have formed at 12,800-11,500 cal. yrs BP (M8) and 9,300-8,900 cal. yrs BP (M12) (Bakke *et al.*, 2005a). Additionally, three inset moraines at Blåvatnet's eastern margin (M10, M11, and M12; ~1.8 km from the present-day glacier front) were dated to 10,400-10,300, 9,800-9,400 and 9,300-8,900 cal. yrs BP, respectively (Bakke *et al.*, 2005a). Then, following the deposition of M12 no additional moraines were formed until the LIA maximum moraine (M13) at around 1890-1928 (Bakke *et al.*, 2005a), with this age established using the lichenometric dating framework of Ballantyne (1990).

6.4. Methods

6.4.1. Glacial geomorphological mapping and ice sheet reconstructions

Geomorphological mapping of the entire study area (Fig. 1a) was conducted using multiple image types and is described in detail by Leigh et al. (2021). In brief, mapping used high-resolution georectified orthophotographs (0.25 m pixel resolution; courtesy of the The Norwegian Mapping Authority, www.norgeibilder.no), medium-resolution 2018/19 multispectrial satellite imagey (10 m pixel resolution Sentinel-2A imagery) and Digital Elevation Models (DEMs; 10 m DEM and 2 m ArcticDEM mosaics; courtesy of The Norwegian Mapping Authority and The Polar Geospatial Center, respectivly).

Glacial landforms were identified and digitally mapped as either vector lines or polygons using ESRIs ArcGIS software. The geomorphological features mapped include moraines, ridges within areas of discrete debris accumulations (DDAs), flutings, eskers, irregular mounded terrain, lineations, glacially streamlined bedrock, possible glacially streamlined terrain, pronival ramparts, rock glaciers, and lithalsas. Additional mapping of glaciers and lakes was done using a semi-automated process on 2018/19 multispectral satellite imagery with manual correction of mapped units (e.g. glaciers/lakes cast under shadow, glaciers obscured by debris, glaciers terminating in proglacial lakes, or where snow patches were erroneously classified as glaciers) to produce the most up to date outlines as possible. Use of the recent satellite imagery implies that references to a 'present-day' glacier refers to the glacier/ice cap dimensions in 2018/2019.

Reassessment of prior ice sheet outlines was achieved by re-drawing the DATED-1 SIS margin shapefiles (Hughes *et al.*, 2016) based on the glacial geomorphological mapping presented by Leigh et al. (2021) and our glacier chronology. Mapping was also guided by topography using the 2 m resolution ArcticDEM (Porter *et al.*, 2018). Existing dating controls throughout the region were also utilised to help set the revised margins into a chronological sequence. Where the prior ice sheet outlines of Hughes et al., (2016) matched relevant moraines, these were left un-edited and shown as thick lines on the map. Where revisions were made, these were drawn from the existing outlines following our new interpretations and shown as thin lines. The old positions were left as dashed lines on the map to provide context for the revisions. Furthermore, new reconstructions of plateau ice cap and mountain glacier extent again followed the geomorphological mapping of Leigh et al.

(2021) and was guided by the topography, present-day ice outlines, and our Rotsund Valley dating. Owing to the relatively sparse geomorphological signature on the mountain plateau surfaces relative to the valley systems, there is a greater amount of uncertainty in these areas.

6.4.2. Field data

When in the field, three subsidiary valleys in the Rotsund Valley (Hjemtverrdalen, Sorbmevággi, and Goahtevággi; Figure 6.1b) were examined alongside one valley on the Lyngen Peninsula (Strupskardet).

In the Rotsund Valley, Sorbmevággi hosts the most extensive, best preserved, and easily accessible moraines. Therefore, this valley was chosen as the baseline from which comparisons are made. Within Sorbmevággi there are five clearly defined moraines that lead up to (not including) the LIA moraine, which has been previously dated to 1822 by Leigh et al., (2020). All five pre-LIA moraines were sampled with the aim to establish moraine formation ages. All moraines that were examined and discussed in the text are identified sequentially starting at M1, which denotes the furthest down valley. For example SM1, whereby the first letter indicates the valley name (S = Sorbmevággi), the second letter indicates the feature in question (M = Moraine), and the number indicates position in the sequence (1 = furthest down valley/terminal moraine).

On all moraines, Schmidt hammer readings and soil profiles were recorded from the frontal and lateral portions, where possible, and only where there was an absence of soil or surface boulders were these measurements not made. Additionally, samples were collected for Terrestrial Cosmogenic Nuclide Dating (TCND) from stable boulders on the Sorbmevággi moraines and a series of perched boulders on a bedrock lip above the SM5 moraine and within the main Rotsund Valley. However, due to ongoing issues with laboratory closures in light of the COVID-19 pandemic, it has not been possible to present and discuss the results of the TCND at the time of thesis submission.

In Strupskardet (Figure 6.1c) there is an extensive sequence of at least 13 moraines, previously investigated and dated (M1-M13; Bakke *et al.*, 2005a). The moraines, with age controls from dating of proglacial lake sediments indicating YD/Holocene, were the primary targets for sampling (moraines M8-M12). At these

moraines, owing to the bouldery nature of most ridges Schmidt hammer readings were prioritised.

6.4.2.1. Schmidt hammer dating

Measurements of rock-surface hardness were taken using a Novatest 'N-type Schmidt hammer', with a specified impact energy of 2.207 N/m. A careful assessment of all boulders was carried out prior to sampling and only large, stable, schist boulders, located on or near moraine crests were sampled. The same operator recorded 10 rebound (R-) values from each boulder, with 10 boulders sampled per moraine. The mean was then calculated from the 100 R-values, and this value is used as the basis for assigning calibrated ages. The use of a selective sampling approach with fewer readings per boulder is considered optimal, as it reduces the field effort relative to other strategies but, more importantly, reduced hammer wear (cf. Shakesby *et al.*, 2011). Minimising Schmidt hammer wear is crucial as it can increase the variability of rebound readings, in turn leading to reduced dating accuracy and precision (cf. Shakesby *et al.*, 2011).

Impacts were made on horizontal or near-horizontal surfaces and were separated by at least a plunger tip width. Readings were made on dry surfaces, away from the edge of boulders or any visible cracks, and rock surfaces were not abraded by carborundum treatment before measurements (e.g. Day, 1977; Shakesby *et al.*, 2006; Wilson *et al.*, 2019). Most boulders within Strupskardet and the Rotsund Valley are above the treeline. In the few cases where moraines are below the treeline, we avoided boulders directly beneath trees, as these were often covered by grasses, moss, and foliose lichen.

6.4.2.2. Soil chronosequencing

Three or more soil pits were excavated into the crests of moraines that pre-date the LIA maxima. In the Rotsund Valley, 30 soil pits were excavated until the C-horizon (unaltered parent material) was reached. The geomorphological context and vegetation coverage of each moraine/soil pit location were recorded alongside details of crest elevation, approximate height from the valley floor, and locality with respect to running and/or standing water. Where possible, pits were confined to sharp crested

portions of moraines (cf. McCarroll and Ware, 1989; Evans, 1999a). Both lateral and end moraines were sampled, and pits were excavated in areas where surface boulders were fewest, in the hope of encountering fewer obstacles with depth.

Soil horizons were identified in the field based on distinct colour changes (see Birkeland, 1999 for rationale and applications to Quaternary soils). From the middle of each identified horizon (and the top of the C-horizon) ~100g of soil was collected and retained for laboratory analysis of dry and wet colour, soil pH, and loss on Ignition (LOI). In each pit, the depth of soil to the base of the B-horizon (top of the C-horizon) and the thickness of each identified horizon (excluding C-horizon) were measured (cf. Evans, 1999a).

In the laboratory, the colours of the wet and dry soil samples were determined using a Munsell soil colour chart. Soil colour enrichment of each horizon was then calculated following the Colour Development Equivalent (CDE) of Buntley and Westin (1965), whereby the chroma is multiplied by a soil colour value (e.g. 10R = 7; 2.5YR = 6; 5YR = 5; 7.5YR = 4; 10YR = 3; 2.5Y = 2 and 5Y = 1). This provides a metric for soil reddening and thus an indication of the maturity of soil development. Soil pH was measured from a 1:2.5 suspension (10 g of dry soil: 25 ml of distilled water). LOI was used to provide an indication of total organic matter content. Around 5 g of each sample was dried overnight at 105°C to determine moisture content, and the samples were then ignited at 550°C for four hours in a furnace to determine percentage LOI.

Relative age dating using the development stage of pedogensis is often converted to calibrated chronologies using equivalent soils from moraines that have independent age control (e.g. from prior absolute/calibrated dating studies). This has been achieved on mountain moraine sequences where a range of soil properties, especially depth, on moraine ridge crests are used to estimate moraine age (e.g. Birkeland, 1978; Bockheim, 1979a, 1979b; Evans and Rogerson, 1986; McCarroll and Ware, 1989; Evans, 1999a; Bentley *et al.*, 2007).

6.5. Results

6.5.1. Central Troms and Finnmark moraine morphology

The time-transgressive nature of the changing ice masses across, between, and within catchments reflects the retreat of the SIS and the development of topographically constrained plateau, valley, and cirque glacial systems. The geomorphological record depicts an extensive series of features which are both spatially and temporally controlled (cf. Leigh *et al.*, 2020) and predominately attributable to four distinct landsystems that likely existed and/or developed throughout the Holocene; the plateau icefield landsystem, the glaciated valley and cirque landsystem, and the periglacial landsystem.

The largest moraine complexes across the region are those that mirror the large fjords and valley systems known as the Tromsø-Lyngen moraines formed ~10,200-11,900 yrs BP (Andersen, 1968) and first identified and described in detail by Helland (1899) and Vogt (1913) and later revisited by Grønlie (1940), Marthinussen (1962), and Holmes and Andersen (1964). Tromsø-Lyngen moraines can be traced near continuously across the study area and frontal portions are clearly identifiable at the fjord heads (cf. Leigh *et al.*, 2020). Within the study area the most clearly identifiable portion of the Tromsø-Lyngen moraine complex is the Spåkenes moraine (Marthinussen, 1962), found at the head of Lyngen fjord (Figure 6.2a-b). Additional large moraine complexes are found in the south/south-east of the region, across the upland plateau (Figure 6.2g-j). Age constraints for these moraines are lacking; however, it is likely that these moraines represent a dynamic and complex ice sheet margin during deglaciation. This is because the close spacing of several arcuate moraine sequences likely represents short-term fluctuations of a highly sensitive ice sheet responding to topography and climate (e.g. Figure 6.2g-h).

The north-eastern side of the Lyngen Peninsula and the coastal islands of Kågen and Ulløya (Figure 6.1) are outside the limits of the Tromsø-Lyngen moraines and thus would most likely have been isolated from the SIS during the YD/Tromsø-Lyngen event (Kverndal and Sollid, 1993; Evans *et al.*, 2002; Hughes *et al.*, 2016). At these sites, the glaciated valley landsystem dominates (Figure 6.2c-d). There is also some evidence of periglacial activity following deglaciation, evidenced by the development of several large rock glacier complexes (cf. Leigh *et al.*, 2020). The north-west orientated valleys of northern Lyngen and the north-east orientated Kågen and

Ulløya valleys have some of the most extensive, numerous, and distinctive inset sequences of moraines throughout the region (e.g. Figure 6.2c-d) and bracketing ages on a select few moraines indicate that some may have been formed prior to the YD, like those of Strupskardet (Bakke *et al.*, 2005a).

In the mountains of southern Lyngen, north and south of Kåfjord, the Kvænangstinden massif (after the tallest mountain Store Kvænangstinden, 1,178 m a.s.l), as well as across the Riehppe plateau, a diverse mixture of glacial geomorphological features are found (cf. Leigh *et al.*, 2020). Most notable are the smaller, but well-defined moraine sequences found just beyond the valley mouths and inset up-valley (e.g. Figure 6.2k-l) often extending to the present-day glacier margins, or into empty cirques. There are also sporadic moraines radiating around the mountain plateaus; these fragmentary deposits likely record the presence of old plateau icefields emerging from the flat-topped summits. On the isolated plateaus throughout the study area the present-day glaciers that remain (e.g. glaciers 157 and 158 (Noammerjiehkki) in the Kåfjord mountains) are currently in a phase of rapid disintegration (Leigh *et al.*, 2020). These glaciers retain the form of small mountain icefields, with small ice tongues filling topographic depressions (Figure 6.2e-f). Finally, a substantial proportion of rock glaciers are also found within these valley systems, representing a key record of mountain deglaciation recording a signal of glacial debuttressing and the evolution from a glacial to rock glacier transition.

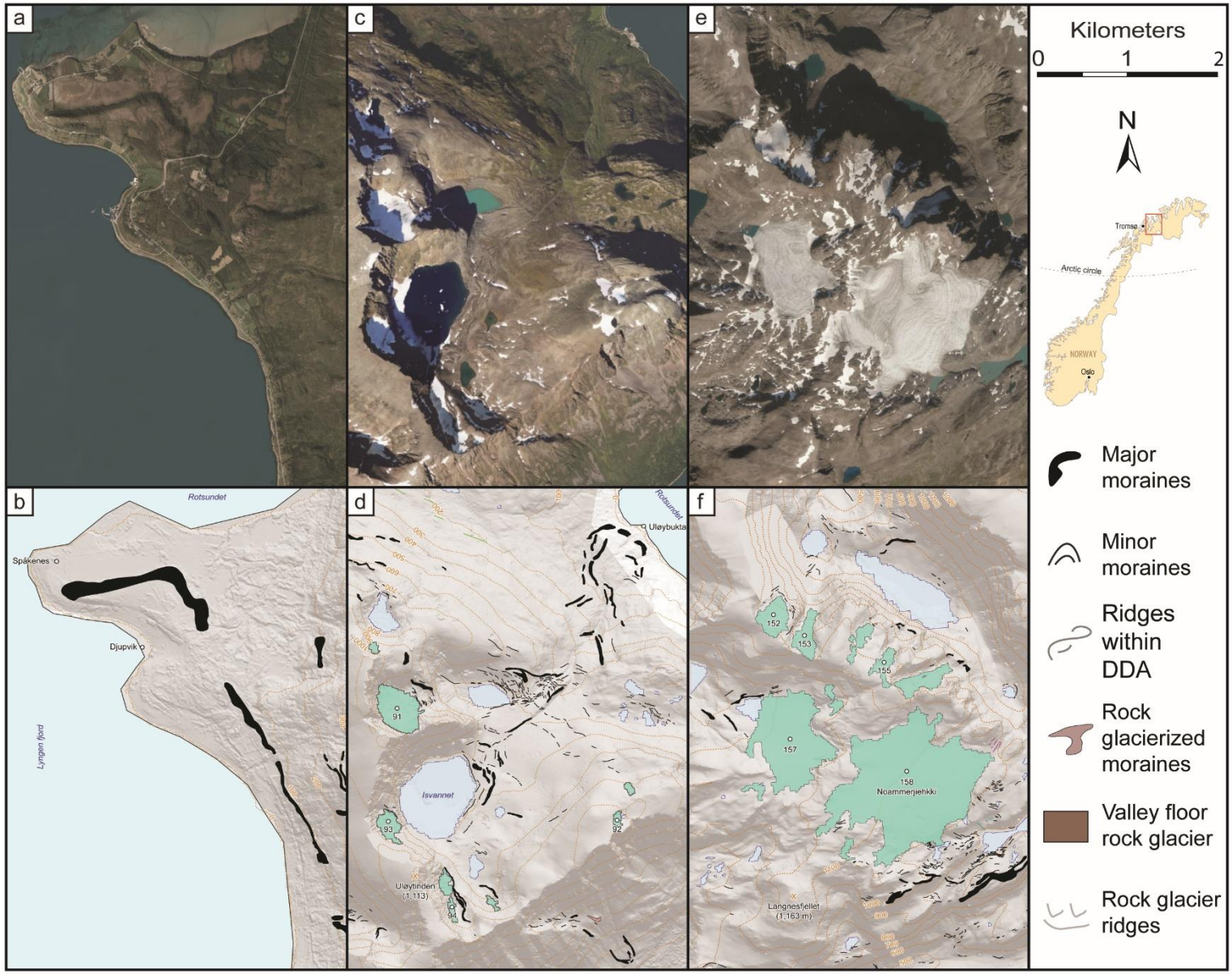
a
c
e
b
d
f
Kilometers
0
1
2
N
Tromsø
Arctic circle
NORWAY
Oslo
Major moraines
Minor moraines
Ridges within DDA
Rock glacierized moraines
Valley floor rock glacier
Rock glacier ridges
Rotsundet
Spåkenes
Djupvik
Lyngen fjord
Uløybukta
Isvannet
Uløytinden (1,113)
Langnesfjellet (1,163 m)
Noammerjiehkki
91
92
93
94
152
153
155
157
158

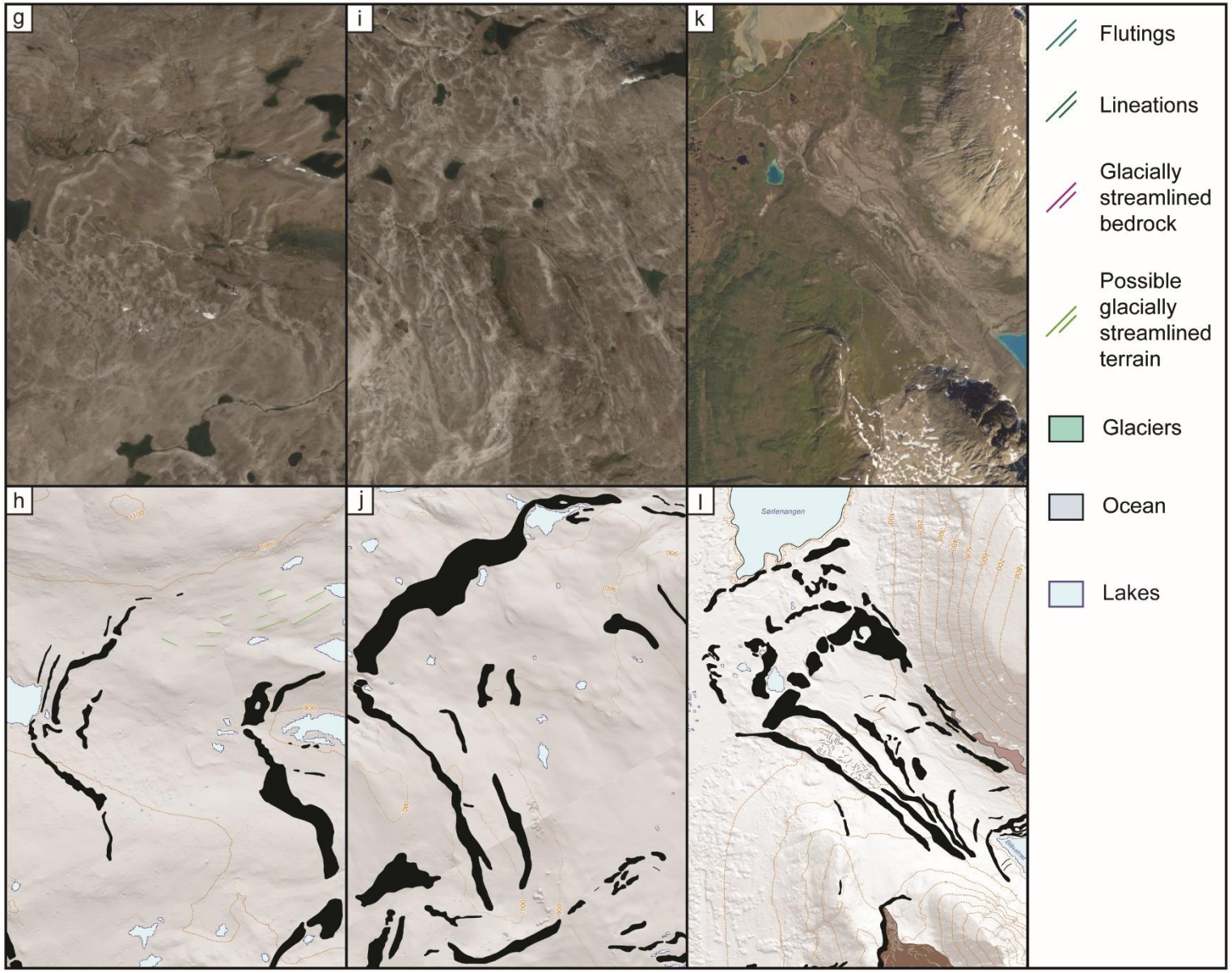
g
i
k
h
j
l
Sørlenangen
Flutings
Lineations
Glacially streamlined bedrock
Possible glacially streamlined terrain
Glaciers
Ocean
Lakes

Figure 6.2. *Exerts from the mapping of Leigh et al. (2021) showing: (a-b) the Spåkenes moraine, part of the Tromsø-Lyngen moraine complex, found at the head of Lyngen fjord; (c-d) the large valley moraine system on the island of Ulløya, with latero-frontal moraine extending to near sea level; (e-f) the disintegrating Noammerjiehkki plateau ice cap and surrounding glaciers in the Kåfjord mountains; (g-h) a series of inset arcuate moraines large moraines north-west of lake Guolasjávri; (i-j) closely spaced arcuate moraines on the inaccessible upland plateau; (k-l) well-defined moraines in Strupskardet formed from just beyond the valley mouth showing a distinct and nearly equally spaced up-valley. Imagery in the top panels (a, c, e, g, i, k) was captured on 24.08.2016 and is from www.norgeibilder.no. Maps in the bottom panels (b, d, f, h, j, l) use Leigh et al. (2021) mapping over a hill-shaded ArcticDEM. All panels are presented at a 1:20,000 scale.*

6.5.2. Rotsund Valley moraine morphology

6.5.2.1. Hjemtverrdalen

In Hjemtverrdalen (forelands of glaciers 115 and 117; Figure 6.1bi and 6.3a) a series of three near-continuous latero-frontal moraines were studied. The oldest frontal moraine (HM1; Figure 6.3a) extends ~1 km into the main Rotsund Valley and has a steep, 20 m high distal slope and shallow proximal slope both rising to a well-defined crest up to ~5 m wide. Inside HM1 and located ~160 m up-valley is a smaller frontal moraine, HM2 (Figure 6.3a), which is characterised by a ~7 m high distal slope and a broad crest. The youngest moraine examined (HM3; Figure 6.3a) is located ~190 m up-valley from HM2 and is characterised by a very steep and ~30 m high distal slope with broad crested (~5 m wide) lateral ridges and narrower (2-3 m wide) frontal ridge.

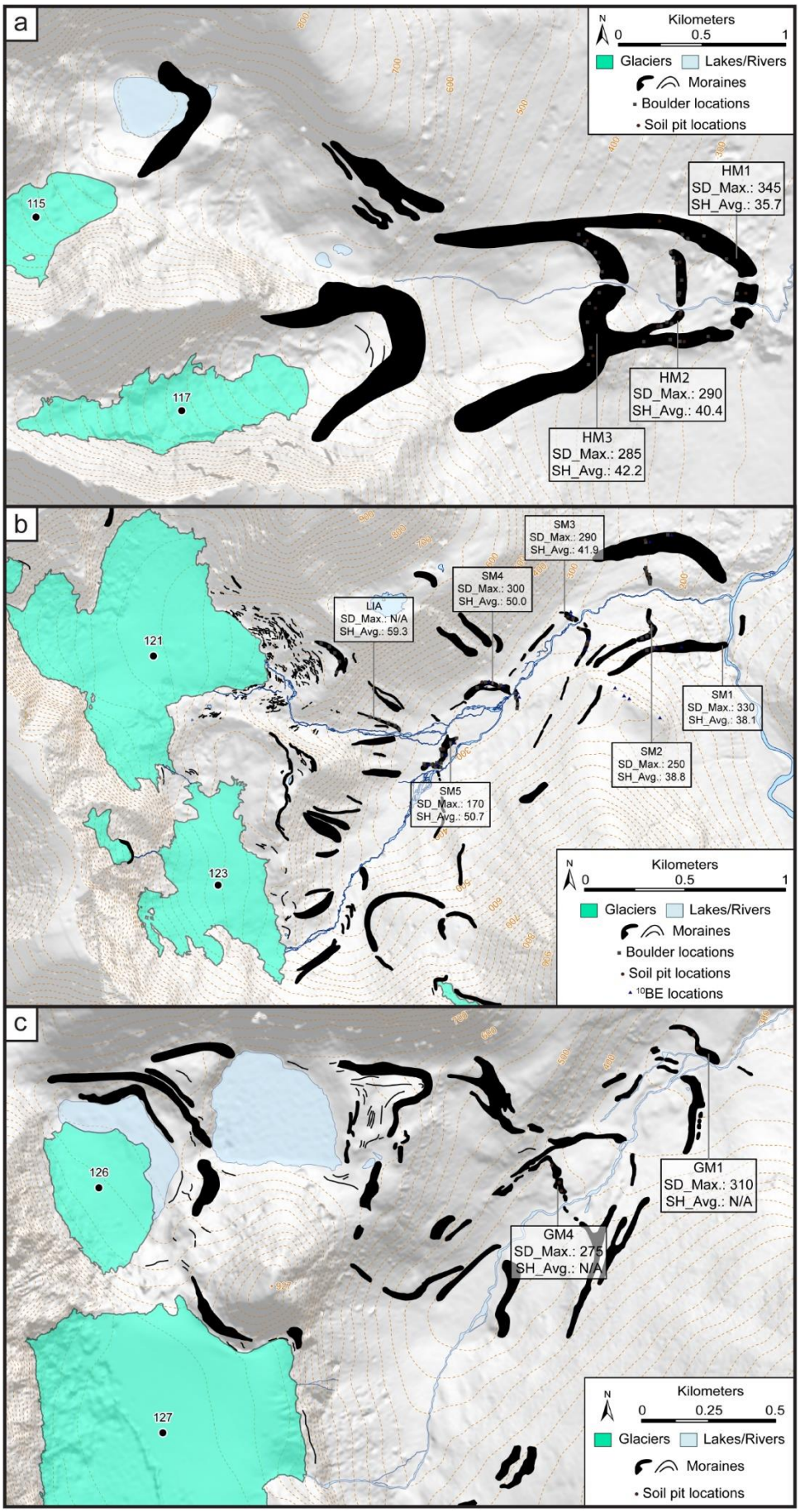
a
N
Kilometers
0
0.5
1
Glaciers
Lakes/Rivers
Moraines
Boulder locations
Soil pit locations
HM1
SD_Max.: 345
SH_Avg.: 35.7
HM2
SD_Max.: 290
SH_Avg.: 40.4
HM3
SD_Max.: 285
SH_Avg.: 42.2
115
117
b
SM3
SD_Max.: 290
SH_Avg.: 41.9
SM4
SD_Max.: 300
SH_Avg.: 50.0
LIA
SD_Max.: N/A
SH_Avg.: 59.3
SM1
SD_Max.: 330
SH_Avg.: 38.1
SM2
SD_Max.: 250
SH_Avg.: 38.8
SM5
SD_Max.: 170
SH_Avg.: 50.7
121
123
Kilometers
0
0.5
1
Glaciers
Lakes/Rivers
Moraines
Boulder locations
Soil pit locations
10BE locations
c
GM1
SD_Max.: 310
SH_Avg.: N/A
GM4
SD_Max.: 275
SH_Avg.: N/A
126
127
Kilometers
0
0.25
0.5
Glaciers
Lakes/Rivers
Moraines
Soil pit locations

Figure 6.3. *Moraine mapping of the three subsidiary valleys within the Rotsund Valley; (a) Hjemtverrdalen, (b) Sorbmejiehkki, (c) Goahtevággi. All sampled moraines are labelled with their associated maximum soil depth (depth to top of C-horizon; SD_Max), average Schmidt hammer R-value (SH_Avg). Base image is the Arctic DEM (courtesy of the Polar Geospatial Centre).*

6.5.2.2. Sorbmevággi

Sorbmevággi (foreland of glaciers 121 and 123; Figure 6.1bii and 6.3b) contains a complex sequence of moraines, of which five were studied in detail. The oldest moraine (SM1; Figure 6.3b and Figure 6.4a) extends ~0.8 km out of Sorbmevággi into the main Rotsund Valley (between 2.6 and 2.9 km from the present-day glaciers 121 and 123, respectively). In its lateral portions it has a steep distal slope with a height of ~10 m, rising to a well-defined crest on the true right (up to ~5m wide), while on the true left, the crest is poorly defined with multiple ridge features recording either moraine de-stabilisation (e.g. melt of buried ice core) or post depositional reworking (e.g. input from rock-avalanche deposits). The proximal slope is steep and ~10 m high, and, on the true right, has smaller ridges inset against it.

Inside the SM1 lateral moraine is a small, recessional moraine (SM2; Figure 6.3b and Figure 6.4b), which is the most subdued moraine in the sequence with a near symmetrical proximal and distal slope. It rises to a height of ~7m on the true right but only ~2 m on the true left. SM2 is positioned at the edge of the treeline with well-established Birch trees having colonised its slopes.

Located ~400 m up valley and at the head of Sorbmevággi, is an imposing latero-frontal moraine (SM3; Figure 6.3b and Figure 6.4c), which extends across the whole valley floor. Its frontal portion has a steep distal slope more than 10 m high, a well-defined crest ~2-3 m wide, and a steep proximal slope (~5 m high), best preserved on the true left. On the true right, a series of complex ridges within DDAs occur on the proximal slopes of SM3. The DDAs are small areas of complex, hummocky, terrain manifest as a disorganised ridge and furrow network separated by a mix of sediment veneer, rocky and bouldery debris, and vegetated ground (Leigh *et al.*, 2021). The lateral portion of SM3 sits low on the valley sides. On the true left it extends only part way into Sorbmevággi where it is overlain by colluvium; on the true right it can be

traced for an additional ~340 m before it becomes indistinguishable from the area of DDA.

Located ~450 m up valley from SM3 is another latero-frontal moraine (SM4; Figure 6.3b and Figure 6.4d) with steep distal and proximal slopes <10 m high and a broad crest, which in some places is poorly defined. The lateral portions are clearly defined on both sides of the valley for ~130 m, after which colluvium on the true left overrides the feature and DDA is developed on the true right.

Inside SM4, on the true right side of Sorbmevággi and located ~350 m up valley, and ~250 m outside the LIA moraine, is a fragmented latero-frontal moraine (SM5; Figure 6.3c and Figure 6.4e). The distal slope is steep and ranges from ~5 to ~15 m high. The crest is well defined (2-3 m wide) and the proximal slope is short and shallow. SM5 has been fragmented, presumably by post-depositional meltwater drainage, and is identifiable as a ~160 m long frontal portion and a 180 m long lateral portion that grades up to the valley side bedrock face. In the frontal portion of SM5, the distal slope is partly superimposed by an area of rock slope failure deposits, clearly distinguishable from the glacial deposits by their size, angularity, and positioning within the valley. On the true right, SM5 shows signs of bifurcation where two ridges emerge from one in its central portion. This may have been caused by melt out of buried glacial ice or by a dynamic frontal margin.

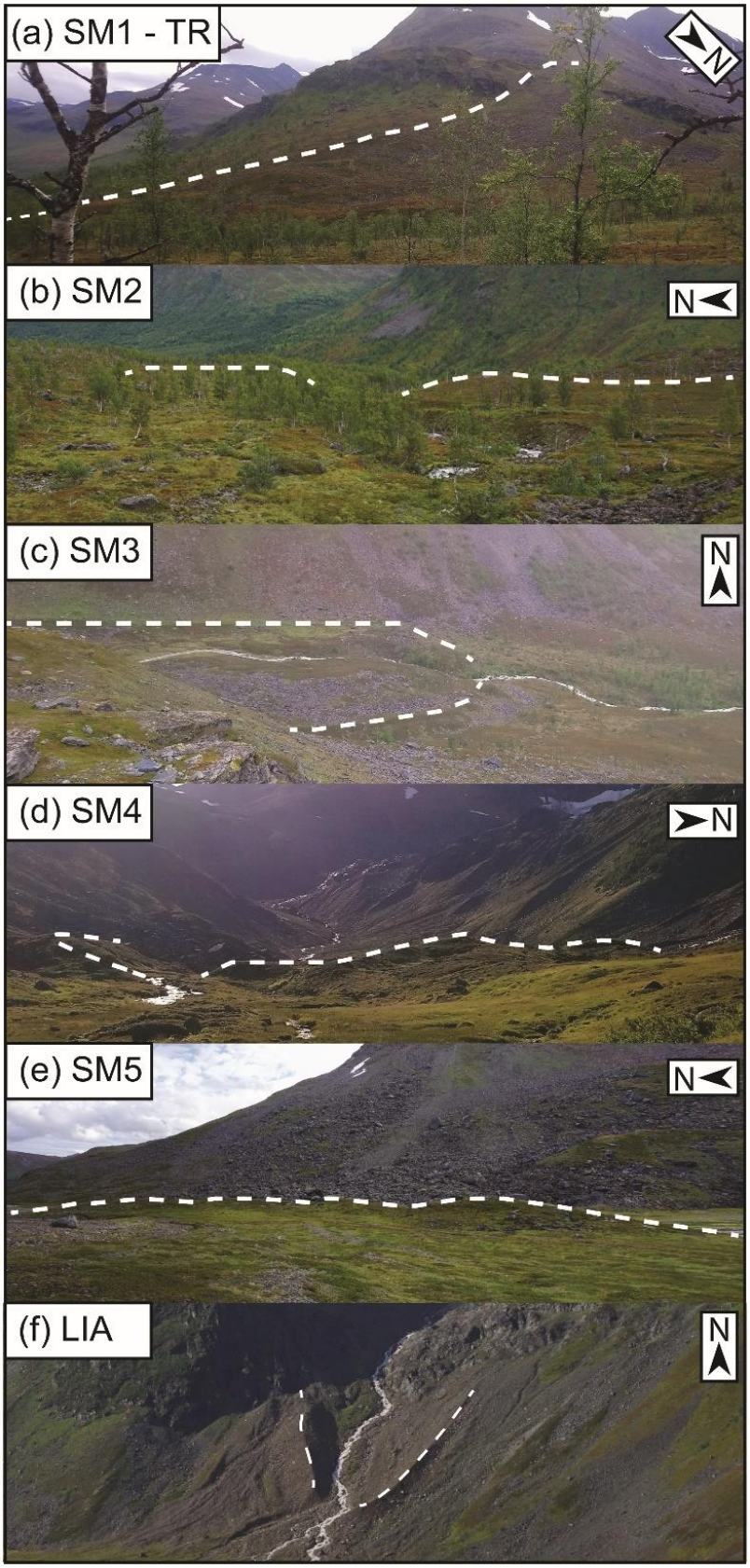

Figure 6.4. *Photographs showing the Sorbmejiehkki moraine sequence from the terminal moraine (SM1) to the LIA moraine (Leigh et al, 2020). The white dashed line represents the moraine crest. Imagery: J.R. Leigh.*

6.5.2.3. Goahtevággi

In Goahtevággi (foreland of glaciers 126, 127, 129, 131, and 132; Figure 6.1biii and 6.3c) only two moraines were studied. These moraines do not contain large, exposed boulders on their crest and, therefore, it was not possible to collect Schmidt hammer R-values. Unlike the other valleys, the oldest moraine (GM1; Figure 6.3c) does not extend into the main Rotsund Valley but is instead situated at the head of Goahtevággi and only accessible on its true left. GM1 is a low-lying, broad feature situated on a wide, flat surface ~130 m higher than the main Rotsund Valley floor. The moraine has a steeper and higher proximal slope than distal slope and cannot be traced along the valley sides. Overall, GM1 is the most fragmented and subdued feature studied, likely resulting from post depositional re-working.

Around 700 m up valley from GM1 is a much larger latero-frontal moraine that spans the full width of Goahtevággi (GM4; Figure 6.3c) and is ~1.2 km distal to the present-day glacier 127. There are two additional moraines between this moraine (GM4) and the outermost moraine (GM1), but GM4 was selected for sampling as it was presumably the last moraine that was formed when all glaciers in this catchment were confluent and should provide an indication of glacier activity midway through the whole moraine sequence. GM4 can be traced along the valley walls and is only broken by the Goahtejohka river channel. Its distal slope is steep and ~30 m high and it has a broad crest (~15 m wide) and shallower proximal slope that is overlain/overlapped by multiple ridges and ridge-like features (DDA).

6.5.3. Schmidt hammer data

A total of 110 boulders were sampled from moraines in Strupskardet and the Rotsund Valley, with a total of 1,100 readings (R-values). The range in mean R-values across our entire dataset is broad, extending from 59 on the Sorbmevággi LIA moraine (SM LIA; Table 6.1) to 35 on the Hjemtverrdalen terminal moraine (HM1; Table 6.1). While there is a high variability in the R-values on individual boulders, there is an overall down valley decrease in R-values, consistent with results from other investigations that have used the Schmidt hammer to establish moraine ages in Norway and elsewhere (e.g. Matthews and Winkler, 2011; Winkler, 2014; Tomkins *et al.*, 2018b, 2018a).

Table 6.1. Schmidt hammer R-values from moraines within Strupskardet and the Rotsund Valley.

Site	Moraine age*[#] (cal. yr. BP) Or Moraine ID[#]	Moraine mean R-value ±95% CI[+]	Feature skewness	Feature kurtosis
Strupskardet	9,300-8,900 (M12)*	41.2 ±1.2	0.06	-0.20
	9,800-9,400 (M11)*	38.1 ±2.3	0.48	0.74
	12,000-11,600* (M9)*	36.0 ±1.5	0.33	-0.04
	12,600-12,400* (M8)*	36.4 ±1.2	0.05	-1.09
Sorbmevággi	SM LIA	59.3 ±1.2	-0.89	0.86
	SM5	50.7 ±1.5	-0.37	0.26
	SM4	50.0 ±1.2	-0.78	0.63
	SM3	41.9 ±1.3	-0.19	-0.27
	SM2	38.8 ±1.7	-0.05	-0.52
	SM1	38.1 ±1.6	-0.06	-0.51
Hjemtverrdalen	HM3	42.2 ±1.3	-0.56	0.56
	HM2	40.4 ±2.8	-0.27	-0.54
	HM1	35.7 ±1.6	0.04	-0.22

*Bracketing moraine ages and moraine IDs from Bakke et al. (2010)

[+]Confidence intervals

[#]Locations detailed in Appendix B

6.5.3.1. Strupskardet

The R-values from the moraines of Strupskardet (Table 6.1, Figure 6.5 and 6.6) show a clear decrease with distance down valley (i.e. moraine relative age). Use of a two-sample t-test indicates that mean R-values from most moraines represent significantly different populations (p-values <0.05). The 12,000-11,600 and 12,600-12,400 cal. yrs BP moraines, as dated by Bakke et al. (2005a), however, have p-values >0.05 (0.67) and therefore cannot be defined as statistically different populations.

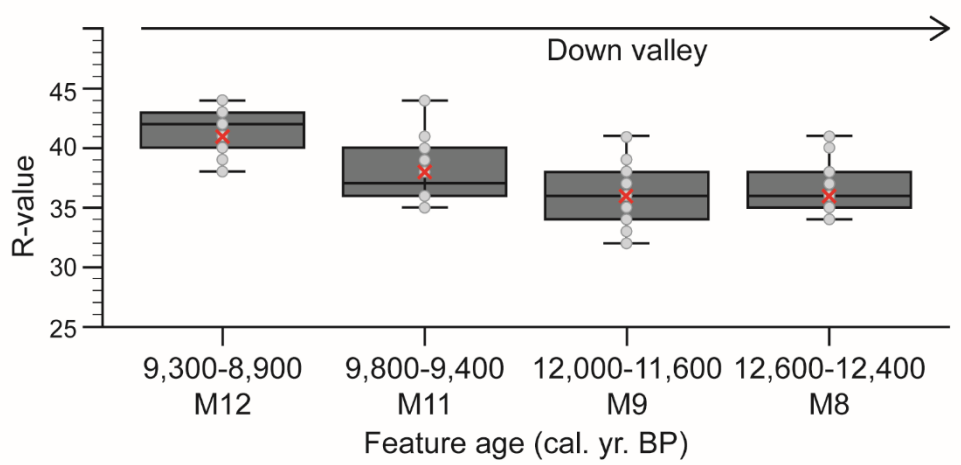

Figure 6.5. *Box plots of Schmidt hammer R-values from Strupskardet moraines with independent age control. Light grey dots represent the mean R-values from individual boulders, while the red crosses represent the mean R-value for each moraine. Dark grey box shows the interquartile range, the black horizontal line the median, and whiskers show the minimum and maximum R-values for each moraine.*

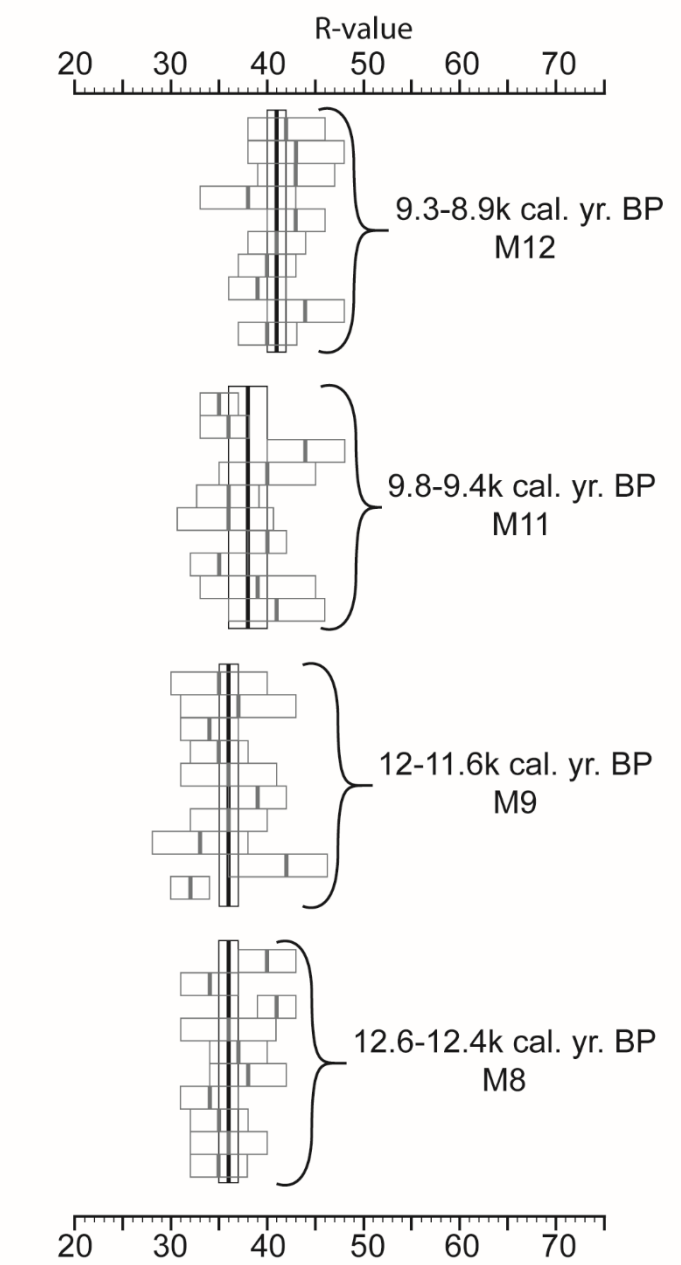

Figure 6.6. *Mean R-value and ±95% confidence intervals for each boulder (grey box and line) and mean R-value from all boulders on a feature (black box and line) from each moraine sampled in Strupskardet.*

6.5.3.2. The Rotsund Valley

Schmidt hammer measurements were only possible within Hjemtverrdalen and Sorbmevággi and not in Goahtevággi. The most extensive Schmidt hammer dataset was established in Sorbmevággi, thereby constituting a suitable baseline from which comparisons of rock surface hardness and hence relative moraine age can be made. The R-values from the moraines of Sorbmevággi (Table 6.1, Figure 6.3b, 6.7a, and 6.8a) show a clear decrease in R-value with distance down valley (i.e. moraine relative age). Use of a two-sample t-test confirms that mean R-values from four out of the six moraines represent significantly different populations. Moraines SM5 and SM4, alongside SM2 and SM1, however, have p-values >0.05.

The R-values from the moraines of Hjemtverrdalen (Table 6.1, Figure 6.3a, 6.7b and 6.8b) suggest two sets of moraines that show a significant reduction in R-value with distance down valley (i.e. moraine relative age). Use of a two-sample t-test indicates that HM3 and HM2 do not represent significantly different populations, but HM3/HM2 and HM1 represent significantly different populations.

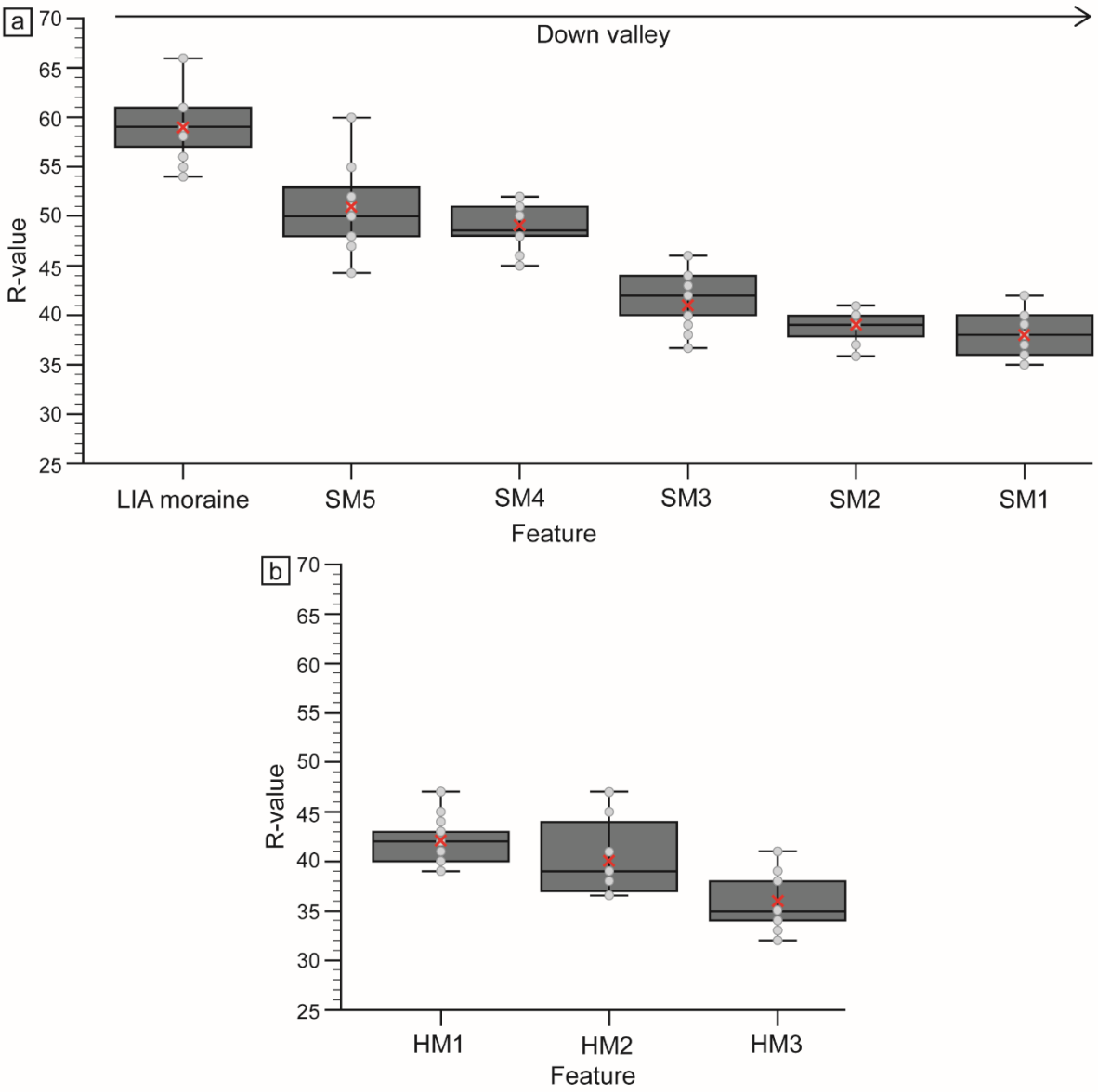

Figure 6.7. *Box plots of Schmidt hammer R-values from: (a) Sorbmevággi moraines, and (b) Hjemtverrdalen moraines. Light grey dots represent the mean R-values from individual boulders, while the red crosses represent the mean R-value for each moraine. Dark grey box shows the interquartile range, the black horizontal line the median and whiskers show the minimum and maximum R-values for each moraine.*

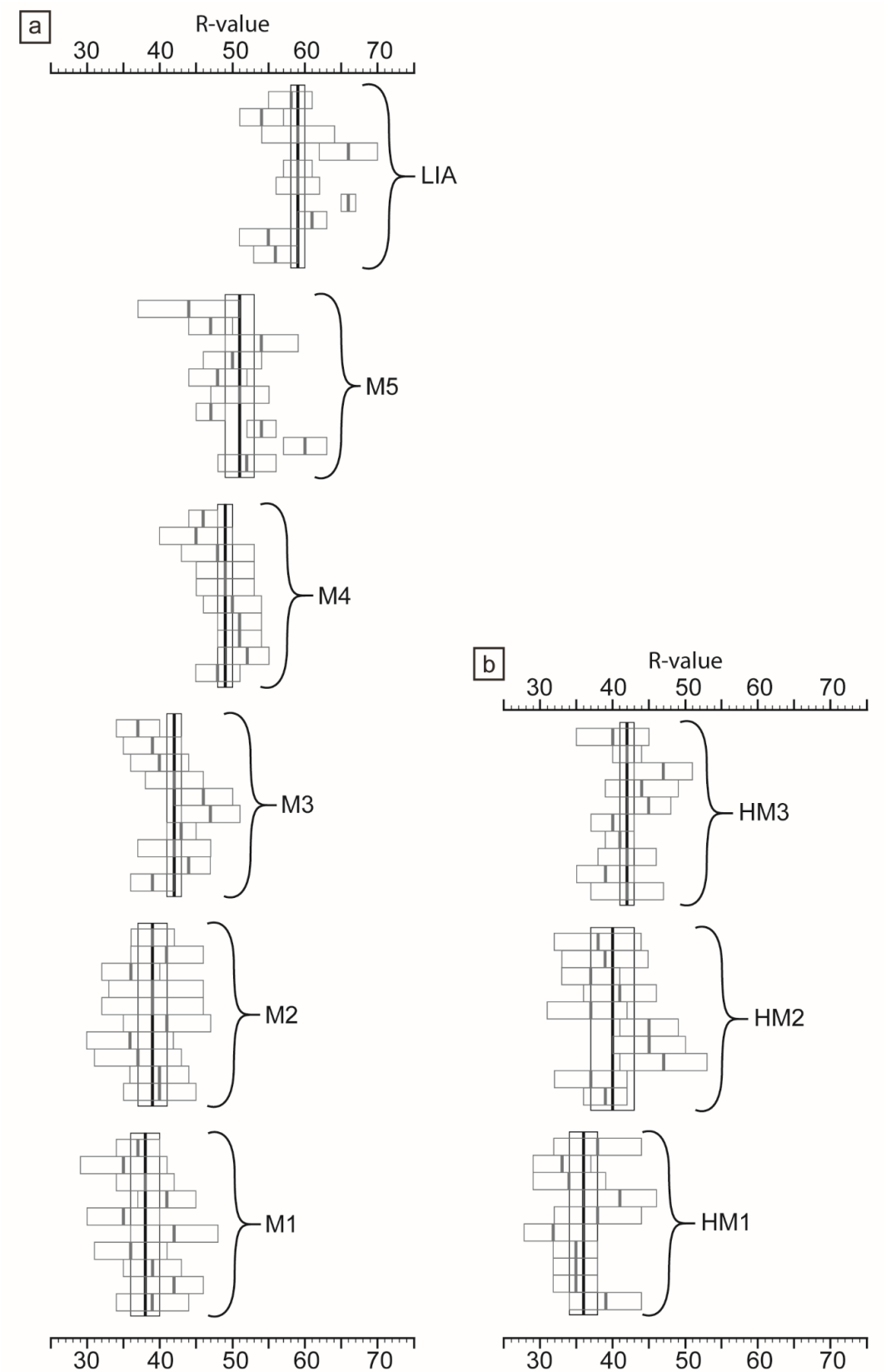

Figure 6.8. *Mean R-value and ±95% confidence intervals for each boulder (grey box and line) and mean R-value from all boulders on a feature (black box and line) from each moraine in (a) Sorbmevágg and (b) Hjemtverrdalen.*

6.5.4. Soil Chronosequences

For most soil pits excavated in the Rotsund Valley, the surface vegetation consisted of a dispersed to thick matt of plants from the *Vaccinium* and *Empetrum* genus of dwarf shrubs (e.g. bilberry and/or crowberry) and/or a variety of mosses and lichens such as juniper haircap moss (*Polytrichum juniperinum*) and reindeer lichen (*Cladonia rangiferina*). Additionally, some soil pits were within the treeline of well-established downy birch (*Betula pubescens*). Owing to the mountainous terrain and isolation of the sites, it is assumed no major anthropogenic land management has occurred since deglaciation. Hence the soils are unaltered and present a natural chronosequence of soil development.

Of the 30 soil pits examined, 29 are classified as Haplic Podzols (Ellis, 1979; cf. Bridges, 1997) exhibiting a distinct E-horizon of ash-grey colour (Figure 6.9), and one pit (RV-19-SP18) was considered a Cambic Podzol (Bridges, 1997) on the basis that no distinct grey E-horizon was present. The podsolization of the soils is indicative of the long, cold winters and short mild summers of the region, and the Taiga biome that dominates the forelands at the elevations of the moraines examined (Fitzpatrick, 1983; Evans, 1999a; Sauer *et al.*, 2007).

The examined soils (e.g. Figure 6.9) generally comprised a thin layer of organic matter and vegetation on the surface (O-horizon), directly underlain by a very dark (near black) layer of soil (A-horizon), rich in organic material and in many cases held together by a thick matt of roots. Below the A-horizon is the characteristic eluvial E-horizon, forming a striking ‘ash-grey’ layer from which minerals have been leached. Beneath the E-horizon is the illuvial B-horizon, comprising parent material which has been altered by pedogenic processes and in which minerals accumulate, having been leached from the E-horizon above. The B-horizon is firmer in texture than the horizons above, with a darker brown colour and often intermixed with larger clasts. Finally, the B-horizon transitions sharply into a compact C-horizon of unaltered parent material, often with closely packed, larger clasts. The C-horizon is also recognisable by its lighter colour than the soil above, its coarser texture, and the lack of visible organic material (e.g. roots). In one instance (RV-19-SP08), a layer of soil between the B and C-horizon was found and identified as a layer of oxidised parent material and denoted as a Cox-horizon (oxidised C horizon; Birkeland, 1978).

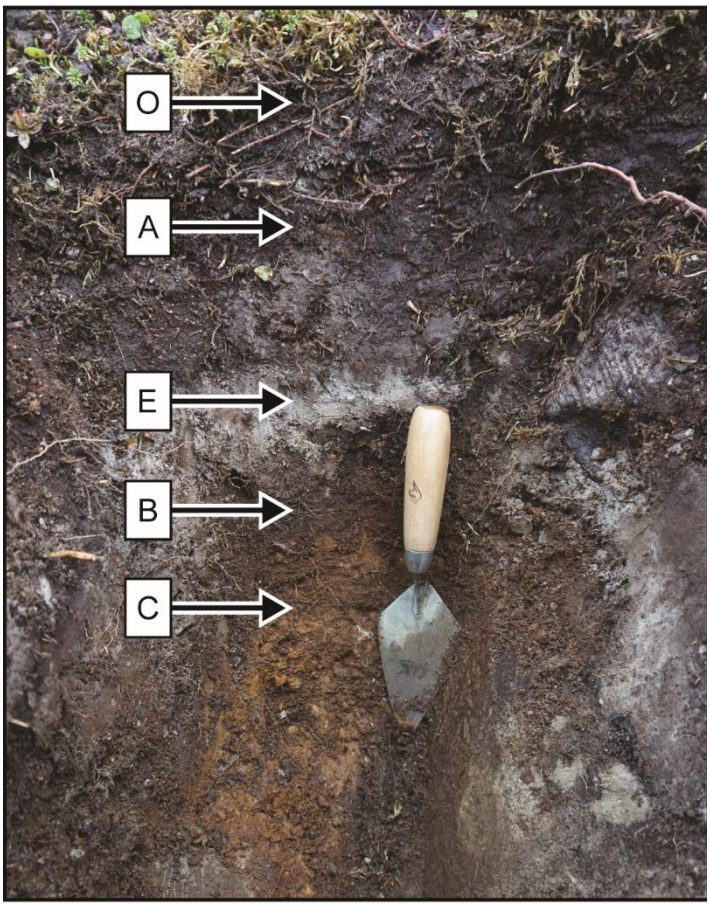

Figure 6.9. *Soil profile found in Rotsund Valley (pit RV-19-SP22) from the moraine crest, with major soil horizons labelled (see text for explanation). Note: The trowel is 127 mm long. Imagery: J.R. Leigh.*

6.5.4.1. The Rotsund Valley

Of the three subsidiary valleys within the Rotsund Valley (Hjemtverrdalen, Sorbmevággi, and Goahtevággi), the most extensive chronosequence was established in Sorbmevággi. Thus, the Sorbmevággi chronosequence was used as a baseline from which comparisons of soil development within Hjemtverrdalen and Goahtevággi are made. The general soil profiles of Sorbmevággi (Figure 6.4b, and 6.10) reveal that, although there is some intra-landform variation between soil pits, the overall trend is one of increasing soil depth with distance down valley (i.e. with moraine relative age; SM5-SM1). For example, the youngest pre-LIA moraine (SM5) has a maximum soil depth to the base of the B-/top of C-horizon of 170 mm, whereas the oldest moraine (SM1) has a maximum depth of 330 mm (Table 6.2). There is, however, one notable outlier to this trend; the small end moraine (SM2) has considerably thinner

and shallower soils than was expected based upon its position within the moraine sequence. The specific B-horizon characteristics from each soil pit in Sorbmevággi (Table 6.2) show a mix of changes in the CDE of both wet and dry B-horizons and indicate no strong pattern of increasing soil reddening with increasing distance down valley (i.e. with increasing moraine relative age), as might have been expected based on previous work with alpine soils in Norway (e.g. Evans, 1999a). Generally, the pH of the B-horizon is that of decreasing acidity with distance down valley with the outermost soils being the most alkaline. Finally, the percentage of organic matter in the B-horizon of each moraine, established via LOI, generally increases down valley (SM5-SM2), indicating increased penetration and/or build-up of plant material in the older soils. In part, this may be linked with the larger plants which are present on the outer moraines and having had greater duration to establish and grow thus decreasing acidity of the soil over time.

Although it was not possible to establish a full chronosequence in either Hjemtverrdalen or Goahtevággi, the outermost moraines (HM1 and GM1) were sampled at each site, with at least one other recessional moraine, to provide some context of the glacial history in these two valleys. The specific B-horizon characteristics from moraines within Hjemtverrdalen and Goahtevággi are presented in Table 6.2 and generalised soil profiles are shown in Figures 6.11 and 6.12. There is again a consistent trend of deepening soils with distance down valley (i.e. with increasing moraine relative age; Figures 6.11 and 6.12), with the outermost moraines HM1 and GM1 both having maximum soil depths >300 mm. The specific B-horizon characteristics of Hjemtverrdalen and Goahtevággi show a similar range of values as those in Sorbmevággi, with some clear down valley trends including a thickening of B-horizon, a clear and consistent increase in the CDE (reddening) of wet soils, and decreasing acidity of the B-horizon (all the outermost moraines have pH values >5.0; Table 6.2).

Overall, there is a clear pattern of increasing moraine crest soil depth with distance down valley (Table 6.2). Soil deepening is attributable to a thickening of both the E- and B-horizons. Additional soil properties such as pH, organic content, and colour show fewer clear trends. Where boulders are not present on the moraine crest (such as in Goahtevággi), soil chronosequences provide a valuable alternative means of relative age dating, enabling expansion of geochronological investigations into additional (local) sites.

Table 6.2. *Soil characteristics from moraines within the Rotsund Valley*

Site	Moraine ID	Soil pit ID	Soil Sample ID[#]	B-Horizon											
				CDE[1]	Mean CDE[1]	CDE[2]	Mean CDE[2]	Organic content (%)	Mean organic content	pH	Mean pH	Thickness (mm)	Mean thickness (mm)	Depth* (mm)	Mean Depth* (mm)
Sorbmevággi	M5	SM5(P1)	RV-19-SP03B	4		16		7		4.5		45		165	
		SM5(P2)	RV-19-SP04B	10	6.7	16	16	11	9	4.8	5.0	90	70	170	165
		SM5(P3)	RV-19-SP05B	6		16		9		5.6		75		160	
	M4	SM4(P1)	RV-19-SP06B	5		12		9		4.5		80		300	
		SM4(P2)	RV-19-SP07B	5	6.7	10	11.3	9	10	4.6	4.5	155	100	285	277
		SM4(P3)	RV-19-SP08B	10		12		13		4.5		65		245	
	M3	SM3(P1)	RV-19-SP09B	6		24		14		4.9		120		290	
		SM3(P2)	RV-19-SP11B	10	8.7	12	20	8	11	4.7	4.8	150	112	290	295
		SM3(P3)	RV-19-SP12B	10		24		10		4.7		65		305	
	M2	SM2(P1)	RV-19-SP01B	20		24		15		5.2		100		230	
		SM2(P2)	RV-19-SP02B	20	20	18	20	16	16	5.0	5.2	85	95	250	240
		SM2(P3)	RV-19-SP15B	20		18		17		5.4		100		240	
	M1	SM1(P1)	RV-19-SP10B	24		18	20	6		5.7		150		330	
		SM1(P2)	RV-19-SP13B	8	13.3	24		10	9	5.1	5.4	125	125	325	328
		SM1(P3)	RV-19-SP14B	8		18		10		5.5		100		330	

Hjemtverrdalen		HM3(P1)	RV-19-SP16B	10		16		-		4.9		70		270	
	M3	HM3(P1)	RV-19-SP17B	3	5.7	12	17.3	-	-	5.1	5.3	80	90	230	262
		HM3(P3)	RV-19-SP18B	4		24		-		5.8		120		285	
		HM2(P1)	RV-19-SP22B	8		12		-		4.9		55		290	
	M2	HM2(P1)	RV-19-SP23B	8	8	18	18	-	-	4.9	5.0	80	63	220	252
		HM2(P3)	RV-19-SP24B	8		24		-		5.1		55		245	
		HM1(P1)	RV-19-SP19B	24		18		-		5.3		145		345	
	M1	HM1(P1)	RV-19-SP20B	10	15.3	18	18	-	-	5.9	5.5	135	130	265	305
		HM1(P3)	RV-19-SP21B	12		18		-		5.4		110		305	
Goahtevággi		GM_(P1)	RV-19-SP28B	4		12		-		5.0		65		225	
	M4	GM_(P2)	RV-19-SP29B	2	3.3	16	12	-	-	5.3	5.4	70	60	240	247
		GM_(P3)	RV-19-SP30B	4		8		-		5.8		45		275	
		GM1(P1)	RV-19-SP25B	10		18		-		4.9		85		290	
	M1	GM1(P2)	RV-19-SP26B	10	9.3	18	18	-	-	5.4	5.2	110	105	310	297
		GM1(P3)	RV-19-SP27B	8		18		-		5.4		120		290	

[1] CDE of wet soil (Buntley and Westin, 1965)

[2] CDE of dry soil (Buntley and Westin, 1965)

[#] Location detailed in Appendix B

* Depth to base of B-horizon/top of C-Horizon

- Measurements not possible due to COVID-19 laboratory closures

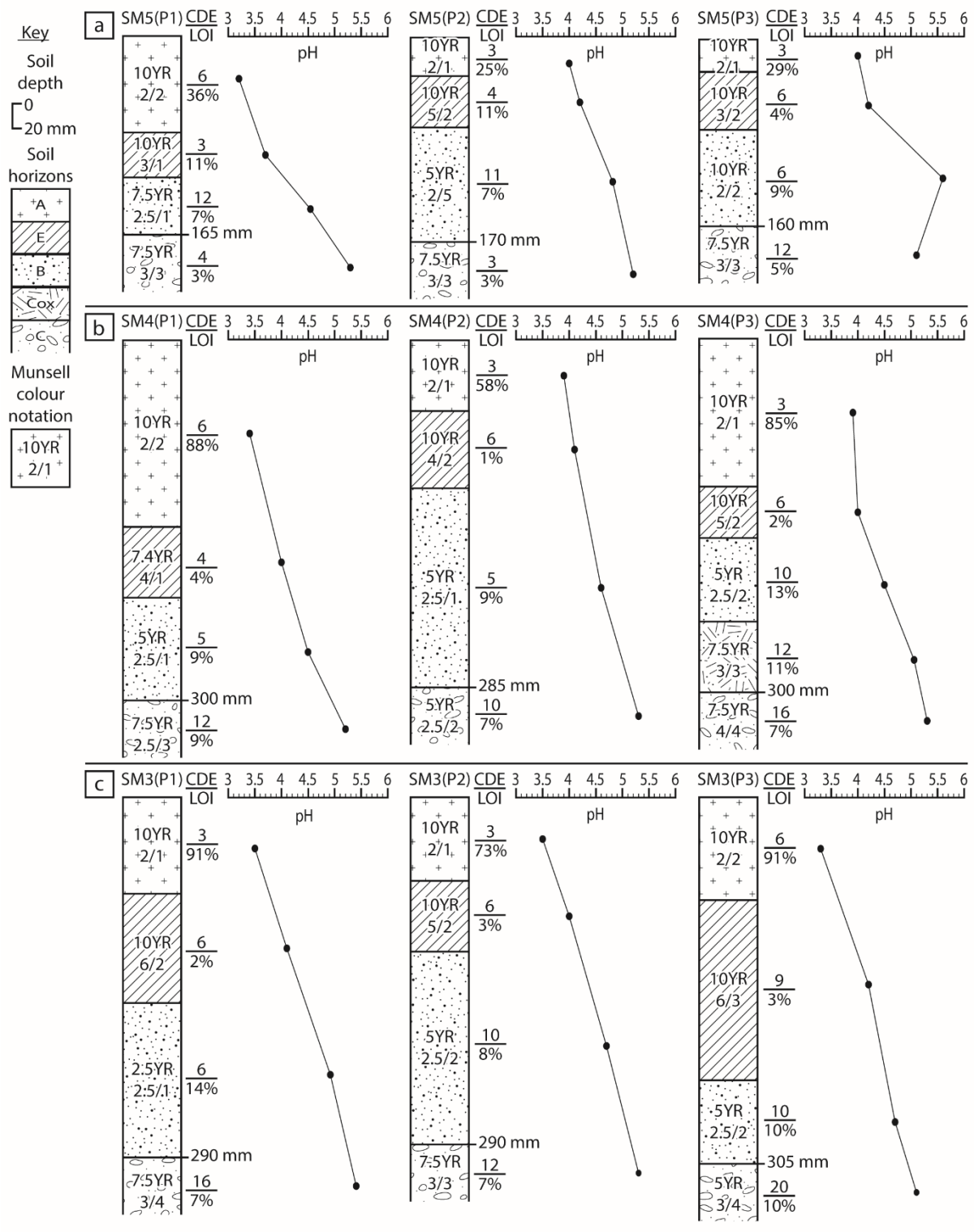
Key
Soil depth
0
20 mm
Soil horizons
A
E
B
Cox
C
Munsell colour notation
10YR 2/1
a
SM5(P1)
CDE
LOI
3 3.5 4 4.5 5 5.5 6
pH
10YR 2/2
6
36%
10YR 3/1
3
11%
7.5YR 2.5/1
12
7%
165 mm
7.5YR 3/3
4
3%
SM5(P2)
10YR 2/1
3
25%
10YR 5/2
4
11%
5YR 2/5
11
7%
170 mm
7.5YR 3/3
3
3%
SM5(P3)
10YR 2/1
3
29%
10YR 3/2
6
4%
10YR 2/2
6
9%
160 mm
7.5YR 3/3
12
5%
b
SM4(P1)
10YR 2/2
6
88%
7.4YR 4/1
4
4%
5YR 2.5/1
5
9%
300 mm
7.5YR 2.5/3
12
9%
SM4(P2)
10YR 2/1
3
58%
10YR 4/2
6
1%
5YR 2.5/1
5
9%
285 mm
5YR 2.5/2
10
7%
SM4(P3)
10YR 2/1
3
85%
10YR 5/2
6
2%
5YR 2.5/2
10
13%
7.5YR 3/3
12
11%
300 mm
7.5YR 4/4
16
7%
c
SM3(P1)
10YR 2/1
3
91%
10YR 6/2
6
2%
2.5YR 2.5/1
6
14%
290 mm
7.5YR 3/4
16
7%
SM3(P2)
10YR 2/1
3
73%
10YR 5/2
6
3%
5YR 2.5/2
10
8%
290 mm
7.5YR 3/3
12
7%
SM3(P3)
10YR 2/2
6
91%
10YR 6/3
9
3%
5YR 2.5/2
10
10%
305 mm
5YR 3/4
20
10%

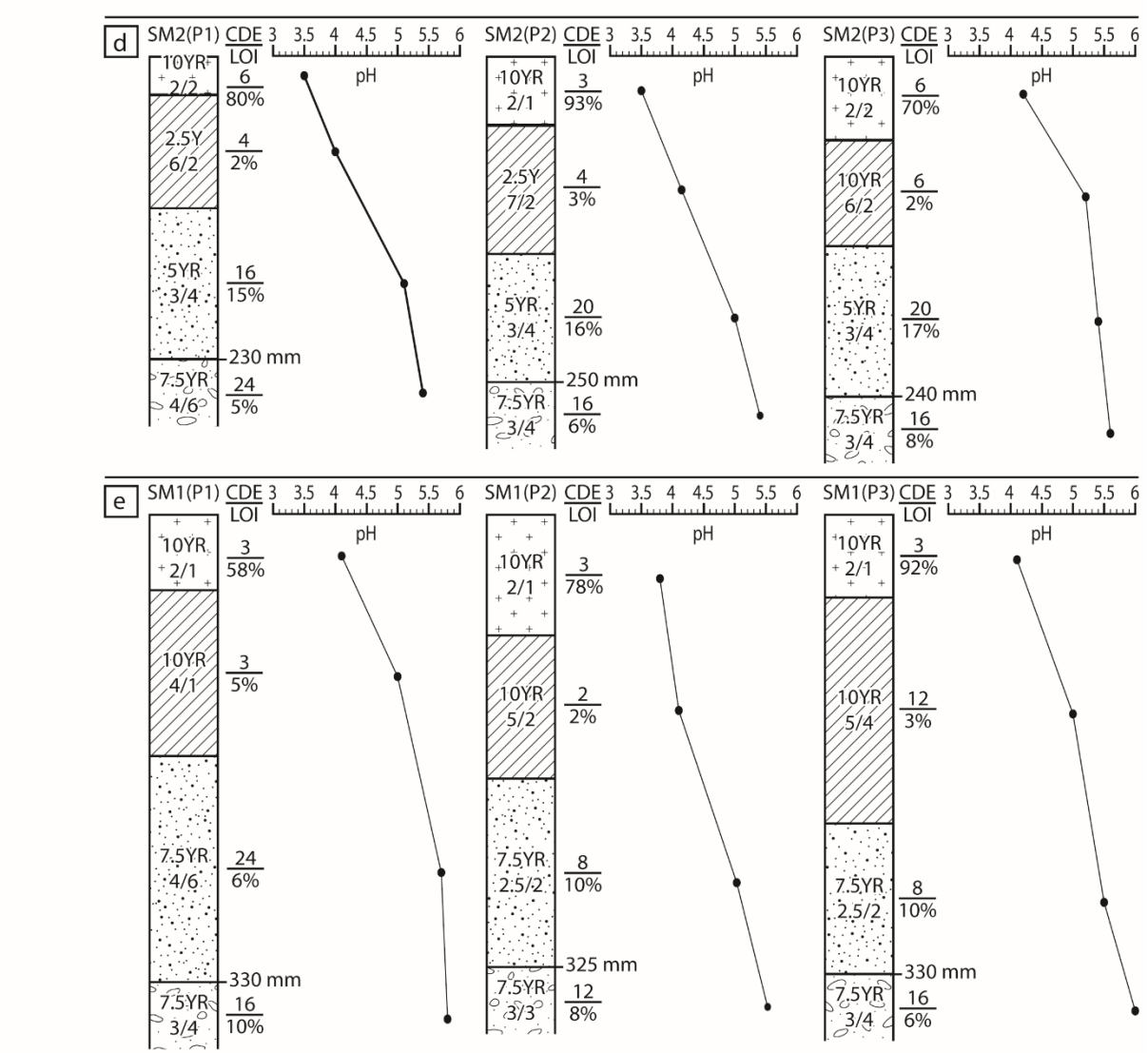

Figure 6.10. *Soil profiles from each soil pit on the moraines sampled in Sorbmevággi: (a) SM5, (b) SM4, (c) SM3, (d) SM2, and (e) SM1. Showing soil horizons (A to C-horizon), wet soil colour (using Munsell colour notation), wet soil CDE (following Buntley and Westin, 1965), LOI values, and soil pH.*

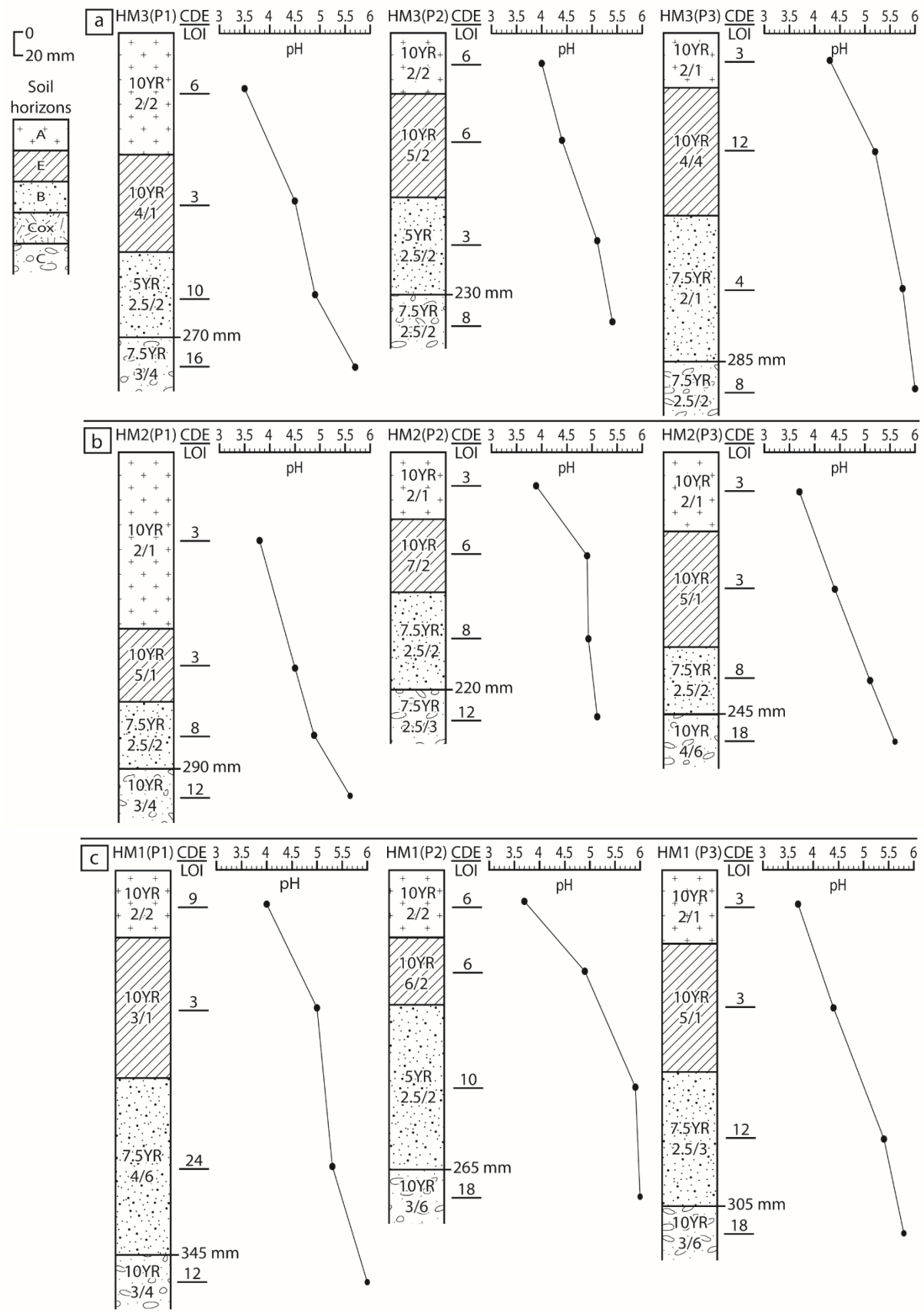
0
20 mm
Soil horizons
A
E
B
Cox
C
a
HM3(P1)
CDE
LOI
3 3.5 4 4.5 5 5.5 6
pH
10YR 2/2
6
10YR 4/1
3
5YR 2.5/2
10
270 mm
7.5YR 3/4
16
HM3(P2)
10YR 2/2
6
10YR 5/2
6
5YR 2.5/2
3
230 mm
7.5YR 2.5/2
8
HM3(P3)
10YR 2/1
3
10YR 4/4
12
7.5YR 2/1
4
285 mm
7.5YR 2.5/2
8
b
HM2(P1)
10YR 2/1
3
10YR 5/1
3
7.5YR 2.5/2
8
290 mm
10YR 3/4
12
HM2(P2)
10YR 2/1
3
10YR 7/2
6
7.5YR 2.5/2
8
220 mm
7.5YR 2.5/3
12
HM2(P3)
10YR 2/1
3
10YR 5/1
3
7.5YR 2.5/2
8
245 mm
10YR 4/6
18
c
HM1(P1)
10YR 2/2
9
10YR 3/1
3
7.5YR 4/6
24
345 mm
10YR 3/4
12
HM1(P2)
10YR 2/2
6
10YR 6/2
6
5YR 2.5/2
10
265 mm
10YR 3/6
18
HM1 (P3)
10YR 2/1
3
10YR 5/1
3
7.5YR 2.5/3
12
305 mm
10YR 3/6
18

Figure 6.11. *Soil profiles from each soil pit on the moraines sampled in Hjemtverrdalen: (a) HM1, (b) HM2, (c) HM3. Showing soil horizons (A to C-horizon), wet soil colour (using Munsell colour notation), wet soil CDE (following Buntley and Westin, 1965), LOI values, and soil pH.*

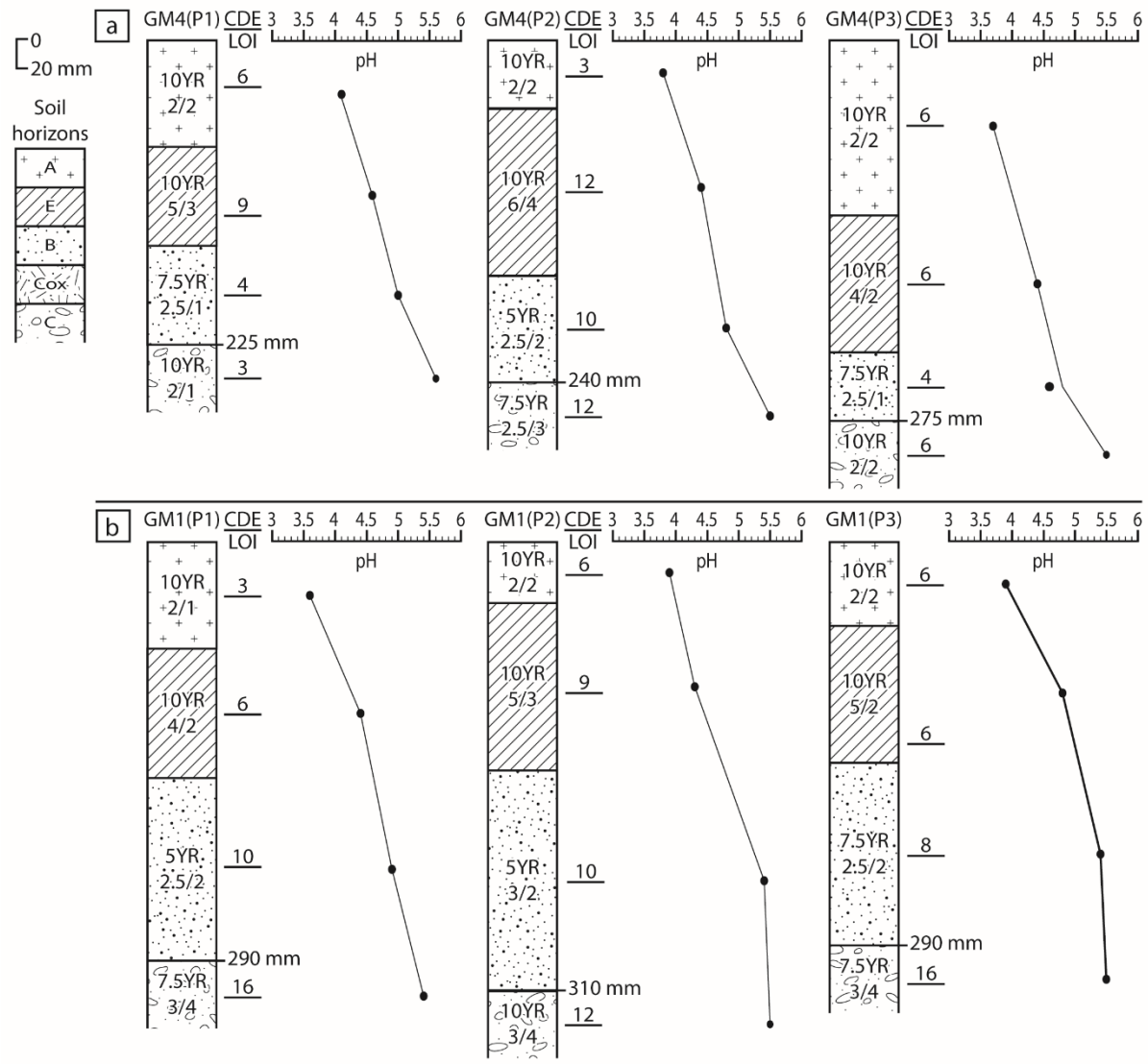

Figure 6.12. *Soil profiles from each soil pit on the moraines sampled in Goahtevággi: (a) GM4, (b) GM1. Showing soil horizons (A to C-horizon), wet soil colour (using Munsell colour notation), wet soil CDE (following Buntley and Westin, 1965), LOI values, and soil pH.*

6.5.5. Establishing Schmidt hammer and soil chronosequence dating calibration curves

6.5.5.1. Strupskardet: establishing a Schmidt hammer dating calibration-curve

Using multiple moraines with independent age control, primarily established from radiocarbon dating (Bakke *et al.*, 2005a), enables a Schmidt hammer R-value-dating calibration curve to be developed. Using the data from the four moraines sampled within Strupskardet, combined with the LIA moraine from Sorbmevággi (Leigh *et al.*, 2020), we test the shape of the R-value-age relationship. Following the approach of Shakesby et al. (2011) we test three different regression equations: linear, second-order polynomial, and logarithmic (Figure 6.13).

Both the second-order polynomial and logarithmic regression plots show better representation of the R-value-age relationship compared to the linear plot (Figure 6.13). Furthermore, second-order polynomial and logarithmic calibration show a slow decline in the rate of R-value lowering with age, implying that over time a small decrease in R-value represents an increasingly large time duration, reflective of a reduction in weathering rates with time (cf. Colman, 1981). Ultimately, the logarithmic dating curve (Figure 6.13c) is used to establish calibrated ages in the Rotsund Valley because the logarithmic curve has the highest correlation coefficient (R^2 = 0.9804; Figure 6.13), and other recent Schmidt hammer investigations have shown R-value-age relationships are best represented by logarithmic regression (e.g. Tomkins *et al.*, 2018a).

Using our logarithmic calibration curve (Figure 6.13c), we calculated calibrated ages and their 95% confidence limits for moraines within the Rotsund Valley (Table 6.3). The resulting ages of the Sorbmevággi moraines reveal a sequence spanning ~6,700 years, with the outermost moraine (SM1) dating to 10,588 (9,587-11,601) cal. yrs BP and the innermost pre-LIA moraine (SM5) dating to 3,877 (3,177-4,599) cal. yrs BP (Table 6.3). The largest errors are from the HM2 moraine which, unsurprisingly, has the greatest scatter in the Schmidt hammer data and the lowest confidence interval (see Table 6.1, Figure. 7.6b and 7.7b).

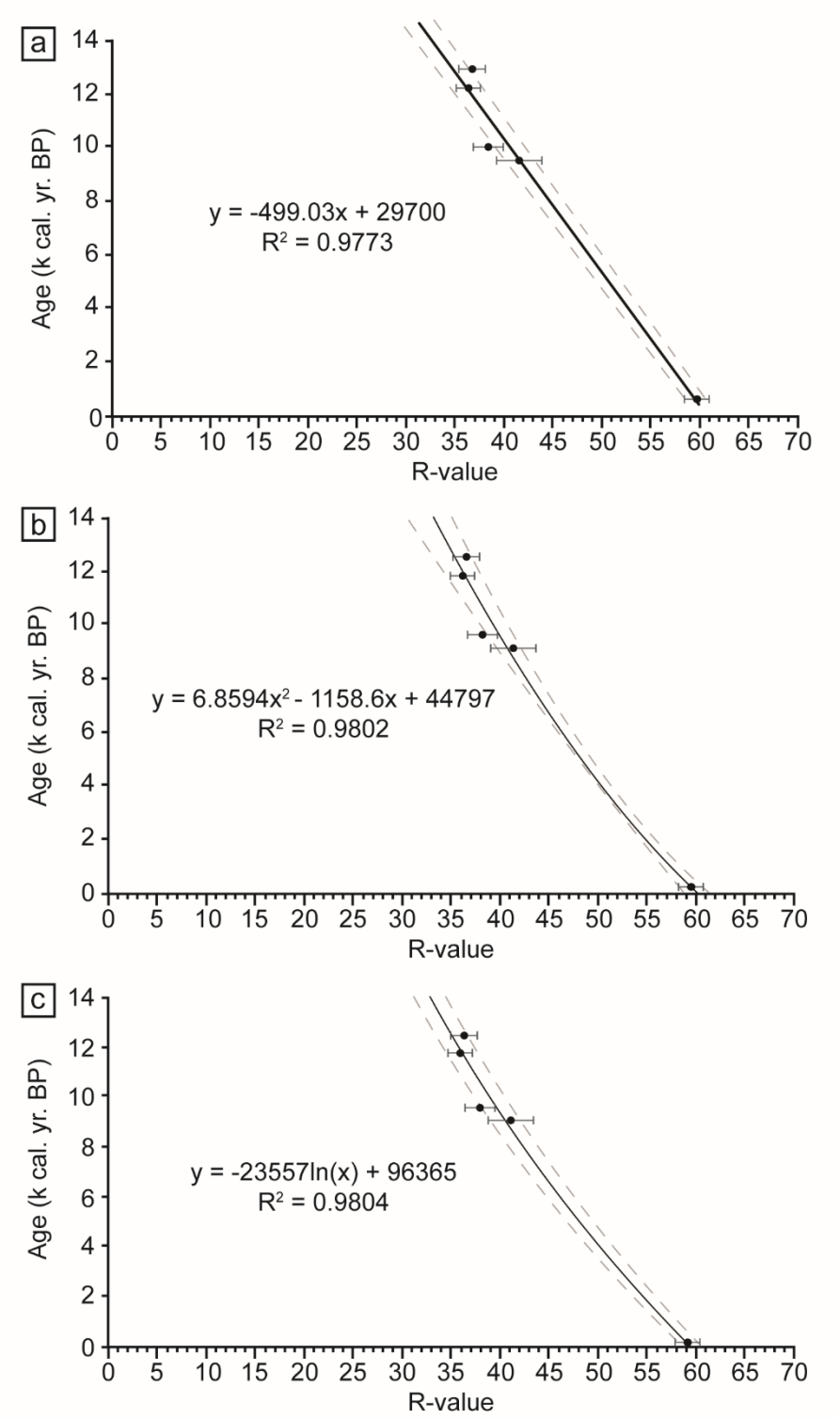

Figure 6.13. *Schmidt hammer R-value-age calibration curves using data collected from moraines of known age in the Strupskardet valley (Bakke et al., 2005a) and the LIA moraine from Sorbmevággi (Leigh et al., 2020): (a) linear, (b) 2nd-order polynomial, (c) logarithmic.*

Table 6.3. *Schmidt hammer exposure ages with 95% confidence intervals (CI) generated from the Strupskardet age-calibration curve (Figure 6.13c) based on independently dated moraines. Confidence intervals show the positive and negative error resulting from curvilinear regression.*

Regression equation	Site	Moraine ID	Feature mean R-value ±95% CI	Calculated age (yrs BP)	+95% CI (-yrs)	-95% CI (+yrs)	Bracketing age
y = -23557ln(x) + 96365	Sorbmevággi	SM5	50.71 ±1.5	**3,877**	700	722	3,177-4,599
		SM4	48.99 ±1.2	**4,690**	582	597	4,108-5,287
		SM3	41.92 ±1.3	**8,362**	697	718	7,665-9,080
		SM2	38.76 ±1.7	**10,208**	1,010	1,055	9,198-11,263
		SM1	38.14 ±1.6	**10,588**	971	1,013	9,587-11,601
	Hjemtverrdalen	HM3	42.20 ±1.3	**8,205**	729	753	7,476-8,958
		HM2	40.44 ±2.8	**9,208**	1,580	1,694	7,628-10,902
		HM1	35.73 ±1.6	**12,125**	1,005	1,049	11,120—13,174

6.5.5.2. Establishing a relative soil chronosequence dating calibration-curve

Using the soil properties recorded from the pre-LIA moraines within Sorbmevággi (SM1-SM5), we attempt to establish a relative soil chronosequence dating calibration curve. Moraines SM1-SM5 must date to the period after the SIS retreat from the continental shelf, likely covering the period since the termination of the YD. However, there is no absolute age control in at the Sorbmevággi site and, therefore, it is considered best to avoid further extrapolation of the relative Schmidt hammer sequence and instead opt to use soil dating as a relative technique, assigning likely correlation between moraines based on soil properties alone.

Previous research has shown the best parameter for relative age dating using soil chronosequences to be simply soil depth and B-horizon thickness (McCarroll and Ware, 1989; Evans, 1999a). Our data shows that maximum depth to the base of the B-/top of C-horizon is the most consistent value with greatest correlation between sites (Table 6.2). We therefore develop curves plotting maximum B-horizon depth and, following Evans (1999a), our soil chronosequence calibration curves use a logarithmic regression (Figure 6.14).

Using these logarithmic curves (dashed grey line on Figure 6.14), we attempt relative dating of moraines in Hjemtverrdalen and Goahtevággi (Table 6.4). Results show that different soil parameters have the potential to produce different calibrated ages (Table 6.4). For example, when comparing the outermost moraine, which logically indicates the oldest moraines in each sequence, there are only slight differences in the maximum soil data: SM1 has two 330 mm deep soils, one of which has a 150 mm thick B-horizon; HM1 has a 345 mm deep soil and a 145 mm thick B-horizon; and GM1 has a 310 mm deep soil and a 120 mm thick B-horizon (Table 6.2). The resulting relative calibration for the terminal moraines (when excluding the anonymously shallow soils of SM2) implies that HM1 would have been formed at a similar time to that of SM1 (Table 6.4), whereas GM1 would be of similar age to SM3. The position in the sequence of GM1 indicates that this calibrated age is too young, indicating that the soils on these moraines are anomalously shallow.

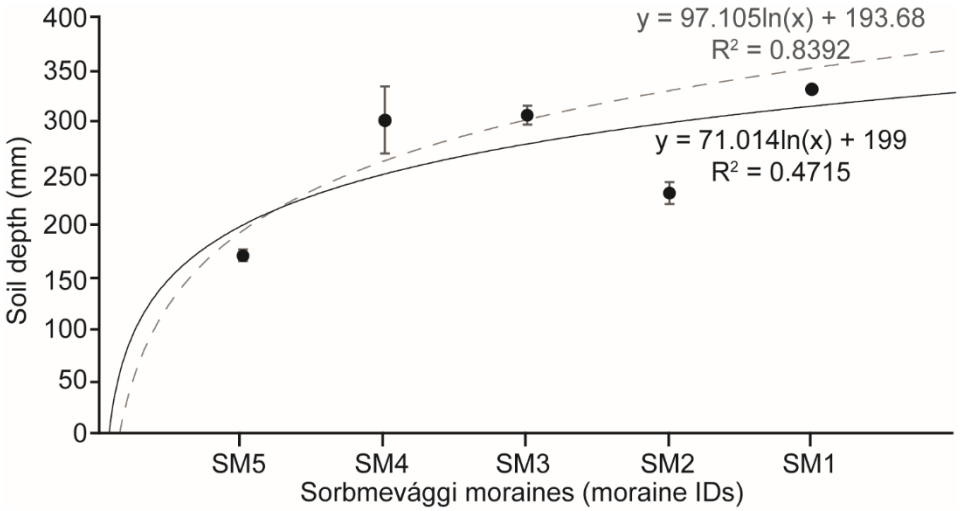

Figure 6.14. *Soil chronosequence relative calibration curves using maximum soil depth collected from moraines within Sorbmevággi and a logarithmic curve. The solid black line is a curve fitted to all the data points whereas the dashed grey line is a curve that excludes the anomalously shallow soil data from SM2.*

Table 6.4. *Results of soil chronosequence relative moraine dating using mean soil thickness and mean soil depth logarithmic calibration curves. The final column shows the calibrated "age" relative to the Sorbmevággi moraine sequence from which the dating curve is based; a relative age of 1.1 would indicate the moraine is of similar age to the SM1 moraine but does not correspond exactly, and an age of 1.5 would indicate the moraine was formed in between the formation ages of SM1 and SM2. The emboldened relative ages are considered most representative of relative moraine age.*

Curve type	Site	Moraine ID	Maximum B-horizon depth (mm ±95% CI)	Relative age in relation to moraines SM1 – SM5
Soil depth all moraines (Fig. 9b, solid black line)	Hjemtverrdalen	HM3	285 ±32	2.6
		HM2	290 ±40	2.4
		HM1	345 ±45	<1
	Goahtevággi	GM4	275 ±29	1.2
		GM1	310 ±13	3.1
Soil depth no SM2 (Fig. 9b, dashed grey line)	Hjemtverrdalen	HM3	285 ±32	**3.4**
		HM2	290 ±40	**3.3**
		HM1	345 ±45	**1.2**
	Goahtevággi	GM4	275 ±29	**3.7**
		GM1	310 ±13	**2.7**

6.6. Discussion

6.6.1. Rotsund Valley glacial chronology, links with Holocene climatic events, and other Scandinavian glacier records

The derived moraine age calculations using the Schmidt hammer dating curve indicate a sequence of glacial events, from the YD (HM1, ~12,125 cal. yrs BP; Table 6.3) throughout the Holocene, to the early-Neoglacial (SM5, ~3,877 cal. yrs BP; Table 6.4). This glacial chronology is broadly consistent with existing interpretations of mountain deglaciation following the retreat of the SIS across Norway (e.g. Nesje *et al.*, 2008; Nesje, 2009).

6.6.1.1. Younger Dryas-Holocene transition

Throughout the Kåfjord Alps, large moraines at the foot of subsidiary valleys are observed and these likely correspond with the outermost moraines in the Rotsund Valley sequence, HM1, SM1, and GM1 (Figure 6.3). The calibrated ages indicate that the Hjemtverrdalen terminal moraine (HM1) formed at ~12,125 (11,120-13,174) cal. yrs BP and the Sorbmevággi terminal moraine (SM1) formed at ~10,588 (9,587-11,601) cal. yrs BP (Table 6.3), thus representing maximum valley glacier extent at the end of the YD. While the Hjemtverrdalen moraine HM1 apparently formed ~1,500 years earlier than the equivalent Sorbmevággi moraine SM1, there is considerable overlap in the 95% confidence intervals (Table 6.3). It is, therefore, likely that the terminal moraines HM1 and SM1 represent the same glacial maxima, sometime during the late-YD. This inference is further supported by the soil data, which show both moraines have similar maximum soil depths and B-horizon thicknesses (Table 6.2).

Some asynchronicity could be expected given the substantially smaller catchment area of Hjemtverrdalen (~2 km^2) compared to the neighbouring Sorbmevággi (~8 km^2), meaning a glacial advance within Hjemtverrdalen might be initiated earlier. A further consideration should be made to the higher elevation and more exposed position of HM1, which might result in enhanced weathering and hence lower R-values and greater rates of soil development than on moraines of comparable age in more sheltered positions.

Support for a late-YD glacial maximum in the Rotsund Valley is provided by other studies from across Norway. In northernmost Norway, absolute ages of ice sheet retreat map and date major YD moraines to ~11,900 ± 1,200 years (Romundset *et al.*,

2017). Similarly, in western Norway reconstructions of the SIS have YD maximum was not achieved until ~11,600-11,700 cal. yrs BP, with ice retreat initiating ~11,500 cal. yrs BP (e.g. Bondevik and Mangerud, 2002; Lohne *et al.*, 2012; Mangerud *et al.*, 2016). Bakke et al. (2005a) also suggest that, contrary to the cold and dry climate during the period 13,000-12,500 cal. yrs BP (Alm, 1993; Birks, 1994; Rea and Evans, 2007), by the late-YD the climate of northern Norway was ameliorating. This climatic amelioration prompted ELA lowering, on the Lyngen Peninsula, to ~620-650 m a.s.l, roughly 350 m lower than at present-day (Bakke *et al.*, 2005a). Given the evidence of a late-YD increase in precipitation, relative to that of the early-YD, across the Lyngen Peninsula (cf. Bakke *et al.*, 2005a), it is highly likely that conditions would have also been more favourable to glacier growth across the whole central Troms and Finnmark region, helping to explain the timing of the Rotsund Valley YD maximum.

6.6.1.2. Early-Holocene

The calibrated ages for SM2 and HM2 (Figure 6.3) indicate an early-Holocene moraine forming event between ~10,208 (9,198-11,263) and ~9,208 (7,628-10,902) cal. yrs BP for SM2 and HM2, respectively (Table 6.3). The overlap in moraine ages around 10,000-9,000 cal. yrs BP corresponds with the Norwegian Erdalen Event (between 10,100 and 9,500 cal. yrs BP; Andersen, 1980; Corner, 1980; Nesje *et al.*, 1991; Dahl *et al.*, 2002). The proximity of SM2 and HM2 to the terminal moraines (SM1 and HM1, <500 m down-valley) fits with the pattern of early-Holocene moraines forming within a short distance of YD moraines yet substantially outside LIA limits, as reported elsewhere in Norway (e.g. Nesje, 1984; Nesje *et al.*, 1991; Matthews *et al.*, 2008; Matthews and Winkler, 2011; Aa and Sønstegaard, 2019). At this time, summer temperature reconstructions from southern Norway have shown temperatures approximately 1.5°C lower with a substantial wetting, such that winter precipitation levels were nearly twice that of the early-21st century and allowing glaciers to expand for a short duration (Velle, 1998; Dahl *et al.*, 2002). Reconstructions of ELAs during the period ~10,000-9,000 cal. yrs BP suggest that relative to the present-day ELAs underwent a maximum lowering of ~205 m at Hardangerjøkulen, southern Norway (Dahl and Nesje, 1996); ~230 m at Nigardsbreen, western southern Norway (Dahl *et al.*, 2002); ~120 m at Austre Okstindbreen, northern central Norway (Bakke *et al.*, 2010) and as much as ~354 m at Strupskardet, northern Norway (Bakke *et al.*, 2005a).

Moving up-valley from the YD/ Erdalen Event moraines in the Sorbmevággi and Hjemtverrdalen sequence, the SM3 and HM3 moraines located at the individual valley heads (Figure 6.4) show remarkably similar calibrated ages and are dated to 8,362 (7,665-9,080) and 8,205 (7,476-8,958) cal. yrs BP, respectively (Table 6.3). These ages indicate that SM3 and HM3 moraines were likely formed during the rapid climatic deterioration of the '8.2 ka event'. During the interval 8,200-7,850 cal. yrs BP, pollen stratigraphy from western Norway indicates that maritime areas experienced wetter conditions (Nesje *et al.*, 2006; Balascio and Bradley, 2012). Additionally, speleothem temperature reconstructions from Søylegrotta, northern Norway indicate a notable temperature reduction centred around 8,200 cal. yrs BP (Lauritzen and Lundberg, 1999) and Norwegian Sea sea-surface temperature reconstructions suggest a ~3°C surface cooling (Risebrobakken *et al.*, 2003). Furthermore, temperature and precipitation changes have been linked to a large glacier advance at Leirdalsbreen, an outlet glacier of the Høgtuvbreen ice cap, northern Norway, (Jansen *et al.*, 2016). Jansen et al. (2016) noted that it is the maritime nature of the Høgtuvbreen ice cap which enabled a readvance at this time, owing to the abrupt precipitation increase resulting in an ~300-year period of a ~140 m lower ELA.

An '8.2 ka event' moraine in the central Troms and Finnmark region is of particular significance, as previous studies documenting Holocene glacier recession throughout this area of northern Norway have not found moraines or other glacial identifiers attributable to this event (e.g. Bakke *et al.*, 2005a; Wittmeier *et al.*, 2015). There are, however, several key differences between the studied glaciers of Bakke et al. (2005) and Wittmeier et al. (2015) which, when compared to the Rotsund Valley, might provide some explanation to the apparent disparities in moraine sequences. Firstly, the Rotsund Valley glaciers are smaller in size, taking on the form of Alpine style small mountain glaciers which are known to have simpler and faster response times to climatic perturbations than those of large outlet glaciers from ice caps and mountain icefields (e.g. Jóhannesson *et al.*, 1989; Bahr *et al.*, 1998; Klingbjer *et al.*, 2005; Masiokas *et al.*, 2009; Theakstone, 2010; Moran *et al.*, 2016b; Le Roy *et al.*, 2017). In northern Sweden, valley glaciers have been shown to have response times of approximately 80 years, with glaciers experiencing marked readvance as a response to climatic deterioration on timescales of <100 years (Klingbjer *et al.*, 2005). Secondly, these glaciers are found in narrower and steeper alpine type valleys and the moraines in question are at higher elevations (SM3 at ~260 m a.s.l. and HM3 at

~380 m a.s.l.), indicating both topography and local ELA may be a contributing factor. For example, a minor lowering of the ELA may have enabled the small alpine glaciers of the Rotsund Valley to readvance while the larger icefields/ice caps and their outlet glaciers required a greater ELA depression to enable substantial readvance (Rosqvist and Østrem, 1989). Finally, the steep valley walls were likely responsible for heightened debris supply to the glacier surface and not only provided ample material for moraine formation, but possibly also contributed increased mass input that in turn promoted advance (Vacco *et al.*, 2010; Reznichenko *et al.*, 2011; Menounos *et al.*, 2013). Indeed, proximal to and in contact with SM3, and within a similar position in Goahtevággi, are broad areas of DDA, indicative of high debris supply at the ice margin (Evans, 2008; Vacco *et al.*, 2010).

6.6.1.3. Late-Holocene (Neoglacial)

After the early-Holocene, no moraines appear to have developed within Sorbmevággi for a period of ~3,700 years, likely representing substantial glacier recession (possibly disappearance) during the peak HTM (6,600-6,300 cal. yrs BP; Nesje 2009). The apparent formation of SM4 at ~4,690 (4,108-5,287) cal. yrs BP and SM5 at ~3,877 (3,177-4,599) cal. yrs BP (Table 6.3), most likely indicates glacier advance or regrowth following the onset of Neoglacial fluctuations within northern Norway. Furthermore, the relative age of GM4, as shown by the soil depth (Table 6.4), indicates that this moraine was formed at a similar time to SM4, or perhaps slightly before. These calibrated ages (and relative sequences) fit with the known pattern of millennial-scale Neoglacial events across Scandinavia during the late-Holocene, with two such events having occurred ~4800-3900 and ~3200-2550 cal. yrs BP (Matthews and Dresser, 2008).

The apparent ages of ~4,690 cal. yrs BP for SM4 and ~3,877 cal. yrs BP for SM5 (Table 6.3) are, however, earlier, and more extensive than compared to other Neoglacial readvances in this region. For example, at the nearby Langfjordjøkelen ice cap on the Bergsfjord Peninsula, lacustrine sediments indicate no glacier activity in the catchment until ~4,110 cal. yrs BP (Wittmeier *et al.*, 2015), with glacier activity increasing until an apparent maximum during the LIA. Conversely, at other sites in northern Norway, such as the Høgtuvbreen ice cap in Nordland County (66°25'N 13°39'E), a distinct 120-year glacier readvance has been reported ~4,420 cal. yrs BP which is suggested to indicate the start of Neoglaciation (Jansen *et al.*, 2016). There

are even earlier Neoglacial events reported further south at Austre Okstindbreen in Nordland County (N66°00' E14°16'). Radiocarbon dating of buried soils and subsequent dating of lacustrine sediments indicates neoglaciation initiating as early as 5,000 cal. yrs BP with a period of heightened glacier activity ~4,500 cal. yrs BP (Griffey and Worsley, 1978; Bakke *et al.*, 2010). Furthermore, on the south-eastern coast of Vestvågøya, northern Norway, lake sediment records have been used to indicate temperature decrease initiating ~4,800 cal. yrs BP with a marked increase in precipitation after ~4,300 cal. yrs BP (Balascio and Bradley, 2012). This evidence combined indicates that the climate of northern, maritime, Norway after 5,000 cal. yrs BP was suitable for Neoglacial glacier regrowth/readvance.

Similar studies in northern Sweden, while less extensive than those of Norway, provide a valuable reference to the onset of Neoglacial conditions across northern Scandinavia. In particular Karlén (1988) and Karlén and Kuylenstierna (1996) document notable cold events and glacial readvances between 5,100 and 4,200 cal. yrs BP, subsequently linked with Dansgaard-Oeschger events and a reduction in northerly heat transport. Advanced glacier positions at around 4,300 and 3,100 cal. yrs BP are also inferred from lake sediments in northern Sweden (Rosqvist *et al.*, 2004). Furthermore, in the maritime western Norway, lacustrine sediments from Ålfotbreen, (61°44'N 05°36'E) were used to propose initial Neoglacial activity as early as ~5,400 cal. yrs BP (Gjerde *et al.*, 2016). Whereas in a more continental, high-frequency glacier fluctuations at Hardangerjokulen (60°33'N 7°25'E) are proposed to have started ~4,800 cal. yrs BP (Dahl and Nesje, 1994). Thus early-Neoglacial (re)advance is not isolated to the maritime regions of northern Norway, instead it appears to be a consistent pattern at mountain glaciers across northern Scandinavia.

As discussed above, it is considered that the specific glacial characteristics of the Rotsund Valley glaciers (size, topography, elevation, maritime location) enabled them to react quickly to short-term climatic deterioration (Ivy-Ochs *et al.*, 2009) and, in turn, exceed the positions achieved during the LIA, which is often considered to represent Neoglacial maxima for larger glaciers across Norway (e.g. Matthews, 1991b; Dahl *et al.*, 2002; Winkler, 2003; Gurney and White, 2005; Nesje, 2009). The maximum extent for Neoglacial advance in the Rotsund Valley is demarcated by moraine SM4 (~4,690 cal. yrs BP; Table 6.3) shown in Figure 6.4 and with consideration to other glacial investigations from northern Scandinavia, this age, while unique, does not seem unreasonable.

6.6.2. Ice sheet margins and Holocene glacier reconstructions of the central Troms and Finnmark region: patterns of advance/retreat

Combining the detailed mapping of Leigh et al. (2021) and the moraine chronology from the Rotsund valley, new reconstructions of ice sheet deglaciation and mountain glacier fluctuation are produced from 14,000 cal. yrs BP to the present-day.

Reassessment of the “most credible” SIS outlines as drawn by Hughes et al. (2016) has revealed a more complex ice sheet margin that not only fills the fjords, but backfills into feeder valleys, and flows around topographic features across the plateau area. Interpretations of the glacial geomorphology indicate a complex transition appears to have taken place following ice sheet deglaciation, with development of mountain plateau icefields and subsequent valley glacier systems:

- At ~14,000 cal. yrs BP (Figure 6.15a) the whole mainland and most of the outlying islands appear to have been covered by ice, with only the northernmost portion of the Lyngen Peninsula, the Maurn Peninsula and the Kvænangstinden massif remaining ice free. We propose that the ice sheet separated around the Maurn Peninsula, flowing through the trough at Hamneidet and entering the Maursundet strait where it butted up against the southern margin of Kågen.
- At ~13, 000 cal. yrs BP (Figure 6.15b) the ice sheet margin has been redrawn with the large outlet glaciers filling greater portions of the fjords and aligning more with the higher moraine systems that track the length of the fjords and valleys, although the Rotsund Valley and Riehppe Plateau appear to be isolated from the ice sheet. On the plateau east of Reisadalen, the ice margin appears more dynamic, with the emergence of small lobes and ice tongues recorded by large lobate moraines (e.g. Figure 6.2i-j). Revised ice front positions are supported by a range of radiocarbon dates from sedimentary deposits near Svensby in Ullsfjord dating to 11,020 and 11,500 ^{14}C yrs BP or 12,562 and 12,970 cal. yrs BP (Andersen, 1968; Plassen and Vorren, 2003). At this time-step there is likely the first emergence of plateau icefields across the mountain plateaus that are separated from the ice sheet (e.g. the Lyngen Peninsular, the Riehppe Plateau, parts of the Kåfjord Alps and Kvænangstinden massif), with these sites producing large outlet glaciers as evidenced by large moraines at,

or just beyond, valley mouths (e.g. Figure 6.2k-l). The glaciers at ~13, 000 cal. yrs BP likely represent the greatest ice extent in northern Norway following the main ice sheet deglaciation.

- At ~12,000 cal. yrs BP (Figure 6.15c) the margin has again been remapped further down the fjords, notably with positions at Skarmunken in Ullsfjord, Spåkenes in Lyngenfjord, and at Straumfjordnes and Bakkeby in Resiafjord. Based on a series of moraines that can be traced around the mountains of Ajit (one of the county's northernmost summits over 1,400 m outside of the Lyngen Alps and ~10 km east of Skibotn), we propose that the mountain tops here may have been ice free at this period, possibly emerging as nunataks ~13,000 cal. yrs BP or earlier (Figure 6.15b, c). Revised ice front positions are supported by a range of radiocarbon dates from sedimentary deposits, with dates of 10,800 ^{14}C yrs BP (12,262 cal. yrs BP) at Skarmunken (Nydal, 1960; Andersen, 1965) and 10,760 ^{14}C yrs BP (12,152 cal. yrs BP) at Spåkenes (Nydal, 1960; Andersen, 1965).
- At ~11,000 cal. yrs BP (Figure 6.15d) we propose substantial revisions to the prior ice margin positions, with glacier outlets occupying the head of Storfjord, the entrance to Skibotndalen, mid-way up Buntadalen, and ~30 km up Reisadalen (near the town of Sappen), with large parts of the inland plateau area to the south/south-east remaining ice covered. While at the very limits of our study area, we also suggest a revision of the margin to skirt around the southernmost edge of the Lyngen Peninsula and likely terminating near the head of Blasfjord. North-west of the large lake Guolasjávri (at the head of the Kåfjord valley) there lies a series of at least three inset arcuate moraines (Figure 6.2g-h). There is no age control on these features, so the 11,000 cal. yrs BP ice front position is tentatively drawn along the outermost moraine ridge. More generally, revised ice front positions are supported by a range of radiocarbon dates from sedimentary deposits with dates of 10,290 ^{14}C yrs BP (11,448 cal. yrs BP) at Birtavarre (Nydal, 1960) and 9,995/9,555 ^{14}C yrs BP (10,987/10,409 cal. yrs BP) within Blasfjord (Forwick and Vorren, 2002). The southernmost margins of the Lyngen Peninsular and mountains to the east have been exposed at this time step, revealing a similar pattern of small mountain plateau icefields having developed. All these glaciated sites are defined by large latero-

frontal moraine systems extending along valley sides and out beyond the confines of the main valleys, which are now inset with extensive sequences of well-defined recessional moraines (e.g. Figure 6.2k-l) and distinct areas of ice-moulded bedrock and till sheets in the in the upper and lower reaches, respectively.

- During the peak HTM between 6,600 and 6,300 cal. yrs BP (Figure 6.15e) it is unknown what would have happened to all the mapped ice masses in response to heightened temperatures. Did all the glaciers melt completely or were the high mountains and elevated plateaus areas of refuge for smaller ice masses? As noted in Section 6.3.1, most glacier reconstructions indicate complete deglaciation, including the studies of Bakke et al. (2005) within Strupskardet (northern Lyngen) and Wittmeier et al. (2015) at Landgfordjoknen (Bergsfjord Peninsula). However, in Nordland county (bordering the Arctic Circle at 66°00' N, 14°16'E), Bakke et al. (2010) suggest that at high-elevation sites, substantially shrunken glaciers may have survived the HTM with regional ELAs at 1,600-1,500 m a.s.l. As such, a speculative minimum elevation threshold of 1,000 m is applied to our Neoglacial outlines. This results in only a small number of glaciers at elevations above 1,000 m remaining, thus indicating that these glaciers may have been able to survive the HTM (Figure 6.15e). In some areas (e.g. the Riehppe Plateau) this elevation threshold has resulted in glaciers at this time-step remaining larger than at the present-day. It should, however, be noted that given there is currently no geochronological or geomorphological data to corroborate these mapped extents, they should be regarded with caution.
- The Neoglacial maximum extent (Figure 6.15f) is mapped following our calibrated age dating in the Rotsund Valley, whereby several moraines outside of the LIA maximum were dated to the late-Holocene (4,690-3,877 cal. yrs BP). Following our dating, we reconstruct glacier extent based on moraines up to 600 m distal to LIA type deposits (Leigh *et al.*, 2020; Weber *et al.*, 2020). In cases where no moraines are evidenced immediately outside the LIA margins, the Neoglacial maximum is represented by the LIA maximum moraines; dated to between 1814-1877 in the Rotsund Valley and as late as 1920-1930 on the Lyngen Peninsula (Ballantyne, 1990; Leigh *et al.*, 2020). Mapping indicates that

Neoglaciation is dominated by mountain valley glacier systems, and only in areas where valley heads connect with mountain plateaus (on southern Lyngen centred around Jiekkevarre, north of Kåfjord at the locality of the present-day Noammerjiehkki ice cap, and on the Riehppe Plateau) were these valley systems likely connected with and supplemented by the small plateau icefields. Within some valleys, reconstructed Neoglacial glacier boundaries cover areas that host present-day rock glaciers situated on the valley floor and butted against LIA moraines, and sometimes connected to present-day glacier margins. In turn, this indicates that many of the valley floor rock glaciers mapped throughout the region (Leigh *et al.*, 2021) were likely formed during the late-Holocene when rockfall rates were heightened owing to mountain destabilisation that followed the complete or near-complete deglaciation of the mid-Holocene. These interpretations are supported by the earlier works of Whalley (1976), Griffey and Whalley (1979), and Whalley (1992), who investigated rock glaciers on the Lyngen Peninsula and concluded they were formed in the late-Holocene, often with their impressive size being attributable to higher rock debris input than the small glaciers could not have provided alone.

- Present-day glaciation across most of the central Troms and Finnmark region is dominated by isolated cirques and rapidly shrinking ice caps; only on the Lyngen Peninsula are large valley glaciers still found. Recent glacier change assessments from northern Norway indicate rapid recession since the mid-20th century, with some of the highest known rates of glacier shrinkage across the whole of mainland Norway (e.g. Andreassen *et al.*, 2012b; Giesen *et al.*, 2014; Weber *et al.*, 2020). There are predictions that many glaciers will not survive beyond the mid- to late-21st century (Andreassen *et al.*, 2012b; Stokes *et al.*, 2018; Leigh *et al.*, 2020; Weber *et al.*, 2020).

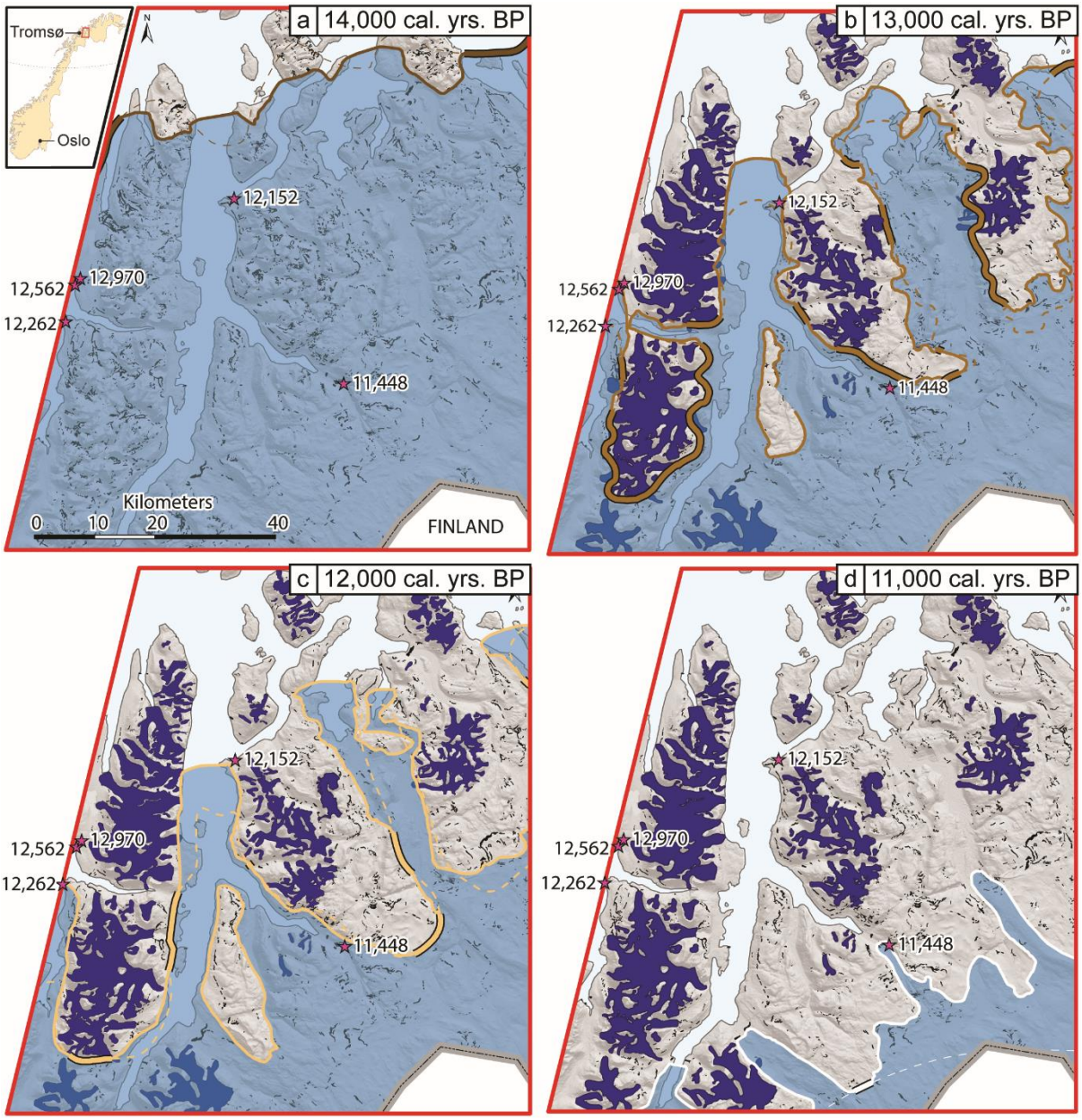
a 14,000 cal. yrs. BP
Tromsø
Oslo
N
12,152
12,562
12,970
12,262
11,448
Kilometers
0 10 20 40
FINLAND
b 13,000 cal. yrs. BP
12,152
12,562
12,970
12,262
11,448
c 12,000 cal. yrs. BP
12,152
12,562
12,970
12,262
11,448
d 11,000 cal. yrs. BP
12,152
12,562
12,970
12,262
11,448

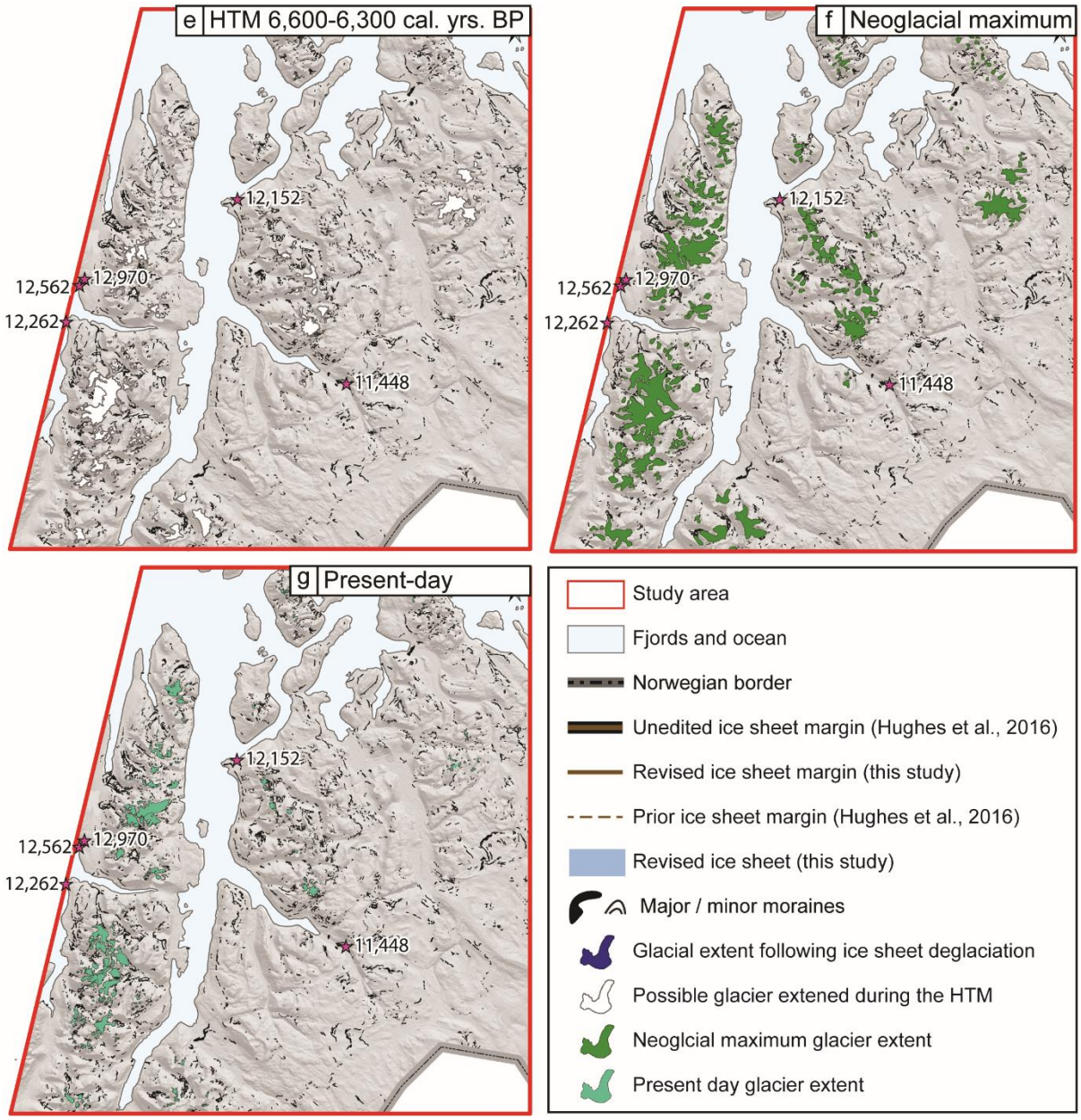

Figure 6.15. *Revised ice sheet margin positions of the Scandinavian Ice Sheet from 14,000-11,000 cal. yrs BP and glacier reconstructions during the Holocene in the central Troms and Finnmark region of Northern Norway. The thick two-tone solid line and thin dashed line represents the unedited most credible ice sheet margin from Hughes et al. (2016) while the thin solid line and solid blue infill represents the revised margin and ice extent. Revised ice sheet margins and new glacier outlines are based on the mapping of Leigh et al. (2021).*

6.7. Conclusions

This paper presents a new Holocene glacial chronology for the mountain glaciers of the Rotsund Valley in central Troms and Finnmark County, northern Norway. Both Schmidt hammer dating and soil chronosequencing are shown to hold promise for calibrated and relative age dating of glacial landforms throughout northern Norway. The new localised chronology reaffirms earlier regional mapping, depicting the main Rotsund Valley as ice free during the Younger Dryas. The mountain glaciers in the area reached their maximum extent just beyond the confines of their subsidiary valleys between 12,125 (11,120-13,174) and 10,588 (9,587-11,601) cal. yrs BP (Table 6.3). In the subsidiary valleys Hjemtverrdalen, Sorbmevággi, and Goahtevággi glaciers formed extensive series of inset moraine sequences and dating indicates notable moraine forming events occurred at around 10,208-9208, at 8,362-8,205, and 4,690 cal. yrs BP. These are attributed to key climatic events; the Erdalen Event, the 8.2 ka event, and the onset of the Neoglacial, respectively (Table 6.3). Notably, this is the first time that these events have been linked to readvances of small mountain glaciers on mainland northern Norway. Moreover, the hypothesised identification of moraines attributable to the 8.2 ka event is unique in this region, indicating that small maritime mountain glaciers were able to respond to short-term climatic perturbations, a behaviour currently not detected at larger glaciers and ice caps in the region. Within Troms and Finnmark County, identification of multiple Neoglacial moraines, outside the dated LIA limits, also challenges the long-held notion that the most extensive glacial readvance of the late Holocene was that of the LIA. This in turn lends support to the work of Bakke et al. (2010) who suggested that glaciers in Nordland County (66º00'N 14º16'E) experienced multiple Neoglacial advances of which at least one, occurring ~1,300 cal. yrs BP , was greater than that of the LIA maximum.

Additionally, using the extensive glacial geomorphological mapping of Leigh et al. (2021) and the new moraine chronology (this study) it has been possible to produce an updated ice margin chronology for the Scandinavian Ice Sheet and mountain glaciers from 14,000 cal. yrs BP to the present-day (Figure 6.15). Glacier extent is summarised at key climatic events, including a period of minimum glaciation during the Holocene Thermal Maximum (Figure 6.15). Mapping indicates that the ice sheet margins were likely more extensive and had more dynamic margins than previously depicted (Figure 6.15). Furthermore, new evidence and reconstructions of plateau

icefields in the central mountain regions of the study area is provided. These early-Holocene icefields have previously been unreported, and it is postulated that some of the high mountains and plateaus might have provided refugia for small glaciers to have endured the HTM before substantial Neoglacial readvance (Figure 6.15).

This work fills a gap in our understanding of glacier extent in the central Troms and Finnmark regions and proves a strong case for further examination of sites across the region to establish detailed glacial chronologies and palaeoglaciological reconstructions for the numerous regions that contained and often still contain plateau icefields, valley, and cirque glaciers.

6.8. Acknowledgments

JRL thanks Robert Leigh, James Linighan, Richard Jones, and Callum Pearson for fieldwork assistance. The 2018 fieldwork was also supported by Lexus Norway, who provided a vehicle for JRL to use during fieldwork and by the Alpkit Foundation who provided monetary funding. The high-resolution Arctic DEMs were provided by the Polar Geospatial Centre under NSF-OPP awards 1043681, 1559691, and 1542736, and aerial orthophotographs were kindly provided by the Norwegian Mapping Authority (Kartverket). We also thank ESA and USGS for providing free satellite imagery and the Geological Survey of Norway (NGU) for providing freely available geological data (made available by the Norwegian license for public data; NLOD). Prior glacier data as collated by the CryoClim project were also used, including glacier outlines downloaded directly from the Norwegian Water Resources and Energy Directorate (NVE) website (https://www.nve.no/hydrology/glaciers/glacier-data/). Scandinavian Ice Sheet margin positions and associated geochronological control data were sourced from the DATED-1 database and time-slice reconstruction map as editable GIS files (downloaded from: http://doi.pangaea.de/10.1594/PANGAEA.848117).

CHAPTER 7

Discussion

Taking a break from digging soil pits and looking up towards Goahtejiehkki *(glacier ID 127), perched on the rocky cirque threshold.*
Photograph date: 03rd September 2019 (by J.R. Leigh)

“Climb, to new heights, and tell me, tell me what you hear...
A whisper from the wind, and I can't help but listen,
It warns us of disaster, and I can't help but wonder,
Can anyone hear the same distress call?”
(Reynolds, 2007)

7.1. Introduction

This chapter synthesises the findings of Chapters 3-6 and discusses the results in the context of the broader picture. Section 7.1 is a discussion on the theme of very small glaciers, highlighting the need for them to be fully considered when assessing glacier change (as first detailed in Chapter 3) and how varying nomenclature can impede cross compatibility between similar studies. Section 7.2 reviews the data on LIA maximum for the central Troms and Finnmark region (Chapter 4) and assesses this against regional studies. The geomorphology of LIA maximum moraines is evaluated and there is consideration to other potential avenues for future research. This section ends with an assessment of lichenometry (as used in Chapter 4) and soil chronosequencing (as used in Chapter 6), highlighting their benefits in situations where Schmidt hammer or ^{10}Be exposure dating is not possible; their usage as an appropriate geochronological technique is reaffirmed. Section 7.3 utilises the new glacial and periglacial geomorphological mapping (Chapter 5) to compare and reassess prior studies, in turn showcasing the ability for higher resolution imagery facilitate the reinterpretation or identification of small-scale features. This section is closed with a brief review of the ongoing debate surrounding rock glacierized features. Section 7.4 provides a detailed comparison of Norwegian ice sheet deglaciation and Holocene glacier fluctuation with that of other Arctic regions and the European Alps, giving context for the Holocene reconstructions established in Chapter 6. Finally, the discussion ends with Section 7.5 which suggests areas for future research with consideration to the results presented in this thesis.

7.2. Mapping very small glaciers and their fate in a warming climate

Small mountain glaciers are an important part of the cryosphere and tend to respond rapidly to climate warming and yet very small glaciers (e.g. <0.05 km^2) can often be overlooked and/or discounted from regional and global glacier maps or assessments of glacier change (cf. Parkes and Marzeion, 2018). The importance of recognising very small glaciers, especially with regards to their protection, or lack thereof, under environmental law has also recently been discussed in science journalism (e.g. Fraser, 2017; Tollefson and Rodríguez-Mega, 2017; Fernández *et al.*, 2021). Most recently, the American Geophysical Union's (AGU) Eos magazine drew attention to the plight of Chile's small glaciers and ice bodies, highlighting how governments, corporations, and activists view these vulnerable cryosphere components differently (Fernández *et al.*, 2021). When considering the legislative efforts to enact a glacier protection law in Chile, Fernández et al. (2021) highlight the uncertainties and omissions in the legislation and emphasised how they lacked detailed scientific grounding and failed to fully consider the potential future impacts to local communities.

Chapter 3 demonstrated how mapping very small glaciers has often been subjective and, to counter this issue, a scoring system for the objective identification and mapping of very small glaciers was established. Remote sensing using appropriate high-resolution imagery is shown to provide an opportunity to improve mapping capabilities and that, when aided by predefined systems and guidelines for mapping, glaciers smaller than 0.01 km^2 and/or those in sub-optimal settings such as within a niche on a hillside/rock wall can be identified and distinguished from (perennial) snow patches. Furthermore, the time of image capture and resolution of the imagery is also noted to play a substantial role in the ability to accurately identify and map very small glaciers. Image capture date and time will impact not only on the intensity of shading but also the angle at which the shadow will be cast and the extent of seasonal snow cover, while resolution will reflect the level of detail that can be ascertained. A good example of this can be found in the Rotsund Valley, where a very small partially debris covered ice/snow unit is situated in an alcove below a steep rock wall, with its lateral-frontal margins impounded by a relatively large moraine (Figure 7.1). This glacier was not included in any of the prior Norwegian glacier inventories, nor was it included in any historic or current topographic maps (Figure 4.4; Chapter 4) and thus can be considered as a "new" glacier. Figure 7.1 demonstrates that while this

ice/snow unit can be seen on recent satellite and aerial imagery neither of these image types enable a conclusive definition as to its nature (e.g. perennial snow vs. glacier) and it is only through ground truthing or by confirming its presence on older imagery that it can be confirmed. Glacier change assessments as carried out in Chapter 4 reveal that this glacier shrank from 0.07 km^2 in 1989 to 0.03 km^2 in 2018.

In the roughly 9,600 km^2 central Troms and Finnmark study area alone, new glacier mapping (Chapter 4) using a combination of methods, image types and resolutions (as described in Chapter 3) showed that there were potentially 78 glaciers that were not included within the 2012 Inventory of Norwegian Glaciers (Andreassen *et al.*, 2012a). Of these 78 glaciers, 23 were classified as *certain*, 10 classified as *probable*, and 45 were classified as *possible* (Table 4.3). Most of the newly mapped glaciers were found in the mountain regions where heavy shading, higher debris supply, and longer lasting seasonal snow present substantial obstacles for remote sensing. Overall, the addition of 78 newly identified and mapped glaciers represented a ~55% increase in number of mapped glaciers. It is, therefore, not unreasonable to speculate that there is a possibility for other glaciers across Norway to have been missed in prior glacier inventories or regional change assessments. Indeed, even in case of the 2012 Inventory of Norwegian Glaciers (Andreassen *et al.*, 2012a), the authors were able to map 907 more glaciers than the prior inventory, owing to improvements in image quality, resolution, and ubiquity, combined with more traditional methods for glacier mapping (Andreassen *et al.*, 2012a). Continued improvements in available imagery will likely facilitate further improvements in glacier mapping. This has just been evidenced by a new yet currently unpublished glacier inventory by NVE (Andreassen et al., in review), which has added 2,370 newly mapped ice bodies, ranging in size from <0.001 to 0.202 km^2. New glacier mapping would, therefore, benefit from consideration as to how recent changes to glacier extent might result in previously unmapped glaciers now having areas lower than mapping thresholds (e.g. 0.01 km^2). Thus, glacier inventorying should utilise old and new imagery when trying to establish long term change assessments to ensure inclusion of presently very small glaciers and even those which may have transitioned from a glacier *sensu strictu* to that of a non-glacier.

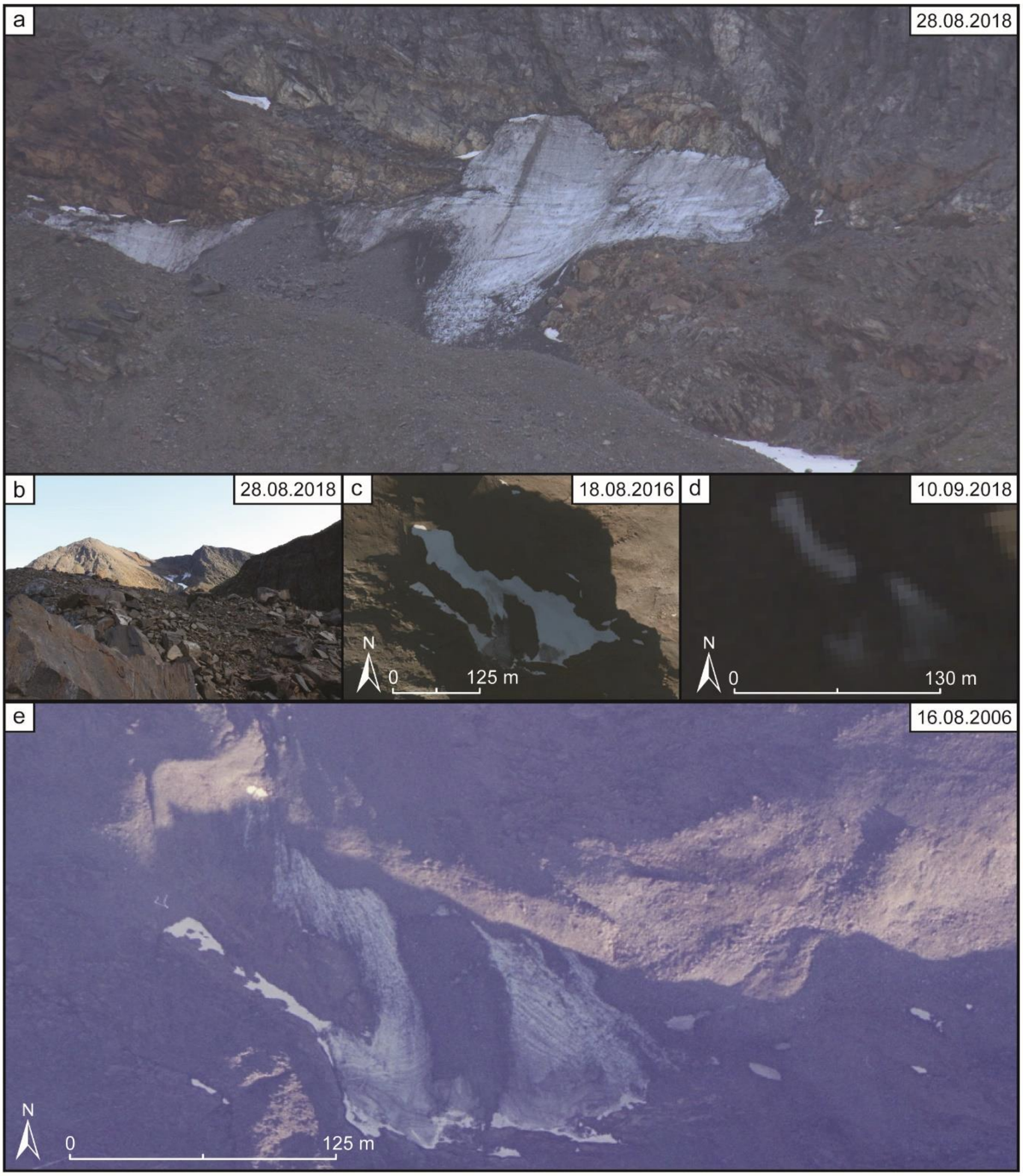

Figure 7.1. *A ~0.03 km^2, partially debris covered glacier in an alcove below a rock wall and impounded by a large moraine, first identified and assessed over time in Chapter 4: (a) zoomed oblique field photograph revealing bare ice and debris banding; (b) wide angle photograph showing the broader setting; (c) aerial imagery from 2016 showing the unit with pervasive snow cover and heavy supraglacial debris; (d) Sentinel2 imagery, on which the general shape of the ice unit can be determined, although debris cover obscures most snow/ice; (e) aerial imagery from www.norgibilder.no captured on 24.08.2006, which clearly shows debris banding in glacier ice which appears to be deforming downslope. Approx. location 69°43'N, 20°40'E.*

One unresolved question which arises from the work presented in Chapter 3 is: do glaciologists need separate terminology for glaciers smaller than 0.5 or even 0.01 km^2 when mapped remotely? Within Chapter 3 glaciers <0.5 km^2 were referred to as simply 'very small glaciers' to avoid any confusion. The issue of differing nomenclature is, however, pervasive with various terminology having been used to describe small glaciers, compounded by scientists using these terms to describe glaciers at different size thresholds and with different interpretations. Glaciers smaller than 0.5 km^2 have been termed very small glaciers (e.g. Huss and Fischer, 2016; De Marco *et al.*, 2020), glacierets (e.g. Gikov *et al.*, 2009; Nojarov *et al.*, 2019), ice aprons (e.g. Thomson *et al.*, 2011; Guillet and Ravanel, 2020), niche glaciers (e.g. Grove, 1961; Hughes, 2018), glacier remnants (e.g. Rabatel *et al.*, 2018; Čekada *et al.*, 2020), microglaciers (e.g. Grünewald and Scheithauer, 2008; Gachev, 2009), or even just ice bodies/units (Cullen *et al.*, 2013; Weber *et al.*, 2019). While most of these terms have been specifically defined (see Table 7.1) there remains occasional overlap in their definitions. Furthermore, outside of the key texts listed in Table 7.1, there are a multitude of different and sometimes conflicting usages of these terms, as noted by Evans (2006) when assessing glacier distribution across the Alps.

The varied and complex terminology for glaciers smaller than 0.5 km^2 creates room for confusion and this is apparent from the literature. Authors do not always recognise glacier terminologies in their strictest sense. Thus, when reviewing literature and comparing studies it is often difficult to assess similarities and/or differences and may even lead to some studies being overlooked. It is, therefore, suggested that the glaciological community reassess current terminology and associated definitions, especially giving the increasing frequency with which small glaciers are being observed and measured in a warming climate. Future studies need consistent terminology to aid in cross comparison and avoid unnecessary confusion, particularly in those cases where reports on glacier change are conveyed to a wider non-specialist audience (e.g. the public).

Table 7.1. *Various glacier terminology and associated definitions from key sources.*

Terminology	Definition
Glacier	*A perennial mass of ice, and possibly firn and snow, originating on the land surface by the recrystallization of snow or other forms of solid precipitation and showing evidence of past or present flow (Cogley et al., 2011, p. 45).* **Glossary of Glacier Mass Balance and Related Terms**
Glacieret	*A very small glacier, typically less than 0.25 km^2 in extent, with no marked flow pattern visible at the surface. To qualify as a glacieret, an ice body must persist for at least two consecutive years. Glacierets can be of any shape, and usually occupy sheltered parts of the landscape (Cogley et al., 2011, pp. 46).* **Glossary of Glacier Mass Balance and Related Terms**
Niche glaciers	*A small glacier in a gully or depression, elongate downslope (Cogley et al., 2011, pp. 70).* **Glossary of Glacier Mass Balance and Related Terms** *An ice body controlled by a niche or rock bench in a mountain or valley side (Benn and Evans, 2010, pp. 9).* **Glaciers and Glaciation**
[Glacier] Remnant	*An isolated melting mass of glacier ice, that has become detached from its source and the remainder of the glacier. Some remnants cover many square miles (Molnia, 2004).* ***USGS Glossary of Glacier Terminology***
Ice apron	*(1) A synonym of mountain apron glacier [a small glacier of irregular outline, elongate along slope, in mountainous terrain]; (2) A conglomerate of snow, refrozen meltwater and blocks of ice resulting from dry calving, found fringing the base of a steep terminus, typically that of a cold glacier* (Cogley et al., 2011, pp. 52). **Glossary of Glacier Mass Balance and Related Terms** *The smallest glacier ice masses, ice aprons, are thin snow and ice accumulations adhering to mountain sides (Benn and Evans, 2010, pp. 9)* **Glaciers and Glaciation**
Ice body	*Any continuous mass of ice, possibly including snow and firn, at or beneath the Earth's surface. Glaciers, ice shelves, ice floes, icebergs, a continuous*

	cover of sea ice, ice wedges in permafrost, and accumulations of ice in caves are all examples of ice bodies (Cogley et al., 2011, pp. 52). **Glossary of Glacier Mass Balance and Related Terms**
Ice patch	*Ice patches are ice bodies without movement by flow or internal motion. They are differentiated from snow patches by their ice content and from glaciers by the absence of internal motion . . . If the ice mass deforms, then it should be considered a glacier (Serrano et al., 2011, p. 58).* **Ice patch origin, evolution and dynamics . . .**
Snowfield	*A more or less extensive and persistent mass of snow. Snowfields are more extensive than snowpatches, but the distinction is not made precisely in common usage. A snowfield that is perennial may be difficult to distinguish from a glacier (Cogley et al., 2011, pp. 83).* **Glossary of Glacier Mass Balance and Related Terms**.
Snowpatch	*A mass of snow of restricted extent, especially one that persists through most or all of the ablation season. Snowpatches are less extensive than snowfields, but the distinction is not made precisely in common usage. A snowpatch that is perennial may be difficult to distinguish from a glacieret (*Cogley et al., 2011, pp. 83). **Glossary of Glacier Mass Balance and Related Terms**.

When assessing changes to these very small glaciers it is important to consider how they are likely to respond in the future. Chapter 4 has shown that while glaciers smaller than 1 km^2 are experiencing less reduction to their areas in absolute (km^2) values, their relative (%) area reductions are the highest throughout the central Troms and Finnmark region. Furthermore, as glaciers shrink, their area-length reduction ratios change, reflecting the transition to a more spherical unit with an upland cirque hypsometry; thus, the response of very small glaciers to changes in climate will likely be markedly different when compared to larger valley glaciers. While it was predicted that many of the glaciers mapped in the central Troms and Finnmark study area will likely melt away before the end of the century (Chapter 4), it is noted that it will not necessarily be the smallest glaciers that are the first to disappear. It is postulated that the glaciers on the exposed and higher elevation plateaux will be amongst the first glaciers to melt away. This is due to, their relatively short response times, small ice thicknesses, and greater sensitivity to changes in ELA, whereby a small rise in ELA

will lead to a large increase in the size of the ablation area (e.g. Rea *et al.*, 1999; Margreth *et al.*, 2014; Boston and Lukas, 2019; Weber *et al.*, 2019). Conversely, the very small glaciers have already experienced substantial recession and now currently exist in very sheltered positions, which, while not being conducive for high mass input and substantial glacier development, are optimally situated for sustaining very small ice bodies, i.e. through reduced insolation. Furthermore, a likely increase in mountain rockfalls owing to climate warming (e.g. Gruber and Haeberli, 2007; Huggel *et al.*, 2012; Stoffel and Huggel, 2012) will further insulate small cirque and valley glaciers to climate warming and may play a key role in the glacier to rock glacier transition (cf. Jones *et al.*, 2019b). There is also the distinct probability that many small glaciers will transition to ice patches over the coming decades, and these will likely be able to survive for a prolonged period; this has already been realised in Norway with present-day ice patches having been evidenced to contain old glacier ice (Ødegård *et al.*, 2011; Finstad *et al.*, 2016; Ødegärd *et al.*, 2017).

7.3. The Little Ice Age in northern Norway

The maximum LIA glacier extent in the Rotsund Valley is dated by lichenometry to between 1814 and 1877 (Table 4.2) and, as noted in Chapter 4, these dates are younger than those ascertained on the nearby Lyngen Peninsula (Ballantyne, 1990). Lichenometric dating across 21 glacier forelands by Ballantyne (1990) indicated that while the 11 largest glaciers studied on the Lyngen Peninsula achieved LIA maxima in the mid-18th century (with no specific date assigned to these features) others (n = 9) attained their maximum extent at the start of the 20th century; of these, five achieved their LIA maximum between 1910-1920 and four between 1920-1930, with their large size being attributed to the overriding of earlier deposits. Ballantyne (1990) also noted that four glaciers had moraines which were dated to between 1825-1845 (n = 1) and 1865-1880 (n = 4), but that these moraines were inside a larger moraine dated to the mid-18th century. Furthermore, as outlined in the literature review (Section 2.4.2.6.3.), the recent work of Wittmeier (2020) on the island of Arnøya further complicates the picture. Their assessment of LIA moraines, using ^{10}Be cosmogenic nuclide dating, indicates maximum LIA extent was reached in 1532 ±20 yrs (1512-1552), with a second LIA moraine <100 m up-valley, formed in 1622 ±100 yrs (1522-1722; Wittmeier *et al.*, 2020). The LIA maximum on Arnøya is thus, roughly 372 years earlier than Ballantyne (1990) reported for the Lyngen Peninsula (using a mid-point of 1925), and 313 years sooner than Leigh et al. (2020) reported in the Rotsund Valley (using a mid-point of 1845; see Chapter 4). Furthermore, the early-16th century LIA maxima for Arnøya is considerably earlier than even the mid-18th century LIA maxima, in central and southern Norway, and stands as an outlier even when viewed in a northern hemispheric or global context (Grove, 2004b, 2004a). This is surprising, and the authors give little attention to this substantial disparity in moraine ages when compared to other similar Norwegian LIA chronologies, or those from the northern Hemisphere more generally. No explanation as to the cause of an early-16th century glacier maximum across Arnøya is given. Furthermore, Wittmeier et al's. (2020) proposed Arnøya LIA maximum seems at odds with nearby Holocene temperature reconstructions; at Barheivatn on the northern Lyngen Peninsula, pollen and plant macrofossil analysis indicates that the most severe late-Holocene climatic deterioration occurred at the start of the 1800s (Bjune *et al.*, 2004). As such, there is currently little available evidence across this region of northern Norway that supports

Wittmeier et al's. (2020) early LIA maximum. Their work does, however, provide the foundations for further research to corroborate these findings and assess the extent to which mountain glaciers on the islands and coastal mountains of northern (Arctic) Norway achieved an early-16th century glacier maximum.

7.3.1. Identifying Little Ice Age glacial geomorphology

A key aspect of Chapter 4 is the demonstration of how LIA maximum moraines in northern Norway are distinct from the other moraine assemblages in the valley sequence, both up and down valley. Specifically, LIA maximum moraines are large, sharp-crested, with little evidence of slumping and/or reworking, and found at a pronounced vegetation trimline (see Figure 4.5). Furthermore, Weber et al. (2019, 2020) recently presented mapped LIA limits of the ice caps Hardangerjøkulen and Langfjordjøkelen using a combination of remote sensing, supported by field surveying. Using moraine identifiers similar to those described above, Weber et al. (2019, 2020) suggested that fresh looking, sparsely vegetated glacial drift alongside distinct erosional/weathering boundaries (including trimlines) can be identified on high-resolution imagery and give a reliable indication of LIA glacial extent.

Using these descriptive characteristics it is possible to assess the presence of other likely LIA moraines and/or LIA glacial extent throughout the Troms and Finnmark region. Using www.norgeibilder.no, it is possible to observe numerous sites that host moraines of similar visual form and distance down valley to those identified and dated in Chapter 4; these sites (examples of which are shown in Figure 7.2) present opportunities for remote sensing analysis, but more importantly have moraines of presumed LIA origin that would be suitable for age dating. Additional age constraint on LIA moraines (across a transect of increasing continentality), will help refine the current disparity in timing of LIA maximum that have been proposed across the Troms and Finnmark region (e.g. Ballantyne, 1990; Leigh *et al.*, 2020; Weber *et al.*, 2020; Wittmeier *et al.*, 2020).

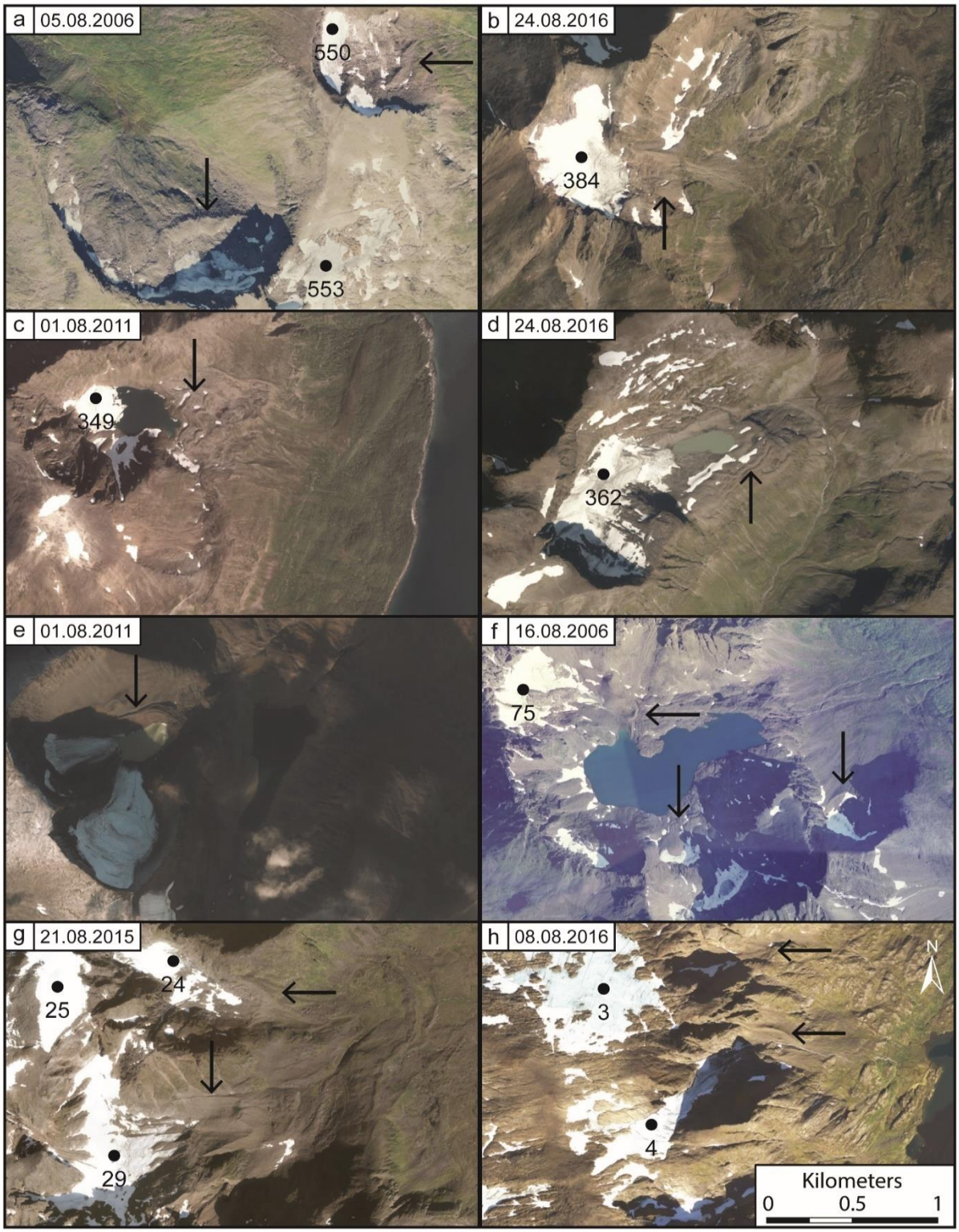

Figure 7.2. *Example of apparent LIA moraines Troms and Finnmark. Labelled from most westerly to most easterly (a-h); (a) 68°38'48.27"N 17°27'14.21"E, (b) 69°30'14.20"N 18°38'0.91"E, (c) 69°48'5.85"N 19°41'34.74"E, (d) 69°15'20.08"N 20°12'20.92"E, (e) 68°58'27.38"N 20°11'39.26"E, (f) 69°57'50.20"N 21°27'1.04"E, (g) 70°13'29.43"N 22°1'34.65"E, (h) 70°26'41.70"N 23° 8'15.57"E. Note: all imagery from www.norgeibilder.no and coordinates generated in Google Earth.*

7.3.2. Review of geochronological methods

7.3.2.1. Lichenometry

Although lichenometry has recently been criticised, with claims that lichenometric results are suspect (Osborn *et al.*, 2015), there are currently few suitable alternatives that offer low-cost, extensive, and reliable dating of features created in the recent past (e.g. within the last 300 years). Lichenometry, therefore, remains the best option where historical evidence is lacking and moraine ages are required (O'Neal, 2016). It is not without appreciation of recent critiques (McCarthy, 2013; Osborn *et al.*, 2015; Rosenwinkel *et al.*, 2015) that lichenometry was used in this thesis to assign calculated ages. Sampling strategies and analyses followed simple and well-established methods, ensuring transparency and allowing a high degree of cross-comparability. Where possible, all moraine surfaces were surveyed, mitigating potential influence of micro-environmental variations (Erikstad and Sollid, 1986; Karlén and Black, 2002). Indeed, Leigh (2016) showed that no moraine side or aspect, for example, had any greater likelihood to host larger lichens, with lichen populations randomly distributed across a moraine. Furthermore, while some authors have argued that methods relying on largest lichens should be dropped (e.g. Bull, 2018), it is not always feasible to adopt other approaches (e.g. size-frequency methods), which involve extensive and exhaustive lichen sampling strategies (i.e. due to time or funding constraints). Hence, the application of the five largest lichen approach was chosen because it is considered the optimum lichenometric index (Innes, 1984b), as supported by numerous reports documenting its use and success (e.g. Haworth *et al.*, 1986; O'Neal, 2006; Sikorski *et al.*, 2009; Carturan *et al.*, 2014; Evans *et al.*, 2019a).

The lichenometric dates used for this research are based on the construction of site-specific dating curves, accounting for differences in hygrocontinentality across mainland Norway (Chapter 4; Section 4.6.1.1). Extrapolation past the last known control is undesirable but, within the region of investigation, no other reliably dated surfaces were present; extrapolation therefore remained the only option. Limiting extrapolation to cover only the last 300 years minimises magnification of errors and is the most prudent approach. As such, lichenometry facilitates a fundamental understanding of the timing and extent of LIA glacial maximum and provides a key geochronological tool to help decipher the timing, extent, and pattern of recent glacial maxima across a variety of environments.

7.3.2.1. Soil chronosequences

Soil development within the Rotsund Valley shows a clear pattern of increasing thickness and depth with apparent moraine age (Table 6.2). However, the individual moraine crest soil properties vary between neighbouring forelands, even when moraines occupy similar positions within the geochronological sequence. The clearest example of dissimilarity in age approximations is seen with the terminal moraines (SM1, HM1, GM1; Table 6.4).

In a geochronological context, whereby differences in the soil profile (e.g. soil depth) are attributable to the varying increments of time since a specific geomorphological feature was formed, the soils in question must form with: (1) an environment of relatively comparable climate; (2) similar parent materials; (3) similar relief; and (4) with minimal variation in biotic factors (Jenny, 1941; Stevens and Walker, 1970; Huggett, 1998; Sauer, 2015). Considering that the three subsidiary valleys are all within 4 km of each other, orientated in similar directions and on the eastern flanks of the same mountain range, it is unlikely that climatic differences can account for the differing soil depths. Furthermore, the lithology is consistent between sites and all soil pits were excavated into the moraine crests so that the measured soils would have developed on similar parent material with comparable conditions in terms of drainage. We therefore consider the most likely variable causing the apparent dissimilarity in soil development between the three valleys is that of biotic factors.

The outermost moraines in the Sorbmevággi sequence are all within an area of boreal woodland with a well-established herbaceous layer. Regular input of organic litter to the moraine/soil surface coupled with the interaction of roots within the soil profile and the encouragement of soil dwelling organisms will likely result in increased rates of soil formation and enhanced onset of podzolization (Bridges, 1997; Phillips and Fitzpatrick, 1999; D'Amico *et al.*, 2014). With the small number of soil pits excavated on each moraine it is, however, difficult to identify any intra-site anomalies that could account for variable soil depths/development.

As a result, it is recommended that further investigation, utilising a greater number of soil pits per moraine (e.g. five-ten) should be undertaken. This would allow a critical and definitive assessment of the applicability of soil chronosequences for relative and/or calibrated dating of Holocene moraines.

7. 4. Glacial and periglacial geomorphology

7.4.1. Glacial landsystems in the upland regions of Troms

Having discussed the principles and signatures of glacial landsystems in Chapter 2 it is worth considering the glacial landsystems within the central upland regions of Troms and Finnmark County (including the Rotsund Valley/Kåfjord Alps field site). In the present-day, the upland regions are predominantly hosts to small cirque glaciers and perennial snow patches, with the exception of a few disintegrating plateau glaciers (the largest two of which are glacier ID 157 and 158; see Figure 3.5 and Figure 6.2). The valley systems are composed of a complex mix of glacial, glaciofluvial, and colluvial sediments and these range from being completely exposed in the recently deglaciated areas to heavily vegetated at the valley mouths. Extensive moraine systems are found throughout the region, forming distinctive latero-frontal systems extending from subsidiary valleys, fragmented minor ridges, and chaotic assemblages of ridges and furrows (e.g. DDAs). On the valley flanks, gelifluction is evident in the form of mass wasting (e.g. ploughing boulders) and at sharp breaks in slope there are areas of glacially polished bedrock and roches moutonnées. Across the higher plateau areas and flat-topped mountain summits there is a surficial covering of weathered residuum, occasionally showing evidence of periglacial activity (e.g. patterned ground). Collectively, the geomorphological characteristics are indicative of the landsystems that have existed since the deglaciation of the region ~13,000 cal. yrs. BP (see Section 6.6.2).

The topography and geomorphology of the upland regions of Troms and Finnmark County is indicative of a plateau icefield landsystem that would likely have evolved following deglaciation, which then transitioned through a valley glacier landsystem into the present-day cirque/peripheral glacier and periglacial landsystems (e.g. Section 2.4.1.1. to Section 2.4.1.6.). The region is dominated by small massifs of isolated, jagged peaks and sharp aretes and areas of upland plateaux, with steep sided as well as some gently sloping glacial valleys.

In plateau uplands of central Troms and Finnmark County, such as the Riehppe Plateau (Figure 7.3), there is ample evidence that plateau icefield landsystems developed following recession of the SIS. Within nearly all the valley systems radiating out from the main plateau, sequences of moraines can be found extending as looped features outside the valley systems, then forming recessional deposits up valley to

where they meet valley head backwalls which are often gently sloping and covered by perennial and late lying ice/snow and gently transitioning to the plateau surface. In a few instances moraines in these valleys can be traced back up onto the plateau surface (Figure 7.3 and see main map; Appendix A and online: doi.org/10.1080/17445647.2021.1950580). On the plateau areas blockfield is widespread, however, without any direct observation and/or age control it is not possible to assess if they have been protected beneath cold-based ice and thus pre-date the recent plateau exposure (Rea et al., 1996; Boston et al., 2015; Bickerdike et al., 2018). As the climate ameliorated and the extensive plateau icefield shrank, with valley glaciers likely having become disconnected, glacial landsystems would have evolved independently. In some areas of the Riehppe Plateau, ice may have extended to the plateau edge and carved into the valleys below, acting as an additional source of ice/snow feeding the valley glaciers; as has been hypothesised and indeed observed elsewhere in the central Troms and Finnmark region (e.g. Whalley, 1973; Forbes 1853).

Across other mountain regions of the central Troms and Finnmark County uplands dominated by series of steep-sided valleys, distinct valley glacial landsystems likely developed contemporaneously with the recession of the SIS and the development of plateau systems described above (e.g. Figure 7.4). The primary characteristics of these landsystems are the distinct sequences of (latero-frontal) recessional moraines and occasional areas of DDAs. Where present, DDAs are predominantly found abutting the proximal sides of large moraines, and rarely covering substantial proportions of the valleys (e.g. Figure 7.4). The infrequent and isolated nature of these DDAs indicate an origin by localised supraglacial loading, likely having occurred in isolated RSF incidents typical of mountain destabilisation during deglaciation (Fenton et al., 2011; McColl, 2012; Curry, 2021). Between moraines, valley floors are generally flat, with braided river systems having reworked the intervening tills; in some instances, moraine dammed lakes have developed. Using the Rotsund Valley reconstructions in Chapter 6, it is possible to postulate that valley glacier systems reacted relatively quickly to the warming of the early-Holocene; glacier recession up valley likely occurred in two to three main stages (e.g. Figure 6.3 and Table 6.3).

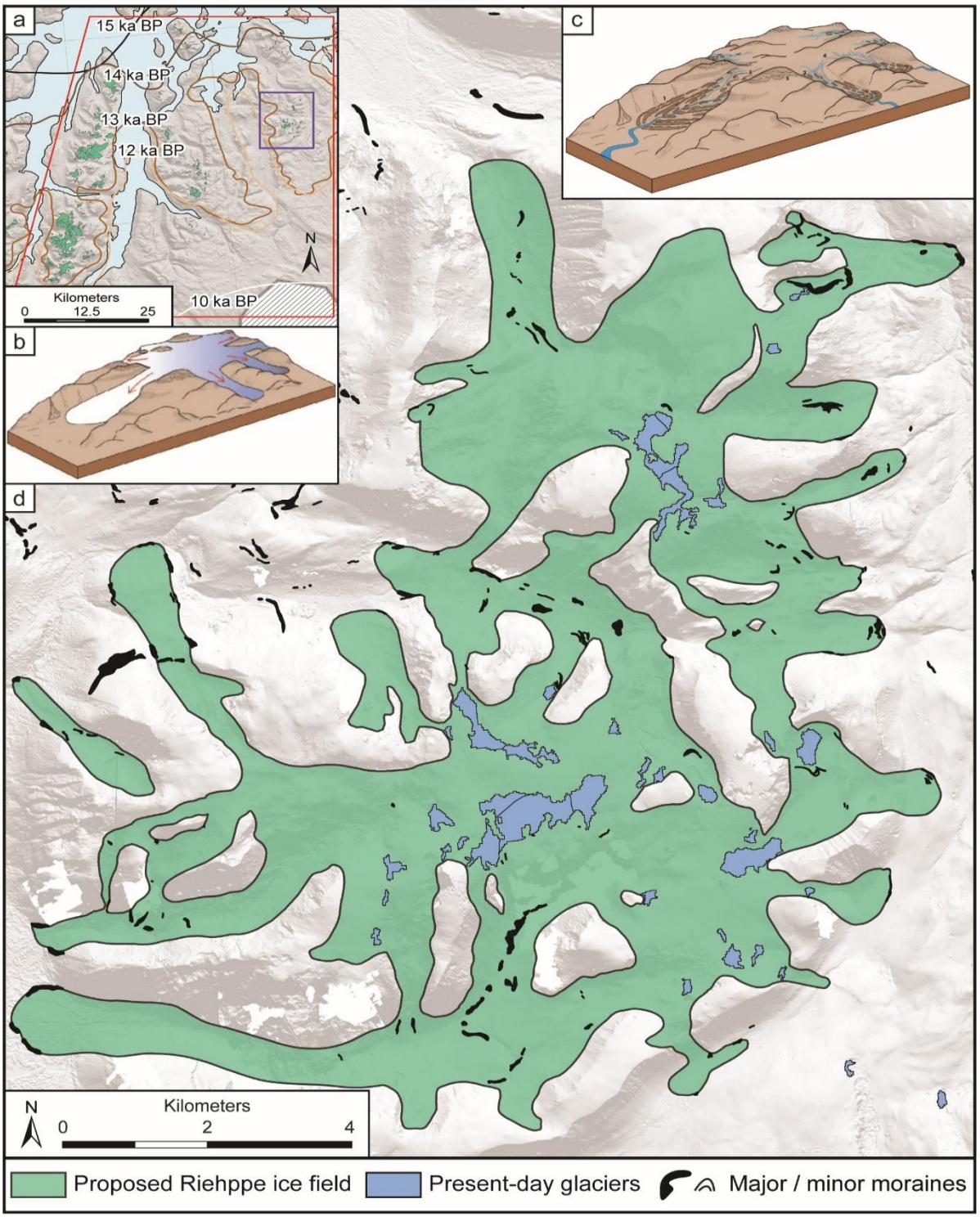

Figure 7.3. *The Riehppe ice field and present-day ice extent. Location of the Riehppe icefield in the upland region of central Troms and Finnmark County (a). Panel (b) and (c) show schematic diagrams of a plateau icefield and plateau icefield landsystem proposed by Bickerdike et al. (2018, pp. 205 and 210). Moraine mapping and glacial reconstructions (d) demonstrate the transition from plateau icefield landsystem to that of a cirque/peripheral glacier landsystem. Base image in (a) and (d) is a 2 m hill shaded Arctic DEM tile.*

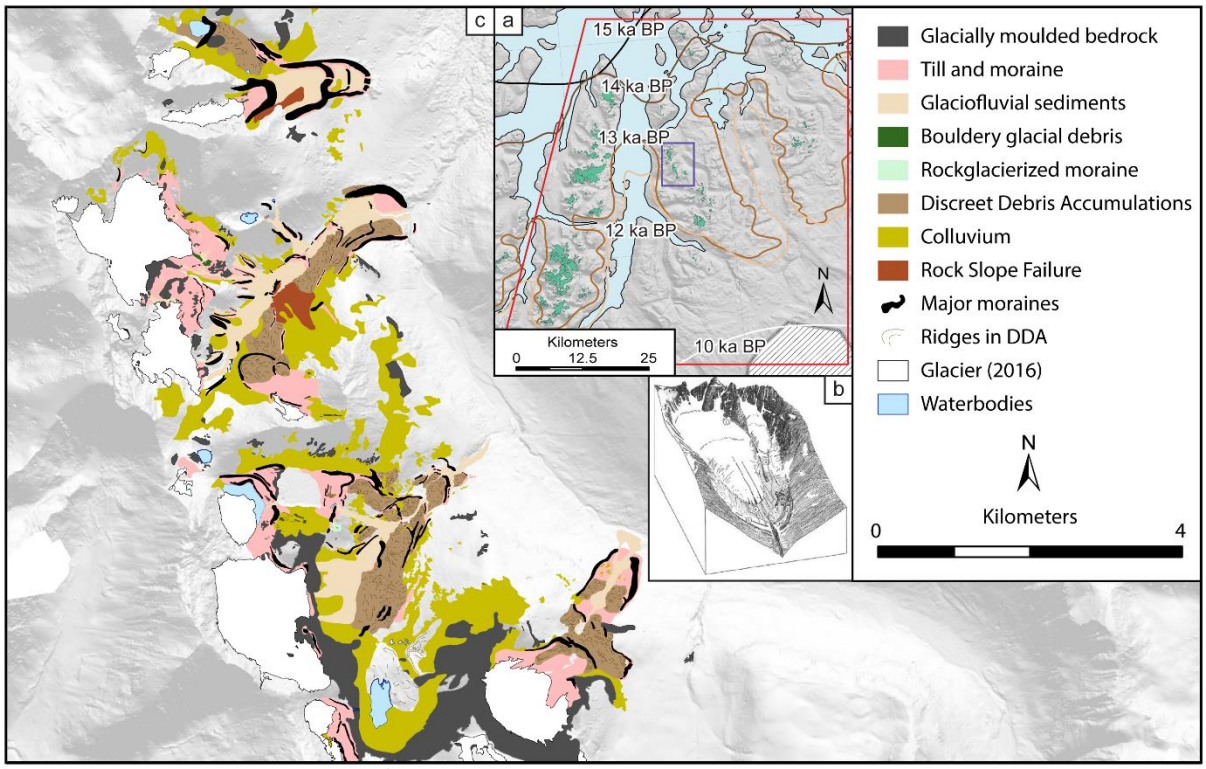

Figure 7.4. The *valley glacier landsystems of the Rotsund Valley. Location of the Rotsund Valley is shown in (a), and the schematic diagram (b) demonstrates the typical components of a valley glacier landsystem (from Benn et al., 2003, pp. 379). The main map in (c) demonstrates the key geomorphological components within the Rotsund Valley in the upland region of central Troms and Finnmark County. Base image in (a) and (c) is a 2 m hill shaded Arctic DEM tile.*

In the present-day glaciers are predominantly found in isolated cirques, rarely extending more than 1 km from cirque headwalls. These glaciers can be categorised within the cirque glacier landsystem (see Section 2.4.1.4.). As discussed in Chapter 4, the present-day glaciers of the Rotsund Valley exist well within their LIA limits, demarcated by large, steep sided, and unvegetated moraines (e.g. Figure 4.5) and are of two distinct types. In the steep narrow valleys which dominate the region there is little evidence of active glacial recession. Instead these glaciers have seemingly experienced relatively un-interrupted retreat or have frontal margins covered in supraglacial debris, producing areas of chaotic DDA (e.g. Figure 4.2). Conversely, at sites where a wider, flatter-floored cirques have formed, glaciers have developed an active temperate cirque landsystem. Across the forelands, numerous regularly spaced and relatively uniformly-sized minor moraines have been constructed, interspersed

with areas of supraglacial debris and dissected by active glacial-fluvial processes. The clearest example of this style of active temperate cirque glacier landsystem is found at Glacier 121, where the foreland was surveyed in the field and mapped in detail (Figure 7.5).

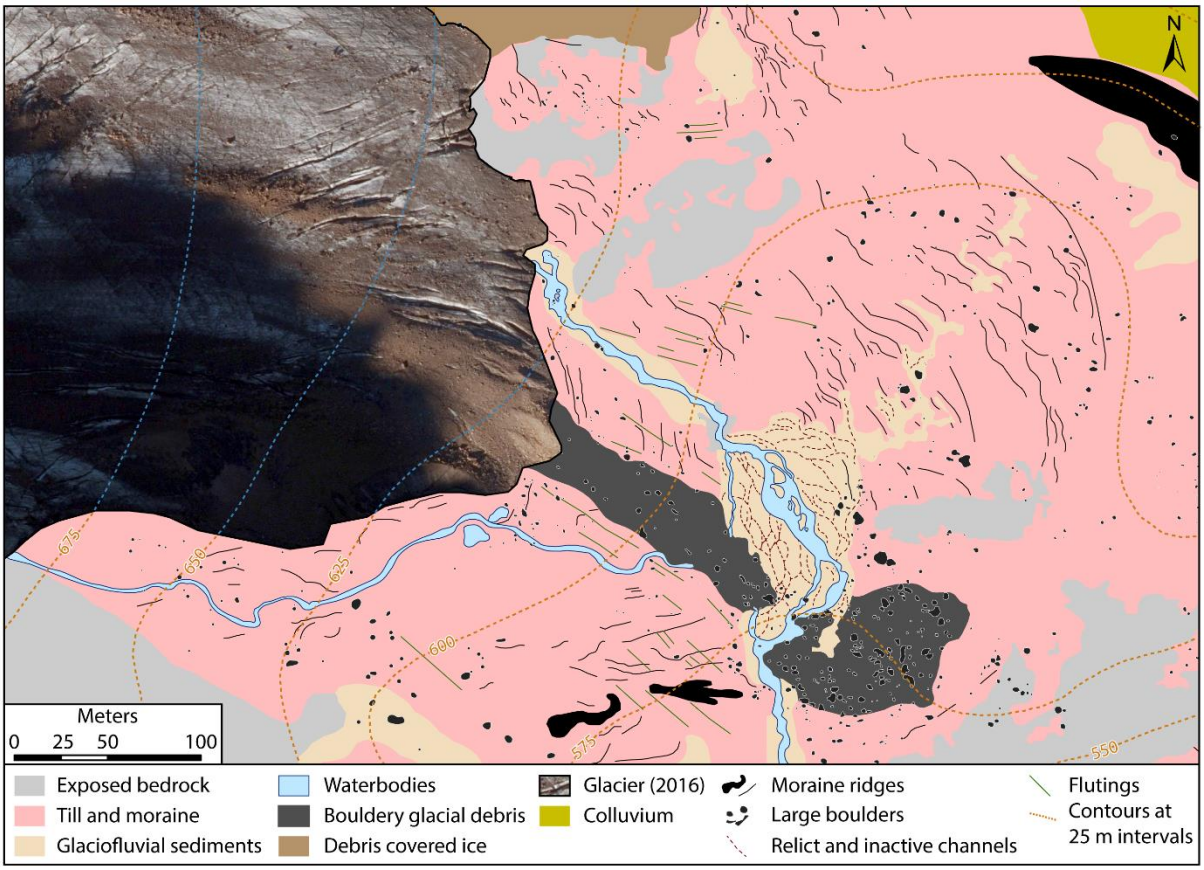

Figure 7.5. *Glacial geomorphological map of glacier 121's foreland, in the Rotsund Valley, northern Norway. The closely spaced, small recessional moraine ridges were likely formed annually during deglaciation in the late-20th and early-21st century and represent an active temperate cirque glacier margin. Modified from the mapping of Leigh et al.* (2020).

Within the valleys that are not occupied by present-day glaciers, the landsystems that now exist are those which have been conditioned by RSF and rock glacierization, with RSF deposits and rock glaciers sometimes occupying large proportions of the valley sides and floors. Other, smaller deposits such as pronival ramparts are also present and these occasionally show evidence of downslope deformation, likely indicating the presence of localised permafrost. In some areas,

moraines also show evidence of post-depositional deformation or rock glacierization (e.g. Figure 7.3).

7.4.2. Rock glaciers: glacial vs. periglacial and the glacier-rock glacier transition

In Chapter 5 the ongoing and unresolved debate surrounding terminology and formation/development processes of many rock glacierized features is briefly discussed (cf. Berthling, 2011; Hedding, 2016b). A clear example of the issues surrounding terminology is seen when looking at the most subtle rock glacierized landforms that occur where there is ample debris supply at the valley side and valley floor interface, with names such as: 'protalus lobes' (e.g. Lindner and Marks, 1985; Harrison *et al.*, 2008; García *et al.*, 2017); 'protalus rock glaciers' (e.g. Gray, 1970; Ballantyne and Harris, 1994; Curry *et al.*, 2001); 'talus-foot rock glaciers' (e.g. Ballantyne and Kirkbride, 1986; Sandeman and Ballantyne, 1996; Matthews *et al.*, 2013); and 'embryonic rock glacier' (Zhu *et al.*, 1996; Serrano and López-Martínez, 2000; Matthews *et al.*, 2017) all used in the literature. Although all these terms are used to describe similar features, the term 'protalus lobe' is the most common.

In Chapter 5, rock glaciers are classified as 'valley floor rock glaciers' and 'valley wall rock glaciers' but it is likely that further field investigations could necessitate and indeed facilitate further subdivision and genetic interpretation, specifically in relation to whether they are glacially or periglacially derived. Furthermore, Figure 7.6 (see also Fig. 5.11c, d) presents an example of a hybrid rock glacier landform containing both valley wall and valley floor type rock glaciers. The largest part of this landform, filling a substantial portion of the cirque, is a 'valley floor rock glacier' with clearly defined ridges within the rock debris that extend up to the glacier margin. The unbroken transition from rock debris to glacier ice, therefore, likely represents the remnants of a heavily debris covered snout which has transitioned into that of an active rock glacier. Additionally, at the foot of the talus slope on the northern margin, yet distinctly separate from the valley floor feature, is a 'valley wall rock glacier'. The lack of evidence on the headwall of a large rock slope failure leads to the reasonable conclusion that this is a deforming pronival rampart (e.g. a protalus lobe). The convexity of both features combined with the absence of vegetation encroachment, indicates the presence of deforming ice within the rock debris, which over time will likely result in the merging of these two landforms. If, or indeed once, the landforms

merge, it is likely that the presently well-defined boundaries will be lost, blurring the hybrid nature of the landform. If it were not for the available image documentation, this would make inferences as to its origin more difficult.

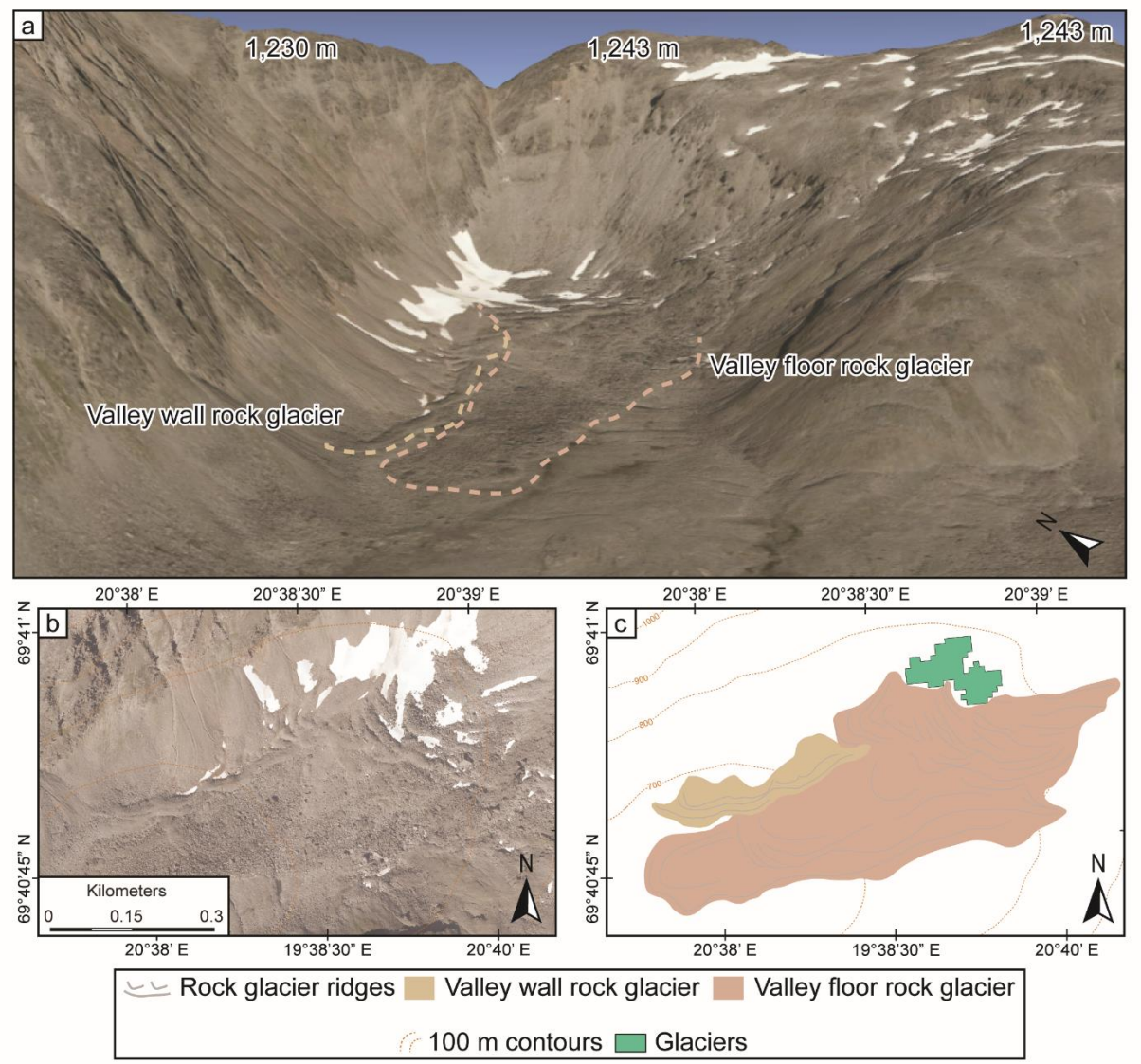

Figure 7.6. A *hybrid rock glacier landform containing both valley wall and valley floor type rock glaciers: (a) 3D render of the area overlain with 0.5 resolution aerial imagery; (b) vertical aerial orthophotograph; (c) mapping of the hybrid landform presented at the same scale as in panel b. Imagery source: www.norgeibilder.no (imagery date: 24.08.2016). Approx. location 69°40'50.97"N, 20°38'24.74"E.*

7.4.3. Comparison with previous mapping

Here a specific example is used to compare the mapping conducted in Chapter 5 (see the main map in the Appendix and online: doi.org/10.1080/17445647.2021.1950580) with previous geomorphological maps of the study area.

The impressive dual lobed rock glacier within Veidalen (see Figure 7.7), originally identified and mapped by Griffey and Whalley (1979), was re-assessed during the mapping undertaken in Chapter 5. The shape and extent of the glacier-derived rock glacier as shown by the map of Griffey and Whalley (1979) was maintained, but the new mapping identified further individual ridges and lobes contained within the rock glacier complex (red box in Figure 7.7b). Distal to the rock glacier it has also been possible to map a series of minor moraines, some of which have been dissected by the rock glacier's advance. Up-valley from the main moraine and rock glacier complex numerous closely spaced inset moraines on the till plain were identified (green box in Figure 7.7b). These moraines are evenly sized and likely represent a period of active ice retreat, geochronological control on these moraines would provide key indication as to their ages and the duration of active ice retreat at this site. Finally, fronting the cirque glacier ID 188, another rock glacier has been mapped alongside a rock glacierized moraine (pink box in Figure 7.7b). The rock glacier's main lobe extends from the till plain in front of glacier 189, continues into the small cirque and at its uppermost extent merges seamlessly with the 2016 ice margin. The rock glacier itself is likely glacier-derived, formed during glacier recession after the LIA maximum, while the rock glacierized moraine possibly demarcates the lateral maximum LIA extent of glacier 189. The new mapping and interpretations (e.g. Figure 7.7) highlight the advantages of modern aerial orthophotograph and GIS software (e.g. higher resolution colour imagery and ease of image adjustments) when mapping remotely. It also shows how it remains important to revisit sites to reassess changes to the local geomorphology, especially given recent glacier recession and associated landscape changes.

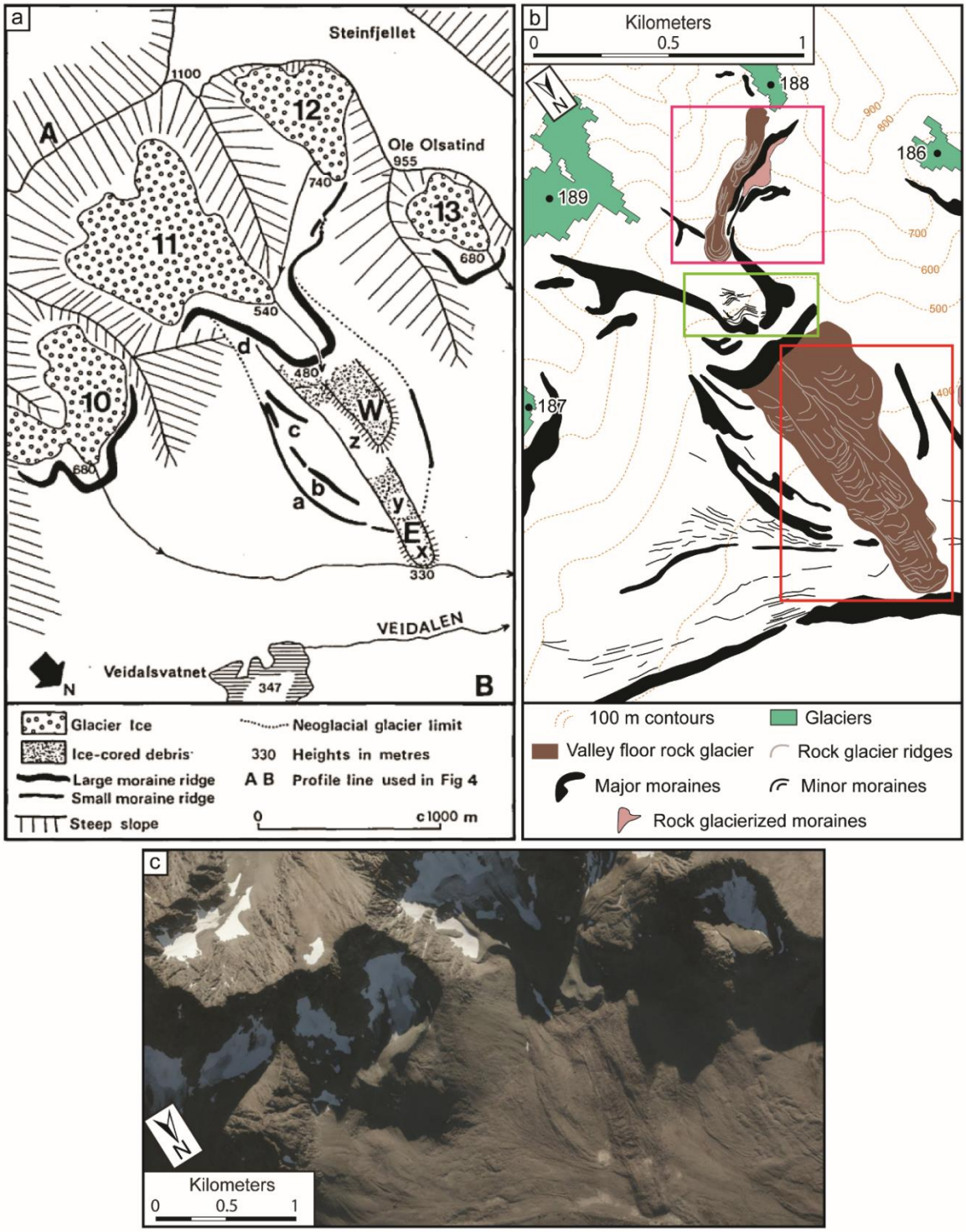

Figure 7.7. *Comparison of mapping interpretation and depiction: (a) the geomorphic map of Griffey and Whalley* (1979)*; (b) re-mapping of the same area; (c) 0.5 resolution aerial imagery of the area (image source: www.norgeibilder.no; 24.08.2016). Additional details include mapping of individual rock glacier ridges within the main rock glacier complex (see red box), an additional rock glacier and a rock glacierized moraine on the foreland of glacier 188 (see pink box), and glacially overridden moraines (see green box). Approx. location 69°45'37"N, 20°3'49"E.*

7.5. Ice sheet deglaciation and the Holocene glacial history

Chapters 5 and 6 have shown that following recession of the SIS (~13,000 cal. yrs BP) small mountain glaciers in the Rotsund Valley, northern Norway achieved their maximum glacial extent during the late-YD (dated to between ~12,000 and 10,500 cal. yrs BP; Table 6.3). Throughout the Holocene, notable moraine forming events occurred around 10,000-9,000, 8,400-8,200, 4,700, 3,900 cal. yrs BP, and the early-1900s (Table 4.2 and 6.3), likely representing the Erdalen Event, 8.2 ka event, several Neoglacial advances, and the LIA. In Sections 6.6.1.1. to 6.6.1.3., the Rotsund Valley Holocene chronology is briefly compared with that of other similar Scandinavian chronologies; the following sub-sections examine and discuss, in greater detail, the similarities and differences in the Rotsund Valley glacial chronology (e.g. Figure 7.8) with reference to other Arctic and Alpine chronologies. The aim is to assess synchronicity, or lack thereof, of Holocene glacier fluctuations from varying sites across the Northern Hemisphere, putting a local chronology into a hemispheric context and enabling a tentative assessment of its reliability.

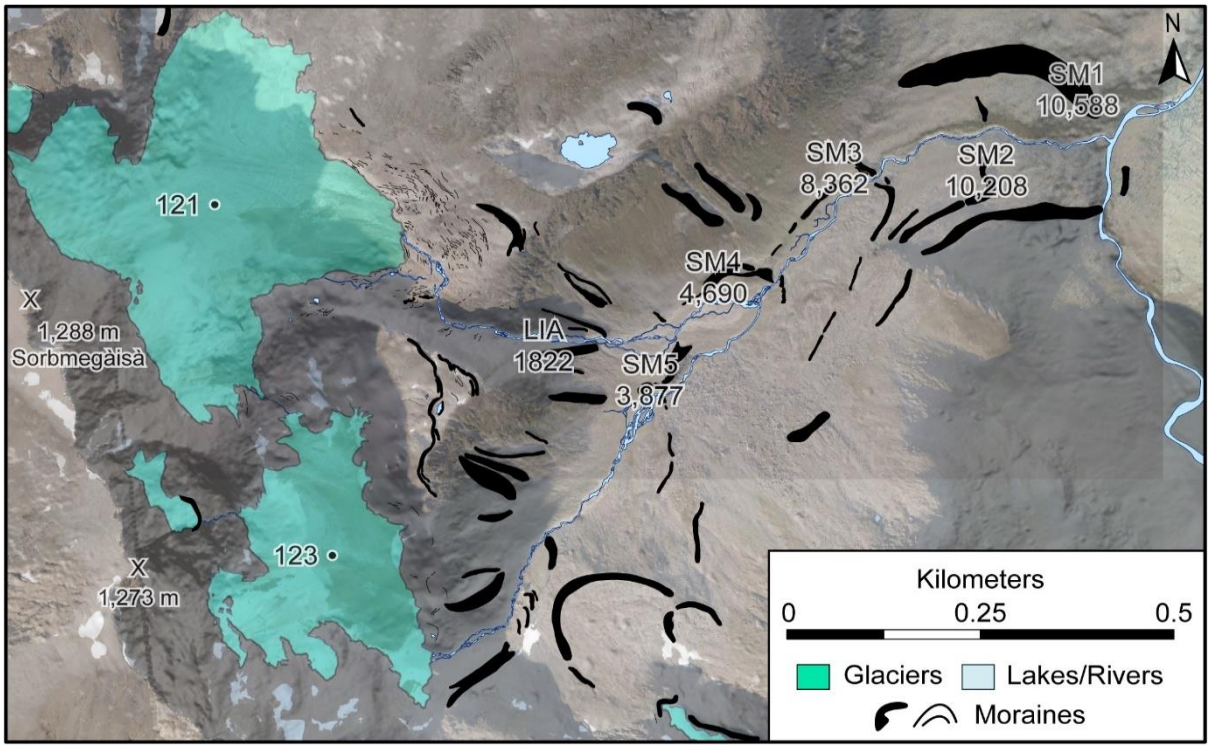

Figure 7.8. *The full moraine sequence of Sorbmevággi extending from a late-YD moraine (SM1) up to the 2016 ice margin. Moraines are annotated with their calculated ages (from Schmidt hammer and Lichenometry; see Chapters 4 and 6). Base image is a 2 m ArcticDEM overlaid on a 0.25 cm aerial orthophotograph mosaic (24.08.2016).*

7.5.1. Palaeo-significance of Rotsund Valley moraines

Throughout Chapters 4 and 6 the well-defined and relatively uniform moraine assemblages found within the individual valley systems of the Rotsund Valley have been linked to key climatic events via the use of calibrated age dating. It is, however, prudent to consider other non-climatic mechanisms that may have resulted in moraine formation.

In the first instance, glacier surging is ruled out as a trigger for moraine formation within the Rotsund Valley. While there are some areas of DDA in the lower forelands of the larger valley systems (sometimes used to evidence surge-type glaciers; Clayton et al., 1985; Drozdowski, 1986) there are no other key characteristic landforms such as zig-zag eskers, crevasse-squeeze ridges, or thrust-block moraines (cf. Evans et al., 2003). Furthermore, the near uniform pattern of moraine sequences within neighbouring valleys indicates that adjacent glaciers are responding in a similar spatio-temporal pattern, which would be unlikely if these glaciers were experiencing surge events.

An alternative non-climatic trigger for glacier advance is that of supraglacial debris loading from valley side RSFs. In brief, heavy debris cover shields the glacier from solar radiation, in turn reducing ablation and resulting in a change to the glaciers mass balance and basal friction, triggering glacier advance (Shulmeister et al., 2009; Vacco et al., 2010). Examples of non-climatically debris-forced advance have been widely documented in New Zealand's Southern Alps (e.g. Shulmeister et a., 2009; Vacco et al. 2010; Reznichenko et al., 2011) and due to anthropogenic debris loading from mining activities (cf. Jamieson et al., 2015; Evans et al., 2016a). There is possible evidence of past supraglacial debris loading (e.g. extensive areas of within-valley DDAs; see Section 6.5.2.2.) having resulted in the deposition of larger and further reaching moraine systems within the Sorbmevággi valley. However, this pattern is not observed across many other valleys within the Rotsund Valley/Kåfjord Alps and, as such, is likely a site-specific example of debris loading enhancing an otherwise synchronous moraine forming event.

Without evidence of an alternative explanation, it is therefore reasonable to hypothesize (as in Chapter 6) that Rotsund Valley moraines represent a synchronous climatic signal. This interpretation is further supported by the range of calibrated ages assigned to key moraines that are coeval with substantial and widely recognised

climatic events (see Chapter 6). Whether these moraines formed because of a climatically driven glacial readvance or stillstand during net retreat is, however, a more difficult question to answer. Further field analysis examining the internal sedimentological structures alongside numerical modelling experiments might provide the opportunity to better understand the triggers of moraine formation at the timesteps as defined in Chapter 6 (Table 6.3).

7.5.2. Comparison with other Arctic regions

7.5.1.1. The early-Holocene

At the onset of the Holocene, fjord systems across the Svalbard archipelago were rapidly deglaciating. However, mountain glacier systems were experiencing multiple episodes of readvance (Farnsworth, 2018; Farnsworth *et al.*, 2020). Most notably, during the period 11,000-10,000 cal. yrs BP it is proposed that mountain glaciers experienced as many as 11 readvances (cf. Farnsworth *et al.*, 2020), with other early-Holocene deposits forming as late as ~9,100 cal. yrs BP (Marks and Wysokiński, 1986; Forwick *et al.*, 2010; Farnsworth *et al.*, 2020). Similarly, on Baffin Island, Arctic Canada, glacial meltwater deposits are attributed to glacier advance between 9,500 and 8,500 cal. yrs BP (Andrews and Ives, 1978; Briner *et al.*, 2016); and in the Disko Bugt region of West Greenland there is evidence of large moraines deposited at, or shortly after, 10,000 cal. yrs BP (Ingólfsson *et al.*, 1990; Briner *et al.*, 2016). In contrast, across Iceland, Geirsdóttir et al. (2009) indicated that by 10,300 cal. yrs BP glaciers had retreated rapidly to the Icelandic highlands, with ice rafted debris delivery to the fjords also having terminated by this time (Geirsdóttir *et al.*, 2002, 2009). Only recently were Brynjólfsson et al. (2015) able to demonstrate a period of early-Holocene glacier readvance on northwest Iceland. Using ^{36}Cl dating of boulders situated on a large moraine at the mouth of Leirufjörður, Brynjólfsson et al. (2015) discovered a formation age around 9,300 cal. yrs BP. Although none of the early-Holocene glacier advances from other Arctic regions have been explicitly linked to the advanced glacier positions of the Norwegian Erdalen Events (10,000-9,500 cal. yrs BP), the marked similarity in their ages indicates that they are all likely attributable to the same early-Holocene cooling. At this time, decreases in δ^{13}C values and observable increase in ice-rafted debris in North Atlantic deep-sea cores are linked with ocean surface cooling and reduction in North Atlantic Deep Water production (cf. Oppo et al., 2010; Wanner et

al., 2011). The Rotsund Valley moraines immediately up-valley from the YD ice limits and dated to 10,208 and ~9,208 cal. yrs BP (Table 6.3, Figure 7.8) appear, therefore, comparable to other similar moraines throughout the Arctic.

In the Rotsund Valley, there are large latero-frontal moraines at the entrances to the subsidiary valleys (e.g. SM3; Figure 7.8), and these are attributed to the 8.2 ka event (Chapter 6). While similar moraine evidence is lacking across Troms and Finnmark County, in Arctic Canada and south-east Greenland a series of deposits, including terminal moraines and pro-glacial lake sediments, have been correlated to the 8.2 ka event (e.g. Young *et al.*, 2012; Balascio *et al.*, 2015; Briner *et al.*, 2016), thus indicating a pan Arctic response to the 8.2 ka event. These results highlight that even at sites lacking moraines, a distinct glacial signal is still evident in other chronological archives (e.g. pro-glacial lake sediments), which has been evidenced across Norway (cf. Nesje, 2009). However, there are also some Arctic regions where no 8.2 ka glacial response is detected; Across Svalbard, Farnsworth et al. (2020) reported that glaciers were in a period of rapid retreat after ~10,000 cal. yrs BP, with little geomorphological evidence to indicate glacier still-stands or readvances during the 8.2 ka event. Although, a distinct period of cooling between 9,000 and 8,200 cal. yrs BP has been evidenced by marine sediments in fjords/coast of Svalbard which show a decline in mollusc remains at this time (Mangerud and Svendsen, 2018; Farnsworth *et al.*, 2020).

7.5.1.2. The mid-Holocene

After the 8.2 ka event moraine, no moraines are evident in the Rotsund Valley until the Neoglacial moraine (e.g. Figure 7.8), representing the mid-Holocene glacial minima. A similar pattern is observed across Norway (cf. Nesje, 2009) and other Arctic regions. On Svalbard, most catchments deglaciated and remained ice-free during the mid-Holocene, with the glacial minima having occurred between 8,000 and 6,000 cal. yrs BP (Farnsworth *et al.*, 2020). It has, however, been postulated that some glaciers in the Nordaustlandet and eastern Spitsbergen region of Svalbard survived the HTM owing to their elevation and distance from the West Spitsbergen Current (Fjeldskaar *et al.*, 2018). In northeast Canada, the Laurentide ice sheet delayed the peak temperatures of the HTM to between 7,000 and 6,000 cal. yrs BP, whereas in Alaska and northwest Canada it is shown to be synchronous with orbital-induced summer

insolation at 11,000-9,000 cal. yrs BP (Renssen *et al.*, 2009). On Baffin Island, it has been demonstrated that while the Foxe Basin ice cap collapsed during the HTM, alpine glaciers in coastal settings were able to survive (Briner *et al.*, 2009). Similarly, on Greenland, while the ice sheet lost as much as 100 Gt/yr for several millennia during the period 7,000-4,000 cal. yrs BP, resulting in a total ice extent substantially smaller than during the 2010s, mountain glaciers and small ice caps remained throughout the Holocene and did not melt away with peak HTM temperatures (Larsen *et al.*, 2015, 2019). Suggestions as to the timing of minimum ice extent of the Greenland ice sheet ranges from 6,000-2,000 cal. yrs BP (cf. Briner *et al.*, 2016). On Iceland, renewed interest in the presence of glaciers during the HTM led Harning et al. (2016) to re-assess glacier presence using lake sediment analysis, leading them to conclude, in-line with most prior studies, that the Drangajökull (like other Icelandic ice caps) melted completely during the peak warm of the HTM, between 9,000 and 6,9000 cal. yrs BP (cf. Harning *et al.*, 2016).

The general patterns of substantial mid-Holocene Arctic deglaciation are broadly in-line with those of the whole of mainland Norway. However, across Norway past research indicated complete deglaciation of the mainland (cf. Nesje *et al.*, 2008; Nesje, 2009), whereas in other Arctic regions (e.g. Svalbard) small, isolated, ice caps and glaciers are shown to have survived the HTM (e.g. Briner *et al.*, 2009; Fjeldskaar *et al.*, 2018; Larsen *et al.*, 2019). These glaciers were optimally situated in mountain regions, often in proximity to the coast, and away from the direct influence of warm air currents (e.g. Briner *et al.*, 2009; Fjeldskaar *et al.*, 2018; Larsen *et al.*, 2019). More recently, however, Bakke et al. (2010) found evidence to suggest that Austre Okstindbreen (a large glacier just south of the Arctic Circle) persisted throughout the HTM, and they liked its perseverance to its higher elevation and distance from the coast. Connecting the survival of Austre Okstindbreen (Bakke *et al.*, 2010) with the survival of many other Arctic glaciers (e.g. Briner *et al.*, 2009; Fjeldskaar *et al.*, 2018; Larsen *et al.*, 2019) would support the inference that some optimally situated glaciers in Troms and Finnmark County, may too have survived the peak warmth of the HTM, as postulated in Figure 6.14.

7.5.1.3. The late-Holocene

Neoglaciation in the Rotsund Valley appears to have reached a maximum ~4,690 cal. yrs BP (Chapter 6; Table 6.3). Across other Arctic regions late-Holocene environmental reconstructions show cooling initiating at: ~5,000 cal. yrs BP in the Svalbard archipelago (Farnsworth *et al.*, 2020) and throughout the Canadian Arctic (Briner *et al.*, 2016), subsequent to 4,000 cal. yrs BP on Greenland (Briner *et al.*, 2016), and after 6,000 cal. yrs BP across Iceland (Geirsdóttir *et al.*, 2009). This in turn triggered enhanced Neoglacial activity from 4,500-4,000 cal. yrs BP across Iceland, 4,000 cal. yrs BP across Greenland, and between 3,000 and 4,000 cal. yrs BP throughout the Canadian Arctic and Svalbard (Geirsdóttir *et al.*, 2009; Briner *et al.*, 2013, 2016; Farnsworth *et al.*, 2020). Furthermore, contrary to the majority of work on mainland Norway, many of the aforementioned studies present details of early-Neoglacial glacier advances more extensive than that of the LIA (e.g. Reusche *et al.*, 2014; Philipps *et al.*, 2017; Larsen *et al.*, 2018; Pawłowska *et al.*, 2020). The evidence of multiple Neoglacial events triggering extensive glacier (re)advance presents a strong link with the chronology depicted in Chapter 6 and strengthens the argument to support a Neoglacial maximum prior to the LIA at some mountain glaciers in Arctic Norway (e.g. Figure 7.8).

7.5.3. Comparison with the European Alps

7.5.2.1. The early-Holocene

Across the European Alps, the first notable Holocene climatic event triggering glacier readvance is linked with a Pre-Boreal Oscillation, which is also recorded in palaeobotanical records (Tinner and Kaltenrieder, 2005; Ivy-Ochs *et al.*, 2009). At this time, Alpine glaciers are believed to have several oscillations during the period ~11,700-10,400, forming large moraines which exceed LIA limits (e.g. Ivy-Ochs *et al.*, 2006; Schimmelpfennig *et al.*, 2012, 2014; Moran *et al.*, 2016a; Protin *et al.*, 2019). Furthermore, in their review of the Alpine glacier chronologies, Ivy-Ochs et al. (2009) noted that after 10,500 cal. yrs BP large glaciers retreated and remained confined to the high-mountains, well within their LIA extents. Yet small glaciers (defined as only a having a size of only a few km^2 or less) reacted more dynamically, with a brief period of glacier advance equal to, and occasionally greater than, LIA maxima, having occurred ~10,500-10,400 cal. yrs BP (Ivy-Ochs *et al.*, 2006). There are also large rock

glaciers, now relict, which are thought to have formed during this period and they remained active at ~10,500 cal. yrs BP when there was a distinct climate shift to warmer and drier conditions (Ivy-Ochs *et al.*, 2009), leading to rapid tree line expansion to higher elevations (Tinner and Kaltenrieder, 2005). Subsequent bulldozing and burial of trees by advancing glaciers in more recent Holocene periods provides a precious resource for ^{14}C dating, helping to pinpoint periods of glacier advance (e.g. Le Roy *et al.*, 2015).

At some of the smaller glaciers in the Eastern Alps, there is also evidence of readvance correlated to the 8.2 ka event, with some glaciers seemingly able to just exceed their LIA extents (Nicolussi and Patzelt, 2001; Kerschner *et al.*, 2006; Kerschner and Ivy-Ochs, 2008; Nicolussi and Schlüchter, 2012). Given the apparent limited glacial response to the 8.2 ka event, it is somewhat surprising that from high-altitude bogs in Austria, Kofler et al. (2005) were able to see a distinct distribution in pollen deposits which is categorically attributable to the 8.2 ka cold event. Subsequently, an 8.2 ka signal has been discovered in speleothems found in a mid-altitude Austrian cave (Boch *et al.*, 2009) and a chironomid record from an high-altitude Austrian Lake (Ilyashuk *et al.*, 2011).

Thus, mountain glaciers across the European Alps in the early-Holocene behaved differently to those of Norway and the Arctic, with Alpine glaciers experiencing their largest advances during the termination of the YD (~12,000 cal. yrs BP) and Pre-Boreal period (~11,000 cal. yrs BP). In contrast, Norway experienced its largest early-Holocene re-advance during the Erdalen Event (10,100-9,500 cal. yrs BP), at the Pre-Boreal to Boreal transition (Matthews *et al.*, 2008; Ivy-Ochs *et al.*, 2009; Nesje, 2009). The substantially differing climates of Norway and the Alps, related to the proximity to the North Atlantic and remnants of the SIS, is likely the driving factor responsible for these different environmental responses. Evidence of climatic perturbations centred around 8,200 cal. yrs BP are, however, broadly similar, with some glacial deposits directly attributable to readvance at this time alongside other sites lacking moraines yet showing distinct glacial signals in other proxy records such as lake sediments (e.g. Dahl and Nesje, 1994; Kofler *et al.*, 2005; Nesje *et al.*, 2006; Ilyashuk *et al.*, 2011).

7.5.2.2. The mid- and late-Holocene

Across the Alps, following the initial re-advance at the very start of the Holocene, most large glaciers receded after 10,500 cal. yrs BP and remained at substantially shrunken sizes for most of the mid-Holocene (Ivy-Ochs *et al.*, 2009). Towards the very end of the HTM, during the period 5,300-3,700 cal. yrs BP, some large catchments are shown to have completely deglaciated, with radiocarbon dating of archaeological evidence (e.g. the Ötztal Ice Man and hunting bows) supporting these observations (e.g. Bellwald, 1992; Suter *et al.*, 2005; Ivy-Ochs *et al.*, 2009; Hafner, 2012). The deglaciation of many catchments matches that proposed for Norway, albeit it at a later time-period.

The first evidence of Neoglacial activity in the central Alps is the apparent glacial advance at ~5,500-5,000 cal. yrs BP (Magny and Haas, 2004; Ivy-Ochs *et al.*, 2009). In the southern French Alps, ^{10}Be dating revealed that multiple late-Holocene moraines exist outside known LIA limits, with the Neoglacial maximum at Bonnepierre Glacier dated to 4,250 ±440 cal. yrs BP (Le Roy *et al.*, 2017). However, a widespread Neoglacial signal is not seen until ~3,500 cal. yrs BP, when large glaciers, such as the Grosser Aletschgletscher advanced (Leemann and Niessen, 1994; Holzhauser, 1997; Holzhauser *et al.*, 2005; Ivy-Ochs *et al.*, 2009). After the initial onset of Neoglaciation, glaciers fluctuated regularly throughout the European Alps, with Matthews (2007) proposing as many as 17 readvances all of similar magnitude and correlating with low solar irradiance. An early-Neoglacial Alpine glacier advance between 5,500 and 5,000 cal. yrs BP while not clearly documented in many Arctic records, could be linked to the earliest Neoglacial moraine in the Rotsund Valley, dated to 4,690 (4,108-5,287) cal. yrs BP (SM4; Table 6.3, Figure 7.8).

7.6. Further research

The conclusions and implications of this thesis highlight several potential areas for continued research which could fruitfully build on the findings presented throughout.

7.6.1. Expanded dating of Little Ice Age moraines in northern Norway and production of a complete Norwegian Little Ice Age maximum glacier inventory

In Chapter 4, 15 LIA moraines were identified in the Kåfjord mountains. When examining the Troms and Finnmark region more broadly, it is possible to observe numerous additional glacier forelands that host moraines of similar visual form and distance down valley (Figure 7.2). Furthermore, field investigations and dating assessments (using techniques such as lichenometry, terrestrial cosmogenic nuclide dating, lake sediment analysis, or dendrochronology) would help test observations regarding timing of LIA maxima and the subsequent rate of change over the following years as made in Chapter 4. A more extensive dataset of LIA deposits would provide substantial clarity on timing of the LIA in the region, as these currently range from ~1532 (Wittmeier *et al.*, 2020) to between 1814-1877 (Leigh *et al.*, 2020) and ~1930 (Ballantyne, 1990). All of these contrast with the mid-1700s date established for southern and central Norway (cf. Nesje *et al.*, 2008).

A more extensive dataset of LIA moraines in northern Norway would also help facilitate a complete LIA inventory for the whole of mainland Norway. A complete Norwegian LIA inventory would be a novel and important resource and could be used for a variety of applications. For example it would enable a better understanding of recent (e.g. past 200-300 years) landsystem transitions and how landscapes are responding to deglaciation (changing stream flow patterns, changing ecology, increasing rockfall risk etc.), help refine numerical models of glacier change, and help to better understand the impacts and implications of anthropogenically-forced climate warming.

7.6.2. Assessing the likelihood of Neoglacial advance or readvance of Rotsund Valley mountain glaciers

As outlined in Chapter 6, moraine dating reveals that mountain glaciers in the Rotsund Valley likely experienced their Neoglacial maximum around ~4,600 cal. yrs BP (Table

7.3). However, what remains unknown is whether these moraines represent readvance of much smaller ice masses that existed in sheltered cirques and were able to survive the peak HMT, or if they represent a glacier maximum of newly reformed glaciers after complete disappearance. Investigations into the downstream sediment archive constrained within the stream bank mires outside of the Neoglacial moraines might help to clarify the presence or absence of glaciers within the catchment throughout the HMT. This would prove an interesting comparison against the work of Bakke et al. (2010), enabling us to assess whether mountain glaciers in the maritime Arctic Norway were able to respond similarly to those continental mountain glaciers, south of the Arctic Circle. Furthermore, gaining insight into minor glacier fluctuations (e.g. such as those recorded in the pro-glacial sediment archive) would help us to understand whether we can identify past climate thresholds for complete deglaciation. If we can identify at what parameters glaciers disappeared in the past, it will better inform our predictions of glacial survival in a warming climate and when such thresholds might be crossed in the future.

7.6.3. Calibration of numerical models

Modelling of the mountain glaciers and ice caps in northern Norway has yet to be systematically undertaken. As such it is unclear how glaciers over the whole region responded to the short-term climatic fluctuations of the Holocene, how they will respond to future warming, and if/when northern Norway will be completely deglaciated. This thesis (particularly chapters 4-6) provides rigorous reconstructions of mountain glaciers and ice caps since the termination of the YD, throughout the Holocene, and including the LIA, alongside a large dataset of mapped moraines and other glacial landforms. These extensive datasets provide the means to compare and calibrate glacier and ice sheet models. Combining the dataset from this thesis, alongside further mapping and dating across northern Norway and further afield (e.g. Sweden and Finland), will improve our understanding of Holocene glacier and climate change across northern Scandinavia. Similar research has proven successful in glacier and ice sheet reconstructions in southern Norway (e.g. Åkesson *et al.*, 2017, 2018, 2020), but has yet to been undertaken for ice caps and mountain glaciers across northern Norway.

7.6.4. Developing constraints on ice thickness

The glacial reconstruction in Chapter 4 provides useful information on glacial extent during the past ~200 years yet lack sufficient data to reliably reconstruct and/or estimate ice thickness. Improved ice thickness estimates are a necessity for detailed, accurate, and reliable glaciological and hydrological investigations (e.g. Koerner, 1977; Dowdeswell and Evans, 2004; Andreassen *et al.*, 2015; Farinotti *et al.*, 2017). Measured constraints of present-day mountain glacier ice thickness would allow better assessment of future glacier changes making a useful addition to our understanding on the state of present-day glaciation (cf. Andreassen *et al.*, 2015). Data on present-day ice thicknesses of the small mountain and cirque glaciers would provide substantial improvements to our understanding of ice content, likely contribution to local hydrological regimes, and help refine their preservation potential under the warming climate of the mid- to late-21st century. Currently, no ice thickness data exist for any mountain glaciers throughout the Troms and Finnmark region. Only on the Langfjordjøkelen ice cap have direct measurements of ice thickness been undertaken (Andreassen *et al.*, 2012b).

7.6.5. Investigating the glacier to rock glacier transition

Glacial and periglacial mapping (Chapter 5) has revealed several valley glacier systems that exhibit well developed valley floor rock glaciers and heavily rock glacierized moraines immediately in front of, or adjoining, present-day glacier margins. These features likely represent a key element of a transitioning glacial system under a warming climate, where glaciers exist in areas of high debris input. Rock glacierisation may also serve to protect glaciers from climate warming and prolong their future preservation. Further research into the glacier to rock glacier transition in (northern) Norway is needed before any substantial inferences and/or conclusions can be made on this subject.

7.6.6. Developing landsystem interpretations

Initial work investigating glacial geomorphology in the central Troms and Finnmark region identified several landsystems that likely existed periodically during the Holocene. This research was predominantly based on remotely sensed observations

and lacks widespread field surveying or subsurface (e.g. sedimentological) investigations. Additional field work on sediment-landform associations would help to expand our existing templates for mountain-centred glacial landsystems and thereby improve our understanding of former glacial dynamics across the region. This would be best focused at those sites which display multiple present-day landsystems, which can be used to evidence landsystem transitions, and/or need field data to corroborate remotely sensed observations, especially at sites where the geomorphological signature is faintest (e.g. at plateau glacier landsystems).

7.6.7. Reassessing soil chronosequences for relative and calibrated age dating of Norwegian Holocene deposits

As outlined in Section 7.4.3 and demonstrated in Chapter 6, soil chronosequences hold potential for use in both relative and calibrated age dating of Holocene deposits and could play a crucial role at sites where other techniques are not possible (e.g. moraines that lack surface boulders for Schmidt hammer or cosmogenic nuclide dating or sites with periglacial reworking of surface boulders). Additional research into the applicability of soil profiles would require further soil data to be collected from a greater number of soil pits from each feature investigated. A greater number of samples would better enable the identification of outliers and provide a more comprehensive understanding of soil development across a feature. Additional testing of soil samples from northern Norway using more advanced techniques, such as examining clay formation using X-ray diffraction and chemical analyses (Righi *et al.*, 1999) or assessing crystallinity ratio of free iron oxides (Longhi *et al.*, 2020) may also provide a means for more reliable geochronological assessments. Furthermore, combining the available soil data from this thesis with TCND (currently being processes) would enable the creation of a calibrated soil dating framework, using site-specific absolute ages controls. Ultimately, any subsequent investigation into Holocene, soils in the Arctic which provides greater utility in terms of a wider spectrum of soil characters will improve the application of the soil chronosequence technique to glacial reconstructions.

CHAPTER 8

Conclusions

Lenangsbreen (glacier ID 201) reflected in Aspevatnet at sunset.

Photograph date: 09th September 2019 (by J.R. Leigh)

“It's over now and I'm a little bit petrified
Of what's to come, yeah my head's a bit stir-fried”
(Reynolds, 2017)

8.1. Conclusions

This thesis set out with two overarching aims (Section 1.2): (1) to put the reconstructed centennial-millennial scale changes in glacier extent into a present-day context; and (2) to reconstruct glacial changes of the central Troms and Finnmark region of Arctic Norway, with a particular emphasis on the Holocene glacial chronology following the recession of the SIS.

Using new data and established evidence, this thesis builds a coherent picture of the extent, style, and rates of shrinkage of mountain glaciers in an Arctic setting across timescales of 10s to 1,000s of years. Using high-resolution aerial orthophotographs (<1 m) and medium resolution satellite imagery (30-15 m) it has been possible to reassess methods for identifying and mapping very small glaciers (Chapter 3) and subsequently undertake more detailed assessments of 20th-21st century glacier change throughout the central Troms and Finnmark region (Chapter 4). This has enabled the first assessments of glacier change within the mountain regions between the Lyngen and Bergsfjord Peninsulas (e.g. the Kåfjord Alps) with the timing of major moraine forming events having been linked to key climatic oscillations in northern Norway. Additionally, new glacial chronologies from the YD to the LIA, were established in the Rotsund Valley (Chapters 4 and 6) and detailed regional scale geomorphological mapping (Chapter 5) complement the prior research that is sporadically spaced throughout the region. The objectives outlined in Chapter 1 are now briefly evaluated to provide a conclusion to this thesis.

8.1.1. Evaluation of 'Objective 1': Assess the number and extent of present-day glaciers and their response to rapid anthropogenically forced climate change

Remote sensing using satellite imagery (30-15 m resolution) and aerial orthophotographs (0.25 m resolution) enabled the identification and mapping of 219 glaciers (Chapter 4). Of these 219 glaciers, 78 were additional to the 2012 Inventory of Norwegian Glaciers (Table 4.3; Chapter 4) and this was a direct result of detailed analysis of aerial orthophotographs and evaluations of methods for identification of very small glaciers (Chapter 3). Tracking these 219 glaciers at five-year time-steps from 1989 to 2018 has revealed a 35.4 km^2 (35%) reduction in glacial area within the central Troms and Finnmark region. Glaciers were shown to fragment as they shrink,

resulting in 252 glacier units being mapped on the 2018 imagery. Additionally, over the 29-year period of satellite observation, 36 individual glaciers shrunk below the 0.01 km^2 minimum size-threshold (selected for accurate mapping on satellite imagery, see Chapter 3) and are thus, no-longer recorded in our glacier change assessments. Finally, it was also predicted that under future warming scenarios, and based on prior rates of glacier shrinkage in the region (e.g. 71% of all mapped glaciers having lost more than 50% of their area over the period 1989-2018), many of the glaciers across central Troms and Finnmark County will disappear altogether within the next 50-100 years.

8.1.2. Evaluation of 'Objective 2': compile a detailed map of the glacial and periglacial geomorphology throughout the central Toms and Finnmark region

A new glacial and periglacial geomorphological map, presented at a 1:115,000 scale, covering central Troms and Finnmark County has been produced using GIS software (Chapter 5). Around 23,500 glacial features and 1,200 periglacial features have been mapped, and of particular interest are the extensive moraine systems that are depicted throughout the region. In total, 14,798 individual moraine crests were mapped with large terminal and recessional moraine complexes mainly located at the heads of and within mountain valleys. It is postulated that the valley moraines record glacier re-advance during the YD, and several subsequent episodes of substantial glacial (re)advance throughout the Holocene. The resulting map and GIS shapefiles are available for detailed analysis of individual areas and/or geomorphological units

8.1.3. Evaluation of 'Objective 3': Identify the presence and age of Little Ice Age moraines fronting a series of small valley glaciers in an area of central Troms and Finnmark County that has not previously been investigated

Large, unvegetated and sharp crested moraines within the previously un-investigated Rotsund Valley, formed <400 m down valley from the 2018 glacier margins and bordering a pronounced vegetation trimline, were dated using a regionally controlled lichenometric dating framework. The resulting ages of these moraines ranged from 1814 to 1877, indicating an early- to mid-19th century LIA maximum (Table 4.2; Chapter 4). These moraines are, therefore, considered to represent the maximum

extent of LIA glacier readvance within the Rotsund Valley and this mountain chain (the Kåfjord Alps) more generally. The 19th century LIA maximum is earlier than that of an early-20th century maximum proposed on the nearby Lyngen Peninsula (Ballantyne, 1990), and later than that of central and southern Norway, where a mid-18th century maximum is reported by regional dating studies and historical documentation (Grove, 2004b; Nesje *et al.*, 2008). However, it matches that of the near ubiquitous mid-19th century (1850) LIA maximum as shown for the European Alps (Grove, 2004b; Ivy-Ochs *et al.*, 2009).

8.1.4. Evaluation of 'Objective 4': Extend the established chronology to determine the ages for the full suite of moraines beyond the Little Ice Age maximum moraines, using a combination of dating techniques

Within the numerous valley systems of Troms and Finnmark County, there exists an extensive sequence of well-defined moraines beyond the LIA limits (as identified in Chapters 4-6). Using detailed mapping and various geochronological techniques it has been possible to date a full sequence of moraines in the Rotsund Valley (see Chapter 6). Calibrated Schmidt hammer dating indicates that, following deglaciation of the main ice sheet across the region, mountain glaciers in the Rotsund Valley attained their maximum extent between approximately 12,000 (11,120-13,174) and 10,600 (9,587-11,601) cal. yrs BP before undergoing recession, with several moraine building events interrupting net retreat. For the first time in this region of northern Norway, moraines have been directly attributed to key Holocene climatic events, including a readvance/stillstand during the Erdalen Event (10,100 and 9,700 cal. yrs BP) and the 8.2 ka event (~8,200 cal. yrs BP). The Neoglacial maximum appears to have occurred around 4,700 (4,108-5,287) cal. yrs BP and was more extensive than that of the LIA. It is, however, not clear whether this Neoglacial episode represents glacial regrowth after complete HTM deglaciation, or the readvance of small glaciers that survived the HTM. Furthermore, using the new glacial chronology and regional geomorphological mapping (Chapters 5 and 6) it has been possible to produce an updated ice margin chronology for the SIS and mountain glaciers from 14,000 cal. yrs BP to the present-day (see Figure 6.15). It is concluded that ice sheet margins were likely more extensive and dynamic than previously depicted with large areas of upland plateau and mountain topography likely covered by icefields following regional deglaciation.

REFERENCES

Aa, A. R. and Sønstegaard, E. (2019) Early-Holocene glacier fluctuations of northern Grovabreen, western Norway. *The Holocene*, **29**(2), 187–196.

Aall, C. and Hoyer, K. G. (2005) Tourism and climate change adaptation: The Norwegian case. In Higham, J. E. S. and Hall, C. M. (eds) Tourism, Recreation, and Climate Change. Bristol: Channel View Publications, 209–223.

Abbot, D. S., Walker, C. C. and Tziperman, E. (2009) Can a convective cloud feedback help to eliminate winter sea ice at high CO2 concentrations? *Journal of Climate*, **22**(21), 5719–5731

Aitkenhead, N. (1960) Observations on the drainage of a glacier-dammed lake in Norway, *Journal of Glaciology*, **3**(27), 607–609.

Åkesson, H., Nisancioglu, K. H., Giesen, R. H. and Morlighem M. (2017) Simulating the evolution of Hardangerjøkulen ice cap in southern Norway since the mid-Holocene and its sensitivity to climate change. *The Cryosphere*, **11**(1), 281–302.

Åkesson, H. Gyllencreutz, R., Mangerud, J., Svendsen, J. I., Nick, F. M. and Nisancioglu, K. H. (2020) Rapid retreat of a Scandinavian marine outlet glacier in response to warming at the last glacial termination. *Quaternary Science Reviews*, **250**, 1–17.

Åkesson, H., Nisancioglu, K. H. and Nick, F. M. (2018) Impact of fjord geometry on grounding line stability. *Frontiers in Earth Science*, **6**, 1–16.

Alexanderson, H., Adrielsson, L., Hjort, C. Möller, P., Antonov, O., Eriksson, S. and Pavlov M. (2002) Depositional history of the North Taymyr ice-marginal zone, Siberia - A landsystem approach. *Journal of Quaternary Science*, **17**(4), 361–382.

Allen, M. R. et al. (2018) Framing and Context, Global Warming of 1.5°C. An IPCC Special Report on the impacts of global warming of 1.5°C above pre-industrial levels and related global greenhouse gas emission pathways, in the context of strengthening the global response to the threat of climate change. In Masson-Delmotte. V. et al. (eds) Sustainable Development, and Efforts to Eradicate Poverty. Geneva, IPCC, 41–91.

Alley, R. B., Alley, R. B., Finkel, R. C., Nishiizumi, K., Anandakrishnan, S., Shuman, C. A., Mershon, G., Zielinski, G. A. and Mayewski, P. A. (1993) Changes in continental and sea-salt atmospheric loadings in central Greenland during the most recent deglaciation: model-based estimates. *Journal of Glaciology*, **41**(139), 503–514.

Alley, R. B., Alley, R. B., Mayewski, P. A., Sowers, T., Stuiver, M., Taylor, K. C. and Clark, P. U. (1997) Holocene climatic instability: A prominent, widespread event 8200 yr ago. *Geology*, **25**(6), 483–486.

Alley, R. B. and Ágústsdóttir, A. M. (2005) The 8k event: Cause and consequences of a major Holocene abrupt climate change. *Quaternary Science Reviews*, **24**(10–11), 1123–1149.

Alm, T. (1993) Ovre Erisvatn - palynostratigraphy of a 22,000 to 10,000 BP lacustrine record on Andmya, northern Norway. *Boreas*, **22**, 171–188.

AMAP (2012) Arctic climate issues 2011: Changes in Arctic snow, water, ice and permafrost. Oslo, Arctic Monitoring and Assessment Programme, 1–97

AMAP (2017) Snow, Water, Ice and Permafrost in the Arctic (SWIPA) 2017. Oslo, Arctic Monitoring and Assessment Programme, 1–269

Andersen, B. G. (1965) Glacial Chronology of Western Troms, North Norway. *Geological Society of America Special Papers*, **84**, 35–54.

Andersen, B. G. (1968) Glacial Geology of Western Troms, North Norway. *Norges Geologiske Undersøkelse*, **256**, 1–160.

Andersen, B. G. (1980) The deglaciation of Norway after 10,000 B.P. *Boreas*, **9**(4), 211–216.

Andersen, B. G., Mangerund, J., Sørensen, R., Reite, A. and Sveian, H.(1995a) Younger Dryas Ice-Marginal Deposits in Norway. *Quaternary International*, **28**, 147–169.

Andersen, B. G., Lundqvist, J. and Saarnisto, M. (1995b) The Younger Dryas margin of the Scandinavian Ice Sheet - An introduction. *Quaternary International*, 28, 145–146.

Andersen, J. L. and Sollid, J. L. (1971) Glacial Chronology and Glacial Geomorphology in the Marginal Zones of the Glaciers, Midtdalsbreen and Nigardsbreen, South Norway. *Norsk Geografisk Tidsskrift - Norwegian Journal of Geography*, **25**(1), 1–38.

Andersson, G. (1998) Genesis of hummocky moraine in the Bolmen area, southwestern Sweden. *Boreas*, **27**(1), 55–67.

Andreassen, L. M., Kjøllmoen, B., Kundsen, N. T., Whalley, W. B. and Fjellanger J. (2000) Regional change of glaciers in northern Norway. Oslo, Norwegian Water Resources and Energy Directorate (NVE), 1–122

Andreassen, L. M. Andreassen, L. M., Elvehøy, H., Kjøllmoen, B., Engeset, R. V. and Haakensen, N. (2005) Glacier mass-balance and length variation in Norway. *Annals of Glaciology*, **42**, 317–325.

Andreassen, L. M. Paul, F., Kääb, A. and Hausberg, J.E. (2008) Landsat-derived glacier inventory for Jotunheimen, Norway, and deduced glacier changes since the 1930s. *The Cryosphere*, **2**(2), 131–145.

Andreassen, L. M., Winsvold, S. H., Paul, F. and Hausberg, J. E. (2012a) Inventory of Norwegian glaciers. Edited by Andreassen L. M. and Winsvold S. H. Oslo: Norwegian Water Resources and Energy Directorate (NVE), 1-236

Andreassen, L. M., Nordli, Ø., Rasmussen, A. and Melvold, K. (2012b) Langfjordjøkelen, a rapidly shrinking glacier in northern Norway. *Journal of Glaciology*, **58**(209), 581–593.

Andreassen, L. M., Huss, M., Melvold, K., Elvehøy, H. and Winsvold, S. H. (2015) Ice thickness measurements and volume estimates for glaciers in Norway. *Journal of Glaciology*, **61**(228), 763–775.

Andreassen, L. M., Elvehøy, H., Kjøllmoen, B. and Belart, J. M. (2020) Glacier change in Norway since the 1960s - An overview of mass balance, area, length and surface elevation changes. *Journal of Glaciology*, **66**(256), 313–328.

Andreassen, L. M., Elvehøy, H. and Kjøllmoen, B. (2002) Using aerial photography to study glacier changes in Norway. *Annals of Glaciology*, **34**, 343–348.

Andrews, J. T. and Ives, J. D. (1978) "Cockburn" Nomenclature and the Late Quaternary History of the Eastern Canadian Arctic. *Arctic and Alpine Research*, **10**(3), 617–633.

Anjar, J., Akçar, N., Lakeman, T., Larsen, E. A. and Seiler, M. (2020) ^{10}Be surface exposure dating of the deglaciation of northernmost Norway and Finland. *Boreas*, **50**(2), 369–380

Antonsson, K. and Seppä, H. (2007) Holocene temperatures in Bohuslän, southwest Sweden: A quantitative reconstruction from fossil pollen data. *Boreas*, **36**(4), 400–410.

Arenson, L. U. and Jakob, M. (2015) Periglacial Geohazard Risks and Ground Temperature Increases. In Lollino, G. et al. (eds) Engineering Geology for Society and Territory. Volume 1. Basil: Springer, 233–237.

Armstrong, R. A. (2011) The biology of the crustose lichen Rhizocarpon geographicum. *Symbiosis*, **55**(2), 53–67.

Árnason, A. and Hafsteinsson, S. B. (2020) A funeral for a glacier: Mourning the more-than-human on the edges of modernity. *Thanatos*, **9**, 46–71.

Arrhenius, S. (1896) On the influence of carbonic acid in the air upon the temperature of the ground. *The London, Edinburgh, and Dublin Philosophical Magazine and Journal of Science*, **41**(251), 237–276.

Attig, J. W. and Clayton, L. (1993) Stratigraphy and origin of an area of hummocky glacial topography, northern Wisconsin, U.S.A. *Quaternary International*, **18**, 61–67.

Augland, L. E., Andresen, A., Gasser, D. and Steltenpohl, M.G. (2014) Early Ordovician to Silurian evolution of exotic terranes in the Scandinavian Caledonides of the Ofoten–Troms area – terrane characterization and correlation based on new U–Pb zircon ages and Lu–Hf isotopic data. *Geological Society, London, Special Publications*, **390**(1), 655–678.

Augustinus, P., Bleakley, N., Deng, Y., Shane, P. and Cochran, U. (2008) Rapid change in early Holocene environments inferred from Lake Pupuke, Auckland City, New Zealand. *Journal of Quaternary Science*, **23**(5), 435–447.

Azócar, G. F. and Brenning, A. (2010) Hydrological and geomorphological significance of rock glaciers in the dry Andes, Chile (27°-33°s). *Permafrost and Periglacial Processes*, **21**(1), 42–53.

Bahr, D. B., Pfeffer, W. T., Sassolas, C. and Meier, M. F. (1998) Response time of glaciers as a function of size and mass balance: 1. Theory. *Jurnal of Geophysical Research: Solid Earth*, **103**(B5), 9777–9782.

Bajracharya, S. R. Maharjan, S. B., Shrestha, F. and Shrestha, B. (2011) Chapter 3: Data Collection and Glacier Mapping Methodology. In Bajracharya, S. R. and Shrestha, B. R. (eds) The Status of Glaciers in the Hindu Kush-Himalayan Region. Kathmandu: International Centre for Integrated Mountain Development, 7–13.

Bakke, J., Bakke, J., Dahl, S. O., Paasche, Ø., Løvlie, R. and Nesje, A. (2005a) Glacier fluctuations, equilibrium-line altitudes and palaeoclimate in Lyngen, northern Norway, during the Lateglacial and Holocene. *The Holocene*, **15**(4), 518–540.

Bakke, J., Lie, Ø., Nesje, A., Dahl, S. O. and Paasche, Ø. (2005b) Utilizing physical sediment variability in glacier-fed lakes for continuous glacier reconstructions during the Holocene, northern Folgefonna, western Norway. *The Holocene*, **15**(2), 161–176.

Bakke, J., Dahl, S. O., Paasche, Ø., Simonsen, J. R., Kvisvik, B., Bakke, K. and Nesje, A. (2010) A complete record of Holocene glacier variability at Austre Okstindbreen, northern Norway: an integrated approach. *Quaternary Science Reviews*, **29**(9–10), 1246–1262.

Bakke, J., Dahl, S. O. and Nesje, A. (2005c) Lateglacial and early Holocene palaeoclimatic reconstruction based on glacier fluctuations and equilibrium-line altitudes at northern Folgefonna, Hardanger, western Norway. *Journal of Quaternary Science*, **20**(2), 179–198.

Balascio, N. L. and Bradley, R. S. (2012) Evaluating Holocene climate change in northern Norway using sediment records from two contrasting lake systems. *Journal of Paleolimnology*, **48**(1), 259–273.

Balascio, N. L., D'Andrea, W. J. and Bradley, R. S. (2015) Glacier response to North Atlantic climate variability during the Holocene. *Climate of the Past*, **11**(12), 1587–1598.

Ballantyne, C. K. (1986) Protalus rampart development and the limits of former glaciers in the vicinity of Baosbheinn, Wester Ross. *Scottish Journal of Geology*, **22**(1), 13–25.

Ballantyne, C. K. (1987) Some Observations on the Morphology and Sedimentology of Two Active Protalus Ramparts, Lyngen, Northern Norway. *Arctic and Alpine Research*, **19**(2), 167–174.

Ballantyne, C. K. (1990) The Holocene glacial history of Lyngshalvoya, northern Norway: Chronology and climatic implications. *Boreas*, **19**, 93–117.

Ballantyne, C. K. (2000) Paraglacial adjustment of rock slopes: causes and consequences. *Indian Journal of Geography and Environment*, **5**, 1–22.

Ballantyne, C. K. (2002) Paraglacial Geomorphology. *Quaternary Science Reviews*, **21**, 1935–2017.

Ballantyne, C. K. (2003) Chapter 17: Paraglacial Landsystems. In Evans, D. J. A. (ed.) Glacial Landsystems. London: Arnold, 432–460.

Ballantyne, C. K. (2008) After the ice: Holocene geomorphic activity in the Scottish Highlands. *Scottish Geographical Journal*, **124**(1), 8–52.

Ballantyne, C. K. (2013) Trimlines and Palaeonunataks. In Elias, S. A. (ed.) Encyclopedia of Quaternary Science, Second Edition. Amsterdam: Elsevier, 918–928.

Ballantyne, C. K. (2018) Periglacial Geomorphology. New Jersey: John Wiley & Sons Ltd.

Ballantyne, C. K. and Benn, D. I. (1994) Glaciological constraints on protalus rampart development. *Permafrost and Periglacial Processes*, **5**(3), 145–153.

Ballantyne, C. K. and Harris, C. (1994) The Periglaciation of Great Britain. Cambridge: Cambridge University Press.

Ballantyne, C. K. and Kirkbride, M. P. (1986) The characteristics and significance of some lateglacial protalus ramparts in upland Britain. *Earth Surface Processes and Landforms*, **11**(6), 659–671.

Ballantyne, C. K. and Stone, J. O. (2013) Timing and periodicity of paraglacial rock-slope failures in the Scottish Highlands. *Geomorphology*, **186**, 150–161.

Barcaza, G., Nussbaumer, S. U., Tapia, G., Valdés, J., García, J. L., Videla, Y., Albornoz, A. and Arias, V. (2017) Glacier inventory and recent glacier variations in the Andes of Chile, South America. *Annals of Glaciology*, **58**(75pt2), 1–15.

Barnekow, L. (1999) Holocene tree-line dynamics and inferred climatic changes in the Abisko area, northern Sweden, based on macrofossil and pollen records. *The Holocene*, **9**(3), 253–265.

Barnett, T. P., Adam, J. C. and Lettenmaier, D. P. (2005) Potential impacts of a warming climate on water availability in snow-dominated regions. *Nature*, **438**(7066), 303–309.

Barr, I. D. and Lovell, H. (2014) A review of topographic controls on moraine distribution. *Geomorphology*, **226**, 44–64.

Barry, R. G. (2006) The status of research on glaciers and global glacier recession: A review. *Progress in Physical Geography*, **30**(3), 285–306.

Barsch, D. (1996) Rockglaciers: indicators for the present and former geoecology in high mountain environments. Berlin: Springer.

Baumann, S. C. (2009) Mapping, analysis, and interpretation of the glacier inventory data from Jotunheimen, south Norway, since the maximum of the 'Little Ice Age. Unpublished PhD thesis. The Julius Maximilian University of Würzburg.

Baumann, S., Winkler, S. and Andreassen, L. M. (2009) Mapping glaciers in Jotunheimen, South-Norway, during the "Little Ice Age" maximum. *The Cryosphere*, **3**, 231–243.

Te Beest, M., Sitters, J., Ménard, C. B. and Olofsson, J. (2016) Reindeer grazing increases summer albedo by reducing shrub abundance in Arctic tundra. *Environmental Research Letters*, **11**(12), 1–13.

Bellwald, W. (1992) Drei spätneolithisch/frühbronzezeitiche Pfeilbogen aus dem Gletschereis am Lötschenpass. *Archäologie Schweiz*, **15**, 166–171.

Bendle, J. M. and Glasser, N. F. (2012) Palaeoclimatic reconstruction from Lateglacial (Younger Dryas Chronozone) cirque glaciers in Snowdonia, North Wales. *Proceedings of the Geologists' Association*, **123**(1), 130–145.

Benedict, J. B. (1990) Experiments on lichen growth. I. Seasonal patterns and environmental controls. *Arctic & Alpine Research*, **22**(3), 244–254.

Benedict, J. B. (2008) Experiments on lichen growth, III. The shape of the age-size curve. *Arctic, Antarctic, and Alpine Research*, **40**(1), 15–26.

Bengtsson, L., Semenov, V. A. and Johannessen, O. M. (2004) The early twentieth-century warming in the arctic - A possible mechanism. *Journal of Climate*, **17**(20), 4045–4057.

Benn, D. I. (1989) Debris transport by Loch Lomond readvance glaciers in Northern Scotland: Basin form and the within-valley asymmetry of lateral moraines. *Journal of Quaternary Science*, **4**(3), 243–254.

Benn, D. I. (1992) The genesis and significance of "hummocky moraine": Evidence from the Isle of Skye, Scotland. *Quaternary Science Reviews*, **11**(7–8), 781–799.

Benn, D. I. (1994) Fluted moraine formation and till genesis below a temperate valley glacier: Slettmarkbreen, Jotunheimen, southern Norway. *Sedimentology*, **41**, 279–292.

Benn, D. I. Benn, D. I., Kirkbride, M. P., Owen, L. A. and Brazier, V. (2003) Chapter 15: Glaciated Valley Landsystems. In Evans, D. J. A. (ed.) Glacial Landsystems. London: Arnold, 372–405.

Benn, D. I. and Evans, D. J. A. (2010) Glaciers and Glaciation, Second Edition. Oxford: Routledge.

Benn, D. I. and Lukas, S. (2006) Younger Dryas glacial landsystems in North West Scotland: an assessment of modern analogues and palaeoclimatic implications. *Quaternary Science Reviews*, **25**(17–18), 2390–2408.

Bennett, G. L., Bennett, G. L., Evans, D. J. A, Carbonneau, P. and Twigg, D. R (2010) Evolution of a debris-charged glacier landsystem, kvíárjökull, Iceland. *Journal of Maps*, **6**, 40–67.

Bennett, M. R. and Boulton, G. S. (1993) A reinterpretation of Scottish "hummocky moraine" and its significance for the deglaciation of the Scottish Highlands during the Younger Dryas or Loch Lomond Stadial. *Geological Magazine*, **130**(3), 301–318.

Bennett, M. R., Huddart, D. and Glasser, N. F. (1999) Large-scale Bedrock Displacement by Cirque Glaciers. *Arctic, Antarctic, and Alpine Research*, **31**(1), 99–107.

Bennett, M. R., Huddart, D. and Mccormick, T. (2000a) An integrated approach to the study of glaciolacustrine landforms and sediments: A case study from Hagavatn, Iceland. *Quaternary Science Reviews*, **19**(7), 633–665.

Bennett, M. R., Huddart, D. and McCormick, T. (2000b) The glaciolacustrine landform-sediment assemblage at Heinabergsjokull, Iceland. *Geografiska Annaler, Series A: Physical Geography*, **82**(1), 1–16.

Bentley, M. J., Evans, D. J. A., Fogwill, C. J., Hansom, J. D., Sugden, D. E. and Kubik, P. W. (2007) Glacial geomorphology and chronology of deglaciation, South Georgia, sub-Antarctic. *Quaternary Science Reviews*, **26**(5–6), 644–677.

Berghuijs, W. R., Woods, R. A. and Hrachowitz, M. (2014) A precipitation shift from snow towards rain leads to a decrease in streamflow. *Nature Climate Change*, **4**(7), 583–586.

Bergstrom, B. and Neeb, P. R. (1978) Reisadalen. Kvartaergeologisk kart 1734 III - Map. 1:50,000. Trondheim: Norges Geologiske Undersøkelse.

Berthling, I. (2011) Beyond confusion: Rock glaciers as cryo-conditioned landforms. *Geomorphology*, **131**(3–4), 98–106.

Berthling, I., Eiken, T. and Sollid, J. L. (2001) Frost heave and thaw consolidation of ploughing boulders in a Mid-Alpine environment, Finse, Southern Norway. *Permafrost and Periglacial Processes*, **12**(2), 165–177.

Beschel, R. E. (1950) Flechten als Altersmasstab rezenter Moranen. *Zeitschrift fur Gletscherkunde und Glazialgeologie*, **1**(2), 152–161.

Beschel, R. E. (1961) Dating rock surfaces by lichen growth and its application to glaciology and physiography (lichenometry). In Raasch, G. O. (ed.) Geology of the Arctic. Toronto: University of Toronto Press, 1044–1062.

Bhambri, R., Bolch, T. and Chaujar, R. K. (2011) Mapping of debris-covered glaciers in the Garhwal Himalayas using ASTER DEMs and thermal data. *International Journal of Remote Sensing*, **32**(23), 8095–8119.

Bhardwaj, A., Joshi, P. K., Singh, M. K., Sam, L. and Gupta, R. D. (2014) Mapping debris-covered glaciers and identifying factors affecting the accuracy. *Cold Regions Science and Technology*, **106**, 161–174.

Bickerdike, H. L. (2016) The Glacial Geomorphology of the Loch Lomond (Younger Dryas) Stadial in Britain. Unpublished PhD thesis. Durham University, Department of Geography.

Bickerdike, H. L., Evans, D. J. A., Ó Cofaigh, C. and Stokes, C. R., (2016) The glacial geomorphology of the Loch Lomond Stadial in Britain: a map and geographic information system resource of published evidence. *Journal of Maps*, **12**(5), 1178–1186.

Bickerdike, H. L., Ó Cofaigh, C., Evans, D. J. A. and Stokes, C. R. (2018a) Glacial landsystems, retreat dynamics and controls on Loch Lomond Stadial (Younger Dryas) glaciation in Britain. *Boreas*, **47**(1), 202–224.

Bickerdike, H. L., Evans, D. J. A., Stokes, C. R. and Ó Cofaigh, C. (2018b) The glacial geomorphology of the Loch Lomond (Younger Dryas) Stadial in Britain: a review. *Journal of Quaternary Science*, **33**(1), 1–54.

Bickerton, R. W. and Matthews, J. A. (1992) On the accuracy of lichenometric dates: an assessment based on the “Little Ice Age’’ moraine sequence of Nigardsbreen, southern Norway. *The Holocene*, **2**(3), 227–237.

Bickerton, R. W. and Matthews, J. A. (1993) “Little ice age” variations of outlet glaciers from the jostedalsbreen ice-cap, Southern Norway: A regional lichenometric-dating study of ice-marginal moraine sequences and their climatic significance. *Journal of Quaternary Science*, **8**(1), 45–66.

Birkeland, P. W. (1978) Soil development as an indication of relative age of Quaternary deposits, Baffin Island, N.W.T., Canada. *Arctic and Alpine Research*, **10**(4), 733–747.

Birkeland, P. W. (1999) Soils and Geomorphology, Third Edition. Oxford: Oxford University Press.

Birks, H. H. (1994) Late-glacial vegetational ecotones and climatic patterns in Western Norway. *Vegetation History and Archaeobotany*, **3**(2), 107–119.

Birks, H. H., Kristensen, D. K., Dokken, T. M. and Andersson, C. (2005) Exploratory Comparisons of Quantitative Temperature Estimates Over the Last Deglaciation in Norway and the Norwegian Sea. *Geophysical Monograph-American Geophysical Union*, **158**, 341–355.

Birks, H. H. (2015) South to north: Contrasting late-glacial and early-Holocene climate changes and vegetation responses between south and north Norway. *The Holocene*, **25**(1), 37–52.

Birks, H. J. B. and Birks, H. H. (2008) Biological responses to rapid climate change at the Younger Dryas-Holocene transition at Kråkenes, western Norway. *Holocene*, **18**(1), 19–30.

Bjune, A., Birks, H. J. B. and Seppä, H. (2004) Holocene vegetation and climate history on a continental-oceanic transect in northern Fennoscandia based on pollen and plant macrofossils. *Boreas*, **33**(3), 211–223.

Bjune, A. E., Bakke, J., Nesje, A. and Birks, H. J. B (2005) Holocene mean July temperature and winter precipitation in western Norvay inferred from palynological and glaciological lake-sediment proxies. *The Holocene*, **15**(2), 177–189.

Blagborough, J. W. and Breed, W. J. (1967) Protalus ramparts on Navajo Mountain, Utah. *American Journal of Science*, **265**, 759–753.

Blake, K. P. and Olsen, L. (1999) Deglaciation of the Svartisen area, northern Norway, and isolation of a large ice mass in front of the Fennoscandian Ice Sheet. *Norsk Geografisk Tidsskrift - Norwegian Journal of Geography*, **53**(1), 1–16.

Blaschek, M. and Renssen, H. (2013) The Holocene thermal maximum in the Nordic Seas: the impact of Greenland Ice Sheet melt and other forcings in a coupled atmosphere–sea-ice–ocean model. *Climate of the Past*, 9(4), 1629–1643.

Blikra, L. H. and Christiansen, H. H. (2014) A field-based model of permafrost-controlled rockslide deformation in northern Norway. *Geomorphology*, **208**, 34–49.

Bliss, A., Hock, R. and Cogley, J. G. (2013) A new inventory of mountain glaciers and ice caps for the Antarctic periphery. *Annals of Glaciology*, **54**(63), 191–199.

Le Blond, A. (1908) Mountaineering in the Land of the Mindnight Sun. London: Fischer Unwin.

Boch, R., Spötl, C. and Kramers, J. (2009) High-resolution isotope records of early Holocene rapid climate change from two coeval stalagmites of Katerloch Cave, Austria. *Quaternary Science Reviews*, **28**(23–24), 2527–2538.

Bockheim, J. G. (1979a) Properties and relative age of soils of southwestern Cumberland Peninsula, Baffin Island, Northwest Territories, Canada. *Arctic and Alpine Research*, **11**(3), 289–306.

Bockheim, J. G. (1979b) Relative age and origin of soils in eastern Wright Valley, Antarctica. *Soil Science*, **128**(3), 142–152.

Bockheim, J. G. (2014) Distribution, properties and origin of viscous-flow features in the McMurdo Dry Valleys, Antarctica. *Geomorphology*, **204**, 114–122.

Boelhouwers, J., Holness, S. and Sumner, P. (2003) The maritime Subantarctic: A distinct periglacial environment. *Geomorphology*, **52**(1–2), 39–55.

Böhme, M., Oppikofer, T., Longva, O., Jaboyedoff, M., Hermanns, R. L. and Derron, M. H. (2015) Analyses of past and present rock slope instabilities in a fjord valley: Implications for hazard estimations. *Geomorphology*, **248**, 464–474.

Böhme, M., Hermanns, R. L. and Lauknes, T. R. (2020) Landscape Formation and Large Rock Slope Instabilities in Manndalen, Northern Norway. In Arbanas, Ž. Bobrowsky P.T., Konagai K., Sassa K., Takara K. (eds) Understanding and Reducing Landslide Disaster Risk. Cham: Springer, 325–330.

Bolch, T., Menounos, B. and Wheate, R. (2010) Landsat-based inventory of glaciers in western Canada, 1985-2005. *Remote Sensing of Environment*, **114**(1), 127–137.

Bonan, D. B., Christian, J. E. and Christianson, K. (2019) Influence of North Atlantic climate variability on glacier mass balance in Norway, Sweden and Svalbard. *Journal of Glaciology*, **65**(252), 580–594.

Bond, G., Showers, W., Cheseby, M., Lotti, R., Almasi, P., DeMenocal, P., Priore, P., Cullen, H., Hajdas, I. and Bonani, G. (1997) A pervasive millennial-scale cycle in North Atlantic Holocene and glacial climates. *Science*, **278**(5341), 1257–1266.

Bond, G., Kromer, B., Beer, J., Muscheler, R., Evans, M. N., Showers, W., Hoffmann, S., Lotti-Bond, R., Hajdas, I. and Bonani, G. (2001) Persistent solar influence on North Atlantic climate during the Holocene. *Science*, **294**(5549), 2130–2136.

Bond, G. C., Showers, W., Elliot, M., Evans, M., Lotti, R., Hajdas, I., Bonani, G. and Johnson, S. (1999) The North Atlantic's 1-2 kyr climate rhythm: Relation to Heinrich events, Dansgaard/Oeschger cycles and the Little Ice Age. *Geophysica*, **112**, 35–58.

Bondevik, S. and Mangerud, J. (2002) A calendar age estimate of a very late Younger Dryas ice sheet maximum in western Norway. *Quaternary Science Reviews*, **21**(14–15), 1661–1676.

Bosson, J. B. and Lambiel, C. (2016) Internal Structure and Current Evolution of Very Small Debris-Covered Glacier Systems Located in Alpine Permafrost Environments. *Frontiers in Earth Science*, **4**(39), 1–17.

Boston, C., Lovell, H., Weber, P. and Chandler, B. (2017) Formation of geometrical ridge networks at a non-surging temperate glacier, Østre Svartisen, Norway. *Geophysical Research Abstracts*, **19**, 17562.

Boston, C. M. and Lukas, S. (2019) Topographic controls on plateau icefield recession: insights from the Younger Dryas Monadhliath Icefield, Scotland. *Journal of Quaternary Science*, **34**(6), 433–451.

Boston, C. M., Lukas, S. and Carr, S. J. (2015) A Younger Dryas plateau icefield in the Monadhliath, Scotland, and implications for regional palaeoclimate. *Quaternary Science Reviews*, **108**, 139–162.

Boulton, G. S. (1976) The Origin of Glacially Fluted Surfaces-Observations and Theory. *Journal of Glaciology*, **17**(76), 287–309.

Boulton, G. S. (1978) Boulder shapes and grain-size distributions of debris as indicators of transport paths through a glacier and till genesis. *Sedimentology*, **25**, 773–799.

Boulton, G. S. (1986) Push-moraines and glacier-contact fans in marine and terrestrial environments. *Sedimentology*, **33**(5), 677–698.

Boulton, G. S., Dongelmans, P., Punkari, M. and Broadgate, M. (2001a) Palaeoglaciology of an ice sheet through a glacial cycle: the European ice sheet through the Weichselian. *Quaternary Science Reviews* **20**(4), 591–625.

Boulton, G. S., Dobbie, K. E. and Zatsepin, S. (2001b) Sediment deformation beneath glaciers and its coupling to the subglacial hydraulic system. *Quaternary International*, **86**(1), 3–28.

Boulton, G. S. and Eyles, N. (1979) Sedimentation by valley glaciers: a model and genetic classification. *Moraines and Varves*, **33**, 11–23.

Bourriquen, M., Mercier, D., Baltzer, A., Fournier, J., Costa, S. and Roussel, E. (2018) Paraglacial coasts responses to glacier retreat and associated shifts in river floodplains over decadal timescales (1966–2016), Kongsfjorden, Svalbard. *Land Degradation and Development*, **29**(11), 4173–4185.

Bowman, D., Eyles, C.H., Narro-Pérez, R. and Vargas, R. (2018) Sedimentology and Structure of the Lake Palcacocha Laterofrontal Moraine Complex in the Cordillera Blanca, Peru. *Revista de Glaciares y Ecosistemas de Montaña*, **5**, 27–42.

Box, J. E., Box, J. E., Colgan, W. T., Christensen, T. R., Schmidt, N. M., Lund, M., Parmentier, F. J. W., Brown, R., Bhatt, U. S., Euskirchen, E. S., Romanovsky, V. E. and Walsh, J. E. (2019) Key indicators of Arctic climate change: 1971-2017. *Environmental Research Letters*, **14**(4), 1–18

Bradwell, T. (2010) Studies on the growth of Rhizocarpon geographicum in NW Scotland, and some implications for lichenometry. *Geografiska Annaler, Series A: Physical Geography*, **92**(1), 41–52.

Bradwell, T., Stoker, M. and Krabbendam, M. (2008) Megagrooves and streamlined bedrock in NW Scotland: the role of ice streams in landscape evolution. *Geomorphology*, **97**(1–2), 135–156.

Braumann, S. M., Schaefer, J. M., Neuhuber, S. M., Reitner, J. M., Lüthgens, C. and Fiebig, M. (2020) Holocene glacier change in the Silvretta Massif (Austrian Alps) constrained by a new ^{10}Be chronology, historical records and modern observations. *Quaternary Science Reviews*, **245**, 1–21.

Brázdil, R., Pfister, C., Wanner, H., Von Storch, H. and Luterbacher, J. (2005) Historical climatology in Europe - The state of the art. *Climatic Change*, **70**(3), 363–430.

Brennand, T. A. (2000) Deglacial meltwater drainage and glaciodynamics: Inferences from Laurentide eskers, Canada. *Geomorphology*, **32**(3–4), 263–293.

Bridges, E. M. (1997) World Soils. Third edition. Cambridge: Cambridge University Press.

Briner, J. P., McKay, N. P., Axford, Y., Bennike, O., Bradley, R. S., de Vernal, A., Fisher, D., Francus, P., Fréchette, B., Gajewski, K. and Jennings, A. (2016) Holocene climate change in Arctic Canada and Greenland. *Quaternary Science Reviews*, **147**, 340–364.

Briner, J. P., Davis, P. T. and Miller, G. H. (2009) Latest Pleistocene and Holocene glaciation of Baffin Island, Arctic Canada: key patterns and chronologies. *Quaternary Science Reviews*, **28**(21–22), 2075–2087.

Briner, J. P., Håkansson, L. and Bennike, O. (2013) The deglaciation and neoglaciation of upernavik isstrøm, Greenland. *Quaternary Research*, **80**(3), 459–467.

Ten Brink, N. W. (1973) Lichen Growth Rates in West Greenland. *Arctic and Alpine Research*, **5**(4), 323–331.

Brodzikowski, K. and van Loon, A. J. (1987) A Systematic Classification of Glacial and Periglacial Environments, Facies and Deposits. *Earth-Science Reviews*, **24**, 297–381.

Brook, M. S., Kirkbride, M. P. and Brook, B. W. (2006) Cirque development in a steadily uplifting range: rates of erosion and long-term morphometric change in alpine cirques in the Ben Ohau Range, New Zealand. *Earth Surface Processes and Landforms*, **31**, 1167–1175.

Brown, J., Harper, J. and Humphrey, N. (2010a) Cirque glacier sensitivity to 21st century warming: Sperry Glacier, Rocky Mountains, USA. *Global and Planetary Change*, **74**(2), 91–98.

Brown, R., Derksen, C. and Wang, L. (2010b) A multi-data set analysis of variability and change in Arctic spring snow cover extent, 1967-2008. J*ournal of Geophysical Research: Atmospheres*, **115**(16), 1–16.

Brugger, K. A., Laabs, B., Reimers, A. and Bensen, N. (2019) Late Pleistocene glaciation in the Mosquito Range, Colorado, USA: Chronology and climate. *Journal of Quaternary Science*, **34**(3), 187–202.

Brugger, K. A., Evenson, E. B. and Stewart, R. A. (1983) Chronology and style of glaciation in the Wildhorse Canyon area: Idaho. *INQUA Symposia on the genesis and lithology of quaternary deposits*, 151–175.

Brynjólfsson, S., Schomacker, A., Ingólfsson, Ó. and Keiding, J. K. (2015) Cosmogenic ^{36}Cl exposure ages reveal a 9.3 ka BP glacier advance and the Late Weichselian-Early Holocene glacial history of the Drangajökull region, northwest Iceland. *Quaternary Science Reviews*, **126**, 140–157.

Brynjólfsson, S., Ingólfsson, Ó. and Schomacker, A. (2012) Surge fingerprinting of cirque glaciers at the Tröllaskagi. *Jökull*, **62**, 1–16.

Bull, W. B. (2018) Accurate surface exposure dating with lichens. *Quaternary Research*, **90**(1), 1–9.

Buntley, G. J. and Westin, F. C. (1965) A comparative study of developmental colour in a Chestnut-Chernozem-Brunizem soil climosequence. *Soil Science Society of America Journal*, **29**(5), 579–582.

Burki, V., Larsen, E., Fredin, O. and Margreth, A. (2009) The formation of sawtooth moraine ridges in Bødalen, western Norway. *Geomorphology*, **105**(3–4), 182–192.

Burns, P. and Nolin, A. (2014) Using atmospherically-corrected Landsat imagery to measure glacier area change in the Cordillera Blanca, Peru from 1987 to 2010. *Remote Sensing of Environment*, **140**, 165–178.

Calkin, P. E. and Ellis, J. M. (1980) A lichenometric dating curve and its application to Holocene glacier studies in the Central Brooks Range, Alaska. *Arctic and Alpine Research*, **12**(3), 245–264.

Capt, M., Bosson, J. B., Fischer, M., Micheletti, N. and Lambiel, C. (2016) Decadal evolution of a very small heavily debris-covered Glacier in an Alpine permafrost environment. *Journal of Glaciology*, **62**(233), 535–551.

Carlson, A. E. et al. (2007) Rapid Holocene deglaciation of the Labrador sector of the Laurentide Ice Sheet. *Journal of Climate*, **20**(20), 5126–5133.

Carr, S. and Coleman, C. (2007) An improved technique for the reconstruction of former glacier mass-balance and dynamics. *Geomorphology*, **92**(1–2), 76–90.

Carrivick, J. L., James, W. H., Grimes, M., Sutherland, J. L. and Lorrey, A. M., (2020) Ice thickness and volume changes across the Southern Alps, New Zealand, from the Little Ice Age to present. *Scientific Reports*, **10**(1), 1–10.

Carrivick, J. L. and Tweed, F. S. (2013) Proglacial Lakes: Character, behaviour and geological importance. *Quaternary Science Reviews*, **78**, 34–52.

Carturan, L. Baroni, C., Carton, A., Cazorzi, F., Fontana, G. D., Delpero, C., Salvatore, M. C., Seppi, R. and Zanoner, T. (2014) Reconstructing fluctuations of la mare glacier (eastern Italian Alps) in the late Holocene: New evidence for a Little Ice Age maximum around 1600 AD. *Geografiska Annaler, Series A: Physical Geography*, **96**(3), 287–306.

Carturan, L. Cazorzi, F., De Blasi, F. and Dalla Fontana, G. (2015) Air temperature variability over three glaciers in the Ortles-Cevedale (Italian Alps): Effects of

glacier fragmentation, comparison of calculation methods, and impacts on mass balance modelling. *Cryosphere*, **9**(3), 1129–1146.

Cave, J. A. S. and Ballantyne, C. K. (2016) Catastrophic Rock-Slope Failures in NW Scotland: Quantitative analysis and implications. *Scottish Geographical Journal*, **132**(3–4), 185–209.

Čekada, M. T., Radovan, D., Lipuš, B. and Mongus, D. (2020) Very small glaciers as Geoheritage: Combining a spatio-temporal visualisation of their development and related effects of climate change. *Geoheritage*, **12**(4), 1-11.

Chandler, B. M. P., Evans, D. J. A., Roberts, D. H., Ewertowski, M. and Clayton, A. I. (2016a) Glacial geomorphology of the Skálafellsjökull foreland, Iceland: A case study of "annual" moraines. *Journal of Maps*, **12**(5), 904–916.

Chandler, B. M. P., Lovell, H., Boston, C. M., Lukas, S., Barr, I. D., Benediktsson, Í. Ö., Benn, D. I., Clark, C. D., Darvill, C. M., Evans, D. J. and Ewertowski, M. W. (2018) Glacial geomorphological mapping: A review of approaches and frameworks for best practice. *Earth-Science Reviews*, **185**, 806–846.

Chandler, B. M. P., Lukas, S., Boston, C. M. and Merritt, J. W. (2019) Glacial geomorphology of the Gaick, Central Grampians, Scotland. *Journal of Maps*, **15**(2), 60–78.

Chandler, B. M. P. et al. (2020a) Sub-annual moraine formation at an active temperate Icelandic glacier. *Earth Surface Processes and Landforms*, **45**(7), 1622–1643.

Chandler, B. M. P., Chandler, S. J., Evans, D. J., Ewertowski, M. W., Lovell, H., Roberts, D. H., Schaefer, M. and Tomczyk, A. M. (2020b) The glacial landsystem of Fjallsjökull, Iceland: Spatial and temporal evolution of process-form regimes at an active temperate glacier. *Geomorphology*, **361**, 1–28.

Chandler, B. M. P., Boston, C. M., Lukas, S. and Lovell, H. (2021) Re-interpretation of "hummocky moraine" in the Gaick, Scotland, as erosional remnants: Implications for palaeoglacier dynamics. *Proceedings of the Geologists' Association*, **132**, 506–524.

Chandler, B. M. P., Evans, D. J. A. and Roberts, D. H. (2016b) Characteristics of recessional moraines at a temperate glacier in SE Iceland: Insights into patterns, rates and drivers of glacier retreat. *Quaternary Science Reviews*, **135**, 171–205.

Chandler, B. M. P., Evans, D. J. A. and Roberts, D. H. (2016c) Recent retreat at a temperate Icelandic glacier in the context of the last ~80 years of climate change in the North Atlantic region. *Arktos*, **2**(1), 1–13.

Chandler, B. M. P., Lukas, S. and Boston, C. M. (2020c) Processes of “hummocky moraine” formation in the Gaick, Scotland: insights into the ice-marginal dynamics of a Younger Dryas plateau icefield. *Boreas*, **49**(2), 248–268.

Chandler, B. M. P. and Lukas, S. (2017) Reconstruction of Loch Lomond Stadial (Younger Dryas) glaciers on Ben More Coigach, north-west Scotland, and implications for reconstructing palaeoclimate using small ice masses. *Journal of Quaternary Science*, **32**(4), 475–492.

Charbonneau, A. A. and Smith, D. J. (2018) An inventory of rock glaciers in the central British Columbia Coast Mountains, Canada, from high resolution Google Earth imagery. *Arctic, Antarctic, and Alpine Research*, **50**(1), 1–24.

Chattopadhyay, G. P. (1984) A fossil valley-wall rock glacier in the Cairngorm mountains. *Scottish Journal of Geology*, **20**(1), 121–125.

Chenet, M., Roussel, E., Jomelli, V. and Grancher, D. (2010) Asynchronous Little Ice Age glacial maximum extent in southeast Iceland. *Geomorphology*. **114**(3), 253–260.

Church, M. and Ryder, J. M. (1972) Paraglacial sedimentation: A consideration of fluvial processes conditioned by glaciation. *Geological Society of America Bulletin*, **83**, 3059–3072.

Chylek, P., Folland, C. K., Lesins, G., Dubey, M. K. and Wang, M. (2009) Arctic air temperature change amplification and the Atlantic Multidecadal Oscillation. *Geophysical Research Letters*, **36**(14), 2–6.

Clapperton, C. M. (1971) Evidence of Cirque Glaciation in the Falkland Islands. *Journal of Glaciology*, **10**(58), 121–125.

Clark, C. D. (1993) Mega-scale glacial lineations and cross-cutting ice-flow landforms. *Earth Surface Processes and Landforms*, **18**, 1–29.

Clark, C. D. (1997) Reconstructing the evolutionary dynamics of former ice sheets using multi-temporal evidence, remote sensing and GIS. *Quaternary Science Reviews*, **16**(9), 1067–1092.

Clark, C. D., Tulaczyk, S. M., Stokes, C. R. and Canals, M. (2003) A groove-ploughing theory for the production of mega-scale glacial lineations, and implications for ice-stream mechanics. *Journal of Glaciology*, **49**(165), 240–256.

Clarke, G. K. C., Leverington, D. W., Teller, J. T. and Dyke, A. S. (2004) Paleohydraulics of the last outburst flood from glacial Lake Agassiz and the 8200 BP cold event. *Quaternary Science Reviews*, **23**(3–4), 389–407.

Clayton, L. and Moran, S. R. (1982) A Glacial Process-Form Model. In Coates, D. R. (ed.) Glacial Geomorphology. Dordrecht: Springer, 89–119.

Clayton, L., Teller, J. T. and Attig, J. W. (1985) Surging of the southwestern part of the Laurentide Ice Sheet. *Boreas*, **14**, 235–241.

Cogley, J. G., Arendt, A. A., Bauder, A., Braithwaite, R. J., Hock, R., Jansson, P., Kaser, G., Moller, M., Nicholson, L., Rasmussen, L. A. and Zemp, M. (2011) Glossary of Glacier Mass Balance and Related Terms. *IHP-VII Technical Documents in Hydrology*, **86**. Paris: UNESCO-IHP

Coker-Dewey, J., Steltenpohl, M. G. and Andresen, A. (2000) Geology of western Ullsfjord, North Norway, with emphasis on the development of an inverted metamorphic gradient at the top of the Lyngen Nappe Complex. *Norsk Geologisk Tidsskrift*, **80**(2), 111–127.

Colgan, P. M., Mickelson, D. M. and Cutler, P. M. (2003) Ice-Marginal Terrestrial Landsystems: Southern Laurentide Ice Sheet Margin. In Evans, D. J. A. (ed.) Glacial Landsystems. London: Arnold, 11–142.

Colhoun, E. A. and Synge, F. M. (1980) The Cirque Moraines at Lough Nahanagan, County Wicklow, Ireland. *Proceedings of the Royal Irish Academy. Section B: Biological, Geological, and Chemical Science*, **80B**, 25–45.

Colman, S. M. (1981) Rock-weathering rates as functions time. *Quaternary Research*, **15**(3), 250–264.

Colucci, R. R. (2016) Geomorphic influence on small glacier response to post-Little Ice Age climate warming: Julian Alps, Europe. *Earth Surface Processes and Landforms*, **41**(9), 1227–1240.

Coquin, J., Mercier, D., Bourgeois, O. and Decaulne, A. (2019) A paraglacial rock-slope failure origin for cirques: A case study from Northern Iceland. *Geomorphologie: Relief, Processus, Environnement*, **25**(2), 117–136.

Corner, G. D. (1980) Preboreal deglaciation chronology and marine limits of the Lyngen-Storfjord area, Troms, North Norway. *Boreas*, **9**(4), 239–249.

Cossart, E., Mercier, D., Decaulne, A. and Feuillet, T. (2013) An overview of the consequences of paraglacial landsliding on deglaciated mountain slopes:

Typology, timing and contribution to cascading fluxes. *Quaternaire*, **24**(1), 13–24.

Craps, S. (2020) Introduction: Ecological grief. *American Imago*, **77**(1), 1–7.

Cuffey, K. M., Alley, R.B., Grootes, P.M., Bolzan, J.M. and Anandakrishnan, S. (1994) Calibration of the $\delta^{18}O$ isotopic paleothermometer for central Greenland, using borehole temperatures. Journal of Glaciology, **40**(135), 341–349.

Cullen, N. J., Sirguey, P., Mölg, T., Kaser, G., Winkler, M. and Fitzsimons, S. J. (2013) A century of ice retreat on Kilimanjaro: The mapping reloaded. *The Cryosphere*, **7**(2), 419–431.

Curry, A. M. (2000) Observations on the distribution of paraglacial reworking of glacigenic drift in western Norway. *Norsk Geografisk Tidsskrift - Norwegian Journal of Geography*, **54**, 139–147.

Curry, A. M. (2021) Paraglacial rock-slope failure following deglaciation in Western Norway. In Beylich, A. A. (ed.) World Geomorphological Landscapes. Cham: Springer, 97–130.

Curry, A. M., Walden, J. and Cheshire, D. A. (2001) The Nant Ffracon "protalus rampart": Evidence for late pleistocene paraglacial landsliding in Snowdonia, Wales. *Proceedings of the Geologists' Association*, **112**(4), 317–330.

Curry, R. R. (1969) Holocene climatic and glacial history of the central Sierra Nevada, California. *Special Paper of the Geological Society of America*, **123**, 1–47.

Cuzzone, J. K., Clark, P. U., Carlson, A. E., Ullman, D. J., Rinterknecht, V. R., Milne, G. A., Lunkka, J. P., Wohlfarth, B., Marcott, S. A. and Caffee, M. (2016) Final deglaciation of the Scandinavian Ice Sheet and implications for the Holocene global sea-level budget. *Earth and Planetary Science Letters*, **448**, 34–41.

D'Amico, M. E., Freppaz, M., Filippa, G. and Zanini, E. (2014) Vegetation influence on soil formation rate in a proglacial chronosequence (Lys Glacier, NW Italian Alps). *Catena*, **113**, 122–137.

Dahl, R. (1966) Block fields, weathering pits and tor-like forms in the Narvik Mountains Nordland, Norway. *Geografiska Annaler: Series A, Physical Geography*, **48**(2), 55–85.

Dahl, S. O., Nesje, A., Lie, Ø., Fjordheim, K. and Matthews, J. A., (2002) Timing, equilibrium-line altitudes and climatic implications of two early-Holocene glacier readvances during the Erdalen Event at Jostedalsbreen, western Norway. *The Holocene*, **12**(1), 17–25.

Dahl, S. O., Bakke, J., Lie, Ø. and Nesje, A. (2003) Reconstruction of former glacier equilibrium-line altitudes based on proglacial sites: An evaluation of approaches and selection of sites. *Quaternary Science Reviews*, **22**(2–4), 275–287.

Dahl, S. O. and Nesje, A. (1994) Holocene glacier fluctuations at Hardangerjøkulen, central-southern Norway: A high-resolution composite chronology from lacustrine and terrestrial deposits. *The Holocene*, **4**(3), 269–277.

Dahl, S. O. and Nesje, A. (1996) A new approach to calculating Holocene winter precipitation by combining glacier equilibrium-line altitudes and pine-tree limits: A case study from Hardangerjøkulen, central southern Norway. *The Holocene*, **6**(4), 381–398.

Dahl, S. O., Nesje, A. and ØVstedal, J. (1997) Cirque glaciers as morphological evidence for a thin Younger Dryas ice sheet in east-central southern Norway. *Boreas*, **26**(3), 161–180.

Darvill, C. M., Stokes, C. R., Bentley, M. J. and Lovell, H., (2014) A glacial geomorphological map of the southernmost ice lobes of Patagonia: the Bahía Inútil - San Sebastián, Magellan, Otway, Skyring and Río Gallegos lobes. *Journal of Maps*, **10**(3), 500–520.

Darvill, C. M., Stokes, C. R., Bentley, M. J., Evans, D. J. A. and Lovell, H. (2017) Dynamics of former ice lobes of the southernmost Patagonian Ice Sheet based on a glacial landsystems approach. *Journal of Quaternary Science*, **32**(6), 857–876.

Day, M. J. (1977) Field assessment of rock hardness using the Schmidt hammer. *British Geomorphological Research Group Technical Bulletin*, **18**, 19–29.

DeBeer, C. M. and Sharp, M. J. (2007) Recent changes in glacier area and volume within the southern Canadian Cordillera. *Annals of Glaciology*, **46**, 215–221.

DeBeer, C. M. and Sharp, M. J. (2009) Topographic influences on recent changes of very small glaciers in the Monashee Mountains, British Columbia, Canada. *Journal of Glaciology*, **55**(192), 691–700.

Delaney, C. (2002) Sedimentology of a glaciofluvial landsystem, Lough Ree area, Central Ireland: Implications for ice margin characteristics during Devensian deglaciation. *Sedimentary Geology*, **149**(1–3), 111–126.

Delworth, T. L. and Knutson, T. R. (2000) Simulation of early 20th century global warming. *Science*, **287**(5461), 2246–2250.

Demuth, M., Pinard, V., Pietroniro, A., Luckman, B. H., Hopkinson, C., Dornes, P. and Comeau, L. (2008) Recent and past-century variations in the glacier resources of the Canadian Rocky Mountains: Nelson River system. *Terra Glacialis*, **11**(248), 27–52.

Déry, S. J. and Brown, R. D. (2007) Recent Northern Hemisphere snow cover extent trends and implications for the snow-albedo feedback. *Geophysical Research Letters*, **34**, 2–7.

Dowdeswell, J. A. and Evans, S. (2004) Investigations of the form and flow of ice sheets and glaciers using radio-echo sounding. *Reports on Progress in Physics*, **67**(10), 1821–1861.

Dowling, L., Eaves, S., Norton, K., Mackintosh, A., Anderson, B., Hidy, A., Lorrey, A., Vargo, L., Ryan, M. and Tims, S. (2021) Local summer insolation and greenhouse gas forcing drove warming and glacier retreat in New Zealand during the Holocene. *Quaternary Science Reviews*, **266**, 1–15.

Drozdowski, E. (1986) "Surge moraines". In Gardiner, V. (ed) International Geomorphology Part II. Wiley: Chichester, 675–692.

Du, Y., Zhang, Y., Ling, F., Wang, Q., Li, W. and Li, X. (2016) 'Water bodies' mapping from Sentinel-2 imagery with Modified Normalized Difference Water Index at 10-m spatial resolution produced by sharpening the SWIR band. *Remote Sensing*, **8**(4), 1–19.

Dyke, A. S., Andrews, J. T. and Miller, G. H. (1982) Quaternary Geology of Cumberland Peninsula, Baffin Island, District of Franklin. Ottawa: Geological Survey of Canada.

Dyrrdal, A. V. (2009) Trend analysis of number of snow days per winter season in Norway. Oslo: Norwegian Meteorological Institute

Dyrrdal, A. V., Saloranta, T., Skaugen, T. and Stranden, H. B. (2013) Changes in snow depth in Norway during the period 1961-2010. *Hydrology Research*, **44**(1), 169–179.

Dyurgerov, M. B. (2005) Mountain glaciers are at risk of extinction. In Huber, U. M., Bugmann, H. K. M., and Reasoner, M. A. (eds) Global Change in Mountain Regions. Dordrecht: Springer Netherlands, 177–185.

Earl, L. and Gardner, A. (2016) A satellite-derived glacier inventory for North Asia. *Annals of Glaciology*, **57**(71), 50–60.

Eckerstorfer, M., Eriksen, H. Ø., Rouyet, L., Christiansen, H. H., Lauknes, T. R. and Blikra, L. H. (2018) Comparison of geomorphological field mapping and 2D-InSAR mapping of periglacial landscape activity at Nordnesfjellet, northern Norway. *Earth Surface Processes and Landforms*, **43**(10), 2147–2156.

Egholm, D. L., Pedersen, V. K., Knudsen, M. F. and Larsen, N. K. (2012) Coupling the flow of ice, water, and sediment in a glacial landscape evolution model. *Geomorphology*, **141**, 47–66.

Ellis, S. (1979) The identification of some Norwegian mountain soil types. *Norsk Geografisk Tidsskrift - Norwegian Journal of Geography*, **33**(4), 205–212.

Elven, R. (1978) Subglacial plant remains from the Omnsbreen glacier area, south Norway. *Boreas*, **7**(2), 83–89.

Engeset, R. V., Schuler, T. V. and Jackson, M. (2005) Analysis of the first jökulhlaup at Blamannsisen, northern Norway, and implications for future events. *Annals of Glaciology*, **42**(1), 35–41.

England, J. (1978) Glacial geology of northeastern Ellesmere Island, N.W.T., Canada. *Canadian Journal of Earth Sciences*, **15**, 603–617.

England, M. R. Eisenman, I., Lutsko, N. J. and Wagner, T. J. W. (2021) The recent emergence of Arctic Amplification. *Geophysical Research Letters*, **48**(15), 1–10.

Eriksen, H. Rouyet, L., Lauknes, T. R., Berthling, I., Isaksen, K., Hindberg, H., Larsen, Y. and Corner, G. D. (2018) Recent acceleration of a rock glacier complex, Ádjet, Norway, Documented by 62 years of remote sensing observations. *Geophysical Research Letters*, **45**(16), 8314–8323.

Eriksen, H. Ø., Bergh, S. G., Larsen, Y., Skrede, I., Kristensen, L., Lauknes, T. R., Blikra, L. H. and Kierulf, H. P. (2017) Relating 3D surface displacement from satellite-and ground-based inSAR to structures and geomorphology of the Jettan Rockslide, northern Norway. *Norsk Geologisk Tidsskrift*, **97**(4), 283–303.

Erikstad, L. and Sollid, J. L. (1986) Neoglaciation in South Norway using lichenometric methods. *Norsk Geografisk Tidsskrift - Norwegian Journal of Geography*, **40**(2), 85–105.

Evans, D. J. A. (1990a) The effect of glacier morphology on surficial geology and glacial stratigraphy in a high arctic mountainous terrain. *Zeitschrift für Geomorphologie*, **34**(4), 481–503.

Evans, D. J. A. (1993) High-latitude rock glaciers: A case study of forms and processes in the Canadian Arctic. *Permafrost and Periglacial Processes*, **4**(1), 17–35.

Evans, D. J. A. (1999a) A soil chronosequence from Neoglacial moraines in western Norway. *Geografiska Annaler, Series A: Physical Geography*, **81**(1), 47–62.

Evans, D. J. A. (1999b) Glacial debris transport and moraine deposition: A case study of the Jardalen cirque complex, Sogn-og-Fjordane, western Norway. *Zeitschrift fur Geomorphologie*, **43**(2), 203–234.

Evans, D. J. A., Rea, B. R., Hansom, J. D. and Whalley, W. B. (2002) Geomorphology and style of plateau icefield deglaciation in fjord terrains: The example of Troms-Finnmark, north Norway. *Journal of Quaternary Science*, **17**(3), 221–239.

Evans, D. J. A. (ed.) (2003a) Glacial Landystems. London: Arnold.

Evans, D. J. A. (2003b) Ice-marginal Terrestrial Landsystems: Active Temperate Glacier Margins. In Evans, D. J. A. (ed.) Glacial Landsystems. London: Arnold, 12–43.

Evans, D. J. A. (2003c) Introduction to glacial landsystems. In A., E. D. J. (ed.) Glacial Landsystems. Reprint. London: Arnold, 1–532.

Evans, D. J. A., Rea, B. R., Hiemstra, J. F. and Ó Cofaigh, C. (2006a) A critical assessment of subglacial mega-floods: a case study of glacial sediments and landforms in south-central Alberta, Canada. *Quaternary Science Reviews*, **25**(13–14), 1638–1667.

Evans, D. J. A. (2008) Geomorphology: Avalanches and moraines. *Nature Geoscience*, **1**(8), 493–494.

Evans, D. J. A. (2009a) Controlled moraines: origins, characteristics and palaeoglaciological implications. *Quaternary Science Reviews*, **28**(3–4), 183–208.

Evans, D. J. A. (2009b) Special theme: Modern analogues in Quaternary palaeoglaciological reconstruction. *Quaternary Science Reviews*, **28**(3–4), 181–182.

Evans, D. J. A. (2010) Controlled moraine development and debris transport pathways in polythermal plateau icefields: Examples from Tungnafellsjökull, Iceland. *Earth Surface Processes and Landforms*, **35**(12), 1430–1444.

Evans, D. J. A. (2011) Glacial landsystems of Satujökull, Iceland: A modern analogue for glacial landsystem overprinting by mountain ice caps. *Geomorphology*, **129**(3–4), 225–237.

Evans, D. J. A., Harrison, S., Vieli, A. and Anderson, E. (2012) The glaciation of Dartmoor: The southernmost independent Pleistocene ice cap in the British Isles. *Quaternary Science Reviews*, **45**, 31–53.

Evans, D. J. A. (2013a) Geomorphology and Retreating Glaciers. In Shroder, J. (ed.) Treatise on Geomorphology. Cambridge: Academic Press, 460–478

Evans, D. J. A., Rother, H., Hyatt, O. M. and Shulmeister, J. (2013) The glacial sedimentology and geomorphological evolution of an outwash head/moraine-dammed lake, South Island, New Zealand. *Sedimentary Geology*, **284**, 45–75.

Evans, D. J. A. (2016) Landscapes at the periphery of glacierization – Retrospect and Prospect. *Scottish Geographical Journal*, **132**(2), 140–163.

Evans, D. J. A., Ewertowski, M., Jamieson, S. S. R. and Orton, C. (2016a). Surficial geology and geomorphology of the Kumtor Gold Mine, Kyrgyzstan: human impacts on mountain glacier landsystems. *Journal of Maps*, **12**(5), 757-769.

Evans, D. J. A., Ewertowski, M., Orton, C., Harris, C. and Guðmundsson, S. (2016b) Snæfellsjökull volcano-centred ice cap landsystem, West Iceland. *Journal of Maps*, **12**, 1128–1137.

Evans, D. J. A. (ed.) (2018) Glacial landsystems of southeast Iceland - Quaternary applications. London: Quaternary Research Association.

Evans, D. J. A., Ewertowski, M., Orton, C. and Graham, D. J. (2018) The glacial geomorphology of the ice cap piedmont lobe landsystem of east Mýrdalsjökull, Iceland. *Geosciences*, **8**(6), 194.

Evans, D. J. A., Guðmundsson, S., Vautrey, J. L., Fearnyough, K. and Southworth, W. G. (2019a) Testing lichenometric techniques in the production of a new growth-rate (curve) for the Breiðamerkurjökull foreland, Iceland, and the analysis of potential climatic drivers of glacier recession. *Geografiska Annaler, Series A: Physical Geography,* **101**(3), 225–248.

Evans, D. J. A. (2020) 'Bodmin Moor'. In Goudie, A. and Migoń, P. (eds) Landscapes and Landforms of England and Wales. Cham: Springer, 257–268.

Evans, D. J. A., Archer, S. and Wilson, D. J. H. (1999a) A comparison of the lichenometric and Schmidt hammer dating techniques based on data from the

proglacial areas of some Icelandic glaciers. *Quaternary Science Reviews*, **18**(1), 13–41.

Evans, D. J. A., Butcher, C. and Kirthisingha, A. V. (1994) Neoglaciation and an early “Little Ice Age” in western Norway: Lichenometric evidence from the Sandane area. *The Holocene*, **4**(3), 278–289.

Evans, D. J. A., Clark, C. D. and Rea, B. R. (2008) Landform and sediment imprints of fast glacier flow in the southwest Laurentide Ice Sheet. *Journal of Quaternary Science*, **22**(3), 249–272.

Evans, D. J. A. and England, J. (1992) Geomorphological evidence of Holocene climatic change from northwest Ellesmere Island, Canadian high Arctic. *The Holocene*, **2**(2), 148–158.

Evans, D. J. A., Ewertowski, M. and Orton, C. (2016b) Eiríksjökull plateau icefield landsystem, Iceland. *Journal of Maps*, **12**(5), 747–756.

Evans, D. J. A., Ewertowski, M. and Orton, C. (2016c) Fláajökull (north lobe), Iceland: active temperate piedmont lobe glacial landsystem. *Journal of Maps*, **12**(5), 777–789.

Evans, D. J. A., Ewertowski, M. and Orton, C. (2017a) Skaftafellsjökull, Iceland: Glacial geomorphology recording glacier recession since the Little Ice Age. *Journal of Maps*, **13**(2), 358–368.

Evans, D. J. A., Ewertowski, M. and Orton, C. (2017b) The glaciated valley landsystem of Morsárjökull, Southeast Iceland. *Journal of Maps*, **13**(2), 909–920.

Evans, D. J. A., Ewertowski, M. W. and Orton, C. (2019b) The glacial landsystem of Hoffellsjökull, SE Iceland: contrasting geomorphological signatures of active temperate glacier recession driven by ice lobe and bed morphology. *Geografiska Annaler, Series A: Physical Geography*, **101**(3), 249–276.

Evans, D. J. A. and Hiemstra, J. F. (2005) Till deposition by glacier submarginal, incremental thickening. *Earth Surface Processes and Landforms*, **30**(13), 1633–1662.

Evans, D. J. A., Kalyan, R. and Orton, C. (2017c) Periglacial geomorphology of summit tors on Bodmin Moor, Cornwall, SW England. *Journal of Maps*, **13**(2), 342–349.

Evans, D. J. A., Lemmen, D. S. and Rea, B. R. (1999b) Glacial landsystems of the southwest Laurentide ice sheet: Modern Icelandic analogues. *Journal of Quaternary Science*, **14**(7), 673–691.

Evans, D. J. A., Nelson, C. D. and Webb, C. (2010a) An assessment of fluting and “till esker” formation on the foreland of Sandfellsjökull, Iceland. *Geomorphology*. **114**(3), 453–465.

Evans, D. J. A. and Rea, B. R. (1999) Geomorphology and sedimentology of surging glaciers: A land-systems approach. *Annals of Glaciology*, **28**, 75–82.

Evans, D. J. A., Shulmeister, J. and Hyatt, O. (2010b) Sedimentology of latero-frontal moraines and fans on the west coast of South Island, New Zealand. *Quaternary Science Reviews*, **29**(27–28), 3790–3811.

Evans, D. J. A. and Twigg, D. R. (2002) The active temperate glacial landsystem: A model based on Breioamerkurjökull and Fjallsjökull, Iceland. *Quaternary Science Reviews*, **21**(20–22), 2143–2177.

Evans, D. J. A., Twigg, D. R. and Shand, M. (2006b) Surficial geology and geomorphology of the þórisjökull plateau icefield, west-central Iceland. *Journal of Maps*, **2**(1), 17–29.

Evans, D. J. A., Young, N. J. P. and Ó Cofaigh, C. (2014) Glacial geomorphology of terrestrial-terminating fast flow lobes/ice stream margins in the southwest Laurentide Ice Sheet. *Geomorphology*, **204**, 86–113.

Evans, I. S. (1990b) Climatic effects on glacier distribution across the southern Coast Mountains, B.C., Canada. *Annals of Glaciology*, **14**, 58–64.

Evans, I. S. (1999c) Was the cirque glaciation of Wales time-transgressive, or not? *Annals of Glaciology*, **28**, 33–39.

Evans, I. S. (2006) Glacier distribution in the alps: Statistical modelling of altitude and aspect. *Geografiska Annaler, Series A: Physical Geography*, **88**(2), 115–133.

Evans, I. S. (2007) Glacial Landforms, Erosional Features: Major Scale Forms. In Elias, S. A. (ed.) Encyclopedia of Quaternary Science. Amsterdam: Elsevier, 838–852.

Evans, I. S. (2009c) A brief report on recent change in small glaciers in British Columbia, Canada. *Quaternary Newsletter*, **118**, 28–31.

Evans, I. S. (2013b) The Erosion of Glaciated Mountains. In Stoddart, D. (ed.) Process and Form in Geomorphology. London: Routledge, 145–174.

Evans, I. S. (2021) Glaciers, rock avalanches and the “buzzsaw” in cirque development: Why mountain cirques are of mainly glacial origin. *Earth Surface Processes and Landforms*, **46**(1), 24–46.

Evans, I. S. and Cox, N. (1974) Geomorphometry and the Operational Definition of Cirques. *The Royal Geographical Society*, **6**(2), 150–153.

Evans, J. A. and Rogerson, J. (1986) Glacial geomorphology and chronology in the Selamiut Range - Nachvak Fiord area, Torngat Mountains, Labrador. *Canadian Journal of Earth Sciences*, **23**, 66–76.

Eyles, N. (1983) The glaciated valley landsystem. In Eyles, N. (ed.) Glacial Geology. Oxford: Pergamon Press, 91–110.

Farbrot, H., Isaksen, K. and Etzelmüller, B. (2008) Present and past distribution of mountain permafrost in Gaissane Mountains, Northern Norway. *Proceedings of the 9th International Conference on Permafrost*, 427–432.

Farinotti, D., Brinkerhoff, D. J., Clarke, G. K., Fürst, J. J., Frey, H., Gantayat, P., Gillet-Chaulet, F., Girard, C., Huss, M., Leclercq, P. W. and Linsbauer, A. (2017) How accurate are estimates of glacier ice thickness? Results from ITMIX, the Ice Thickness Models Intercomparison eXperiment. *Cryosphere*, **11**(2), 949–970.

Farnsworth, W. R. (2018) Holocene glacier history of Svalbard: Retracing the style of (de)glaciation. Unpublished PhD thesis. UiT, The Arctic University of Norway, Faculty of Science and Technology, Department of Geosciences.

Farnsworth, W. R., Allaart, L., Ingólfsson, Ó., Alexanderson, H., Forwick, M., Noormets, R., Retelle, M. and Schomacker, A. (2020) Holocene glacial history of Svalbard: Status, perspectives and challenges. *Earth-Science Review*s, **208**, 1–28.

Federici, P. A. and Pappalardo, M. (2010) Glacier retreat in the Maritime Alps area. *Geografiska Annaler: Series A, Physical Geography*, **92**(3), 361–373.

Fernández, A., MacDonell, S., Somos-Valenzuela, M. and González-Reyes, Á. (2021) Chile's Glacier Protection Law Needs Grounding in Sound Science. American Geophysical Union Eos Magazine. https://eos.org/opinions/chiles-glacier-protection-law-needs-grounding-in-sound-science. Accessed on: 09.07.2021

Finstad, E., Martinsen J., Hole, R. and Pilø, L. (2016) Prehistoric and medieval skis from glaciers and ice patches in Norway. *Journal of Glacial Archaeology*, **3**(1), 43–58.

Fischer, M., Huss, M., Barboux, C. and Hoelzle, M. (2014) The New Swiss Glacier Inventory SGI2010: Relevance of using high-resolution source data in areas dominated by very small glaciers. *Arctic, Antarctic, and Alpine Research*, **46**(4), 933–945.

Fischer, M. (2018) Understanding the response of very small glaciers in the Swiss Alps to climate change. Unpublished PhD thesis. University of Fribourg, Department of Geosciences.

Fitzpatrick, E. A. (1983) Soils: Their formation, classification and distribution. London: Longman.

Fjeldskaar, W., Bondevik, S. and Amantov, A. (2018) Glaciers on Svalbard survived the Holocene thermal optimum. *Quaternary Science Reviews*, **199**, 18–29.

Fleisher, P. J., Bailey, P. K. and Cadwell, D. H. (2003) A decade of sedimentation in ice-contact, proglacial lakes, Bering Glacier, AK. *Sedimentary Geology*, **160**(4), 309–324

Forbes, J. D. (1853) Norway and Its Glaciers: Visited in 1851; followed by journals of excursions in the high Alps of Dauphiné, Berne and Savoy. Edinburgh: Adam & Charles Black.

Forwick, M. Vorren, T. O., Hald, M., Korsun, S., Roh, Y., Vogt, C. and Yoo, K. C. (2010) Spatial and temporal influence of glaciers and rivers on the sedimentary environment in Sassenfjorden and Tempelfjorden, Spitsbergen. *Geological Society Special Publication*, **344**, 163–193.

Forwick, M. and Vorren, T. O. (2002) Deglaciation history and post-glacial mass movements in Balsfjord, northern Norway. *Polar Research*, **21**(2), 259–266.

Foss, M. (1802) Justedalens kortelige beskrivelse. In Berg, J. C. (ed.) *Magazin for Danmarks og Norges topographiske, oekonomiske og statistiske deskrivelse*, **2**: 3-44.

Fraser, B. (2017) Argentine scientist indicted over design of glacier inventory. Science. https://www.science.org/news/2017/12/argentine-scientist-indicted-over-design-glacier-inventory. Accessed on: 14.03.2018

Frauenfelder, R. and Kääb, A. (2000) Towards a palaeoclimatic model of rock glacier formation in the Swiss Alps. *Annals of Glaciology*, **31**, 281–286.

French, H. M. (2017) The Periglacial Environment. Fourth edition. New Jersey: John Wiley & Sons Ltd.

Frey, H., Paul, F. and Strozzi, T. (2012) Compilation of a glacier inventory for the western Himalayas from satellite data: Methods, challenges, and results. *Remote Sensing of Environment*, **124**, 832–843.

Furunes, T. and Mykletun, R. J. (2012) Frozen Adventure at Risk? A 7-year Follow-up Study of Norwegian Glacier Tourism. *Scandinavian Journal of Hospitality and Tourism*, **12**(4), 324–348.

Gachev, E. (2009) Indicators for modern and recent climate change in the highest mountain areas of Bulgaria. *Landform Analysis*, **10**, 33–38.

Gachev, E., Stoyanov, K. and Gikov, A. (2016) Small glaciers on the Balkan Peninsula: State and changes in the last several years. *Quaternary International*, **415**, 33–54.

Ganyushkin, D. A, Chistyakov, K. V., Volkov, I. V., Bantcev, D. V., Kunaeva, E. P. and Terekhov, A. V. (2017) Present Glaciers and Their Dynamics in the Arid Parts of the Altai Mountains. *Geosciences*, **7**(4), 1–32.

García-Ruiz, J. M., Palacios, D., De Andrés, N., Valero-Garcés, B. L., López-Moreno, J. I. and Sanjuán, Y. (2014) Holocene and “Little Ice Age” glacial activity in the Marboré Cirque, Monte Perdido Massif, Central Spanish Pyrenees. *The Holocene*, **24**(11), 1439–1452.

García, M. G., Cañadas, E. S., Blasco, J. S. and Trueba, J. G. (2017) Surface dynamic of a protalus lobe in the temperate high mountain. Western Maladeta, Pyrenees. *Catena*, **149**, 689–700.

Gauthier, M. S., Kelley, S. E. and Hodder, T. J. (2020) Lake Agassiz drainage bracketed Holocene Hudson Bay Ice Saddle collapse. *Earth and Planetary Science Letters*, **544**, 1–11.

Geikie, A. (1866) Notes for a Comparison of the Glaciation of the West of Scotland with that of Arctic Norway. *Proceedings of the Royal Society of Edinburgh*, **5**, 530–556.

Geirsdóttir, Á., Andrews, J. T., Ólafsdóttir, S., Helgadóttir, G. and Hardardóttir, J. (2002) A 36 Ky record of iceberg rafting and sedimentation from north-west Iceland. *Polar Research*, **21**(2), 291–298.

Geirsdóttir, Á., Miller, G. H., Axford, Y. and Ólafsdóttir, S. (2009) Holocene and latest Pleistocene climate and glacier fluctuations in Iceland. *Quaternary Science Reviews*, **28**(21–22), 2107–2118.

Gellatly, A. F., Gordon, J. E., Whalley, W. B. and Hansom, J. D. (1988) Thermal regime and geomorphology of plateau ice caps in northern Norway: observations and implications. *Geology*, **16**(11), 983–986.

Gellatly, A. F., Whalley, W. B., Gordon, J. E., Hansom, J. D. and Twigg, D. S. (1989) Recent glacial history and climatic change, Bergsfjord, Troms-Finnmark, Norway. *Norsk Geografisk Tidsskrift - Norwegian Journal of Geography*, **43**(1), 19–30.

Gellatly, A. F., Whalley, W. B. and Gordon, J. E. (1986) Topographic control over recent glacier changes in southern Lyngen Peninsula, North Norway. *Norsk Geografisk Tidsskrift - Norwegian Journal of Geography*, **40**(4), 211–218.

Geological Survey of Norway (2015) Berggrunn: national bedrock database. Available at: http://geo.ngu.no/kart/berggrunn/?lang=English. Accessed on: 02.08.2018.

Giesen, R. H., Andreassen, L. M., Oerlemans, J. and Van Den Broeke, M. R. (2014) Surface energy balance in the ablation zone of Langfjordjøkelen, an Arctic, maritime glacier in northern Norway. *Journal of Glaciology*, **60**(219), 57–70.

Gikov, A., Gikov, A., Zlatinova, C. and Blagoev, B. (2009) Present state of Bulgarian glacierets. *Landform Analysis,* **11**, 16–24.

Giles, D. P., Griffiths, J. S., Evans, D. J. A. and Murton, J. B. (2017) Geomorphological framework: Glacial and periglacial sediments, structures and landforms. In Griffiths, J. S. and Martin, C. J. (eds) Engineering Geology and Geomorphology of Glaciated and Periglaciated Terrains – Engineering Group Working Party Report. London: The Geological Society of London, 59–368.

Gisnås, K., Etzelmüller, B., Lussana, C., Hjort, J., Sannel, A. B. K., Isaksen, K., Westermann, S., Kuhry, P., Christiansen, H. H., Frampton, A. and Åkerman, J. (2017) Permafrost Map for Norway, Sweden and Finland. *Permafrost and Periglacial Processes*, **28**(2), 359–378.

Gjerde, M., Bakke, J., Vasskog, K., Nesje, A. and Hormes, A. (2016) Holocene glacier variability and Neoglacial hydroclimate at Ålfotbreen, western Norway. *Quaternary Science Reviews*, **133**, 28–47.

Glasser, N. F., Harrison, S., Jansson, K. N., Anderson, K. and Cowley, A. (2011) Global sea-level contribution from the Patagonian Icefields since the Little Ice Age maximum. *Nature Geoscience*, **4**(5), 303–307.

Glasser, N. F. and Bennett, M. R. (2004) Glacial erosional landforms: Origins and significance for palaeoglaciology. *Progress in Physical Geography*, **28**(1), 43–75.

Glasser, N. F., Harrison, S. and Jansson, K. N. (2009) Topographic controls on glacier sediment-landform associations around the temperate North Patagonian Icefield. *Quaternary Science Reviews*, **28**(25–26), 2817–2832.

Goehring, B. M., Brook, E. J., Linge, H., Raisbeck, G. M. and Yiou, F. (2008) Beryllium-10 exposure ages of erratic boulders in southern Norway and implications for the history of the Fennoscandian Ice Sheet. *Quaternary Science Reviews*, **27**(3–4), 320–336.

Golledge, N. R. (2007) An ice cap landsystem for palaeoglaciological reconstructions: characterizing the Younger Dryas in western Scotland. *Quaternary Science Reviews*, **26**(1–2), 213–229.

Gordon, J. E., Whalley, W. B., Gellatly, A. F. and Vere, D. M. (1992) The formation of glacial flutes: Assessment of models with evidence from Lyngsdalen, North Norway. *Quaternary Science Reviews*, **11**(7–8), 709–731.

Grab, S. W. (1996) The occurrence of a Holocene rock glacier on Mount Kenya: Some observations and comments. *Permafrost and Periglacial Processes*, **7**(4), 381–389.

Graham, D. J., Bennett, M. R., Glasser, N. F., Hambrey, M. J., Huddart, D. and Midgley, N. G. (2007) Comment on: “A test of the englacial thrusting hypothesis of ‘ hummocky ’ moraine formation”. *Boreas*, **36**(1), 103–107.

Gray (1970) Mass wasting studies in the Ogilvie and Wernecke mountains, Central Yukon territory. *Geological Survey Canada Papers,* **70**, 192–195.

Greig, D. (2011) Moraine chronology and deglaciation of the northern Lyngen Peninsula, Troms, Norway. Unpublished MSc Thesis. UiT, The Arctic University of Norway, Faculty of Science and Technology, Department of Geosciences.

Gribbon, P. W. F. (1964) Recession of Glacier Tasîssârssik A, East Greenland. *Journal of Glaciology*, **5**(39), 361–363.

Griffey, N. J. and Whalley, W. B. (1979) A rock glacier and moraine-ridge complex, Lyngen Peninsula, north Norway. *Norsk Geografisk Tidsskrift - Norwegian Journal of Geography*, **33**(3), 117–124.

Griffey, N. J. and Worsley, P. (1978) The pattern of Neoglacial glacier variations in the Okstindan region of northern Norway during the last three millennia. *Boreas*, **7**(1), 1–17.

Grønlie, O. T. (1931) Breer i Balsfjorden. *Norsk Geografisk Tidsskrift - Norwegian Journal of Geography*, **12**, 265–289.

Grønlie, O. T. (1940) On the traces of the ice ages in Nordland, Troms, and the south-western part of Finnmark in northern Norway. *Norsk Geografisk Tidsskrift - Norwegian Journal of Geography*, **20**, 1–70.

Groom, G. E. (1959) Niche Glaciers in Bünsow Land, Vestspitsbergen. *Journal of Glaciology*, **3**(25), 368–376.

Grove, J. M. (1961) Some notes on Slab and Niche Glaciers, and the characteristics of Proto-Cirque hollows. *International Association of Scientific Hydrology*, **54**, 281–287.

Grove, J. M. (1988) The Little Ice Age. London: Methuen.

Grove, J. M. (2001) The initiation of the “Little Ice Age” in regions round the North Atlantic. *Climatic Change*, **48**(1), 53–82.

Grove, J. M. (2004a) Little Ice Ages: Ancient and Modern (Volume 1). Second edition. London: Routledge.

Grove, J. M. (2004b) Little Ice Ages: Ancient and Modern (Volume 2). Second edition. London: Routledge.

Gruber, S. and Haeberli, W. (2007) Permafrost in steep bedrock slopes and its temperatures-related destabilization following climate change. *Journal of Geophysical Research: Earth Surface*, **112**(2), 1–10.

Grudd, H. (1990) Small Glaciers as Sensitive Indicators of Climatic Fluctuations. *Geografiska Annaler: Series A, Physical Geography*, **72**(1), 119–123.

Grünewald, K. and Scheithauer, J. (2008) Microglaciers in the Pirin mountains. *Problems of Geography*, **1**, 164–180.

Guillet, G. and Ravanel, L. (2020) Variations in surface area of six ice aprons in the Mont-Blanc massif since the Little Ice Age. *Journal of Glaciology*, **66**(259), 777–789.

Gunnar, Ø. (1964) Ice-Cored Moraines in Scandinavia. *Geografiska Annaler*, **46**(3), 282–337.

Gurney, S. D. and White, K. (2005) Sediment magnetic properties of glacial till deposited since the Little Ice Age maximum for selected glaciers at Svartisen and Okstindan, northern Norway. *Boreas*, **34**(1), 75–83.

Haeberli, W. (1985) Creep of mountain permafrost: internal structure and flow of alpine rock glaciers. *Mitteilungen der Versuchsanstalt für Wasserbau, Hydrologie und Glaziologie der ETH Zürich*, **77**, 1–142.

Haeberli, W. (2000) Modern research perspectives relating to permafrost creep and rock glaciers: A discussion. *Permafrost and Periglacial Processes*, **11**(4), 290–293.

Haeberli, W. (2005) Investigating glacier-permafrost relationships in high-mountain areas: Historical background, selected examples and research needs. *Geological Society Special Publication*, **242**, 29–37.

Haeberli, W., Hallet, B., Arenson, L., Elconin, R., Humlum, O., Kääb, A., Kaufmann, V., Ladanyi, B., Matsuoka, N., Springman, S. and Mühll, D. V. (2006) Permafrost creep and rock glacier dynamics. *Permafrost and Periglacial Processes*, **17**, 189–214.

Haeberli, W., Hoelzle, M., Paul, F. and Zemp, M. (2007) Integrated monitoring of mountain glaciers as key indicators of global climate change: the European Alps. *Annals of Glaciology*, **46**, 150–160.

Haeberli, W., Paul, F. and Zemp, M. (2013) Vanishing glaciers in the European Alps. *Pontifical Academy of Sciences, Scripta Varia*, **118**, 1–9.

Hafner, A. (2012) Archaeological discoveries on Schnidejoch and at other ice sites in the European Alps. *Arctic*, **65**, 189–202.

Hambrey, M. J., Huddart, D., Bennett, M. R. and Glasser, N. F. (1997) Genesis of "hummocky moraines" by thrusting in glacier ice: Evidence from Svalbard and Britain. *Journal of the Geological Society*, **154**(4), 623–632.

Hamilton, S. J. (1995) Age determinations of rock glaciers using lichenometry. Unpublished PhD thesis. Queen's University of Belfast, School of Natural Built Environment.

Hamilton, S. J. and Whalley, B. W. (1995) Rock glacier nomenclature: A re-assessment'. *Geomorphology*, **14**, 73–80.

Hanáček, M., Flašar, J. and Nývlt, D. (2011) Sedimentary petrological characteristics of lateral and frontal moraine and proglacial glaciofluvial sediments of Bertilbreen, Central Svalbard. *Czech Polar Reports*, **1**, 11–33.

Hansen, E. S. (2010) A review of lichen growth and applied lichenometry in Southwest and Southeast Greenland. *Geografiska Annaler, Series A: Physical Geography*, **92**(1), 65–79.

Hanssen-Bauer, I., Førland, E. J., Haddeland, I., Hisdal, H., Mayer, S., Nesje, A., Nilsen, J. E. Ø., Sandven, S., Sandø, A. B., Sorteberg og, A. and Ådlandsvik,

B. (2015a) Klima i Norge 2100. Oslo: The Norwegian Climate Service Center (NKSS)

Hanssen-Bauer, I. et al. (2017) Climate in Norway 2100 - a knowledge base for climate adaptation. Oslo: The Norwegian Climate Service Center (NKSS)

Harbitz, C. B., Glimsdal, S., Løvholt, F., Kveldsvik, V., Pedersen, G. K. and Jensen, A. (2014) Rockslide tsunamis in complex fjords: From an unstable rock slope at Åkerneset to tsunami risk in western Norway. *Coastal Engineering*, **88**, 101–122.

Harning, D. J., Geirsdóttir, Á., Miller, G. H. and Zalzal, K. (2016) Early Holocene deglaciation of Drangajökull, Vestfirðir, Iceland. *Quaternary Science Reviews*, **153**, 192–198.

Harris, C., Kern-Luetschg, M., Smith, F. and Isaksen, K. (2008) Solifluction Processes in an Area of Seasonal Ground Freezing, Dovrefjell, Norway. *Permafrost and Periglacial Processes*, **19**, 31–47.

Harris, C. and Bothamley, K. (1984) Englacial Deltaic Sediments as Evidence for Basal Freezing and Marginal Shearing, Leirbreen, Southern Norway. *Journal of Glaciology*, **30**(104), 30–34.

Harris, S. A. (1993) Palsa-like mounds in a mineral substrate, Fox Lake Yukon Territory. In Proceedings of the 6th International Conference on Permafrost, Beijing, China. Wushan Guangzhou: South China University of Technology, 238–243.

Harrison, S., Glasser, N., Winchester, V., Haresign, E., Warren, C. and Jansson, K. (2006) A glacial lake outburst flood associated with recent mountain glacier retreat, Patagonian Andes. *The Holocene*, **16**(4), 611–620.

Harrison, S., Anderson, E. and Passmore, D. G. (1998) A small glacial cirque basin on Exmoor, Somerset Stephan Harrison. *Proceedings of the Geologists' Association*, **109**, 149–158.

Harrison, S., Whalley, B. and Anderson, E. (2008) Relict rock glaciers and protalus lobes in the British Isles: implications for Late Pleistocene mountain geomorphology and palaeoclimate. *Journal of Quaternary Science*, **23**(3), 287–304.

Harrison, S., Winchester, V. and Glasser, N. (2007) The timing and nature of recession of outlet glaciers of Hielo Patagónico Norte, Chile, from their Neoglacial IV

(Little Ice Age) maximum positions. *Global and Planetary Change*, **59**(1–4), 67–78.

Hartmeyer, I., Delleske, R., Keuschnig, M., Krautblatter, M., Lang, A., Schrott, L. and Otto, J. C. (2020) Current glacier recession causes significant rockfall increase: The immediate paraglacial response of deglaciating cirque walls. *Earth Surface Dynamics*, **8**(3), 729–751.

Hastings, G. (1899) The Lyngen district. *Alpine Journal,* **19**, 356–363.

Hättestrand, C. and Clark, C. D. (2006) The glacial geomorphology of Kola Peninsula and adjacent areas in the Murmansk Region, Russia. *Journal of Maps*, **2**(1), 30–42.

Haworth, L. A., Calkin, P. E. and Ellis, J. M. (1986) Direct measurement of lichen growth in the Central Brooks Range, Alaska, U.S.A., and its application to Lichenometric dating. *Arctic and Alpine Research*, **18**(3), 289–296.

Hedding, D. W., Sumner, P. D., Holness, S. D. and Meiklejohn, K. I. (2007) Formation of a pronival rampart on sub-Antarctic Marion Island. *Antarctic Science*, **19**(4), 443–450.

Hedding, D. W. (2011) Pronival rampart and protalus rampart: A review of terminology. *Journal of Glaciology*, **57**(206), 1179–1180.

Hedding, D. W. (2016a) Pronival ramparts: A review. *Progress in Physical Geography*, **40**(6), 835–855.

Hedding, D. W. (2016b) Pronival ramparts: Origin and development of terminology. *Erdkunde*, **70**(2), 141–151.

Hedding, D. W. and Sumner, P. D. (2013) Diagnostic criteria for pronival ramparts: Site, morphological and sedimentological characteristics. *Geografiska Annaler, Series A: Physical Geography*, **95**(4), 315–322.

Heikkilä, M. and Seppä, H. (2003) A 11,000 yr palaeotemperature reconstruction from the southern boreal zone in Finland. *Quaternary Science Reviews*, **22**(5–7), 541–554.

Helama, S., Timonen, M., Holopainen, J., Ogurtsov, M. G., Mielikäinen, K., Eronen, M., Lindholm, M. and Meriläinen, J. (2009) Summer temperature variations in Lapland during the Medieval Warm Period and the Little Ice Age relative to natural instability of thermohaline circulation on multi-decadal and multi-centennial scales. *Journal of Quaternary Science*, **24**(5), 450–456.

Helland, A. (1899) Tromsø Amt I. In Kiær, A., Vibe, J. and Helland, H. (eds) Geologi. Norges Land og Folk. Kristiania (Oslo): Aschehoug.

Helland, A. (1905) XX. Fmmarkens AMT - Første del. In Norges land og folk topografisk-statistisk beskrevet. Kristiania (Oslo): Aschehoug, 804.

Hewitt, K. (2013) The great lateral moraine; Karakoram Himalaya, Inner Asia. *Geografia Fisica e Dinamica Quaternaria*, **36**, 81–94.

Hiemstra, J. F., Matthews, J. A., Evans, D. J. A. and Owen, G. (2015) Sediment fingerprinting and the mode of formation of singular and composite annual moraine ridges at two glacier margins, Jotunheimen, southern Norway. *The Holocene*, **25**(11), 1772–1785.

Hilger, P., Hermanns, R. L., Gosse, J. C., Jacobs, B., Etzelmüller, B. and Krautblatter, M. (2018) Multiple rock-slope failures from Mannen in Romsdal Valley, western Norway, revealed from Quaternary geological mapping and ^{10}Be exposure dating. *The Holocene*, **28**(12), 1841–1854.

Hjort, J., Ujanen, J., Parviainen, M., Tolgensbakk, J. and Etzelmüller, B. (2014) Transferability of geomorphological distribution models: Evaluation using solifluction features in subarctic and Arctic regions. *Geomorphology*, **204**, 165–176.

Hjort, J., Karjalainen, O., Aalto, J., Westermann, S., Romanovsky, V. E., Nelson, F. E., Etzelmüller, B. and Luoto, M. (2018) Degrading permafrost puts Arctic infrastructure at risk by mid-century. *Nature Communications*, **9**(1), 1-9.

Hoel, A. and Werenskiold, W. (1962) Glaciers and snowfields in Norway. Norsk Polarinstitutt Skrifter. Oslo: Oslo Universiy Press.

Holmes, G. W. and Andersen, B. G. (1964) Glacial chronology of Ullsfjord, northern Norway. *United States Geological Survey Professional Paper D*, **475**, 159–163.

Holzhauser, H. (1997) Fluctuations of the Grosser Aletsch Glacier and the Gorner Glacier during the last 3200 years, new results. In Frenzel, B. (ed.) Glacier fluctuations during the Holocene. Stuttgart: Gustav Fischer, 35–58.

Holzhauser, H., Magny, M. and Zumbühl, H. J. (2005) Glacier and lake-level variations in west-central Europe over the last 3500 years. *The Holocene*, **15**(6), 789–801.

Hoppe, G. and Schytt, V. (1953) Some Observations on Fluted Moraine Surfaces. *Geografiska Annaler*, **35**(2), 105–115.

Huggel, C., Allen, S., Deline, P., Fischer, L., Noetzli, J. and Ravanel, L. (2012) Ice thawing, mountains falling-are alpine rock slope failures increasing. *Geology Today*, **28**(3), 98–104.

Huggett, R. J. (1998) Soil chronosequences, soil development, and soil evolution: A critical review. *Catena*, **32**(3–4), 155–172.

Hughes, A. L. C., Gyllencreutz, R., Lohne, Ø. S., Mangerud, J. and Svendsen, J. I. (2016) The last Eurasian ice sheets - a chronological database and time-slice reconstruction, DATED-1. *Boreas*, **45**, 1–45.

Hughes, P. D. (2018) Little Ice Age glaciers and climate in the Mediterranean mountains: A new analysis. *Cuadernos de Investigación Geográfica*, **44**(1), 15–45.

Hughes, P. D., Gibbard, P. L. and Woodward, J. C. (2003) Relict rock glaciers as indicators of Mediterranean palaeoclimate during the Last Glacial Maximum (Late Würmian) in northwest Greece. *Journal of Quaternary Science*, **18**(5), 431–440.

Humlum, O. (1978) Genesis of layered lateral moraines: implications for palaeoclimatology and lichenometry. *Geografiska Tidsskrift*, **77**, 65–72.

Humlum, O. (1998) The climatic significance of rock glaciers. *Permafrost and Periglacial Processes*, **9**(4), 375–395.

Hurrell, J. W., Kushnir, Y., Ottersen, G. and Visbeck, M. (2003) An overview of the North Atlantic Oscillation. *Geophysical Monograph-American Geophysical Union*, **134**, 1–35.

Huss, M. (2011) Present and future contribution of glacier storage change to runoff from macroscale drainage basins in Europe. *Water Resources Research*, **47**(7), 1–14.

Huss, M. and Fischer, M. (2016) Sensitivity of very small glaciers in the Swiss Alps to future climate change. *Frontiers in Earth Science*, **4**(34), 1–17.

Ikeda, A. and Matsuoka, N. (2002) Degradation of talus-derived rock glaciers in the upper Engadin, Swiss Alps. *Permafrost and Periglacial Processes*, **13**(2), 145–161.

Ilyashuk, E. A., Koinig, K. A., Heiri, O., Ilyashuk, B. P. and Psenner, R. (2011) Holocene temperature variations at a high-altitude site in the Eastern Alps: A chironomid record from Schwarzsee ob Sölden, Austria. *Quaternary Science Reviews*, **30**(1–2), 176–191.

Imhof, P., Nesje, A. and Nussbaumer, S. U. (2012) Climate and glacier fluctuations at Jostedalsbreen and Folgefonna, southwestern Norway and in the western Alps from the “Little Ice Age” until the present: The influence of the North Atlantic Oscillation. *The Holocene*, **22**(2), 235–247.

Ingólfsson, Ó., Frich, P., Funder, S. and Humlum, O.L.E., (1990) Paleoclimatic implications of an early Holocene glacier advance on Disko Island, West Greenland. *Boreas*, **19**(4), 297–311.

Innes, J. L. (1983) Development of lichenometric dating curves for Highland Scotland. *Transactions of the Royal Society of Edinburgh: Earth Sciences*, **74**(1), 23–32.

Innes, J. L. (1984a) Lichenometric dating of moraine ridges in northern Norway: Some problems of application. *Geografiska Annaler: Series A, Physical Geography*, **66**(4), 341–352.

Innes, J. L. (1984b) The Optimal Sample Size in Lichenometric Studies. *Arctic and Alpine Research*, **16**(2), 233–244.

Innes, J. L. (1985) Lichenometry. *Progress in Physical Geography*, **9**, 187–254.

Innes, J. L. (1986) Dating exposed rock surfaces in the Arctic by lichenometry: The problem of thallus circularity and its effect on measurement errors. *Arctic*, **39**(3), 253–259.

Intrieri, J. M., Fairall, C. W., Shupe, M. D., Persson, P. O. G., Andreas, E. L., Guest, P. S. and Moritz, R. E. (2002) An annual cycle of Arctic surface cloud forcing at SHEBA. Journal *of Geophysical Research: Oceans*, **107**(10), 1–14.

IPCC (2013) Climate Change 2013: The Physical Science Basis, Contribution of Working Group I to the Fifth Assessment Report of the Intergovernmental Panel on Climate Change. Cambridge: Cambridge University Press.

IPCC (2019) Special Report: The Ocean and Cryosphere in a Changing Climate. Cambridge: Cambridge University Press.

IPCC (2021) Climate Change 2021: The Physical Science Basis, Contribution of Working Group I to the Sixth Assessment Report of the Intergovernmental Panel on Climate Change. Cambridge: Cambridge University Press.

Ipsen, H. A., Principato, S. M., Grube, R. E. and Lee, J. F. (2018) Spatial analysis of cirques from three regions of Iceland: implications for cirque formation and palaeoclimate. *Boreas*, **47**(2), 565–576.

Isarin, R. F. B. (1997) Permafrost distribution and temperatures in Europe during the Younger Dryas. *Permafrost and Periglacial Processes*, **8**(3), 313–333.

Iturrizaga, L. (2011) Paraglacial landscape transformations. In Singh, V. P., Singh, P., and Haritashya, U. K. (eds) Encyclopedia of Earth Sciences Series. Dordrecht: Springer, 817–823.

Ives, J. D. (1978) The maximum extent of the Laurentide Ice Sheet along the east coast of North America during the Last Glaciation. *Arctic*, **31**(1), 24–53.

Ives, J. D., Andrews, J. T. and Barry, R. G. (1975) Growth and decay of the Laurentide Ice Sheet and comparisons with Fenno-Scandinavia. *Die Naturwissenschaften*, **62**(3), 118–125.

Ivy-Ochs, S., Kerschner, H., Reuther, A., Maisch, M., Sailer, R., Schaefer, J., Kubik, P. W., Synal, H. and Schluchter, C. (2006) The timing of glacier advances in the northern European Alps based on surface exposure dating with cosmogenic ^{10}Be, ^{26}Al, ^{36}Cl, and ^{21}Ne. *Special Paper of the Geological Society of America*, **415**, 43–60.

Ivy-Ochs, S., Kerschner, H., Maisch, M., Christl, M., Kubik, P. W. and Schlüchter, C. (2009) Latest Pleistocene and Holocene glacier variations in the European Alps. *Quaternary Science Reviews*, **28**, 2137–2149.

Jackson, M. and Ragulina, G. (2014) Inventory of glacier-related hazardous events in Norway. Oslo: Norges Vassdrags-og Energidirektorat (NVE).

Jamieson, S. S. R., Ewertowski, M. W. and Evans, D. J. A. (2015) Rapid advance of two mountain glaciers in response to mine-related debris loading. *Journal of Geophysical Research: Earth Surface*, **120**(7), 1418-1435.

Jansen, H. L., Simonsen, J. R., Dahl, S. O., Bakke, J. and Nielsen, P. R. (2016) Holocene glacier and climate fluctuations of the maritime ice cap Høgtuvbreen, northern Norway. *The Holocene*, **26**(5), 736–755.

Jaskólski, M. W., Pawłowski, Ł. and Strzelecki, M. C. (2017) Assessment of geohazards and coastal change in abandoned Arctic town, Pyramiden, Svalbard. In: Rachlewicz, G. (ed.), Cryosphere reactions against the background of environmental changes in contrasting high-Arctic conditions in Svalbard. Institute of Geoecology and Geoinformation A. Mickiewicz University in Poznań Polar Reports, vol. 2, Bogucki Wydawnictwo Naukowe: 51–64.

Jensen, C. and Vorren, K.-D. (2008) Holocene vegetation and climate dynamics of the boreal alpine ecotone of northwestern Fennoscandia. *Journal of Quaternary Science*, **23**(8), 719–743.

Jiskoot, H., Juhlin, D., St Pierre, H. and Citterio, M. (2012) Tidewater glacier fluctuations in central East Greenland coastal and fjord regions (1980s-2005). *Annals of Glaciology*, **53**(60), 35–44.

Jiskoot, H. and Mueller, M. S. (2012) Glacier fragmentation effects on surface energy balance and runoff: Field measurements and distributed modelling. *Hydrological Processes*, **26**(12), 1862–1876.

Johannessen, O. M., Bengtsson, L., Miles, M. W., Kuzmina, S.I., Semenov, V. A., Alekseev, G. V., Nagurnyi, A. P., Zakharov, V. F., Bobylev, L. P., Pettersson, L. H. and Hasselmann, K. (2004) Arctic climate change: observed and modelled temperature and sea-ice variability. *Tellus A: Dynamic Meteorology and Oceanography*, **56**(4), 328–341.

Jóhannesson, T., Raymond, C. F. and Waddington, E. D. (1989) A simple method for determining the response time of glaciers. In Oerlemans, J. (ed.) Glacier fluctuations and climatic change. Dordrecht: Springer, 334–352.

Johnsen, S. J., Clausen, H. B., Dansgaard, W., Fuhrer, K., Gundestrup, N., Hammer, C. U., Iversen, P., Jouzel, J. and Stauffer, B. (1992) Irregular glacial interstadials recorded in a new Greenland ice core. *Nature*, **359**, 311–313.

Johnson, B. G., Thackray, G. D. and Van Kirk, R. (2007) The effect of topography, latitude, and lithology on rock glacier distribution in the Lemhi Range, central Idaho, USA. *Geomorphology*, **91**(1–2), 38–50.

Johnson, E. and Rupper, S. (2020) An examination of physical processes that trigger the albedo-feedback on glacier surfaces and implications for regional glacier mass balance across high mountain Asia. *Frontiers in Earth Science*, **8**, 1–18.

Johnson, L. M. (2019) How to Mourn a Glacier. The New Yorker, https://www.newyorker.com/news/dispatch/how-to-mourn-a-glacier. Accessed on: 20.10.2020.

Johnson, M. D. and Clayton, L. (2003) Supraglacial Landsystems in Lowland Terrain. In Evans, D. J. A. (ed.) Glacial Landsystems. London: Arnold, 228–258.

Johnson, M. D. and Mickelson, D. M. (1995) Composition and genesis of glacial hummocks, western Wisconsin, USA. *Boreas*, **24**, 97–116.

Johnson, P. G. (1980) Glacier-rock glacier transition in the southwest Yukon Territory, Canada. *Arctic and Alpine Research*, **12**(2), 195–204.

Johnson, W. H. and Menzies, J. (2002) Supraglacial and ice-marginal deposits and landforms. In Menzies, J. (ed.) Modern and Past Glacial Environments. Oxford: Butterworth-Heinemann, 317–333.

Jomelli, V., Grancher, D., Naveau, P., Cooley, D. and Brunstein, D. (2007) Assessment study of lichenometric methods for dating surfaces. *Geomorphology*, **86**(1–2), 131–143.

Jomelli, V., Grancher, D., Brunstein, D. and Solomina, O. (2008) Recalibration of the yellow Rhizocarpon growth curve in the Cordillera Blanca (Peru) and implications for LIA chronology. *Geomorphology*, **93**(3–4), 201–212.

Jones, D. B., Harrison, S., Anderson, K. and Betts, R. A. (2018a) Mountain rock glaciers contain globally significant water stores. *Scientific Reports*, **8**(1), 1–10.

Jones, D. B., Harrison, S., Anderson, K., Selley, H. L., Wood, J. L. and Betts, R. A. (2018b) The distribution and hydrological significance of rock glaciers in the Nepalese Himalaya. *Global and Planetary Change*, **160**, 123–142.

Jones, D. B., Harrison, S., Anderson, K. and Whalley, W. B. (2019a) Rock glaciers and mountain hydrology: A review. *Earth-Science Reviews*, **193**, 66–90.

Jones, D. B., Harrison, S., Anderson, K., Shannon, S. and Betts, R. A. (2021) Rock glaciers represent hidden water stores in the Himalaya. *Science of the Total Environment*, **793**, 1–8.

Jones, D. B., Harrison, S. and Anderson, K. (2019b) Mountain glacier-to-rock glacier transition. *Global and Planetary Change*, **181**, 1-13

Junttila, J., Aagaard-Sørensen, S., Husum, K. and Hald, M. (2010) Late Glacial-Holocene clay minerals elucidating glacial history in the SW Barents Sea. *Marine Geology*, **276**(1–4), 71–85.

Kamp, U., Byrne, M. and Bolch, T. (2011) Glacier fluctuations between 1975 and 2008 in the Greater Himalaya Range of Zanskar, southern Ladakh. *Journal of Mountain Science*, **8**(3), 374–389.

Karlén, W. (1976) Lacustrine sediments and tree-limit variations as indicators of Holocene climatic fluctuations in Lapland: Northern Sweden. *Geografiska Annaler: Series A, Physical Geography*, **58**(1–2), 1–34.

Karlén, W. (1979) Glacier variations in the Svartisen area, northern Norway. *Geografiska Annaler, Series A: Physical Geography*, **61**(1), 11–28.

Karlén, W. (1981) Lacustrine Sediment Studies. A Technique to Obtain a Continous Record of Holocene Glacier Variations. *Geografiska Annaler: Series A, Physical Geography*, **63**(3), 273–281.

Karlén, W. (1988) Scandinavian glacial and climatic fluctuations during the Holocene. *Quaternary Science Reviews*, **7**, 199–209.

Karlén, W. and Black, J. L. (2002) Estimates of lichen growth-rate in northern Sweden. *Geografiska Annaler, Series A: Physical Geography*, **84**(3–4), 225–232.

Karlén, W. and Kuylenstierna, J. (1996) On solar forcing of Holocene climate: Evidence from Scandinavia. *The Holocene*, **6**(3), 359–365.

Kehew, A. E., Esch, J. M., Kozlowski, A. L. and Ewald, S. K. (2012) Glacial landsystems and dynamics of the Saginaw Lobe of the Laurentide Ice Sheet, Michigan, USA. *Quaternary International*, **260**, 21–31.

Kerschner, H., Hertl, A., Gross, G., Ivy-Ochs, S. and Kubik, P. W. (2006) Surface exposure dating of moraines in the Kromer valley (Silvretta Mountains, Austria) - evidence for glacial response to the 8.2 ka event in the Eastern Alps? *The Holocene*, **16**(1), 7–15.

Kerschner, H. and Ivy-Ochs, S. (2008) Palaeoclimate from glaciers: Examples from the Eastern Alps during the Alpine Lateglacial and early Holocene. *Global and Planetary Change*, **60**(1–2), 58–71.

Kim, K. Y., Kim, J. Y., Kim, J., Yeo, S., Na, H., Hamlington, B. D. and Leben, R. R. (2019) Vertical feedback mechanism of winter Arctic Amplification and sea ice loss. *Scientific Reports*, **9**(1), 1–10.

Kirkbride, M. P. (2000) Ice-marginal geomorphology and Holocene expansion of debris-covered Tasman Glacier, New Zealand. *IAHS Publication*, **264**, 211–217.

Kirkbride, M. P. (2002) Processes of glacial transportation. In Menzies, J. (ed.) Modern and Past Glacial Environments. Oxford: Butterworth-Heinemann, 147–169.

Kirkbride, M. P. (2011) Debris-Covered Glaciers. In Singh, V. P., Singh, P., and Haritashya, U. K. (eds) Encyclopedia of Snow, Ice and Glaciers. Dordrecht: Springer, 190–191.

Kirkbride, M. P. and Deline, P. (2013) The formation of supraglacial debris covers by primary dispersal from transverse englacial debris bands. *Earth Surface Processes and Landforms*, **38**(15), 1779–1792.

Kirkbride, M. and Spedding, N. (1996) The influence of englacial drainage on sediment-transport pathways and till texture of temperate valley glaciers. *Annals of Glaciology*, **22**, 160–166.

Kjøllmoen, B., Andreassen, L. M., Elvehøy, H. and Jackson, M. (2018) Glaciological investigations in Norway 2017. Oslo: Norges Vassdrags-og Energidirektorat (NVE).

Kjøllmoen, B. (2019) Reanalysing a glacier mass balance measurement series - Nigardsbreen 1962-2013. *NVE Rapport*, **30**(2016), 1-59.

Kleman, J. (1994) 'Preservation of landforms under ice sheets and ice caps', Geomorphology, 9(1), 19–32.

Klingbjer, P., Brown, I. A. and Holmlund, P. (2005) Identification of climate controls on the dynamic behaviour of the subarctic glacier Salajekna, northern Scandinavia. *Geografiska Annaler, Series A: Physical Geography*, **87**(1), 215–229.

Knudsen, C. G., Larsen, E., Sejrup, H. P. and Stalsberg, K. (2006) Hummocky moraine landscape on Jæren, SW Norway - implications for glacier dynamics during the last deglaciation. *Geomorphology*, **77**(1–2), 153–168.

Kobashi, T., Severinghaus, J. P., Brook, E. J., Barnola, J. M. and Grachev, A. M. (2007) Precise timing and characterization of abrupt climate change 8200 years ago from air trapped in polar ice. *Quaternary Science Reviews*, **26**(9–10), 1212–1222.

Koenigk, T., Brodeau, L., Graversen, R. G., Karlsson, J., Svensson, G., Tjernström, M., Willén, U. and Wyser, K. (2013) Arctic climate change in 21st century CMIP5 simulations with EC-Earth. *Climate Dynamics*, **40**(11–12), 2719–2743.

Koerner, R. M. (1977) Ice thickness measurements and their implications with respect to past and present ice volumes in the Canadian High Arctic ice caps. *Canadian Journal of Earth Sciences*, **14**, 2697–2705.

Kofler, W., Krapf, V., Oberhuber, W. and Bortenschlager, S. (2005) Vegetation responses to the 8200 cal. BP cold event and to long-term climatic changes in the Eastern Alps: Possible influence of solar activity and North Atlantic freshwater pulses. *The Holocene*, **15**(6), 779–788.

Krabbendam, M. and Bradwell, T. (2011) Lateral plucking as a mechanism for elongate erosional glacial bedforms: Explaining megagrooves in Britain and Canada. *Earth Surface Processes and Landforms*, **36**(10), 1335–1349.

Krüger, J. (1993) Moraine-ridge formation along a stationary ice front in Iceland. *Boreas*, **22**(2), 101–109.

Krüger, J. (1994) Glacial processes, sediments, landforms and stratigraphy in the terminus region of Myrdalsjökull, Iceland: Two interdisciplinary case studies. *Folia Geographica Danica*, **21**, 1–233.

Krüger, J. (1995) Origin, chronology and climatological significance of annual-moraine ridges at Myrdalsjokull, Iceland. *The Holocene*, **5**(4), 420–427.

Krüger, J. (1996) Moraine ridges formed from subglacial frozen-on sediment slabs and their differentiation from push moraines. *Boreas*, **25**(1), 57–64.

Kuhn, M. (1995) The mass balance of very small glaciers. *Zeitschrift für Gletscherkunde und Glazialgeologie*, **31**, 171–179.

Kullman, L. and Kjällgren, L. (2006) Holocene pine tree-line evolution in the Swedish Scandes: Recent tree-line rise and climate change in a long-term perspective. *Boreas*, **35**(1), 159–168.

Kverndal, A.-I. and Sollid, J. L. (1993) Late Weichselian glaciation and deglaciation in northeastern Troms, northern Norway. *Norsk Geografisk Tidsskrift - Norwegian Journal of Geography*, **47**(3), 163–177.

Kvisvik, B. C., Paasche, Ø. and Dahl, S. O. (2015) Holocene cirque glacier activity in Rondane, southern Norway. *Geomorphology*, **246**, 433–444.

Lane, T. P., Paasche, Ø., Kvisvik, B., Adamson, K. R., Rodés, Á., Patton, H., Gomez, N., Gheorghiu, D., Bakke, J. and Hubbard, A. (2020) Elevation changes of the Fennoscandian Ice Sheet interior during the last deglaciation. *Geophysical Research Letters*, **47**(14), 1–10.

Larsen, E., Attig, J. W., Rune Aa, A. and Sønstegaard, E. (1998) Late-glacial cirque glaciation in parts of western Norway. *Journal of Quaternary Science*, **13**(1), 17–27.

Larsen, E., Lysså, A., Rubensdotter, L., Farnsworth, W.R., Jensen, M., Nadeau, M. J. and Ottesen, D. (2018) Lateglacial and Holocene glacier activity in the Van Mijenfjorden area, western Svalbard. *Arktos*, **4**(1), 1–21.

Larsen, N. K. et al. (2015) The response of the southern Greenland ice sheet to the Holocene thermal maximum. *Geology*, **43**(4), 291–294.

Larsen, N. K., Kjær, K. H., Lecavalier, B., Bjørk, A. A., Colding, S., Huybrechts, P., Jakobsen, K. E., Kjeldsen, K .K., Knudsen, K. L., Odgaard, B. V. and Olsen, J.

(2019) Local ice caps in Finderup Land, North Greenland, survived the Holocene Thermal Maximum. *Boreas*, **48**(3), 551–562.

Lauritzen, S. E. and Lundberg, J. (1999) Calibration of the speleothem delta function: An absolute temperature record for the Holocene in northern Norway. *The Holocene*, **9**(6), 659–669.

Leemann, A. and Niessen, F. (1994) Holocene glacial activity and climatic variations in the Swiss Alps: Reconstructing a continuous record from proglacial lake sediments. T*he Holocene*, **4**(3), 259–268.

Leigh, J. R. (2016) Testing the reliability of lichenometric dating in a continental high altitude site: a study in the Austrian Alps. Unpublished MSc thesis. Queen Mary University of London, School of Geography.

Leigh, J. R., Stokes, C. R., Carr, R. J., Evans, I. S., Andreassen, L. M. and Evans, D. J. A. (2019) Identifying and mapping very small (<0.5 km^2) mountain glaciers on coarse to high-resolution imagery. *Journal of Glaciology*, **65**(254), 873–888.

Leigh, J. R., Stokes, C. R., Evans, D. J. A., Carr, R. J. and Andreassen, L. M. (2020) Timing of Little Ice Age maxima and subsequent glacier retreat in northern Troms and western Finnmark, northern Norway. *Arctic, Antarctic, and Alpine Research*, **52**(1), 281–311.

Leigh, J. R., Evans, D. J. A., Stokes, C. R., Andreassen, L. M. and Carr, R. J. (2021) Glacial and periglacial geomorphology of central Troms and Finnmark county, Arctic Norway. *Journal of Maps*, **17**(2), 348–366.

Leuenberger, M. C., Lang, C. and Schwander, J. (1999) Delta ^{15}N measurements as a calibration tool for the paleothermometer and gas-ice age differences: A case study for the 8200 B.P. event on GRIP ice. *Journal of Geophysical Research*, **104**, 163–170.

Lewis, W. V. (1960) The problem of cirque erosion. In Lewis, W. V. (ed.) Norwegian Cirque Glaciers. London: Royal Geographical Society, 97–100.

Lie, Ø., Dahl, S. O., Nesje, A., Matthews, J. A. and Sandvold, S. (2004) Holocene fluctuations of a polythermal glacier in high-alpine eastern Jotunheimen, central-southern Norway. *Quaternary Science Reviews*, **23**(18–19), 1925–1945.

Liermann, S., Beylich, A. A. and van Welden, A. (2012) Contemporary suspended sediment transfer and accumulation processes in the small proglacial

Sætrevatnet sub-catchment, Bødalen, western Norway. *Geomorphology*, **167**, 91–101.

Liestøl, O. (1956) Glacier Dammed Lakes in Norway. *Norsk Geografisk Tidsskrift - Norwegian Journal of Geography*, 15(3-4), 122-149.

Lilleøren, K. S. et al. (2012) The relative age of mountain permafrost - estimation of Holocene permafrost limits in Norway. *Global and Planetary Change*, **92**, 209–223.

Lilleøren, K. S. and Etzelmüller, B. (2011) A regional inventory of rock glaciers and ice-cored moraines in Norway. *Geografiska Annaler: Series A Physical Geography*, **93**(3), 175–191.

Lindahl, I., Stevens, B. P. J. and Zwaan, K. B. (2005) The geology of the Váddás area, Troms: a key to our understanding of the Upper Allochthon in the Caledonides of northern Norway. *Norges Geologiske Undersøkelse*, **445**(5), 5–43.

Lindh, L. (1984) Studies on the transitional form between snowpatch and glacier in the Abisko Mountains, Sweedish Lappland. *Svensk Geografisk Årsbok*, **60**, 145–156.

Lindner, L. and Marks, L. (1985) Types of debris slope accumulations and rock glaciers in South Spitsbergen. *Boreas*, **14**, 139–153.

Linge, H., Brook, E. J., Nesje, A., Raisbeck, G.M., Yiou, F. and Clark, H. (2006) In situ ^{10}Be exposure ages from southeastern Norway: implications for the geometry of the Weichselian Scandinavian ice sheet. *Quaternary Science Reviews*, **25**(9–10), 1097–1109.

Linge, H., Olsen, L., Brook, E. J., Darter, J. R., Mickelson, D. M., Roisbeck, G. M. and Yiou, F. (2007) Cosmogenic nuclide surface exposure ages from Nordland, northern Norway: Implications for deglaciation in a coast to inland transect. *Norsk Geologisk Tidsskrift*, **87**(1–2), 269–280.

Lippl, S., Vijay, S. and Braun, M. (2018) Automatic delineation of debris-covered glaciers using InSAR coherence derived from X-, C- and L-band radar data: A case study of Yazgyl Glacier. *Journal of Glaciology*, **64**(247), 811–821.

Livingstone, S. J., Ó Cofaigh, C. and Evans, D. J. A. (2010) A major ice drainage pathway of the last British-Irish Ice Sheet: the Tyne Gap, northern England. *Journal of Quaternary Science*, **25**(3), 354–370.

Lliboutry, L. A. (1965) Traité de glaciologie. Paris: Masson.

Lochte, A. A., Repschläger, J., Kienast, M., Garbe-Schönberg, D., Andersen, N., Hamann, C. and Schneider, R. (2019) Labrador Sea freshening at 8.5 ka BP caused by Hudson Bay Ice Saddle collapse. *Nature Communications*, **10**(1), 1–9.

Lohne, Ø. S., Mangerud, J. A. N. and Svendsen, J. I. (2012) Timing of the Younger Dryas glacial maximum in Western Norway. *Journal of Quaternary Science*, **27**(1), 81–88.

Longhi, A., Monticelli, D. and Guglielmin, M. (2020) The use of iron chemical analysis of podzols to date the Late Pleistocene – Holocene deglaciation history of the Central Italian Alps. *Journal of Quaternary Science*, **35**(8), 1021–1035.

Loso, M. G. and Doak, D. F. (2006) The biology behind lichenometric dating curves. *Oecologia*, **147**(2), 223–229.

Loso, M. G., Doak, D. F. and Anderson, R. S. (2014) Lichenometric dating of Little Ice Age glacier moraines using explicit demographic models of lichen colonization, growth, and survival. *Geografiska Annaler, Series A: Physical Geography*, **96**(1), 21–41.

Lovell, H., Stokes, C. R. and Bentley, M. J. (2011) A glacial geomorphological map of the Seno Skyring-Seno Otway-Strait of Magellan region, southernmost Patagonia. *Journal of Maps*, **7**(1), 318–339.

Lowe, J. and Walker, M. (2015) Reconstructing Quaternary Environments. 3rd edition. Oxon: Routledge.

Lukas, S. (2005) A test of the englacial thrusting hypothesis of “hummocky” moraine formation: case studies from the northwest Highlands, Scotland. *Boreas*, **34**(3), 287–307.

Lukas, S. (2006) Morphostratigraphic principles in glacier reconstruction - A perspective from the British Younger Dryas. *Progress in Physical Geography*, **30**(6), 719–736.

Lukas, S. (2012) Processes of annual moraine formation at a temperate alpine valley glacier: Insights into glacier dynamics and climatic controls. *Boreas*, **41**(3), 463–480.

Lukas, S. and Bradwell, T. (2010) Reconstruction of a Lateglacial (Younger Dryas) mountain icefield in Sutherland, northwestern Scotland, and its palaeoclimatic implications. *Journal of Quaternary Science*, **25**(4), 567–580.

Lukas, S. and Sass, O. (2011) The formation of alpine lateral moraines inferred from sedimentology and radar reflection patterns: A case study from Gornergletscher, Switzerland. *Geological Society Special Publication*, **354**, 77–92.

Lynch, C. M., Barr, I. D., Mullan, D. and Ruffell, A. (2016) Rapid glacial retreat on the Kamchatka Peninsula during the early 21st century. Cryosphere, **10**(4), 1809–1821.

Mackintosh, A. N., Anderson, B. M. and Pierrehumbert, R. T. (2017). Reconstructing Climate from Glaciers. *Annual Review of Earth and Planetary Sciences*, **45**(1), 649–680.

Magny, M. and Haas, J. N. (2004) A major widespread climatic change around 5300 cal. yr BP at the time of the Alpine Iceman. *Journal of Quaternary Science*, **19**(5), 423–430.

Mangerud, J. (2008) Scandinavian Ice Sheet. In Gornitz, V. (ed.) Encylopedia of Paleoclimatology and Ancient Environments. Dordrecht: Springer, 877–879.

Mangerud, J., Aarseth, I., Hughes, A. L., Lohne, Ø. S., Skår, K., Sønstegaard, E. and Svendsen, J. I. (2016) A major re-growth of the Scandinavian Ice Sheet in western Norway during Allerød-Younger Dryas. *Quaternary Science Reviews*, **132**, 175–205.

Mangerud, J. and Svendsen, J. I. (2018) The Holocene Thermal Maximum around Svalbard, Arctic North Atlantic; molluscs show early and exceptional warmth. *The Holocene*, **28**(1), 65–83.

Mangerund, J. (2004) Ice sheet limits on Norway and the Norwegian continental shelf. In Ehlers, J. and Gibbard, P. (eds) Quaternary Glaciations - Extent and Chronology. Volume 1. Amsterdam: Elsevier, 271–294.

Manley, G. (1955) On the occurrence of ice domes and permanently snow-covered summits. *Journal of Glaciology*, **2**(17), 453–456.

Manley, G. (1959) The late-glacial climate of north-west England. *Geological Journal*, **2**(2), 188–215.

De Marco, J. Carturan, L., Piermattei, L., Cucchiaro, S., Moro, D., Dalla Fontana, G. and Cazorzi, F. (2020) Minor imbalance of the lowermost Italian glacier from 2006 to 2019. *Water*, **12**(9), 1–21.

Margreth, A. Dyke, A. S., Gosse, J. C. and Telka, A. M. (2014) Neoglacial ice expansion and late Holocene cold-based ice cap dynamics on Cumberland

Peninsula, Baffin Island, Arctic Canada. *Quaternary Science Reviews*, **91**, 242–256.

Marks, L. and Wysokiński, L. (1986) Early Holocene glacier advance in the Austfjorden Region, northern Spitsbergen. *Bulletin of the Polish Academy of Sciences*, **34**(41), 437–446.

Marr, P., Winkler, S. and Löffler, J. (2018) Investigations on blockfields and related landforms at Blåhø (Southern Norway) using Schmidt-hammer exposure-age dating: Palaeoclimatic and morphodynamic implications. *Geografiska Annaler, Series A: Physical Geography*, **100**(3), 285–306.

Marren, P. M. (2002) Glacier margin fluctuations, Skaftafellsjökull, Iceland: Implications for sandur evolution. *Boreas*, **31**(1), 75–81.

Marshall, G. J., Dowdeswell, J. A. and Rees, W. G. (1994) The spatial and temporal effect of cloud cover on the acquisition of high quality Landsat imagery in the European Arctic sector. *Remote Sensing of Environment*, **50**(2), 149–160.

Marthinussen, M. (1962) ^{14}C-datings referring to shore lines, transgressions, and glacial substages in northern Norway. *Norsk Geologisk Undersøkelse*, **215**, 37–67.

Martin, H. E. and Whalley, W. B. (1987) Rock Glaciers part 1: rock glacier morphology: classification and distribution. *Progress in Physical Geography*, **11**(2), 260–282.

Martin, J. R. V., Davies, B. J. and Thorndycraft, V. R. (2019) Glacier dynamics during a phase of Late Quaternary warming in Patagonia reconstructed from sediment-landform associations. *Geomorphology*, 337, 111–133.

Marzeion, B., Jarosch, A. H. and Gregory, J. M. (2014) Attribution of global glacier mass loss to anthropogenic and natural causes. *Science*, **345**(6199), 919–921.

Masiokas, M. H. et al. (2009) Little Ice Age fluctuations of small glaciers in the Monte Fitz Roy and Lago del Desierto areas, south Patagonian Andes, Argentina. *Palaeogeography, Palaeoclimatology, Palaeoecology*, **281**(3–4), 351–362.

Matero, I. S. O., Gregoire, L. J., Ivanovic, R. F., Tindall, J. C. and Haywood, A. M. (2017) The 8.2 ka cooling event caused by Laurentide ice saddle collapse. *Earth and Planetary Science Letters*, **473**, 205–214.

Matero, I. S. O., Gregoire, L. J. and Ivanovic, R. F. (2020) Simulating the early Holocene demise of the Laurentide Ice Sheet with BISICLES (public trunk revision 3298). *Geoscientific Model Development*, **13**(9), 4555–4577.

Matthews, J. A. (1991) The late Neoglacial ('Little Ice Age') glacier maximum in southern Norway: new ^{14}C-dating evidence and climatic implications. *The Holocene*, **1**(3), 219–233.

Matthews, J. A., Shakesby, R. A., Berrisford, M. S. and McEwen, L. J. (1998) Periglacial Patterned Ground on the Styggedalsbreen Glacier Foreland, Jotunheimen, Southern Norway: Micro-Topographic, Paraglacial and Geoecological Controls. *Permafrost and Periglacial Processes*, **9**, 147–166.

Matthews, J. A., Dahl, S. O., Nesje, A., Berrisford, M. S. and Andersson, C. (2000) Holocene glacier variations in central Jotunheimen, southern Norway based on distal glaciolacustrine sediment cores. *Quaternary Science Reviews*, **19**(16), 1625–1647.

Matthews, J. A., Berrisford, M. S., Dresser, P. Q., Nesje, A., Dahl, S. O., Bjune, A. E., Bakke, J., John, H., Birks, B., Lie, Ø. and Dumayne-Peaty, L. (2005) Holocene glacier history of Bjørnbreen and climatic reconstruction in central Jotunheimen, Norway, based on proximal glaciofluvial stream-bank mires. *Quaternary Science Reviews*, **24**(1–2), 67–90.

Matthews, J. A. (2005) "Little Ice Age" glacier variations in Jotunheimen, southern Norway: A study in regionally controlled lichenometric dating of recessional moraines with implications for climate and lichen growth rates. *The Holocene*, **15**(1), 1–19.

Matthews, J. A. (2007) Neoglaciation in Europe. In Elias, S. A. (ed.) Encyclopedia of Quaternary Science: Second Edition. Amsterdam: Elsevier, 1122–1133.

Matthews, J. A., Shakesby, R. A., Schnabel, C. and Freeman, S. (2008) Cosmogenic ^{10}Be and ^{26}Al ages of Holocene moraines in southern Norway I: Testing the method and confirmation of the date of the Erdalen Event (c. 10 ka) at its type-site. *The Holocene*, **18**(8), 1155–1164.

Matthews, J. A., Winkler, S., Wilson, P., Tomkins, M. D., Dortch, J. M., Mourne, R. W., Hill, J. L., Owen, G. and Vater, A. E. (2018) Small rock-slope failures conditioned by Holocene permafrost degradation: a new approach and conceptual model based on Schmidt-hammer exposure-age dating, Jotunheimen, southern Norway. *Boreas*, **47**, 1144–1169.

Matthews, J. A. and Briffa, K. R. (2005) The "Little Ice Age": Re-evaluation of an evolving concept. *Geografiska Annaler: Series A, Physical Geography*, **87**(1), 17–36.

Matthews, J. A., Cornish, R. and Shakesby, R. A. (1979) “Saw-Tooth” moraines in front of Bødalsbreen, southern Norway. *Journal of Glaciology*, **22**(88), 535–546.

Matthews, J. A. and Dresser, P. Q. (2008) Holocene glacier variation chronology of the Smørstabbtindan massif, Jotunheimen, southern Norway, and the recognition of century- to millennial-scale European Neoglacial Events. *The Holocene*, **18**(1), 181–201.

Matthews, J. A., McCarroll, D. and Shakesby, R. A. (1995) Contemporary terminal-moraine ridge formation at a temperate glacier: Styggedalsbreen, Jotunheimen, southern Norway. *Boreas*, 24, 129–139.

Matthews, J. A., Nesje, A. and Linge, H. (2013) Relict talus-foot rock glaciers at Øyberget, upper Ottadalen, southern Norway: Schmidt hammer exposure ages and palaeoenvironmental implications. *Permafrost and Periglacial Processes*, **24**(4), 336–346.

Matthews, J. A. and Petch, J. R. (1982) Within-valley asymmetry and related problems of Neoglacial lateral moraine development at certain Jotunheimen glaciers, southern Norway. *Boreas*, **11**(3), 225–247.

Matthews, J. A. and Shakesby, R. A. (1984) The status of the “Little Ice Age” in southern Norway: relative-age dating of Neoglacial moraines with Schmidt hammer and lichenometry. *Boreas*, 13(3), 333–346.

Matthews, J. A. and Whittaker, R. J. (1987) Vegetation succession on the Storbreen glacier foreland, Jotunheimen, Norway: a review. *Arctic & Alpine Research*, **19**(4), 385–395.

Matthews, J. A., Wilson, P. and Mourne, R. W. (2017) Landform transitions from pronival ramparts to moraines and rock glaciers: A case study from the Smørbotn cirque, Romsdalsalpane, southern Norway. *Geografiska Annaler: Series A Physical Geography*, **99**(1), 15–37.

Matthews, J. A. and Winkler, S. (2011) Schmidt-hammer exposure-age dating (SHD): Application to early Holocene moraines and a reappraisal of the reliability of terrestrial cosmogenic-nuclide dating (TCND) at Austanbotnbreen, Jotunheimen, Norway. *Boreas*, **40**(2), 256–270.

McCall, J. G. (1952) The internal structure of a cirque glacier: report on studies of the englacial movements and temperatures. *Journal of Glaciology*, **2**(12),122-131.

McCall, J. G. (1972) The flow characteristics of a cirque glacier and their effect on cirque formation. In Embleton, C. (ed.) Glaciers and Glacial Erosion. London: Palgrave, 205–228.

McCarroll, D., Shakesby, R. A. and Matthews, J. A. (1998) Spatial and temporal patterns of late Holocene rockfall activity on a Norwegian talus slope: A lichenometric and simulation-modeling approach. *Arctic and Alpine Research*, **30**(1), 51–60.

McCarroll, D. and Ware, M. (1989) The variability of soil development on Preboreal moraine ridge crests, Breiseterdalen, southern Norway. *Norsk Geografisk Tidsskrift - Norwegian Journal of Geography*, **43**(1), 31–36.

McCarthy, D. P. (2013) Lichenometry. In Elias, S. and Mock, C. (eds) Encyclopedia of Quaternary Science. Second edition. London: Elsevier, 565–572.

McColl, S. T. (2012) Paraglacial rock-slope stability. *Geomorphology*, **153**, 1–16.

McDougall, D. (2013) Glaciation style and the geomorphological record: Evidence for Younger Dryas glaciers in the eastern Lake District, northwest England. *Quaternary Science Reviews*, **73**, 48–58.

McDougall, D. A. (1998) Loch Lomond Stadial plateau icefields in the Lake District, northwest England. Unpublished PhD thesis. University of Glasgow, Department of Geography and Topographic Science.

McDougall, D. A. (2001) The geomorphological impact of Loch Lomond (Younger Dryas) Stadial plateau icefields in the central Lake District, northwest England. *Journal of Quaternary Science*, **16**(6), 531–543.

McDougall, D. A. and Evans, D. J. A. (2015) The Quaternary of the Lake District: Field Guide. London: Quaternary Research Association.

Medeiros, A. S., Wood, P., Wesche, S. D., Bakaic, M. and Peters, J. F. (2017) Water security for northern peoples: review of threats to Arctic freshwater systems in Nunavut, Canada. *Regional Environmental Change*, **17**(3), 635–647.

Van Der Meer, J. J. M., Menzies, J. and Rose, J. (2003) Subglacial till: The deforming glacier bed. *Quaternary Science Reviews*, **22**(15–17), 1659–1685.

Meier, K. D., Thannheiser, D., Wehberg, J. and Eisenmann, V. (2005) Soils and nutrients in northern mountain birch forests: A case study from Finnmarksvidda, northern Norway. In Wielgolaski, F. E., Karlsson, P. S., and Thannheiser, D. (eds) Plant Ecology, Herbivory, and Human Impact in Nordic Mountain Birch Forests. Berlin: Springer, 19–33

Meier, W. J. H., Grießinger, J., Hochreuther, P. and Braun, M. H. (2018) An updated multi-temporal glacier inventory for the Patagonian Andes with changes between the Little Ice Age and 2016. *Frontiers in Earth Science*, **6**, 1–21.

Mendelová, M., Hein, A. S., Rodes, A., Smedley, R. K. and Xu, S. (2020) Glacier expansion in central Patagonia during the Antarctic Cold Reversal followed by retreat and stabilisation during the Younger Dryas. *Quaternary Science Reviews*, **227**, 1–19.

Menounos, B., Clague, J. J., Clarke, G. K., Marcott, S. A., Osborn, G., Clark, P. U., Tennant, C. and Novak, A. M. (2013) Did rock avalanche deposits modulate the late Holocene advance of Tiedemann Glacier, southern Coast Mountains, British Columbia, Canada? *Earth and Planetary Science Letters*, **384**, 154–164.

Mercier, D. (2008a) Paraglacial and paraperiglacial landsystems: Concepts, temporal scales and spatial distribution. *Géomorphologie: Relief, Processus, Environnement*, **320**(1), 133–144.

Mercier, D. (2008b) Paraglacial geomorphology: Conceptual and methodological revival. *Géomorphologie: Relief, Processus, Environnement*, **4**, 219–222.

Milfont, T. L., Wilson, M. S. and Sibley, C. G. (2017) The public's belief in climate change and its human cause are increasing over time. *PLoS ONE*, **12**(3), 1–9.

Millar, C. I. and Westfall, R. D. (2008) Rock glaciers and related periglacial landforms in the Sierra Nevada, CA, USA; inventory, distribution and climatic relationships. *Quaternary International*, **188**(1), 90–104.

Miller, G. H., Alley, R. B., Brigham-Grette, J., Fitzpatrick, J. J., Polyak, L., Serreze, M. C. and White, J. W. (2010) Arctic amplification: Can the past constrain the future? *Quaternary Science Reviews*, **29**(15–16), 1779–1790.

Molnia, B. F. (2004) Glossary of Glacier Terminology, U.S. Geological Survey. https://pubs.usgs.gov/of/2004/1216/. (Accessed on: 18.06.2018).

Monnier, S. and Kinnard, C. (2015) Reconsidering the glacier to rock glacier transformation problem: New insights from the central Andes of Chile. *Geomorphology*, **238**, 47–55.

Moran, A. P., Ivy-Ochs, S., Schuh, M., Christl, M. and Kerschner, H. (2016a) Evidence of central Alpine glacier advances during the Younger Dryas-early Holocene transition period. *Boreas*, **45**, 398–410.

Moran, A. P., Kerschner, H. and Ochs, S. I. (2016b) Redating the moraines in the Kromer Valley (Silvretta Mountains) – New evidence for an early Holocene glacier advance. *The Holocene*, **26**(4), 655–664.

Morehouse, H. and Cigliano, M. (2021) Cultures and Concepts of Ice: Listening for Other Narratives in the Anthropocene. *Annals of the American Association of Geographers*, **111**(3), 913–920.

Movia, A., Beinat, A. and Crosilla, F. (2016) Shadow detection and removal in RGB VHR images for land use unsupervised classification. *ISPRS Journal of Photogrammetry and Remote Sensing*, **119**, 485–495.

Murton, J. B. (2021) What and where are periglacial landscapes? *Permafrost and Periglacial Processes*, **32**, 186–212.

Murton, J. B. and Ballantyne, C. K. (2017) Periglacial and permafrost ground models for Great Britain. In Griffiths, J. S. and Martin, C. J. (eds) Engineering Geology and Geomorphology of Glaciated and Periglaciated Terrain. London: Geological Society, 501–579.

Muscheler, R., Beer, J. and Vonmoos, M. (2004) Causes and timing of the 8200 yr BP event inferred from the comparison of the GRIP ^{10}Be and the tree ring Δ^{14}C record', *Quaternary Science Reviews*, **23**(20), 2101–2111

Mutz, S., Paeth, H. and Winkler, S. (2016) Modelling of future mass balance changes of Norwegian glaciers by application of a dynamical–statistical model. *Climate Dynamics*, **46**(5–6), 1581–1597.

Naegeli, K. and Huss, M. (2017) Sensitivity of mountain glacier mass balance to changes in bare-ice albedo. *Annals of Glaciology*, **58**(75), 119–129.

Nagy, T. and Andreassen, L. M. (2019) Glacier surface velocity mapping with Sentinel-2 imagery in Norway. *NVE Rapport* **37**, 1–35

Najafi, M. R., Zwiers, F. W. and Gillett, N. P. (2013) Attribution of Arctic temperature change to greenhouse-gas and aerosol influences. In Climate Change 2013: The Physical Science Basis. Contribution of Working Group I to the Fifth Assessment Report of the Intergovernmental Panel on Climate Change. Cambridge: Cambridge University Press.

Narama, C., Kääb, A., Duishonakunov, M. and Abdrakhmatov, K. (2010) Spatial variability of recent glacier area changes in the Tien Shan Mountains, Central Asia, using Corona (~ 1970), Landsat (~ 2000), and ALOS (~ 2007) satellite data. *Global and Planetary Change*, **71**(1–2), 42–54.

Nesje, A. (1984) Kvartærgeologiske undersøkingar i Erdalen, Stryn, Sogn og Fjordane. University of Bergen.

Nesje, A., Kvamme, M., Rye, N. and Løvlie, R. (1991) Holocene glacial and climate history of the Jostedalsbreen region, Western Norway: Evidence from lake sediments and terrestrial deposits. *Quaternary Science Reviews*, **10**(1), 87–114.

Nesje, A., Dahl, S. O., Løvlie, R. and Sulebak, J. R. (1994) Holocene glacier activity at the southwestern part of Hardangerjøkulen, central-southern Norway: Evidence from lacustrine sediments. *The Holocene*, **4**(4), 377–382.

Nesje, A., Dahl, S. O., Andersson, C. and Matthews, J. A. (2000a) The lacustrine sedimentary sequence in Sygneskardvatnet, western Norway: A continuous, high-resolution record of the Jostedalsbreen ice cap during the Holocene. *Quaternary Science Reviews,* **19**(11), 1047–1065.

Nesje, A., Matthews, J. A., Dahl, S. O., Berrisford, M. S. and Andersson, C. (2001) Holocene glacier fluctuations of Flatebreen and winter-precipitation changes in the Jostedalsbreen region, western Norway, based on glaciolacustrine sediment records. *The Holocene*, **11**(3), 267–280.

Nesje, A. (2005) Briksdalsbreen in western Norway: AD 1900-2004 frontal fluctuations as a combined effect of variations in winter precipitation and summer temperature. *The Holocene*, **15**(8), 1245–1252.

Nesje, A., Bjune, A. E., Bakke, J., Dahl, S. O., Lie, Ø. and Birks, H. J. B. (2006) Holocene palaeoclimate reconstructions at Vanndalsvatnet, western Norway, with particular reference to the 8200 cal. yr BP event. *The Holocene*, **16**(5), 717–729.

Nesje, A., Bakke, J., Dahl, S. O., Lie, Ø. and Matthews, J. A. (2008) Norwegian mountain glaciers in the past, present and future. *Global and Planetary Change*, **60**(1–2), 10–27.

Nesje, A. (2009) Latest Pleistocene and Holocene alpine glacier fluctuations in Scandinavia. *Quaternary Science Reviews*, **28**(21), 2119–2136.

Nesje, A. and Dahl, S. O. (1991a) Holocene glacier variations of Blåisen, Hardangerjøkulen, central Southern Norway. *Quaternary Research*, **35**, 25–40.

Nesje, A. and Dahl, S. O. (1991b) Late Holocene glacier fluctuations in Bevringsdalen, Jostedalsbreen region, western Norway (ca 3200-1400 BP). *The Holocene*, **1**(1), 1–7.

Nesje, A. and Dahl, S. O. (2000) Glaciers and Environmental Change. First Edition. London: Routledge.

Nesje, A. and Dahl, S. O. (2001) The Greenland 8200 cal. yr BP event detected in loss-on-ignition profiles in Norwegian lacustrine sediment sequences. *Journal of Quaternary Science*, **16**(2), 155–166.

Nesje, A. and Dahl, S. O. (2003) The “Little Ice Age” - only temperature? *The Holocene*, **13**(1), 139–145.

Nesje, A. and Kvamme, M. (1991) Holocene glacier and climate variations in western Norway: Evidence for early or early Holocene glacier demise and multiple Neoglacial events. *Geology*, **19**, 610–612.

Nesje, A., Lie, Ø. and Dahl, S. O. (2000b) Is the North Atlantic Oscillation reflected in Scandinavian glacier mass balance records? *Journal of Quaternary Science*, **15**(6), 587–601.

Nesje, A. and Matthews, J. A. (2011) The Briksdalsbre Event: A winter precipitation-induced decadal-scale glacial advance in southern Norway in the and 1990s and its implications. *The Holocene*, **22**(2), 249–261.

Newton, M. Evans, D. J. A., Roberts, D. H. and Stokes, C. R. (2018) Bedrock mega-grooves in glaciated terrain: A review. *Earth-Science Reviews*, **185**, 57–79.

NGU (2021) Superficial deposits - National Database (online). http://geo.ngu.no/kart/losmasse_mobil/. Accessed on: multiple times thought-out 2018-2021

Nicolussi, K. and Patzelt, G. (2001) Untersuchungen zur holozänen Gletscherentwicklung von Pasterze und Gepatschferner (Ostalpen). *Zeitschrift fur Gletscherkunde und Glazialgeologie*, **36**, 1–88.

Nicolussi, K. and Schlüchter, C. (2012) The 8.2 ka event-Calendar-dated glacier response in the Alps. *Geology*, 40(9), 819–822.

Nojarov, P., Gachev, E. and Grünewald, K. (2019) Recent behavior and possible future evolution of the glacieret in the cirque Golemiya Kazan in the Pirin Mountains under conditions of climate warming. *Journal of Mountain Science*, **16**(1), 16–29.

Norges Geologiske Undersogelse (2019) Unstable mountain range danger level info. National Database for Unstable Rock Slopes. http://geo.ngu.no/kart/ustabilefjellparti_mobil/. Accessed: 16.08.2021

Norwegian Polar Institute (2021) Climate change in the Arctic. https://www.npolar.no/en/themes/climate-change-in-the-arctic/#tab-id-1. Accessed on: 23.03.2021.

Nussbaumer, S. U., Nesje, A. and Zumbühl, H. J. (2011) Historical glacier fluctuations of jostedalsbreen and folgefonna (southern Norway) reassessed by new pictorial and written evidence. *The Holocene*, **21**(3), 455–471.

Nydal, E. (1960) Trondheim natural radiocarbon measurements II. *Radiocarbon*, **2**, 82–96.

O'Neal, M. A. (2006) The effects of slope degradation on lichenometric dating of Little Ice Age moraines. *Quaternary Geochronology*, **1**(2), 121–128.

O'Neal, M. A. (2016) Lichenometric dating: Science or pseudo-science? - Comment to the paper published by Osborn, McCarthy, LaBrie, and Burke, Quaternary Research, 83, 1–12. *Quaternary Research*, **86**, 242–243.

Ó Cofaigh, C. et al. (1999) Glacial landform-sediment assemblages in the Canadian High Arctic and their implications for late Quaternary glaciation. *Annals of Glaciology*, **28**, 195–201.

Ó Cofaigh, C. and Evans, D. J. A. (2001) Sedimentary evidence for deforming bed conditions associated with a grounded Irish Sea glacier, southern Ireland. *Journal of Quaternary Science*, **16**(5), 435–454.

Ó Cofaigh, C., Evans, D. J. A. and England, J. (2003) Ice-marginal terrestrial landsystems: sub-polar glacier margins of the Canadian and Greenland high Arctic. In Evans, D. J. A. (ed.) Glacial Landsystems. London: Arnold, 44–64.

Ødegård, R. S., Nesje, A., Isaksen, K. and Eiken, T. (2011) Perennial ice patch studies – preliminary results from a case study in Jotunheimen, southern Norway. *Geophysical Research Abstracts*, **13**, EGU2011-12027

Ødegärd, R. S., Nesje, A., Isaksen, K., Andreassen, L. M., Eiken, T., Schwikowski, M. and Uglietti, C. (2017) Climate change threatens archaeologically significant ice patches: Insights into their age, internal structure, mass balance and climate sensitivity. *The Cryosphere*, **11**(1), 17–32.

Oerlemans, J. (1994) Quantifying Global Warming from the Retreat of Glaciers. *Science*, **264**(5156), 243–245.

Oerlemans, J. (2005) Extracting a Climate Signal from 169 Glacier Records. *Science*, **308**(5722), 675–677.

Oerlemans, J. (2007) Estimating response times of Vadret da Morteratsch, Vadret da Palü, Briksdalsbreen and Nigardsbreen from their length records. *Journal of Glaciology*, **53**(182), 357–362.

Oestreich, K. (1906) Die Täler des nordwestlichen Himalaya: Beobachtungen und studien. *Petermanns Mitteilungen*, **155**(33).

Ojha, S., Fujita, K., Asahi, K., Sakai, A., Lamsal, D., Nuimura, T. and Nagai, H. (2016) Glacier area shrinkage in eastern Nepal Himalaya since 1992 using high-resolution inventories from aerial photographs and ALOS satellite images. *Journal of Glaciology*, **62**(233), 512–524.

Olsen, L., Fredin, O. and Olesen, O. (eds) (2013) Quaternary Geology of Norway. Geological. Trondheim: Norges Geologiske Undersøkelse.

Oltmanns, M., Straneo, F. and Tedesco, M. (2019) Increased Greenland melt triggered by large-scale, year-round cyclonic moisture intrusions. *The Cryosphere*, **13**(3), 815–825.

Oppo, D.W., McManus, J.F. and Cullen, J.L. (2003) Deepwater variability in the Holocene epoch. *Nature*, **422**(6929), 277-277.

Osborn, G. (1986) Lateral-Moraine Stratigraphy and Neoglacial History of Bugaboo Glacier, British Columbia. *Quaternary Research*, **178**, 171–178.

Osborn, G., McCarthy, D., LaBrie, A. and Burke, R. (2015) Lichenometric dating: Science or pseudo-science? *Quaternary Research*, **83**(1), 1–12.

Øseth, E. (2011) Climate Change in the Norwegian Arctic: consequences for life in the north, NorACIA. Tromsø: Norwegian Polar Institute

Østrem, G., Haakensen, N. and Melander, O. (1973) Atlas over breer i Nord-Skandinavia (Glacier Atlas of Northern Scandanavia). Norges Vassdrags-og Elektrisitetsvesen og Stockholms Universitet.

Østrem, G., Liestøl, O. and Wold, B. (1976) Glaciological investigations at Nigardsbreen, Norway. *Norsk Geografisk Tidsskrift - Norwegian Journal of Geography*, **30**(4), 187–209.

Overpeck, J., Hughen, K., Hardy, D., Bradley, R., Case, R., Douglas, M., Finney, B., Gajewski, K., Jacoby, G., Jennings, A. and Lamoureux, S. (1997) Arctic environmental changes of the last four centuries. *Science*, **278**(5341), 1251–1256

Owen, L. A. (1994) Glacial and non-glacial diamictons in the Karakoram Mountains and western Himalayas. In Warren, W. P. and Groot, D. G. (eds) Meeting of the

commission on the formation and deformation of glacial deposits. Rotterdam: A. A. Balkema, 9–28.

Owen, L. A. (1998) Timing and Style of Glaciation in the Himalaya. *Himalayan Geology*, **19**(2), 39–47.

Owen, L. A. and Derbyshire, E. (1989) The Karakoram glacial depositional system. *Zeitschrift für Geomorphologie*, **76**, 33–73.

Paasche, Ø., Dahl, S. O., Bakke, J., Løvlie, R. and Nesje, A. (2007) Cirque glacier activity in arctic Norway during the last deglaciation. *Quaternary Research*, **68**(3), 387–399.

Pan, C. G., Pope, A., Kamp, U., Dashtseren, A., Walther, M. and Syromyatina, M. V. (2018) Glacier recession in the Altai Mountains of Mongolia in 1990–2016. *Geografiska Annaler: Series A Physical Geography*, **100**(2), 185–203.

Park, H. S., Kim, S. J., Stewart, A. L., Son, S. W. and Seo, K. H. (2019) Mid-Holocene Northern Hemisphere warming driven by Arctic amplification. *Science Advances*, **5**(12), 1–10.

Parkes, D. and Marzeion, B. (2018) Twentieth-century contribution to sea-level rise from uncharted glaciers. *Nature*, **563**(7732), 551–554.

Paul, F., Kääb, A., Maisch, M., Kellenberger, T. and Haeberli, W. (2004) Rapid disintegration of Alpine glaciers observed with satellite data. Geophysical Research Letters, **31**(21), 12–15.

Paul, F., Barry, R. G., Cogley, J. G., Frey, H., Haeberli, W., Ohmura, A., Ommanney, C. S. L., Raup, B., Rivera, A. and Zemp, M. (2009) Recommendations for the compilation of glacier inventory data from digital sources. *Annals of Glaciology*, **50**(53), 119–126.

Paul, F., Barry, R., Cogley, G., Frey, H., Haeberli, W., Ohmura, A., Ommanney, C. S. L., Raup, B., Rivera, A. and Zemp, M. (2010) Guidelines for the compilation of glacier inventory parameters from digital sources. Zürich: World Glacier Monitoring Service (WGMS), 1–23.

Paul, F., Barrand, N. E., Baumann, S., Berthier, E., Bolch, T., Casey, K., Frey, H., Joshi, S. P., Konovalov, V., Le Bris, R. and Mölg, N. (2013) On the accuracy of glacier outlines derived from remote-sensing data. *Annals of Glaciology*, **54**(63), 171–182.

Paul, F., Bolch, T., Kääb, A., Nagler, T., Nuth, C., Scharrer, K., Shepherd, A., Strozzi, T., Ticconi, F., Bhambri, R. and Berthier, E. (2015) The glaciers climate change

initiative: Methods for creating glacier area, elevation change and velocity products. *Remote Sensing of Environment*, **162**, 408–426.

Paul, F., Winsvold, S. H., Kääb, A., Nagler, T. and Schwaizer, G. (2016) Glacier remote sensing using Sentinel-2. part II: Mapping glacier extents and surface facies, and comparison to Landsat 8. *Remote Sensing*, **8**(7), 1–15.

Paul, F. and Andreassen, L. M. (2009) A new glacier inventory for the Svartisen area (Norway) from Landsat ETM+: Methodological challenges and first results. *Journal of Glaciology*, **55**(192), 607–618.

Paul, F., Frey, H. and Bris, R. L. (2011) A new glacier inventory for the European Alps from Landsat TM scenes of 2003: Challenges and results. *Annals of Glaciology*, **52**(59), 144–152.

Paul, F., Machguth, H. and Kääb, A. (2005) On the impact of glacier albedo under conditions of extreme glacier melt: the summer of 2003 in the Alps. *EARSeL eProceedings*, **4**(2), 139–149.

Paul, F. and Mölg, N. (2014) Hasty retreat of glaciers in northern Patagonia from 1985 to 2011. *Journal of Glaciology*, **60**(224), 1033–1043.

Paus, A. (1995) The Late Weichselian and early Holocene history of tree birch in south Norway and the Bølling Betula time-lag in northwest Europe *Review of Palaeobotany and Palynology*, **85**(3), 243–262.

Paus, A. et al. (2006) Lateglacial nunataks in central Scandinavia: Biostratigraphical evidence for ice thickness from Lake Flåfattjønn, Tynset, Norway. Q*uaternary Science Reviews*, **25**(11), 1228–1246.

Paus, A., Haflidason, H., Routh, J., Naafs, B. D. A. and Thoen, M. W. (2019) Environmental responses to the 9.7 and 8.2 cold events at two ecotonal sites in the Dovre mountains, mid-Norway. *Quaternary Science Reviews*, **205**, 45–61.

Pawłowska, J., Łącka, M., Kucharska, M., Pawlowski, J. and Zajączkowski, M. (2020) Multiproxy evidence of the Neoglacial expansion of Atlantic Water to eastern Svalbard. *Climate of the Past*, **16**(2), 487–501.

Pedro, J. B., Van Ommen, T. D., Rasmussen, S. O., Morgan, V. I., Chappellaz, J., Moy, A. D., Masson-Delmotte, V. and Delmotte, M. (2011) The last deglaciation: Timing the bipolar seesaw. *Climate of the Past*, **7**(2), 671–683.

Pellikka, P. and Rees, W. G. (eds) (2009) Remote Sensing of Glaciers: Techniques for Topographic, Spatial and Thematic Mapping of Glaciers. London: CRC Press.

Pendleton, S. L. Briner, J. P., Kaufman, D. S. and Zimmerman, S. R. (2017) Using Cosmogenic ^{10}Be Exposure Dating and Lichenometry to Constrain Holocene Glaciation in the Central Brooks Range, Alaska. *Arctic, Antarctic, and Alpine Research*, **49**(1), 115–132.

Pfeffer, W. T., Arendt, A. A., Bliss, A., Bolch, T., Cogley, J. G., Gardner, A. S., Hagen, J. O., Hock, R., Kaser, G., Kienholz, C. and Miles, E. S. (2014) The Randolph Glacier Inventory: A globally complete inventory of glaciers. *Journal of Glaciology*, **60**(221), 537–552.

Philipps, W. Briner, J. P., Gislefoss, L., Linge, H., Koffman, T., Fabel, D., Xu, S. and Hormes, A. (2017) Late Holocene glacier activity at inner Hornsund and Scottbreen, southern Svalbard. *Journal of Quaternary Science*, **32**(4), 501–515.

Phillips, D. H. and Fitzpatrick, E. A. (1999) Biological influences on the morphology and micromorphology of selected Podzols (Spodosols) and Cambisols (Inceptisols) from the eastern United States and north-east Scotland. *Geoderma*, **90**(3), 327–364.

Pissart, A., Calmels, F. and Wastiaux, C. (2011) The potential lateral growth of lithalsas. *Quaternary Research*, **75**(2), 371–377.

Pithan, F. and Mauritsen, T. (2014) Arctic amplification dominated by temperature feedbacks in contemporary climate models. *Nature Geoscience*, **7**(3), 181–184.

Plassen, L. and Vorren, T. O. (2003) Sedimentary processes and the environment during deglaciation of a fjord basin in Ullsfjorden, North Norway. *Norsk Geologisk Tidsskrift*, **83**(1), 23–36.

Porter, C., Morin, P., Howat, I., Noh, M., Bates, B., Peterman, K., Keesey, S., Schlenk, M., Gardiner, J. and Tomko, K. (2018) ArcticDEM. Minneapolis: Polar Geospatial Center.

Powell, J. (2017) Scientists reach 100% consensus on anthropogenic global warming. *Bulletin of Science, Technology and Society*, **37**(4), 183–184.

Powell, J. L. (2015) Climate scientists virtually unanimous: Anthropogenic global warming is true. *Bulletin of Science, Technology & Society*, **35**(5–6), 121–124.

Pratt-Sitaula, B., Burbank, D. W., Heimsath, A. M., Humphrey, N. F., Oskin, M. and Putkonen, J. (2011) Topographic control of asynchronous glacial advances: A case study from Annapurna, Nepal. *Geophysical Research Letters*, **38**(24), 1–6.

Price, R. J. (1966) Eskers near the Casement Glacier, Alaska. *Geografiska Annaler: Series A, Physical Geography*, **48**(3), 111–125.

Price, R. J. (1969) Moraines, Sandar, Kames and Eskers near Breidamerkurjökull, Iceland. *Transactions of the Institute of British Geographers*, **46**, 17–43.

Price, R. J. (1970) Moraines at Fjallsjokull, Iceland. *Arctic and Alpine Research*, **2**(1), 27–42.

Price, R. J. (1971) The Development and Destruction of a Sandur, Breidamerkurjokull, Iceland. *Arctic and Alpine Research*, **3**(3), 225–237.

Protin, M., Schimmelpfennig, I., Mugnier, J. L., Ravanel, L., Le Roy, M., Deline, P., Favier, V., Buoncristiani, J. F., Aumaitre, G., Bourlès, D. L. and Keddadouche, K. (2019) Climatic reconstruction for the Younger Dryas/Early Holocene transition and the Little Ice Age based on paleo-extents of Argentière glacier (French Alps). *Quaternary Science Reviews*, **221**, 1–15.

Purdie, H., Gomez, C. and Espiner, S. (2015) Glacier recession and the changing rockfall hazard: Implications for glacier tourism. *New Zealand Geographer*, **71**(3), 189–202.

Putnam, A. E., Denton, G. H., Schaefer, J. M., Barrell, D. J., Andersen, B. G., Finkel, R. C., Schwartz, R., Doughty, A. M., Kaplan, M. R. and Schlüchter, C. (2010) Glacier advance in southern middle-latitudes during the Antarctic Cold Reversal. *Nature Geoscience*, **3**(10), 700–704.

Putnam, A. E., Schaefer, J. M., Denton, G. H., Barrell, D. J., Finkel, R. C., Andersen, B. G., Schwartz, R., Chinn, T. J. and Doughty, A. M. (2012) Regional climate control of glaciers in New Zealand and Europe during the pre-industrial Holocene. *Nature Geoscience*, **5**(9), 627–630.

Rabatel, A., Ceballos, J. L., Micheletti, N., Jordan, E., Braitmeier, M., González, J., Mölg, N., Ménégoz, M., Huggel, C. and Zemp, M. (2018) Toward an imminent extinction of Colombian glaciers? *Geografiska Annaler: Series A Physical Geography*, **100**(1), 75–95.

Racoviteanu, A. E., Paul, F., Raup, B., Khalsa, S. J. S. and Armstrong, R. (2009) Challenges and recommendations in mapping of glacier parameters from

space: Results of the 2008 global land ice measurements from space (GLIMS) workshop, Boulder, Colorado, USA. *Annals of Glaciology*, **50**(53), 53–69.

Racoviteanu, A. E. Arnaud, Y., Williams, M. W. and Manley, W. F. (2015) Spatial patterns in glacier characteristics and area changes from 1962 to 2006 in the Kanchenjunga-Sikkim area, eastern Himalaya. *The Cryosphere*, **9**(2), 505–523.

Randal, B. A. O. (1971) The igneous rocks of the Lyngen Peninsula, Troms, Norway. *Norges Geologiske Undersøkelse*, **269**, 143–146.

Rangecroft, S., Harrison, S., Anderson, K., Magrath, J., Castel, A. P. and Pacheco, P. (2013) Climate change and water resources in arid mountains: An example from the Bolivian Andes. *Ambio*, **42**(7), 852–863.

Rangecroft, S., Harrison, S. and Anderson, K. (2015) Rock glaciers as water stores in the Bolivian Andes: An assessment of their hydrological importance. *Arctic, Antarctic, and Alpine Research*, **47**(1), 89–98.

Rasmussen, L. A. (2007) Spatial extent of influence on glacier mass balance of North Atlantic circulation indices. *Terra Glacialis*, **11**, 43–58.

Rastner, P., Bolch, T., Mölg, N., Machguth, H., Le Bris, R. and Paul, F. (2012) The first complete inventory of the local glaciers and ice caps on Greenland. *The Cryosphere*, **6**(6), 1483–1495.

Raup, B., Kääb, A., Kargel, J. S., Bishop, M. P., Hamilton, G., Lee, E., Paul, F., Rau, F., Soltesz, D., Khalsa, S. J. S. and Beedle, M. (2007) Remote sensing and GIS technology in the Global Land Ice Measurements from Space (GLIMS) Project. *Computers and Geosciences*, **33**(1), 104–125.

Raup, B. and Khalsa, S. J. S. (2010) GLIMS Analysis Tutorial. *GLIMS*, 1–15.

Ravanel, L. and Deline, P. (2011) Climate influence on rockfalls in high-alpine steep rockwalls: The north side of the Aiguilles de Chamonix (Mont Blanc Massif) since the end of the “Little Ice Age”. *The Holocene*, **21**(2), 357–365.

Rea, B. R., Whalley, W. B., Rainey, M. M. and Gordon, J. E. (1996) Blockfields, old or new? Evidence and implications from some plateaus in northern Norway. *Geomorphology*, **15**, 109–121.

Rea, B. R., Whalley, W. B., Evens, D. J. A., Gordon, J. E. and McDougall, D. A. (1998) Plateau Icefields: Geomorphology and dynamics. *Quaternary Proceedings*, **6**, 35–54.

Rea, B. R., Whalley, W. B., Dixon, T. S. and Gordon, J. E. (1999) Plateau icefields as contributing areas to valley glaciers and the potential impact on reconstructed

ELAs: A case study from the Lyngen Alps, North Norway. *Annals of Glaciology*, **28**, 97–102.

Rea, B. R. and Evans, D. J. A. (2003) Plateau Icefield Landsystems. In Evans, D. J. A. (ed.) Glacial Landsystems. London: Arnold, 407–431.

Rea, B. R. and Evans, D. J. A. (2007) Quantifying climate and glacier mass balance in north Norway during the Younger Dryas. *Palaeogeography, Palaeoclimatology, Palaeoecology*, **246**(2–4), 307–330.

Reichert, B. K., Bengtsson, L. and Oerlemans, J. (2002) Recent glacier retreat exceeds internal variability. *Journal of Climate*, **15**, 3069–3081.

Reinardy, B. T. I., Leighton, I. and Marx, P. J. (2013) Glacier thermal regime linked to processes of annual moraine formation at Midtdalsbreen, southern Norway. *Boreas*, **42**(4), 896–911.

Rekstad, J. (1892) Om Svartisen og dens gletchere. *Norsk Geografisk Selskabs Aarbog*, **3**, 71–90.

Rekstad, J. (1900) Om periodiske forandringer hos norske braser. *Norges Geologiske Undersogelse*, **28**(4), 1–15.

Rekstad, J. (1904) Fra Jostedalsbræen. *Bergens Museums Aarbog*, **1**, 1–69.

Rekstad, J. (1910) Forandringer ved norske breer i aaret 1908-09. *Bergens Museums Aarbog*, **4**, 2–12.

Rekstad, J. (1915) Forandringer ved norske bræer i äret 1913–14. *Bergen Museums Arbok*, **7**, 1–5.

Renssen, H., Seppä, H., Heiri, O., Roche, D. M., Goosse, H. and Fichefet, T. (2009) The spatial and temporal complexity of the Holocene Thermal Maximum. *Nature Geoscience*, **2**(6), 411–414.

Renssen, H., Seppä, H., Crosta, X., Goosse, H. and Roche, D. M. (2012) Global characterization of the Holocene Thermal Maximum. *Quaternary Science Reviews*, **48**, 7–19.

Renssen, H., Goosse, H. and Fichefet, T. (2002) Modelling the effect of freshwater pulses on the early Holocene climate: The influence of high-frequency climate variability. *Paleoceanography*, **17**(2), 10–16

Reusche, M., Winsor, K., Carlson, A. E., Marcott, S. A., Rood, D. H., Novak, A., Roof, S., Retelle, M., Werner, A., Caffee, M. and Clark, P. U. (2014) ^{10}Be surface exposure ages on the late-Pleistocene and Holocene history of Linnébreen on Svalbard. *Quaternary Science Reviews*, **89**, 5–12.

Reyes, A. V. and Clague, J. J. (2004) Stratigraphic evidence for multiple Holocene advances of Lillooet Glacier, southern Coast Mountains, British Columbia. *Canadian Journal of Earth Sciences*, **41**(8), 903–918.

Reynolds, R. (2007) Jonny Sniper. Take to the Skies (album) - Enter Shikari. St. Albans, UK: Ambush Reality.

Reynolds, R. (2012) System... A Flash Flood of Colour (album) - Enter Shikari. St. Albans, UK: Ambush Reality.

Reynolds, R. (2015a) Myopia. The Mindsweep (album) - Enter Shikari. St. Albans, UK: Ambush Reality.

Reynolds, R. (2015b) The Appeal & The Mindsweep Part I. The Mindsweep (album) - Enter Shikari. St. Albans, UK: Ambush Reality.

Reynolds, R. (2017) The Sights. The Spark (album) - Enter Shikari. St. Albans, UK: Ambush Reality.

Reynolds, R. (2020) Modern Living. Nothing Is True & Everything Is Possible (album) - Enter Shikari. St. Albans, UK: Ambush Reality.

Reznichenko, N. V., Davies, T. R. H. and Alexander, D. J. (2011) Effects of rock avalanches on glacier behaviour and moraine formation. *Geomorphology*, **132**(3–4), 327–338.

Richardson, C. and Holmlund, P. (1996) Glacial cirque formation in northern Scandinavia. *Annals of Glaciology*, **22**, 102–106.

Richter, R. and Müller, A. (2005) De-shadowing of satellite/airborne imagery. *International Journal of Remote Sensing*, **26**(15), 3137–3148.

Righi, D., Huber, K. and Keller, C. (1999) Clay formation and podzol development from postglacial moraines in Switzerland. *Clay Minerals*, **34**, 319–332.

Risebrobakken, B., Jansen, E., Andersson, C., Mjelde, E. and Hevrøy, K. (2003) A high-resolution study of Holocene paleoclimatic and paleoceanographic changes in the Nordic Seas. *Paleoceanography*, **18**(1), 1–14

Rizzi, J., Nilsen, I. B., Stagge, J. H., Gisnås, K. and Tallaksen, L. M. (2018) Five decades of warming: Impacts on snow cover in Norway. *Hydrology Research*, ***49***(3), 670–688.

Robinson, Z. P., Fairchild, I. J. and Russell, A. J. (2008) Hydrogeological implications of glacial landscape evolution at Skeiðarársandur, SE Iceland. *Geomorphology*, **97**(1–2), 218–236.

Roe, G. H., Baker, M. B. and Herla, F. (2017) Centennial glacier retreat as categorical evidence of regional climate change. *Nature Geoscience*, **10**(2), 95–99.

Rogers, J. C. and Mchugh, M. J. (2002) On the separability of the North Atlantic Oscillation and Arctic Oscillation. *Climate Dynamics*, **19**, 599–608.

Rohling, E. E. and Pälike, H. (2005) Centennial-scale climate cooling with a sudden cold event around 8,200 years ago. *Nature*, **434**(7036), 975–979.

Romundset, A., Akçar, N., Fredin, O., Tikhomirov, D., Reber, R., Vockenhuber, C., Christl, M. and Schlüchter, C. (2017) Lateglacial retreat chronology of the Scandinavian Ice Sheet in Finnmark, northern Norway, reconstructed from surface exposure dating of major end moraines. *Quaternary Science Reviews*, **177**, 130–144.

Romundset, A., Bondevik, S. and Bennike, O. (2011) Postglacial uplift and relative sea level changes in Finnmark, northern Norway. *Quaternary Science Reviews*, **30**(19–20), 2398–2421.

Roof, S. and Werner, A. (2011) Indirect growth curves remain the best choice for lichenometry: Evidence from directly measured growth rates from Svalbard. *Arctic, Antarctic, and Alpine Research*, **43**(4), 621–631.

Rosén, P., Segerström, U., Eriksson, L., Renberg, I. and Birks, H. J. B. (2001) Holocene climatic change reconstructed from diatoms, chironomids, pollen and near-infrared spectroscopy at an alpine lake (Sjuodjijaure) in northern Sweden. *The Holocene*, **11**(5), 551–562.

Rosenwinkel, S., Korup, O., Landgraf, A. and Dzhumabaeva, A. (2015) Limits to lichenometry. *Quaternary Science Reviews*, **129**, 229–238.

Rosqvist, G., Jonsson, C., Yam, R., Karlén, W. and Shemesh, A. (2004) Diatom oxygen isotopes in pro-glacial lake sediments from northern Sweden: A 5000 year record of atmospheric circulation. *Quaternary Science Reviews*, **23**(7–8), 851–859.

Rosqvist, G. C. and Østrem, G. (1989) The sensitivity of a small ice cap to climatic fluctuations. *Geografiska Annaler: Series A Physical Geography*, **71**(1), 99–103.

Le Roy, M., Nicolussi, K., Deline, P., Astrade, L., Edouard, J.L., Miramont, C. and Arnaud, F. (2015) Calendar-dated glacier variations in the western European Alps during the Neoglacial: The Mer de Glace record, Mont Blanc Massif. *Quaternary Science Reviews*, **108**, 1–22.

Le Roy, M., Deline, P., Carcaillet, J., Schimmelpfennig, I., Ermini, M. and ASTER Team, (2017) ^{10}Be exposure dating of the timing of Neoglacial glacier advances in the Ecrins-Pelvoux massif, southern French Alps. *Quaternary Science Reviews*, **178**, 118–138.

Roy, P. S., Behera, M. D. and Srivastav, S. K. (2017) Satellite remote sensing: Sensors, applications and technique. *Proceedings of the National Academy of Sciences, India Section A: Physical Sciences*, **87**(4), 465–472.

Ryder, J. M. (1971) The stratigraphy and morphology of para-glacial alluvial fans in south-central British Columbia. *Canadian Journal of Earth Sciences*, **8**, 279–298.

Rye, N., Nesje, A., Lien, R. and Anda, E (1987) The Late Weichselian ice sheet in the Nordfjord - Sunnmøre area and deglaciation chronology for Nordfjord, western Norway. *Norsk Geografisk Tidsskrift - Norwegian Journal of Geography*, **41**(1), 23–43.

Sagredo, E. A. Kaplan, M. R., Araya, P. S., Lowell, T. V., Aravena, J. C., Moreno, P. I., Kelly, M. A. and Schaefer, J. M. (2018) Trans-pacific glacial response to the Antarctic Cold Reversal in the southern mid-latitudes. *Quaternary Science Reviews*, **188**, 160–166.

Sandeman, A. F. and Ballantyne, C. K. (1996) Talus rock glaciers in Scotland: Characteristics and controls on formation. *Scottish Geographical Magazine*, **112**(3), 138–146.

Sanders, J. W., Cuffey, K. M., MacGregor, K. R., Kavanaugh, J. L. and Dow, C. F. (2010) Dynamics of an alpine cirque glacier. *American Journal of Science*, **310**(8), 753–773.

Sanders, J. W., Cuffey, K. M., MacGregor, K. R., Kavanaugh, J. L. and Dow, C. F. (2018) Variations in the surface velocity of an alpine cirque glacier. *Journal of Glaciology*, **64**(248), 969–976.

Sanjaume, E. and Tolgensbakk, J. (2005) Raised beach forms and evidence of submarine permafrost on the Varanger Peninsula, North Norway. *Journal of Coastal Research*, **49**, 3–8.

Sanjaume, E. and Tolgensbakk, J. (2009) Beach ridges from the Varanger Peninsula (Arctic Norwegian coast): Characteristics and significance. *Geomorphology*, **104**(1–2), 82–92.

Sattler, K., Anderson, B., Mackintosh, A., Norton, K. and de Róiste, M. (2016) Estimating permafrost distribution in the maritime southern Alps, New Zealand, based on climatic conditions at rock glacier sites. *Frontiers in Earth Science*, **4**, 1–17.

Sauer, D., Sponagel, H., Sommer, M., Giani, L., Jahn, R. and Stahr, K. (2007) Podzol: Soil of the year 2007. A review on its genesis, occurrence, and functions. *Journal of Plant Nutrition and Soil Science*, **170**(5), 581–597.

Sauer, D. (2015) Pedological concepts to be considered in soil chronosequence studies. *Soil Research*, **53**(6), 577–591.

Schaffer, N., MacDonell, S., Réveillet, M., Yáñez, E. and Valois, R. (2019) Rock glaciers as a water resource in a changing climate in the semiarid Chilean Andes. *Regional Environmental Change*, **19**(5), 1263–1279.

Schimmelpfennig, I., Schaefer, J. M., Akçar, N., Ivy-Ochs, S., Finkel, R. C. and Schlüchter, C. (2012) Holocene glacier culminations in the Western Alps and their hemispheric relevance. *Geology*, **40**(10), 891–984.

Schimmelpfennig, I., Schaefer, J. M., Akçar, N., Koffman, T., Ivy-Ochs, S., Schwartz, R., Finkel, R. C., Zimmerman, S. and Schlüchter, C. (2014) A chronology of Holocene and Little Ice Age glacier culminations of the Steingletscher, Central Alps, Switzerland, based on high-sensitivity beryllium-10 moraine dating. *Earth and Planetary Science Letters*, **393**, 220–230.

Schleier, M., Hermanns, R. L., Rohn, J. and Gosse, J. C. (2015) Diagnostic characteristics and paleodynamics of supraglacial rock avalanches, Innerdalen, Western Norway. *Geomorphology*, **245**, 23–39.

Schomacker, A. (2008) What controls dead-ice melting under different climate conditions? A discussion. *Earth Science Reviews*, **90**(3–4), 103–113.

Screen, J. A. and Simmonds, I. (2010) The central role of diminishing sea ice in recent Arctic temperature amplification. *Nature*, **464**(7293), 1334–1337.

Seierstad, J., Nesje, A., Dahl, S. O. and Simonsen, J. R. (2002) Holocene glacier fluctuations of Grovabreen and Holocene snow-avalanche activity reconstructed from lake sediments in Grøningstølsvatnet, western Norway. *The Holocene*, **12**(2), 211–222.

Sejrup, H. P., Seppä, H., McKay, N. P., Kaufman, D. S., Geirsdóttir, Á., de Vernal, A., Renssen, H., Husum, K., Jennings, A. and Andrews, J. T. (2016) North Atlantic-

Fennoscandian Holocene climate trends and mechanisms. *Quaternary Science Reviews*, **147**, 365–378.

Seppä, H. and Birks, H. J. B. (2002) Holocene climate reconstructions from the Fennoscandian tree-line area based on pollen data from Toskaljavri. *Quaternary Research*, **57**(2), 191–199.

Seppä, H., Hammarlund, D. and Antonsson, K. (2005) Low-frequency and high-frequency changes in temperature and effective humidity during the Holocene in south-central Sweden: Implications for atmospheric and oceanic forcings of climate. *Climate Dynamics*, **25**(2–3), 285–297.

Seppä, H., Hannon, G. E. and Bradshaw, R. H. W. (2004) Holocene history of alpine vegetation and forestline on Pyhäkero mountain, northern Finland. *Arctic, Antarctic, and Alpine Research*, 36(4), 607–614.

Serrano, E., González-trueba, J. J., Sanjose, J. J. and Del Rio, L. M. (2011) Ice patch origin, evolution and dynamics in a temperate high mountain environment: The Jou Negro, Picos de Europa (NW Spain). *Geografiska Annaler: Series A Physical Geography*, **93**(2), 57–70.

Serrano, E., Oliva, M., González-García, M., López-Moreno, J. I., González-Trueba, J., Martín-Moreno, R., Gómez-Lende, M., Martín-Díaz, J., Nofre, J. and Palma, P. (2018) Post-Little Ice Age paraglacial processes and landforms in the high Iberian mountains: A review. *Land Degradation and Development*, **29**(11), 4186–4208.

Serrano, E. and López-Martínez, J. (2000) Rock glaciers in the South Shetland Islands, Western Antarctica. *Geomorphology*, 35(1–2), 145–162.

Serreze, M. C. and Barry, R. G. (2011) Processes and impacts of Arctic amplification: A research synthesis. *Global and Planetary Change*, **77**(1–2), 85–96.

Serreze, M. C. and Francis, J. A. (2006) The arctic amplification debate. *Climatic Change*, **76**(3–4), 241–264.

Shahtahmassebi, A., Yang, N., Wang, K., Moore, N. and Shen, Z. (2013) Review of shadow detection and de-shadowing methods in remote sensing. *Chinese Geographical Science*, **23**(4), 403–420.

Shakesby, R. A. (1997) Pronival (protalus) ramparts: A review of forms, processes, diagnostic criteria and palaeoenvironmental implications. *Progress in Physical Geography*, **21**(3), 394–418.

Shakesby, R. A., Matthews, J. A., Karlén, W. and Los, S. O. (2011) The Schmidt hammer as a Holocene calibrated-age dating technique: Testing the form of the R-value-age relationship and defining the predicted-age errors. *The Holocene*, **21**(4), 615–628.

Shakesby, R. A. Matthews, J. A., Winkler, S., Fabel, D. and Dresser, P. Q. (2020) Early-Holocene moraine chronology, Sognefjell area, southern Norway: evidence for multiple glacial and climatic fluctuations within the Erdalen Event (~10.2–9.7 ka). *Norwegian Journal of Geology Early-Holocene*, **100**(1), 1–28.

Shakesby, R. A., Matthews, J. A. and Owen, G. (2006) The Schmidt hammer as a relative-age dating tool and its potential for calibrated-age dating in Holocene glaciated environments. *Quaternary Science Reviews*, **25**(21–22), 2846–2867.

Shakesby, R. A., Matthews, J. A. and Schnabel, C. (2008) Cosmogenic ^{10}Be and ^{26}Al ages of Holocene moraines in southern Norway II: evidence for individualistic responses of high-altitude glaciers to millennial-scale climatic fluctuations. *The Holocene*, **18**(8), 1165–1177.

Shapiro, L. G. and Stockman, G. C. (2001) Computer Vision. New Jersey: Prentice Hall.

Sharp, M. (1984) Annual moraine ridges at Skalafellsjokull, southeast Iceland. *Journal of Glaciology*, **30**(104), 82–93.

Sharp, M. (1985) Sedimentation and Stratigraphy at Eyjabakkajökull - An Icelandic Surging Glacier. *Quaternary Research*, **24**(3), 268–284.

Sharpe, D. R. and Cowan, W. R. (1990) Moraine formation in northwestern Ontario: product of subglacial fluvial and glaciolacustrine sedimentation. *Canadian Journal of Earth Sciences*, **27**(11), 1478–1486.

Shepherd, A., Ivins, E. R., Geruo, A., Barletta, V. R., Bentley, M. J., Bettadpur, S., Briggs, K. H., Bromwich, D. H., Forsberg, R., Galin, N. and Horwath, M. (2012) A reconciled estimate of ice-sheet mass balance. *Science*, **338**(6111), 1183–1189.

Shilts, W. W., Aylsworth, J. M., Kaszycki, C. A., Klassen, R. A. and Graf, W. L. (1987) Canadian Shield. *Geomorphic Systems of North America*, **2**, 119–161

Shroder, J. F., Bishop, M. P., Copland, L. and Sloan, V. F. (2000) Debris-covered glaciers and rock glaciers in the Nanga Parbat Himalaya, Pakistan. *Geografiska Annaler: Series A Physical Geography*, **82**(1), 17–31.

Shulmeister, J., Davies, T. R., Evans, D. J. A., Hyatt, O. M. and Tovar, D. S. (2009) Catastrophic landslides, glacier behaviour and moraine formation–A view from an active plate margin. *Quaternary Science Reviews*, **28**(11-12), 1085-1096

Sikorski, J. J., Kaufman, D. S., Manley, W. F. and Nolan, M. (2009) Glacial-geologic evidence for decreased precipitation during the Little Ice Age in the Brooks Range, Alaska. *Arctic, Antarctic, and Alpine Research*, **41**(1), 138–150.

Sissons, J. B. (1974) A Late-Glacial Ice Cap in the Central Grampians, Scotland. *Transactions of the Institute of British Geographers*, **62**, 95–114.

Sissons, J. B. (1977) The Loch Lomond readvance in southern Skye and some palaeoclimatic implications. *Scottish Geographical Journal*, **1**, 23–36.

Sissons, J. B. (1979) The Loch Lomond advance in the Cairngorm Mountains. *Scottish Geographical Magazine*, **95**(2), 66–82.

Sissons, J. B. (1980) The Loch Lomond Advance in the Lake District, northern England. *Earth and Environmental Science Transactions of the Royal Society of Edinburgh*, **71**(1), 13–27.

Skuce, A. G., Jacobs, P., Green, S. A., Rice, K., Winkler, B., Richardson, M., Cook, J. and Skuce, A.G. (2016) Does It Matter if the Consensus on Anthropogenic Global Warming Is 97% or 99.99%? *Bulletin of Science, Technology & Society*, **36**(3), 150–156.

Slaymaker, O. (2009) Proglacial, periglacial or paraglacial? *Geological Society Special Publication*, **320**, 71–84.

Slingsby, W. C. (1898) Mountaineering in Arctic Norway. *Alpine Journal*, **9**, 414–437.

Slingsby, W. C. (1904) Norway, the Northern playground. Sketches of climbing and mountain exploration in Norway between 1872 and 1903. Edinburgh: David Douglas.

Smith, M. J. and Clark, C. D. (2005) Methods for the visualization of digital elevation models for landform mapping. *Earth Surface Processes and Landforms*, **30**(7), 885–900.

Sollid, J. L., Andersen, S., Hamre, N., Kjeldsen, O., Salvigsen, O., Sturød, S., Tveitå, T. and Wilhelmsen, A. (1973) Deglaciation of Finnmark, North Norway. *Norsk Geografisk Tidsskrift - Norwegian Journal of Geography*, 27(4), 233–325.

Solomina, O., Ivanov, M. and Bradwell, T. (2010) Lichenometric studies on moraines in the Polar Urals. *Geografiska Annaler: Series A Physical Geography*, **92**(1), 81–99.

Solomina, O. N., Bradley, R. S., Hodgson, D. A., Ivy-Ochs, S., Jomelli, V., Mackintosh, A. N., Nesje, A., Owen, L. A., Wanner, H., Wiles, G. C. and Young, N. E. (2015) Holocene glacier fluctuations. *Quaternary Science Reviews*, **111**, 9–34.

Solomina, O. N., Bradley, R. S., Jomelli, V., Geirsdottir, A., Kaufman, D. S., Koch, J., McKay, N. P., Masiokas, M., Miller, G., Nesje, A. and Nicolussi, K. (2016) Glacier fluctuations during the past 2000 years. *Quaternary Science Reviews*, **149**, 61–90.

Song, C., Sheng, Y., Wang, J., Ke, L., Madson, A. and Nie, Y. (2017) Heterogeneous glacial lake changes and links of lake expansions to the rapid thinning of adjacent glacier termini in the Himalayas. Geomorphology, **280**, 30–38.

Spedding, N. and Evans, D. J. A. (2002) Sediments and landforms at Kvíárjökull, southeast Iceland: A reappraisal of the glaciated valley landsystem. *Sedimentary Geology*, **149**(1–3), 21–42.

Speight, J. G. (1963) Late Pleistocene historical geomorphology of the Lake Pukaki area, New Zealand. *New Zealand Journal of Geology and Geophysics*, **6**(2), 160–188.

Statistics Norway (2020) Urban settlements: population and area, by municipality, Population and land area in urban settlements. https://www.ssb.no/en/befolkning/folketall/statistikk/tettsteders-befolkning-og-areal. Accessed on: 17.08.2021.

Stevens, P. R. and Walker, T. W. (1970) The chronosequence concept and soil formation. *The Quarterly Review of Biology*, **45**(4), 333–350.

Stewart, E. J., Wilson, J., Espiner, S., Purdie, H., Lemieux, C. and Dawson, J. (2016) Implications of climate change for glacier tourism. *Tourism Geographies*, **18**(4), 377–398.

Stibal, M., Bradley, J. A., Edwards, A., Hotaling, S., Zawierucha, K., Rosvold, J., Lutz, S., Cameron, K. A., Mikucki, J. A., Kohler, T. J. and Šabacká, M. (2020) Glacial ecosystems are essential to understanding biodiversity responses to glacier retreat. *Nature Ecology and Evolution*, **4**(5), 686–687.

Stjern, C. W., Lund, M. T., Samset, B. H., Myhre, G., Forster, P. M., Andrews, T., Boucher, O., Faluvegi, G., Fläschner, D., Iversen, T. and Kasoar, M. (2019) Arctic Amplification response to individual climate drivers. *Journal of Geophysical Research: Atmospheres*, **124**(13), 6698–6717.

Stocker, T. F. and Johnsen, S. J. (2003) A minimum thermodynamic model for the bipolar seesaw. *Paleoceanography*, **18**(4), 1–9.

Stoffel, M. and Huggel, C. (2012) Effects of climate change on mass movements in mountain environments. *Progress in Physical Geography*, **36**(3), 421–439.

Stoffel, M., Tiranti, D. and Huggel, C. (2014) Climate change impacts on mass movements - Case studies from the European Alps. *Science of the Total Environment*, **493**, 1255–1266.

Stokes, C. R., Spagnolo, M., Clark, C. D., Cofaigh, C. Ó., Lian, O. B. and Dunstone, R. B. (2013) Formation of mega-scale glacial lineations on the Dubawnt Lake Ice Stream bed: 1. size, shape and spacing from a large remote sensing dataset. *Quaternary Science Reviews*, **77**, 190–209.

Stokes, C. R., Corner, G. D., Winsborrow, M. C., Husum, K. and Andreassen, K. (2014) Asynchronous response of marine-terminating outlet glaciers during deglaciation of the Fennoscandian Ice Sheet. *Geology*, **42**(5), 455–458.

Stokes, C. R., Andreassen, L. M., Champion, M. R. and Corner, G. D. (2018) Widespread and accelerating glacier retreat on the Lyngen Peninsula, northern Norway, since their “Little Ice Age” maximum. *Journal of Glaciology*, **64**(243), 100–118.

Storrar, R. D., Evans, D. J. A., Stokes, C. R. and Ewertowski, M. (2015) Controls on the location, morphology and evolution of complex esker systems at decadal timescales, Breidamerkurjökull, southeast Iceland. *Earth Surface Processes and Landforms*, **40**(11), 1421–1438.

Storrar, R. D., Ewertowski, M., Tomczyk, A. M., Barr, I. D., Livingstone, S. J., Ruffell, A., Stoker, B. J. and Evans, D. J. A. (2020) Equifinality and preservation potential of complex eskers. *Boreas*, **49**(1), 211–231.

Storrar, R. D. and Livingstone, S. J. (2017) Glacial geomorphology of the northern Kivalliq region, Nunavut, Canada, with an emphasis on meltwater drainage systems. *Journal of Maps*, **13**(2), 153–164.

Storrar, R. D., Stokes, C. R. and Evans, D. J. A. (2014) Morphometry and pattern of a large sample (>20,000) of Canadian eskers and implications for subglacial drainage beneath ice sheets. *Quaternary Science Reviews*, **105**, 1–25.

Stroeven, A. P., Hättestrand, C., Kleman, J., Heyman, J., Fabel, D., Fredin, O., Goodfellow, B. W., Harbor, J. M., Jansen, J. D., Olsen, L. and Caffee, M. W.

(2016) Deglaciation of Fennoscandia. *Quaternary Science Reviews*, **147**, 91–121.

Strzelecki, M. C., Szczuciński, W., Dominiczak, A., Zagórski, P., Dudek, J. and Knight, J. (2020) New fjords, new coasts, new landscapes: The geomorphology of paraglacial coasts formed after recent glacier retreat in Brepollen (Hornsund, southern Svalbard). *Earth Surface Processes and Landforms*, **45**(5), 1325–1334.

Suter, P. J. J., Hafner, A. and Glauser, K. (2005) Prähistorische und frühgeschichtliche Funde aus dem Eis: der wiederentdeckte Pass über das Schnidejoch. *Archäologie der Schweiz*, **28**(4), 16–23.

Sutinen, R., Aro, I., Närhi, P., Piekkari, M. and Middleton, M. (2014) Maskevarri Ráhppát in Finnmark, northern Norway - Is it an earthquake-induced landform complex? *Solid Earth*, **5**(2), 683–691.

Sveian, H., Riiber, K., Bergstrøm, B. and Reite, A. J. (2005) Troms Fylke, løsmassekart M 1:310,000. Trondheim: Norges Geologiske Undersøkelse.

Svensson, H. (1962) Note on a type of patterned ground on the Varanger peninsula, Norway. *Geografiska Annaler*, **44**(3–4), 413–413.

Svensson, H. (1963) Tundra polygons. Photographic interpretation and field studies in North-Norwegian polygon areas. *NGU Series*, **223**, 298–327.

Teller, J. T., Leverington, D. W. and Mann, J. D. (2002) Freshwater outbursts to the oceans from glacial Lake Agassiz and their role in climate change during the last deglaciation. *Quaternary Science Reviews*, **21**(8–9), 879–887.

Tennant, C., Menounos, B., Wheate, R. and Clague, J. J. (2012) Area change of glaciers in the Canadian rocky mountains, 1919 to 2006. *The Cryosphere*, **6**(6), 1541–1552.

Thackeray, C. W. and Fletcher, C. G. (2016) Snow albedo feedback: Current knowledge, importance, outstanding issues and future directions. *Progress in Physical Geography*, **40**(3), 392–408.

Thackeray, S. J., Robinson, S. A., Smith, P., Bruno, R., Kirschbaum, M., Bernacchi, C., Byrne, M., Cheung, W., Cotrufo, M. F., Gienapp, P. and Hartley, S. (2020) Civil disobedience movements such as School Strike for the Climate are raising public awareness of the climate change emergency. *Faculty of Science, Medicine and Health - Papers: Part B.* Wollongong: University of Wollongong, 1–3.

Theakstone, W. H. (1965) Recent Changes in the Glaciers of Svartisen. *Journal of Glaciology*, **5**(40), 411–431.

Theakstone, W. H. (1990) Twentieth-century glacier change at Svartisen, Norway: the influence of climate, glacier geometry and glacier dynamics. *Annals of Glaciology*, **14**(1981), 283–287.

Theakstone, W. H. (2010) Glacier changes at Svartisen, northern Norway, during the last 125 years: Influence of climate and other factors. *Journal of Earth Science*, **21**(2), 123–136.

Thoman, R. L., Richter-Menge, J. and Druckenmiller, M. L. (2020) Arctic Report Card 2020. Washington, D.C.: National Oceanic and Atmospheric Administration

Thomas, E. R., Wolff, E. W., Mulvaney, R., Steffensen, J. P., Johnsen, S.J., Arrowsmith, C., White, J. W., Vaughn, B. and Popp, T. (2007) The 8.2 ka event from Greenland ice cores. *Quaternary Science Reviews*, **26**(1–2), 70–81.

Thompson, D. W. J. and Wallace, J. M. (1998) The Arctic Oscillation signature in the wintertime geopotential height and temperature fields. *Geophysical Research Letters*, **25**(9), 1297–1300.

Thompson, D. W. J. and Wallace, J. M. (2000) Annular modes in the extratropical circulation. Part I: Month-to-month variability. *Journal of Climate*, **13**(5), 1000–1016.

Thompson, H. R. (1957) Pangnirtung Pass: An exploratory geomorphology. Unpublished PhD thesis. McGill University, Department of Earth and Planetary Sciences.

Thomson, L. I., Osinski, G. R. and Ommanney, C. S. L. (2011) Glacier change on Axel Heiberg Island, Nunavut, Canada. *Journal of Glaciology*, **57**(206), 1079–1086.

Tinner, W. and Kaltenrieder, P. (2005) Rapid responses of high-mountain vegetation to early Holocene environmental changes in the Swiss Alps. *Journal of Ecology*, **93**(5), 936–947.

Tolgensbakk, J. and Sollid, J. L. (1988) Kåjford. Kvartaergologisk og geomorfologi 1634 II, M. 1:50,000. Oslo: Geografisk Institutt, Universitete i Oslo.

Tollefson, J. and Rodríguez-Mega, E. (2017) Argentinian geoscientist faces criminal charges over glacier survey. Nature. https://www.nature.com/articles/d41586-017-08236-y. Accessed on: 14.03.2018.

Tomkins, M. D., Dortch, J. M., Hughes, P. D., Huck, J. J., Stimson, A. G., Delmas, M., Calvet, M. and Pallàs, R. (2018a) Rapid age assessment of glacial landforms

in the Pyrenees using Schmidt hammer exposure dating (SHED). *Quaternary Research*, **90**(1), 26–37.

Tomkins, M. D., Huck, J. J., Dortch, J. M., Hughes, P. D., Kirbride, M. P. and Barr, I. D. (2018b) Schmidt Hammer exposure dating (SHED): Calibration procedures, new exposure age data and an online calculator. *Quaternary Geochronology*, **44**, 55–62.

Torsnes, I., Rye, N. and Nesje, A. (1993) Modern and Little Ice Age Equilibrium-Line Altitudes on outlet valley glaciers from Jostedalsbreen, western Norway: An evaluation of different approaches to their calculation. *Arctic and Alpine Research*, **25**(2), 106–116.

Turnbull, J. M. and Davies, T. R. H. (2006) A mass movement origin for cirques. *Earth Surface Processes and Landforms*, **31**(9), 1129–1148.

Turner, J. and Marshall, G. J. (2011) The Holocene. In Climate Change in the Polar Regions. Cambridge: Cambridge University Press, 194–255.

Vacco, D. A., Alley, R. B. and Pollard, D. (2010) Glacial advance and stagnation caused by rock avalanches. *Earth and Planetary Science Letters*, **294**(1–2), 123–130.

Vargas Bedemar, E. R. von. (1819) Reise nach dem hohen Norden durch Schweden, Norwegen und Lappland: in den Jahren 1810, 1811, 1812 und 1814 / von Vargas Bedemar. Volume 1. Lausanne: University of Lausanne.

Vavrus, S., Waliser, D., Schweiger, A. and Francis, J. (2009) Simulations of 20th and 21st century Arctic cloud amount in the global climate models assessed in the IPCC AR4. *Climate Dynamics*, **33**(7–8), 1099–1115.

Velle, G. (1998) A palaeoecological study of chironomids (Insecta: Diptera) with special reference to climate. Unpublished PhD thesis. University of Berge, Department of Geography.

Velle, G., Larsen, J., Eide, W., Peglar, S. M. and Birks, H. J. B. (2005) Holocene environmental history and climate of Råtåsjøen, a low-alpine lake in south-central Norway. *Journal of Paleolimnology*, **33**(2), 129–153.

Vere, D. M. and Matthews, J. A. (1985) Rock glacier formation from a lateral moraine at Bukkeholsbreen, Jotunheime, Norway: a sedimentological approach. *Zeitschrift für Geomorphologie Stuttgart*, **29**(4), 397–415.

Vick, L. M., Böhme, M., Rouyet, L., Bergh, S. G., Corner, G. D. and Lauknes, T. R. (2020) Structurally controlled rock slope deformation in northern Norway. Landslides. *Landslides*, **17**(8), 1745–1776.

Vikhamar-Schuler, D., Hanssen-Bauer, I. and Førland, E. (2010) Long-term climate trends of Finnmarksvidda, Northern-Norway. Oslo: Norwegian Meteorological Institute.

Voarintsoa, N. R. G., Railsback, L. B., Brook, G. A., Wang, L., Kathayat, G., Cheng, H., Li, X., Edwards, R. L., Rakotondrazafy, A. F. M. and Madison Razanatseheno, M. O. (2017) Three distinct Holocene intervals of stalagmite deposition and nondeposition revealed in NW Madagascar, and their paleoclimate implications. *Climate of the Past*, **13**(12), 1771–1790.

Voarintsoa, N. R. G., Matero, I. S., Railsback, L. B., Gregoire, L. J., Tindall, J., Sime, L., Cheng, H., Edwards, R. L., Brook, G. A., Kathayat, G. and Li, X. (2019) Investigating the 8.2 ka event in northwestern Madagascar: Insight from data–model comparisons. *Quaternary Science Reviews*, **204**, 172–186.

Vogt, J. H. L. (1913) Om to endemoræne-trin i det nordlige Norge. *Norsk Geografisk Tidsskrift - Norwegian Journal of Geography*, **2**(4), 397–415.

Wang, J. and Ikeda, M. (2000) Arctic oscillation and Arctic sea-ice oscillation. *Geophysical Research Letters*, **27**(9), 1287–1290.

Wanner, H., Beer, J., Bütikofer, J., Crowley, T. J., Cubasch, U., Flückiger, J., Goosse, H., Grosjean, M., Joos, F., Kaplan, J. O. and Küttel, M. (2008) Mid- to Late Holocene climate change: An overview. *Quaternary Science Reviews*, **27**(19–20), 1791–1828.

Wanner, H., Solomina, O., Grosjean, M., Ritz, S. P. and Jetel, M. (2011) Structure and origin of Holocene cold events. *Quaternary Science Reviews*, **30**(21–22), 3109–3123.

Van der Wateren, F. M. (2003) Ice-marginal Terrestrial Landsystems: Southern Scandinavian Ice Sheet Margin. In Evans, D. J. A. (ed.) Glacial Landsystems. London: Arnold, 166–203.

Waters, C. N., Zalasiewicz, J., Summerhayes, C., Barnosky, A.D., Poirier, C., Gałuszka, A., Cearreta, A., Edgeworth, M., Ellis, E.C., Ellis, M. and Jeandel, C. (2016) The Anthropocene is functionally and stratigraphically distinct from the Holocene. *Science*, **351**(6269) 137–147

Watson, C. S., King, O., Miles, E. S. and Quincey, D. J. (2018) Optimising NDWI supraglacial pond classification on Himalayan debris-covered glaciers. *Remote Sensing of Environment*, **217**, 414–425.

Weber, P., Boston, C. M., Lovell, H. and Andreassen, L. M. (2019) Evolution of the Norwegian plateau icefield Hardangerjøkulen since the “Little Ice Age”. *The Holocene*, **29**(12), 1885–1905.

Weber, P. (2020) Ice-marginal processes and retreat dynamics of Norwegian plateau icefields. Unpublished PhD thesis. University of Portsmouth, School of the Environment, Geography & Geosciences.

Weber, P., Lovell, H., Andreassen, L. M. and Boston, C. (2020) Reconstructing the Little Ice Age extent of Langfjordjøkelen, Arctic mainland Norway, as a baseline for assessing centennial-scale icefield recession. *Polar Research*, **39**, 1–21.

Weertman (1971) Shear Stress at the Base of a Rigidly Rotating Cirque Glacier. *Journal of Glaciology*, **10**(58), 31–37.

Werner, A. (1993) Holocene moraine chronology, Spitsbergen, Svalbard: lichenometric evidence for multiple Neoglacial advances in the Arctic. *The Holocene*, **3**(2), 128–137.

West, J. J. and Hovelsrud, G. K. (2008) Climate change in Northern Norway vulnerability of natural resource-dependent sectors and communities. *CICERO Report*, **4**, 1–37.

Westoby, M. J. Rounce, D.R., Shaw, T.E., Fyffe, C.L., Moore, P.L., Stewart, R.L. and Brock, B.W. (2020) Geomorphological evolution of a debris-covered glacier surface. *Earth Surface Processes and Landforms*, **45**(14), 3431–3448.

WGMS (1989) World Glacier Inventory - Status 1988. Edited by W. Haeberli et al. Zurich: IAHS (ICSI) / UNEP / UNESCO.

Whalley, B. (1976) A rock glacier and its relation to the mass balance of corrie glaciers, Strupbreen, Troms, Norway. *Norsk Geografisk Tidsskrift - Norwegian Journal of Geography*, **30**(2), 51–55.

Whalley, B. W., Gordon, J. E., Gellatly, A. F. and Hansom, J. D. (1995a) Plateau and valley glaciers in North Norway: responses to climate change over the last 100 years. *Zeitschrift für Gletscherkunde und Glazialgeologie*, **31**, 115–124.

Whalley, B. W., Hamilton, S. J., Palmer, C. F., Gordon, J. E. and Martin, H. E. (1995b) The dynamics of rock glaciers: data from Tröllaskagi, north Iceland. In

Slaymaker, O. (ed.) Steepland Geomorphology. New Jersey: John Wiley & Sons Ltd., 129–145.

Whalley, B. W., Rea, B. R., Rainey, M. M. and McAlister, J. J. (1997) Rock weathering in blockfields: Some preliminary data from mountain plateaus in north Norway. *Geological Society Special Publication*, **120**, 133–145.

Whalley, W. B. (1971) Observations of the drainage of an ice-dammed lake - Strupvatnet, Troms, Norway. *Norsk Geografisk Tidsskrift - Norwegian Journal of Geography*, **25**(3–4), 165–174.

Whalley, W. B. (1973) A note on the fluctuations of the level and size of Strupvatnet, Lyngen, Troms and the interpretation of ice loss on Strupbreen. *Norsk Geografisk Tidsskrift - Norwegian Journal of Geography*, **27**(1), 39–45.

Whalley, W. B. (1992) A rock glacier in south Ellendalen, Lyngen Alps, Troms. *Norsk Geografisk Tidsskrift - Norwegian Journal of Geography*, **46**(1), 29–31.

Whalley, W. B. (2009) On the interpretation of discrete debris accumulations associated with glaciers with special reference to the British Isles. *Geological Society Special Publication*, **320**, 85–102.

Whalley, W. B. (2012) Using Discrete Debris Accumulations to Help Interpret Upland Glaciation of the Younger Dryas in the British Isles. In Piacentini, T. (ed.) Studies on Environmental and Applied Geomorphology. Rijeka: InTech, 1–20.

Whalley, W. B. (2020) Gruben glacier and rock glacier, Wallis, Switzerland: glacier ice exposures and their interpretation. *Geografiska Annaler: Series A Physical Geography*, **102**(2), 141–161.

Whalley, W. B., Gordon, J. E. and Gellatly, A. F. (1989) Effects of Topographic and Climatic Controls on 19th and 20th Century Glacier Changes in the Lyngen and Bergsfjord Areas, North Norway. In Oerlemans, J. (ed.) Glacier Fluctuations and Climatic Change. Dordrecht: Springer, 153–172.

Whalley, W. B., Gordon, J. E. and Thompson, D. L. (1981) Periglacial Features on the Margins of a receding plateau ice cap, Lyngen, North Norway. *Journal of Glaciology*, **27**(97), 492–496.

Whalley, W. B. and Martin, H. E. (1992) Rock glaciers: II models and mechanisms. *Progress in Physical Geography*, **16**(2), 127–186.

Whalley, W. B., Martin, H. E. and Gellatly, A. F. (1986) The problem of “hidden” ice in glacier mapping. *Annals of Glaciology*, **8**, 181–183.

Widmann, M. (2009) Delayed Holocene warming. *Nature Geoscience*, **2**(6), 380–381.

Wiles, G. C., Barclay, D. J. and Young, N. E. (2010) A review of lichenometric dating of glacial moraines in Alaska. *Geografiska Annaler: Series A Physical Geography*, **92**(1), 101–109..

Williams, J. (1973) Neoglacial chronology of the Fourth of July Cirque, Central Colorado Front Range: Discussion. *Bulletin of the Geological Society of America*, **84**(11), 3761–3766.

Williams, R. S., Hall, D. K. and Benson, C. S. (1991) Analysis of glacier facies using satellite techniques. *Journal of Glaciology*, **37**(125), 120–128.

Wilson, P. (1990) Characteristics and Significance of Protalus Ramparts and Fossil Rock Glaciers on Errigal Mountain, County Donegal. *Proceedings of the Royal Irish Academy. Section B: Biological, Geological, and Chemical Science*, **90B**, 1–21.

Wilson, P. (2009) Rockfall talus slopes and associated talus-foot features in the glaciated uplands of Great Britain and Ireland: Periglacial, paraglacial or composite landforms? *Geological Society Special Publication*, **320**(1), 133–144.

Wilson, P. (2017) Periglacial and Paraglacial Processes, Landforms and Sediments. In Coxon, P., McCarron, S., and Mitchekk, F. (eds) Advances in Irish Quaternary Studies. Paris: Atlantis Press, 217–254.

Wilson, P., Linge, H., Matthews, J. A., Mourne, R. W. and Olsen, J. (2019) Comparative numerical surface exposure-age dating (10 Be and Schmidt hammer) of an early-Holocene rock avalanche at Alstadfjellet, Valldalen, southern Norway. *Geografiska Annaler: Series A, Physical Geography*, **101**(0), 293–309.

Wilson, P. Matthews, J. A., Mourne, R. W., Linge, H. and Olsen, J. (2020) Interpretation, age and significance of a relict paraglacial and periglacial boulder-dominated landform assemblage in Alnesdalen, Romsdalsalpane, southern Norway. *Geomorphology*, **369**, 1–16.

Winkler, S. (2000) The “Little Ice Age” maximum in the Southern Alps, New Zealand: Preliminary results at Mueller Glacier. *The Holocene*, **10**(5), 643–647.

Winkler, S. (2003) A new interpretation of the date of the “Little Ice Age” glacier maximum at Svartisen and Okstindan, northern Norway. *The Holocene*, **13**(1), 83–95.

Winkler, S. (2014) Investigation of late-Holocene moraines in the western Southern Alps, New Zealand, applying Schmidt-hammer exposure-age dating. *The Holocene*, **24**(1), 48–66.

Winkler, S., Elvehøy, H. and Nesje, A. (2009) Glacier fluctuations of Jostedalsbreen, western Norway, during the past 20 years: the sensitive response of maritime mountain glaciers. *The Holocene*, **19**(3), 395–414.

Winkler, S. and Lambiel, C. (2018) Age constraints of rock glaciers in the Southern Alps/New Zealand - Exploring their palaeoclimatic potential. *The Holocene*, **28**(5), 778–790.

Winkler, S. and Matthews, J. A. (2010) Observations on terminal moraine-ridge formation during recent advances of southern Norwegian glaciers. *Geomorphology*, **116**(1–2), 87–106.

Winkler, S. and Nesje, A. (2009) Perturbation of climatic response at maritime glaciers? *Erdkunde*, **63**(3), 229–244.

Winsvold, S. H., Andreassen, L. M. and Kienholz, C. (2014) Glacier area and length changes in Norway from repeat inventories. *The Cryosphere*, **8**(5), 1885–1903.

Wittmeier, H. E., Bakke, J., Vasskog, K. and Trachsel, M. (2015) Reconstructing Holocene glacier activity at Langfjordjøkelen, Arctic Norway, using multi-proxy fingerprinting of distal glacier-fed lake sediments *Quaternary Science Reviews*, **114**, 78–99.

Wittmeier, H. E., Schaefer, J. M., Bakke, J., Rupper, S., Paasche, Ø., Schwartz, R. and Finkel, R. C. (2020) Late Glacial mountain glacier culmination in Arctic Norway prior to the Younger Dryas. *Quaternary Science Reviews*, **245**, 1–13.

Wolfe, S. A., Stevens, C. W., Gaanderse, A. J. and Oldenborger, G. A. (2014) Lithalsa distribution, morphology and landscape associations in the Great Slave Lowland, Northwest Territories, Canada. *Geomorphology*, **204**, 302–313.

Woo, M. K. and Young, K. L. (2014) Disappearing semi-permanent snow in the High Arctic and its consequences. *Journal of Glaciology*, **60**(219), 192–200.

De Woul, M. and Hock, R. (2005) Static mass-balance sensitivity of Arctic glaciers and ice caps using a degree-day approach. *Annals of Glaciology*, **42**, 217–224.

Wrona, F. J. Johansson, M., Culp, J. M., Jenkins, A., Mård, J., Myers-Smith, I. H., Prowse, T. D., Vincent, W. F. and Wookey, P. A. (2016) Transitions in Arctic ecosystems: Ecological implications of a changing hydrological regime. *Journal of Geophysical Research Biogeosciences*, **3**, 650–674.

Xiang, Y., Gao, Y. and Yao, T. (2014) Glacier change in the Poiqu River basin inferred from Landsat data from 1975 to 2010. *Quaternary International*, **349**, 392–401.

Xu, M., Bogen, J., Wang, Z., Bønsnes, T. E. and Gytri, S. (2015) Pro-glacial lake sedimentation from jökulhlaups (GLOF), Blåmannsisen, northern Norway. *Earth Surface Processes and Landforms*, **40**(5), 654–665.

Yang, X. Y., Fyfe, J. C. and Flato, G. M. (2010) The role of poleward energy transport in arctic temperature evolution. *Geophysical Research Letters*, **37**(14), 1–5.

Young, K. L., Brown, L. and Labine, C. (2018) Snowcover variability at Polar Bear Pass, Nunavut. *Arctic Science*, **4**(4), 669–690.

Young, N. E., Briner, J. P., Leonard, E. M., Licciardi, J. M. and Lee, K. (2011) Assessing climatic and nonclimatic forcing of Pinedale glaciation and deglaciation in the western United States. *Geology*, **39**(2), 171–174.

Young, N. E., Briner, J. P., Rood, D. H. and Finkel, R. C. (2012) Glacier extent during the younger dryas and 8.2-ka event on Baffin Island, Arctic Canada. *Science*, **337**, 1130–1333.

Zalasiewicz, J., Waters, C. N., Summerhayes, C. P., Wolfe, A. P., Barnosky, A. D., Cearreta, A., Crutzen, P., Ellis, E., Fairchild, I. J., Gałuszka, A. and Haff, P. (2017) The Working Group on the Anthropocene: Summary of evidence and interim recommendations. *Anthropocene*, **19**, 55–60.

Zalasiewicz, J., Waters, C., Summerhayes, C. and Williams, M. (2018) The Anthropocene. *Geology Today*, **34**(5), 177–181.

Žebre, M. and Stepišnik, U. (2015) Glaciokarst landforms and processes of the southern Dinaric Alps. *Earth Surface Processes and Landforms*, **40**(11), 1493–1505.

Zemp, M. (2008) Global glacier changes: facts and figures. In Zemp, M. and J. van Woerden (eds). Hertfordshire: UNEP/Earthprint, 24–26

Zemp, M., Frey, H., Gärtner-Roer, I., Nussbaumer, S. U., Hoelzle, M., Paul, F., Haeberli, W., Denzinger, F., Ahlstrøm, A. P., Anderson, B. and Bajracharya, S. (2015) Historically unprecedented global glacier decline in the early 21st century. *Journal of Glaciology*, **61**(228), 745–762.

Zemp, M., Huss, M., Thibert, E., Eckert, N., McNabb, R., Huber, J., Barandun, M., Machguth, H., Nussbaumer, S.U., Gärtner-Roer, I. and Thomson, L. (2019) Global glacier mass changes and their contributions to sea-level rise from 1961 to 2016. *Nature*, **568**(7752), 382–386.

Zhang, T. (2005) Influence of the seasonal snow cover on the ground thermal regime: An overview. *Reviews of Geophysics*, **43**(4), 1–23.

Zhang, Y., Gao, T., Kang, S., Shangguan, D. and Luo, X. (2021) Albedo reduction as an important driver for glacier melting in Tibetan Plateau and its surrounding areas. *Earth Science Reviews*, **220**, 1–11.

Zhu, C., Zhang, J. and Cheng, P. (1996) Rock Glaciers in the Central Tianshan Mountains, China. *Permafrost and Periglacial Processes*, **7**(1), 69–78.

APPENDIX A

Glacial and periglacial geomorphology of central Troms and Finnmark county, Arctic Norway. Due to file-size limits the following map is a screengrab, a higher-resolution version of this map can be downloaded from the supplementary information of Leigh et al. (2020): https://doi.org/10.1080/17445647.2021.1950580.

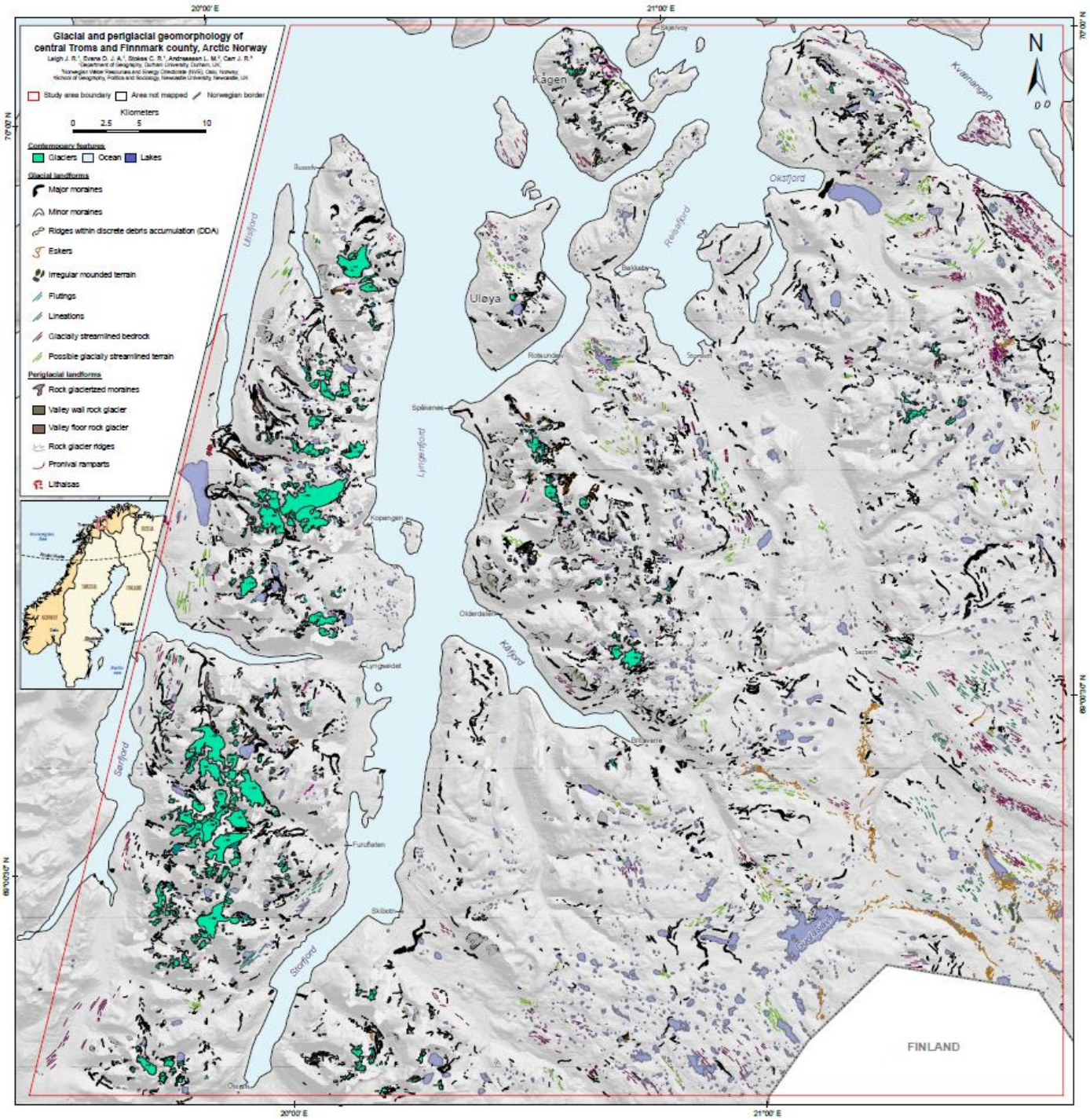

APPENDIX B

A table detailing all key objects (e.g. glaciers, moraines, samples) and their locations. Location details are taken from Google Earth and displayed in degrees, minutes, seconds.

Feature Type	Feature ID/Name	Location (degrees, minutes, and seconds)
Glacier	26 (Svartfjelljøkelen)	70°13'54.33"N, 21°54'42.56"E
Glacier	34	70°11'8.53"N, 22°10'23.24"E
Glacier	38	70°11'11.08"N, 22°8'39.89"E
Glacier	39	70°11'35.20"N, 22°1'27.30"E
Glacier	41	70°11'12.40"N, 22°6'4.25"E
Glacier	43 (Isdaljøkelen)	70°10'20.39"N, 21°56'41.60"E
Glacier	47 (Isfjordjøkelen)	70° 8'14.57"N, 22°4'11.38"E
Glacier	48 (Nerisen)	70° 7'46.55"N, 22°3'49.06"E
Glacier	54 (Langfjord East)	70°07'33.4"N, 21°47'01.8"E
Glacier	62 (Rødhetta)	70° 9'31.03"N, 20°43'31.91"E
Glacier	74	69°58'24.88"N, 21°21'35.88"E
Glacier	115 (Sorbmejiehkki)	69°44'44.08"N, 20°39'8.80"E
Glacier	117	69°44'22.31"N, 20°39'24.24"E
Glacier	121	69°43'41.73"N, 20°38'0.93"E
Glacier	123	69°43'5.29"N, 20°38'36.45"E
Glacier	126	69°42'5.54"N, 20°39'25.50"E
Glacier	127 (Goahtejiehkki)	69°41'29.73"N, 20°39'45.90"E
Glacier	129	69°40'53.57"N, 20°40'33.97"E
Glacier	130	69°40'11.63"N, 20°54'25.15"E
Glacier	131	69°40'37.65"N, 20°40'46.74"E
Glacier	132	69°40'26.42"N, 20°41'15.21"E
Glacier	136	69°38'40.60"N, 20°48'33.29"E
Glacier	138	69°38'26.41"N, 20°48'2.12"E
Glacier	141	69°38'10.51"N, 20°49'25.70"E
Glacier	142	69°37'45.73"N, 20°50'52.97"E
Glacier	151	69°35'21.44"N, 20°52'13.68"E
Glacier	155	69°34'21.95"N, 20°48'12.62"E
Glacier	157	69°34'0.24"N, 20°46'15.53"E
Glacier	158 (Noammerjiehkki)	69°33'43.74"N, 20°48'9.95"E
Glacier	109	69°43'34.44"N, 21°29'6.60"E
Glacier	110	69°43'26.39"N, 21°27'44.66"E
Glacier	111	69°43'32.14"N, 21°26'50.48"E
Glacier	113	69°43'9.66"N, 21°26'35.96"E
Glacier	190	69°44'6.14"N, 20°15'10.22"E
Glacier	199 (west Lenangsbreen)	69°42'42.79"N, 20°2'27.90"E
Glacier	201 (east Lenangsbreen)	69°42'37.48"N, 20°3'39.15"E
Glacier	202	69°42'13.49"N, 20°0'52.15"E
Glacier	204	69°41'42.33"N, 20°0'6.44"E
Glacier	220	69°36'20.89"N, 20°6'8.59"E
Glacier	222 (Kjosen)	69°36'9.89"N, 20°5'8.33"E
Glacier	227 (Kvalvikdalsbreen)	69°31'43.71"N, 20°2'11.93"E

Glacier	234	69°30'26.88"N, 19°59'51.01"E
Glacier	238 (Rypedalsvatnbreen)	69°30'15.4"N, 19°57'15.6"E
Glacier	257 (Sydbreen)	69°27'12.87"N, 19°55'44.50"E
Glacier	264 (north Veidalsbreen)	69°25'28.0"N 19°53'03.9"E
Glacier	364	69°51'2.37"N, 19°14'26.19"E
Glacier	2316 (Briksdalsbreen)	61°39'52.3"N 6°52'54.0"E
Glacier	Unmapped glacier (p. 107)	69°38'8.66"N, 20°35'24.46"E
Glacier	Unmapped glacier (p. 113)	69°38'10.57"N, 20°32'38.75"E
Mountain	Jiehkkevárri	69°28'3.39"N, 19°52'46.47"E
Geomorphological	Lateral moraine	69°44'31.96"N, 20°40'14.36"E
Mountain	Jettan rockslide	69°33'23.62"N, 20°24'48.04"E
Geomorphological	Ploughing boulder	69°43'19.72"N, 20°42'7.48"E
Geomorphological	Erdalen Event moraine	61°50'36.4"N 7°10'35.1"E
Geomorphological	Barheivatn (lake)	69°41'58.02"N, 19°51'13.68"E
Geomorphological	Dalmutladdo (lake)	69°11'23.8"N 20°43'54.6"E
Geomorphological	Øvrefetene (Finse Site)	60°34'25"N, 7°30'54"E
Geomorphological	Nigardsbreen LIA moiraine	61°39'16.8"N 7°16'30.4"E
Geomorphological	Engabreen LIA moiraine	66°42'10"N, 13°43'21"E
Geomorphological	Sør-Tverrfjorddalen	70°11'2.58"N, 21°41'35.63"E
Mountain	Goahtegáisá	69°41'23.59"N, 20°38'44.40"E
Landmark	Rotsundelv churchyard	69°47'18.30"N, 20°42'30.58"E
Landmark	Storslett churchyard	69°46'11.88"N, 21° 2'5.43"E
Geomorphological	115 M1 (Table 4.1)	69°44'52.04"N, 20°39'49.25"E
Geomorphological	117 M1 (Table 4.1)	69°44'25.50"N, 20°40'31.34"E
Geomorphological	117 M2 (Table 4.1)	69°44'27.05"N, 20°40'31.30"E
Geomorphological	117 M3 (Table 4.1)	69°44'30.01"N, 20°40'29.81"E
Geomorphological	121 M1 (Table 4.1)	69°43'27.43"N, 20°40'6.89"E
Geomorphological	121 M2 (Table 4.1)	69°43'27.98"N, 20°39'57.90"E
Geomorphological	121 M3 (Table 4.1)	69°43'44.61"N, 20°39'24.16"E
Geomorphological	121 M6 (Table 4.1)	69°43'39.38"N, 20°39'24.95"E
Geomorphological	121 M7 (Table 4.1)	69°43'39.66"N, 20°39'22.82"E
Geomorphological	121 M8 (Table 4.1)	69°43'40.11"N, 20°39'16.65"E
Geomorphological	123 M1(1) (Table 4.1)	69°42'56.55"N, 20°39'35.45"E
Geomorphological	123 M1(2) (Table 4.1)	69°43'2.41"N, 20°39'26.58"E
Geomorphological	123 M2 (Table 4.1)	69°42'56.83"N, 20°39'31.95"E
Geomorphological	123 M4 (Table 4.1)	69°42'59.88"N, 20°39'9.74"E
Geomorphological	123 M5 (Table 4.1)	69°43'10.75"N, 20°39'3.94"E
Geomorphological	123 M6 (Table 4.1)	69°42'57.64"N, 20°39'7.31"E
Geomorphological	123 M8 (Table 4.1)	69°43'10.56"N, 20°38'57.68"E
Glacier	Unmapped glacier (p. 276)	69°42'42.16"N, 20°40'28.64"E
Geomorphological	Rock glaciers	69°45'37.93"N, 20°3'49.83"E
Sample (soil)	RV19SP01	69°43'48.30"N, 20°42'8.52"E
Sample (soil)	RV19SP02	69°43'48.09"N, 20°42'8.57"E
Sample (soil)	RV19SP03	69°43'21.22"N, 20°40'18.03"E
Sample (soil)	RV19SP04	69°43'21.15"N, 20°40'22.73"E
Sample (soil)	RV19SP05	69°43'23.56"N, 20°40'27.25"E
Sample (soil)	RV19SP06	69°43'32.67"N, 20°40'55.64"E
Sample (soil)	RV19SP07	69°43'33.34"N, 20°40'52.57"E
Sample (soil)	RV19SP08	69°43'33.69"N, 20°40'47.88"E
Sample (soil)	RV19SP09	69°43'42.88"N, 20°41'30.43"E
Sample (soil)	RV19SP10	69°43'53.86"N, 20°42'10.45"E
Sample (soil)	RV19SP11	69°43'38.19"N, 20°41'37.66"E
Sample (soil)	RV19SP12	69°43'36.34"N, 20°42'12.92"E

Sample (soil)	RV19SP13	69°43'40.73"N, 20°41'35.26"E
Sample (soil)	RV19SP14	69°43'36.38"N, 20°42'7.95"E
Sample (soil)	RV19SP15	69°43'40.05"N, 20°42'7.40"E
Sample (soil)	RV19SP16	69°44'37.35"N, 20°41'32.99"E
Sample (soil)	RV19SP17	69°44'28.86"N, 20°41'31.65"E
Sample (soil)	RV19SP18	69°44'25.64"N, 20°41'34.13"E
Sample (soil)	RV19SP19	69°44'37.56"N, 20°41'55.73"E
Sample (soil)	RV19SP20	69°44'30.75"N, 20°42'12.67"E
Sample (soil)	RV19SP21	69°44'26.67"N, 20°41'57.77"E
Sample (soil)	RV19SP22	69°44'28.04"N, 20°41'53.47"E
Sample (soil)	RV19SP23	69°44'30.81"N, 20°41'58.73"E
Sample (soil)	RV19SP24	69°44'33.61"N, 20°41'59.34"E
Sample (soil)	RV19SP25	69°42'16.60"N, 20°43'1.23"E
Sample (soil)	RV19SP26	69°42'18.24"N, 20°43'0.42"E
Sample (soil)	RV19SP27	69°42'19.15"N, 20°42'57.24"E
Sample (soil)	RV19SP28	69°42'4.13"N, 20°42'6.82"E
Sample (soil)	RV19SP29	69°42'1.95"N, 20°42'8.94"E
Sample (soil)	RV19SP30	69°42'0.94"N, 20°42'9.35"E
Sample (S-hammer)	RV19G121M1B1	69°43'54.42"N, 20°42'20.03"E
Sample (S-hammer)	RV19G121M1B2	69°43'53.62"N, 20°42'9.66"E
Sample (S-hammer)	RV19G121M1B3	69°43'36.95"N, 20°42'22.46"E
Sample (S-hammer)	RV19G121M1B4	69°43'36.83"N, 20°42'23.08"E
Sample (S-hammer)	RV19G121M1B5	69°43'36.64"N, 20°42'8.13"E
Sample (S-hammer)	RV19G121M1B6	69°43'36.83"N, 20°42'23.08"E
Sample (S-hammer)	RV19G121M1B7	69°43'36.38"N, 20°42'5.06"E
Sample (S-hammer)	RV19G121M1B8	69°43'35.55"N, 20°42'1.44"E
Sample (S-hammer)	RV19G121M1B9	69°43'54.55"N, 20°42'17.82"E
Sample (S-hammer)	RV19G121M1B10	69°43'53.66"N, 20°42'7.85"E
Sample (S-hammer)	RV19G121M2B1	69°43'38.47"N, 20°42'4.89"E
Sample (S-hammer)	RV19G121M2B2	69°43'38.82"N, 20°42'6.43"E
Sample (S-hammer)	RV19G121M2B3	69°43'39.17"N, 20°42'7.62"E
Sample (S-hammer)	RV19G121M2B4	69°43'39.55"N, 20°42'8.13"E
Sample (S-hammer)	RV19G121M2B5	69°43'40.67"N, 20°42'7.65"E
Sample (S-hammer)	RV19G121M2B6	69°43'47.27"N, 20°42'9.81"E
Sample (S-hammer)	RV19G121M2B7	69°43'47.76"N, 20°42'9.42"E
Sample (S-hammer)	RV19G121M2B8	69°43'47.97"N, 20°42'9.53"E
Sample (S-hammer)	RV19G121M2B9	69°43'48.98"N, 20°42'8.42"E
Sample (S-hammer)	RV19G121M2B10	69°43'49.57"N, 20°42'8.14"E
Sample (S-hammer)	RV19G121M3B1	69°43'43.61"N, 20°41'30.36"E
Sample (S-hammer)	RV19G121M3B2	69°43'43.06"N, 20°41'30.36"E
Sample (S-hammer)	RV19G121M3B3	69°43'35.84"N, 20°41'33.76"E
Sample (S-hammer)	RV19G121M3B4	69°43'37.05"N, 20°41'35.82"E
Sample (S-hammer)	RV19G121M3B5	69°43'42.66"N, 20°41'31.83"E
Sample (S-hammer)	RV19G121M3B6	69°43'43.14"N, 20°41'30.05"E
Sample (S-hammer)	RV19G121M3B7	69°43'43.21"N, 20°41'30.80"E
Sample (S-hammer)	RV19G121M3B8	69°43'36.17"N, 20°41'34.27"E
Sample (S-hammer)	RV19G121M3B9	69°43'38.27"N, 20°41'37.77"E
Sample (S-hammer)	RV19G121M3B10	69°43'40.93"N, 20°41'35.49"E
Sample (S-hammer)	RV19G121M4B1	69°43'31.20"N, 20°41'2.99"E
Sample (S-hammer)	RV19G121M4B2	69°43'30.84"N, 20°41'2.93"E
Sample (S-hammer)	RV19G121M4B3	69°43'33.73"N, 20°40'49.57"E
Sample (S-hammer)	RV19G121M4B4	69°43'32.76"N, 20°40'55.91"E
Sample (S-hammer)	RV19G121M4B5	69°43'32.76"N, 20°40'55.91"E

Sample (S-hammer)	RV19G121M4B6	69°43'32.64"N, 20°40'53.34"E
Sample (S-hammer)	RV19G121M4B7	69°43'33.36"N, 20°40'51.35"E
Sample (S-hammer)	RV19G121M4B8	69°43'33.66"N, 20°40'49.92"E
Sample (S-hammer)	RV19G121M4B9	69°43'33.64"N, 20°40'49.27"E
Sample (S-hammer)	RV19G121M4B10	69°43'32.78"N, 20°40'42.93"E
Sample (S-hammer)	RV19G121M5B1	69°43'21.27"N, 20°40'17.93"E
Sample (S-hammer)	RV19G121M5B2	69°43'21.14"N, 20°40'21.96"E
Sample (S-hammer)	RV19G121M5B3	69°43'22.61"N, 20°40'26.46"E
Sample (S-hammer)	RV19G121M5B4	69°43'24.42"N, 20°40'31.01"E
Sample (S-hammer)	RV19G121M5B5	69°43'21.37"N, 20°40'24.76"E
Sample (S-hammer)	RV19G121M5B6	69°43'20.91"N, 20°40'22.69"E
Sample (S-hammer)	RV19G121M5B7	69°43'21.39"N, 20°40'23.66"E
Sample (S-hammer)	RV19G121M5B8	69°43'23.56"N, 20°40'27.13"E
Sample (S-hammer)	RV19G121M5B9	69°43'24.52"N, 20°40'31.40"E
Sample (S-hammer)	RV19G121M5B10	69°43'25.11"N, 20°40'34.14"E
Sample (S-hammer)	RV19G117M1B1	69°44'26.89"N, 20°41'55.16"E
Sample (S-hammer)	RV19G117M1B2	69°44'26.66"N, 20°41'57.66"E
Sample (S-hammer)	RV19G117M1B3	69°44'26.66"N, 20°41'57.66"E
Sample (S-hammer)	RV19G117M1B4	69°44'26.73"N, 20°42'4.86"E
Sample (S-hammer)	RV19G117M1B5	69°44'28.05"N, 20°42'12.28"E
Sample (S-hammer)	RV19G117M1B6	69°44'30.66"N, 20°42'12.69"E
Sample (S-hammer)	RV19G117M1B7	69°44'34.27"N, 20°42'12.18"E
Sample (S-hammer)	RV19G117M1B8	69°44'36.36"N, 20°42'6.81"E
Sample (S-hammer)	RV19G117M1B9	69°44'36.26"N, 20°42'2.17"E
Sample (S-hammer)	RV19G117M1B10	69°44'36.68"N, 20°41'59.55"E
Sample (S-hammer)	RV19G117M2B1	69°44'28.19"N, 20°41'53.24"E
Sample (S-hammer)	RV19G117M2B2	69°44'28.54"N, 20°41'55.21"E
Sample (S-hammer)	RV19G117M2B3	69°44'28.55"N, 20°41'56.69"E
Sample (S-hammer)	RV19G117M2B4	69°44'29.21"N, 20°41'58.25"E
Sample (S-hammer)	RV19G117M2B5	69°44'31.00"N, 20°41'58.23"E
Sample (S-hammer)	RV19G117M2B6	69°44'31.29"N, 20°41'58.34"E
Sample (S-hammer)	RV19G117M2B7	69°44'32.34"N, 20°41'59.64"E
Sample (S-hammer)	RV19G117M2B8	69°44'33.83"N, 20°41'58.95"E
Sample (S-hammer)	RV19G117M2B9	69°44'34.48"N, 20°41'58.24"E
Sample (S-hammer)	RV19G117M2B10	69°44'34.80"N, 20°41'57.05"E
Sample (S-hammer)	RV19G117M3B1	69°44'37.41"N, 20°41'32.80"E
Sample (S-hammer)	RV19G117M3B2	69°44'36.51"N, 20°41'34.92"E
Sample (S-hammer)	RV19G117M3B3	69°44'35.58"N, 20°41'36.43"E
Sample (S-hammer)	RV19G117M3B4	69°44'34.77"N, 20°41'36.96"E
Sample (S-hammer)	RV19G117M3B5	69°44'33.96"N, 20°41'37.86"E
Sample (S-hammer)	RV19G117M3B6	69°44'31.83"N, 20°41'36.23"E
Sample (S-hammer)	RV19G117M3B7	69°44'30.83"N, 20°41'33.52"E
Sample (S-hammer)	RV19G117M3B8	69°44'30.83"N, 20°41'33.52"E
Sample (S-hammer)	RV19G117M3B9	69°44'26.32"N, 20°41'32.78"E
Sample (S-hammer)	RV19G117M3B10	69°44'24.87"N, 20°41'31.60"E
Sample (S-hammer)	SV19M8B1	69°44'0.55"N, 20°2'10.04"E
Sample (S-hammer)	SV19M8B2	69°44'0.59"N, 20°2'8.48"E
Sample (S-hammer)	SV19M8B3	69°44'0.95"N, 20°2'5.58"E
Sample (S-hammer)	SV19M8B4	69°44'1.91"N, 20°2'0.88"E
Sample (S-hammer)	SV19M8B5	69°44'2.55"N, 20°1'58.03"E
Sample (S-hammer)	SV19M8B6	69°44'3.01"N, 20°1'53.94"E
Sample (S-hammer)	SV19M8B7	69°44'3.06"N, 20°1'46.59"E
Sample (S-hammer)	SV19M8B8	69°44'2.91"N, 20°1'40.59"E

Sample (S-hammer)	SV19M8B9	69°44'1.75"N, 20°1'31.75"E
Sample (S-hammer)	SV19M8B10	69°44'0.43"N, 20°1'23.67"E
Sample (S-hammer)	SV19M9B1	69°43'56.82"N, 20°1'49.65"E
Sample (S-hammer)	SV19M9B2	69°43'56.82"N, 20°1'49.65"E
Sample (S-hammer)	SV19M9B3	69°43'56.81"N, 20°1'47.69"E
Sample (S-hammer)	SV19M9B4	69°43'56.79"N, 20°1'45.62"E
Sample (S-hammer)	SV19M9B5	69°43'55.93"N, 20°1'37.54"E
Sample (S-hammer)	SV19M9B6	69°43'55.93"N, 20°1'33.61"E
Sample (S-hammer)	SV19M9B7	69°43'56.51"N, 20°1'28.90"E
Sample (S-hammer)	SV19M9B8	69°43'56.63"N, 20°1'24.43"E
Sample (S-hammer)	SV19M9B9	69°43'56.73"N, 20°1'22.43"E
Sample (S-hammer)	SV19M9B10	69°43'56.57"N, 20°1'19.41"E
Sample (S-hammer)	SV19M11B1	69°43'48.22"N, 20°2'26.82"E
Sample (S-hammer)	SV19M11B2	69°43'47.24"N, 20°2'29.37"E
Sample (S-hammer)	SV19M11B3	69°43'46.59"N, 20°2'30.80"E
Sample (S-hammer)	SV19M11B4	69°43'43.33"N, 20°2'36.59"E
Sample (S-hammer)	SV19M11B5	69°43'43.15"N, 20°2'37.22"E
Sample (S-hammer)	SV19M11B6	69°43'41.43"N, 20°2'41.65"E
Sample (S-hammer)	SV19M11B7	69°43'41.43"N, 20°2'41.65"E
Sample (S-hammer)	SV19M11B8	69°43'41.15"N, 20°2'42.26"E
Sample (S-hammer)	SV19M11B9	69°43'41.04"N, 20°2'42.98"E
Sample (S-hammer)	SV19M11B10	69°43'40.67"N, 20°2'43.65"E
Sample (S-hammer)	SV19M12B1	69°43'40.71"N, 20°2'38.38"E
Sample (S-hammer)	SV19M12B2	69°43'41.04"N, 20°2'37.49"E
Sample (S-hammer)	SV19M12B3	69°43'42.23"N, 20°2'35.70"E
Sample (S-hammer)	SV19M12B4	69°43'42.23"N, 20°2'35.70"E
Sample (S-hammer)	SV19M12B5	69°43'42.23"N, 20°2'35.70"E
Sample (S-hammer)	SV19M12B6	69°43'42.23"N, 20°2'35.70"E
Sample (S-hammer)	SV19M12B7	69°43'43.90"N, 20°2'31.56"E
Sample (S-hammer)	SV19M12B8	69°43'44.50"N, 20°2'29.73"E
Sample (S-hammer)	SV19M12B9	69°43'45.96"N, 20°2'27.38"E
Sample (S-hammer)	SV19M12B10	69°43'46.68"N, 20°2'23.80"E